

**Utilising airborne scanning laser (LiDAR) to  
improve the assessment of Australian native  
forest structure**

**Alex C. Lee**

**BSc, MSc (Auckland)**

**Submitted in fulfilment of the requirements for the degree of  
Doctor of Philosophy  
at the Australian National University**

**October 2008**





**River Red Gum (*E. camaldulensis*) located on an island in the Murray river, NE Victoria.**

---

---

## TABLE OF CONTENTS

---

<b>List of Figures.....</b>	<b><i>x</i></b>
<b>List of Tables.....</b>	<b><i>xvi</i></b>
<b>List of Equations.....</b>	<b><i>xviii</i></b>
<b>List of Abbreviations.....</b>	<b><i>xix</i></b>
<b>Certificate of Authorship.....</b>	<b><i>xxi</i></b>
<b>Preface.....</b>	<b><i>xxii</i></b>
<b>Acknowledgements.....</b>	<b><i>xxiii</i></b>
<b>Abstract.....</b>	<b><i>xxiv</i></b>
<b>Chapter 1. Introduction.....</b>	<b>1</b>
<b>1.1 Introduction .....</b>	<b>1</b>
1.1.1 The requirement for forest information.....	1
1.1.2 Forest assessment in Australia .....	4
<i>State of the Forest Reporting .....</i>	<i>4</i>
<i>Continental Forest Monitoring .....</i>	<i>7</i>
1.1.3 Dealing with scale in remote sensing of forests .....	10
1.1.4 Summary .....	13
<b>1.2 Thesis Research Question .....</b>	<b>15</b>
1.2.1 Primary research question .....	15
<i>Rationale and Research Objectives.....</i>	<i>15</i>
<i>Objective 1: Measuring forest cover using LiDAR.....</i>	<i>16</i>
<i>Objective 2: Measuring forest height using LiDAR.....</i>	<i>17</i>
1.2.2 Research delimitations .....	18
<b>1.3 Outline of Thesis.....</b>	<b>20</b>
<b>Chapter 2. Research issues .....</b>	<b>21</b>
<b>2.1 Introduction .....</b>	<b>21</b>

---

<b>2.2</b>	<b>Continental Forest Measurement in Australia .....</b>	<b>22</b>
2.2.1	Description of Australian forests.....	22
2.2.2	Defining and measuring Australia’s forests .....	24
	<i>National Vegetation Information System .....</i>	25
	<i>Current National Forest Inventory reporting .....</i>	26
	<i>Limitations with NFI forest height and cover reporting .....</i>	30
2.2.3	Utilising data within integrated sampling schemes .....	33
	<i>Sampling strategies overview.....</i>	33
	<i>Random, systematic, and stratified random sampling .....</i>	36
	<i>Model based sampling.....</i>	37
	<i>Using field data for remote sensing calibration.....</i>	38
<b>2.3</b>	<b>Remote Sensing of Forests.....</b>	<b>40</b>
2.3.1	Overview .....	40
2.3.2	LiDAR remote sensing of forests .....	46
	<i>Overview .....</i>	46
	<i>Large footprint LiDAR.....</i>	50
	<i>LiDAR for Australian forests.....</i>	51
	<i>LiDAR calibration studies.....</i>	52
2.3.3	Tree crown delineation using high resolution remote sensing .....	54
	<i>Local minima location.....</i>	55
	<i>Minima contouring.....</i>	56
	<i>Template matching and object-oriented analyses .....</i>	57
	<i>Delineation limitations.....</i>	58
<b>2.4</b>	<b>Scale in Remote Sensing .....</b>	<b>60</b>
2.4.1	Overview .....	60
	<i>Modifiable Areal Unit Problem.....</i>	62
	<i>Hierarchy theory and Landscape Ecology.....</i>	63

---

2.5	Summary .....	65
<b>Chapter 3. Data Analysis Methodology .....</b>		<b>67</b>
3.1	Introduction .....	67
3.2	Research Design Overview .....	69
3.2.1	Multi-scale strategy overview .....	69
	<i>Developing a hierarchical multi-scale modelling framework.....</i>	<i>69</i>
	<i>Applying the multi-scale hierarchical framework.....</i>	<i>71</i>
3.3	Data Collection .....	75
3.3.1	Introduction .....	75
3.3.2	Queensland study site.....	75
	<i>Overview of Queensland multi-stage sampling.....</i>	<i>78</i>
	Stage III: LiDAR data capture .....	79
	Stage IV: Field sampling.....	81
	Stage V: Georeferencing of photography to LiDAR .....	83
3.3.3	NE Victorian study site .....	85
	<i>Plot location site descriptions .....</i>	<i>88</i>
3.3.4	Data descriptions for both sites .....	91
	<i>Ancillary data.....</i>	<i>91</i>
	<i>Summary of Queensland and NE Victorian field data .....</i>	<i>91</i>
	<i>API classification comparisons with NFI.....</i>	<i>91</i>
3.4	Phase 1 – LiDAR Plot / Stand Scale Forest Structure Assessment.....	94
3.4.1	Introduction .....	94
3.4.2	LiDAR pre-processing .....	94
	<i>Stage VI: Bare ground surfaces .....</i>	<i>94</i>
	<i>Site Characteristics and terrain complications.....</i>	<i>96</i>
3.4.3	Estimating Tree Height for Plot / Stand .....	98
	<i>Stage VIII: Maximum and predominant height from LiDAR.....</i>	<i>98</i>

---

	<i>Plot scale LiDAR apparent vertical profiles .....</i>	99
	<i>Creating apparent vertical profiles using field data .....</i>	102
	<i>Growth stage assessment using apparent vertical profiles .....</i>	103
3.4.4	Estimating plot scale canopy cover .....	104
	<i>Stage VIII: Foliage and Crown cover .....</i>	104
<b>3.5</b>	<b>Phase II –Tree and Component Scale Structure Modelling .....</b>	<b>106</b>
3.5.1	Tree scale modelling strategy .....	106
	<i>HSCOI Stage IX: Calculation of stem diameter.....</i>	107
3.5.2	Individual crown segmentation and delineation.....	109
	<i>Conceptual overview.....</i>	109
	<i>Stage I - Empirical functions for general crown templates.....</i>	110
	<i>Stage II - Creating individual crown segments.....</i>	114
	<i>Stage III - Classification of crown segments.....</i>	116
	<i>Stage IV - Creating crown objects .....</i>	121
3.5.3	Tree component scale LiDAR modelling.....	127
	<i>Branch radius calculation.....</i>	130
<b>3.6</b>	<b>Phase 3 – Multi-Scale Calibration and Validation Case Studies .....</b>	<b>131</b>
3.6.1	Introduction .....	131
3.6.2	Multi-scale assessment of height and cover .....	131
	<i>Multi-scale predominant height assessment.....</i>	131
	<i>Multi-scale canopy cover assessment .....</i>	136
	<i>LiDAR and API crown cover comparison.....</i>	137
	<i>Crown Separation method test.....</i>	138
3.6.3	Landsat cover investigation and validation .....	139
3.6.4	ICESat calibration with airborne LiDAR.....	142
	<i>Vegetation comparisons.....</i>	143
	<i>ICESat footprint derivation and attribute extraction.....</i>	143

---

3.7	<b>Summary</b> .....	150
<b>Chapter 4. Results</b> .....		<b>152</b>
4.1	<b>Introduction</b> .....	152
4.2	<b>Field Plot Representativeness</b> .....	153
4.3	<b>Multi-Scale Height Results</b> .....	155
4.3.1	Plot scale height results .....	155
	<i>Maximum canopy height</i> .....	155
	<i>Predominant canopy height</i> .....	157
4.3.2	LiDAR height results with different assessment areas.....	159
	<i>Multi-scale variation of LiDAR height in NE Victoria</i> .....	159
	<i>Multi-scale variation of LiDAR height at Injune</i> .....	164
4.3.3	Apparent vertical profiles.....	166
	<i>Simulating apparent vertical profiles</i> .....	166
	<i>Growth stage and disturbance assessment using profiles</i> .....	168
4.4	<b>Multi-scale Canopy Cover results</b> .....	176
4.4.1	Plot scale cover results .....	176
	<i>Comparisons between cover using field data</i> .....	176
	<i>Crown cover comparison between LiDAR and photography</i> .....	180
	<i>LiDAR foliage-branch cover comparisons with field data</i> .....	182
	<i>SLATS foliage projective cover comparison with LiDAR cover</i> ....	184
	<i>Correlations between cover metrics and data sources</i> .....	186
	<i>Crown separation method test results</i> .....	189
4.4.2	Forest cover assessment at a range of scales .....	192
4.5	<b>Tree Scale Stem and Crown Delineation Results</b> .....	198
4.5.1	Tree stem density and location.....	198
	<i>Stem mapping at Injune</i> .....	198
	<i>Tree scale stem diameter derived from height</i> .....	200

---

4.5.2	Tree crown delineation results .....	201
<b>4.6</b>	<b>Multi-Scale Calibration Results .....</b>	<b>209</b>
4.6.1	Landsat pixel scale LiDAR cover calibration .....	209
4.6.2	Crown and foliage cover translation function .....	211
4.6.3	ICESAT case study calibration using LiDAR height and cover .....	215
4.6.4	Stand reconstruction results using tree components.....	218
<b>4.7</b>	<b>Summary .....</b>	<b>225</b>
<b>Chapter 5.</b>	<b>Discussion .....</b>	<b>227</b>
<b>5.1</b>	<b>Introduction .....</b>	<b>227</b>
<b>5.2</b>	<b>Improving the Assessment of Forest Structure using LiDAR.....</b>	<b>228</b>
5.2.1	Improving forest structure measurement using LiDAR.....	228
5.2.2	Improving forest height assessment using LiDAR.....	233
	<i>Maximum canopy height .....</i>	<i>233</i>
	<i>Predominant canopy height .....</i>	<i>234</i>
	<i>Apparent Vertical Profiles .....</i>	<i>236</i>
	<i>Maximum stand height at a range of assessment scales .....</i>	<i>239</i>
	<i>Predominant Height at a range of assessment scales .....</i>	<i>240</i>
	<i>National Forest Inventory Reporting .....</i>	<i>241</i>
5.2.3	Improving forest cover assessment using LiDAR.....	241
	<i>Field data comparisons.....</i>	<i>242</i>
	<i>LiDAR cover comparisons with field and CASI.....</i>	<i>243</i>
	<i>LiDAR to API comparisons .....</i>	<i>245</i>
	<i>LiDAR to Landsat TM comparisons.....</i>	<i>247</i>
	<i>Landscape sampling.....</i>	<i>248</i>
	<i>Multi-scale sampling and reporting of cover .....</i>	<i>249</i>
5.2.4	Assessment of the Height Scaled Crown Openness Index (HSCOI)	251
	<i>HSCOI derived stem density .....</i>	<i>251</i>



---

<i>HSCOI derived stem height and diameter</i> .....	253
<i>HSCOI crown delineation</i> .....	253
5.2.5 Calibration case study examples using LiDAR.....	256
<i>Landsat TM calibration using LiDAR structural output</i> .....	256
<i>Foliage-branch cover-to-crown cover translation function</i> .....	257
<i>ICESat calibration for continental monitoring</i> .....	258
<i>Stand reconstruction modelling for SAR simulation</i> .....	259
<b>5.3 Practical Implications, Limitations and Recommendations</b> .....	<b>262</b>
5.3.1 Practical implications .....	262
5.3.2 Limitations and recommendations for future research.....	264
<b>Chapter 6. Conclusion</b> .....	<b>267</b>
<b>6.1 Thesis Conclusion</b> .....	<b>267</b>
<b>References</b> .....	<b>269</b>
<b>Appendix A</b> .....	<b>289</b>
Ancillary Results.....	289
<b>Appendix B</b> .....	<b>320</b>
Plot data illustrations for NE Victoria.....	320
<b>Appendix C</b> .....	<b>326</b>
List of Published Papers.....	326
Statement of Author Contribution to Published Papers.....	327
<b>Appendix D</b> .....	<b>332</b>
Hemispherical photo calibration methodology overview .....	332

---

---

## LIST OF FIGURES

---

Figure 1: CFMF multi-tier design illustrating the potential role of airborne LiDAR as a Tier 2 dataset (after Wood, <i>et al.</i> , 2006).....	10
Figure 2: Distribution of NFI forest types in Australia. Source – State of the Forests Report, 2003 (NFI, 2003). .....	28
Figure 3: Illustration of different cover measurement sensors and range of scale and spatial resolution, both field and remotely sensed (McDonald, <i>et al</i> 1998; McCloy, 2006).....	29
Figure 4: Graphical representation of the elements of a small footprint airborne scanning laser (LiDAR) system. GPS refers to Global Positioning System, INS is Inertial Navigation System. Note that the graphic and elements are illustrative only and not to scale.....	49
Figure 5: Methods chapter layout showing major components of LiDAR assessment of forest structure. ....	68
Figure 6: Thesis conceptual overview outlining linkages between multi-scale hierarchal modelling and applications for modelling forests with LiDAR. ....	72
Figure 7: Flowchart of multi-scale calibration modelling and application strategy ..	74
Figure 8: Location of the 37 x 60 km Injune study area, within south-central Queensland. ....	76
Figure 9: Sketch of the Maranoa River by the explorer Thomas Mitchell in 1846 (upper) (Mitchell, 1846); and a photo of the Maranoa from a nearby location in 2004 (lower). ....	77
Figure 10: Landsat ETM image (2003) of study area and systematic photo and LiDAR plot layout, with field plot locations circled. State Forests are the light green hashed areas. Study area boundary was 37 km x 60 km, and sampling units are 4 km apart.....	80
Figure 11: True colour 1:4000 stereo aerial photograph of PSU 138 overlain with the 500 x 150 m primary sampling unit and 30 secondary sampling units (50 x 50 m). Polygon vectors mapped through API delineate different forest communities (based on dominant species composition and cover)....	84
Figure 12: Location of the secondary study site within the Broken and Ovens catchments in NE Victoria.....	85
Figure 13: Layout of LiDAR data collection with ancillary NVIS vegetation data aggregated to broad species classes (NLWRA, 2001) within the NE Victorian study area.....	87
Figure 14: Field plot site information summary (LiDAR derived) with max tree height (LiDAR), dominant species groups (field), and broad landform zone (derived) (Wood <i>et al.</i> , 2006). ....	88
Figure 15: Original DEM TIN created with all ground returns, for PSU 142 .....	95
Figure 16: Final spatially refined DEM TIN for PSU 142 .....	95
Figure 17: DEM difference surface - original DEM subtracted from final DEM for PSU 142. ....	95
Figure 18: LiDAR representations – raw points profile across Qld plot width (p81-11), vertical profile of summed returns per 1m height interval, and cumulative height percentage curve summary. ....	101
Figure 19: Steps to generate foliage branch cover, and CHM crown cover from LiDAR .....	105

Figure 20: (a) Height-to-D <sub>130</sub> translation function using 80% of field measured stems and (b) validation using remaining 20% of field stems.....	108
Figure 21: Hollows function derived from field data measurements (outside field plots), and applied to LiDAR derived stems. ....	108
Figure 22: Flowchart of crown delineation methodology.....	111
Figure 23: Calibration using 80% of field data trees (Upper) and validation using 20% of field data trees (Lower) for estimating crown area from height, for (a) Eucalypt and Angophora trees, and (b) Callitris and Acacia trees (live trees 5cm+ D <sub>130</sub> ). ....	113
Figure 24: Crown segmentation using surface generated from a 1m circular (a) and 5x5m rectangular (b) moving window. ....	115
Figure 25: Smoothing of segmentations (a) and segment clipping with HSCOI derived crown boundary delineation (b).....	115
Figure 26: Illustration of different apparent vertical profiles for the two main structural types.....	118
Figure 27: Examples of the two broad genus groups based mature tree structural crown forms.....	119
Figure 28: Crown structural classification into two broad genus categories at (a) segment <sub>1m</sub> and (b) segment <sub>5m</sub> scales. Green is <i>Callitris-Acacia</i> and light brown is <i>Eucalypt-Angophora</i> . ....	119
Figure 29: Derivation of circular crown shape assumption, using all field live stems 5cm+ D <sub>130</sub> (n = 2708) and comparing crown north-south length versus east-west length. ....	122
Figure 30: Final crown structural classification (a) and delineation after spatial assessment (b).....	123
Figure 31: Voxel groups associated with branch clusters within an individual <i>E. populnea</i> tree from PSU 142, with a planimetric view (upper) and 3D view (lower).....	129
Figure 32: Predominant stand height assessment using LiDAR 10m cells at different spatial extents at CFMF plot 212 (Ovens river). ....	132
Figure 33: Illustration of CFMF plot p212 with plot, transect and stand scales of assessment. The LiDAR point data slice was approx. 100m deep....	133
Figure 34: Multi-scale assessment of predominant height for NE Victorian sites, with example for plot 212 shown. ....	135
Figure 35: Example of predominant height assessment at a range of scales for Injune (PSU 142 shown, with 10m cells within 30 larger 0.25ha SSU's).....	135
Figure 36: Illustration of the multiple scales of FBC circular assessment for NE Victorian plots. LiDAR (2m+) for plot 212 has red/orange colour as highest returns (~ 40 m), with lowest non-ground dark blue. Background image was Landsat ETM. ....	137
Figure 37: Vector pixel layer example for PSU 142, derived from Landsat SLATS FPC grid (background). Values within cells indicate FPC.....	141
Figure 38: LiDAR return density (all returns) for PSU 142. Values within cells indicate LiDAR FBC.....	141
Figure 39: HSCOI derived stems for PSU 142. Values within cells indicate stem density per FPC pixel (stems per hectare).....	141
Figure 40: HSCOI derived crown delineations for PSU 142. Values within cells indicate LiDAR crown cover percent per pixel area. ....	141
Figure 41: ICESat transects (light blue) with the airborne LiDAR transects (yellow) and numbered overlap locations across CFMF pilot region in NE Victoria. ....	142

---

Figure 42: Examples of the ICESat footprint size and shape attributes derived using airborne LiDAR. a) single footprint with returns that are within the footprint (black) and over 2m in height (light blue); and b) two footprints from different dates showing different shapes due to different laser sensors used. ....	146
Figure 43: Layout of the Results chapter showing the major components of the strategy for using LiDAR to improve forest structure measurement. ....	153
Figure 44: Comparison of the LiDAR structural (height and cover) range of field plots and all SSU's ....	154
Figure 45: Comparison of maximum height between field and LiDAR at Injune for; (a) field plots; and (b) individual tree height for 100 manually selected, isolated overstorey trees ....	156
Figure 46: Comparisons field and LiDAR for NE Victorian plots for; a) max plot height for field plot and transect areas; and b) frequency distribution of maximum LiDAR height. ....	156
Figure 47: Frequency distribution of LiDAR maximum height at Injune for: (a) field plots; and (b) all 4500 SSUs. ....	157
Figure 48: Injune field plot predominant height (10m cells) for: (a) from field data and LiDAR at different sampling rates, and (b) frequency distribution of LiDAR heights. ....	158
Figure 49: NE Victoria field plot predominant height (10m cells) for: (a) from field data and LiDAR at different sampling rates, and (b) frequency distribution of LiDAR heights. ....	158
Figure 50: Frequency distributions for predominant height at Injune for 4500 SSUs derived from transfer function using 90 <sup>th</sup> percentile LiDAR height. .	159
Figure 51: Representativeness test for field plot (~0.09 ha) and transect area (~1 ha) versus swath overlap area (~25ha) for LiDAR (a) predominant height, and (b) maximum height, in NE Victoria. ....	160
Figure 52: LiDAR predominant height assessment at a range of spatial scales for NE Victorian sites where field plots are located. ....	162
Figure 53: Comparison of sampling strategies for estimating stand (~20ha) predominant height for field plots in NE Victoria using (a) single locations (field or LiDAR); and (b) multiple samples within stand. ....	163
Figure 54: LiDAR predominant height assessment at a range of spatial scales for 12 PSUs at Injune. Dominant species codes are given in Chapter 3. ....	165
Figure 55: Comparisons between apparent vertical profile from LiDAR and field cubic modelling for matches that are: (a) good (p142-02), and (b) not as good (p81-11). ....	167
Figure 56: Correlation of percentage of cubes at each 1m height interval, with LiDAR and field apparent vertical profiles for matches that are; (a) good (p142-02), and (b) not as good (p81-11). ....	167
Figure 57: Field data summary for SSU 124-19, illustrating tree growth stage and genus distribution by stem diameter (total Basal Area = 4.30m <sup>2</sup> ) and stocking ( $n = 603$ ). ....	169
Figure 58: Apparent vertical profiles from LiDAR (black) and field (grey) cubic modelling for SSU 124-19. ....	169
Figure 59: Growth stage example using indicative LiDAR vertical profiles from NE Victoria. For the LiDAR profiles the x-axis is percentage of canopy returns, y-axis is height above ground (m). ....	171
Figure 60: LiDAR apparent vertical profile showing the potential difference in fire intensity between two high country plots on steep slopes. (a) plot 562, less intensity fire impact, with understorey and lower canopy still	

	present. (b) plot 558, intense fire impact, no understorey or lower canopy left and scorched crowns. ....	172
Figure 61:	Comparison of LiDAR apparent vertical profiles and plot photos for plots in NE Victorian <i>E. radiata</i> forests, illustrating a potential understorey fire recovery sequence, based on the last recorded fire within; (a) 1 year (p313), (b) 12 years ago (p550), and (c) 64 years ago (p463).....	173
Figure 62:	Assessment of stand structure using apparent vertical profiles at a range of scales, for the Injune study area .....	175
Figure 63:	Injune field data comparisons for transect FPC versus transect FBC (left), and transect FBC (2000) versus field hemi-photo FBC (2004) (right). ....	177
Figure 64:	Comparison of FBC field plot measurements: a) transects in 2000 and 2004; and b) transects and hemispherical photo in 2004.....	178
Figure 65:	Estimated hemispherical photo view extent, based on calibration results for p142-13. HSCOI crown delineations are shown for reference. The field plot boundaries and transects are approximately 50m long .....	178
Figure 66:	Comparison of field tree-map CC measurements: a) with transect FBC; and b) with hemispherical-photo FBC. ....	179
Figure 67:	NE Victorian plot tree-map CC correspondence with hemispherical photo FBC.....	179
Figure 68:	Injune API CC (mid-point of class) correspondence with the LiDAR CC sample within the API polygon. ....	181
Figure 69:	Comparison of individual API polygon CC (mid-point of class) and LiDAR CC (mean, min and max) based on 25m cells within the PSU. Individual polygon IDs have been removed for clarity. ....	181
Figure 70:	NE Victorian API CC (mid-point of class) correspondence with the LiDAR CC field plot and transect area sample within the API polygon. ....	182
Figure 71:	Comparisons of LiDAR FBC at 0.5 and 2 m height thresholds, with a) field transect FBC; and b) FBC derived from hemispherical-photographs. ....	183
Figure 72:	LiDAR FBC distribution from a) Injune field plots; and b) 4500 SSUs across study area.....	183
Figure 73:	SLATS Landsat derived FPC distribution for the Injune study area (220,000ha). NFI forest classes are shown.....	184
Figure 74:	SLATS Landsat derived FPC distribution for the NE Victoria study area. NFI forest classes are shown. ....	185
Figure 75:	Crown separation transect method for p142-13. Field mapped stems are solid orange circles (proportional to $D_{130}$ ) and open circles (proportional to mean crown radius). LiDAR point sampling density (grey) and HSCOI crown delineations (green) are shown. Field plot boundaries and transects are 50m long. ....	190
Figure 76:	Crown separation transect method for p81-16. Map elements are described in the Figure 75 caption. Field plot boundaries and transects are 50m long. ....	190
Figure 77:	Apparent vertical profiles for p142-13 (a) and p81-16 (b), highlight different vertical foliage characteristics, which may contribute to the different cover results observed. ....	191
Figure 78:	Comparison of FBC from LiDAR and hemispherical photos, in a) field plot area; and b) transect area. ....	194
Figure 79:	Comparison of FBC from LiDAR in transect area and field plot hemispherical-photo. ....	194

Figure 80: Comparison of FBC for different data and pixel sizes, within the LiDAR swath for NE Victorian plot 220. ....	194
Figure 81: LiDAR FBC at plot locations with increasing assessment area, for Floodplain ecozone. ....	195
Figure 82: LiDAR FBC at plot locations with increasing assessment area, for Foothills ecozone. ....	195
Figure 83: LiDAR FBC at plot locations with increasing assessment area, for Subalpine ecozone. ....	195
Figure 84: LiDAR FBC at plot locations with increasing assessment area, for the NE Victorian Montane ecozone. ....	196
Figure 85: LiDAR FBC at plot locations with increasing assessment area for Injune. ....	197
Figure 86: Crown/clusters and stem locations identified using the HSCOI surface generated for PSU 142. Darker areas in the HSCOI <sub>stand</sub> surface indicate crowns that are taller and contain a greater density of canopy elements. Internal squares are SSU field plot locations numbered (from left to right) as 02, 13, 18 and 20. ....	199
Figure 87: Correspondence between field-measured $D_{130}$ , and height derived $D_{130}$ from HSCOI derived stems. ....	200
Figure 88: Correspondence between plot-level basal area, for stems measured in the field and estimated from LiDAR HSCOI modelling. ....	201
Figure 89: Correlation between field estimated crown area and area derived from LiDAR HSCOI crown delineations, aggregated into broad class types. ....	205
Figure 90: Comparison of crown diameter for; a) field and HSCOI trees from plots 142-13 and 81-16, and b) NE Victorian plot CC comparison between field tree-map buffer and HSCOI crowns. ....	207
Figure 91: NE Victorian LiDAR crown delineation examples and associated field plot centre photos. (a) Plot 382 with a good match between plot level crown cover and stem density; and (b) Plot 562 with a poor match for plot level crown cover and stem density. ....	208
Figure 92: Comparisons of SLATS FPC and LiDAR FBC at 0.5m (left) and 2m (right) thresholds. ....	210
Figure 93: Comparison of SLATS FPC and LiDAR CC. ....	210
Figure 94: Comparisons of LiDAR stem density and FBC at 0.5m (left) and 2m (right) thresholds. ....	210
Figure 95: Comparisons of LiDAR stem density and Landsat FPC (left), and LiDAR CC (right). ....	210
Figure 96: Comparison between LiDAR CC and SLATS FPC within 12 PSU's using all 25 m cells where $CC \geq FPC$ ( $n = 855$ ). ....	212
Figure 97: Derivation of translation function between SLATS FPC and LiDAR CC within 12 PSU's, using 80% of 25 m cells where $CC \geq FPC$ ( $n = 683$ ). ....	212
Figure 98: Validation of translation function between SLATS FPC and LiDAR CC within 12 PSU's, using 20 % of 25 m cells ( $n = 172$ ) where $CC \geq FPC$ . ....	212
Figure 99: Comparison between LiDAR CC and FBC within 1161 x 25 m pixel sized areas from 12 PSU's. ....	214
Figure 100: Comparison between LiDAR CC and FBC for Injune SSU's (50 m), NE Victorian field plots (30 m), and selected ICESat footprints from NE Victoria (50 - 100m). Red arrows indicate current NFI CC-FPC translation thresholds. ....	214

---

Figure 101: Airborne LiDAR from three ICESat footprints from ALS tile 26 displayed on a 1 m LiDAR derived DEM. ....	216
Figure 102: Perspective view of LiDAR within ICESat footprint areas. See Figure 101 for legend. ....	216
Figure 103: Sample of mapped tree stems, crowns, and primary (thicker lines) and secondary (thinner lines) branch distributions in PSU 142 derived from the LiDAR data. Inset extent is marked as a dashed box. ....	219
Figure 104: Perspective view of a portion of PSU 142 showing mapped tree stems, crowns, and voxels derived from the LiDAR analyses. The view extent of Figure 103 is in the foreground. ....	219
Figure 105: (a) <i>E. populnea</i> -dominated forest at PSU_142. (b) Graphical output of part of the reconstructed canopy from the DSTO radar simulation (Lucas <i>et al.</i> , 2006c). ....	220
Figure 106: Injune correspondence between field data and LiDAR allometric and component estimated biomass – all assessed stems ( $n = 200$ ) ....	221
Figure 107: Injune correspondence between field data and LiDAR allometric and component estimated biomass – LiDAR modelling outlier stems removed ( $n = 185$ ) ....	222
Figure 108: Injune correspondence between field data and LiDAR allometric and component estimated biomass – LiDAR modelling and highly different field outlier stems removed ( $n = 170$ ) ....	222
Figure 109: Injune correspondence between LiDAR allometric and LiDAR component estimated biomass – all assessed stems ( $n = 200$ ) ....	223
Figure 110: Summary of predominant and max height for each CFMF field plot, by ecozone. ....	294
Figure 111: Comparison of stand sampling strategies for estimating stand (~20ha) predominant height by ecozone. ....	295
Figure 112: SLATS Landsat FPC (2000) spatial distribution at the Injune study site. ....	305
Figure 113: NE Victorian SLATS FPC (uncalibrated) from two Landsat scenes. Systematic field plots are yellow, additional calibration plots are pink. ....	306
Figure 114: Injune cover matrix graphs. All scales are percent cover. ....	311
Figure 115: NE Victoria cover matrix graphs. All scales are percent cover. ....	312
Figure 116: LiDAR derived tree stem basal area (per pixel) versus SLATS FPC, for 1114 Landsat pixels in 12 PSUs at Injune. ....	319
Figure 117: Registration of calibration images using Nikon fisheye lens, showing effective view area, zenith rings, and gaps in extent with the merged photos. ....	333
Figure 118: Calibration images taken at ANU showing area imaged, and the same effective view extent with (a) Nikon lens, and (b) Minolta lens. ....	334
Figure 119: Effect of background colour and pixel brightness threshold in hemispherical photo analysis on cover estimates, using Nikon and Minolta lenses. ....	335
Figure 120: Simulated viewsheds at different zenith angles for Nikon fisheye photos when taken along Qld transects within a field plot ....	336
Figure 121: Assessing potential hemispherical photo view areas for NE Victorian plots against of LiDAR returns (FBC) clipped at a range of circular areas. ....	338
Figure 122: Assessing view area of NE Victorian plot hemispherical photos against LiDAR (FBC) % circular area assessment for plot and transect areas respectively. ....	339

---

---

## LIST OF TABLES

---

Table 1: Area of NFI forest types ('000 ha) across the States and Territories in Australia. Source: National Forest Inventory State of the Forests Report, 2003. .....	27
Table 2: NFI translation between foliage projective cover (FPC) and crown cover (CC) (National Forest Inventory, 1998). .....	31
Table 3: Advantages and disadvantages assumptions of different hierarchal processing levels for forest assessment using LiDAR.....	70
Table 4: Main stages in the acquisition, processing and analysis of field and remotely sensed data (Tickle, <i>et al.</i> , 2006).....	79
Table 5: Estimated year of last fire and logging for NE Victorian plots (DSE, 2003) .....	90
Table 6: NFI, Victorian SFRI , and Queensland API crown cover class standards...	92
Table 7: Height class and ranges for NFI, Victorian SFRI, and Queensland API standards .....	93
Table 8: Illustration of a selection of terrain complications on canopy height estimates .....	97
Table 9: Translation between LiDAR and field estimation methods for predominant height .....	99
Table 10: Growth Stage type using SFRI and EMC classifications .....	103
Table 11: Overview of processing stages for the HSCOI.....	107
Table 12: Genus probability selection criteria .....	120
Table 13: Spatial criteria for merging a segment with neighbouring segments.....	123
Table 14: Spatial criteria for splitting a segment .....	126
Table 15: Functions used to calculate branch start and end radius .....	130
Table 16: Multi-scale predominant height assessment buffer selection areas for NE Victorian plot locations. ....	134
Table 17: Formulae utilised for footprint dimension and area calculations: .....	143
Table 18: ICESat attributes extracted for comparison with airborne LiDAR.....	144
Table 19: Variables extracted or calculated for footprint size estimation. ....	144
Table 20: Assignment of LiDAR returns within ICESat footprint .....	145
Table 21: ICESat case study footprints; description, full waveform, and LiDAR apparent vertical profiles .....	147
Table 22: Description of LiDAR attributes utilised for ICESat calibration and validation .....	148
Table 23: Representativeness of Injune forest structure sampling, comparing LiDAR from 4500 SSUs across the landscape with LiDAR from field plots (in parentheses), by NFI class. ....	154
Table 24: Representativeness of NE Victorian forest structure sampling, comparing continental NFI data with field plot LiDAR (in parentheses). ....	154
Table 25: Maximum height comparison between field and LiDAR for Injune and NE Victoria plots .....	155
Table 26: Comparisons of predominant height: field and LiDAR for Injune and NE Victoria plots .....	159
Table 27: LiDAR height comparisons at a range of assessment area scales for NE Victoria .....	160
Table 28: Summary statistics for predominant height at a range of assessment scales, per NE Victorian ecozone .....	163



Table 29: Summary of matrix results for the field plot area.....	166
Table 30: Plot descriptions for three plots illustrating growth progression with time since fire. ....	172
Table 31: Comparison of relative accuracy of CC estimates between API and LiDAR CC, across different LiDAR sampling ranges of the API polygon. ...	180
Table 32: Comparison of NFI forest cover class distribution across the Injune landscape using SLATS FPC for study area, and LiDAR PSU sample (1,125ha) for FBC and CC. ....	184
Table 33: NE Victotian SLATS FPC for study area compared to LiDAR and hemi-photo data in field plot and transect areas, using percentage of 20km systematic samples in each NFI forest class.....	185
Table 34: Matrix of correlations for cover metrics across a range of datasets and measurement scales, for the Injune field plots * .....	187
Table 35: Matrix of correlations for cover metrics across a range of datasets and measurement scales, for the NE Victorian field plots .....	188
Table 36: Matrix of P-values for cover metric correlations across a range of datasets and measurement scales, for the NE Victorian field plots .....	188
Table 37: Crown separation test comparison for p142-13 and p81-16.....	189
Table 38: FBC comparison between field plot and transect area combinations for NE Victoria. ....	192
Table 39: Summary of LiDAR FBC at different scales, averaged per NE Victorian ecozone. ....	193
Table 40: Tree stem density per plot correspondence for Injune and NE Victoria from HSCOI modelling.....	199
Table 41: Description of LiDAR crown delineation validation classification types. ....	202
Table 42: Summary of crown delineation validation comparison of 90 trees aggregated by type. ....	202
Table 43: Examples of LiDAR crown delineation classification types found in the validation. ....	203
Table 44: Genus probably modelling accuracy assessment by delineation type, using 90 randomly selected trees .....	206
Table 45: SLATS FPC comparisons with LiDAR derived cover and stem density metrics for Injune .....	211
Table 46: LiDAR CC comparisons with SLATS FPC and LiDAR FBC, for Injune and NE Victoria.....	211
Table 47: LiDAR and ICESat attributes from the riparian strip footprint f (ICE-id = 484 ).....	217
Table 48: LiDAR and ICESat attributes from the mid-slope footprint (ICE-id = 480) .....	217
Table 49: LiDAR and ICESat attributes from the ridge top footprint (ICE-id = 475) .....	217
Table 50: Comparison of structural attributes between field data (4 plots) and LiDAR stand modelling for PSU 142 .....	218
Table 51: Summary of biomass estimates for PSU 142 plots from field, LiDAR stem allometric, and LiDAR component sources. ....	223
Table 52: Summary of biomass functions using field data and LiDAR stem and components.....	224
Table 53: Major knowledge limitations for LiDAR utilisation in multi-scale sampling schemes.....	227
Table 54: Description of different types of LiDAR and field error with stand reconstruction using component modelling, for SAR simulation. ....	261
Table 55: Species name and API codes for Injune trees.....	289

---

Table 56: Injune field plot height results from field and LiDAR data for max and predominant height, and at different measurement scales.....	290
Table 57: NE Victorian field plot height results across a range of datasets and measurement scales. All values are in metres. ....	292
Table 58: Results from correlation and Kolmogorov-Smirnov test comparisons between LiDAR and field cubic modeling derived apparent vertical profiles for Injune. ....	296
Table 59: Injune field plots apparent vertical profiles using modelled field data (red) and LiDAR returns (blue), and plot centre hemispherical photo. ....	297
Table 60: Injune field plot percentage cover results across a range of datasets, cover metrics, and measurement scales.....	307
Table 61: NE Victorian field plot percentage cover results across a range of datasets, cover metrics, and measurement scales. All values in percentage cover. ....	309
Table 62: Crown Separation ratio calculation test for p142-13 .....	313
Table 63: Crown Separation ratio calculation test for p81-16 .....	314
Table 64: Slope and intercept significance values for calibration and validation functions .....	315
Table 65: LiDAR return density at different height thresholds for Injune plots.....	317
Table 66: LiDAR return density at different height thresholds for NE Victorian plots. ....	318
Table 67: NE Victorian field plot data (left to right) - LiDAR CHM surfaces, LiDAR apparent vertical profiles, and plot centre hemispherical photos. With CHM surfaces dark blue is ground, red-brown is tallest canopy. Refer to LiDAR profile for respective heights (m). ....	320

---

## LIST OF EQUATIONS

---

Equation 1 .....	104
Equation 2 .....	107
Equation 3 .....	112

---

---

## LIST OF ABBREVIATIONS

---

AIRSAR	Airborne Synthetic Aperture Radar
AGO	Australian Greenhouse Office
API	Aerial Photographic Interpretation
BA	Basal Area
CASI	Compact Airborne Spectral Imager
CC	Crown Cover
CFMF	Continental Forest Monitoring Framework
CHM	Canopy Height Model
CRCGA	Cooperative Research Centre for Greenhouse Accounting
D <sub>130</sub>	Diameter of tree stem at 130 cm height above ground
DEM	Digital Elevation Model
DNRE	Department of Natural Resources and Environment (Victoria)
DPI	Department of Primary Industries (Queensland)
DSTO	Defence Science and Technology Organisation
DTM	Digital Terrain Model
EMC	Ecological Maturity Classification
FBC	Foliage-Branch Cover
FPC	Foliage Projective Cover
GIS	Geographic Information Systems
GPS	Global Positioning System
HSCOI	Height Scaled Crown Openness Index
ICESat	Ice, Cloud, and land Elevation Satellite
IBRA	Interim Biogeographical Regionalisation for Australia
JERS	Japanese Earth Resources Satellite
LiDAR	Light Detection And Ranging
MAUP	Modifiable Areal Unit Problem

---

MODIS	MODerate-resolution Imaging Spectroradiometer
NFI	National Forest Inventory
NFPS	National Forest Policy Statement
NLWRA	National Land and Water Resources Audit
NVIS	National Vegetation Information System
PSU	Primary Sampling Unit
QDNRM	Queensland Department of Natural Resources and Mines
RSE	Residual Standard Error
RWG2	Research Working Group 2
$\delta$	Standard Deviation
SAR	Synthetic Aperture Radar
SFRI	Statewide Forest Resource Inventory (Victoria)
SLATS	Statewide Landcover And Trees Study (Queensland)
SLR	Single Lens Reflex (camera)
SPOT	Satellite Pour l'Observation de la Terre
SOFR	State of the Forests Report
SSU	Secondary Sampling Unit
TIN	Triangulated Irregular Network
TM / ETM	Thematic Mapper / Enhanced Thematic Mapper
UTM	Universal Transverse Mercator

---

---

## CERTIFICATE OF AUTHORSHIP

---

I hereby declare that this submission is my own work and that, to the best of my knowledge and belief, it contains no material previously published or written by another person nor material which to a substantial extent was accepted for the award of any other degree or diploma at the Australian National University or any other educational institution, except where due acknowledgement is made in the thesis. Any contribution made to the research by colleagues with whom I have worked at the Australian National University or elsewhere during my candidature is fully acknowledged.

---

Alex Lee

Date:

---

---

## PREFACE

---

Parts of the description of the Injune study area in Chapter 3 of this thesis was published in:

Tickle, P. K., Lee, A., Lucas, R. M., Austin, J. and Witte, C. (2006) Quantifying Australian forest floristics and structure using small footprint LiDAR and large scale aerial photography. *Forest Ecology and Management*, 223, 379-394.

Description of the Height Scaled Crown Openness Index (HSCOI) in Chapter 3, 4, and 5 was published in:

Lee, A. C. and Lucas, R. M. (2007) A LiDAR-derived Canopy Density Model for Tree Stem and Crown Mapping in Australian Forests. *Remote Sensing of Environment*, 111, 493-518.

Description and discussion of the LiDAR modelling for stand reconstruction for SAR simulation was published in:

Lucas, R. M., Lee, A. C. and Williams, M. L. (2006) Enhancing SAR simulations using LiDAR for understanding the relations between forest structure and SAR imagery. *IEEE Transactions on Geoscience and Remote Sensing*, 44, 2736-2754.

In Tickle *et al.*, (2006) and Lucas *et al.*, (2006) all LiDAR related processing and discussion was undertaken by me.

Appendix 3 provides a more detailed description of author contributions to the above papers.

---

---

## ACKNOWLEDGEMENTS

---

I would like to express my gratitude and appreciation for all the people who helped me in various ways as I undertook this research. In particular, I sincerely thank the members of my supervisory panel for their guidance and support – Dr Cris Brack, Dr Brian Lees, Dr Brendan Mackey, and especially Dr Richard Lucas for being such a willing and energetic colleague on field trips, conference, and late night online writing sessions from opposite sides of the globe. I also extend my thanks to:

- The Fenner School of Environment and Society for financial and academic support, and for making the almost home away from home bearable. In particular I thank the IT and other support staff for their continual help.
- The Cooperative Research Centre for Greenhouse Accounting for financially supporting the research, and providing a both academically stimulating and challenging forum to test my ideas out.
- The staff of the various government agencies that provided resources for field work, supplied data, and technical support. So, a big thank you to everyone at the Bureau of Rural Sciences, the Queensland Department of Natural Resources and Mines, and the Victorian Department of Natural Resources and Environment.
- My parents, Myrene and Ray Lee for always believing in me and supporting any crazy idea that I wanted to do. I also thank Sue and Justin McCarthy (and the rest of the McCarthy clan) for endless support to our long studying (or suffering?) family with child minding and the rest.
- Finally, to my lovely wife Tess whom I owe so much, for keeping me sane when there was so much more to do, and being able to look after our sons, and for not going too crazy while trying to complete her own PhD. Lastly, I thank my magic little man Max, who would always cheerfully waved goodbye to Daddy as he disappeared off to “nooni”. We can now finally spend more time together.

---

---

## ABSTRACT

---

Enhanced understanding of forest stocks and dynamics can be gained through improved forest measurement, which is required to assist with sustainable forest management decisions, meet Australian and international reporting needs, and improve research efforts to better respond to a changing climate. Integrated sampling schemes that utilise a multi-scale approach, with a range of data sourced from both field and remote sensing, have been identified as a way to generate the required forest information. Given the multi-scale approach proposed by these schemes, it is important to understand how scale potentially affects the interpretation and reporting of forest from a range of data.

To provide improved forest assessment at a range of scales, this research has developed a strategy for facilitating tree and stand level retrieval of structural attributes within an integrated multi-scale analysis framework. The research investigated the use of fine-scale (~1m) airborne Light Detection and Ranging (LiDAR) data (1,125 ha in central Queensland, and 60,000 ha in NE Victoria) to calibrate other remotely sensed data at the two study sites. The strategy refines forest structure mapping through three-dimensional (3D) modelling combined with empirical relationships, allowing improved estimation of maximum and predominant height, as well as foliage and crown cover at multiple scales. Tree stems (including those in the sub-canopy) were located using a height scaled crown openness index (HSCOI), which integrated the 3D density of canopy elements within the vertical profile into a two-dimensional spatial layer. The HSCOI modelling also facilitated the reconstruction of the 3D distribution of foliage and branches (of varying size and orientation) within the forest volume.

Comparisons between forests at the Queensland and NE Victorian study sites indicated that accurate and consistent retrieval of cover and height metrics could be achieved at multiple scales, with the algorithms applicable for semi-automated use in other forests with similar structure. This information has facilitated interpretation and evaluation of Landsat imagery and ICESat satellite laser data for forest height and canopy cover retrieval. The development of a



---

forest cover translation matrix allows a range of data and metrics to be compared at the plot scale, and has initiated the development of continuous transfer functions between the metrics and datasets. These data have been used subsequently to support interpretation of SAR data, by providing valuable input to 2D and 3D radar simulation models. Scale effects have been identified as being significant enough to influence national forest class reporting in more heterogeneous forests, thus allowing the most appropriate use and integration of remote sensed data at a range of scales. An empirically based forest minimum mapping area of 1 ha for reporting is suggested. The research has concluded that LiDAR can provide calibration information just as detailed and possibly more accurately than field measurements for many required forest attributes. Therefore the use of LiDAR data offers a unique opportunity to bridge the gap between accurate field plot structural information and stand to landscape scale sampling, to provide enhanced forest assessment in Australia.

---

# CHAPTER 1. INTRODUCTION

---

## 1.1 Introduction

### 1.1.1 The requirement for forest information

To manage forests sustainably, meet national and international reporting requirements and provide input to climate change research, it is important to accurately measure forest stocks and dynamics. To this end the Australian National Forest Inventory has proposed the Continental Forest Monitoring Framework (CFMF) as a way to address these challenges. Integrated sampling schemes such as the proposed CFMF utilise a multi-scale approach with a range of data, sourced from both field and remotely sensed. Given the multi-scale approach of the proposed CFMF, it is important to understand how scale affects the interpretation and reporting of forest measures using both high resolution data (spatial and spectral), such as aerial photography or airborne Light Detection and Ranging (LiDAR) and moderate spatial resolution data (e.g., Landsat TM, radar). Specifically, the thesis will investigate how higher spatial resolution data such as airborne scanning LiDAR can improve the calibration of a range of lower spatial resolution data (Landsat, radar and ICESat satellite based laser data), and lead to an improvement in the assessment of forest at scales ranging from local, regional to continental.

As a signatory to international agreements, including the United Nations Framework Convention on Climate Change (UNFCCC) and the Montreal Process Working Group for sustainable forest management, Australia is increasingly required to provide accurate and quantitative information on forest species/community composition (herein referred to as floristics), structure (e.g., height and cover) and condition over the entire continent (Richards and Brack, 2004). Additionally, to effectively respond to a changing climate, there is a need to improve forest and vegetation assessment methods, particularly as the dynamics (direction and magnitude) of potential change need to be identified as well as the current stock (Burrows *et al.*, 2002). This presents many research challenges as a greater range of information is required, which previously had not been widely or consistently collected (Wood *et al.*, 2006; Thackway

*et al.*, 2007). In addition, such information is required by governments, industry, private landholders and the public to detect trends in commercial, biodiversity and greenhouse values, assess the performance of management practices and public policies, guide sustainable development, and forecast the future condition of these ecosystems (Henry *et al.*, 2002; National Forest Inventory, 2003, Brack, 2007).

However, undertaking such assessments within Australia represents a significant challenge for two main reasons. First, Australia has an estimated 164 million hectares (ha) of native forests and woodlands, which are widely distributed, and generally located around the outer margins of the continent. Second, around 70 % of these forests are under private management, with less than 10 % in commercial public forest estate. Traditionally, forest information collected from publicly managed forests had improved spatial resolution, temporal collection, and a greater range of attributes. In the areas under private management, the information available on structure and condition is especially limited (National Forest Inventory, 2003). The development of efficient and cost-effective methods for retrieving this essential information is therefore critical if national and international obligations are to be better fulfilled and the sustainable development and conservation of forest resources optimised (Thackway *et al.*, 2007). Such information is also vital if Australia is to continue to contribute in a meaningful way to Kyoto Protocol related discussions (Brack *et al.*, 2006).

Landscapes are spatially heterogeneous geographic areas characterised by diverse interacting (spatially and temporally) patches or ecosystems, ranging from relatively natural terrestrial and aquatic systems such as forests, grasslands and lakes to human-dominated environments including agricultural and urban areas (Turner and Gardner, 1991; Forman, 1995). In natural forests and woodlands, or those where a diversity of management practices occur, traditional point or plot (herein defined as an area used to collect floristic and or structural data that can be any size, but for practical field survey purposes is generally not more than 1 ha (McDonald *et al.*, 1998)) based measurements of structure, biomass and species composition are difficult to extrapolate to the landscape because of the inherent complexity of the system. Such variability arises from natural disturbance, different processes of regeneration and succession, as

well as human interaction and management practices that occur at a range of spatial and temporal scales. The difficulty in quantifying this inherent variability leads, therefore, to uncertainties in local to regional extrapolations of the attribute of interest (Norman *et al.*, 2003). However, the integration of remotely sensed data, acquired by airborne and/or spaceborne sensors across the electromagnetic spectrum, and at a range of scales, provides a more appropriate mechanism for extrapolation (Patenaude *et al.*, 2005). This is because data from different sensors can provide unique and specific information (e.g., on height, cover and productivity) in several dimensions that relate directly to the state and dynamics of forested landscapes (Tickle *et al.*, 2006).

In the assessment of forest stocks and dynamics within landscapes, individual trees (herein defined as a woody plant more than 2 m tall with a single stem or branches well above the base (McDonald *et al.*, 1998)) can be considered as one fundamental unit of measurement. Where this scale of assessment is a requirement, then ideally, full accounting across the landscape would be generated using tree level information. However, this is currently not achievable or practical because of cost, effort, processing and storage issues. In some cases it may not even be necessary to have this level of detail to adequately answer some research questions. For this reason, a census of a landscape commonly uses remotely sensed data with spatial resolutions ranging from 10 m ~ 1 km. However, the information that can be extracted from this data is generally more useful for landscape scale assessments, as individual trees cannot usually be discerned.

Conversely, fine scale (high spatial and/or spectral resolution) remotely sensed data (herein defined as pixels or data elements < 5 m) or field data can provide much more information at the plot level, but is usually limited to a small sample of the landscape (Wulder, 1998). Therefore, in order to better understand the complexity of forest dynamics within the landscape, what is required is an ability to discern broad-scale patterns and processes, and relate these to finer scales at which human investigations are most familiar (Hay *et al.*, 2001). Hence, and as a compromise, there is a need to make use of medium scale data to provide a census of the landscape, but to use the finer spatial resolution data to provide critical calibration and

validation data, algorithms, and perspectives that allow the knowledge gap to be bridged. When this is undertaken within appropriate landscape sampling schemes which integrate data across scales, then the landscape variability can be adequately captured, described, and ultimately modelled (McCloy, 2006).

### **1.1.2 Forest assessment in Australia**

In Australia, the primary national level initiative for investigating forest assessment using multi-scale data analyses that includes remote sensing is undertaken by the National Forest Inventory (NFI) with the State of the Forests reports, and proposed Continental Forest Monitoring Framework (CFMF).

#### ***State of the Forest Reporting***

State of the Forest reports utilise the Montreal Process criteria and indicators framework as a basis for describing the state of Australia's forests. The Montreal Process 'Santiago Declaration' aims to report on a set of criteria and indicators developed by 12 member countries that have temperate and boreal forests, to better undertake sustainable forest management. Criteria are defined as broad categories of forest values that we desire to maintain, whilst indicators are measurable aspects of these criteria. The Montreal Process identified seven broad criteria important for sustainable forest management: biological diversity, productive capacity, ecosystem health and vitality, soil and water resources, global carbon cycles, socio-economic benefits, and an effective legal, institutional and economic framework. Some 67 indicators have been identified for reporting against these criteria at a national level, though implementing the framework is voluntary and not legally binding. In Australia, Commonwealth, State and Territory forestry and conservation Ministers have endorsed the Montreal Process as a regional reporting framework for forests. Criteria and indicators can be used over time to describe the state of a nation's forests and assess progress towards the goals of sustainable forest management (National Forest Inventory, 1998).

The Australian Commonwealth government has produced a number of national reports on Australia's forests that draw on the Montreal Process framework. Australia's First Approximation Report for the Montreal Process (Commonwealth of Australia, 1997) provides an initial report against the national level criteria and indicators. Australia's State of the Forests Reports (National Forest Inventory, 1998; National Forest Inventory, 2003), provides a comprehensive description of Australia's forests, and cover most aspects of the Montreal Process criteria and indicators. These reports highlight accomplishments such as the development of the Comprehensive Regional Assessment regional framework, and links with domestic and international activities, including Regional Forest Agreements in the late 1990's, and current research and development projects. The reports present data and issues about progress to date on reporting those indicators that are most easily assessed (National Forest Inventory, 2003).

Prior to the establishment of the National Forest Inventory (NFI) in 1988, capacity to report nationally on Australia's forests was limited. The Australian Commonwealth, State and Territory governments signed the National Forest Policy Statement (NFPS) in 1992, and in so doing, endorsed the existence and aims of the NFI. NFPS policy pursues broad national goals within a regionally based planning framework that integrates environmental and commercial objectives (National Forest Inventory, 1998).

Since establishment, the NFI has compiled a near complete and relatively consistent baseline snapshot of Australia's forest extent and basic characteristics. The NFI had to rely on a compilation approach, primarily from State and Territory agencies, for national reporting due to limited resources, demands for immediate reporting and the system of government and resource management responsibilities. This meant that data was compiled from a variety of pre-existing sources and collected to a variety of standards. It has been noted by the NFI that, in general, higher quality data (i.e., as noted previously, higher spatial and temporal resolution, with greater attribute range and measurement consistency) on forests is found on the part of the public land estate that is vested in public forest management agencies. Data for forests on land in public conservation reserves is generally of poorer quality, when compared to data from publicly

managed forests. There are large data gaps for forests on private and leasehold land (National Forest Inventory, 2003). Between State and Territories there are differences in definitions for data types reported under Montreal Process indicators (for an example, see Chapter 3, section 3.3.4). While all States and Territories are moving towards adopting standard national classification systems and definitions for indicators such as forest type, tenure and plantation regions, there are still issues with adapting existing forest data to standard national definitions and classification systems. This has resulted in large data gaps, and spatial data that are inconsistent or unavailable nationally for some of the indicators (National Forest Inventory, 2003).

The utility of existing forest and vegetation mapping for detecting and monitoring change is limited because this information is compiled from data sourced from a range of scales, acquired over different time periods, and obtained for a variety of purposes. Historically, information was derived from a combination of field survey and aerial photography (Skidmore and Turner, 1987), with more recent programs utilising satellite imagery (QDNRM, 2005). New mapping programs, for example the National Vegetation Information System (NLWRA 2001), are not efficient for monitoring and determining change or trends as each update effectively creates a new baseline. This contrasts with updates made within an efficient and repeatable monitoring system, and at a level of detail that is increasingly being required to answer ever more complex management questions. Another important factor concerning existing data is the absence of precision (or quality) estimates of key attributes relating to, for example, forest structure. Differences in attributes estimated using new data or techniques cannot definitively be interpreted as a real change, as they may be a result of improved measurement. Therefore there is a need to develop rigorous monitoring systems that enable accurate and timely reporting, which can be used as early warning signals of inappropriate management actions and a trigger for adaptive management (Norman *et al.*, 2003).

Scale also impacts on the implementation of the Montreal Process, particularly as much of the existing data does not adequately represent the variation present in Australian forests, for example, local scale vegetation species/community composition and structure. National to

regional scale mapping has management implications in that it under-represents rare forest types, hence efforts to ensure ecological diversity may not be focused on the required areas. The process of compiling regional and national datasets also potentially presents a barrier to land owner and local community involvement in the mapping and monitoring process. Given the Montreal Process requires Australia to report on trends in attributes, the NFI is leading the establishment of a Continental Forest Monitoring Framework (CFMF) (Norman *et al.*, 2003). This framework will be discussed in the next section.

### ***Continental Forest Monitoring***

The proposed CFMF was initiated to provide an integrated, scientifically reliable, nationally consistent inventory and monitoring program to determine trends in extent, structure, composition, health, status, use, and management of all types and tenures of Australia's forests. The framework will use a range of sampling and mapping methodologies to monitor the condition and management of Australia's forests and woodlands. This will constitute a major change in direction for forest inventory from a largely static, passive "snap-shot" approach that relies heavily on State and Territory based mapping, to one in which existing mapped data can be integrated with results from a consistently collected continental monitoring framework (Lee *et al.*, 2003).

Currently there are major knowledge gaps for forests under private management (70 % of Australia's forest) and in conservation reserves (13% of Australia's forest), which limit current assessment and reporting requirements (Norman *et al.*, 2003). A continental monitoring framework aims to be cost effective, readily applied, repeatable, transparent and verifiable. The information will be able to inform and evaluate national policy, regional decisions on trans-boundary issues, and to support sub-regional monitoring activities aimed at evaluating management actions. As described in Norman *et al.*, (2003), the CFMF will be designed with political and economic, as well as scientific, requirements and constraints in mind, to:



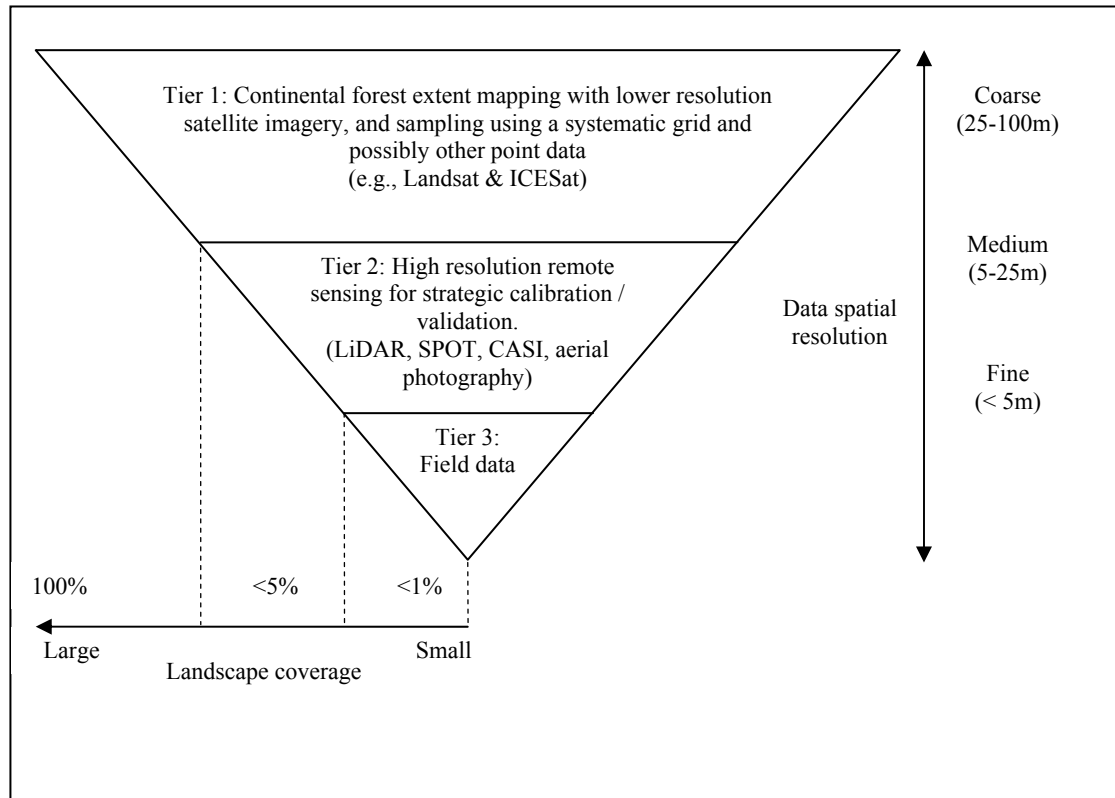
1. Report average trends but also to detect outliers where possible, while still maintaining statistical validity for, as a minimum, ecozones with an area of 1 million hectares or greater.
2. Measure relevant biophysical metrics objectively, consistently, and preferably directly, using technology independent means, and use continuous variables rather than categorical variables where possible, as well as providing for adaptive re-measurement.
3. Involve permanent site-based measurement using the most cost-effective sampling approach integrated with a range of remotely sensed data collected at a range of scales within a system that integrates sample and map-based assessments.
4. Provide accurate estimates of change for all metrics at 5 yearly intervals for as long as such reporting remains relevant to national needs.
5. Retain the flexibility to respond to emerging priorities from broader natural resource management interests and changes in indicators and technology and utilise existing data sources to the maximum extent possible.

In the light of these parameters and in consideration of international experience combined with the present state of inventory knowledge and technologies, a multi-tier data collection design was chosen by the CFMF Technical Advisory Committee (Figure 1) (Norman, *et al.*, 2006; Wood *et al.*, 2006). The design takes advantage of opportunities presented by recent developments in remote sensing at a range of scales, whilst retaining the ability to incorporate new more efficient data collection technologies as they become available. The design features three interrelated tiers of data collection. Tier 1 maps land cover type and vegetation canopy density across all areas using medium scale remotely sensed data, for example from Landsat Thematic Mapper (TM), Moderate Resolution Imaging Spectroradiometer (MODIS). Tier 1 mapping products could be enhanced through information from the Ice, Cloud and land Elevation Satellite (ICESat) which could provide a sample of vegetation heights reasonably consistently collected across the continent. Tier 2 utilises high spatial or spectral resolution remote sensing across a relatively large ( $\geq 5\%$ ) representative sample, at the intersections of a regular grid (nominally 20-50 km) across the whole country, to

assess a greater range of forest attributes. Potential datasets include: airborne datasets such as Light Detection And Ranging (LiDAR), aerial photography, or hyperspectral data such as that from the Compact Airborne Spectrographic Imager (CASI), and/or higher spatial resolution satellite imagery such as SPOT5 or equivalent. This data collection is integrated closely with the Tier 3 level where the full set of attributes are directly measured periodically on the ground at a relatively small (< 0.1%) representative sub-sample of the Tier 2 sample (Wood *et al.*, 2006).

Small footprint LiDAR is an active sensor that uses laser beams in the near infrared spectral range directed towards the ground. The laser scanner determines distance between aircraft and a point on the earth's surface based on the known speed of light, and measured time difference between emission of a light pulse and reception of the reflected signal. By combining range or distance, scanning angle, aircraft attitude (pitch, yaw, roll) and position (from Global Positioning Systems (GPS)) the exact x,y,z coordinate of the point on the earth's surface can be calculated. The resulting data is a 3D point cloud from terrain, vegetation, and other surface features (e.g., buildings) often with several million measurements per square kilometre (Lim *et al.*, 2003b). The point density and ground coverage is a function of the scanning mechanism, aircraft flying parameters, topography and the requirements of the project survey which all impact on the quality and accuracy of results generated. Where multiple users of the data are present, (e.g., hydrologists, foresters, urban planners) there are usually trade-offs in the utility of the data for each group, as a given point density may not meet the needs of all users. Many surveys utilised for forest assessment typically acquire a point density of 1 or 2 returns per square metre, and this point density is generally adequate for detailed terrain mapping, for individual trees to be discernable, and to provide an indication of the presence or absence of understorey foliage. However, improved results are obtained with higher sampling densities (which are also often required for urban planning), though at the expense of smaller area covered due to a lower flying height (and therefore higher cost per hectare) and greater computational and storage requirements (Reutebuch *et al.*, 2005). The ability to generate a high level of detail, often at the same accuracy as field plot estimates across large swaths of the

landscape (Lim *et al.*, 2003b), is the reason the CFMF investigated the use of LiDAR in the framework. However, more research is required to fully realise the potential of the data for improving the accuracy of forest structure assessment (Wood *et al.*, 2006).



**Figure 1: CFMF multi-tier design illustrating the potential role of airborne LiDAR as a Tier 2 dataset (after Wood, *et al.*, 2006).**

### 1.1.3 Dealing with scale in remote sensing of forests

In remote sensing, scale typically refers to the resolution and extent of an assessment unit, and scaling is the process of translating or extrapolating information from one resolution to another (Wu and Qi, 2000). An appreciation of scale and scaling is important to better understand broad-scale patterns and processes, and effectively relate them to fine scale measurements with which we are most familiar. Accurately transferring information between scales is necessary because many environmental and resource management problems can only be dealt with effectively at broad scales (Wu and Qi, 2000).

To improve our understanding of how scale can be utilised effectively when using remote sensing, it is first necessary to define the terms and theory. In this study, two broad

types of scale are defined: absolute and relative. *Absolute* scale is an objective assessment that is referenced to some independent baseline. Absolute scale is a practical, standard system used to partition geographical space in operational spatial or temporal units (Wu and Qi, 2000; Hay *et al.*, 2001). Ecologists recognise two aspects of scale: *grain*, which is the smallest spatial unit over which observations are made, and *extent*, which is the range or total area over which observations of a specified grain are undertaken. In remote sensing, spatial resolution is equivalent to grain, in that it is the smallest unit for which a sensor averages observations (either actively or passively) of the Earth's surface (Hay *et al.*, 2001). For optical imagery and Synthetic Aperture Radar (SAR), these units are generally rectangular (e.g., pixel), whilst for Light Detection And Ranging (LiDAR) these are circular or elliptical. Cartographically, scale refers to the ratio of map distances represented with respect to actual distances on the ground (Dungan, 2001). In a *relative scale* framework, scale is intrinsically linked to both the spatial entities and relationships between these entities, and can be expressed as ratios. Relative scale can be defined as the window through which an investigator views the world. As such, the choice of scale becomes linked to the phenomenon under observation and the questions being posed about it (Hay *et al.*, 2001). This thesis seeks to utilise scale in both the absolute and relative sense.

To make progress on scale issues, it must be recognised that all remotely sensed data and spatial analyses are sensitive to the size, shape and orientation of the data collection units. The collective descriptor of these elements in geostatistics is termed “support” (Atkinson and Curran, 1995; Dungan, 2001). This recognition is critical when minimizing bias in characterising forested landscapes and to avoid developing misleading relationships. Remotely sensed data, when represented as raster data models, have enforced a limited, though much more consistent, set of supports in the form of pixels. The change of support, (e.g., aggregating pixels or classified elements from smaller to larger sizes) is one precisely defined aspect of up-scaling and down-scaling (Ju *et al.*, 2005). Appropriate use of scaling requires an explicit acknowledgment that increasing support involves decreasing variance, increasing symmetry for univariate distributions, and introducing potentially unpredictable effects on multivariate

distributions. Regression based approaches to ‘calibrate’ remotely sensing information to canopy variables or other regionalised variables are reliant on the specifications of support for all variables involved. When discussing the variability of a quantity expressed for a region, it is essential that reference is made to the support on which it is measured (Dungan, 2001).

Scaling effects on spatial analyses have been identified since the 1930’s (Gehlke and Biehl, 1934), and a well known aspect of this, as identified in the statistical and geographical literature, is termed the “*Modifiable Areal Unit Problem*” (MAUP) (Openshaw, 1984). The MAUP consists of two inter-related concepts that occur when analysing spatial data. The first is the “scale or aggregation problem”, where the same set of spatial data are aggregated into several sets of larger areal units (i.e., the *size* of the support), with each combination leading to different data values and inferences. The magnitude of potential error will depend on the inherent heterogeneity of the forest and the nature and extent of the sampling strategy. The second aspect of the MAUP is the “zoning problem”, where a given set of areal units are recombined into zones that are of the same size but located differently (i.e., the *shape* of support). This again results in variation in data values and consequently, different conclusions might be formed (Jelinski and Wu, 1996; Fotheringham *et al.*, 2000).

The identification and use of basic attributes or geographical entities defining the objects under investigation was researched as a way to avoid MUAP issues (Fotheringham, 1989). Given the diversity of geographical problems and strategies that are currently being addressed and implemented, this approach may not be relevant or even possible in all cases of spatial analysis. Nevertheless, it is a fundamental practical exercise that should be undertaken to ensure the validity of any scientific enquiry, and therefore is at the core of the scale issue (Marceau, 1999). For forest assessment, the basic entity approach is appealing because the basic spatial unit of a forest can be easily defined as a tree (and the spaces between trees). While individual trees are readily discernable in fine spatial resolution remotely sensed data, automated tree extraction is still an emerging field that requires further research (Bunting and Lucas, 2006). If entities (such as trees), and relationships between related variables, emerge at specific scales (e.g., from tree, to forest patch, and to landscape mosaic), there must be a way to

define them and to relate them across discrete levels of organisation. This practical problem is raised when building a digital database in which individual objects must be identified, and their spatial and temporal topology built (Marceau, 1999). This idea is also at the foundation of new sets of techniques for feature extraction from digital imagery referred to as multi-scale object-specific techniques, where the focus is on the detection and identification of individual objects appearing on an image when the appropriate scale is reached (Burnett and Blaschke, 2003; Hay *et al.*, 2005).

#### **1.1.4 Summary**

This chapter has outlined the current situation with forest assessment at the national scale in Australia. The review has identified the need to improve national level reporting of forest structure, in order to meet the many challenges Australia faces in relation to sustainable management of forest resources and ecosystem services, especially in response to a changing climate. For example, it is difficult to generate a comprehensive understanding of Australia's forest estate due to the large continental area and dispersed nature of the forests. Additionally, much of the forest estate is located on private or leasehold land where accurate and up-to-date measurements are very rare or difficult to acquire.

The National Forest Inventory has begun to address these issues by proposing the Continental Forest Monitoring Framework as a new approach to inventory of the national forest estate. The integrated sampling framework seeks to utilise medium scale remotely sensed data for national mapping, combined with fine scale field data and high-spatial/spectral resolution airborne imagery for calibration and validation. This strategy aims for an efficient balance between the level of attribute detail and the spatial coverage. As with most new approaches, there is often uncertainty as to how it should be implemented, and what the best combinations of sensors and methodologies are. One of the key concepts of the proposed framework is the use of continuous rather than categorical measurements of forest structure, generated from a range of data sources and at multiple scales.

Therefore, there is a need to be able to accurately translate between assessment scales. As scale issues affect all remotely sensed data in some way, there is a requirement to understand the magnitude of the potential impacts so error in forest structural modelling and reporting can be minimised. Investigations into scale issues have indicated that using basic geographic entities or objects (e.g., trees) are an effective way to reduce, mitigate, or at least better understand the effects of scale on forest assessment when using remote sensing.

LiDAR data has known potential for generating continuous assessments of forest structure that can be equivalent to field measurements, but over much larger areas that can be surveyed on the ground. This provides a source of calibration data that can sample more of the landscape variability at fine scales, allowing improvements in the accuracy of reporting from medium scale data. What is currently missing is a strategy for using LiDAR to link fine scale field data with medium scale data within multi-scale integrated sampling schemes. An integral part of a multi-scale strategy is the use of basic geographic entities. There is a current research gap for generating structural information at a tree scale (crowns and/or stems) from LiDAR data in Australian forests. These requirements form the basis of the primary research question that will be addressed in this thesis.

## 1.2 Thesis Research Question

### 1.2.1 Primary research question

Section 1.1 identified the need for a strategy to utilise fine scale remotely sensed data to link field data with forest structure mapping data across a range of scales, for example within multi-scale frameworks. Airborne small footprint scanning LiDAR is a dataset that has shown promise to date in being able to meet many of the requirements for a multi-scalable dataset, however there is limited research on the utility of LiDAR for Australian forest structural assessment in the context of a multi-scale monitoring strategy. Therefore, in order to evaluate the utility of LiDAR as an effective multi-scale calibration dataset, the primary research question of this thesis is:

**How can airborne LiDAR improve Australian forest structure assessment?**

#### *Rationale and Research Objectives*

Forest structure can be broadly defined depending on the research interest. The assessment of structure can encompass a wide range of metrics and be valid at a range of scales Lund, (2002). For example, Specht and Specht (1999) state that plant community structure reflects its position in space and time, and illustrates the spatial distribution of plant community biomass, as well as indicating the effects of prevailing disturbance patterns. A range of life-forms can be recognised, and whilst these life-forms often intergrade, often broad divisions are apparent, with strata or layers emerging. For example, overstorey development can be indicative of the time since disturbance, the competitive ability of different species and the quality of the site (Specht and Specht, 1999).

For the purposes of this thesis, the concept of forest structure is defined as a measure of density: that is, the density of tree stems within a unit area, the density of crown branches and foliage originating from those stems (i.e. crown and foliage cover), and the density of foliage at different heights throughout the forest volume. A multi-scale calibration strategy incorporating basic geographic entities would allow a better understanding of the potential impacts of scale on



the assessment of forest structure. For example, how different assessment sizes may cause variation in what is reported as 'forest'. As scale issues are inherent with analyses of remotely sensed data, particular emphasis will be placed on the development of a strategy to use LiDAR for forest structure assessment at multiple scales. This will incorporate knowledge of scale and use a framework based around ecological hierarchy theory. Given the above, and in order to answer the primary research question, two objectives are defined, which delimit the boundaries of the research. These objectives specifically address two metrics that constitute forest structure, defined here as height and cover.

***Objective 1: Measuring forest cover using LiDAR***

The first objective seeks to understand how forest cover reporting can be enhanced using airborne LiDAR. The rationale for objective one is as follows. The NFI uses the crown cover (CC) metric to report on forest, which is defined as the percentage of a sample area within the vertical projection of the periphery of tree crowns, where crown are treated as opaque (McDonald, et al. 1998). Traditionally the source of this data for the NFI was estimated from field transects and air photo interpretation (API) (QDNR, 2000). API may be a relatively inexpensive dataset to acquire, but there are high costs and long timeframes (if a wide range of attributes are required) involved with the interpretation, and the results can be subjective and hard to objectively validate or repeat consistently. The results are generally categorical which has limitations for monitoring. New satellite based forest cover estimation use the foliage projective cover (FPC) metric (defined as is the percentage of a sample area occupied by the vertical projection of foliage only (McDonald, *et al.* 1998)), in semi-automated and repeatable programs, which generate continuous data which is more suited to classification at a range of scales, and monitoring (QDNR, 2004). Whilst monitoring programs (such as the proposed CFMF) seek to use continuous variables from a range of sources at different scales for monitoring, there are limitations in the current translation between FPC and CC, and especially when data is compiled from individual States and Territories. The current translation uses very broad classes and there is large variation between environments. Thus there is a need for

additional empirical refinement in order to move towards a more robust and repeatable continuous transfer function between metrics.

Because airborne LiDAR spans a range of spatial resolutions between potential data sources, there is potential to provide consistent calibration and translation between data sources, different cover measurement metrics, and at a range of assessment scales. As a result, new methods to provide calibration and translation metrics will be investigated as part of research objective one. For example, crown cover will be explicitly mapped using tree level LiDAR multi-scale modelling, in order to provide a source of crown cover data that can be up-scaled to calibrate other data at the most appropriate resolution. The results of the modelling will then be used to develop an initial empirical (continuous) transfer function between foliage and crown cover, and tested on a range of medium scale data.

### ***Objective 2: Measuring forest height using LiDAR***

The second objective seeks to identify how forest height reporting can be enhanced using airborne LiDAR. The rationale for objective two is as follows. Currently the NFI uses mean stand height categorised into a few broad height classes for reporting. Traditionally forest height has been estimated from field data or as classes of mean stand height from API. However the categorical data have limited potential for effective monitoring, and can be difficult to accurately measure from API in tall or dense forests, especially where the ground is not visible (VDNRE, 2000). With laser data from sensors such as ICESat satellite becoming increasingly available, there is the opportunity to enhance the height information available for national reporting and monitoring, if an effective understanding of the strengths and weaknesses of the data can be obtained.

In addition to spanning the proposed CFMF data spatial resolution range, airborne LiDAR may also offer the unique ability to rapidly assess of canopy height, in an accurate and repeatable manner. Therefore, in order to address objective two, different height metrics will be generated from airborne LiDAR and compared to field estimates. Then the impact of scale on height metrics when reporting forest different assessment scales will be investigated. Finally,

utilising the knowledge gained from field calibration and potential effects of scale, initial correlations will be developed between LiDAR and ICESat derived forest height metrics. This will indicate how accurate ICESat data may be when utilised for continental forest structure monitoring.

The anticipated outcomes of achieving the two research objectives include: the improved understanding of how different structural metrics are correlated between data sources, and assist in the development of empirical transfer functions between structural metrics to improve the calibration of remotely sensed data. In this context, improvement can be defined as increasing the efficiency of assessments when compared to current methods. This may be achieved by generating assessments at the same level of accuracy that is achieved with current methods, but the new method can generate results faster, with lower costs and less effort, and/or over larger areas. Improvement can also occur with the development of new metrics, to produce the required information more effectively or provide new insights (Brack, 2000).

The primary research question and associated objectives form the basis of significant new work in the field of high spatial resolution remote sensing of forests. The development of correlations among structural measurements through the use of basic geographic entities, and utilisation of these for multi-scale calibration and validation for Australian forest assessment, provides an important new contribution to national forest inventory and carbon monitoring initiatives.

### **1.2.2 Research delimitations**

To establish the boundaries of the present research, the following elements are demarcated. The primary source of small footprint LiDAR and additional data for calibration and validation was from data collected at existing study sites in south central Queensland (ex CRC Greenhouse Accounting and Australian Research Council SPIRT funded project; Tickle *et al.*, 2006; Lucas *et al.*, 2006a) and in North East Victoria (from the National Forest Inventory CFMF pilot study area; Wood *et al.*, 2006).

In order to address the primary research questions, this thesis makes several assumptions. First, that plot data drawn from existing landscape sampling schemes is representative of forest across the landscapes under investigation (Tickle *et al.*, 2006; Wood *et al.*, 2006). As the sampling strategies at the study sites had already been established and data collected prior to this thesis, research will be limited to testing the representativeness of field plot information using the available data. Second, whilst the two study areas utilised in this research may well span a broad range of Australian forest types, the conclusions reached about the utility of LiDAR to improve the assessment of forest structure will primarily be applicable to the forest types found at the study sites, and in particular, where LiDAR and field data were coincident. Third, that field data is the most accurate source of forest structural data with which to compare and calibrate remotely sensed data. This assumption will be investigated and discussed with respect to the conceptual similarities and differences between the metric measurement methods.

Due to the exploratory nature of the primary research question, emphasis will be on developing descriptive comparisons between data, in relation to the structural metric under investigation. Comparison correlations will utilise simple linear regression techniques as the primary statistical tool in the first instance.

### 1.3 Outline of Thesis

There are a total of six chapters in this thesis. The current chapter, Chapter 1, has presented a brief introduction to the central research question of this thesis. It has discussed the requirements for forest information, dealing with scale issues in remote sensing of forests, forest remote sensing strategies, and the current state of national forest assessment in Australia. The need to investigate how LiDAR can improve forest structure assessment has been identified.

Chapter 2 provides a review of LiDAR remote sensing of forests and dealing with scale in the analyses of remotely sensed data. Descriptions of Australia's forests and their definition at the national level are provided, and an overview of the current field based methods for forest structural assessment.

Chapter 3 describes in detail the research methodology that was designed to test and address the research question. It will outline the two study areas, the data utilised, multi-scale analysis, and calibration of other remotely sensed data for forest structure.

Chapter 4 outlines the results of the multi-scale strategy and data analyses, using LiDAR to assess forest structural metrics, as outlined in Chapter 3.

Chapter 5 discusses the findings of the research, and demonstrates that small footprint LiDAR can improve forest structural assessment. It will revisit the research question from Chapter 1 and state the extent to which the research achieved its goal. Chapter 5 will also discuss the theoretical and practical implications of the research, limitations, and the future directions for forest assessment utilising small footprint LiDAR. The thesis is concluded in Chapter 6.

Appendices A and B contain additional tabular and graphical information and examples that support the primary results presented in Chapter 4. Appendix C contains copies of key papers progressively published as a result of my research. Appendix D contains additional calibration information from the hemispherical photograph analyses for plot scale cover.

## CHAPTER 2. RESEARCH ISSUES

---

### 2.1 Introduction

The aim of this research is to determine how LiDAR can improve the assessment of Australian forest structure. As such, it is inherently about improving forest measurement strategies in order to provide a better understanding of forest stocks and dynamics, assist with sustainable forest management decisions, and meet national and international reporting needs.

This chapter provides a review of the relevant literature and background for measuring and monitoring Australia's forests using remote sensing. Section 2.2 of this chapter examines the definition and location of forest in Australia, and outlines current national forest assessment methods and limitations. The important elements for linking field and remotely sensed data within different sampling strategies are also outlined. Section 2.3 introduces forest measurement using both passive optical (e.g., Landsat TM) and active (e.g., radar, LiDAR) sensors. An extensive overview of LiDAR remote sensing of forests is provided including its use (either singularly or in conjunction with other remotely sensed data), for calibration of medium scale data, and for structural assessment (e.g., including tree crown delineation). Given the multi-scale approach of integrated sampling schemes, such as the proposed CFMF, it is important to understand how scale potentially affects the integration, interpretation and reporting of forest structure from field and remotely sensed data. Therefore a theoretical perspective on scale is presented in section 2.4. Finally, the chapter is summarised in section 2.5.

## 2.2 Continental Forest Measurement in Australia

### 2.2.1 Description of Australian forests

Within Australia, the structural characteristics and distribution of plant communities are largely a function of tectonic, geologic, pedologic and climatic (e.g., rainfall, fire) related influences (Peel *et al.*, 2005). Forest occurs across a wide range of environments, from dense wet tropical rainforests to sparse dry desert woodlands, and from coastal plains to alpine high country. Most Australian native forest tree species trace their origins back to the super-continental Gondwanan landmass. After the final break-up of this super-continent about 38 million years ago, and subsequent shift northwards, sclerophyllous vegetation that was better adapted to hotter and drier conditions gradually replaced the previously dominant rainforest. In this environment, sclerophyllous vegetation evolved hard, spiky or shiny leaves to reduce moisture loss and to cope with the nutrient-deficient, weathered, shallow and fragile soils that formed over much of the continent (Boland, *et al.*, 1992). These conditions, along with an increased fire frequency, resulted in *Eucalyptus* and *Acacias* flourishing, while species dependent on constant high levels of moisture were confined to relatively small areas of the continent. Over the last two million years, the climate has fluctuated between warm, wet periods and cool, dry periods, with the forests advancing and retreating in response to these changes (Wardell-Johnson *et al.*, 1997; National Forest Inventory, 1998).

As a result of regular burning by humans over tens of thousands of years, major effects on vegetation structure and composition are evident although the extent and implications of this are still debated. In Australia, indigenous people arrived about 50,000 years ago, and used fire as a hunting and land management tool, with widely varying use across the country. European settlement after 1788 resulted in more varied and widespread impacts on forests, with large areas cleared for agriculture and urban use. Estimates indicate that around 33 % of the original forested area was cleared and another 40 % was affected by timber harvesting at some stage (National Forest Inventory, 1998). Changes in fire and grazing regimes, especially with the removal of Indigenous practices, may have encouraged regeneration in some areas where previously forests with a more open or sparse understorey occurred (Walker *et al.*, 1993;

Burrows *et al.*, 2002). New plantations have been also been established, composed of both exotic and native species (National Forest Inventory, 1998).

According to the 2003 State of the Forests report (National Forest Inventory, 2003), approximately 164 million hectares (21 %) of the Australian continent (768 million hectares) is covered in forests (see Table 1 and Figure 2). The genus *Eucalyptus*, which occurs naturally predominantly in Australia, and *Acacia* both account for the majority of the country's forests in terms of area. There are more than 700 species of eucalypts, as well as many other genera of trees (such as rainforest and native conifers), in a rich array of ecosystems that vary in their floristic composition, structure and the fauna they support. Current forest distribution is mainly confined to regions where average rainfall exceeds 500 millimetres per year, largely in the northern, eastern and south-western coastal zones, including Tasmania. In drier parts of the country open woodland and mallee forests are found. In some places, for example the Eastern Goldfields region of Western Australia, the stature and extent of the native forest is greater than would be expected from the low rainfall. In these drier locations trees have developed survival mechanisms to withstand the conditions, relying on groundwater stores or occasional floods (Wardell-Johnson *et al.*, 1997; National Forest Inventory, 2003).

Most native forests are more open-crowned, with canopy covers of less than 70 % and comprised of species with architectures that are markedly dissimilar to those found in both temperate and tropical closed forests (Barlow, 1994). The vegetation is mostly woody, sclerophyllous and evergreen, and is characterised by leaves which tend to be vertically orientated in response to the high sun intensity. The dimensions (area and depth) of crowns in the upper canopy are highly variable, ranging from large and expansive (typical to many *Eucalyptus* and *Angophora* species) to small and compact (typical to *Callitris* species). In many cases, both crown types occur in the same stand but often in different strata, and variation in tree height, crown size, shape and density (which is high even within species) occurs as a function of the volume and type of soil that can be exploited for water and nutrients. Crown size is also indicative of the area a plant will influence through, for example, shading and litter deposition (Jupp and Walker, 1996).



### 2.2.2 Defining and measuring Australia's forests

Information about vegetation and vegetation dynamics is increasingly being recognised as a fundamental dataset that is required to inform public debate with regard to audits of resource condition. Therefore, vegetation information is required to effectively plan and report on resource development based on biophysical, social and economic aspirations (Thackway *et al.*, 2007). There are two primary national level forest and vegetation mapping initiatives currently underway in Australia: the National Forest Inventory (NFI) and the National Vegetation Information System (NVIS). NVIS will be briefly described in this section followed by an outline of current NFI forest assessments and limitations. The proposed CFMF design was previously described in Chapter 1. A summary of the typical requirements and rationale for permanent plot based sampling strategies are outlined in this chapter, and a description of different sampling systems is given. The integration of field data for remote sensing calibration is discussed in terms of data sources, accuracy, and compilation issues. This provides context and rationale for the assessment of the utility of LiDAR to improve forest structure measurement, within integrated sampling schemes.

A consistent and practical definition of forest is fundamental to monitoring and reporting effectively Australia's forest estate. The current definition of forest that was adopted by Australia's National Forest Inventory and used in State of the Forests Reports (National Forest Inventory, 1998; 2003), as well as by the Australian Greenhouse Office (AGO) (Richards, 2002) is:

An area, incorporating all living and non-living components, that is dominated by trees having usually a single stem and a mature or potentially mature stand height exceeding two metres and with existing or potential crown cover of overstorey strata about equal to or greater than 20 per cent. This includes Australia's diverse native forests and plantations, regardless of age. It is also sufficiently broad to encompass areas of trees that are sometimes described as woodlands.

*(National Forest Inventory, 1998)*

The definition is based on the 1992 National Forest Policy Statement, signed by all State, Territories and the Australian Government, but modified to remove uncertainty relating to

crown cover and height, and to meet operational implementation requirements. The minimum potential crown cover to qualify an area of trees as forest is now 20 %, which puts into effect the National Forest Policy Statement requirements that 'forest' is to include what has sometimes been called 'woodland'. The definition also refers to 'trees having usually a single stem' and sets the lower tree height limit at two metres, which allowed the inclusion of the forest-forming mallees. Shrublands are excluded, even if they are taller than two metres, because of the requirement to be of tree formation. This definition is biologically based, rather than focused on particular forest uses (Hnatiuk, *et al.*, 2003). It is similar to the single internationally agreed definition used by the United Nations Food and Agriculture Organisation, which is:

Land with tree crown cover (or equivalent stocking level) of more than 10 per cent and area of more than 0.5 hectares. The trees should be able to reach a minimum height of 5 metres at maturity in situ. May consist either of closed forest formations where trees of various storeys and undergrowth cover a high proportion of the ground; or of open forest formations with a continuous vegetation cover in which tree crown cover exceeds 10 per cent.

(FAO, 1998)

### ***National Vegetation Information System***

The National Vegetation Information System is a consistent attribute and database framework for describing, translating and compiling existing mapped information for all vegetation types across the whole landscape, and at regular intervals by the respective Australian State and Territory land and vegetation management agencies (NLWRA, 2001). The NVIS framework describes native vegetation using the concept of a 'definitive vegetation type', which details the structure and floristics of vegetation at the association or sub-association level and within mapped vector polygons (NLWRA, 2001). This is in contrast with the NFI requirement to only measure forest at the genus level with a broad structural classification (National Forest Inventory, 2003). The NVIS structure was developed in response to an increasing requirement to provide information for the long-term sustainable use and integrated natural resource management of regional ecosystems. However, as indicators of resource condition have yet to be fully developed, it is necessary to investigate approaches that encompass all vegetation information across landscapes at a level of detail relevant to regional

decision-making. Whilst ‘definitive vegetation types’ represent an integration or aggregation of many attributes (i.e., structure and floristics), they are not readily suited for measuring and monitoring trends, mainly due to the categorical nature of the vegetation type descriptions (Thackway *et al.*, 2007).

### ***Current National Forest Inventory reporting***

At the national level Australia’s native forests are classified into three crown cover classes: woodland (20–50 %), open (50–80 %), and closed (80–100 %). Three height categories are used to classify Australia’s native forests: low (2-10 m), medium (11-30 m), and tall (> 30 m). Almost two-thirds of the native forest estate is woodland, with around 70 % being of medium height (Table 1). In New South Wales, Victoria and the Australian Capital Territory the majority of the forests are classified as open forest (Figure 2).

Traditionally, the primary sources of cover information that the States and Territories feed into the NFI compilation process are derived from air photo interpretation, and more recently satellite imagery (Hnatiuk, *et al.*, 2003) (see Figure 3 for a range of sources). Crown cover (CC) is interpreted over generally homogeneous areas from aerial photography. Crown cover is expressed as the percentage of crown area projection per unit land area, with crown area defined as the total area contained within the external boundaries of the tree crown, where crowns are considered opaque (McDonald, *et al.*, 1998). Foliage projective cover (FPC) is based on the vertical projection of the crown foliage, and is derived from satellite imagery (e.g., Landsat TM). A related measure, foliage-branch cover (FBC) also includes branch elements in the assessment of cover, rather than just foliage. With both foliage measures, the density can vary according to species, crown type, age, location and time of year (National Forest Inventory, 2003; VicDNRE, 2000). Foliage projective cover is considered to provide a better indication of the photosynthetic potential of a plant community because trees generally have irregular canopy shape and low foliage density (Specht and Specht 1999). However, McDonald, *et al.*, (1998) recommend that crown cover be used as the primary structural attribute because foliage cover can seasonally vary, but crown size will remain constant unless major disturbance occurs.

**Table 1: Area of NFI forest types ('000 ha) across the States and Territories in Australia. Source: National Forest Inventory State of the Forests Report, 2003.**

Forest type	Australian Capital Territory	New South Wales	Northern Territory	Queensland	South Australia	Tasmania	Victoria	Western Australia	Australia	Percent of native forest
Acacia	0	1 251	1 613	6 984	1 939	74	63	4 563	16 488	10
Callitris	0	1 240	386	387	261	1	56	0	2 330	1
Casuarina	0	1 000	14	216	763	1	4	40	2 039	1
Eucalypt	116	22 218	27 911	38 706	7 849	2 476	7 562	20 184	127 024	78
Eucalypt mallee woodland	0	9	0	122	5 180	0	1 171	3 918	10 400	–
Eucalypt mallee open	0	13	0	0	864	0	0	1 051	1 929	–
Eucalypt low woodland	3	114	16 368	1 373	1 207	65	246	2 616	21 992	–
Eucalypt medium woodland	18	2 269	5 532	32 696	554	1 274	598	10 321	53 263	–
Eucalypt tall woodland	0	91	0	1 130	0	289	219	0	1 728	–
Eucalypt low open	4	72	257	0	1	0	273	22	629	–
Eucalypt medium open	63	15 921	5 703	3 326	42	7	2 809	2 048	29 920	–
Eucalypt tall open	28	3 729	0	59	1	841	2 246	170	7 073	–
Eucalypt low closed	0	0	18	0	0	0	0	8	27	–
Eucalypt medium closed	0	0	33	0	0	0	0	30	63	–
Eucalypt tall closed	0	0	0	0	0	0	0	0	0	–
Mangrove	0	3	355	196	19	0	2	173	749	<1
Melaleuca	0	44	1 593	5 301	1	19	96	0	7 056	4
Rainforest	0	486	224	2 885	0	598	16	5	4 214	3
Other	0	415	738	1 059	34	0	135	398	2 780	2
Total native forest	117	26 658	32 836	55 734	10 866	3 169	7 935	25 365	162 680	100
Total forest (2003) <sup>1</sup>	133	26 981	32 843	55 942	11 015	3 364	8 295	25 717	164 290	
Total land area	240	80 160	134 620	172 720	98 400	6 780	22 760	252 550	768 230	
<i>Forest as per cent of land area</i>	55	34	24	32	11	50	36	10	21	

1 – Includes plantations

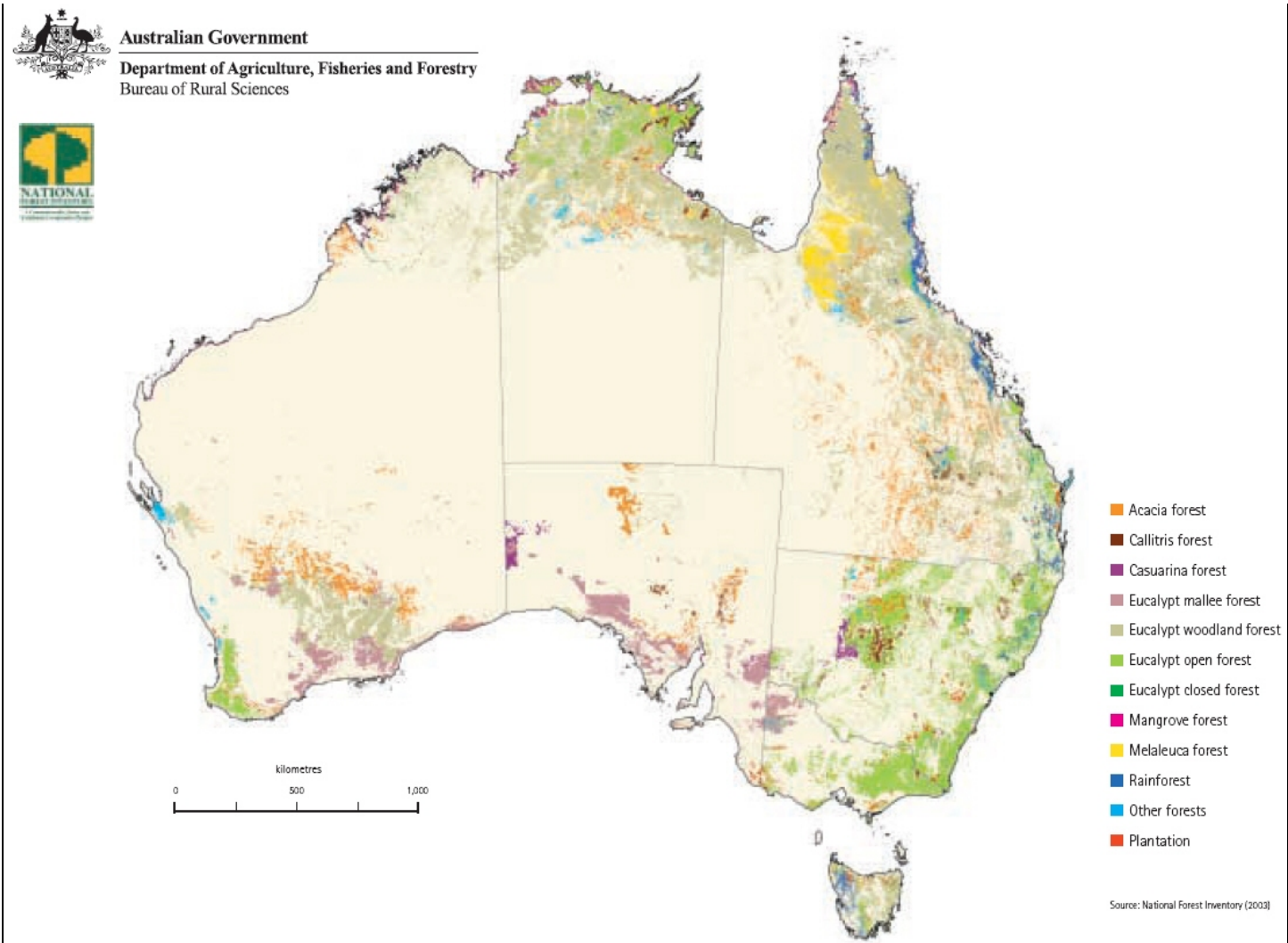


Figure 2: Distribution of NFI forest types in Australia. Source – State of the Forests Report, 2003 (NFI, 2003).

Scale	Tree component			Tree crown						Plot			Stand				Landscape					census						
	Resolution	10cm	50cm	1m	2m	5m	10m	15m	20m	25m	30m	40m	50m	100m	250m	500m	1km	sample 1%	2%	5%	25%		50%	100%				
Field data				Field transects - e.g. 1m interval, 50m long - <b>FBC, FPC</b>																								
				Hemispherical photos - e.g. a single photo with estimated 50m view - <b>FBC</b>																								
				Plot tree map and crown measurements - <b>CC</b>																								
Remotely sensed data	LiDAR returns			Crown delineations - <b>CC</b>																								
				voxels - <b>FBC</b>																								
													Aerial Photo Interpretation (API) - polygons with broad <b>CC</b> classes only															
													Hyperspectral & high resolution imagery - <b>CC</b> - (e.g. Ikonos, Quickbird, CASI - 2m crowns; Hymap 5-10m crowns)															
									ETM+ pan				Landsat TM derived <b>FPC</b> (e.g. Qld SLATS)															
													pan (2.5m) SPOT5 - <b>CC or FPC?</b>															
														ICESat footprints (50-100m) - varies between <b>CC or FBC</b>														
														2 bands	MODIS - <b>FPC</b>													
													SAR or other imagery - theoretical cover assessment ability, but need further research															

Figure 3: Illustration of different cover measurement sensors and range of scale and spatial resolution, both field and remotely sensed (McDonald, *et al* 1998; McCloy, 2006).

According to the NFI, there is currently no nationally consistent standard for mapping tree height, and it was noted that mapping compiled for national level reporting had nearly 150 different height classes (Wood, *et al.*, 2006). Accurate and consistent height information is not extensively available across the continent due to the time, effort and resources required to collect the data in the field or interpret from stereo aerial photography. Generally, the majority of accurate height information is only available for areas that are, or were, managed as State Forests (National Forest Inventory, 2003). Height information in other forested areas are usually broad estimates from a few field plots, or infrequent high quality study sites that have API or LiDAR for example. These measurements are then extrapolated to similar environmental and/or forest conditions within broad scale datasets.

### ***Limitations with NFI forest height and cover reporting***

The National Forest Inventory compiles national scale forest information using data from the States and Territories. A major difficulty with this approach is that each source of data is provided at different assessment scales (e.g., pixel spatial resolution or aerial photographic scale), level of attribute detail, accuracy (spatial and attribute) and dates of collection (Wood *et al.*, 2006). Mismatches between categorical cover and height classes are observed when compiling and translating API derived data into National Forest Inventory classes. The observed mismatches make accurate national aggregation of the height or cover class area difficult, and limit the effective use of the data in modelling and calibration of other data. Examples of mismatches between height and cover classes when using National Forest Inventory, Queensland and Victorian API schemes are given in Chapter 3. A related issue is that, due to large class ranges and subjective interpretation, there is low sensitivity to change when comparing data from different dates, unless it occurs at a class boundary. The low sensitivity with the current classes prevents effective monitoring other than at very broad scales (Scarth *et al.*, 2001).

To integrate different sources of cover information, the National Forest Inventory provides a broad conversion between foliage projective cover and crown cover (Table 2). With

continuous cover information now available from satellite imagery (e.g., Landsat TM derived foliage projective cover; QDRM, 2003), a continuous and objective transfer function is needed to make better use of both historical and current/future information. Whilst there are methods for translating between cover metrics when using field data (e.g., McDonald *et al.*, 1998), these require the subjective assessment of canopy openness, which cannot be done using medium scale remotely sensed data. This issue is highlighted by the AGO, who state that there is no direct relationship between tree crown cover and woody foliage projective cover, but that generally 20 % tree crown cover equates to around 10-15 % woody foliage projective cover (Table 2), with the relationship varying according to geography and vegetation community (AGO, 2003). Therefore a major research gap exists in the development of an objective translation between cover metrics, derived from different remotely sensed data.

**Table 2: NFI translation between foliage projective cover (FPC) and crown cover (CC) (National Forest Inventory, 1998).**

Cover Class	FPC range	CC range	Forest Cover Type
1	0-10%	0-20%	Non Forest
2	10-30%	20-50%	Woodland
3	30-70%	50-80%	Open Forest
4	70-100%	80-100%	Closed forest

There is a need for an integrated sampling framework for forest assessment due to the current ‘snap-shot’ data compilation approach used by National Forest Inventory and National Vegetation Information System. For example, when comparing the two forest area estimates made in the 1998 and 2003 State of the Forests Reports (SOFR), the forest extent in 2003 was an increase over that reported in 1998. However, it was determined that the increase largely represents more comprehensive forest mapping of the continent rather than an actual increase in the area of forest (National Forest Inventory, 2003). Current information on woody cover change indicates that total forest cover in Australia is in fact decreasing, though because of recent State and Federal legislation, the rate of current forest clearance has reduced from the higher rates experienced in the 1970s and early 1980s (AGO, 2005). The confusion arising from incomplete compilation and reporting, and a reliance on a wide range of data sources and processing methodology, highlights the need for an integrated continental sampling and



monitoring strategy. Such a strategy is required if accurate reporting across large areas with detailed information is to be achieved (Wood *et al.*, 2006).

The lack of an appropriate minimum area for defining forest is another limitation of the current National Forest Inventory mapping process. In Australia, the Australian Greenhouse Office uses a minimum woody area of 0.2 ha, and for Kyoto Protocol reporting the minimum area of forest ranges from 0.05-1.0 ha (Furby, 2002; AGO, 2005). The variable application of a minimum forest area by different agencies within a country is a common issue (Lund, 2002). Currently for the National Forest Inventory, sensor spatial resolution or public reporting scale determines the minimum area of forest. For example, the National Forest Inventory aggregates 25 m Landsat TM derived cover pixels to a minimum reporting level of 100 m, which is considered suitable for national reporting (Wood *et al.*, 2006). Conversely, API mapped forest polygons are converted to 100 m raster grid cells, with the resultant issues for accuracy in area and shape when converting from vector to raster formats. API can readily utilise a standard minimum area based on the interpreter's ability to discern homogeneous regions at the scale of the photo (e.g., 3 ha in Tasmania, with 1:20,000 scale photography; Stone, (1998)). However, there is no nationally consistent minimum area available due to the range of photographic scales in use (Wood *et al.*, 2006). When using satellite imagery to classify forest cover, the pixel size becomes the minimum area defined as woody cover (e.g., a Landsat TM 25 m pixel is 0.0625 ha). If the strict NFI definition of 'forest' is applied to each pixel, then the vegetation has to be  $\geq 20\%$  crown cover and  $\geq 2$  m height within the pixel. Without appropriate calibration and validation of the assumed cover and height thresholds, the resulting forest classification can be inaccurate, and generate potentially large variation in national level spatial and temporal estimates of the forest estate (Lund, 2002).

When defining a minimum area, there is the issue of when does a tree or group of trees with  $\geq 20\%$  crown cover per unit area become classifiable as a forest? With moderate scale image spatial resolutions ( $\sim 25$  m+) it is conceivable that a single pixel will, in theory, be larger than all but the very largest tree crowns. In sparser forests, it is possible that a single tree can be found within a single pixel, and be large enough to register greater than the 20% cover

threshold. This single tree per pixel as ‘forest’ concept, whilst currently meeting a strictly applied definition of NFI forest, is unlikely to be of use to ecologists or foresters (or other users) that may have different perceptions of, or requirements for, what a “forest” should be. Whatever the perceptions, it is likely that users of the forest data consider that a forested area should (or does) contain more than one tree, and it should at least be a self-sustaining area made up of a number of trees (Lund, 2002). Additionally, when using automated crown delineation routines to derive then aggregate individual tree crown objects into ‘forest’ (however defined), a fundamental requirement is the minimum area of the reporting unit. For example, a requirement could be that the forest area is made up of more than one tree. The issue then becomes one of how to empirically and objectively determine the minimum area and density that is required to meet these criteria. Wood *et al.*, (2006) state that the NFI Steering Committee is still examining the best way to define a minimum area for national forest compilation and reporting. This research gap will form a component of the methods and results undertaken in this thesis to address the primary research question.

### **2.2.3 Utilising data within integrated sampling schemes**

#### ***Sampling strategies overview***

It is important to understand the strengths and limitations of different sampling schemes in order to have confidence in the collected data, and to provide avenues of query to test assumptions of representativeness at multiple scales. The following section provides a brief outline of common sampling designs, and a summary of the use of field data for remote sensing calibration within integrated sampling schemes. The use of remotely sensed data for forest assessment is described in Section 2.3.

Permanent plot-based inventory systems utilising representative sampling are not new to forest assessment, and provide the most direct and effective measurement of trends in forest change and tree growth (Norman *et al.*, 2003). Trends have been estimated either through comparison of successive aggregate values from single-measure temporary plots, aggregation of

---

compared successive measures of individual permanent plots, or through a hybrid of these approaches, such as sampling with partial replacement (Scott, 1998). These inventory systems are widely utilised throughout the world, with Canada, New Zealand, Scandinavia and the United States of America (USA) all having similar forest assessment, management and implementation issues (Norman *et al.*, 2003). For example, these countries have extensive areas of relatively undisturbed natural forests over which the accessibility, level of existing knowledge and management intervention is relatively limited. Inventory sampling used by these countries is based on simple and flexible (though less efficient) systematic grids using permanent field plots with limited pre-stratification (or none at all) (Norman *et al.*, 2003). Systems are commonly two-or three stage (or phase) incorporating remotely sensed data from API or satellite based remote sensing. For example, the USA uses a three phase system, where aerial photos (and increasingly satellite imagery) are used on a one kilometre grid in the first phase to stratify locations to place field plots (phase 2 and 3 plots), and to determine expansion factors for strata (e.g., forest, non forest) (Smith, 2002).

New Zealand (Coomes *et al.*, 2002) and Canada (Wulder *et al.*, 2004) employ similar strategies but rely more heavily on remotely sensed data to provide some of the required forest attributes. New methodologies are continually being developed, for example in Canada the Forest Research Partnership developed Enhanced Inventory Project as well as the Earth Observation for Sustainable Development of Forests, which have the main objectives of testing and evaluating new technology to develop an enhanced forest resource inventory to replace the current aerial photographic and ground sampling approach. Key components of the project were the integration of airborne LiDAR, multi-band orthophotography and other remotely sensed data (e.g. hyperspectral, SAR) to generate digital terrain models, canopy surfaces, stand variables by species, stand level diameter distributions, and an increased understanding of the LiDAR data collection variables on estimation of forest variables (Natural Resources Canada, 2007).

In Scandinavian countries, forest inventory is well advanced, with many countries utilising private companies for resource assessment, for example FORAN Remote Sensing

(<http://forangroup.com/>) in Sweden. In Norway and Sweden conventional inventory methods use either systematic field plots and/or aerial photography to delineate stands and carry out stand inventory of floristics and structure. Research into LiDAR inventory has been widely taken up and has now become a practical and economic alternative. LiDAR based inventory utilises aerial photography for stand delineation and stratification, followed by LiDAR and field sampling for stand assessment (e.g. height, mean diameter, basal area, stocking and volume) (Næsset, 2004; Holmgren, and Jonsson, 2004). In Finland, major changes are underway in national forest inventory, for example, it is planned that from 2010 all forest inventory conducted by Forest Centres will be based on laser scanning, aerial photography and deliberately positioned field plots. Non-parametric plot based methods will be applied to generate estimates by forest stand by species of age, height, diameter and volume (Finnish Forest Association, 2008).

There is wide variation between countries for plot dimensions, orientation and sample density. The same issues facing these countries also occur in Australia, and the NFI is utilising the international experience in the development of the proposed CFMF (Wood *et al.*, 2006).

Within any sampling framework, errors in measurement, estimation and sampling are commonly recognised. *Measurement error* may occur in estimating structural attributes, such as tree height. *Estimation errors* are associated with the prediction of new attributes, many of which are difficult to measure (e.g., biomass) from measured attributes (e.g., diameter at 130 cm height ( $D_{130}$ )). Within a sampling strategy, a key component is to reduce both the measurement and estimation errors at the site level and from both field and remotely sensed data. (Schreuder and Gregoire, 1993; West, 2004) *Sampling errors* relate to how well the sample represents the entire population or region. When designing sampling strategies, consideration needs to be given to the intensity of samples required to adequately represent the area or population. Samples too close together will tend to duplicate information creating a wasteful (and expensive) design. However, samples too far apart will give rise to large sampling variances (potential error) and so be inefficient (Scott, 1998).

---

***Random, systematic, and stratified random sampling***

The simplest and easiest technique to sample a population is to select an unbiased sample across the area to be assessed. This is achieved by randomly locating samples until the desired number have been collected. A limitation with simple random sampling is that often clusters of sites are generated in some parts of the area and no observations in others, which, depending on the research interest, can limit the suitability of the method for effective spatial sampling (Haining, 1990). This limitation can be offset with stratified random sampling, where an independent random selection is made within partitioned regions or strata. This strategy allows the variances of the estimators from each stratum to be combined to obtain variances of estimators for the whole population (Thompson, 2002).

Stratification schemes are most efficient when the population is partitioned such that the units within the stratum are as similar as possible. Whilst variance between strata may be high, a stratified sample with adequate units from each stratum in the population will tend to be representative of the population as a whole (Thompson, 2002). Stratified random samples become inefficient when the distance between samples is less than a predefined optimal distance used in a systematic sample. Therefore, some form of systematic sampling may be desirable which keeps sites at some optimal distance apart while providing full coverage of the area under investigation. If attributes under investigation tend towards highly variable distributions, then a relatively dense network of sites is required so that the variable nature of the area can be characterised (Haining, 1990).

Whilst random allocation of sites reduces bias toward any particular spatial attribute, clustering can occur even with stratification, for example near strata boundaries (Thompson, 2002). Theoretical evidence stresses the effectiveness of systematic sampling in a variety of spatial situations. However, issues can arise with aligned systematic sampling because of spatial variability occurring at a range of measurement scales, discontinuous spatial variation, or where there are features that are not easily sampled using a regular grid (e.g., riparian vegetation; Haining, 1990). Practical issues also influence sampling design. While a potentially optimal design may use a dense network of sites on a regular grid, when cost,

timeliness of survey, and access (especially to private land or remote/difficult terrain) are considered then it is likely that not all potential sites can be used. In these instances, an increased sampling error has to be accepted or a different sampling methodology used (Thompson, 2002).

### ***Model based sampling***

An example of a potentially powerful sampling design, developed to address some of the issues of random and systematic sampling, is model-based sampling. With this strategy, a regression model is used to determine the value of the attribute of interest, based on its relationship to an easily observed variable that was measured on every sampling unit in the population (West, 2004). Multiple covariate attributes can be utilised in the regression model, so long as they are all available in the sampled population (i.e., remote sensed data), which can often result in improved model prediction accuracies. Model based sampling designs have been used at local and regional levels for over 20 years (Biggs *et al.*, 1985; Wood and Schreuder, 1986; Hamilton and Brack, 1999). However, whilst the application of model based sampling at continental scales was proposed (Brack, 2004), and forms a key part of the Australian Greenhouse Office NCAS methodology (Brack *et al.*, 2006), the sampling strategy has not yet been implemented for national forest monitoring.

An advantage of a model-based strategy is that it utilises the full power of regression analysis in establishing relationships between the variable of interest (often something more difficult to measure – such as field data) and one or more covariates that can be (generally more easily) measured in the population (e.g., using remote sensing). Generally, all that is required is that the data collected covers most of the value range of the covariates occurring in the population, and that the sample is objectively selected (West, 2004). These criteria allow field data collected for purposes other than forest inventory to be utilised more often, thereby reducing cost and resource requirements.

Disadvantages of model-based sampling are that (as with most stratified designs) some prior knowledge or data is required in order to develop the regression models. If there are large

uncertainties in the existing data, or gaps in the extent or knowledge of the range of values in the population, then the resultant models may have large variances and poor prediction ability when applied to new areas. Second, a model-based sampling strategy could become potentially confusing and unwieldy (and therefore difficult to ‘sell’ and implement) when a large number of variables of interest are being investigated, with each requiring a separate regression model to be developed. This may be mitigated to some extent if there is correlation between forest metrics, thereby allowing a smaller set of variables to predict a larger range of metrics. Despite these potential disadvantages, where cost is a factor, the ability to predict a required attribute based on readily available remotely sensed data can provide a relatively inexpensive initial estimate (with confidence levels), especially if the required information was not available previously, or is available but has low spatial or spectral resolution and limited attributes (Brack, 2007).

### ***Using field data for remote sensing calibration***

Field data are used to enhance the extraction of information from remotely sensed sources, through calibration of the data and information, and to provide an assessment of the accuracy of derived information. This methodology is a core part of the strategy for integrated sampling schemes. The following section outlines current knowledge and theory on the data integration process, and provides guidance for addressing the primary research question, in terms of linking and calibrating LiDAR with field estimates of forest structure.

Field data can be defined as independently verifiable, more detailed and accurate (spatially and in information content), and collected using proven and repeatable techniques, usually at a fine spatial resolution (Curran and Williamson, 1985). Field data are collected at key locations determined through appropriately designed sampling strategies, as outlined previously (Curran and Williamson, 1986). The field site concept is defined by McDonald *et al.*, (1998) as a small area of land that is considered to be representative of the vegetation, landform, or land surface / features associated with the observations. It is noted that whilst the extent of a site is arbitrary, a square or rectangular site of 400 m<sup>2</sup> is appropriate for sampling

vegetation, however this may vary depending on the surrounding land cover. What is required with all field data collections used with remotely sensed data is a clear definition of the purpose of the data, and a specification of the criteria that the field data must meet, such as (but not limited to) the types or intended use, spatial resolution, timeliness and accuracy of the data collected (Zhou *et al.*, 1998; Fisher *et al.*, 2006).

When using field data to validate remote sensing derived information, accuracy is defined as the closeness of derived values to field estimates (Cooke and Harris, 1970). However, as field data are rarely totally accurate, the accuracy assessment is not necessarily an estimate of the closeness to the “true” values (although it may be close). This also suggests that field data should not be called “ground truth”, as it is also an estimate of the attribute of interest (Brogaard and Ólafsdóttir, 1997). Two other concepts related to the usefulness of field data for calibration deal with bias and precision. Bias is defined as the difference between the mean value from a set of repeated measurements and its ‘true’ value. Precision is defined as the variation in a set of repeated measurements (West, 2004).

Three different types of accuracy can be recognised with respect to remote sensing analyses: classification accuracy, parameter estimate accuracy and location accuracy. *Classification accuracy* can be undertaken at a pixel level, where the classification result is compared to field estimates for each pixel in a sample, and a commission and omission error table generated. When object-oriented analyses are undertaken on the data, objects (e.g., crops, fields or forest patches) that are generated from a number of pixels (or segments / clusters) can be assessed for accuracy for both class attributes and area / boundary location (Van Gendern *et al.*, 1978).

*Parameter estimate accuracy* compares the estimate of a physical attribute (e.g., forest height or cover) with ground measurements, usually with correlation and regression analyses to establish the relationship and set confidence ranges (Thompson, 2002). Whilst the assessment process is generally simple (depending on the metric being compared), accuracy estimates can be compromised when there is a mismatch between the sensor spatial resolution and the scale at which *in-situ* measurements are collected. The use of *in-situ* measurements for model



calibration and validation therefore requires robust and defensible methods to adequately sample or spatially aggregate ground measurements to the scale (e.g., size and shape) at which the remotely sensed data are acquired (Curran and Williamson 1986; Atkinson and Curran 1995; Baccini, *et al.*, 2007).

*Location accuracy* assessments between field and remotely sensing data compare points, lines, or polygon area features. Assessments generally rely on specialised field survey techniques (e.g., through the use of ground control points) and/or Global Positioning Systems (GPS), for the registration and geo-rectification of the remotely sensed data (Lund, 1998). Where both field and remotely sensed data have utilised the same ground control points, and thus have the same inherent positional error, it can be difficult to judge which source provides a more accurate estimate of the object location, particularly when fine scale remotely sensed data are used.

## **2.3 Remote Sensing of Forests**

### **2.3.1 Overview**

Remotely sensed imagery records the spectral reflectance from the surface of the Earth, and is a useful source of information about the spatial distribution of vegetation. Applications for mapping the location of vegetation, its quality, quantity and dynamics are numerous and continually expanding. There is also a correspondingly intensive research effort for improving analytical methods (Dungan, 2001). The scale of the land surface unit under observation (pixel size) and spectral range combine to determine the amount of information that can be derived from these sensors; thus an understanding of potential scale effects is critical to effective use of remotely sensed data (Hay *et al.*, 2005).

Remote sensing use within forest inventory has been steadily increasing over the last 60 years. The first use began with black and white aerial photography after the First World War, with major utilisation and colour photography occurring after World War II. There has been an

ever expanding use of satellite remote sensing from the 1970's, with the spatial resolution, extent, diversity (multi-spectral, hyper-spectral, microwave/radar, laser), and reliability of remote sensing technologies improving rapidly over the last decade (Wulder, 1998). Additionally, the increasing adoption of a range of remote sensing instruments in multi-resource inventories has produced more accurate information, particularly for defining forest boundaries and producing national level maps (Lund, 1998; McRoberts and Tomppo, 2007).

Methods for processing moderate spatial resolution (~20 m+) remote sensing to produce forest and land cover information are well developed and accepted (e.g., Richards *et al.*, 2000; Cihlar, 2000; Donoghue, 2000; Patenaude *et al.*, 2005). Broad scale forest mapping and monitoring worldwide has been undertaken primarily using NASA's Landsat series, the Advanced Very High Resolution Radiometer (AVHRR) (e.g., Lu *et al.*, 2003), the Satellite Pour l'Observation de la Terre (SPOT) series, and more recently with the Moderate Resolution Imaging Spectroradiometer (MODIS) sensors (Wulder, 1998; Hill *et al.*, 2006). Processing methods for determining forest cover from moderate spatial resolution sensors like Landsat TM, range from band ratio combinations such as NDVI (e.g., Miura *et al.*, 2006) to more complex modelling using, for example, regression based modelling (Lucas, *et al.*, 2006c) or Geo-Optical (GO) and radiative transfer methods (Li and Strahler 1985; Li *et al.*, 1995, McCloy, 2006). With GO methods for example, pixel radiance is modelled as the area-weighted combination of the range of sunlit and shaded tree objects and background components visible to the sensor. GO models are used to estimate the bidirectional reflectance distribution function using discrete 3D objects, where the shape, density and patterns control the reflectance response to illumination and different view angles. In the Li-Strahler GO model a spherical shape is assumed for the partially illuminated tree crowns that make up the vegetation canopy (Jupp and Walker, 1996; Scarth and Phinn, 2000).

The Landsat series of satellites have been in operation since 1972, and have been utilised for a broad range of applications in Australia. The latest sensors - Landsat 5 Thematic Mapper (TM) and Landsat 7 Enhanced Thematic Mapper (ETM) - have 30 m spatial resolution across 7 spectral bands, with Landsat 7 having an additional 15 m panchromatic band (NASA,

2008). A fault developed in Landsat 7 during 2003 resulting in data gaps, rendering its data unusable for National Forest Inventory applications; however more recent research into increasingly sophisticated data blending algorithms incorporating MODIS and Landsat, the SLC-off limitation is becoming less of an issue (Gao *et al.*, 2006; Wulder *et al.*, 2008). This also highlights the requirement for CFMF data collection methods to be technology independent (Principle 4), or at least not substantially reliant on any one sensor (Wood, *et al.*, 2006). In Australia, two major users of Landsat TM imagery for state and national level forest measurement and monitoring are the Queensland Statewide Land-cover And Trees Study (SLATS) program and the Australian Greenhouse Office National Carbon Accounting System (NCAS).

SLATS use Landsat TM imagery from 1989-to-present for estimating the extent and change in woody vegetation. A multiple regression vegetation index developed using field site data sampled throughout Queensland, is used to calculate a gradient of woody foliage projective cover, and seeks to detect woody vegetation to the lowest possible detection limit (QDNRM, 2003; Lucas *et al.*, 2006b). This vegetation index compensates for the difference in background soil colour which can otherwise cause significant overestimation (for black soil) or underestimation (for red soil) of woody vegetation cover. Dry season imagery (July – September) is used to minimise the variability in image quality due to atmospheric haze and cloud, and to provide the maximum differentiation between pasture and forest canopy (Lucas, *et al.*, 2006b). For purposes of vegetation management, SLATS detects all woody vegetation, with a minimum threshold of approximately 7 % foliage projective cover in most cases, but the minimum threshold may be up to 12 % where image quality is poorer (AGO, 2003; QDNRM, 2003). Recently airborne LiDAR data were collected at a number of test sites, and research is underway to use the LiDAR to improve the Landsat TM derived foliage cover estimation models (J. Armston, *pers. com.*).

NCAS use Landsat TM data to identify change in forest cover status to feed into national carbon accounting models. The primary mission of NCAS is to support Australia's position in the international development of policy and guidelines for terrestrial greenhouse gas

sinks and emissions. NCAS estimates continental biomass stock and flux at sub-hectare resolution using Geographic Information Systems (GIS) based process models (3PGs) combined with empirical data (Richards and Brack, 2004; Richards and Evans, 2004). Maps of biomass potential are interpolated from mapped multi-temporal productivity layers, calibrated with measurements of mature forest biomass. Biomass accumulation is estimated with simple growth formulae, linked to site productivity (predicted using soil and climate factors) and combined with stand age estimated from disturbance analyses derived from Landsat MSS and TM images spanning 1972-2002 (Richards, 2002). NCAS was developed using a process of continuous improvement, and this allows for enhanced capability for monitoring, scenario modelling, and capability to support climate change mitigation initiatives (Brack *et al.*, 2006). For example, vegetation layers used in the modelling for stratification and allocation of mature biomass estimation functions were derived initially from a combination of the Resource Assessment Commission survey (RAC, 1992) and Carnahan (AUSLIG, 1990) mapping (Richards, 2002). A more recent update includes the National Vegetation Information System data (ESCAVI, 2003).

The NCAS, according to international guidelines, measures a claimed constant minimum threshold of 20 % interpreted tree crown cover at 2 m height, and identifies only verifiable, deliberate land use change (i.e. from a forest to a non-forest use). It was noted in the NCAS documentation that the 20 % crown cover is at the lower limit of cover that can be accurately resolved using Landsat TM data (Richards, 2002). However it should be noted that non-stereo optical data is inherently asymptotic to vertically distributed structural elements (McCloy, 2006), so while the NCAS may claim to utilise a 2 m height threshold, in practise this can only be assumed or roughly estimated based on temporal analyses. Actual fine scale active data sources such as LiDAR would be required to quantitatively apply a specific height threshold to the modelling. Whilst seeking to develop a consistent and comprehensive assessment of vegetation across the continent, these data still contain knowledge gaps and issues with mapping scale, currency, and use (e.g., determining a 2 m height threshold using passive

optical data), which can introduce error when assessed, utilised, or validated at the sub-hectare level.

Synthetic Aperture Radar (SAR) is another potential source of forest information. Knowledge of the information content of this data source acquired over forest environments, and in particular microwave interaction with different components (leaves, trunks, branches) is required to support the retrieval of their biomass, structure and floristic composition at an operational level (Hyypä *et al.*, 2000). Such knowledge is increasingly important given the deployment of lower frequency spaceborne radar sensors (e.g., Japan's Advanced Land Observing Satellite (ALOS) Phased Array L-band SAR) to complement the current suite of C-band sensors observing the Earth. Active microwave sensors can penetrate the canopy and so provide information about the entire vertical depth of the forest, as well as being sensitive to a range of forest parameters, including the geometric structure of tree components (Liang *et al.*, 2005).

Another benefit of SAR systems is the ability to make all-weather (although results can be negatively impacted by wet conditions e.g., de Jong *et al.*, 2002) and night-time observations at high spatial resolution, and at a range of frequencies and polarizations. In gaining such knowledge, a number of approaches can be adopted, including the use of empirical relationships (Dobson *et al.*, 1995; Lucas *et al.*, 2000; Le Toan *et al.*, 2004) and modelling by distributing tree components of varying size, geometry and dielectric properties within two-dimensional (2D) layers (e.g., Durden *et al.*, 1989; Lucas *et al.*, 2004; Liang *et al.*, 2005). More recent modelling have utilised 3D cubes (e.g., Sun *et al.*, 2002) and simulated microwave interaction, overall backscatter coefficient, and the magnitude of contributory mechanisms (e.g., single bounce, volume scattering). In the latter case, the cubes or "voxels" (volumetric pixels) have typically been constructed around artificial trees or those that have been measured from field data. However, at the present time these systems and methodological approaches tend to be best suited for structurally homogeneous forest types, and those in the lower biomass range (30-200 Mg ha<sup>-1</sup>) due to issues of sensor saturation (Imhoff, 1992; Lucas *et al.*, 2006a).

LiDAR remote sensing directly measures both horizontal and vertical spatial elements of forest structure. Many studies utilising either both small footprint (< 0.5 m radius) or large footprint (10 m +) waveform digitization airborne LiDAR, have demonstrated an ability to recover structural elements such as tree and canopy height, canopy cover and volume, canopy height profiles, biomass and basal area at accuracies near equivalent to (and sometimes better than) field survey (Magnussen and Boudewyn, 1998; Lim *et al.*, 2003b; Riano *et al.*, 2004; Gobakken and Naesset, 2005; Lefsky *et al.*, 2005b). LiDAR remote sensing of forests will be covered in more detail in section 2.3.2.

When mapping forest structure, an optimal integration strategy would include finely detailed measurements that field sampling (or field equivalent remotely sensed data) provides, combined with the broad spatial coverage of moderate spatial resolution remote sensing. Although this level of forest structural information cannot be provided by any current single technology, advancements in SAR and LiDAR have the potential to lead to broad-scale mapping of both horizontal and vertical structure in the near future (Reutebuch *et al.*, 2005). However, intermediate scale mapping of forest structure is possible through statistical analyses such as model based sampling, and/or fusion of information from multiple sensors. This process takes advantage of the highly detailed vertical measurements provided by LiDAR: either detailed full waveform-digitizing (where available e.g., SLICER / LVIS (Harding *et al.*, 2001)) or ICESat (Lefsky *et al.*, 2005a), or less detailed but more available small footprints systems (Lim *et al.*, 2003b). The LiDAR is then combined with the broad-scale mapping capabilities of passive optical sensors, for example Landsat TM (Hudak *et al.*, 2002; Wulder and Seemann, 2003; Donoghue and Watt, 2006), or hyperspectral (Bunting and Lucas, 2006; Koetz *et al.*, 2007; Addink *et al.*, 2007; Lucas *et al.*, 2008), or the coarse sensitivity to horizontal and vertical structure afforded by SAR (Reutebuch *et al.*, 2005; Hyde *et al.*, 2006; Lucas *et al.*, 2006a).

### 2.3.2 LiDAR remote sensing of forests

#### *Overview*

As described previously, LiDAR is increasingly being utilised in the calibration between field data and other remotely sensed data. The following section outlines the research into the application of LiDAR for forest assessment, including strengths and limitations for assessing forest cover and height. This provides context and direction for discussing the utility of LiDAR to improve measures of forest structure, which is presented in Chapter 5.

In recent years, the retrieval of forest structural attributes across the landscape has been advanced considerably following the development of remote sensing technology, and particularly multiple (discrete) return and full waveform LiDAR (Lim *et al.*, 2003b). Small footprint LiDAR is an active sensor that uses a laser beam in the near infrared spectral range directed towards the ground. The time and intensity of any return signals from the original pulse are used to measure the distance to an object. Depending upon flying height, the footprint size may vary from 0.1 to 5.0 m and the interval between laser returns may range from 0.25 to 5 m. With the aid of real-time differential GPS (with base stations) and sophisticated inertial navigation systems (INS) that measure aircraft pitch, yaw and roll, most LiDAR are now capable of achieving absolute spatial accuracies of  $< \pm 1$  m in the x and y directions, and  $< 0.25$  m in the z direction (i.e., elevation). In most systems, the laser pulse is emitted via a rotating mirror, which creates a zigzag swath of laser returns either side of the aircraft (Figure 4). For forest assessment purposes, LiDAR provides a highly precise dataset of points representing a sample of terrain and vegetation. The high geo-registration accuracies now makes it possible to “image” individual tree crowns, and to locate the same trees on the ground using, for example, hand-held GPS (Lovell *et al.*, 2003).

Over the last 15 years, the use of small footprint airborne LiDAR for retrieving ground surface and vegetation parameters has been demonstrated. The data have been used primarily to retrieve commonly measured forest attributes, namely tree-based estimates of top height and crown dimensions (Leckie *et al.*, 2003; Solberg *et al.*, 2006), or stand-based estimates of mean or maximum canopy height (Mean *et al.*, 2000; Naesset, 2002), basal area and stem volume

(Holmgren *et al.*, 2003), canopy cover (Todd *et al.*, 2003; Riaño *et al.*, 2004), timber volume (Maltamo *et al.*, 2004) and/or biomass (Lim and Treitz, 2004). Algorithms have typically been developed through empirical relationships with ground data, and their success was reported by referring to a testing ground dataset and utilizing standard statistical descriptors (e.g., the coefficient of variation,  $r^2$ ). This work has now matured to the state where direct estimates of structural variables (e.g., tree heights, canopy cover) routinely achieve  $r^2$  values approaching or exceeding 0.90 (e.g., Suarez *et al.*, 2005). Hyypä *et al.*, (2001) demonstrated that LiDAR could provide more precise stand-based estimates than conventional field-based inventory.

To date, the research and development effort has largely been undertaken by timber companies, government organizations and the academic scientific community. Research into LiDAR application have often been in close collaboration due to the high cost of acquisition, mission planning, collection of associated field data, along with computer storage and processing software. Most studies have been conducted across a range of forested biomes (boreal, temperate, subtropical and/or tropical) in the US (Lefsky, *et al.*, 1999; Hall *et al.*, 2005), Canada, (Magnussen and Boudewyn, 1998; Lim and Treitz, 2004), Australasia (Lovell *et al.*, 2003; Tickle *et al.*, 2006; Goodwin *et al.*, 2006) and Europe (Hyypä *et al.*, 2001; Gaveau and Hill, 2003). When retrieving forest structural attributes, the majority of studies have utilised LiDAR height information, which has generally been in the form of canopy height surfaces or models (CHM) interpolated from point data from the outer surface on the canopy. In earlier studies using LiDAR data, emphasis was placed on retrieving tree or stand height from the canopy height models or information on the vertical stratification of foliage and branch elements (e.g., Magnussen and Boudewyn, 1998; Todd *et al.*, 2003; Lovell *et al.*, 2005).

Whilst most LiDAR studies have utilised a scanning mode sensor since they offer a larger measurement area and the ability to delineate individual crowns, profiling systems were initially trialled before being superseded by scanners. Profiling LiDAR systems use a single beam emitted below the aircraft to sample the ground and features, generating a single line transect of points, rather than a scan of an area. More recently profiling systems have been investigated again as a less expensive alternative to scanners, especially for regional or

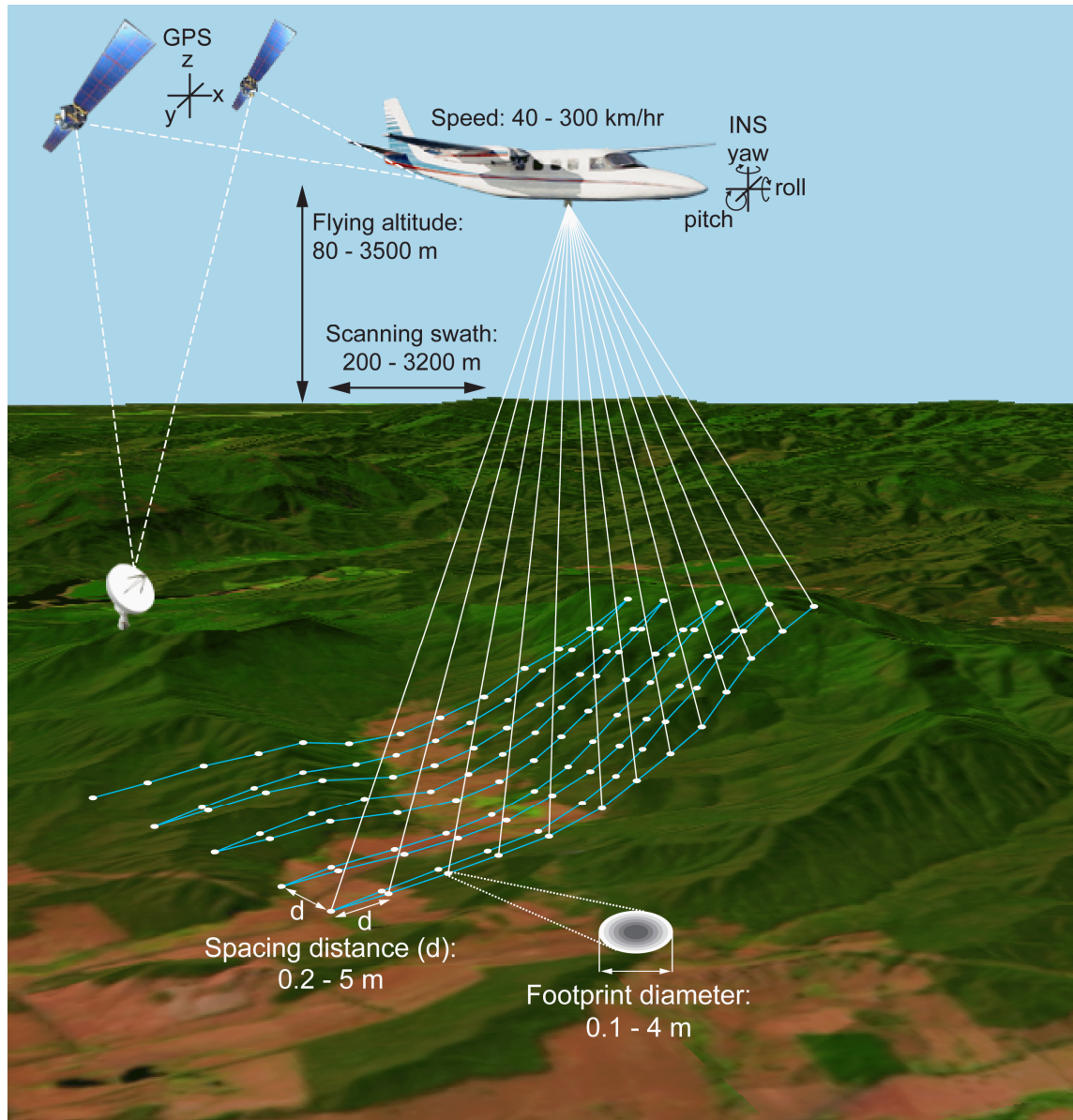


continental sampling. In Australia, a profiler system was used to assess foliage projective cover and canopy height, with  $R^2$  values greater than 0.9 with field estimates reported. Monitoring of changes in cover and height resulting from logging or growth, were shown to be successful (Weller *et al.*, 2003).

In North America both the USA and Canada have reported LiDAR profiler trials. In the state of Delaware, USA, a single set of airborne laser-profiling data acquired in 2000 was used to assess forest wood volume and biomass, with estimates within 22% of US Forest Service county level estimates. Mature forest stands that provided suitable habitat of endangered species were successfully identified and mapped. The studies concluded that line intercept sampling techniques used in conjunction with a relatively inexpensive, portable airborne laser-profiling system should be utilised as a regional (hundreds of thousands of hectares or larger) assessment tool for assessing and monitoring a wide range of natural resources (Nelson *et al.*, 2003; Nelson *et al.*, 2004). In Canada, two coincident LiDAR profiler transects were integrated with Landsat ETM+ imagery to monitor boreal forest change over a 5 year period (1997 and 2002) along an approximate 600 km corridor. The results indicated that key canopy attributes (including forest canopy height) were stable over the five-year period. It was found that, as expected, forest growth occurred incrementally over broad areas; with losses being very evident and spatially constrained. It was concluded that the approach held potential for investigating the impacts of climate change across a boreal forest latitudinal gradient (Wulder *et al.*, 2007).

At present, attention is increasingly turning to the estimation of a greater range of forest attributes as processing methods become more sophisticated. Desirable attributes include tree density (e.g., Holmgren *et al.*, 2003; Leckie *et al.*, 2003), basal area or biomass (e.g., Lefsky *et al.*, 1999; Lim and Treitz, 2004; Lefsky *et al.*, 2005a) and measures of canopy cover (Riaño *et al.*, 2004; Chen *et al.*, 2004). For the purpose of retrieving these attributes, measures derived from the LiDAR CHM (maximum, mean or percentiles) and/or the percentage of canopy strikes per unit area or volume have typically been considered. For estimating stem density, several studies have simply counted crowns delineated using the CHM (e.g., Hyypä *et al.*, 2001; Leckie *et al.*, 2003; Suarez *et al.*, 2005), whilst others have used more complex transfer

functions based on specific percentiles of the height distribution of canopy LiDAR pulses or mathematical functions (e.g., Weibull (Lovell *et al.*, 2003; Maltamo *et al.*, 2004); or Johnson's SB (Jerez, *et al.*, 2005) that describe apparent vertical profiles.



**Figure 4: Graphical representation of the elements of a small footprint airborne scanning laser (LiDAR) system. GPS refers to Global Positioning System, INS is Inertial Navigation System. Note that the graphic and elements are illustrative only and not to scale.**

Plot and stand-level descriptions (e.g., density, mean height and canopy cover) have been obtained through aggregation of tree level information (e.g., Popescu *et al.*, 2003). However, success in locating and attributing stems occurring in high density young forests or beneath overstorey canopies and integrating these with those of the overstorey trees for stand-

based estimates were limited to only a few studies (e.g., Hyypä *et al.*, 2001; Leckie *et al.*, 2003; Gaveau and Hill, 2003; Suarez *et al.*, 2005; Koukoulas and Blackburn, 2005).

Some studies have examined the potential to integrate existing API with LiDAR. For example, St-Onge *et al.*, (2004) assessed the potential for improved utilisation of historical aerial photography for tree height measurement by using LiDAR derived ground Digital Terrain Models (DTM). The study used LiDAR to derive ground elevation (base of tree), and then using stereo photogrammetry to measure tree height. This allowed the improvement of photo interpretation and measurement of height even in more dense forests, which traditionally were more difficult to interpret due to higher cover in lower or understorey strata. As the ground terrain was unlikely to change in a major way (unless there has been significant disturbance/erosion), then the same DTM could be used with historical photography, thus expanding the utility of historical aerial photo archives.

### ***Large footprint LiDAR***

The majority of studies have focused on small footprint LiDAR, largely because of the earlier development of this technology but also because of the wider availability of commercial systems in many countries. By contrast, full waveform large footprint airborne systems are still experimental in the USA, and not yet commercially available. This limitation is being addressed to some extent by spaceborne LIDAR platforms such as the Geoscience Laser Altimeter System (GLAS) on the current NASA Ice, Cloud, and land Elevation Satellite (ICESat). The GLAS sensor is a full-waveform laser with an approximate ellipsoid footprint of 70 m diameter on average (variable between 50 m diameter circle to 60 x 120 m ellipse), with samples approximately every 200 m along track, and 183 day repeat cycle path. Investigations into forest height extraction have been initiated, and are currently ongoing (Ranson, *et al.*, 2004; Lefsky, *et al.*, 2005a; Harding and Carabajal, 2005).

These and other full waveform LiDAR data (e.g., SLICER and LVIS) are showing considerable promise for forest assessment. Depending on foliage canopy, they are capable of sampling almost the full canopy profile within each footprint. The high level of sampling

provides information on the distribution of strata (including the sub canopy), the canopy volume and other stand attributes (e.g., growth stage) which have proved difficult to obtain with small footprint LiDAR or other methods (Lefsky, *et al.*, 1999; Harding, *et al.*, 2001; Lim *et al.*, 2003b; Lefsky *et al.*, 2005b). However, whilst providing stand level descriptions, these systems have proved limited for retrieving tree level information such as the location of individual stems and their associated crowns dimensions. This occurs largely because the diameter of the footprint, (generally 8 – 70 m; Lim *et al.*, 2003b), presents a lower bound on the horizontal spatial resolution. Also, it is often difficult to relate field scale data or provide absolute measures of the foliage height distribution (Harding, *et al.*, 2001).

This is in contrast to the small footprint systems within which tree crowns can be readily discerned and information on the vertical profile also obtained. Large footprint systems generate a full waveform for each footprint, resulting in large volumes of complex data requiring sophisticated processing. Small footprint systems also generate large volumes of data but the data themselves are relatively simple (i.e., in terms of spatial location, elevation and intensity) and are more readily available for immediate use and analysis. Even so, the representation of the canopy vertical profile is at a lower spatial resolution and can be biased toward the upper parts of the canopy, thus potentially affecting foliage cover estimates derived from LiDAR, as identified in Lovell *et al.*, (2003).

### ***LiDAR for Australian forests***

A key benefit of all LiDAR systems is that they provide information on the distribution of plant elements in the sub-canopy and, in Australia, this information is sought as it has relevance to managing flora and faunal species, understanding both forest health and condition, and the capacity of forests to regenerate, especially following fire, drought or harvesting (Stone *et al.*, 2000). Such knowledge is also required for improved carbon accounting of both current and future carbon stocks (Dean *et al.*, 2004), and for risk assessment in relation to fire fuel loads and crown fires (Riaño *et al.*, 2003; Andersen *et al.*, 2005). However, useable algorithms for retrieving information on the sub-canopy of forests in Australia from LiDAR have been difficult

to obtain, partly because most have been developed on, and are applicable to, single-layered forests or those that are multi-layered but with a relatively uniform structure. Such structures are common to forests in northern hemisphere temperate regions, which are composed primarily of coniferous (e.g., Hall *et al.*, 2005) and/or broadleaved (e.g., Patenaude *et al.*, 2005) species, and also the tropics (Drake *et al.*, 2002; Clark *et al.*, 2004).

Native forests typical to Australia differ from these formations in that many are more open, and comprised of a mix of species with markedly different architectures. In particular, the dimensions (area and depth) of crowns in the upper canopy are highly variable, ranging from large and expansive (typical to many *Eucalyptus* and *Angophora* species) to small and compact, such as those typical to *Callitris* species (Specht and Specht, 1999). In many cases, both crown types occur in the same stand but often in different strata, which present significant challenges for deriving estimates of tree density, basal area and crown cover from LiDAR canopy height models. Specifically, when locating individual trees within the canopy height model, many trees partially or wholly in the sub-canopy or understorey are not identified (Hyyppä *et al.*, 2001), high points in crowns often do not necessarily correspond to the location of the stem (Lee *et al.*, 2001), and multiple high points within a single crown may occur that falsely indicate the presence of several separate trees (Florence, 1996). Stand-based basal area estimates may also be inaccurate, particularly if these are generated by counting locally high points from the LiDAR canopy height model and subsequently applying regression equations relating height and stem diameter at 130 cm height ( $D_{130}$ ), as many trees are omitted or attributed with incorrect height values. Estimates of stand-based crown cover are also often based on arbitrary thresholds of the canopy height model rather than on a measure that better relates to the distribution of foliage and branch elements.

### ***LiDAR calibration studies***

In parallel with LiDAR research for extracting forest metrics of interest, a number of studies have examined the interaction and responses of LiDAR data from different forest structural configurations, and with different sensor parameters. This has enabled, to some

degree, an ability to compare results between sensors and forests. However, given the large range of forests and structures found worldwide, and the ever increasing sophistication of sensors, there is still much research to be undertaken. Assessment of sensor and forest structure interactions can be categorised into three broad research topics – forest simulation studies, multi-sensor and multi-forest type comparisons, and comparisons between ground and airborne LiDAR systems.

Forest simulation studies have sought to better understand the LiDAR interactions, such as the effect of scan angle and return sampling density in different forest structures and terrain, by controlling all aspects of the interaction through modelling. The modelling can be used to account for bias in actual LiDAR data and optimise sensor configurations for differing forest types. Models have included 3D ray-tracing simulation, relatively simple forest stand simulation such as plantations, and recently more sophisticated forest stand simulations where a range of structural configurations simulate trees with variable heights, crown dimensions and foliage clumping (Holmgren *et al.*, 2003; Lovell *et al.*, 2005; Goodwin *et al.*, 2007). Simulation results have been impressive with correlations between the simulated and actual LiDAR results having an  $r^2$  exceeding 0.9. Results have identified linear relationships between LiDAR return spacing and predominant height (Lovell *et al.*, 2005), height estimation differences of less than 2.5 m (Goodwin *et al.*, 2007), and canopy profiles that have a similar form to LiDAR profiles, but which can have a systematic overestimation of 2.5 m (Holmgren *et al.*, 2003).

A number of studies have had access to sensor systems that allowed different parameters to be tested over the same forest location, or similar systems across a range of different forest types. This has facilitated an improved understanding of how different sensor parameter combinations measure the forest. For example, in both Canada and Australia the influence of flying altitude, beam divergence, mean point spacing, and pulse repetition frequency on return intensities and vertical frequency distributions were investigated (Chasmer *et al.*, 2006a; Goodwin *et al.* 2006; Thomas, *et al.*, 2006; Hopkinson, 2007). Results showed that platform altitude and footprint size did not have a major influence on standard forest structure attributes (height, basal area, and biomass) and normalised canopy height profile

estimation. However, there was a positive relationship between platform altitude and the underestimation of tree crown area and crown volume, with higher altitudes and/or lower return spacing resulting in greater error (Goodwin *et al.*, 2006; Thomas, *et al.*, 2006).

A few studies have utilised ground based laser ranging sensors in combination with airborne LiDAR, to either compare both laser based methods of forest assessment with field data (e.g., in Australia - Lovell *et al.*, 2003) or directly compare the results from the two laser systems (Chasmer *et al.*, 2004; Chasmer *et al.*, 2006b). A high percentage of airborne LiDAR pulses were found to be intercepted at the top of the canopy, with fewer returns from within the canopy and understory. Additionally, a statistically significant tree height difference between field measurements and the maximum laser pulse return from both airborne and terrestrial LiDAR was found, with an underestimate of tree height by one metre on average from the maximum airborne laser pulse returns (Chasmer *et al.*, 2006b). It was concluded that future research should focus on improving understanding of how laser pulse returns are "triggered" within vegetated environments, and how canopy properties or data acquisition parameters may influence the location of this "trigger" event (Chasmer *et al.*, 2006b).

### **2.3.3 Tree crown delineation using high resolution remote sensing**

Developing a crown cover dataset that can be utilised at multiple scales is a significant component of this thesis and is undertaken in order to address the primary research question. This section provides background to tree crown delineation methods using fine spatial resolution remote sensing and focuses mainly on those that have utilised LiDAR data. Bunting and Lucas, (2006) provide a detailed review of crown delineation methods. Some of the concepts and issues to address presented here will be utilised as part of the research design presented in Chapter 3.

Common approaches to defining and/or delineating tree crowns firstly involve the development of a forest/non-forest mask, with thresholds of reflectance for optical images (e.g., Bunting and Lucas, 2006) or height with LiDAR based methods (Hyypä *et al.*, 2001). Once a mask was applied to the image or layer, then individual crowns or crown apices are found

through either (or a combination of) locating local maxima, identifying crown boundaries at minima in the reflectance or height surface topology, and /or using templates of different crown sizes and shapes.

### ***Local minima location***

Many studies have utilised a range of spatial methods to detect crown centroids and boundaries. These methods begin by finding local maxima in the image, which may have been initially smoothed using low pass-filters to remove apparent noise (often small internal crown gaps). Filters of different sizes and shapes, related to the expected crown size found in the area, can be used to iteratively determine the maxima most likely to equate to tree centroids. Local minima are identified and used to map crown boundaries through region-growing from local maxima, combined with watershed based segmentation methods (Chen *et al.*, 2006). Various clustering and optimising approaches have sought to refine the number of maxima and minima and have tended to limit crown splitting during segmentation, often combined with knowledge-based assumptions on the shape of trees. (e.g., Wulder *et al.*, 2000; Hyypä *et al.*, 2001; Culvenor, 2002; Culvenor, 2003; Popescu *et al.*, 2003; Popescu and Wynne, 2004).

The minima and maxima finding methods tend to be most accurate in mature or early-mature coniferous stands. They were more limited in dense young stands, in dense clusters of deciduous trees, or mature heterogeneous forests where single trees could not be identified in the complex canopy. In dense stands, the crown area was found to be underestimated, because of partly interlocked crowns (Pouliot *et al.*, 2002; Koch *et al.*, 2006). Reported accuracies were variable and depended on the forest types, with the modelled crown mapping successfully identifying between 60-80 % of the field mapped crowns. Stem detection accuracy was found to be no longer obtainable in any stand condition with a density greater than approximately 2,200 stems ha<sup>-1</sup> (Rowell *et al.*, 2006)

The use of a calibration model to correct the segmented areas was suggested by Hyypä *et al.*, (2001). It was observed that whilst crowns in the top layer were detected, smaller trees underneath were not found. Coops *et al.*, (2004) applied Culvenor's (2002) tree identification



and delineation algorithm (TIDA) to both fine spatial resolution multi-spectral imagery, and discrete-return LiDAR data, with the LiDAR performing better at crown matching when compared to field data. The authors concluded that the optimal result was obtained when tree crowns were delineated using both LiDAR and multi-spectral data.

### ***Minima contouring***

Methods that use valley following (or contouring) along canopy reflectance or height topographical minima extend the minima-finding concepts described previously. Reflectance topography is formed by the brighter reflectance from the tops of trees, and darker intensities on the crown sides or gaps between trees due to shading. After high spectral resolution (both multi- and hyperspectral) images are smoothed using a range of filters, height or reflectance minima are identified using a range of search kernels, and the minima contour is followed in a clockwise manner such that similar sized, symmetrical and non-overlapping crown shapes are formed. Often rule-based isolation models are used to improve the segmentation results (e.g., Leckie *et al.*, 2003; Leckie *et al.*, 2005; Gougeon and Leckie, 2006). These methods have been extended using image contouring procedures and supervised feature extraction to generate polygons, which are manipulated based on geometrical and spatial properties of known tree crowns (e.g., Koukoulas and Blackburn, 2005). Accuracy of the valley following methods ranged from 50–60 % of field measured tree delineations being identified when only using spectral imagery, to 80–90 % when LiDAR and multi-spectral imagery were combined. Common errors found by the studies were delineating a single cluster that actually consisted of two or three crowns, and a consistent height underestimation of 1.3 m on average by the LiDAR derived delineations. Overall, results indicated that the LIDAR produced better results in semi-natural forests, whereas delineations from spectral images (e.g., aerial photography) were more accurate in broadleaved deciduous plantations.

---

### ***Template matching and object-oriented analyses***

A further refinement of geometric and spatial crown modelling approaches uses template matching algorithms within object-orientated segmentation. These methods link physical models of trees to the imagery, canopy height models or point data using template (2D and 3D) matching techniques, and often at different scale-levels. Templates of known growth stage and species are associated with potential crowns in the image that have the most similar template (e.g., Persson *et al.*, 2002; Solberg *et al.*, 2006). The methodology can be enhanced when very high sampling rate LiDAR (12 returns per square meter) is used to detect trees (Brandtberg *et al.*, 2003). The accuracy of earlier methods was up to 71 % of all trees (> 5 cm stem diameter) detected (and 91 % of the stem volume), and later methods identifying up to 93 % of the dominant trees and 19 % of the sub-canopy trees. Standard error estimates for height and crown diameter were around 1.2 m and 1.1 m respectively, with crown diameter overestimated by 0.8 m (Solberg *et al.*, 2006). It was observed that the segmentation technique generated crown diameters that were too small for trees with intersecting tree crowns because segments could not overlap.

The template concept is further extended by using Definiens eCognition Expert-based object-oriented image classification and segmentation methods (e.g., Suárez *et al.*, 2005; Bunting and Lucas, 2006). Forest features from different spectral types are identified using scale and homogeneity metrics obtained from reflectance parameters, and height from a LiDAR can be added if available. Object maxima within larger potential crowns were used as seed pixels, which were expanded to the edges of the reflectance topology. The final crowns were generated after classification-based splitting or merging using scale dependent templates. Results suggested that LiDAR can predict tree tops more efficiently for smaller-diameter than for larger-diameter trees, with the discrepancy related to the fact that these trees are generally sub-dominants and have canopy heights below the mean height of the surrounding trees (Suárez *et al.*, 2005). In forests with a high density of individuals (e.g., regrowth), local maxima were counted to approximate density within clusters, as individual crowns could not be delineated. The delineation process provided accuracies on an average of 70 % (range 48 – 88 %) for

individuals or clusters of the same species (stem diameter > 10 cm), with lower accuracies associated with dense stands containing several canopy layers (Bunting and Lucas, 2006).

### ***Delineation limitations***

The crown delineation methods described above have a number of issues that require further research to resolve. First, some crown centroid and local minima methods apply restrictions based on crown size, shape or spacing. Others may require a user defined kernel, such that a bright point is identified each time the window is moved across the image. TIDA and similar algorithms have had problems with larger gaps between trees, which are erroneously classified as tree segments in some cases, and therefore the algorithm appeared to operate best in more closed forests (Culvenor, 2002). Also, with these methods, crown boundaries are at least one (or more) pixels wide, which is inappropriate for forests with touching or interlocking crowns, or even crowns identified at different height strata. In these cases, a mapped "gap" pixel is an artefact of the method and does not represent an actual gap. However, it could also be said that this is also an artifact of the raster data model used to display the results, rather than the actual delineation method itself. Whilst using vector boundaries would reduce the apparent size of the potential crown boundary, how best to represent interlocking crowns or crowns in different height strata, whilst still maintain a boundary between crown objects is an issue common to all delineation methods, when utilised in 2D GIS or image processing systems. This issue is yet to be resolved.

One possible solution to representing a cluster of trees with interlocking crowns may be to use an outer crown boundary without internal boundaries, but using points to represent tree trunk locations. Attributes could be attached to the points indicating probable crown size and shape that is also related back to the overall cluster size and shape. Alternatively, the crown cluster itself could contain attributes describing the estimated stem density, including sub-canopy stems. For example, Maltamo, *et al.*, (2004) investigated tree crown segmentation methods, where individual single trees were recognised, and tree height and crown area detected. It was observed that while the detection of suppressed trees from a height model

based on LiDAR was difficult, it was possible to predict these trees by using theoretical Weibull distribution functions. Weibull distributions were fitted to the LiDAR detected tree height distribution, in order to predict the number of small trees based on empirical correlation with field data.

An issue with boundary following methods is that they tend to ignore the 3D positioning of crowns. Specifically, assumptions are made that all or most stems have a crown area similar in size, are reasonably symmetrical, do not cast shadows or overlap each other, and have definitive boundaries. Whilst the practicalities are many for this approach when developing new algorithms, in mature or disturbed forests stands, these situations tend to be less common. In a similar manner, template methods require prior knowledge of the range of crown forms throughout different growth stages. In mixed species forests with a range of soil types and landforms, the range of templates are required to match most or all potential forms can be prohibitive to gather and utilise.

## 2.4 Scale in Remote Sensing

### 2.4.1 Overview

An understanding of scale as a fundamental concept in the effective utilisation of remotely sensed data is required for assessing forested landscapes, primarily because scale determines the quality and type of information that can be extracted from data (Wulder, 1998). Forest landscapes are spatially correlated and scale-dependent. Therefore multi-scale information is required to fully describe, understand, manage, and predict the complex hierarchical dynamics that determine structure, processes, and functioning (Hay, *et al.*, 2001; Wu, 2004). Understanding landscape functioning and process is required if improving sustainable forest management and better prediction of the potential impacts of climate change on ecosystems is to be achieved. When scaling or extrapolating fine scale remote sensing or site specific data to medium scales, substantial error can result if the approach is arbitrary or inappropriate (Hay *et al.*, 2001). Interpretation error can also occur when making statistical inferences from medium scale aggregated data or relationships to individuals, with this termed the *ecological fallacy* by Robinson, (1950; in Marceau, 1999). Therefore, the prediction and mitigation of scale and aggregation effects on statistical results and modelling, or exploring improved methods of integrating data across scales, are recognized as major research goals (Marceau, 1999; Atkinson and Tate, 2000). There has been an ever increasing sophistication of analytical research techniques, leading to enhanced prediction accuracy for forest inventory and biophysical parameters when using remotely sensed data (Wulder, 1998).

Initial methods to understand the effects of scale utilised semi-variogram graphs as a way to investigate optimal spatial resolution for a particular investigation (Woodcock and Strahler 1987). These graphs showed how the local variance of a digital image for a scene changed as the resolution-cell size changes, and therefore assisted in selecting an appropriate image scale. Semi-variograms were generated by imaging the scene at fine spatial resolution and then collapsing the image to successively medium spatial resolutions while calculating a measure of local variance (Jupp *et al.*, 1989). Research of this type provided insight into remote sensing scale effects, by indicating that there is an implicit limit to the information content

associated with a particular sensor, and this limit is determined through knowledge of the spatial resolution of the sensor (Wulder, 1998). In pixel based analyses, image classification is a form of simplification, and appropriate simplifications serve to further our understanding of complex issues and problems, and are nearly always based on high-spatial resolution models (Visvalingam, 1991; Dungan, 2001). Typically, each measurement is classified independently of the others; however spatial autocorrelation is an inherent feature of high-spatial resolution images. Where spatial autocorrelation is ignored, significant biases can be introduced that reduce the accuracy of areal inventory (Curran and Williamson, 1986).

Over the last decade, there has been a shift from pixel based remote sensing analysis to that which incorporates multi-scale object-oriented methods (Hay *et al.*, 1997). The main drivers have been the commercial availability of high spatial resolution data (< 5 m) combined with an increase in computing power with decreasing cost, and the cross-fertilisation of object-oriented software developments from the Computer Science and Geographic Information Systems disciplines. These systems incorporate raster processing ability, and in many cases are available as off-the-shelf commercial products (Hay, *et al.*, 2005). An important component of the shift in analysis methods is the conceptual ability to recognise and generate image objects in high-spatial resolution data that are made up of many individual pixels (with generally similar values per object, but not exclusively) and which correspond to real-world geographic entities. This then emulates what human interpreters visualise when analysing an image. Visualisations encompass a scale dependent range of objects of varying shape, size, arrangement, texture, and spatial context (Hay, *et al.*, 2005). Whilst these concepts, termed H-resolution (and the converse case, termed L-resolution, where the cells are larger than the objects being imaged (Strahler *et al.*, 1986)), have been discussed for over 20 years, it is only relatively recently that the tools and data have matured sufficiently to match the conceptual understanding, and thus allowing user requirements to be met.

Object-oriented concepts developed from the recognition that pixels are an arbitrary grid imposed on the surface, where grid boundaries do not have a corresponding real world counterpart. The integration of energy that constitutes the pixel digital number is also derived,

in part, from areas outside the pixel, and thus pixels are not true geographic (or ‘real-world’) entities (Hay *et al.*, 2005). The analysis of H-resolution imagery with object-oriented methods in conjunction spatial statistics provides for stronger relationships and linkages to be created between the image spectral and spatial information, and between ground data. Parameters may be estimated empirically: either with regression-based models, or in a more deterministic fashion, such as deriving stem counts from delineated tree crowns (Wulder, 1998). The advantage of deterministic models is that they lead to a more direct understanding of the nature of the scene, sensor, atmosphere and their joint interactions. Empirical models are useful for data exploration, suggesting relationships that can be refined further by models with more deterministic components. When exercised under conditions for which they have been calibrated, empirical models can produce very accurate scene inference (Dungan, 2001). The combination of empirical and deterministic approaches may provide for an increase in the ability to estimate forest inventory and biophysical parameters (Wulder, 1998).

### ***Modifiable Areal Unit Problem***

Remote sensing technologies represent the primary data source for landscape analysis, but there is often difficulty in extracting accurate, reproducible information from imagery. This is because, as noted previously, the results of spatial analyses are sensitive to the size (scale) of the data collection units. If scale is not accounted for adequately, it can lead to bias and the development of spurious relationships. A well known aspect of scaling effects on spatial analyses is the “*Modifiable Areal Unit Problem*” (MAUP) (Openshaw, 1984; Jelinski and Wu, 1996), which was described previously in Chapter 1. The MAUP issue must be considered when relating field data to image data. For adequate calibration and extraction of accurate information the ground data must represent an areal extent similar to the spatial resolution of the remote-sensing instrument. This is because there is a direct relationship between the size of the objects of interest on the ground and the image (pixel) spatial resolution (Wulder, 1998). Object-based approaches that use basic geographic entities have been put forward as a viable solution to the MAUP issues associated with pixel-based remotely sensing (Fotheringham *et al.*,

2000). By generating basic geographic entities that specifically relate to real-world objects, the resultant remotely sensed analyses are much more likely to be valid, meaningful, and useful (Hay *et al.*, 2005).

Research efforts to better understand the information content of optical remotely sensed data at medium scales have utilised aspects of the multi-scale use of geographical entities. The multi-scale basic entity strategy has also been employed to better predict microwave interactions in the canopy. Both research efforts have led to the development of a range of new vegetation modelling approaches. Models use a range of geometric forms, at varying levels of sophistication in terms of how strata and shading are defined, to physically represent the canopy and canopy gaps. Alternatively, empirical relationships between canopy reflectance and the variable of interest are developed (McCloy, 2006). The main types of physical modelling approaches include the turbid medium (e.g., Combal *et al.*, 2000), the geo-optical (e.g., Li and Strahler, 1985; Jupp and Walker, 1996), ray tracing or flux / radiosity (e.g., Smith and Goltz, 1994; Gastellu-Etcheberry *et al.*, 1996; Casa and Jones, 2005), and hybrids of these such as linear semi-empirical adaptations of physical models (e.g., Fang and Liang, 2005). Depending on the size of the forest stand being modelled, some models can be very computationally intensive, which limits their practical application. In other cases, when forests exhibit a highly clumped nature and contain heterogeneous crown shapes, such as found in Australian woodlands, then assumptions on the size, shape and distribution of canopy elements are often violated, so reducing their accuracy (McCloy, 2006).

### ***Hierarchy theory and Landscape Ecology***

Ecological systems overwhelmingly complex and this complexity must be managed or defined for effective understanding and scaling within the system to occur (Wu, 1999). Hierarchy theory suggests that complex systems have a high degree of redundancy, and description and understanding can be facilitated by simplification through time-space decomposition into a limited number of subsystems (Turner and Gardner, 1991). When applied to a forested landscape for example, a hierarchical model may be composed of drainage basins,



which in turn are composed of local ecosystems or stands, which are in turn composed of individual trees (which in turn are composed of stems, branches and leaves, and so on) and tree gaps (Forman 1995). Hierarchy theory is a part of general systems theory, and has emerged as part of a movement toward a general science of complexity, levels of organization and issues of scale (Simon, 1962; Simon 1973). A concept of duality for interactions within hierarchy theory has been suggested, such as process-structure, and part-whole. For example, Koestler (1967) referred to the notion of a 'holon', defined as a hierarchical entity that is at once a whole and at the same time a part. A holon at once operates as a quasi-autonomous whole that integrates its parts, whilst at the same time integrating itself into an upper level purpose or role. The relationship between two adjacent hierarchical levels is asymmetric: the upper level exerts constraints (e.g., as boundary conditions) and provides context to the lower level, whereas the lower provides initiating conditions and mechanistic understanding to the upper (Wu, 1999).

Recent theoretical developments in landscape ecology have recognised that identifying, and taking advantage of the hierarchical structure and near-decomposability of complex ecological systems may hold the key to improving understanding and prediction through robust simplification and successful scaling (Allen and Starr, 1982; Turner and Gardner, 1991). Wu (1999) summaries the paradigm of hierarchical patch dynamics as being one that integrates hierarchy theory and patch dynamics and, whilst allowing simplification of the complexity of nature, still retains the essence of the system. A hierarchical patch dynamics scaling strategy can be implemented in three stages, each of which may involve a number of steps and methods: (1) identifying appropriate patch hierarchies to decompose complex spatial systems., (2) making observations and developing models of patterns and processes around focal levels, and (3) extrapolation across the domains of scale using a hierarchy of models (Wu, 1999). Generally, decomposing a complex system may invoke a bottom-up (aggregation) or top-down (partitioning) scheme or both (O'Neill et al., 1986). The establishment of an appropriate patch hierarchy then allows patterns and processes to be studied at their characteristic focal levels or domains of scale, through the careful choice of grain (e.g., observation resolution) and extent (Wu, 1999).

## 2.5 Summary

The primary aim of this thesis is to determine how LiDAR can improve the assessment of forest structure. This Chapter has reviewed the current literature to gain an understanding why forest structural measurements need improving, and how LiDAR may assist with this task. The main issues identified in the literature form the basis of the research design (described in Chapter 3), developed to address the primary research question.

This chapter has identified that the National Forest Inventory currently utilises data with categorical classifications, and compiled for national reporting from the States and Territories using a ‘snap-shot’ approach every five years. This methodology is not well suited to effective monitoring of forest stocks and dynamics, especially in response to a changing climate. The National Forest Inventory has proposed the Continental Forest Monitoring Framework (CFMF) as a strategy to overcome the current reporting limitations. One of the key concepts of the proposed framework is the use of continuous measurements for forest structure, gathered within an integrated multi-scale scheme, and utilising a range of data sources. The proposed framework has identified a number of limitations requiring further research. These include the ability to effectively translate between structural metrics using continuous transfer functions, and the derivation of an objective and empirically based minimum area for reporting forest.

Multi-scale integrated sampling strategies are an efficient way to measure the landscape in detail, and involve taking fine scale measurements from a few well-selected field data and calibrating medium scale data that can be applied across the landscape. A limitation of these strategies is that with large landscape variability, it is difficult to achieve a representative sample when limited to surveying relatively few field plots (e.g., due to cost, effort, and access limitations). Effective calibration of medium scale data is therefore limited, which in turn affects the accuracy of regional or national reporting. LiDAR has been shown to have potential for generating information that is equivalent to field measurements, but over much larger areas that can be surveyed on the ground. This then provides a source of calibration data that can sample more of the landscape variability at fine scales, allowing improvements in the accuracy of reporting from medium scale data. What is currently missing is a strategy for using LiDAR

to link fine scale field data with medium scale data (e.g., Landsat TM, ICESat, radar) within integrated sampling schemes for Australian forests.

Scale issues affect all remotely sensed data in some way (e.g., the Modifiable Areal Unit Problem), which can lead to error in forest structural modeling and reporting. Investigations into scale issues have indicated that using basic geographic entities or objects (e.g., trees) within a hierarchical system is an effective way to reduce, mitigate, or at least better understand the effects of scale on forest assessment when using remote sensing. Up-scaling tree level data to match the spatial resolution of the medium scale data can reduce scale issues, and improve calibration and validation of structural measurements. However, the research gap for Australian forests is the ability to generate structural information at a tree scale (crowns and/or stems) from LiDAR data. Ultimately, the results of investigations into the research gaps identified here will enable the primary thesis research question to be addressed, and therefore determine how LiDAR can improve forest structure assessment in Australia.

---

## CHAPTER 3. DATA ANALYSIS METHODOLOGY

---

### 3.1 Introduction

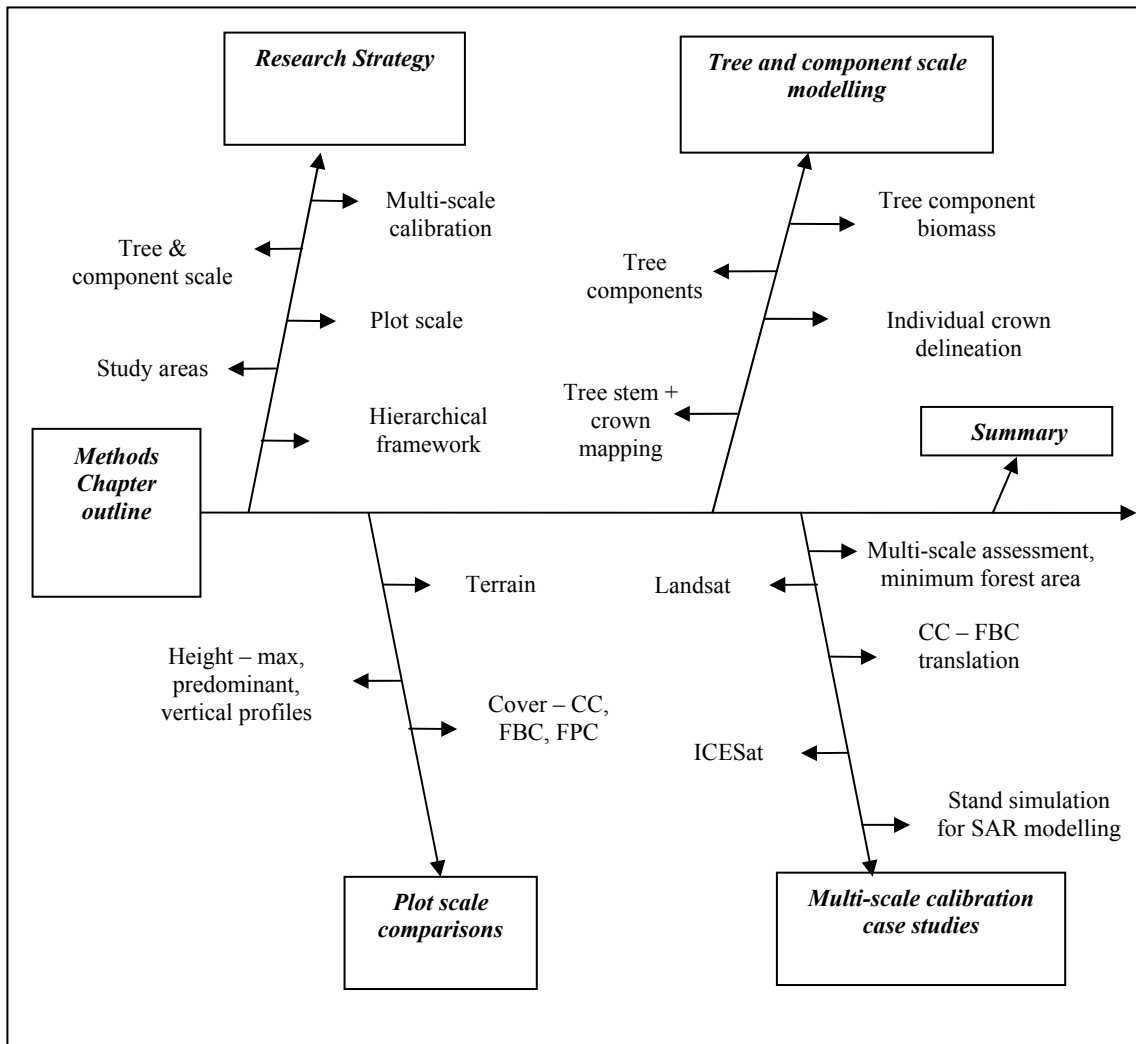
To answer the primary research question and objectives, there is a need to investigate how LiDAR can improve the assessment of forest structure in Australia. The preceding chapter identified a number of limitations with current national forest structure measurement and monitoring. This chapter describes the research design and methodology that will address these limitations, and provide the results to address the research objectives, and therefore answer the primary research question. The research design described in this chapter will encompass:

- 1 A strategy for using LiDAR to link fine scale field data with medium scale data (e.g., Landsat TM, ICESat, radar) within integrated sampling schemes;
- 2 The ability to generate structural information at a tree scale (crowns and/or stems) from LiDAR data for Australian forests, to allow sensor independent up-scaling and improved calibration of medium scale remotely sensed data, for both height and cover metrics;
- 3 The ability to effectively translate between structural metrics using continuous transfer functions, and the derivation of an objective and empirically based minimum area for reporting forest.

This chapter is divided into several sections (Figure 5). Section 3.2 outlines the research design for developing a hierarchical multi-scale framework strategy, which utilises LiDAR to link fine scale field data with medium scale remotely sensed data. Section 3.3 provides an overview of the published procedures were used to collect the field and remotely sensed data at both Queensland and NE Victorian study sites. Section 3.4 describes the methods for plot to stand scale assessment of forest structural metrics relating to height and cover, to allow translation between LiDAR and field data estimates. Section 3.5 outlines the spatial data analysis techniques used to develop the tree and tree component scale results using LiDAR. Section 3.6 describes a number of case studies where exploratory data analysis techniques are

used to calibrate other remotely sensed data using multi-scale LiDAR products. Section 3.7 summarises the main outcomes of the chapter.

It should be noted that, unless otherwise specified, ESRI ArcInfo Arc Macro Language (AML) algorithms written by the researcher performed the iterative calculations and spatial analyses described in the following sections. Statistical analyses were undertaken in SPLUS (version 7).



**Figure 5: Methods chapter layout showing major components of LiDAR assessment of forest structure.**

## 3.2 Research Design Overview

### 3.2.1 Multi-scale strategy overview

To facilitate the improvement of forest structure assessment and specifically measurement of forest height and cover using LiDAR, the research design strategy has two main components. First, a multi-scale analysis strategy is outlined that uses LiDAR to link field data to medium scale remote sensing through the use of basic geographic entities. Second, case studies will be described which highlight the different applications that can be undertaken using the strategy, which were used to address the limitations identified in Chapter 2.

#### *Developing a hierarchical multi-scale modelling framework*

When using LiDAR to effectively link field data with a range of medium scale remotely sensed data, it is necessary to operate at multiple scales. As outlined in Chapter 2, an examination of hierarchy theory from the field of landscape ecology suggests that when one studies a phenomenon or entity at a particular hierarchal level (the focal level, often denoted as Level 0), the mechanistic understanding comes from the next lower level (Level -1), whereas the significance of that phenomenon can only be revealed at the next higher level (Level +1) (Wu, 1999). Thus three adjacent levels or scales are usually necessary for understanding most of the behaviour of ecological systems. When developing a spatially explicit dataset consisting of basic geographic entities, the first task is to define the actual basic entity of analysis. In order to delimit practical and achievable objectives for this thesis, the basic entities for each of the three hierarchal levels are defined as:

- 1 *Level 0*: An individual tree or tree cluster. Clusters are mapped where interlocking crowns or high stem densities preclude individual crown separation. Two entities will be mapped at this level (i.e., tree crowns/clusters of crowns, and individual stems). Mapping individual stems is especially important for interpreting crown clusters, as the cluster area is likely to contain more than one tree.
- 2 *Level +1*: The wider forest stand, which is defined here as the maximum spatial extent of the available LiDAR data. This level can be divided into the plot scale (for direct

comparison with field data), and the stand or landscape scales (to test representativeness of plots within the stand and landscape).

- 3 *Level -1*: Within-tree components, defined as trunks and crowns (from Level 0) containing major branches, and leaves and small branches (represented as canopy voxels). The amount of leaves and small branches is calculated using allometry applied to the Level 0 tree entity structural dimensions and species (species information is derived from externally supplied hyperspectral data). Primary and secondary branches are modelled based on stem location, crown dimensions, and voxel distribution within the crown.

The three hierarchical levels form the basis of the strategy to address the research gap in terms of developing a strategy to link LiDAR structural assessments of height and cover with other data. The assumed advantages and disadvantages of measuring structure at the different levels within the hierarchical strategy are listed in Table 3.

**Table 3: Advantages and disadvantages assumptions of different hierarchal processing levels for forest assessment using LiDAR**

Level	Assumed Advantages	Assumed Disadvantages
Plot or Stand (+1)	<ul style="list-style-type: none"> <li>- Rapid application, conceptually and computationally simple.</li> <li>- Applicable across landscape when using large datasets.</li> <li>- Accurate at plot level with suitable field calibration.</li> </ul>	<ul style="list-style-type: none"> <li>- “Black box” approach; can be difficult to account accurately for effect of within plot variation or intra-plot variation observed.</li> <li>- Within plot structural complexity reduced to a few simple “average” values which limits explanatory ability.</li> <li>- A range of possible component structural arrangements can give the same overall plot result; thus predictive ability is reduced especially in heterogeneous environments.</li> <li>- Ensuring accurate plot boundary location for comparisons can be difficult.</li> </ul>
Tree (0)	<ul style="list-style-type: none"> <li>- More accurate representation of within plot/stand variability.</li> <li>- Can be scaled up or down to any pixel scale within limits of base data.</li> <li>- Stand level stem and crown mapping reasonably computationally quick.</li> </ul>	<ul style="list-style-type: none"> <li>- Takes longer than plot scale to generate.</li> <li>- Assumptions required on tree crown shape, as well as representativeness of LiDAR data penetrating tree crowns (i.e. vertical strata assessment) .</li> <li>- Validation accuracy depends on tree level field data accuracy; issues with GPS locations, incorrect matching of stems and less accurate field measurements (e.g., height) that can lead to poorer correspondence results.</li> </ul>
Tree component (-1)	<ul style="list-style-type: none"> <li>- Much greater level of detail possible; therefore fine spatial resolution remote sensing calibration and ecological modelling can be undertaken.</li> <li>- Suitable for radar volumetric canopy interaction modelling and simulation.</li> </ul>	<ul style="list-style-type: none"> <li>- Long processing times because of level of detail required.</li> <li>- Many assumptions on branch and leaf location, size, density and orientation.</li> <li>- Difficult to validate especially when field data not explicitly collected to same level of detail, therefore validation generally undertaken using medium spatial resolution data.</li> </ul>

Whilst the primary analysis hierarchy is described above, the hierarchical strategy can be applied at other scales depending on the research problem being addressed. The respective entities can be defined along the a scale continuum, ranging from tree components (stems, branches and leaves), trees, forest stands or patches, up to whole forests or forested regions, and ultimately biomes. For example, a hierarchical strategy used to address variability within forest stands would have the focal level as a field plot (or equivalent assessment unit), with the level – 1 being a tree crown or stem map within the plot, and the Level +1 being the wider stand within which the plot is found. Alternatively, if the research was investigating variability between forests stands in the landscape, then the forest stand would be the focal level, with field plot sized areas within the stand constituting Level –1, and the wider landscape being Level +1. Thus a hierarchical multi-scale strategy is a useful approach for improving forests structural measurement, when linking datasets and metrics. This assertion will be revisited in the Discussion chapter, and an assessment made of its validity.

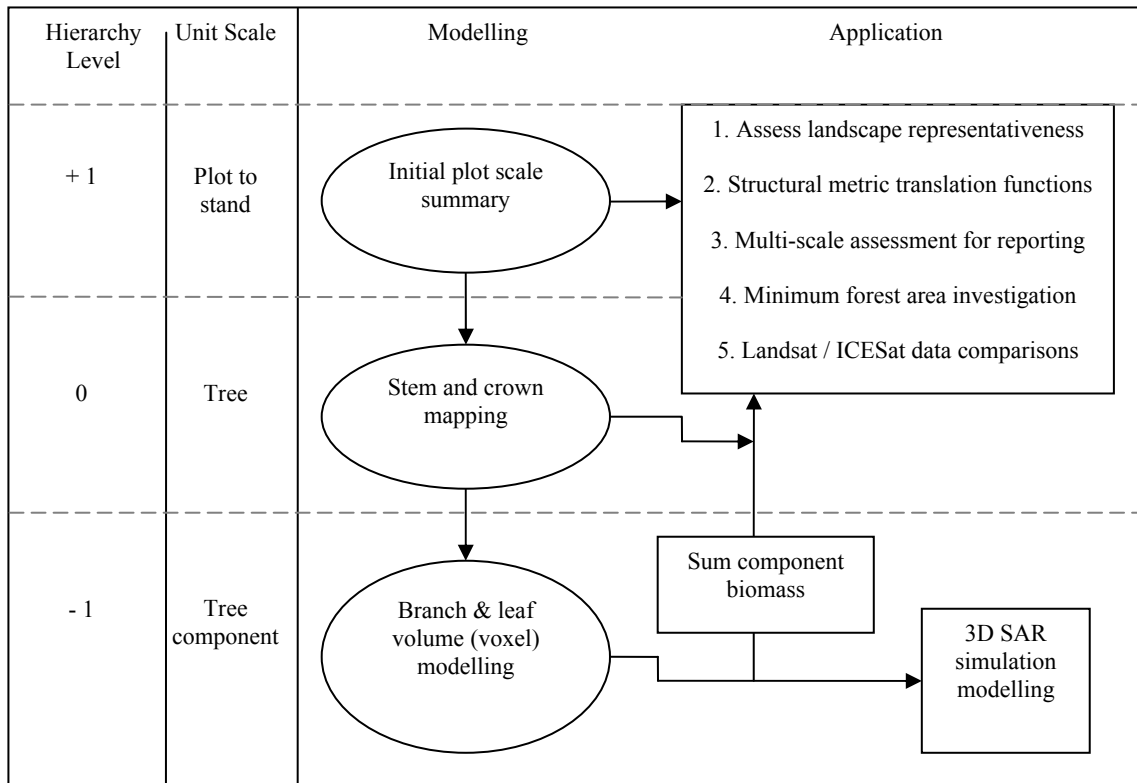
#### ***Applying the multi-scale hierarchical framework***

The multi-scale hierarchical framework uses three processing phases to generate the data required for the strategy. A number of case studies then test the application and overall usefulness of the strategy (Figure 6). The first phase begins at the Level +1 scale, to establish if there were robust relationships between plot scale field data and LiDAR derived metrics for forest height and cover metrics (Lucas *et al.*, 2006a; Tickle *et al.*, 2006). This was done for both study sites, to gain an understanding of any regional differences in metric estimation. After validation to acceptable levels of accuracy, the LiDAR derived height and cover metrics were applied to the full extent of the LiDAR data within both the Injune and NE Victorian landscape-sampling schemes. This then creates a large sample from which to assess the landscape distribution and variability of the structural attributes, and tests field plot representativeness.

The second phase utilises a range of spatial modelling methods to delineate and map Level 0 entities such as tree crowns and stems (Lee and Lucas, 2007). Level 0 entities were



then used to aid in the modelling of Level -1 tree components such as branches and leaf clumps (Lucas *et al.*, 2006c) by providing a bounding area within which to assign individual tree identifiers. Within phase II, height was calculated for individual tree stems, tree crown extent was mapped to determine plot crown cover, which allows quantification of within-plot variability.



**Figure 6: Thesis conceptual overview outlining linkages between multi-scale hierarchal modelling and applications for modelling forests with LiDAR.**

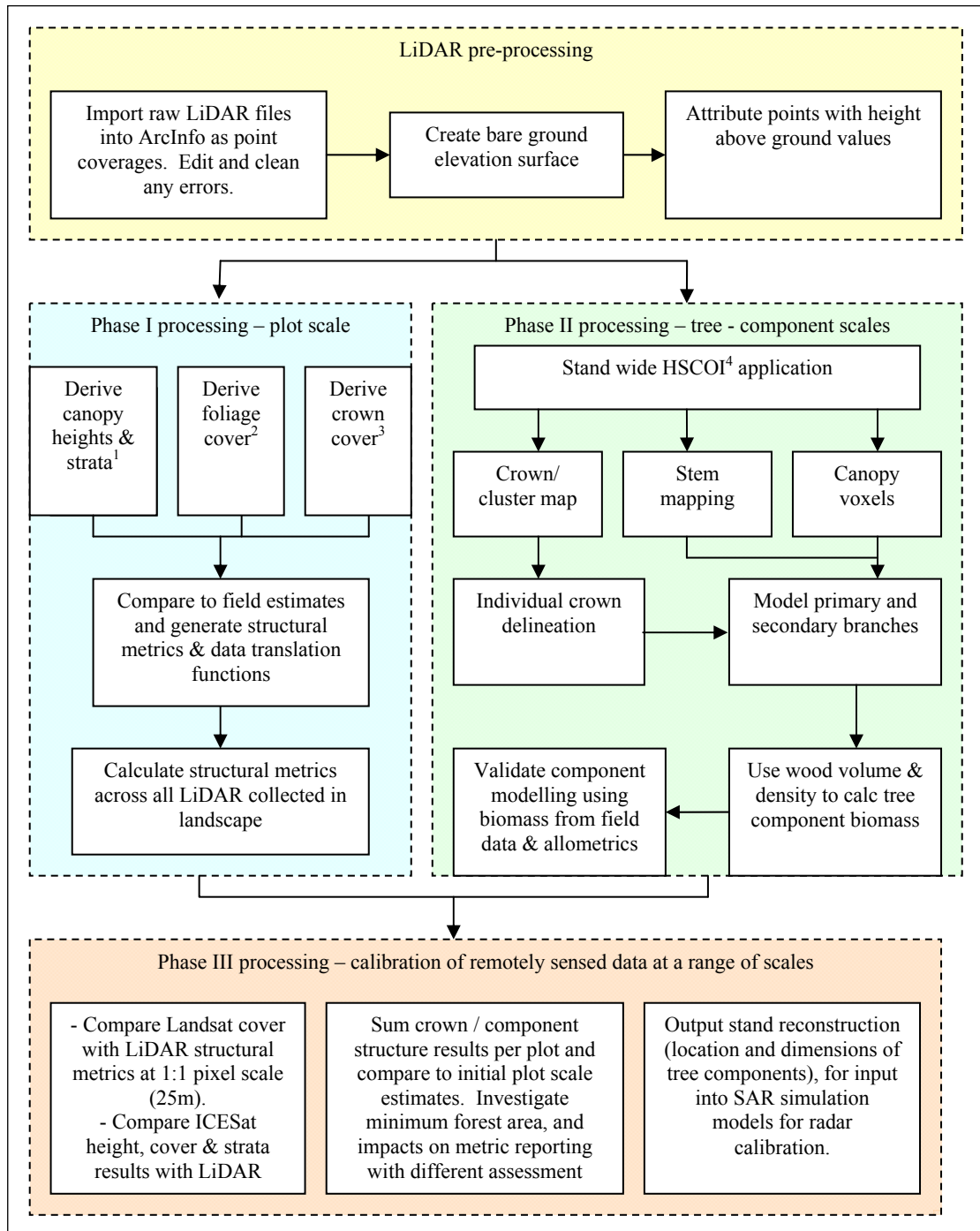
Phase III integrates data across scales, where tree and tree component level data were used to create calibration or validation layers at the most appropriate scale and alignment for the data being investigated. Because the different data used for forest assessment have different pixel sizes and interactions with vegetation, it can be difficult to use one calibration dataset (e.g., field data) for calibration of multiple datasets. As described previously, remotely sensed data can suffer from scale issues such as the MAUP, and a suggested approach to address these issues was through the use of basic geographic entities. A calibration dataset made up of basic geographic entities (e.g., tree crowns, stems, or tree components) can then be re-scaled to any

spatial resolution and shape that is required. This enables an improved match with the sensor being calibrated (e.g., Landsat TM, ICESat, radar), or research question being investigated. To determine overall utility of LiDAR to improve forest structural assessment, and thus address the two research objectives, four case studies are presented:

1. Multi-scale assessment of height and cover. This case study examines the effect of plot or assessment size on the reported height or cover metric when compared to the wider stand. The results will be used to empirically determine an efficient minimum area for reporting forest;
2. Comparison of SLATS Landsat TM derived foliage projective cover with LiDAR estimates of crown and foliage branch cover, stem density and basal area. The comparisons will also aid in the development of a continuous translation function between foliage projective cover and crown cover;
3. Investigation of ICESat full waveform laser data for extracting forest stand height and cover;
4. An illustration of the use of LiDAR tree and tree component modelling to reconstruct a forest stand for coherent SAR simulation modelling, as different wavelengths interact with the respective components in different ways.

Figure 7 illustrates how the datasets used in this research integrate to address the research aim. The utilisation of multi-scale processing feedback loops was identified for the three phases: initial plot scale, tree and component scales (i.e. unpacking the plot “black box”), and then refinement of plot scale methodology and application to other remotely sensed data.

Figure 7: Flowchart of multi-scale calibration modelling and application strategy



1 - from apparent vertical profiles and cumulative percentage summaries.

2 - from percentage of vegetation returns (2m+) (FBC) or through empirical transfer function derived from field transect data (FPC).

3 - from interpolation to TIN model utilising either 2m contour, or rasterise TIN and calculate percentage of cells 2m+

4 – Height Scaled Crown Openness Index – see Section 0

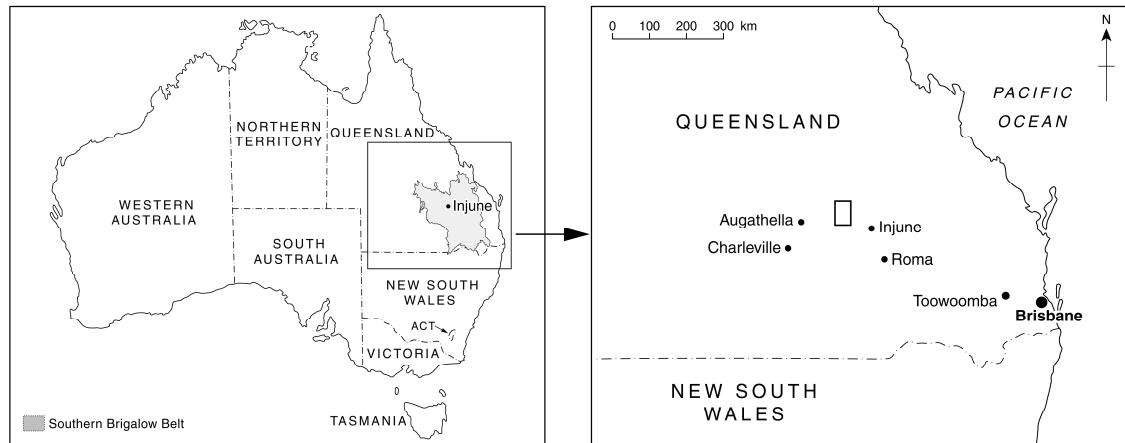
### **3.3 Data Collection**

#### **3.3.1 Introduction**

To address the primary research objectives and question, data from two different forest measurement pilot projects were utilised. The first project undertook data collection in 2000, and concentrated on a study area in the south central Queensland forest and woodlands. The project was funded by the Cooperative Research Centre Greenhouse Accounting (CRCGA) (Tickle, *et al.*, 2006; CRCGA, 2006) and an Australian Research Council SPIRT grant (Lucas, *et al.*, 2004). The Queensland study area was the primary site for this thesis, and was where all development of the models was undertaken. The second project collected data in 2003 as part of a National Forest Inventory Continental Forest Monitoring Framework pilot project in North East Victoria (described in the Introduction chapter). The NE Victorian site was a secondary site for this thesis, and provides validation for the models developed at the Queensland site, and highlights any regional modification that may be required if the LiDAR models were to be utilised in other regions.

#### **3.3.2 Queensland study site**

The Injune study focused on an area of mixed species open forests and woodlands near the town of Injune (Latitude 25° 36' S, Longitude 147° 30' E) in the Southern Brigalow Belt (SBB) Interim Biogeographical Regionalisation for Australia (IBRA) region (Thackway and Cresswell, 1995) (Figure 8). The SBB region, which was one of 16 IBRA regions within Queensland, constitutes 12.5 % of the state's land area. Approximately 8,901,250 ha, or 41.2 %, of the SBB was presently covered by forests and woodlands. The main study site had an area of 221,120 ha, with approximately 192, 153 ha (86.9 %) identified as forests and woodlands. Within the study site elevation varies from 437 - 850 m and the mean annual rainfall was approximately 635 mm, although was variable, with most recorded between December and February (summer). The mean annual maximum temperature was 27°C (Bureau of Meteorology, 2004).



**Figure 8: Location of the 37 x 60 km Injune study area, within south-central Queensland.**

The area was first explored by Europeans in 1846, with Thomas Mitchell travelling north through the eastern portion of the Injune study area following the Maranoa river, and recording landscape and vegetation observations along the way (see Figure 9; Mitchell, 1846). Settlement by graziers mostly likely occurred in the 1860's and railways were constructed in the 1870's. Severe drought in the 1890's forced many landholders off their properties. From the early 1900's the Queensland forestry department began reserving land and timber for wood production, with commercial harvesting of *Callitris* and Ironbark (*Eucalyptus*) species occurring from the 1940's onwards. Throughout the area, selective logging has only occurred once at any one site. The level of timber resource use reflects both the extent of the resource and the relatively slow growth in this area. Growth was influenced by relatively poor soils and low rainfall (B. Howard, Qld DPI, *pers. comm.*). This then indicates that major human induced structural change in the forest of the study area has not been widespread (as indicated in Figure 9).

The forests in the study area contain a diverse range of species, although several dominate, and both excurrent (i.e. conical shape common to many gymnosperms) and decurrent (i.e. round or spreading shape common to most angiosperm trees) structural forms were commonplace (Lucas *et al.*, 2004). White cypress pine (*Callitris glaucophylla*) dominates many stands but this species was selectively harvested, so large individuals were typically absent. Most *Callitris* occur in dense stands comprised of a large number of smaller individuals (up to several trees per m<sup>2</sup>).



**Figure 9: Sketch of the Maranoa River by the explorer Thomas Mitchell in 1846 (upper) (Mitchell, 1846); and a photo of the Maranoa from a nearby location in 2004 (lower).**

*Eucalyptus* species are widespread throughout the area, with Silver-leaved Ironbark (*E. melanaphloia*) and Poplar Box (*E. populnea*) dominating. Tumbledown Red Gum or Baradine Gum (*E. dealbata* var *chlorodata*) and Smooth Barked Apples (*Angophora leiocarpa*) occur along the creeks and at scattered locations throughout the landscape, and individual trees often contribute the greater proportion of the stand biomass. Larger individuals of both *Eucalyptus* and *Angophora* species form the upper canopy of many stands, below which several layers of sub-canopy trees of varying densities occur. Brigalow (*Acacia harpophylla*) and tall understorey shrubs such as Wilga (*Gejeira parviflora*) and Sandalwood Box (*Eremophila mitchelli*) are commonplace. Many stands contain a mix of *Acacia*, *Callitris*, *Eucalyptus* and *Angophora* species. A wide range of growth (and therefore structural forms) exist because of the varying impacts of different soil types, natural fires, droughts, clearing (e.g., pulling, poisoning) and grazing (Tickle *et al.*, 2006).

### ***Overview of Queensland multi-stage sampling***

The following section presents an overview of the Injune study sampling strategy. It should be noted that the sampling strategy and data acquisition were carried out prior to the initiation of this thesis. The methods are described in more detail in Lucas *et al.*, (2006a) and Tickle *et al.*, (2006).

The acquisition of image and field data was undertaken in four main stages (Table 4). In Stage I, a systematic sampling scheme (Schreuder *et al.*, 1993) was implemented to guide the acquisition of large scale aerial photography (LSP) (Stage II) and LiDAR data (Stage III). Following collection and initial interpretation of these data, a stratified random selection strategy was used to select 34 field plots, where forest inventory data were collected (Stage IV). The majority of the fieldwork was carried out during the period of LiDAR data acquisition and within one month of the LSP data acquisition, thereby minimising any seasonal effects and the likely impacts of anthropogenic land cover change at the field sites. Description of processing stages I, II, and VII can be found in Tickle *et al.*, (2006) (Appendix C), whilst stages III, IV, V, VI and VIII are described in subsequent sections.

**Table 4: Main stages in the acquisition, processing and analysis of field and remotely sensed data (Tickle, *et al.*, 2006)**

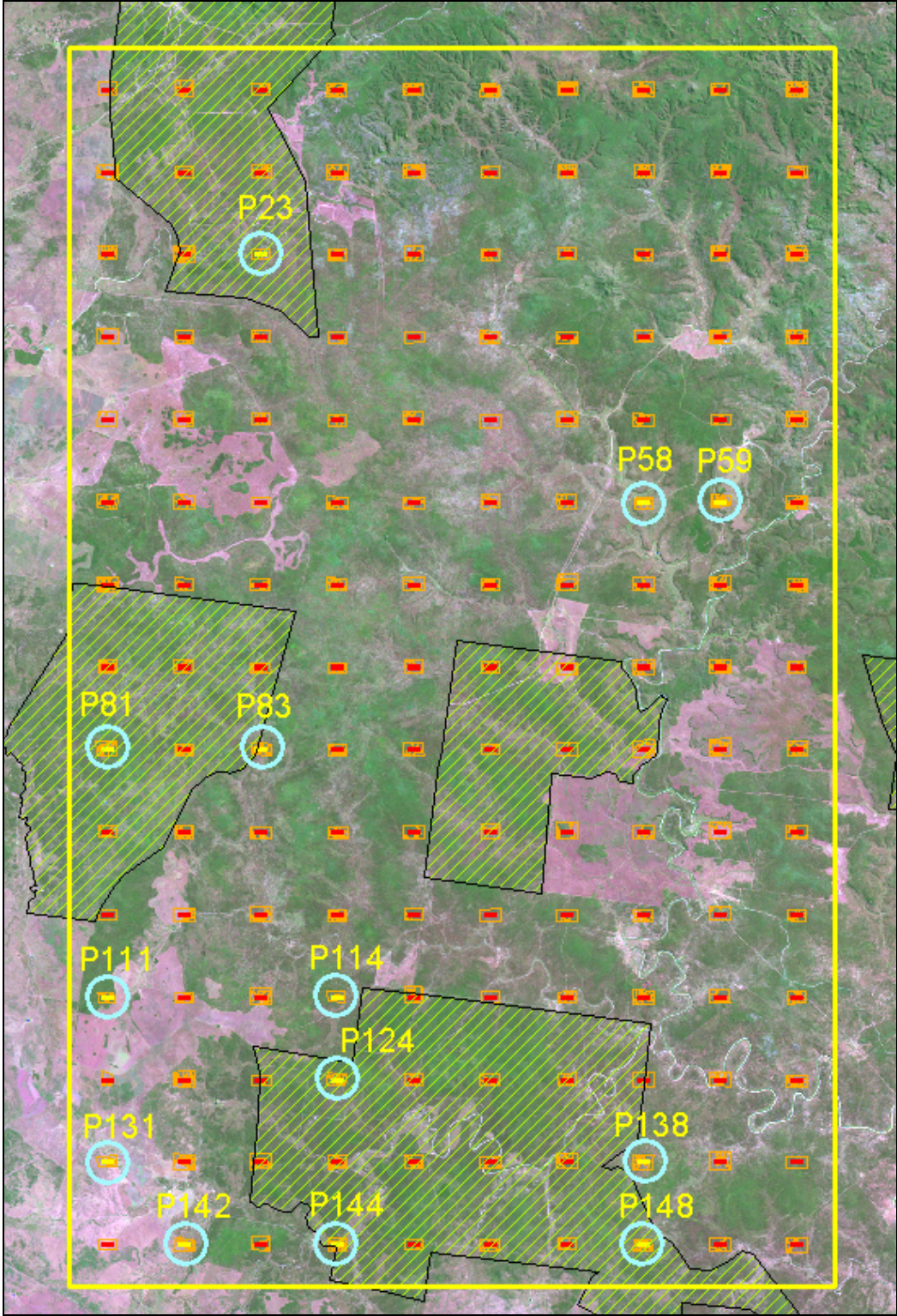
Stage	Task	Purpose
<i>Sampling and data acquisition</i>		
I	Sample design	To select appropriate field sample locations
II	LSP capture and pre-stratification	To allow description of the species/community composition
III	LiDAR capture	To facilitate retrieval of structural attributes (height, crown, foliage and/or branch cover)
IV	Field sampling	To provide ground truth for interpretation of LSP and LiDAR and validation of products.
<i>Post-processing</i>		
V	Georeferencing of LSP to LiDAR	To allow overlay of API vector information
VI	Generation of LiDAR height surfaces	Calculation of a bare earth DEM and vegetation height
<i>Data analysis</i>		
VII	Classification of forest communities based on LSP interpretation	To determine spatial distributions of dominant, co-dominant and sub-dominant species
VIII	Tree height, FBC, FPC and canopy cover retrieval from LiDAR	To provide individual tree and stand level estimates

***Stage III: LiDAR data capture***

Airborne scanning LiDAR data were captured over a one-week period commencing August 24<sup>th</sup> 2000 using an Optech 1020 scanning laser, mounted in a Bell Jet Ranger helicopter. The Optech 1020 measured 5,000 first and last returns and the intensity of each return per second. The LiDAR operated within the near infra-red spectrum with a beam divergence of 0.3 milliradians, a footprint of approximately 7.5 cm and a mean sampling interval of < 1 m.

Data were acquired flying in an east-west direction centred on a 150 x 500 m (7.5 ha) Primary Sampling Units (PSUs) located 3.7 x 4 km apart in the east-west and north-south directions respectively (Figure 10). Each of the 150 primary sampling units was then subdivided into 30 systematically numbered Secondary Sampling Units (SSU) that are 50 x 50 m (0.25 ha) in size. The helicopter flew at a nominal altitude of 250 m, which resulted in a swath width of approximately 200 m. A GPS base station was established for all flights. With full differential GPS corrections, in addition to pitch, yaw and roll compensation from an inertial navigation system, coordinates were guaranteed by the data supplier to an absolute accuracy (standard deviation ( $\sigma$ ) of the control point sample) of < 1 m in the x and y directions and < 0.15 m in the z direction.





**Figure 10: Landsat ETM image (2003) of study area and systematic photo and LiDAR plot layout, with field plot locations circled. State Forests are the light green hashed areas. Study area boundary was 37 km x 60 km, and sampling units are 4 km apart.**

---

***Stage IV: Field sampling***

Field inventory data were collected during August 2000. The collection of field data over the same period as the remotely sensed data acquisition was considered necessary to limit the impact of changes in seasonal foliage cover or land cover (associated with disturbance by fire or clearing) on the subsequent development of relationships with remotely sensed data.

Prior to acquisition of the field data, a 100 x 100 m regular grid on a transparency sheet was overlain on the overlap area of each of the 150 hardcopy large scale photography stereo pairs. A count of dots (located at the intersection of the grid lines) were used to estimate the proportions of land use, land cover and forest types as well as forest height and cover, disturbance regimes and vehicular access (Jones, 2000).

After interpreting the photography, the API codes were used to stratify and identify suitable locations for field sampling. The stratification assumed that the vegetation types contained within the 150 primary sampling units were representative of the proportions across the entire study area. For the purposes of stratification, the different forest types were classified into four distinct structural categories: *Acacia* or sparse vegetation (containing species such as BGL, SWB, BLH, BOK); *Callitris* (e.g., CP-, FMP); *Eucalypt Ironbark* (e.g., SLI, GTI, BRI, NRI); and *Eucalypt Other/Angophora* (e.g., PBX, ECH, SBA, RBA) (see Table 55, Appendix A for the species name and API codes). The Eucalypt class was split as the various Ironbark species were seen to contribute a significant proportion of the mapped landscape. Each forest type was then ranked into three (low, medium and high) potential and relative biomass classes using a combination of API and biomass estimates from the Japanese Earth Resources Satellite (JERS-1) Synthetic Aperture Radar (SAR) data, resulting in 12 vegetation strata (Jones, 2000; Lucas *et al.*, 2000).

It was determined that the field inventory would be limited to 2 - 4 secondary sampling units per day using 2 field crews of 5 staff. Therefore, out of a potential 150 primary sampling units, 13 were selected that contained the necessary strata and met access, travel times, and safety criteria. Within these 13 sampling units, 34 secondary sampling units were randomly selected across the 12 strata (in proportion to their area within the 150 primary sampling units).

Once located, a 50 x 50 m square plot, aligned in a north-south direction, was established using GPS survey and laser range-finding equipment. Tapes of 50 m length were then laid out to produce a 10 x 10 m grid to guide the subsequent location of trees for measurement. Within each plot, the location of all trees > 10 cm in diameter (at 130 cm above ground level) was recorded digitally by placing reflectors at each of the plot corners and then using either a GEOSCAN or CENTURION Laser Rangefinder to record the distance and angle from each tree to the nearest visible reflector. Trees 5 - 10 cm in diameter were located by reading the *x* and *y* distances (in cm) from 50 m tapes placed perpendicularly (at 10 m intervals) across the entire plot. The cover and height of trees and shrubs < 5 cm in diameter was estimated within five 10 x 10 m sub-plots, with the centres of four located at a distance of 10 m from each of the corners and a fifth located at the centre of the plot. Within each plot, each tree was identified to species level and key measurements recorded included trunk diameter (cm, at both 30cm and 130cm) and height (m) to the top of the tree, to the canopy base, and to the first green limb. Three additional secondary sampling units that were identified as non-forest but containing regenerating vegetation, species and structural measures were selected. Within these 'regrowth' plots five 10 x 10 m subplots were located.

Transects were established within the field plot to estimate vegetation cover. Transects consisted of three 50 metre tapes laid out in the north-south direction at 10, 25 and 40 m, moving eastward from the south-west corner. Along each transect the presence or absence of overstorey canopy material was recorded at 1 m intervals. The recording method, after (Specht, 1970), uses a plastic tube which was attached to a 2 m length rod and contains an internal cross-hair. A mirror situated at the base of the tube at an angle of 45° then enables the operator to record the presence or absence of green leaves or wood (trunk or branches) in the canopy vertically above. Foliage-branch projected cover (FBC) and foliage projected cover (FPC) was then calculated as the sum of foliage and/or branch records as a proportion of the total observations. For the purposes of this study, foliage-branch cover relates to the amount of light that would reach the ground, and was the percentage of the plot area occupied by the vertical projection of foliage and branches, while foliage projected cover only considers light

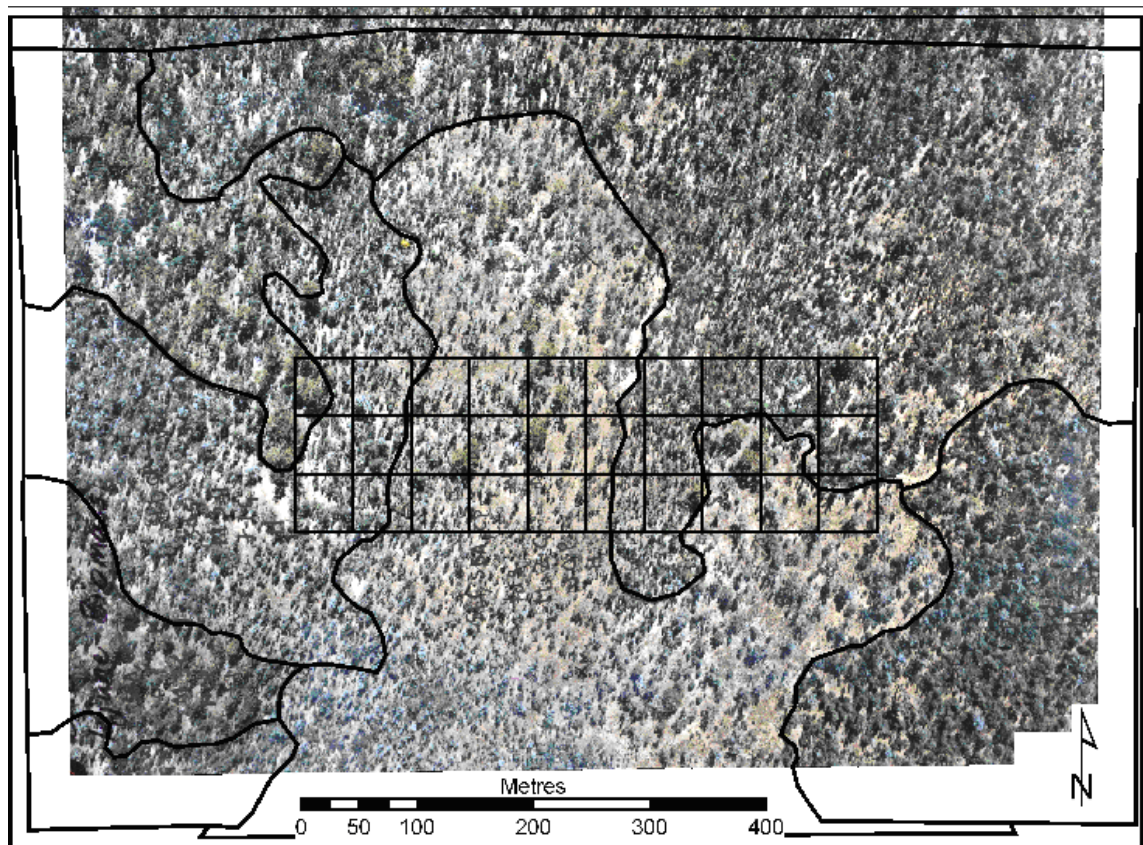
interception by green foliage. Crown cover (CC) was defined as the percentage of the site within the vertical projection of the periphery of crowns, with crowns considered opaque (Walker *et al.*, 1988; McDonald *et al.*, 1998). As part of a subsequent 2004 field trip, an azimuthally independent estimation of foliage projective cover was tested on selected Queensland field plots. This was an improved Queensland Statewide Landcover and Trees Study (SLATS; QDNRM, 2003) field transect collection method, and involved laying out a 50 m transect on a bearing due north from the plot centre, with two other transect at 60° and 120° degrees respectively from the first transect. Canopy measures were then conducted as described previously (J. Armston, *pers com*).

Hemispherical photography was used to gather information on canopy openness and cover for the Injune study site. During the second field campaign to the Injune study area in 2004 to collect additional data for this thesis, hemispherical photographs were taken within 31 field plots at 10 m intervals along the three 50 m north-south transects previously established within each plot. Photos were collected using a Nikon D70 digital SLR 6.1 mega-pixel camera with a 10.5 mm full frame hemispherical prime lens with a tripod. Two photos were taken at each 10 m interval along the transects: one oriented north-south and the other east-west, which were subsequently merged for a single photo. Estimates of foliage cover for the fields plots were generated using Gap Light Analyzer (Version 2) software (Frazer *et al.*, 1999). For comparisons with LiDAR cover estimates, two estimates were made. First, the single photo closest to the plot centre was used, and secondly, three photos from the centre of each transect. Appendix D describes the photographic calibration undertaken to generate estimates of foliage-branch cover from the hemispherical photography.

#### ***Stage V: Georeferencing of photography to LiDAR***

Initial georeferencing of the aerial photography applied known GPS locations from the aircraft navigation unit at the time of the photography acquisition. The GPS coordinates were applied to the centre of the image, and aligned using the image principle points. Additional pseudo-control points were derived based on aircraft flying height and camera parameters such

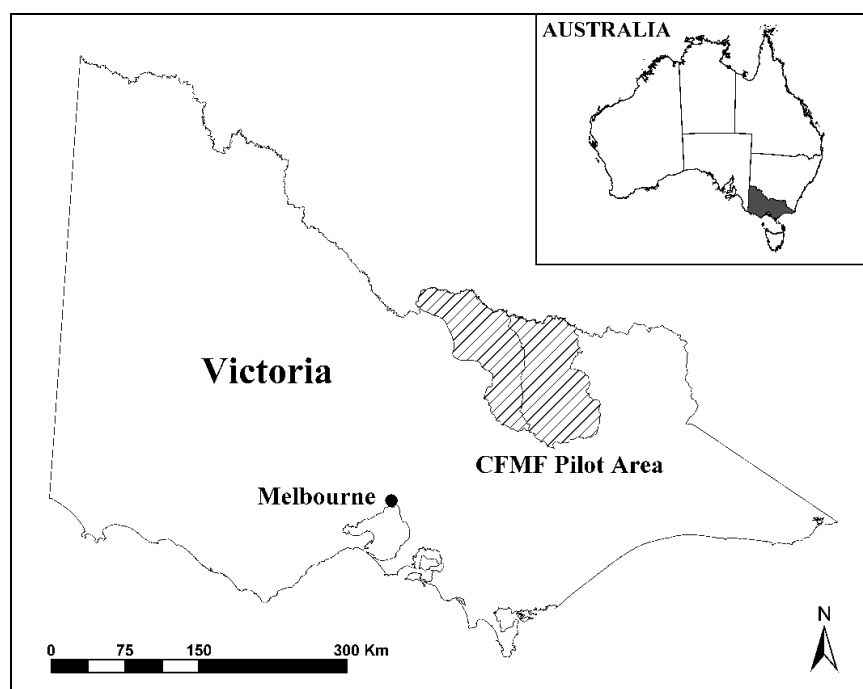
as lens focal length and image pixel resolution. Additional detail on the photographic acquisition and interpretation was found in Jones (2000). The initial georeferencing produced an accuracy of  $\pm 20$  m. Image rectification used a polynomial function with ground control points (GCPs) sourced from the LiDAR data swath, resulted in root mean square errors of  $< \pm 2$  m within the LiDAR strips. Following registration of the photography, floristic and structural mapping was interpreted from the photographs (Jones, 2000). Interpreted crown cover projection was averaged for each mapped forested polygon (for all forest types), and polygons that had clusters of gaps or open areas were dealt with by averaging the overall estimated crown cover class for the polygon (Jones, 2000). The API was then scanned, vectorised and rectified using the same transformation as the digital imagery, allowing GIS overlays of species type with the LiDAR data.



**Figure 11: True colour 1:4000 stereo aerial photograph of PSU 138 overlain with the 500 x 150 m primary sampling unit and 30 secondary sampling units (50 x 50 m). Polygon vectors mapped through API delineate different forest communities (based on dominant species composition and cover).**

### 3.3.3 NE Victorian study site

Both field and LiDAR data was collected as part of a National Forest Inventory Continental Forest Monitoring Framework (CFMF) pilot implementation project in North East Victoria in 2003. The design of the sampling strategy and data collection were determined prior to this thesis, although were implemented during the course of the study. The total area of the two catchments utilised for the pilot study was 1,507,068 hectares (Figure 12). There were 22 field plots (30 x 30 m) measured at forested sites the nodes of the 20 km systematic sampling grid (Figure 13). Within each plot, structural attributes similar to those measured within the Injune study area were recorded (e.g., location, species, height, and crown dimensions for every tree with  $D_{130} \geq 10\text{cm}$ ). Additional tree measurements were made where trees intersected four 45 m transects, located in the north, east, west and south directions from the plot centre (Wood *et al.*, 2006).



**Figure 12: Location of the secondary study site within the Broken and Ovens catchments in NE Victoria.**

At each field plot, digital hemispherical photos were used to provide plot estimates of cover. A Minolta DiMAGE 7Hi 5 mega-pixel digital camera with a fisheye adapter lens, and tripod were used for the photography. The photos were taken at 10 m intervals along the four transects, with an image also taken at plot centre. The plot estimate of canopy cover was

derived from an average of the centre photo and four plot edge photos, located 15 m from the centre along each transect. Calibration and analyses of the images used Gap Light Analyzer (Version 2) software (Frazer *et al.*, 1999). Appendix D outlines the calibration process.

Airborne scanning LiDAR data were captured from 15<sup>th</sup>– 19<sup>th</sup> April 2003, using an Optech 1225 scanning LiDAR mounted in a fixed wing aircraft. The Optech 1225 had a scanning rate of 25,000 Hz, recording both first and last returns, and the intensity of each return. The LiDAR operated within the near infra-red spectrum with a beam divergence of 0.2 milliradians, a footprint of approximately 22 cm, and a mean post spacing of < 1 m. LiDAR was collected over each of the CFMF plots, located at the nodes of the 20 km CFMF sampling grid. The LiDAR was collected as a continuous transect of data, with the swath approximately 400m wide and a total length of 1,485 km (Figure 13). Due to the nature of the sample grid layout, some plots were overflown twice (or three times in one instance) when the plot was on the intersection of the north-south and east-west flight lines. In total, approximately 59,400 ha of LiDAR data was collected (~4 % of the study catchments), with over 1 billion individual data points. The LiDAR data was acquired 2 weeks before the field campaign started. This enabled the calibration of the LiDAR products with field data to be as accurate as possible, given that regeneration of burnt areas was rapidly occurring.

Aerial photography was collected over the field plots at the same time as LiDAR, but was not interpreted for forest structure attributes due to a lack of qualified interpreters. Therefore the existing Victorian Statewide Forest Resource Inventory (SFRI) API polygon layers were used for comparison with LiDAR. Victorian SRFI API quantifies crown cover by comparing a mapped eucalypt forest stand to silhouetted examples of known density classes. Alternatively, a dot grid on transparency sheets was overlaid on the forest stand, and then a comparison was made of the number of dots which fall on tree crowns to the total number of dots in the forest stand. The density fraction was then expressed as a percentage (VicDNRE, 2000). Forest stand height from SFRI API was measured using stereo photogrammetry, and recorded as the average height of the most abundant crown form class (i.e., that which occupied 30 % or more of the stand area) (VicDNRE, 2002).

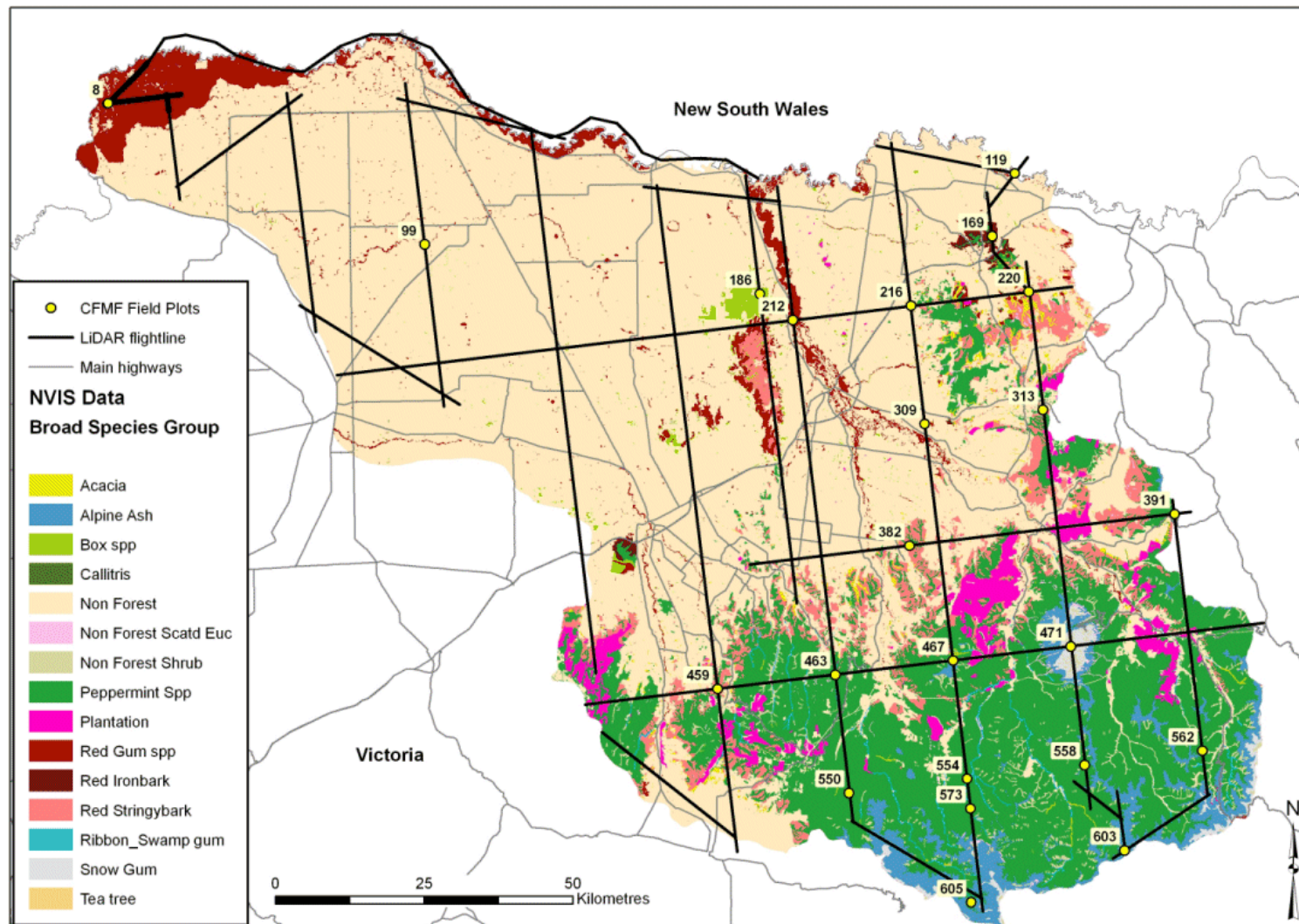
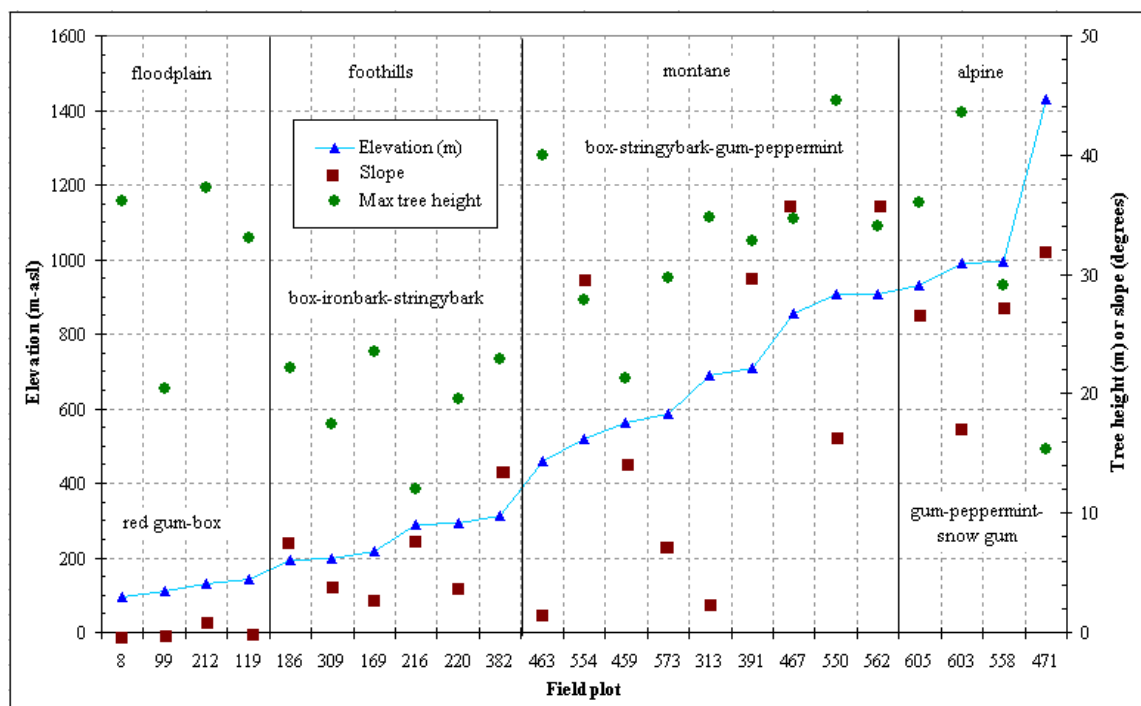


Figure 13: Layout of LiDAR data collection with ancillary NVIS vegetation data aggregated to broad species classes (NLWRA, 2001) within the NE Victorian study area.



### Plot location site descriptions

Site descriptions for the field plot locations combined dominant tree species and broad soils information with initial LiDAR derived site characteristics such as elevation and slope (Figure 14). The field plot locations were broadly classed into four landform or ‘ecozone’ categories based on obvious, but arbitrary, clustering of the attributes. The ecozone boundaries were an initial classification based on the available data, and may change when more data (field or remotely sensed) were analysed from around Australia by the National Forest Inventory (Wood *et al.*, 2006).



**Figure 14: Field plot site information summary (LiDAR derived) with max tree height (LiDAR), dominant species groups (field), and broad landform zone (derived) (Wood *et al.*, 2006).**

The Floodplain zone was generally flat, and dominated by red gum and grey box (*E. camaldulensis*, *E. microcarpa*). These forests can grow quite tall (mean of 35 m), with LiDAR analyses indicating that they can attain a height at least to 50 m. The elevation was below 200 m, and the dominant soils were clay-loam (chromosol). In contrast, the Foothill zone appears to have a significantly lower max tree height (mean of 22 m), possibly relating to poorer site quality (for example less water availability and lower nutrient soils). Slope was more variable, but still generally low (i.e. less than 15°), and the elevation range for this landform / ecozone

class was 200 – 400 m. The dominant eucalypt tree species were box (*E. polyanthemos ssp vesti*, *E. microcarpa*, *E. goniocalyx*), hill red gum (*E. blakelyi*), red ironbark (*E. sideroxylon ssp tricarpa*) and red stringybark (*E. macrorhyncha*). The plots were found on clay-loam (chromosol), sandy-loam (sodosol), and sandy (kurosol) soils.

The Montane landform zone includes plots mainly found on steep mountain slopes, or on river terraces in the valleys, within the elevation range 400-900 m. Slope was highly variable, and it was observed that the plots with the tallest trees were found on the flattest sites, possibly indicating a relationship to water availability (i.e. near to streams) and shelter (i.e. not on exposed ridge-tops). The overall mean tree height was around 30m, but this was variable. The dominant eucalypt species include box (*E. goniocalyx*,) and stringybark (*E. macrorhyncha*,) on the lower elevation sites, with gum (*E. dalrympleana*, *E. rubida ssp rubida*, *E. globulus ssp bicostata*) and peppermint (*E. radiata*, *E. dives*) on the higher elevation sites. Soils were generally light clay (dermosol) dominated, with some clay-loam (chromosol) sites.

Field plots in the Subalpine zone range from 900 - 1450 m, where slopes were generally steep, though variable. The effect of the harsh subalpine environment was evident in the reduction in max tree height from an average of 35 m to 15 m, as the higher elevations are reached. Gum (*E. dalrympleana*, *E. rubida ssp rubida*), ash (*E. delegatensis*), and peppermint (*E. dives*, *E. radiata*) species dominate in the lower elevations within this class, with snow gum (*E. pauciflora ssp pauciflora*) dominant at the highest elevations. These sites have subalpine humus soils (tenosol).

Most areas in NE Victoria have been burnt by wildfire at some stage, with much of the Montane areas burnt in major fires in 1939. Some state forest sites have been also logged to various degrees. Table 5 provides a summary of these disturbances, from available data (as of 2003). It should be noted that some plots have been subjected to wildfire since 2003. These disturbances influence the forest structural attributes extracted from remotely sensed data collected for this thesis, so this background knowledge was useful to assist in interpreting the results, especially when using LiDAR apparent vertical profiles (see Table 67, Appendix B).

**Table 5: Estimated year of last fire and logging for NE Victorian plots (DSE, 2003)**

<b>Plot</b>	<b>Ecozone</b>	<b>Year of last recorded burn</b>	<b>Year of last recorded logging</b>
8	Floodplain	-	-
212	Floodplain	-	-
119	Floodplain	-	-
99	Floodplain	-	-
186	Foothills	-	-
309	Foothills	-	-
169	Foothills	1985	1980 (single tree selection)
216	Foothills	-	-
220	Foothills	2003	-
382	Foothills	1994	1993 (group selection)
463	Montane	1939	1983 (group selection)
554	Montane	1939, 1985	-
459	Montane	1939	-
573	Montane	1939, 1985	-
313	Montane	2003	1986 (group selection)
391	Montane	1939, 1999	-
467	Montane	1939	-
550	Montane	1939, 1991	1989 (single tree selection)
562	Montane	1939, 2003	-
605	Subalpine	1939	-
603	Subalpine	1939, 2003	1979 (group selection)
558	Subalpine	1939, 2003	-
471	Subalpine	1939, 2003	-

### 3.3.4 Data descriptions for both sites

#### *Ancillary data*

For both study areas, a number of existing regional scale datasets were used for additional information and calibration against the fine scale field data. The datasets include the Queensland Statewide Landcover and Trees Study (SLATS) Landsat TM derived foliage projective cover, nominally for 2000, and change in woody/non-woody extent from 1991 to 1999 (QDNRM, 2003) for the Injune study site. For NE Victoria, uncalibrated SLATS data was available that was generated using 2003 Landsat ETM imagery. The number of field plots used to calculate estimates for comparison with foliage projective cover have been clipped to the extent of the Landsat imagery (which was missing 14.3% of the study area) to allow appropriate comparisons between datasets. This results in 33 of the initial 39 systematic grid nodes being used, of which 14 (of the initial 17) were located at forested sites, according to field and high spatial resolution remotely sensed data. The National Vegetation Information System (NVIS) pre-clearing vegetation (nominally 1940-50's) (NLWRA, 2001), and extant vegetation (1995), were used, and which were updated with Queensland Herbarium vegetation data (1999) (NLWRA, 2001) for the Injune study area. For both study sites data from the State of the Forests Reports (National Forest Inventory, 1998, National Forest Inventory, 2003) were used.

#### *Summary of Queensland and NE Victorian field data*

Summaries of field data tree and plot distributions of the key attributes are provided in Lee and Lucas, 2007 (Appendix C). Note that two secondary sampling units in the Queensland data were excluded (i.e.,  $n = 32$ ) because these were only partially covered by LiDAR data.

#### *API classification comparisons with NFI*

When compiling and translating categorical forest cover information derived from aerial photos into National Forest Inventory crown cover classes, a match between classes was generally (although not always) observed. For example, there were two mismatches between National Forest Inventory crown cover class ranges and those used for both the Statewide Forest

Resource Inventory (SFRI) API eucalypt crown cover classes, and those used in Queensland (Table 6) (VicDNRE, 2002; Jones, 2000). The class threshold values between National Forest Inventory and both State-based API standards do not match for the woodland class. Here the National Forest Inventory 20% cover class break was not replicated in the API classes, so there was a 9% difference between the two systems. This was likely to cause either overestimation or underestimation in the data supplied to the National Forest Inventory, depending on how the data (percentage area of cover class) was rounded (up or down) to match the National Forest Inventory classes.

**Table 6: NFI, Victorian SFRI , and Queensland API crown cover class standards**

NFI Crown Cover Class	Victorian SFRI API cover		Queensland API cover	
	Class	Cover range	Class	Cover range
1	1	0–9%	1	< 10%
	2	10–29%	2	10-29%
2	3	30–49%	3	30-49%
	4	50–69%	4	50-79%
3	5	70–84%	5	80-100%
	6	85–100%		

Additionally, for the SFRI classification at the closed forest class there was a 5% difference between the thresholds for closed forest, with this being 85% in the SFRI classification and 80% in the National Forest Inventory class. Table 7 provides a comparison between the National Forest Inventory height classes, and two examples of API height classes for Victoria and Queensland. As Table 7 shows, there were a number of mismatches between classification systems, making accurate national aggregation of the area of the height classes difficult. The Queensland API classification, as described in Jones, (2000), used stand height (mean height of the co-dominant mature trees) into one of the three broad classes described in Table 7. Comparisons with the National Forest Inventory classification show there was a 2 m mismatch between low and medium National Forest Inventory classes, but given the limited

ability to discern this resolution of height measurement through API, it was likely to introduce only minor error into the compilation.

**Table 7: Height class and ranges for NFI, Victorian SFRI, and Queensland API standards**

NFI Height		SFRI API Height		Queensland API Height	
Class	Range (m)	Class	Range (m)	Class	Range (m)
1	2-10	6	<5	1	<12
		5	5-14.9		
2	10-30	4	15-27.9	2	12-30
		3	28-39.9		
		2	40-51		
3	30+	1	>51	3	30+

## 3.4 Phase 1 – LiDAR Plot / Stand Scale Forest Structure Assessment

### 3.4.1 Introduction

This section outlines the methods used to generate plot and stand scale forest structure estimates from LiDAR data. The pre-processing of the LiDAR, for the calculation of bare earth terrain surfaces was presented. Methods for deriving apparent vertical profiles are described, followed by plot scale height and canopy cover assessments.

### 3.4.2 LiDAR pre-processing

#### *Stage VI: Bare ground surfaces*

An initial Digital Elevation Model (DEM) was constructed by interpolating pre-classified first and last ground returns with a 1 m proximal tolerance (where any returns found within 1 m of other returns were excluded) and represented as a Triangulated Irregular Network (TIN) model (Figure 15). However, examination of the resulting surface indicated a certain degree of ‘noise’ and surface variation resulting from on-ground surface features (e.g., logs, grass swards and shrubs). Therefore, and following other studies (e.g., Suarez *et al.*, 2005), a multi-scale filtering strategy was employed. Here the lowest returns (first or last) within local search windows of increasing dimension (1 x 1 m to 5 x 5 m) were selected to generate bare ground surfaces, on the assumption that these were more likely to represent the true elevation surface. The most suitable window size for generating the final elevation surface (Figure 16) was determined by examining a corresponding elevation standard deviation surface generated using a 5 x 5 search window. The standard deviation elevation surface was generated by dividing the PSU into 5 x 5 m kernels, and within these squares the standard deviation of the ground return heights was calculated. Flatter areas were identified from the standard deviation surface in areas of lower deviation in the elevation range, and therefore would only require ground returns from larger search windows or kernels (e.g., 5 x 5 m) to efficiently describe the terrain. Where ground elevation was more variable (e.g., water courses) then returns from smaller kernels were used, with the general rule being that the greater the deviation, the smaller the kernel.

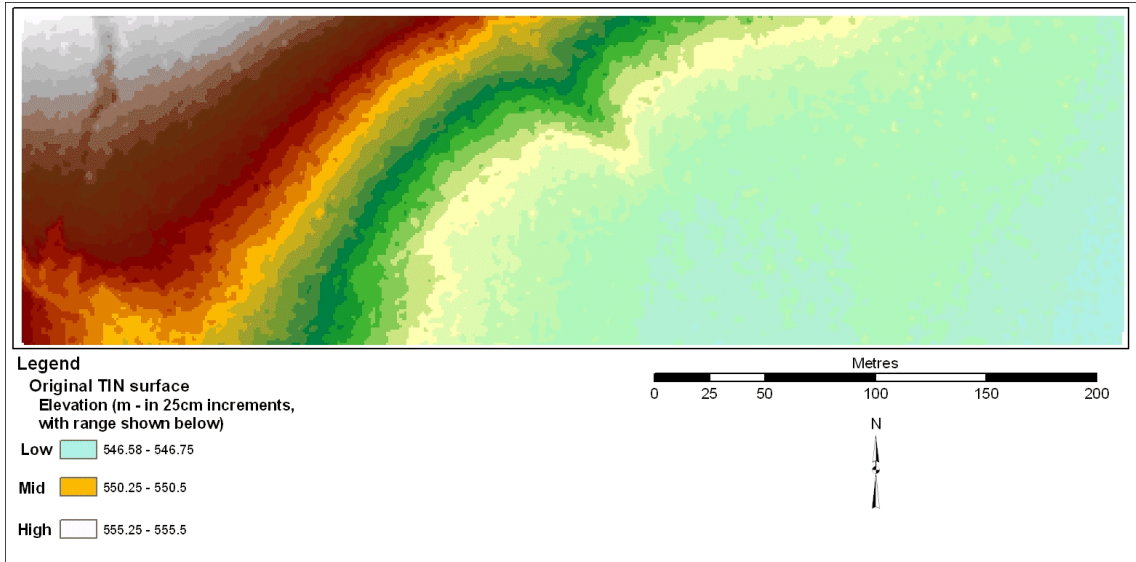


Figure 15: Original DEM TIN created with all ground returns, for PSU 142

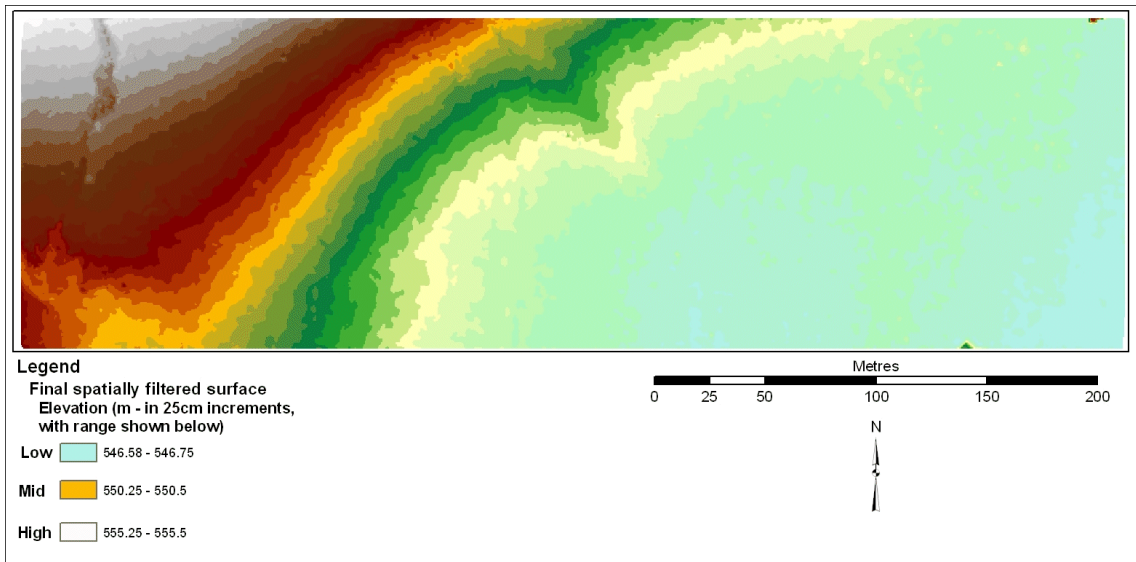


Figure 16: Final spatially refined DEM TIN for PSU 142

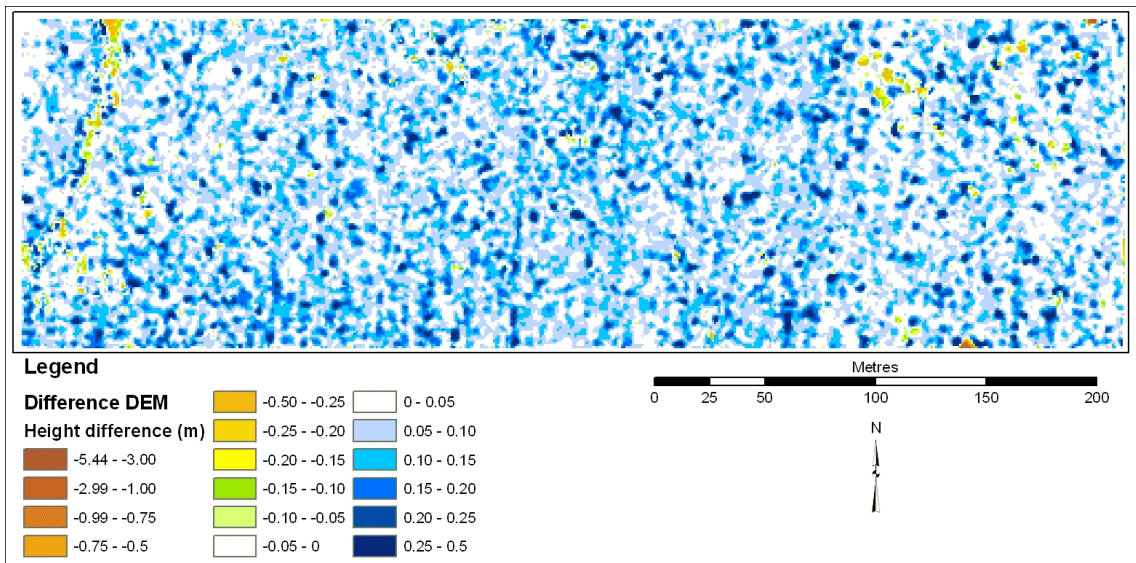


Figure 17: DEM difference surface - original DEM subtracted from final DEM for PSU 142.

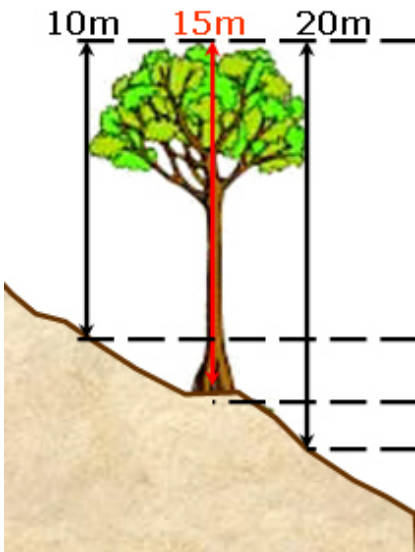


Subtracting the initial TIN ground model from the final spatially filtered surface produced a difference surface (Figure 17). As an example, the surface analysis for primary sampling unit 142 indicated that the spatially filtered elevation layer was lower and differed, on average, by 8 cm (standard deviation ( $\delta$ ) = 8 cm, range = -0.5 to 0.5 m). Similar results were observed within the other primary sampling units, and these compared well to other studies (e.g., Hodgson and Bresnahan, 2004). The on-ground surface features previously identified were also evident within the difference surface, indicating that spatial filtering of the surface was effective in their removal. Once calculated, the height of woody vegetation was determined as the difference in elevation between the final bare ground surface and the first and last vegetation LiDAR returns. Only returns above 0.5 m were subsequently used for canopy assessment, as those below this height were considered to be from shrubs, tall grass, and larger items of woody debris.

#### ***Site Characteristics and terrain complications***

LiDAR ground surfaces were used to assess elevation, slope, aspect, and landscape position of the field plot. In some cases this was the most reliable method to collect this information. Drainage lines and old logging tracks were identified in some cases, providing insight into the history of sites and the local hydrology in the surrounding area. This information can also be used to provide a quality control check for the LiDAR height above ground values. For example in areas of terrain with high ground surface variability, such as when there are cliff lines or rocky outcrops present, then canopy heights might be highly variable, reflecting the ground surface below the tree ( as illustrated in Table 8). Here, when calculating tree top height on steep slopes or when cliffs were present, the down-slope part of the crown will actually have a height ‘higher’ than the crown underneath the trunk or on the up-slope side of the crown. This may not reflect the ‘true’ overstorey canopy variability, potentially giving canopy height values which were inconsistent with a similar stand structure found on sites with less slope.

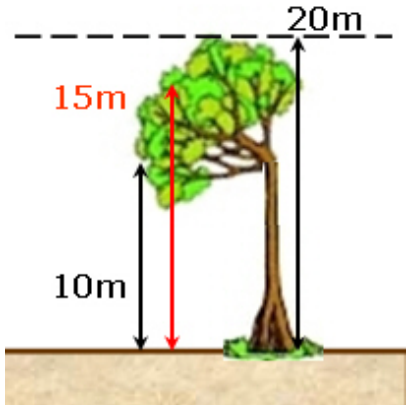
Table 8: Illustration of a selection of terrain complications on canopy height estimates



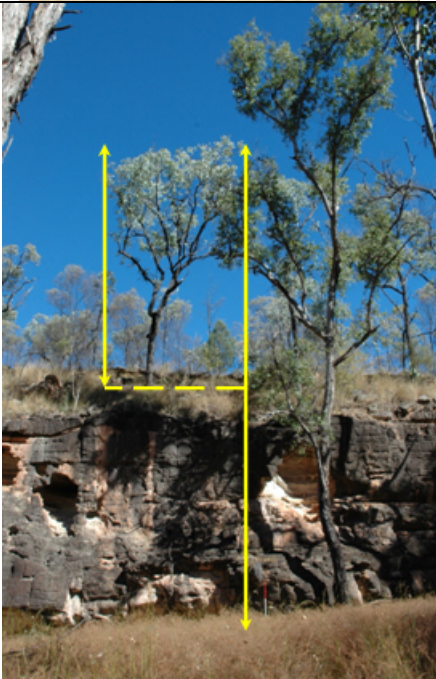
Top of canopy for generally flat topped eucalypts - LiDAR has same elevation “above sea level” values. Height above “ground” could be:

- tree height up-slope (10m)
- tree height at trunk (15m)
- tree height down-slope (20m)

(note – graphic not to scale, for illustration only)



Processing of canopy LiDAR returns to calculate an apparent “height above ground” value. Here trees on steep slopes when represented as canopy height above ground would appear as in the graphic (i.e. 5 m taller). This representation assumes that the trunk was located under the tallest part of the crown.



An extreme example that can occur was where tree canopies overhang cliff edges. The ironbark tree has canopy elements twice as high (above ground) as the actual tree height.

### 3.4.3 Estimating Tree Height for Plot / Stand

#### *Stage VIII: Maximum and predominant height from LiDAR*

Stand height was a required parameter for broad scale reporting at the NFI and NVIS scale. However, in heterogeneous forests when using remote sensing it can be difficult to reliably scale field plot measures of tree height to a consistent, objective and repeatable measure of stand height. For forest monitoring, it was useful to know:

1. The mean or predominant height of the plot or stand at the time of measurement, as an indicator of stand (assuming the plot area was representative of the wider stand) growth stage (i.e. regeneration, young, mature, senescent), and to provide a reference point for subsequent measurements;
2. The maximum height of the plot / stand, as an indicator of potential site quality, and therefore potentially the maximum height the majority of trees in the stand will eventually reach, if it can be established that the tallest trees currently on the plot were mature;
3. Some indication of the variation in tree heights throughout a plot or stand – low tree height variation could indicate an even aged stand, whereas high tree height variation could indicate a mixed age stand.

These three height parameters were measured using LiDAR in the following way. The maximum height was the highest canopy return recorded within the plot or stand. Predominant height was calculated as the mean of the maximum height of the tallest trees (field data) or assessment cells (LiDAR) within a defined area (e.g., field plot). Height variation was assessed using the standard deviation of tree heights or the assessment cells used for predominant height.

Predominant height was generally calculated using a sampling rate of 50 trees ha<sup>-1</sup>, although between the States and Territories this can range 40-75 trees ha<sup>-1</sup> (RWG2, 1999). When using plot scale assessments of LiDAR, the tallest individual trees cannot be automatically selected to directly compare to field estimates (this was undertaken in Phase II LiDAR processing). Therefore, spatial sampling across the plot was used, where a regular grid

creates a number of assessment cells, within which the maximum LiDAR height was recorded. The mean of the cell height then determines the predominant canopy height for the plot. Ideally, the assessment cell size will approximate an individual crown area, so it can be assumed that a cell was equivalent to a single tree for accurate comparisons. A cell size of 10 m was chosen because 93% of CFMF field measured trees have crowns smaller than 10 m diameter, and square plots could be efficiently covered by whole numbers of cells.

However, there was still a conceptual difference between the field-measured predominant ‘stem’ height, and LiDAR cell-based predominant ‘canopy’ height. Therefore, two field sampling rates were chosen to compare to the LiDAR predominant height estimates, as it was unknown how the stem sampling rate compared to the canopy sampling. A sampling rate of 100 trees ha<sup>-1</sup> within a NE Victorian 30 x 30 m plot (0.09 ha), equates to the 9 tallest field trees, and dividing the plot into 10 m cells gave a 3 x 3 array (9 cells in total) (Table 9). A sampling rate of 50 trees ha<sup>-1</sup> equates to the 5 tallest field trees, rounded up to whole trees. The respective sampling rates for the Injune study used more trees due to larger field plots (Table 9).

**Table 9: Translation between LiDAR and field estimation methods for predominant height**

Data Source	Plot size (area)	Sampling rate (trees ha <sup>-1</sup> )	Field tallest trees per plot	LiDAR cell count per plot
NE Victoria				
LiDAR 10 m cell	30 x 30 m (900m <sup>2</sup> )	50	5	9
LiDAR 10 m cell	30 x 30 m (900m <sup>2</sup> )	100	9	9
Injune				
LiDAR 10 m cell	50 x 50 m (2500m <sup>2</sup> )	50	13	25
LiDAR 10 m cell	50 x 50 m (2500m <sup>2</sup> )	100	25	25

### ***Plot scale LiDAR apparent vertical profiles***

As indicated in Chapter two, initial investigations of LiDAR vertical foliage profiles have shown promise in assessing the vertical structure of forests, improving understanding of growth stage, understorey recovery since disturbance, condition, and biomass. Apparent vertical profiles were generated for all field plots at both study sites. Whilst vertical profiles may indicate overstorey and understorey strata, they were termed ‘apparent’ as the literature has identified that they may not be entirely representative of the full vertical structure (Lovell, *et al.*,

2003; Coops *et al.*, 2007). This will be tested by comparing the plot vertical structure profiles from field tree data simulated within  $1\text{m}^3$  reference matrix to those generated from LiDAR (Lee *et al.*, 2004 – Appendix C).

In the simplest sense, apparent vertical profiles are the summation of the number of non-ground LiDAR returns per arbitrary height interval (Figure 18 – left, centre). Most small footprint LiDAR profiles reported in the literature use a 1 m height bin, as this generally equates to the LiDAR post-spacing sampling density, and was an efficient compromise between showing detail in vertical forest structure against the number of returns collected. Height bins with a very small height range would only record a few returns and not show much information, whereas larger height ranges would mask subtle variation and potential strata breaks.

With apparent vertical profiles, larger percentage values indicate where the foliage was most dense and/or the crowns most wide. Strata breaks (i.e. between over and understorey) are most likely to be where there are the least percentage values (Figure 18 - centre). Both of these statements assume a representative sample of the actual vertical foliage distribution. As stated in Chapter 2, Lovell *et al.*, (2003) hypothesise that this may not be the case. Cumulative percentage curves are generated by sorting all non-ground returns (lowest to highest), and calculating the cumulative percentage value for all returns (Figure 18 - right). This provides the height of the vegetation at certain quantiles or class percentiles of LiDAR data, which have been used in multiple regression models for assessing forest structure and biomass (e.g., Magnussen and Boudewyn, 1998). For example, the height of vegetation at 50 % of all the non-ground data in the plot was at approximately 18 m (Figure 18). This indicates a large and relatively tall overstorey canopy was “capturing” at least half of the non-ground returns.

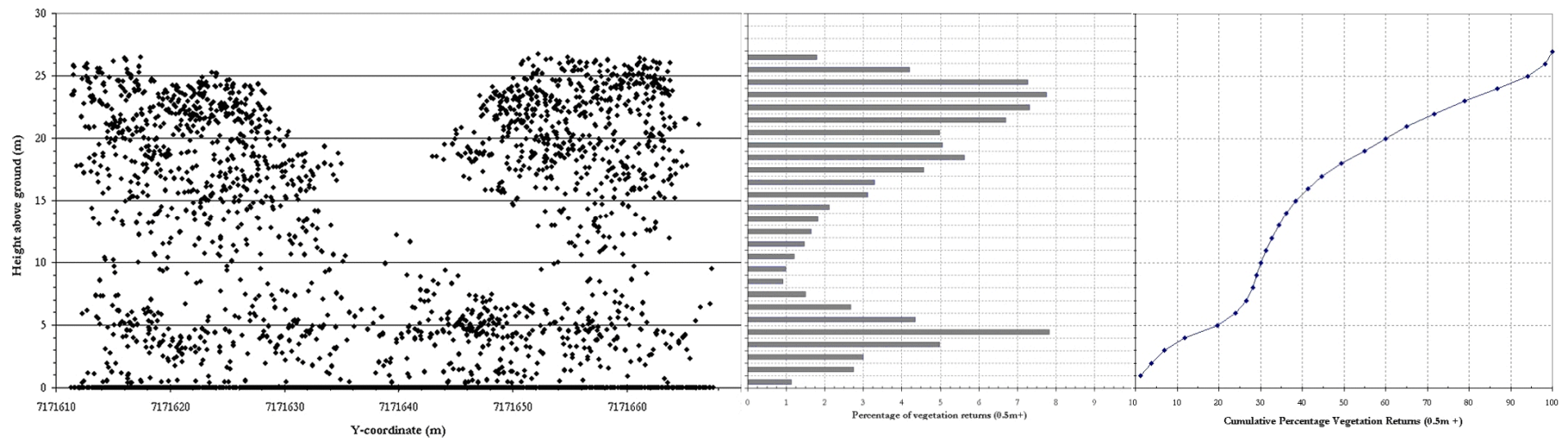


Figure 18: LiDAR representations – raw points profile across Qld plot width (p81-11), vertical profile of summed returns per 1m height interval, and cumulative height percentage curve summary.

---

### ***Creating apparent vertical profiles using field data***

A method to generate apparent vertical profiles from field measurements was developed to be able to objectively quantify obvious strata breaks, to provide validation against LiDAR apparent vertical profiles, and to compare against existing vertical foliage profiles for this environment (e.g., Walker *et al.*, 1986). Additionally, if significant differences were observed between the profiles, then it may indicate that there was bias in the LiDAR profile in terms of it representing the actual foliage distribution. A cubic matrix was developed for vertical profile generation using field data, based on the methodology of Walker and Penridge, (1987). The field modelled profiles were then compared with LiDAR profiles, with a full description given in Lee *et al.*, (2004) (Appendix C).

One method to examine the accuracy of the vertical profile modelling of the field data, similar to that used in Goodwin *et al.*, (2007), was to compare the LiDAR and field estimate percentage of cubes at each height interval. A good correlation will indicate that the profiles were similar; whereas a poor correlation will highlight that there were significant differences in the profile at different heights. This method will work best when there was a reasonably large spread of percentage values, for example one or two large peaks in the profile. Where there was an even distribution of cube percentage values across the height range then the correlation may not represent the accuracy as well, because values will be concentrated within a small range. Where there was a mismatch in top height estimates between LiDAR and field data, this can impact on the accuracy assessment method, as there was likely to be an offset between profiles, which will not reflect the overall profile distribution.

Due to the limitations of the first profile accuracy assessment, additional accuracy assessments were undertaken using a Kolmogorov-Smirnov test. The two-sample Kolmogorov-Smirnov test can be considered as an alternative to an unpaired *t*-test but which actually tests for any difference between the distributions that the two samples came from. A significant difference could mean that the population medians were different, the variances were different, or the shapes of the distributions were different, but the test will not indicate which of these it was. The Kolmogorov-Smirnov test was used because the apparent vertical profile distributions

from LiDAR and field 3D cubic modeling were often not normal, therefore a standard *t*-test would not be appropriate. However, whilst these non-parametric tests were simple to interpret, they are less powerful in being able to detect differences which may actually occur (Townend, 2002). Therefore the results will be used as a guide, rather than providing conclusive evidence, when discussing the relative similarity of the field and LiDAR modeled apparent vertical profiles.

### ***Growth stage assessment using apparent vertical profiles***

A qualitative assessment of forest growth stage for the NE Victorian plots was made using LiDAR apparent vertical profiles, which were linked to growth stage classifications from two different State systems. The State systems were the Victorian State Forest Resource Inventory (SFRI) API based classification, and the Queensland Ecological Maturity Classification (EMC) (FERA, 1998). Based on the growth stage descriptions, the two classification systems have been linked (Table 10). Example LiDAR vertical profiles from NE Victorian field plots were then visually assessed and allocated to one of the classes.

**Table 10: Growth Stage type using SFRI and EMC classifications**

<b>Class number</b>	<b>EMC description</b>	<b>SFRI class</b>
1	Dominant in over-mature trees, trace regeneration / regrowth	late mature
2	Mainly dominant with mature trees with some shorter regrowth	mature
3	Mainly dominant with regrowth, some taller mature trees	early mature
4	Dominant in regeneration /regrowth, trace mature / over-mature	
5		unevenaged (no clear eucalypt age class dominance)
6		Undefined (not measured)



### 3.4.4 Estimating plot scale canopy cover

#### *Stage VIII: Foliage and Crown cover*

LiDAR derived foliage-branch cover (FBC) was calculated as the percentage of all returns that were 2 m or greater in height (Figure 19). The > 2 m threshold was based on the National Forest Inventory definition for forest. It was also useful for comparison with field data that was collected using a sighting tube at eye level. Another height threshold of > 0.5 m was also used for comparison with hemispherical-photo or satellite imagery derived cover, where applying a height threshold cannot be readily done, and it was assumed that almost all canopy material was assessed.

To generate initial plot scale crown cover estimates from LiDAR data, returns > 2 m height were interpolated to a canopy surface / height model, using the highest returns within a defined search radius (typically 1 or 2 m) (Figure 19). Then, crown cover (CC) was calculated for each field plot as:

$$CC(\%) = \frac{\sum x_i}{n} * 100 \quad \text{Equation 1}$$

where  $x$  was the number of 1 m<sup>2</sup> tree crown cells (> 2 m height) and  $n$  was the number of cells in the plot.

A canopy height model (CHM) only utilises the returns from the outer canopy (Figure 19 panel 3). Depending on the shape of the tree, an accurate representation of canopy form or volume may not be generated. An assessment of canopy height model generation and potential issues with crown representation was presented in Lee *et al.*, (2001) (Appendix C). The assessment indicated that when height contours generated from the CHM were displayed in 3D, it was evident that they did not represent the correct shape of the canopy when compared to the LiDAR point cloud. The Height Scaled Crown Openness Index was developed to address these issues (Phase II processing - section 3.5).

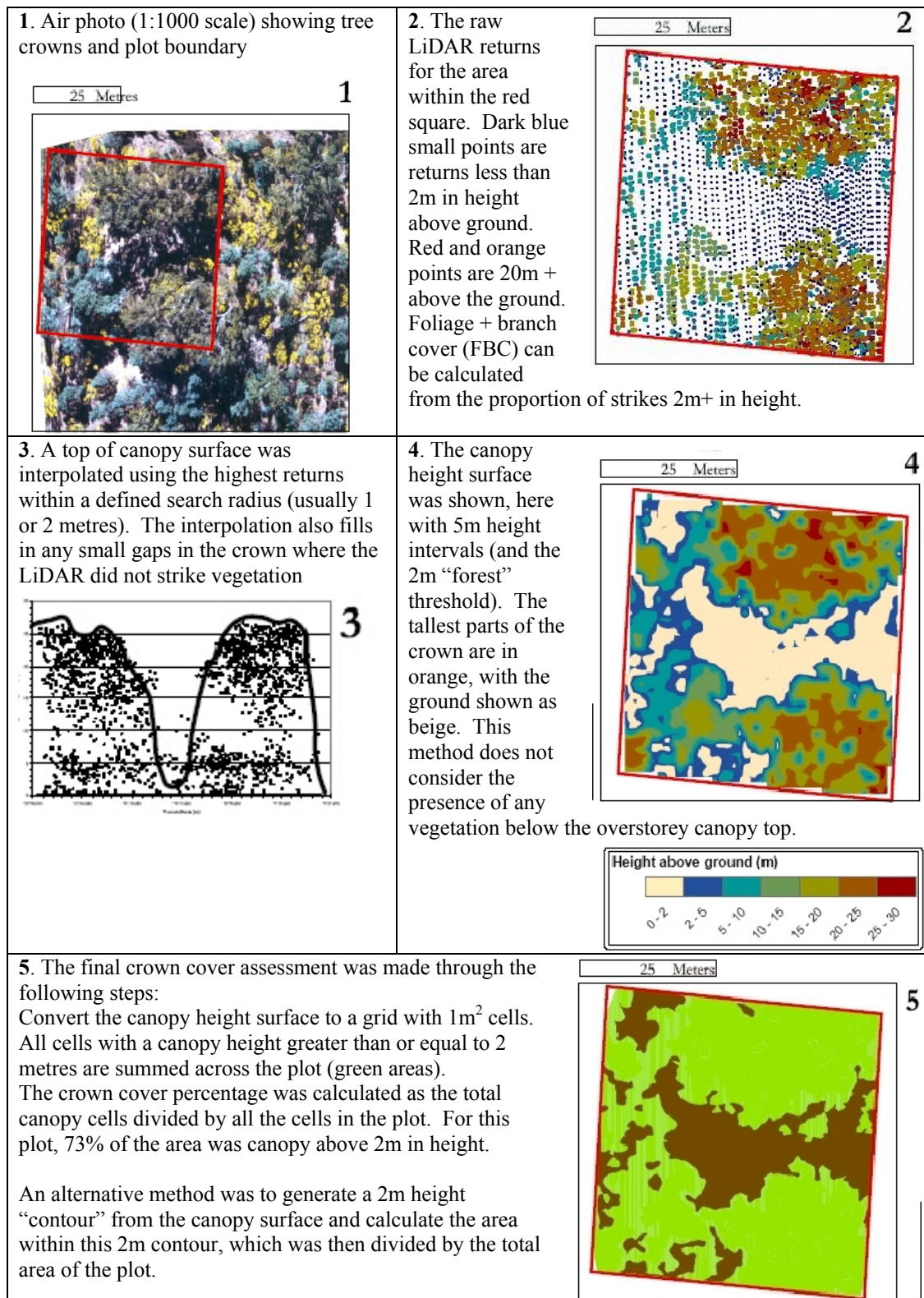


Figure 19: Steps to generate foliage branch cover, and CHM crown cover from LiDAR

## 3.5 Phase II –Tree and Component Scale Structure Modelling

### 3.5.1 Tree scale modelling strategy

In order to answer the primary research question, and determine how LiDAR can improve the assessment of forest structure, the potential impacts of scale must be examined. From a review of the literature in Chapters 1 and 2, it was identified that the use of basic geographic entities enables the potential impacts of scale to be investigated. As outlined in the research design, this thesis uses basic geographic entities of tree and tree components as the basis for enhancing forest structural assessments. The following section describes the development of the tree and component scale geographic entities.

As outlined previously (Lee *et al.*, 2001 – Appendix C), there were a number of issues with using canopy height models (CHM) for tree and stand level assessment, especially when there was a requirement for sub-canopy stem assessment. Therefore, to provide an alternative method for assessing the stand, a Height Scaled Crown Openness Index (HSCOI) method was developed. The analysis of field and LiDAR data was undertaken in several successive stages (Stages I – IX; Table 11). Specifically, the tree scale modelling combined with field data were used to:

1. Evaluate the potential of the LiDAR data for identifying stem locations, including those associated with sub-canopy trees,
2. Support the generation of empirical relationships between LiDAR-derived data (i.e., the canopy height models and HSCOI) and field data tree height and diameter for all identified stems, and
3. Evaluate the potential of the LiDAR for retrieving stand level estimates of stem density, predominant stem height, basal area, and cover and (crown cover and foliage-branch cover).

Each of the stages (except stage IX) was comprehensively described in Lee and Lucas (2007) (Appendix C).

**Table 11: Overview of processing stages for the HSCOI**

	<b>Stage</b>	<b>Purpose</b>
I	Calibration and validation strategy	To ensure a) a sequence of reliable inputs to models and b) data to test model outputs across a range of forest types and environments.
II	Calculation of field plot-based stem density, cover, and sub-canopy tree assessment	To provide calibration and validation sets at the plot level and to establish, based on field data, the accuracy of retrieval.
III	Conceptual development of the Height scaled Crown Openness Index (HSCOI)	To conceptualise and demonstrate the steps required for calculation of the HSCOI.
IV	Calculation of the HSCOI Matrix generation and intersection of LiDAR points. Calculation of LiDAR penetration.	
V	Smoothing of the HSCOI and generation of minima.	To allow detection of stems regardless of crown dimensions and position in the vertical profile.
VI	Stem location using the HSCOI: Stem identification and extraction Filtering multiple scales utilising tree crown area and HSCOI thresholds.	To allow mapping of stems by locating HSCOI minima and refinement of these maps by utilising empirical functions and field-measurements (e.g., height, crown area) for different species.
VII	Crown/cluster area and cover estimation	To identify the forest/non-forest boundary and crowns/crown clusters contained within.
VIII	Estimation of stem height and plot-scale attributes (including density and predominant height).	To indicate stem size at the tree and stand level, thereby facilitating tree and stand level assessment of growth (successional) stage and estimation of biomass.
IX	Estimation of stem diameter ( $D_{130}$ ) and biomass	To provide required inputs for allometric equations, and for SAR simulation calibration.

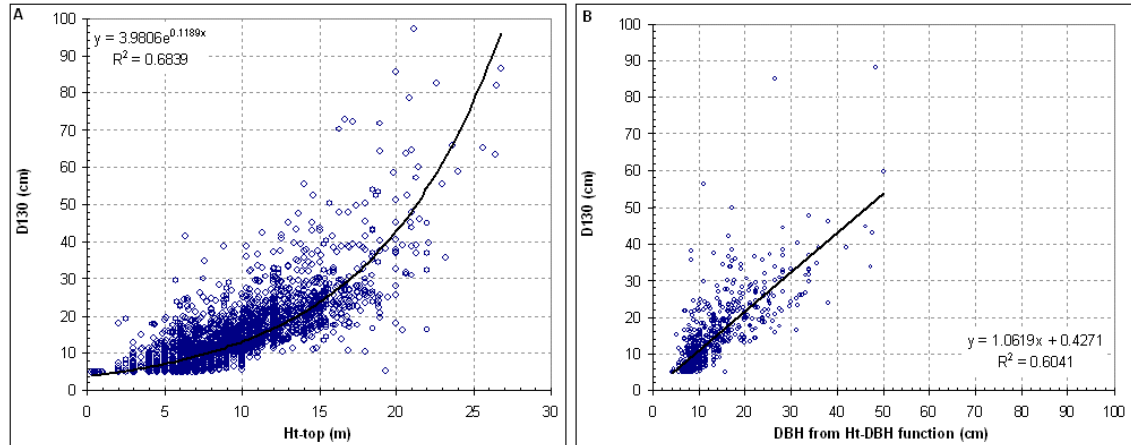
### ***HSCOI Stage IX: Calculation of stem diameter***

Most LiDAR studies have used various metrics of height to determine stem diameter, either at an individual tree level, or at a plot or stand level via basal area. This research used field data to generate a function that predicted stem diameter (at 130 cm:  $D_{130}$ ) from tree height. A random sample (80 %,  $n = 3,016$ ) of field-measured live trees with  $D_{130} \geq 5$ cm, (from 33 field plots) were used (Figure 20a) such that:

$$D_{130} = 3.9806 * \exp^{(0.1189 * H)} \quad \text{Equation 2}$$

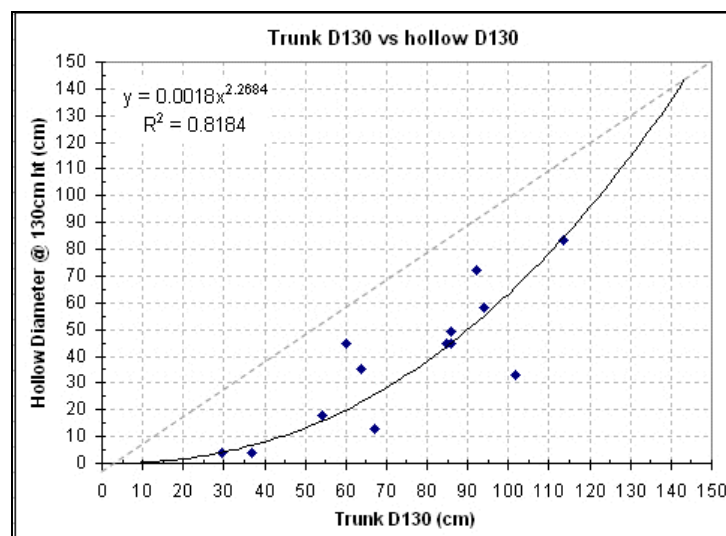
All species were included in the investigation, and the empirical non-linear (power) function was generally applicable across the main genus types. When evaluated against the remaining 20 % of live trees ( $D_{130} \geq 5$ cm,  $n = 755$ ), predictions of  $D_{130}$  were reasonable ( $r^2 = 0.60$ , RSE = 5.97 cm, with the slope and intercept of the best-fit line being 1.06 and 0.43 respectively; Figure 20b). Whilst some scatter was evident, the slope of the best-fit line indicated that stem  $D_{130}$  derived from height measurements approximated actual field-measured

$D_{130}$ . The function could be further refined by splitting into multiple species-specific classes. However, the application would also require species classification and mapping of the remotely sensed data (Lucas *et al.*, 2008).



**Figure 20: (a) Height-to- $D_{130}$  translation function using 80% of field measured stems and (b) validation using remaining 20% of field stems.**

A hollows factor was also applied to the stems, based on a small sample of field data (Figure 21). The hollows factor only applied to trees with the  $D_{130}$  of greater than 30cm  $D_{130}$ , as no trees smaller than this were observed to have substantial hollows that would impact on overall tree biomass using existing allometric equations. The range of observations for the hollows factor could easily utilise a linear function also, which reflects the relatively low number of observations.



**Figure 21: Hollows function derived from field data measurements (outside field plots), and applied to LiDAR derived stems.**

Additionally, the sample was relative small, so further development of this function was recommended. As the hollows factor was only applied to a relatively small set of the trees due to the D130 threshold, the amount of error contributed to the plot or stand total from uncertainty in this function was likely to be small, but should be investigated as a future research option.

### **3.5.2 Individual crown segmentation and delineation**

#### ***Conceptual overview***

As shown in the thesis conceptual flowchart (Figure 7, section 3.1), crown delineation was a key component of developing basic geographic entities. These entities form the building blocks of the multi-scale strategy to improve the assessment of forest structure using LiDAR. An individual tree was defined as the spatial unit of hierarchal Level 0, and the previous section (Lee and Lucas, 2007 – Appendix C) has described how individual tree stems can be mapped. This section outlines the LiDAR methods developed to delineate individual tree crowns, thus completing the second component of Level 0.

Tree crowns were used to provide bounding areas for the tree component modelling, so that field data derived empirical functions can be applied at a tree level. This also allows voxels, branches, and stems to be assigned and constrained to a single crown. Crown cover estimates were generated for the field plots and larger assessment areas (e.g., primary sampling unit or ICESat footprints), to compare to field data. Tree crown cover was also up-scaled and compared with other cover metrics such as foliage-branch cover and foliage projective cover, estimated from a range of sources. As with the initial development of the Height Scaled Crown Openness Index (HSCOI), the crown delineation methodology has primarily been developed for the Queensland Injune data. Due to time constraints, the delineation methods have not yet been calibrated for the NE Victorian field data.

There were four main stages in the LiDAR crown delineation method. These are briefly described below, and illustrated in (Figure 21).

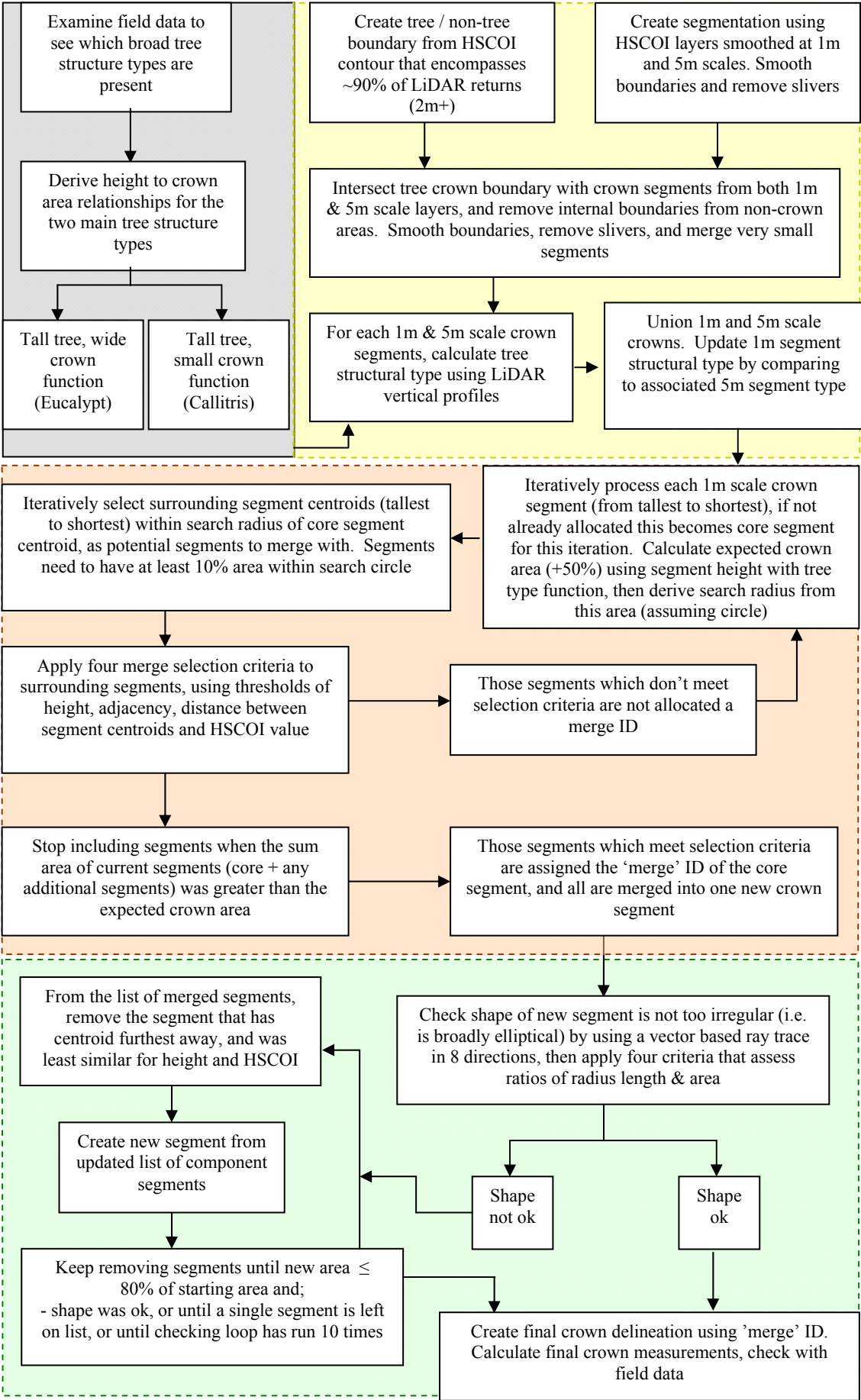
- Empirical functions were deriving from field data for two main tree structural types, thus allowing a simple template approach such that an expected crown area for a given tree height can be utilised.
- HSCOI crown edge segments were generated, as described in Section 3.5.1.
- Crown segments were classified into different structural types utilising LiDAR apparent vertical profiles and multi-scale spatial assessments.
- Individual crown objects were generated from segments using a range of attribute and spatial context criteria. The use of multi-scale adaptive templates allows the merging of small segments or splitting of large crown objects into more accurate crown representations as appropriate. Final crown dimensions were then calculated, and validated against field data.

### ***Stage I - Empirical functions for general crown templates***

The first stage in the individual crown delineation process was the development of crown templates using field data derived empirical functions. The use of minima contouring and template matching methods to assist in crown delineation using high-spatial resolution imagery was described in Chapter 2 (e.g., Koukoulas and Blackburn, 2005; Gougeon and Leckie, 2006; Bunting and Lucas, 2006; Solberg *et al.*, 2006), and crown shape was shown to influence LiDAR response (Nelson, 1997).

An examination of the Injune field data identified two broad categories of crown shape/area (i.e., a template) for taller mature trees – small compact crowns regardless of top-height (i.e., generally less than 50 m<sup>2</sup>), such as those from *Callitris* or *Acacia* genus (or some *Eucalyptus* in heavily stocked stands). The other category had large wide spreading crowns as the maximum height of the tree was attained, which is typical of woodland *Eucalyptus* or *Angophora* genus. Shorter, less mature trees of both types generally had smaller, more compact crowns, with the mean crown area of all trees being less than 10 m<sup>2</sup> (Figure 23).

**Figure 22: Flowchart of crown delineation methodology**





From examination of the range of field data, a basic hypothesis was postulated that the taller the tree, the wider the crown should be, a proposition also put forward by Jack and Long, (1991). Different crown size ranges per tree height were observed for each of the two main crown shape/area categories (Figure 23). It was also observed that the crown area of these two different types could be significantly different for the same tree top-height, especially at the taller end of the observed range (i.e., > 20 m).

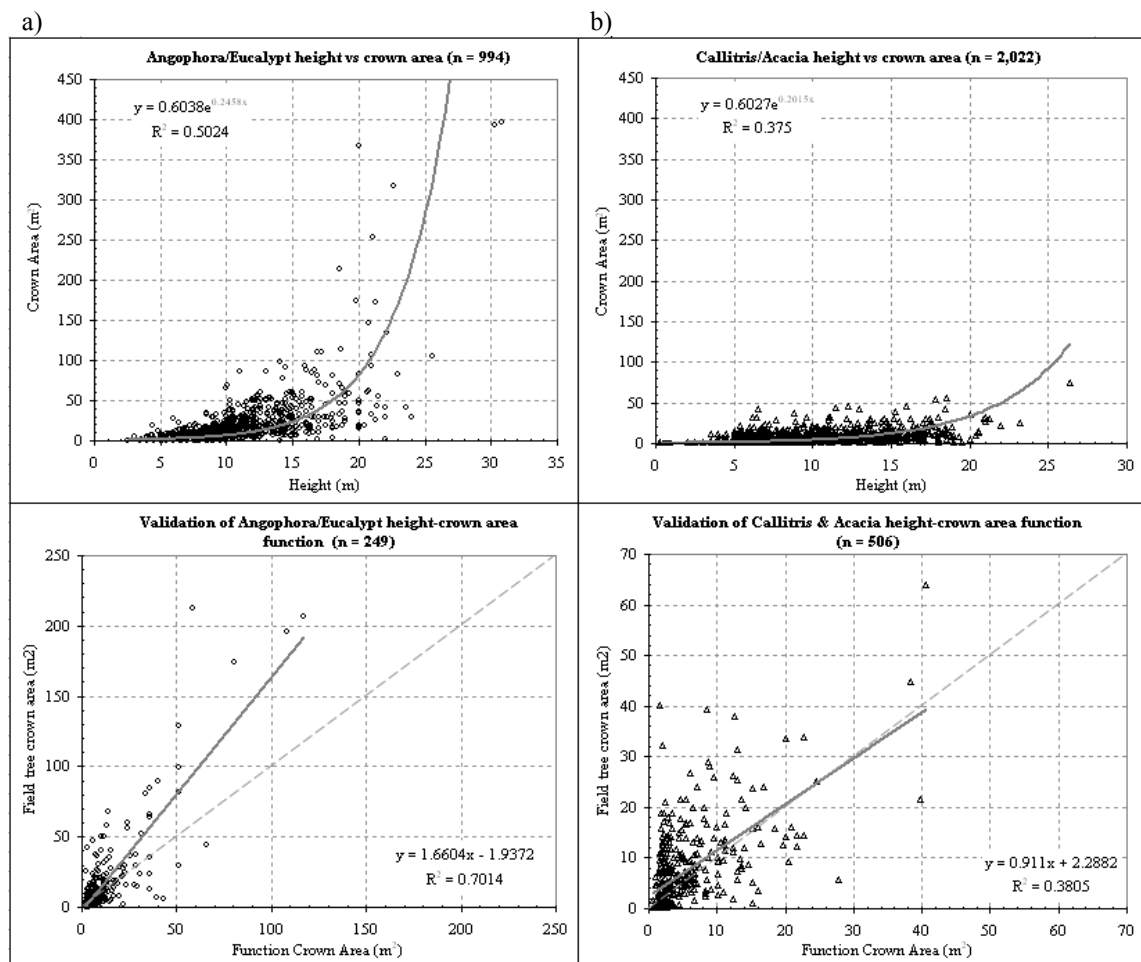
The crown delineation process utilises a multi-scale approach, with a fine scale segmentation to derive crown building blocks (equivalent to a Level -1 in a hierarchy), which were then compared to segmentations derived at medium scales, to put the constituent blocks into context (equivalent to a Level 0 in a hierarchy). The final crown products were a combination of constituent crown segments. The primary processing issue then becomes one of appropriately merging small segments into large (but not too large) segments for trees with wide crowns, whilst retaining small segments for smaller crowned trees. The appropriate sizes were determined from empirical functions derived from field data, which compare tree top height and crown area.

Crown area was based on an assumed circular or elliptical shape, derived from diameter measurements in north-south and east-west directions. The calibration and validation of both functions are shown in Figure 23, with calibration utilising a random selection of 80% of field stems, and validation using the remaining 20% of stems. The *Eucalyptus* function was described in Lee and Lucas (2007) and shown in Figure 23a, with the *Callitris* function given in Equation 3 (Figure 23b).

$$\text{Callitris Crown Area} = 0.6027 * \exp^{(0.2015 * \text{height})} \quad \text{Equation 3}$$

Using randomly selected validation datasets, the *Angophora/Eucalypt* function produced a correspondence ( $r^2 = 0.70$ ,  $\text{RSE} = 16.2 \text{ m}^2$ ,  $n = 249$ ), with a slope and intercept of the best-fit line being 1.66 and -1.937 respectively (Figure 23). The *Callitris/Acacia* function produced a correspondence ( $r^2 = 0.38$ ,  $\text{RSE} = 5.8 \text{ m}^2$ ,  $n = 506$ ), with a slope and intercept of the best-fit line being 0.911 and 2.288 respectively (Figure 23). Whilst there was much scatter in

the *Callitris/Acacia* function validation result, on average the function produced near to the expected field result (as evidenced by the validation best-fit line approximating the 1:1 line). Because the actual crown areas involved were relatively small (i.e. generally less than 50 m<sup>2</sup>), the function was considered adequate for the intended purpose within the delineation modelling.



**Figure 23: Calibration using 80% of field data trees (Upper) and validation using 20% of field data trees (Lower) for estimating crown area from height, for (a) Eucalypt and Angophora trees, and (b) Callitris and Acacia trees (live trees 5cm+ D<sub>130</sub>).**

However, the validation exercise indicated that the expected crown area derived using the *Angophora/Eucalypt* function was consistently underestimated when compared to the field estimated crown area. From the validation graph (Figure 23), the line-of-best-fit was found to show bias in the prediction of actual field measurement value of approximately 1.5 times the translation function value. Therefore to improve the predictive ability of the function when applied to the LiDAR modelling, a crown area expansion factor of 50 % was applied to the initial function result. In the modelling algorithm the final expected crown area calculated by

dividing the initial expected crown area by two, and the result added to the original expected area. The observed bias in the translation function validation was most likely a result of the large natural variation in *Angophora* and *Eucalyptus* height and crown area as measured in the field. This could be linked to different species, stem density influences, soils, nutrient, and water availability (Florence, 1996). Lack of accuracy in the crown area field measurements may also contribute to the observed variation in the relationship between crown area and height.

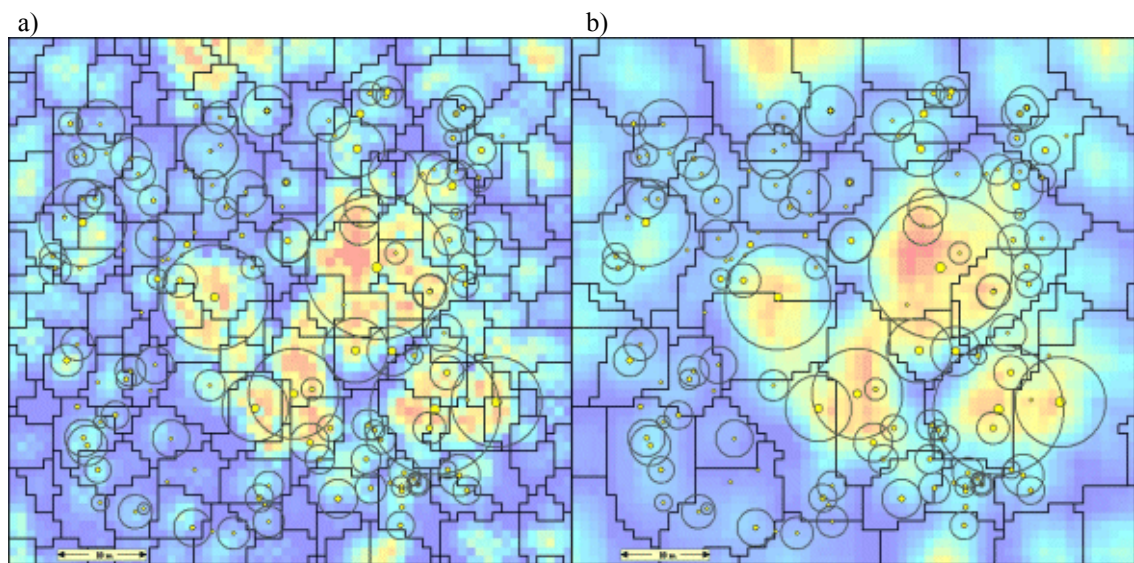
As the height-to-crown area function was exponential, very large crown areas can be generated at the upper end of recorded tree heights. To prevent unrealistic crown area values being produced, an upper crown area bound was applied to the final expected crown area. This upper bound was based on the largest crown area observed in the field data, plus an expansion factor of approximately 10 % to allow for error in the field estimate, and for trees larger than those found in the field plots. For the Queensland data, the largest crown area observed was 455 m<sup>2</sup>, so the upper bound applied was rounded up to 500 m<sup>2</sup>. With the Queensland derived function, the maximum crown area would be derived with a tree height of approximately 27 m or more. When considering all LiDAR in the landscape sample, tree heights up to 35 m were observed, whilst the tallest tree measured in the field was 31 m, so it was therefore possible that larger crowned trees exist in the landscape. Examination of LiDAR (or other high spatial resolution data if available) at the locations with the tallest heights would indicate if the crown width upper bound needs to be increased.

### ***Stage II - Creating individual crown segments***

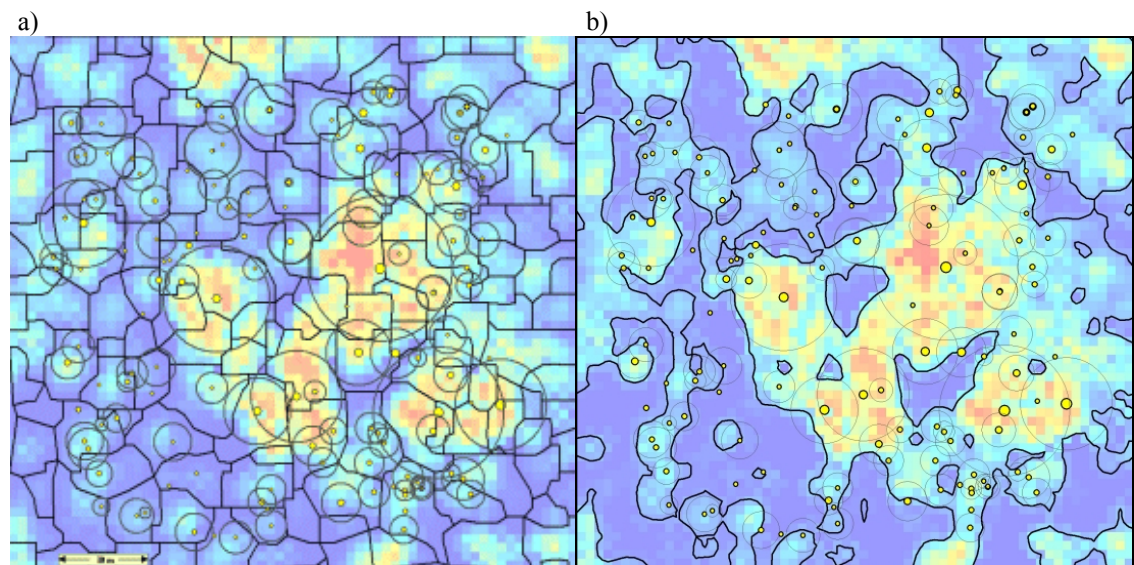
Each crown area was segmented into potential individual tree crowns or tree clusters using ArcGIS hydrological functions (ESRI, 2006), where ‘drainage’ basins were delineated around areas of low foliage density, as indicated by high Height Scaled Crown Openness Index (HSCOI) values. Using the ArcInfo ‘BASIN’ function, ridgelines between basins provided the vectors for the crown delineation. The drainage basins were created by locating the pour points at the edges of the analysis window (where water would pour out of the grid), as well as sinks,

then identifying the contributing area above each pour point. The method of deriving flow direction from a DEM, utilised by ArcGIS, is presented in Jensen and Domingue (1988).

With the initial steps of the crown segmentation process for the Injune test plot (p81-16), basin delineation was done on both the 1 m and 5 m HSCOI<sub>stand</sub> surfaces (herein described as segment<sub>1m</sub> and segment<sub>5m</sub> respectively) (Figure 24). Segmentation vectors were smoothed to remove the blocky appearance resulting from the underlying HSCOI grid (Figure 25). For the figures, the background image was HSCOI<sub>stand</sub>, where dark blue is high openness (bare ground), and red is low openness with the tallest trees (i.e. centre of tree).



**Figure 24: Crown segmentation using surface generated from a 1m circular (a) and 5x5m rectangular (b) moving window.**



**Figure 25: Smoothing of segmentations (a) and segment clipping with HSCOI derived crown boundary delineation (b).**

Field data stems are yellow filled circles proportional to  $D_{130}$ , and open circles are proportional to mean crown radius. Following delineation, the basins were clipped to the  $HSCOI_{stand}$ , crown edge, with those basin vectors outside the tree crown area removed (Figure 25). When initially compared to the field tree maps, the segments<sub>5m</sub> tend to indicate where large crowned trees occur, whilst creating large clusters of many smaller crowned trees. The segments<sub>1m</sub> tend to split the very large crowns into leaf clumps areas, presumably from the major branches, whilst correctly segmenting small trees. Where clusters of many small trees occur, even segments<sub>1m</sub> tend to aggregate these into single segments, where individual crowns cannot be discerned. Each segment was then assigned the highest LiDAR return found within the segment.

### ***Stage III - Classification of crown segments***

The third stage in the crown delineation process applies a genus probability process at multiple spatial scales, using both segments<sub>1m</sub> and segments<sub>5m</sub>. The segment<sub>5m</sub> was used to determine if the genus distinction calculated for the segment<sub>1m</sub> needs modification. This was because large crowned trees (e.g., *Eucalypt* or *Angophora*) were often made up of many smaller segments equivalent to major branch clumps at the finer scale, which can have a similar structural signature to *Callitris* forms. Therefore, if the genus assessment was only done on the segment<sub>1m</sub>, large trees would remain over-segmented. The working hypothesis with these structural assessments was that *Callitris* type trees will tend to have denser foliage concentrated in the upper part of the crown. This results in more LiDAR returns being “captured” in the upper portions of the crown. The resultant LiDAR apparent vertical profile from trees of this type will therefore tend to be strongly skewed towards the top most part of the crown, and the  $HSCOI_{local}$  values will tend to have a smaller range, as the crown was more compact. These concepts were illustrated using examples from two segments, with LiDAR returns by height, and associated apparent vertical profiles for the two representative broad genus types (Figure 26). Figure 27 provides photographic examples of the two broad genus groups.

---

Due to variability in crown form in different environments, a range of criteria were used to determine the probable genus group, as any one test may not give a correct result if applied singly. The four tests were initially developed using nine trees (five *Eucalypt-Angophora* and four *Callitris-Acacia*) from two different field plots (Table 12). When two or more of the four test criteria exceed the relevant threshold then the segments<sub>1m</sub> and segments<sub>5m</sub> were classed as *Callitris-Acacia* forms, otherwise the segment was classed as *Eucalypt-Angophora*.

The two segmentations were then combined, and the genus code from each segment<sub>1m</sub> was compared to the corresponding segment<sub>5m</sub> (Figure 28). When both segment<sub>1m</sub> and segment<sub>5m</sub> were classed as *Callitris-Acacia* then the final genus assignment for segment<sub>1m</sub> was *Callitris-Acacia*. For all other combinations of genus between the two assessment scales the final genus assignment was *Angophora-Eucalypt*. Where more than one segment<sub>5m</sub> overlaps the segment<sub>1m</sub>, then the segment<sub>5m</sub> that has at least 10% of the area overlapping the segment<sub>1m</sub>, and was the larger for area and tallest in height was used. Subsequent validation was done on the rest of the field plots, with the final genus assignment occurring for each assessment scale.

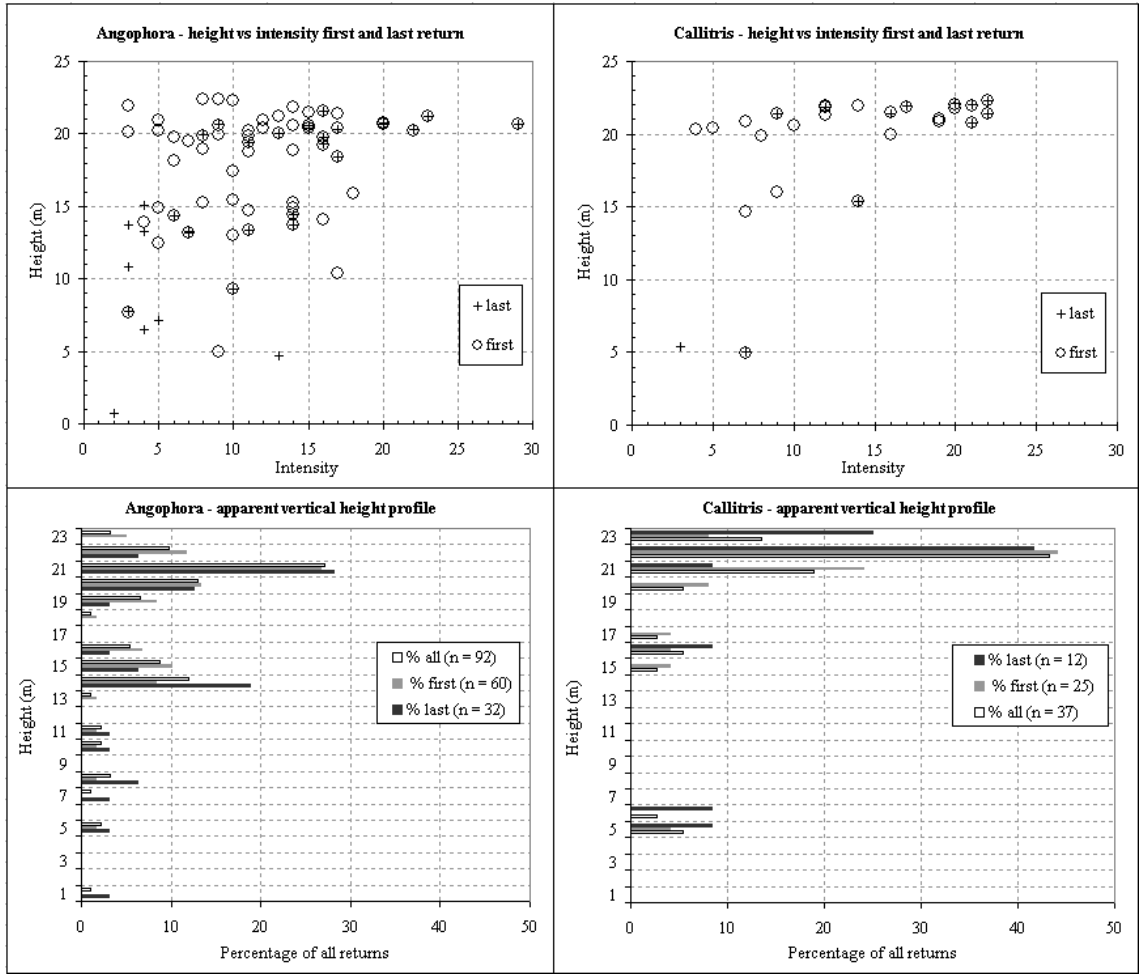


Figure 26: Illustration of different apparent vertical profiles for the two main structural types.



Angophora



Callitris

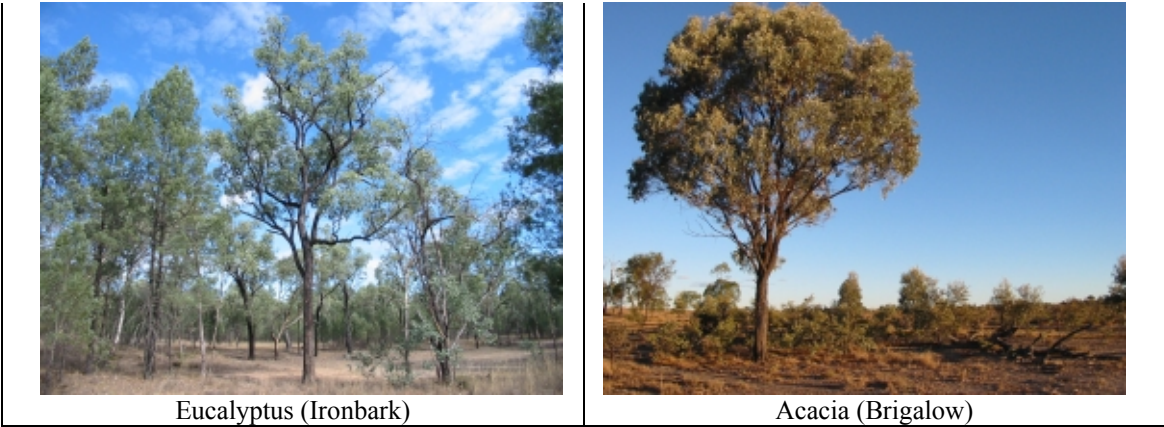


Figure 27: Examples of the two broad genus groups based mature tree structural crown forms

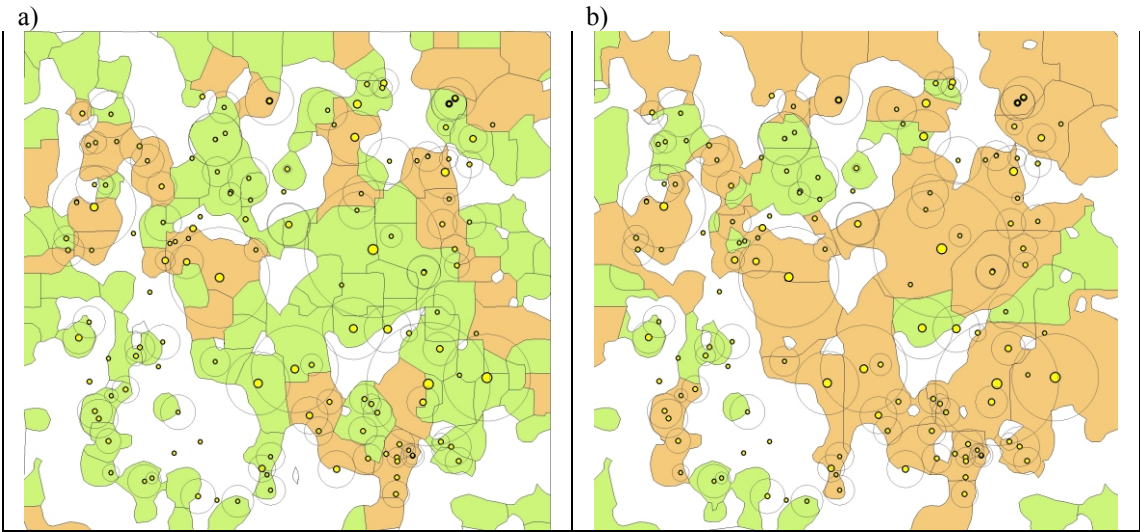
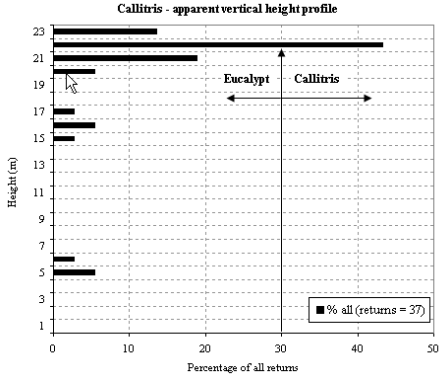
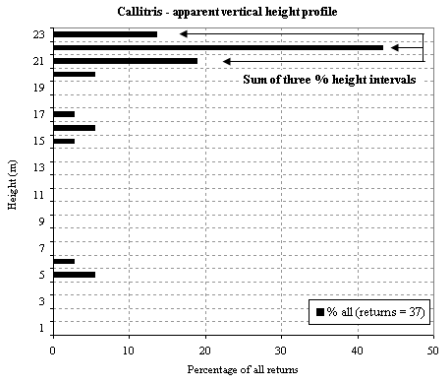
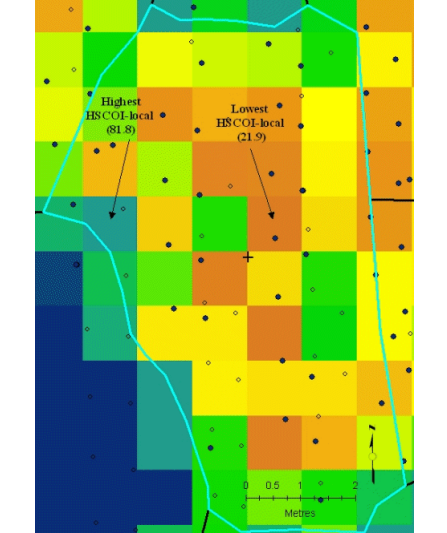
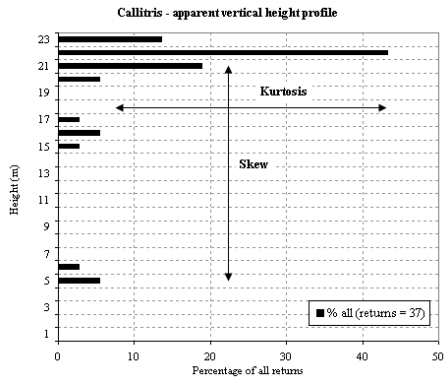


Figure 28: Crown structural classification into two broad genus categories at (a) segment<sub>1m</sub> and (b) segment<sub>5m</sub> scales. Green is *Callitris-Acacia* and light brown is *Eucalypt-Angophora*.



**Table 12: Genus probability selection criteria**

#	Criteria	Example
1	<p>The percentage value of the LiDAR return count at max frequency from the apparent vertical profile.</p> <p><i>Callitris</i> form if result was <math>\geq 30\%</math>.</p> <p>The graphic segment example has a percentage value at maximum LiDAR frequency of 43.2%.</p>	
2	<p>Sum of the percentage values for the LiDAR return frequency from each height interval bordering the maximum frequency height interval, (including the maximum frequency value).</p> <p><i>Callitris</i> form if result was <math>\geq 55\%</math>.</p> <p>The graphic segment example has a sum percentage value of 75.7%.</p>	
3	<p>The range of HSCOI<sub>local</sub> values (max – min) within the segment</p> <p><i>Callitris</i> form if result was <math>\leq 60</math>.</p> <p>The graphic segment example has a HSCOI<sub>local</sub> range of 60% (81.8 – 21.9).</p> <p>The LiDAR canopy returns (0.5m+) used in the apparent vertical profiles for the other criteria are black points. Ground returns are hollow/grey points. Dark blue HSCOI<sub>local</sub> cells indicate bare ground.</p>	
4	<p>Kurtosis or skewness of the LiDAR apparent vertical profile. If either one of these was met or exceeded then the segment was most likely <i>Callitris</i>.</p> <p>For kurtosis a <i>Callitris</i> form if result was <math>\geq 2</math>.</p> <p>For skew a <i>Callitris</i> form if result was <math>\geq 1</math>.</p> <p>The graphic segment example has a kurtosis of 12.14 and skew of 3.32.</p>	

---

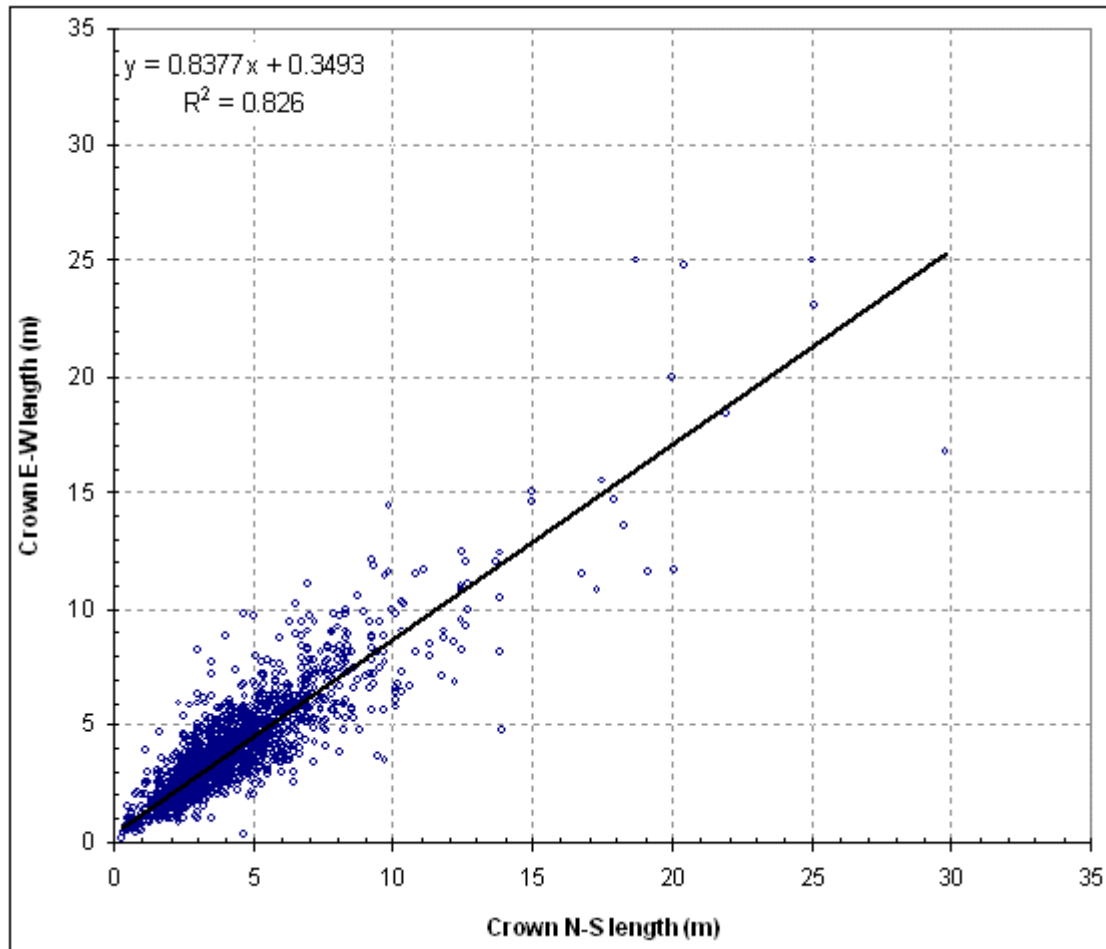
***Stage IV - Creating crown objects***

In stage four of the crown delineation process, objects representing tree crowns were derived from the polygon segment<sub>1m</sub> layer, which were assessed using a range of spatial criteria (see Figure 22 for the overview). The criteria to determine the most likely crown area were based on the field-data derived height-to-crown area relationships, and used the segment LiDAR maximum height. Segments were iteratively processed from the tallest to the shortest tree, and at each stage the segment being processed became the “core” segment. Surrounding segments were then assessed with respect to the core segment. This equates to the “seed” point used in optical crown segmentation literature (see Chapter 2; e.g., Bunting and Lucas, 2006). Once a segment<sub>1m</sub> became the core segment, or it was allocated to be merged with a core segment, it was removed from the processing list, thus preventing larger crowns from being “undone” as the iteration progressed.

Parameters, criteria and thresholds (see Table 13 and Table 14) used to determine if a segment should be merged, split or remain unchanged were initially determined through iterative empirical testing on a selected set of tree crown segments reserved for algorithm calibration. These segments were selected so that they spanned species, height and crown width ranges observed within three different field plots (see Lee and Lucas, 2007 (Appendix 3) for a description of the field plots used for calibration). Validation of the parameters and thresholds was achieved by executing the segmentation algorithm across the all LiDAR in the calibration field plots and comparing the delineation results to the remaining (independent) field data trees. A range of different criteria combinations were iteratively developed to account for the observed natural variability in tree crown dimensions, foliage density, and horizontal and vertical location within the stand.

Overall there were two general assumptions that determine how the criteria and thresholds were applied. First, segments were only merged if they were similar in height, foliage density and location (i.e. adjacent or close by). This assumption was evaluated by comparing initial segment delineations with field data tree maps for a range of species and crown sizes. Second, tree crowns were found to be generally circular/elliptical in shape using

field data measures of the crown extents in the north-south and east-west directions (Figure 29). It was found that, in general, crowns had even diameter distances based on the near 1:1 relationship. Evidence for an assumed circular shape was further bolstered by examination of ground and aerial photographs of the plots and raw LiDAR data of known individual trees (e.g. see Figure 19). Therefore, segments that deviated greatly from this shape were considered to be comprised of crowns of several trees, and were split if constituent segments were available.



**Figure 29: Derivation of circular crown shape assumption, using all field live stems 5cm+ D130 (n = 2708) and comparing crown north-south length versus east-west length.**

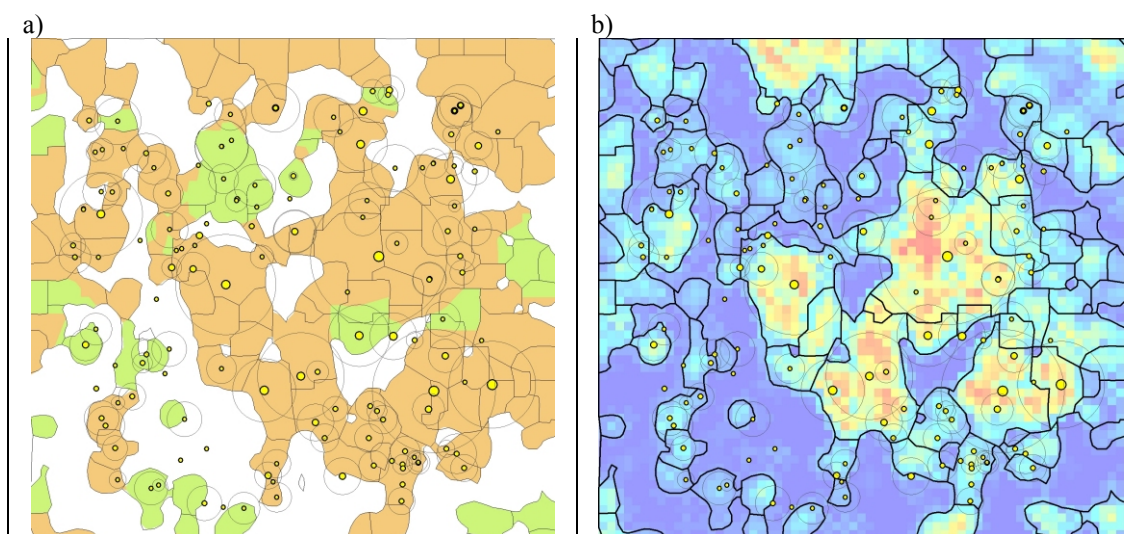
The first part in the crown object delineation stage assessed the area of the core segment. The segment<sub>1m</sub> LiDAR height and probable genus were used to calculate the expected crown area, using the field data relationships described previously. Segments were then defined as being near equal, too small, or too large with respect to the expected area. If the core segment was too small, the surrounding tree segments<sub>1m</sub> that overlapped the segment<sub>5m</sub> within which the core segment centroid was located were selected. This prevented crowns

growing too large by not selecting segments<sub>1m</sub> that may be part of other trees (as identified by the 5 m assessment scale). The selected surrounding crown segments<sub>1m</sub> were processed tallest to shortest, and four criteria were utilised, as described in Table 13:

**Table 13: Spatial criteria for merging a segment with neighbouring segments**

Criteria	Description
1	The selected segment <sub>1m</sub> was adjacent to core segment.
2	The selected segment <sub>1m</sub> had LiDAR height $\geq 73$ % of the height in core segment.
3	The centroid of the selected segment <sub>1m</sub> was within 110 % of the search distance from core segment centroid. The search distance was calculated as the radius of a circle with an area the same as the expected crown area.
4	The selected segment <sub>1m</sub> centroid $HSCOI_{stand}$ was within 25 % of core segment centroid $HSCOI_{stand}$ .

The selected segment<sub>1m</sub> was coded with the core segment ID (termed the “merge ID”) when any of these four combinations of criteria were met – (1 and 2); or ((1 or 2) and 3); or (1 and 3 and 4); or (2 and 3 and 4). Otherwise the surrounding segment<sub>1m</sub> was not added to larger crown, but instead was released back into the iterative processing list. Processing was complete for the core segment when either no more surrounding segment<sub>1m</sub> meet the assessment criteria, or when the total area of the core segment plus any additional segment<sub>1m</sub> that have been allocated to it exceeded the expected crown area. Once all segments<sub>1m</sub> had been processed, the final assigned “merge” ID was used within a ‘dissolve’ process, where any adjacent segments<sub>1m</sub> with the same merge ID were combined to form a larger crown (see Figure 30b).



**Figure 30: Final crown structural classification (a) and delineation after spatial assessment (b).**

If a core segment was too large as indicated by the expected crown area assessment, a range of criteria were used to determine if it should be split. Note that larger segments can only be split into constituent segment<sub>1m</sub> parts, if present. Shape was assessed using four shape criteria, with the segment shape deemed to be too irregular when the criteria for the shape ratio and one of the others were met. When this occurred the segment was coded as available for the splitting process. If the criteria indicate that a segment<sub>1m</sub> was too irregular, but could not be further split due to there not being any constituent segments<sub>1m</sub>, then a flag was entered into the database indicating that the segment was most likely made up of many small stems, but where individual crown areas could not be resolved using the available data and processing scales. The four assessment criteria were summarised below and illustrated in Table 14:

- (1) if the perimeter-to-area shape ratio was greater than or equal to the threshold. If this was the case then the three additional checks were undertaken,
  - (2) if the segment roundness ratio was less than or equal to the threshold,
  - (3) if the elongation ratio was less than or equal to the threshold; or
  - (4) if the eccentricity ratio less than or equal to the threshold.

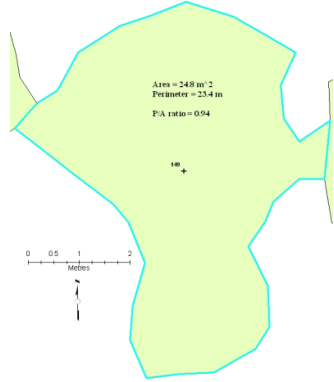
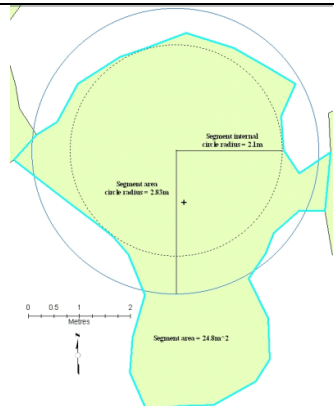
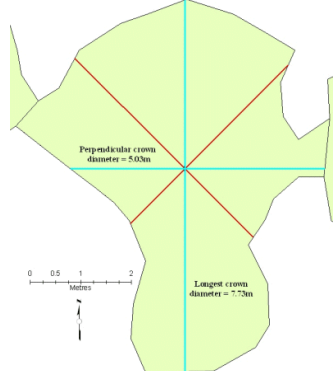
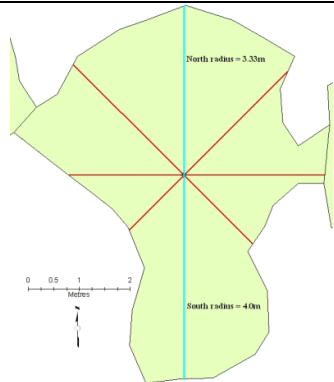
For criterion 1, the expected shape ratio (perimeter-to-area ratio) was calculated for a circle, which was assumed to be the shape of an idealised tree crown. When compared to the actual perimeter-to-area ratio from the segment, the ratio indicated the similarity to a circular shape. The expected perimeter-to-area function was developed empirically for an area ranging from 1 m<sup>2</sup> to 600 m<sup>2</sup>, which was 150 m<sup>2</sup> larger than the largest crown found the Injune field data. The form of the function was  $y = 3.5449x^{-0.5}$ , where  $y$  = perimeter-to-area ratio, and  $x$  = area. The form of the function was modified in Table 14 to be usable in Arc Macro Language, as a power function (other than  $x^2$ ) was not available.

For the second criterion, the circular shape (i.e. an idealised tree crown), was assessed in a different way to support the result of the criterion 1 measure. Here a circle was generated within the segment, as well as a circle with an area the same as that of the segment. The radii of the two circles were then compared as a ratio measure. The rationale of this measure was that the ratio will approach one when the segment was almost circular, and thus more likely to be an

individual crown. If the crown segment was very irregular, then an internal circle would be much smaller than the actual segment area would indicate.

For the third and fourth criteria, an assessment of the length and width of the segment was made. Here, the rationale was that a segment shape that was irregular (and less likely to be an individual tree crown), will have a large divergence of radii measures. These two criteria were developed to provide a more direct comparison to the available field data measurements. To determine the segment length (and therefore shape), a star pattern of 8 arcs was generated from the centroid location, using a length of three times distance of the radius of the largest circle that can fit within the segment. This was undertaken to ensure the assessment arcs extend to the crown edge. The arcs were then clipped to the segment boundary, and the longest arc within the segment identified, as well as the perpendicular arc. The respective diameter or radii lengths compared, and where lengths were relatively even, then the shape was assumed to be roughly circular and thus close to an assumed individual tree crown. The converse situation occurs where there was a large difference in the diameter and radii measures, and the segment was coded for splitting, if constituent segments were present.

Table 14: Spatial criteria for splitting a segment

#	Criteria	Example
1	<p>The shape ratio – the segment perimeter-to-area ratio divided by the expected (for a circle) perimeter-to-area ratio.</p> $C1 = \frac{\left(\frac{\textit{perimeter}}{\textit{area}}\right)}{\left(3.5449 \times \frac{1}{\sqrt{\textit{area}}}\right)}$ <p>The segment was further checked if the result was <math>\geq 1.47</math>.</p> <p>The graphic example has a <math>C1 = 1.32</math> (area = <math>24.8\text{m}^2</math>, perimeter = <math>23.4\text{m}</math>)</p>	
2	<p>The roundness ratio – the radius of the largest circle that can be contained entirely within the segment divided by the radius of a circle with an area the same as the segment area.</p> $C2 = \frac{\textit{circle\_radius\_within\_segment}}{\textit{circle\_radius\_with\_segment\_area}}$ <p>The segment was split if result was <math>\leq 0.61</math>.</p> <p>The graphic example has a <math>C2 = 2.10/2.83 = 0.74</math></p>	
3	<p>The elongation ratio – the perpendicular diameter (of longest crown diameter) divided by the longest crown diameter.</p> $C3 = \frac{\textit{perpendicular\_segment\_diameter\_length}}{\textit{longest\_segment\_diameter\_length}}$ <p>The segment was split if the result was <math>\leq 0.75</math>.</p> <p>The graphic example has a <math>C3 = 5.03/7.73 = 0.65</math></p>	
4	<p>The eccentricity ratio - the two radii that make up the longest crown diameter measurement. The lowest radius was divided by the highest radius.</p> $C4 = \frac{\textit{smaller\_radius\_of\_longest\_diameter}}{\textit{larger\_radius\_of\_longest\_diameter}}$ <p>The segment was split if result was <math>\leq 0.55</math></p> <p>The graphic example has a <math>C4 = 3.33/4.00 = 0.83</math></p>	

### 3.5.3 Tree component scale LiDAR modelling

The previous section outlined the stem mapping and crown delineation methods utilised to develop a hierarchical Level 0 calibration dataset. This section extends the methods to model at the tree component scale (i.e., branches and leaves), in addition to the already derived stems. Modelling components allows more sophisticated SAR simulations to be undertaken, and facilitates a purely structural calculation of biomass, using specific volumes of wood or leaf material multiplied by the species specific weight or density of these components. Components can also be spatially mapped, further enhancing the structural description of the plot that can be achieved.

Prior to the component modelling, each crown was associated with a species type based on CASI data, using procedures outline by Bunting and Lucas, (2006). The attribution of LiDAR crown delineations with CASI derived species is described in Lucas *et al.*, (2006c) (Appendix C). The main steps to model branch and leaf component level information were:

- a) Generate tabular 3D 1 m<sup>3</sup> canopy voxel database, i.e. such as that used for the HSCOI.
- b) Intersect voxels with individual crown polygons, and assign to individual stems within the crown area.
- c) Spatially cluster voxels (in 3 dimensions) into primary branch clumps, with the centre of mass location of voxels becoming the primary branch end. The primary branch start at stem was derived from empirical functions using field data. The secondary branches that emanate from voxels were assigned to a primary branch (see Figure 31 for an example).
- d) Determine branch diameter as function of trunk diameter, where primary branch meets trunk. The branch volume was calculated based on the assumption that the branches were cylinders. Species specific wood density factors were then applied, and the structural woody biomass (including trunk) was calculated.
- e) Use allometrics (using species,  $D_{130}$ , or height) to determine small branch and leaf biomass within voxels.
- f) Sum the estimates of structural biomass per tree and compare to field biomass estimated with allometrics using  $D_{130}$  only, for validation of the modelling.



These steps were comprehensively described in Lucas *et al.*, 2006c (Appendix C), with additional detail on the branch radius calculation given in the next section. Biomass estimation methods at the plot and tree scale were also described in Lucas *et al.*, 2008 (Appendix C).

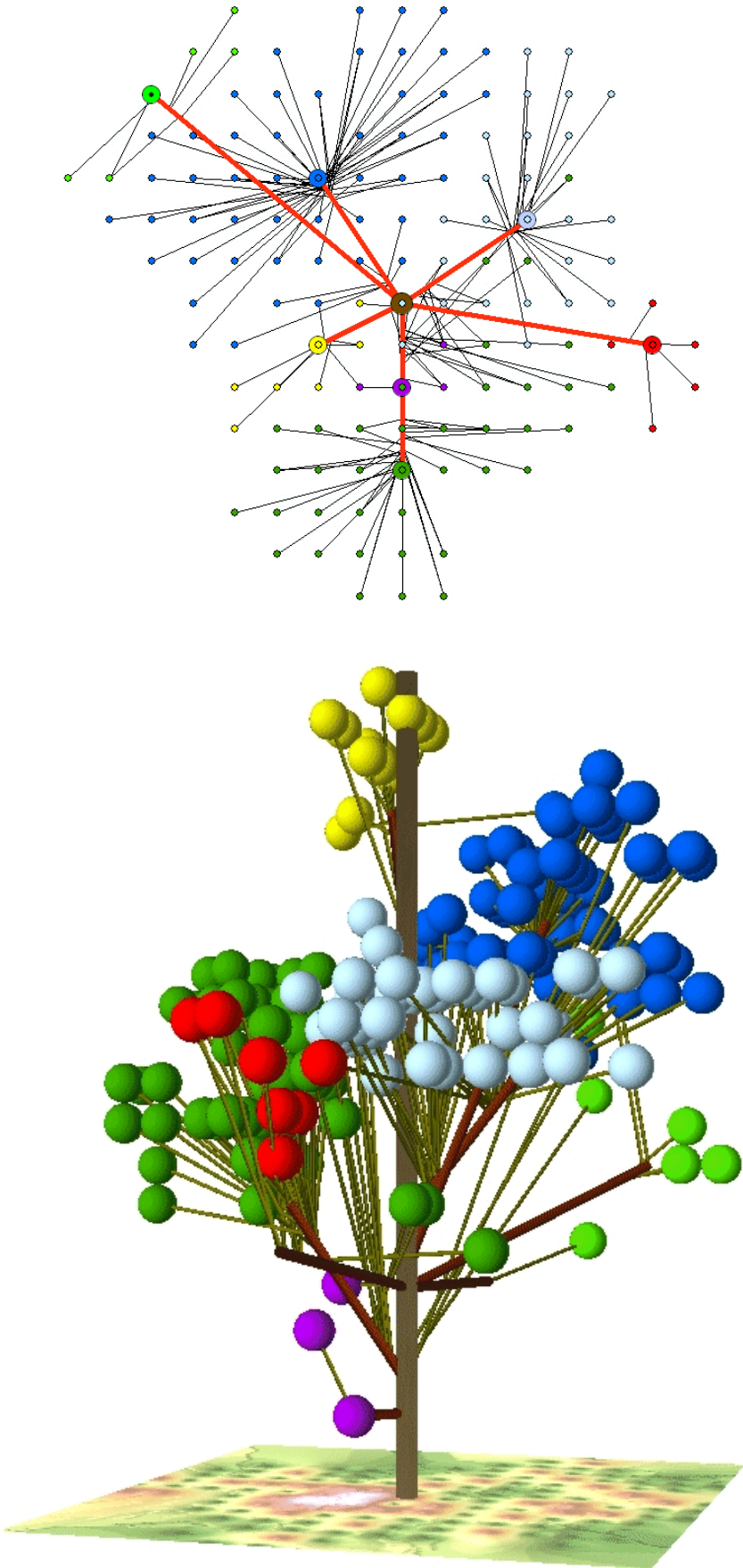


Figure 31: Voxel groups associated with branch clusters within an individual *E. populnea* tree from PSU 142, with a planimetric view (upper) and 3D view (lower).

**Branch radius calculation**

The start and end radii estimates for branches were calculated using the functions shown in Table 15. All branch radius units were reported in metres. Values for the start and end radii of both branch categories were based primarily on trunk and branch diameter data. Primary branch end radius equals the primary start radius multiplied by 0.8015. Here 0.8015 was the linear function parameter derived from field data tree measurements for the species, where  $y = 0.8015x$ , ( $x$  = branch start diameter, and  $y$  = branch end diameter); the intercept was forced through zero, and the range of measurements was 2.7 - 34.7 cm. Secondary branch start radius equals the primary branch end radius, and the secondary branch end radius equals the secondary start radius multiplied by 0.8015.

**Table 15: Functions used to calculate branch start and end radius**

Primary branch start radius = $\frac{(((H_{top} - Tr\_offset - DBH\_ht) - PBst) \times 100)}{\tan(T\_Angle)}$	Tr_offset = trunk end offset = 1.5m DBH_ht = height at DBH = 1.3m PBst = primary branch start height (m)  Primary branch start radius parameters: Htop = tree top height (m), T_Angle = (Taper_A * Pi / 180) (radians). To convert Taper_A to radians (for use in excel) it was multiplied by Pi and divided by 180.
Taper_A = Taper function angle = $ASin\left(\frac{(Tr\_vert\_ht \times 100)}{Tr\_hyp}\right) \times \frac{180}{\pi}$	Taper function angle parameters: Tr_vert_ht = trunk vertical height (m) = (tree top height - Trunk end offset) Tr_hyp = trunk hypotenuse length (m) (i.e. length of outside of trunk to top height).
Tr_hyp = trunk hypotenuse length = $\sqrt{\left(\left(\frac{DBH}{2} + Tr\_e\_radius\right)^2 + (Tr\_vert\_ht * 100)^2\right)}$	Trunk hypotenuse length parameters: DBH = diameter at breast height (1.3m) (cm) Tr_e_radius = radius of trunk at end (cm) Tr_vert_ht = trunk vertical height (m)

## 3.6 Phase 3 – Multi-Scale Calibration and Validation Case Studies

### 3.6.1 Introduction

As described in the introduction to the this chapter, to address the primary research question with respect to the utility of LiDAR to improve forest structural assessment, three case studies were presented:

1. Multi-scale assessment of height and cover. This case study examines the effect of plot or assessment size on the reported height or cover metric (and investigates a minimum reporting area for forest), a comparison of crown cover derived from LiDAR versus API, and a trial of the crown separation “zig-zag” transect method;
2. Comparison of SLATS Landsat TM derived foliage projective cover with LiDAR foliage-branch cover and crown cover, to investigate the development of a foliage projective cover to crown cover translation function;
3. Investigation and calibration of ICESat full waveform LiDAR data for forest stand height and cover.

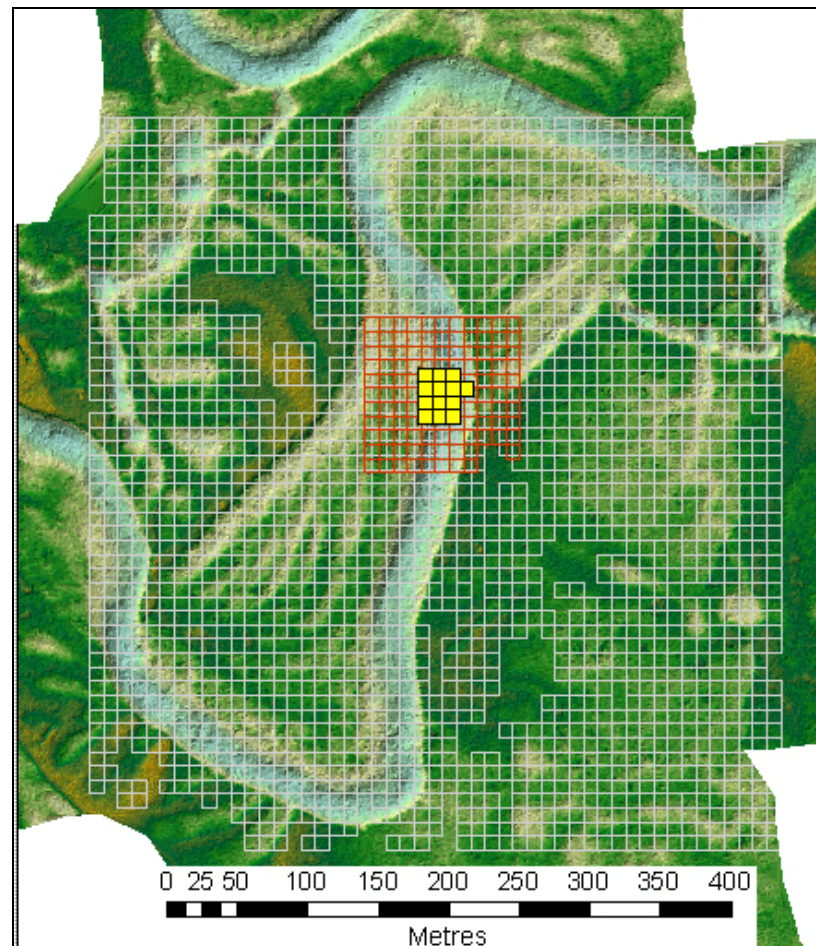
### 3.6.2 Multi-scale assessment of height and cover

#### *Multi-scale predominant height assessment*

This section tests the hypothesis that the scale of assessment (i.e. the defined area of a plot or “stand”) influences the reported stand height. If the assessment area was too small, it may not represent the wider stand. If it was too large then it may include tree heights from other stands with different structure. It was assumed that a “stand” was structurally relatively homogeneous, though it was recognised that in some situations determining homogeneity can be difficult. As described previously, predominant height was calculated as the mean of 10 m cells with a canopy height greater than or equal to 2 m, within a defined area, where the maximum LiDAR return per 10 m cell was used. Because the NE Victorian LiDAR data were collected with a wider swath than Injune, this analysis concentrated on the NE Victorian LiDAR in the first instance. This method was applied at the following scales (Figure 32):

- field plot scale (30 x 30m - 0.09ha) (solid yellow)
- transect area scale (100 x 100m - 1ha) (red outline)
- LiDAR swath overlap scale (~400 x 400m ~ 20ha) (grey outline),

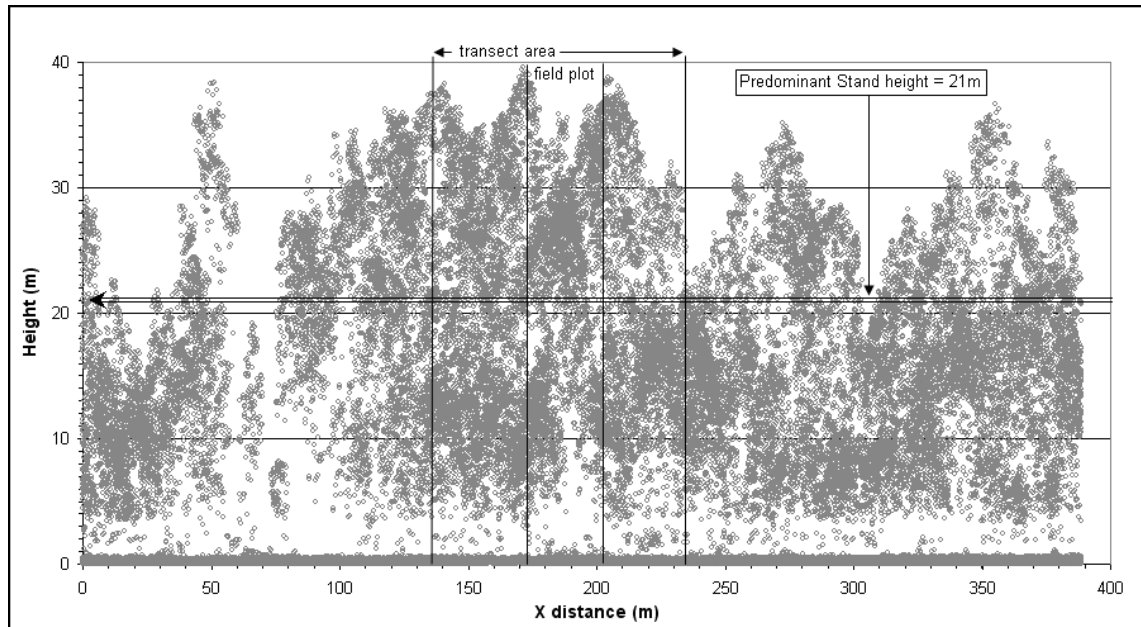
Apparent “holes” in the lattice indicate that no LiDAR returns higher than 2 m were observed for that cell.



**Figure 32: Predominant stand height assessment using LiDAR 10m cells at different spatial extents at CFMF plot 212 (Ovens river).**

An example of the raw LiDAR data in profile, for NE Victorian plot 212, has the data sliced to the full width of the swath, and was approximately 100 m deep (Figure 33). The different scales of assessment, namely field plot, transect area, and swath extent, were indicated. This plot illustrates potential issues with plot height representativeness, as the location may not reflect the wider stand. This issue may be more pronounced in highly variable forest environments such as riparian zones within floodplains (Figure 33). In this example, it can be seen that the field plot was located within a cluster of taller trees, but the wider stand appears to

have tree canopy that was generally shorter. Note that in this illustration the trees appear to have quite narrow crowns. This was an artefact of the display, as the X distance (x-axis) scale was 4 times greater than the tree height scale (y-axis), so it was not indicative of the actual crown shape (see also the plot hemispherical photos in Appendix B).



**Figure 33: Illustration of CFMF plot p212 with plot, transect and stand scales of assessment. The LiDAR point data slice was approx. 100m deep.**

To test whether the actual location of the field plot has an affect on the predominant height result, additional analyses were undertaken. Here field and transect ‘plots’ were randomly located within the LiDAR swath area, and a mean value derived from the respective samples. This was primarily to test if a single field or transect plot was adequately sampling the wider stand (as defined by the LiDAR swath). The analysis method used the 10 x 10 m cell lattice which covers the whole LiDAR swath at the plot location (approx 400 x 400 m or 20 ha). A start cell was randomly selected from within the swath area, and from this start cell a transect area was derived (i.e. 100 cells in a 10 x 10 array, with the start cell located in the lower left corner). At the centre of the transect area, a field plot area (9 cells in 3 x 3 array) was subsequently extracted. The predominant height was calculated for both assessment scales. This process was then repeated 30 times throughout the LiDAR swath area and for each of the plots across the landscape.

For the Injune multi-scale predominant height calculation, the analyses were undertaken using square and rectangular assessment areas respectively, due to the secondary sampling unit layout (Figure 35). The first iteration of assessment begins with the centre secondary sampling unit (# 15), from which the predominant height was calculated based on all 10m cells. The second iteration then adds the 4 adjacent border secondary sampling units (5, 14, 16, and 25) to the selection set, and predominant height calculated. The third iteration selects the 3 x 3 matrix of secondary sampling units centred on secondary sampling unit 15. Subsequent iterations then include additional secondary sampling unit columns of three secondary sampling units on each side (6 in total included per iteration) moving outwards, until the 7<sup>th</sup> iteration calculates the predominant height using all 30 secondary sampling units. Note the outer row/column (for 2 sides) of 10 m cells with a height of 0 m was initially generated to capture any additional LiDAR swath returns caused by adverse aircraft movement. For this analysis, these cells were not used as these 10 m cells were outside the primary sampling unit area.

**Table 16: Multi-scale predominant height assessment buffer selection areas for NE Victorian plot locations.**

<b>iteration</b>	<b>Buffer circle area (ha) (radius (m))</b>	<b>Mean number of 10m cells assessed (&gt;2m height)</b>
1	0.1 (18)	9
2	0.5 (40)	48
3	1.0 (56)	93
4	2.0 (80)	186
5	5.0 (126)	461
6	10 (178)	913
7	15 (219)	1324
8	20 (256)	1666

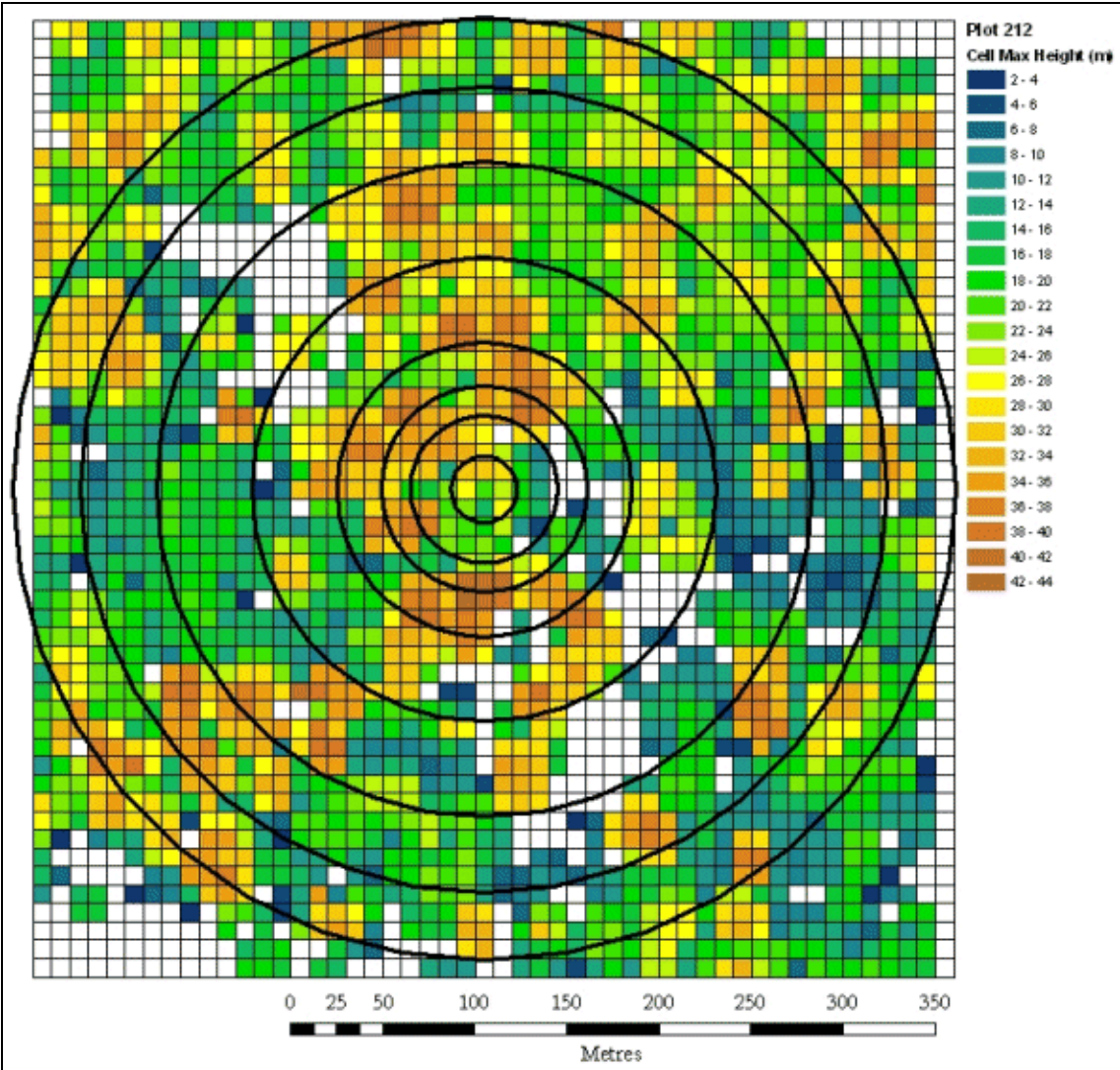


Figure 34: Multi-scale assessment of predominant height for NE Victorian sites, with example for plot 212 shown.

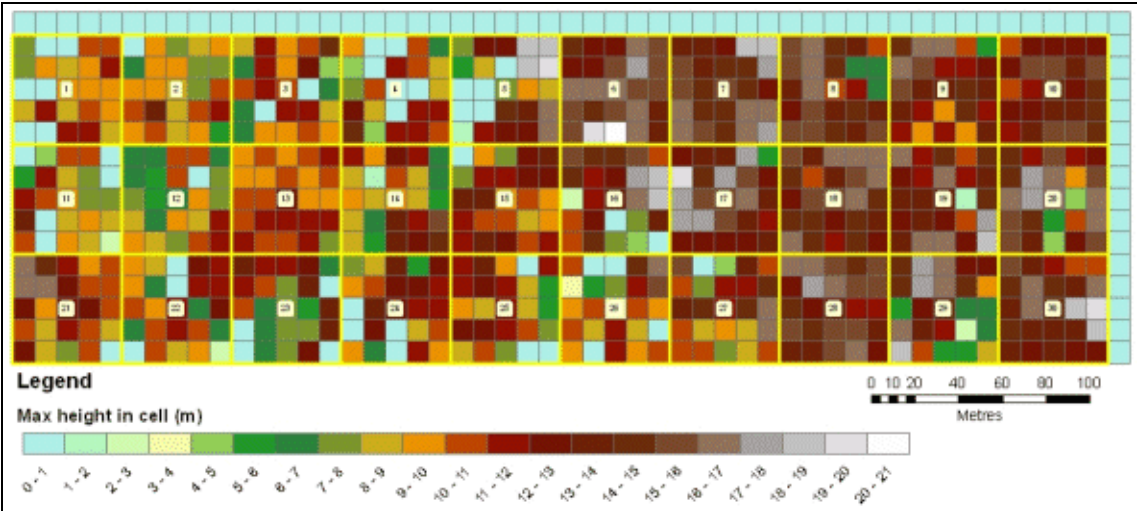


Figure 35: Example of predominant height assessment at a range of scales for Injune (PSU 142 shown, with 10m cells within 30 larger 0.25ha SSU's).

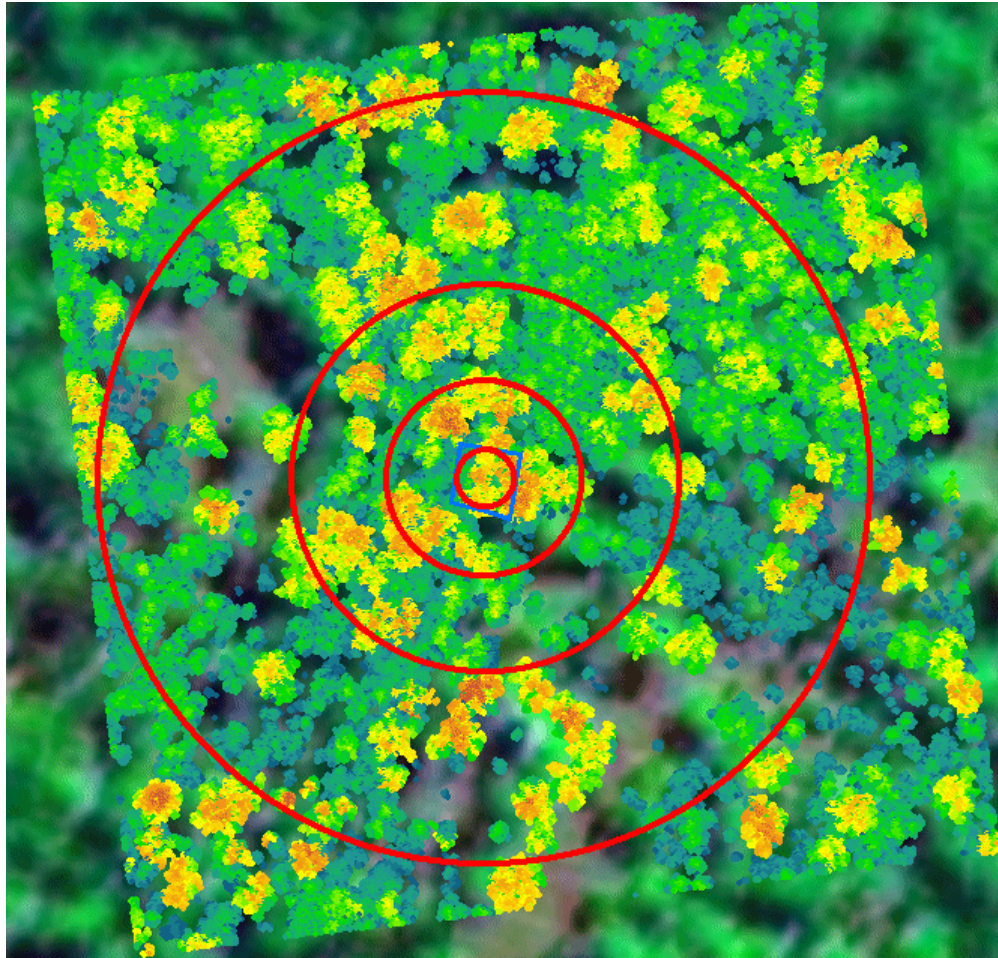


### ***Multi-scale canopy cover assessment***

In a similar process to that used with predominant height, the foliage-branch cover estimates were extended to the swath width using LiDAR at a known range of scales. This was due to the limitation of not precisely knowing the view extent of the hemispherical photography versus the LiDAR. The utility of LiDAR as a multi-scale dataset to compare to a range of other sensors was initially trialled on plot 220 in NE Victoria. At this location the trial of woody non-woody assessment was undertaken for the LiDAR swath area (522 ha), and used LiDAR, SPOT5, and an early version of the Australian Greenhouse Office (AGO) Landsat TM derived woody non-woody layer data as part of the CFMF pilot project. The hemispherical photo value was for the field plot area, to assess if the plot location and this data source were representative of the wider stand.

Subsequently the LiDAR analyses were extended to investigate how foliage-branch cover estimate changed with an increasing circular assessment area, for all plot locations in NE Victoria, and using the full extent of the LiDAR data (approx 400 m x 400 m). The analysis utilised vector rings of increasing radius up to 220 m, to approximate the full swath extent, and which were intersected with the LiDAR point data. Foliage-branch cover was then calculated as the proportion of LiDAR returns  $> 2$  m height above ground, with respect to all returns. Assessment rings were generated in 10 m radius increments, with the addition of 5 m and 15 m rings to increase the spatial resolution of the assessment at finer scales.

For Injune, various sized rectangles were used instead of circles due to the rectangular shape of the primary sampling unit (Figure 35). The Y distance incrementing by 10 m, with 5 and 15 m distance measurements also included to increase the spatial resolution of the assessment at finer scales. The Y distance reached a maximum distance of 150 m, to assess the whole primary sampling unit. It was observed that the X distance of the assessment rectangles were equal to the Y distance multiplied by 3.333.



**Figure 36: Illustration of the multiple scales of FBC circular assessment for NE Victorian plots. LiDAR (2m+) for plot 212 has red/orange colour as highest returns (~ 40 m), with lowest non-ground dark blue. Background image was Landsat ETM.**

### *LiDAR and API crown cover comparison*

Historically, estimates of cover derived from API have been the primary source of information for NFI reporting. However the categorical nature of the estimates can cause difficulties in translating and calibration with other sources or types of forest cover data. The mid-point of the API cover class was chosen as the variable to correlate with a LiDAR derived crown cover estimate, as it provides an indication of the relative accuracy of the cover interpretation. The limitation of this method was that it likely introduces bias as it was derived from a categorical classification, and especially in classes with a large range. The mean and range of LiDAR derived crown cover was calculated using 25 m cells within the API polygon. For this analysis the API polygon extent could range from being smaller than the LiDAR primary sampling unit, to being much larger (Figure 11). As a result, the comparative analysis

included an assessment of the coverage of LiDAR crown cover cells within the API polygon, to investigate if less LiDAR coverage within the polygon also led to a less accurate comparison of cover. The classes chosen for this were arbitrary, but selected such that there was useful class distinction for making assessments about the results, given the difficulties in comparing categorical interpreted data with empirically based crown delineations.

### ***Crown Separation method test***

The current nationally consistent crown cover estimation method as developed by Walker *et al.*,(1988) and Penridge and Walker (1988), was presented in the field survey handbook for soils and vegetation (McDonald *et al.*, 1998). One of the stated limitations of the method was having accurate and realistic crown cover maps with which to calibrate and test the range of assumptions that were inherent in the method (Penridge and Walker, 1988). The development of LiDAR derived crown delineations allows some of the methodological assumptions to be examined in more detail, for both similar and different environments to that used in Penridge and Walker (1988). However, it was beyond the scope of the thesis to undertake a full assessment for all field plots.

An initial comparison was done using two field plots at the Injune field site. This study area was chosen as it has a wider range of consistently collected cover data. One plot (p142-13) was selected that closely matches the environment used to develop the crown separation zig-zag method, namely grazed poplar box (*Eucalyptus populnea*) woodland in central Queensland. The second plot (p81-16) was selected to test the robustness of the crown separation method in a more challenging forest (mature *Angophora-Callitris* woodland with dense understorey of regenerating *Acacia*, *Lysicarpus*, and *Callitris*), whilst still being in the same general landscape (the two plots were 25 km apart). The primary assumption behind the comparison used in this thesis was that the LiDAR tree crown delineations were an accurate representation of the tree crowns, and as would be observed in the field. The crown separation comparison test uses a combination of field data and LiDAR crown delineation. The field stems points were used to determine the zig-zag transect path, and the LiDAR crown delineations were used to calculate

the actual lengths of crown and inter-crown gap along the transect, as per the McDonald *et al.*, (1998) method description.

### 3.6.3 Landsat cover investigation and validation

This section outlines a potential strategy using LiDAR to test and calibrate foliage projective cover at the scale of a Landsat pixel. The methods for extracting foliage projective cover from Landsat data by the SLATS program were described in Chapter 2. SLATS utilises an extensive program of field checking and continuous research into improving the cover products (Lucas *et al.*, 2006b). One aspect of the calibration process was the translation of field data foliage cover to a Landsat TM pixel, where there may be an issue from differences in scale between field transect calibration data and its application to the larger Landsat TM pixel.

Hemispherical photo analyses and LiDAR data sample both the photosynthetic foliage, and non-photosynthetic branch and trunk canopy components, yet it was only photosynthetic material that satellite imagery generally responds to. Therefore, there was a difference between satellite foliage projective cover (such as Landsat), and foliage-branch cover (LiDAR and hemispherical photo observations). With the LiDAR individual crown delineation methods developed in this research, it was now possible to develop consistent translation functions between foliage projective cover, foliage-branch cover and crown cover, thus expanding on existing knowledge (e.g., Specht and Specht, 1999).

The method used to assess the suitability of LiDAR data for calibration was described in the following section. Here, the assumption was made that LiDAR derived foliage-branch cover was close to field based estimates of foliage projective cover and foliage-branch cover, as described in Section 3.3.2. This assumption will be tested with the results presented in Chapter 4, and in the implications discussed in Chapter 5. There were four main stages to the foliage projective cover calibration strategy. First, the Landsat TM derived foliage projective cover layer was used to generate a pixel vector layer, based on the individual raster pixels (Figure 37). Second, the vector 'pixel' layer was used to assign an identification code (pixel-ID) to the LiDAR point data, and the percentage of canopy returns within each pixel area was calculated

(Figure 38). Foliage-branch cover was calculated for canopy returns at 0.5 m (vegetation cover) and 2 m height (forest cover) thresholds. Third, the pixel-ID assignment was repeated for LiDAR mapped stems, to investigate linkages between stem density (per hectare) and foliage projective cover (Figure 39). Finally, the LiDAR-derived crown delineations were clipped within each pixel and tree crown cover was calculated (Figure 40).

The four-stage process was undertaken for 12 primary sampling units that contain field plot data. Any Landsat pixels that were only partially covered by LiDAR data were excluded, giving a final total of 1,161 individual assessment pixel ‘cell’ polygons for comparison. Across the assessment cells the mean return sampling density (all returns) was 1 return per 0.54 m<sup>2</sup> (max – 1 return per 1.49 m<sup>2</sup>, min - 0.14 m<sup>2</sup>, standard deviation - 0.2 m<sup>2</sup>).

It was subsequently noted that a number of cells had Landsat TM foliage projective cover higher than LiDAR crown cover, especially in the lower cover range (see Results chapter). Conceptually this was a logical inconsistency, as with a 2D representation of cover the foliage projective cover should always be less than or equal to crown cover, assuming an opaque crown. Therefore, it appears that foliage additional to that found within the tree crowns was being included in the SLATS foliage projective cover estimate, most likely from shrubs and grasses. In order to provide an appropriate calibration for tree “forest” cover, all cells where foliage projective cover > crown cover by more than 2 % were excluded, and the remaining set (855) used to develop the calibration and validation subsets. The function calibration subset consisted of 80 % randomly selected 25 m cells, with the validation set using the remaining 20 % of randomly selected cells.

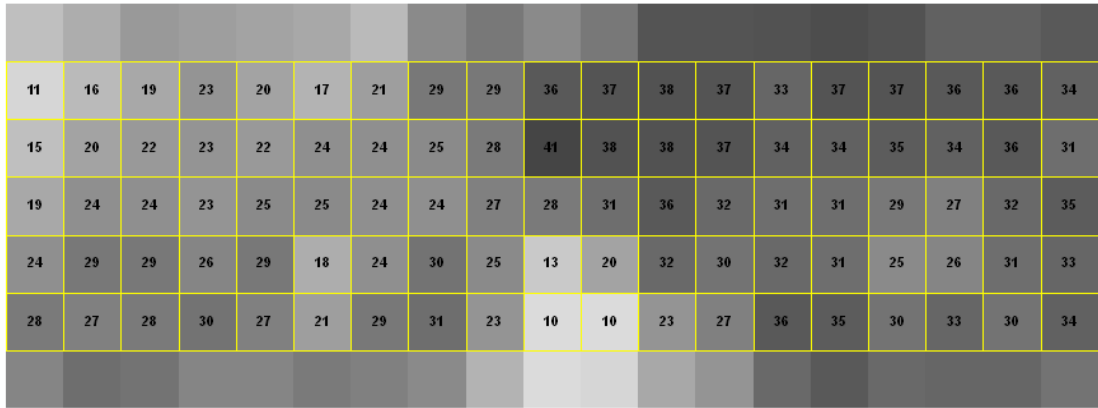


Figure 37: Vector pixel layer example for PSU 142, derived from Landsat SLATS FPC grid (background). Values within cells indicate FPC.

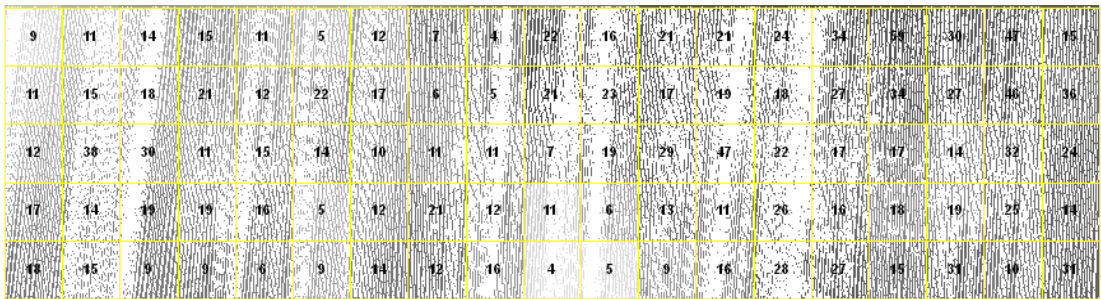


Figure 38: LiDAR return density (all returns) for PSU 142. Values within cells indicate LiDAR FBC.

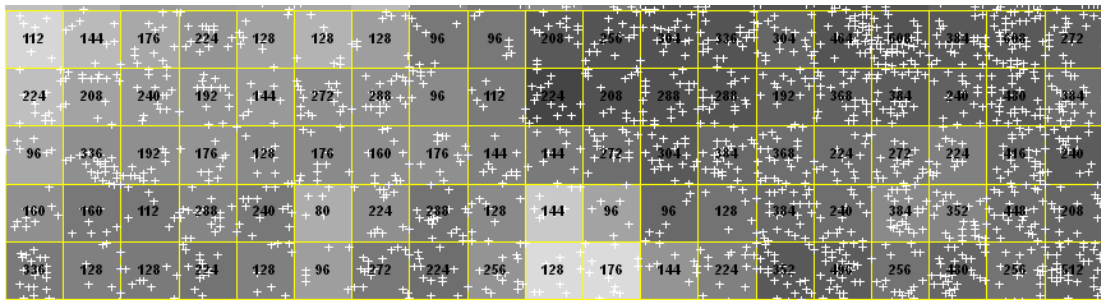


Figure 39: HSCOI derived stems for PSU 142. Values within cells indicate stem density per FPC pixel (stems per hectare).

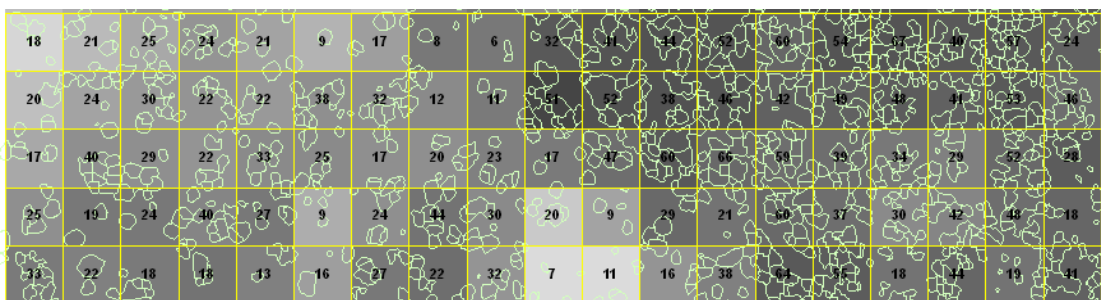


Figure 40: HSCOI derived crown delineations for PSU 142. Values within cells indicate LiDAR crown cover percent per pixel area.

### 3.6.4 ICESat calibration with airborne LiDAR

Chapters 1 and 2 identified the ICESat platform (and associated laser sensors) as a possible solution to the lack of a continental-wide, consistently collected height data source for Australia. Therefore, to investigate the potential for ICESat data to meet this requirement, ICESat data were intersected with the LiDAR transects and a total of 27 overlap locations in NE Victoria were found (Figure 41). The locations cover a wide range of environments, from Floodplains, Foothills, to Montane and Subalpine sites. Land cover varies from dense and closed forests to open woodlands, as well as cropping, horticulture, and grazing. At each overlap site, ICESat footprints were selected that were completely within the airborne LiDAR swath, and which assumed an approximate footprint size of 50 x 75 m, but which varied depending on the collection date. This resulted in a total of 94 individual footprints. For the purposes of this thesis, a case study using three of the initial 94 footprints were selected to highlight the use of LiDAR for calibration. The processing of the LiDAR for calibration and comparison is described in the following sections. The full assessment of all 94 footprints was reported in Lee *et al.*, (2006).

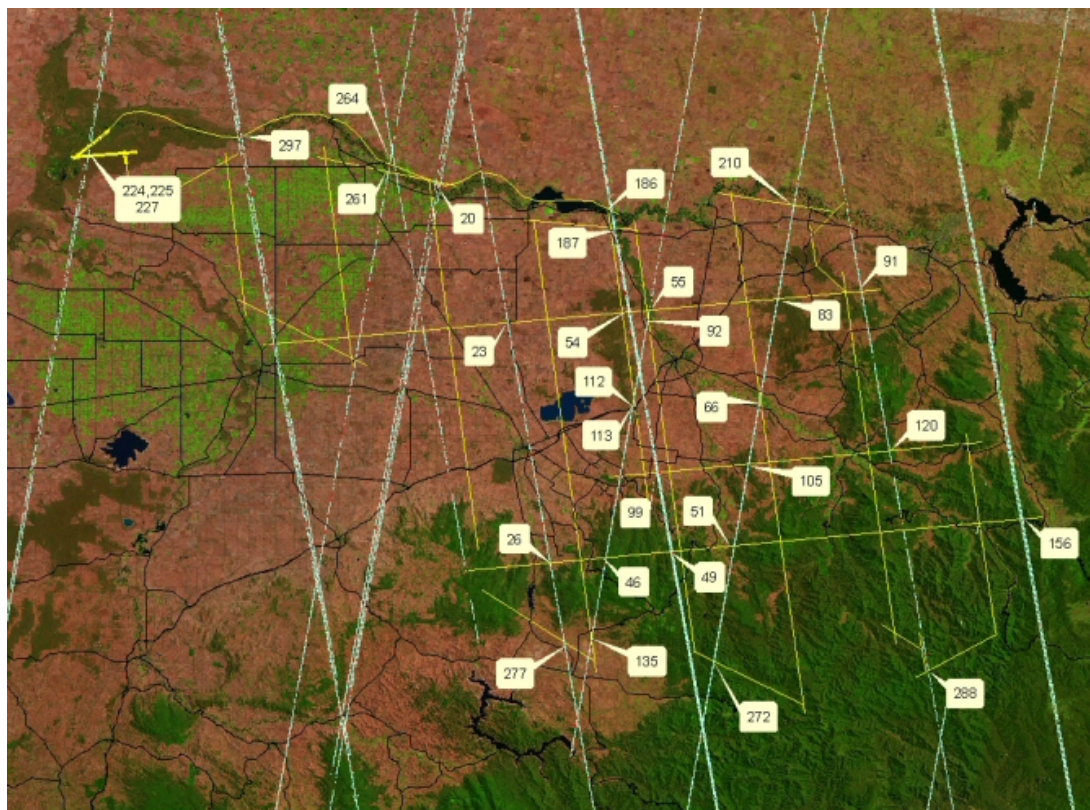


Figure 41: ICESat transects (light blue) with the airborne LiDAR transects (yellow) and numbered overlap locations across CFMF pilot region in NE Victoria.

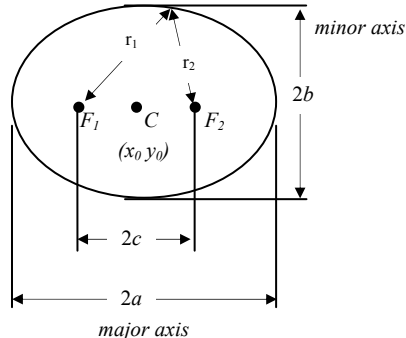
### ***Vegetation comparisons***

Vegetation comparisons required a number of processing stages. First, calculation of approximate ICESat footprint size and shape were undertaken, which allowed representation of the footprint using airborne LiDAR. Second, a range of terrain and vegetation information were extracted from the LiDAR data (such as elevation, slope, predominant and maximum height, canopy cover), within the estimated footprint area. The extracted LiDAR information was then compared with the respective ICESat data.

### ***ICESat footprint derivation and attribute extraction***

To enable the most accurate comparison, the footprint shape and size needed to be accurately portrayed. Data on this was extracted from the ICESat data by Peter Scarth (Lee *et al.*, 2006), and this allowed the most effective selection of the airborne LiDAR data. The formulae used to model ICESat footprint were given in Table 17, using the parameters extracted for each footprint, as listed in Table 18. The parameters were then used to work out which airborne LiDAR returns were within the footprint area. To do this the variables were extracted and calculated, as shown in Table 19.

**Table 17: Formulae utilised for footprint dimension and area calculations:**

 <p><b>Illustration of the major and minor axes for an ellipse</b></p>	$b = \alpha \sqrt{1 - e^2}$ $= \sqrt{a^2 - c^2}$ $c = \sqrt{a^2 - b^2}$ $= \frac{a e}{e}$ $e = \sqrt{1 - \frac{b^2}{a^2}}$ $= \frac{c}{a}$ <p><b>Major and minor axes, and eccentricity (e) derivations</b></p>
$A = \frac{2 \pi}{\sqrt{4 a c - b^2}}$ <p><b>Area of an ellipse – used to cross-check spatial mapping footprint area estimate.</b></p>	



**Table 18: ICESat attributes extracted for comparison with airborne LiDAR.**

Attribute name	Code name in data	Description
Azimuth	tpazimuth	The orientation (from north) of the major axis of the elliptical footprint
Eccentricity	tpeccentri	Gives the shape of the footprint, where values close to 0 give a circle, and close to 1 give a flattened ellipse.
Ellipse major axis	tpmajoraxi	The length (m) of the major axis of the ellipse
Intensity	tpintensit	Intensity of returned pulse
Footprint date	J2000	Julian day from 12pm, January 1 <sup>st</sup> , 2000
Reflectance	reflectance	Amount of energy returned to the satellite
Vegetation reflectance	veg_ref	Proportion of reflectance assumed to be from the non ground waveform peaks
Ground reflectance	gnd_ref	Proportion of reflectance assumed to be from the ground waveform peak
Foliage Projective Cover	veg_fpc	Percentage cover – values range from 0 to 1, with 1 = 100% cover
Centroid height	centroid_ht	Distance from centre of the ground pulse to the centre of the highest veg pulse
Fit height	fit_ht	The third parameter ( $\beta$ ) in the weibull distribution used to fit the cumulative vegetation profile - $(\beta[1]*\exp(-\beta[2]*(\text{height}_x/\beta[3])^{\beta[4]}))$
Veg height	veg_ht	Height where the cumulative FPC greater than 2m crosses 95%
Slope	DEM_slope	In version r_28 of the ICESat data, the SRTM slope was extracted. As this was not done for the r_26 version, then airborne LiDAR derived DEM (1m) slope was utilised instead. This slope was calculated as the mean of slope estimates from a number of 20 x 20m cells that covered the footprint area.

**Table 19: Variables extracted or calculated for footprint size estimation.**

Variable name	Source or calculation	Notes
azim_degree	Icesat item 'tpazimuth'	Azimuth value
azim	[calc 90 - %azim_degree%]	Calculate the offset angle of major axis from horizontal
eccent	Icesat item 'tpeccentri'	Eccentricity value
majorax	Icesat item 'tpmajoraxi'	Diameter of major (long) axis
major_rad	[calc %majorax% / 2]	Radius of major (long) axis
minor_rad	[calc ( %majorax% / 2 ) * [sqrt %min1% ]]	Radius of minor (short) axis
min1	[calc ( 1 - ( %eccent% * %eccent% ) ) ]	Component of minor radius calculation

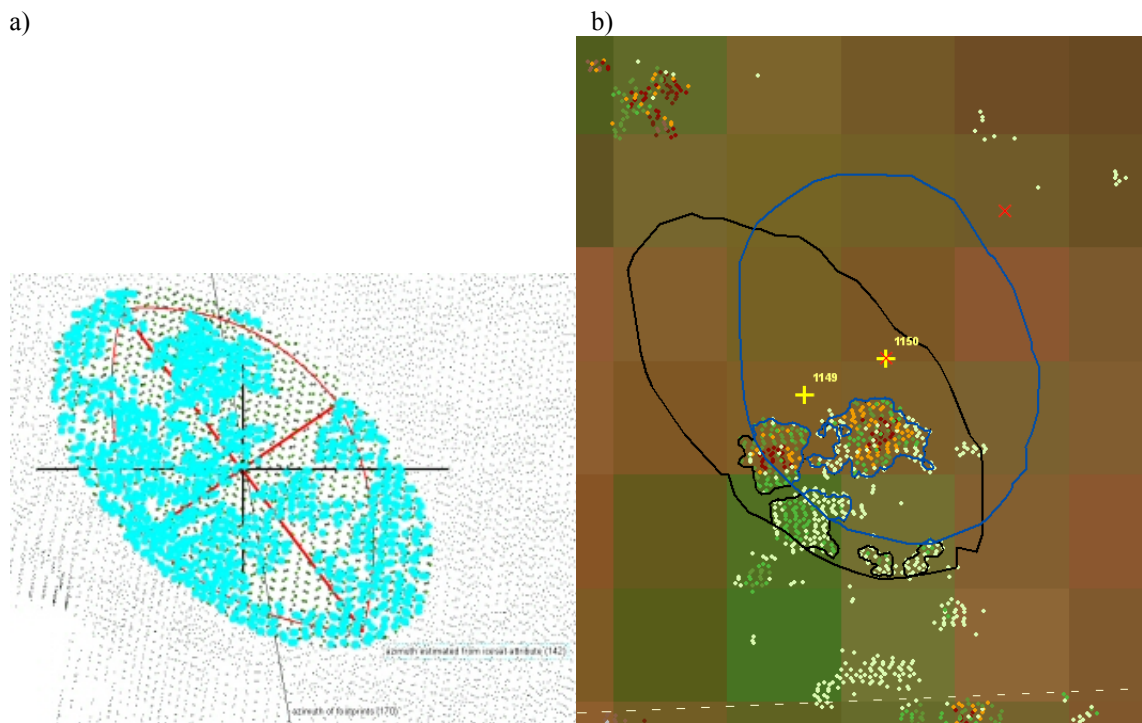
The ICESat footprint centre point coordinates (in geographic decimal degrees (Lat/Long)) were then extracted and reprojected into UTM (GDA94) coordinates (metres), to be used with the airborne LiDAR. The location of each LiDAR return in the area around the footprint was then assessed, and the distance from return location and the ICESat centre point calculated (Table 20). If the LiDAR return was found within the elliptical area of the footprint, then it was coded with the ICESat point ID. In this way, all points within the footprint could be

selected. Where multiple footprints (from different dates) occurred in close proximity, a LiDAR return could fall within the elliptical area of more than one footprint. If this occurred, then the footprint ID was assigned to additional items in the LiDAR spatial database. Up to five ICESat footprint IDs for each return could be accommodated with the current algorithm.

**Table 20: Assignment of LiDAR returns within ICESat footprint**

Variable name	Source or calculation	Notes
Calculate the rotated coordinate system orientation - this was the rotation of the ellipse clockwise from 90 degrees in radians		
x1	[calc %LiDAR_x% - %x_cntr% ]	LiDAR_x = x coordinate, and x_cntr was the ICESat centre x coordinate
y1	[calc %LiDAR_y% - %y_cntr% ]	LiDAR_y = y coordinate, and y_cntr was the ICESat centre y coordinate
azim_rad	[calc 0.0174532925 * %azim%]	convert offset angle to radians
cos_az	[cos %azim_rad%]	result in radians
sin_az	[sin %azim_rad%]	result in radians
x_chk	[calc ( %x1% * %cos_az% ) + ( %y1% * %sin_az% ) ]	
y_chk	[calc ( %y1% * %cos_az% ) - ( %x1% * %sin_az% ) ]	
Calculate the relative distance of the returns from centre to ellipse boundary - if %chk_dist% less than or equal to 1, then it was within ellipse area, and the LiDAR return was coded with the ICESat ID.		
chk_dist	[calc ( ( %x_chk% * %x_chk% ) / ( %major_rad% * %major_rad% ) ) + ( ( %y_chk% * %y_chk% ) / ( %minor_rad% * %minor_rad% ) ) ]	

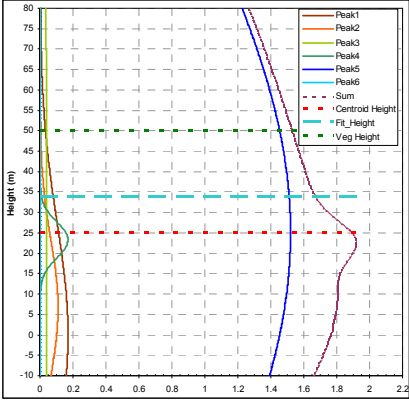
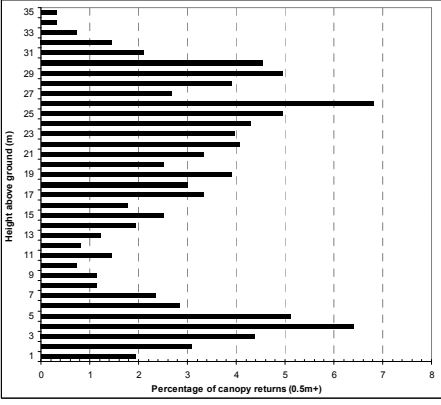
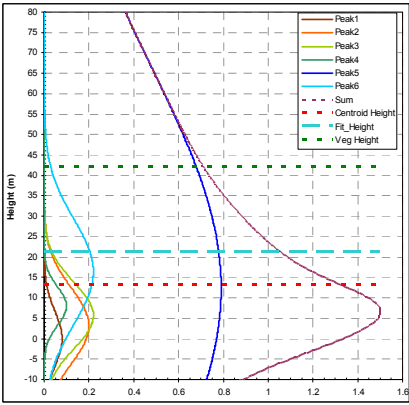
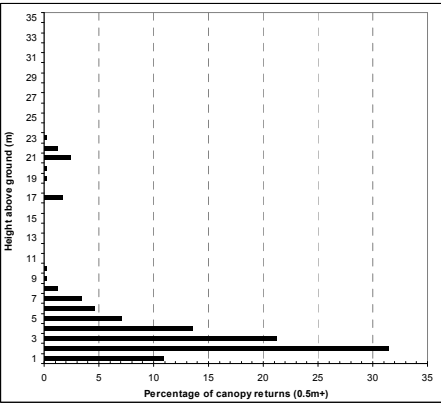
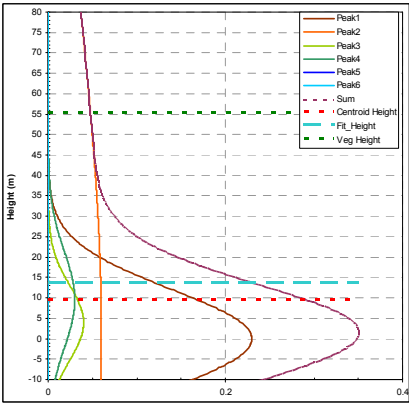
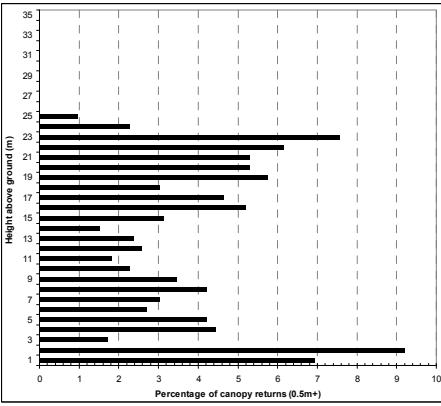
The development of the LiDAR point extraction within an ICESat footprint initially used a location in red gum forest near the Murray River (Figure 42a). Once the parameters had been modelled correctly, all footprints were extracted from within the available LiDAR data. Different footprint shapes were found with different dates of collection, highlighted with an example from the Foothills south of Wangaratta (Figure 42b). In the example, the black footprint was collected in November 2003, and the navy footprint was collected in March 2004, with yellow crosses indicating the respective footprint centres. The background image was the AGO Landsat TM mosaic from 2002 (25 m cells), and the LiDAR returns were coloured by height above ground (blue/green is 2-5 m, orange-brown are taller tree tops ~12-15 m). Vectors generated from the airborne LiDAR tree crown delineation routines enclose the LiDAR returns.



**Figure 42: Examples of the ICESat footprint size and shape attributes derived using airborne LiDAR. a) single footprint with returns that are within the footprint (black) and over 2m in height (light blue); and b) two footprints from different dates showing different shapes due to different laser sensors used.**

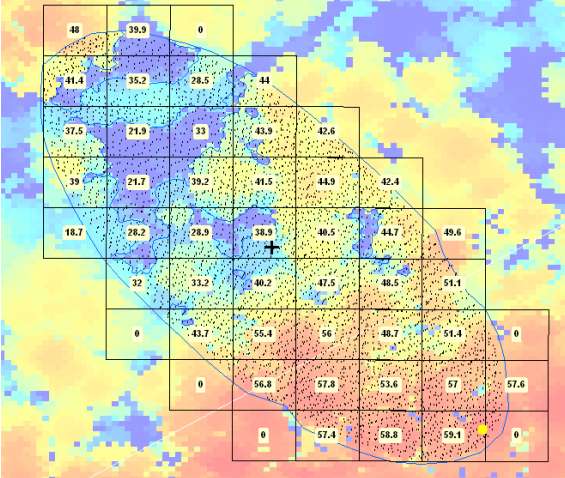
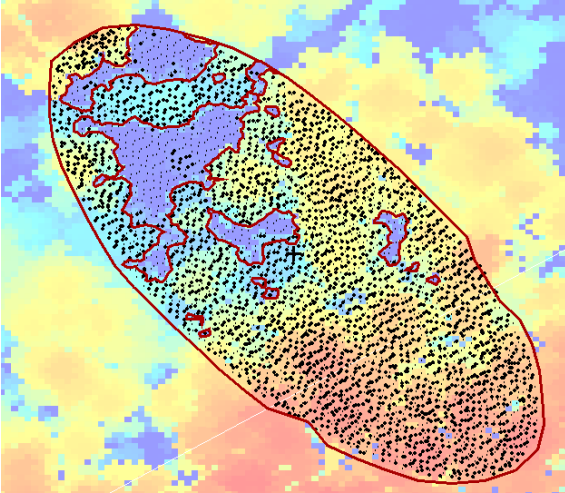
A location approximately 30 km south of Benalla in NE Victoria was chosen as the case study site to examine the potential effects of slope and vegetation density on the extraction of ICESat height and cover attributes. The ICESat waveforms were extracted using the spreadsheet developed by P. Scarth (QDNRM), and then compared to the airborne LiDAR return data and apparent vertical profiles (Table 21). Note that the vertical height scales (Y-axis) between the ICESat and LiDAR profiles were different. Empirical results of the case study comparison are presented in Chapter 4. Table 22 outlines the concept and brief description the different terrain and vegetation attributes calculated using airborne LiDAR that were used to calibrate the extracted ICESat values.

**Table 21: ICESat case study footprints; description, full waveform, and LiDAR apparent vertical profiles**

Case Study Footprint details	ICESat waveform profile	LiDAR apparent vertical profile
<p>ICE-id: 484</p> <p>Collection date: 6-10-2003</p> <p>Major axis length: 89 m</p> <p>Elevation: 304.9 m (asl)</p> <p>No. of LiDAR returns: 1233</p> <p>Location (DD) Latitude: -36.809288 Longitude: 146.04567</p>		
<p>ICE-id: 480</p> <p>Collection date: 6-10-2003</p> <p>Major axis length: 89 m</p> <p>Elevation: 313.9 m (asl)</p> <p>No. of LiDAR returns: 413</p> <p>Location (DD) Latitude: -36.810833 Longitude: 146.04591</p>		
<p>ICE-id: 475</p> <p>Collection date: 6-10-2003</p> <p>Major axis length: 89 m</p> <p>Elevation: 328.8 m (asl)</p> <p>No. of LiDAR returns: 923</p> <p>Location (DD) Latitude: -36.81237 Longitude: 146.0462</p>		

**Table 22: Description of LiDAR attributes utilised for ICESat calibration and validation**

Attribute	Description	Illustration (using ALS tile 288, ICESat ID 71)
Elevation	<p>Elevation for the ICESat footprint was assessed using the mean ground elevation (metres above sea level), across the whole footprint. For the footprint shown in the illustration (right), this means the elevation result value was approximately half way up the slope within the footprint area.</p>	
Mean Slope	<p>The first slope attribute was mean slope (degrees). This was calculated as the mean of a number of 20 m cells that cover the footprint area within the 1 m DEM. Slope was calculated across each 20m cell. In the illustration, the cells shown are 10m (for mean height). The cells used for slope equate to 4 adjacent 10 m cells.</p>	
Absolute slope	<p>The second slope attribute was absolute slope (degrees). This was the maximum slope within the ground elevation range. It was calculated as the slope of the max ground elevation difference (rise) against the mean diameter of the footprint (mean of X and Y coordinate distance max minus min) (run).</p>	
Elevation range	<p>The greatest elevation difference (m) within the footprint, and was calculated as the max vegetation elevation minus minimum ground elevation.</p>	

<p>Max height</p> <p>Mean height</p> <p>Height variability</p>	<p>Maximum vegetation height (metres) - was the highest LiDAR return found in the footprint. Within illustration (right), this was shown with the yellow highlighted return (lower right corner). The 1 m spatial resolution top of canopy height grid was shown, coloured from dark blue (0m) through to red (60m).</p> <p>Predominant vegetation height (metres) - was calculated as the mean of the heights from 10m cells across the footprint. The maximum height in each 10m cell was first calculated. A cell needs to have LiDAR returns across at least 20% of the cell area for the cell to be included in the mean height and standard deviation calculations. This was the reason for some cells on the edge of the footprint having a “0” for the cell maximum height.</p> <p>Canopy height variability (metres) was assessed using the canopy height standard deviation metric. This was the standard deviation of the maximum heights from each of the 10m cells used in the predominant height calculation.</p>	
<p>Vegetation Foliage Cover</p> <p>Forest Foliage Cover</p> <p>Crown Cover</p>	<p>Percentage vegetation foliage cover was calculated as the percentage of all (ground and vegetation) LiDAR returns that are 0.5m or greater in height. Because foliage and branches cannot be differentiated, then the cover was assumed to include both (FBC). The vegetation description refers to the fact that all canopy material taller than 0.5m was sampled, including shrubs and understorey, if present and observable through the overstorey.</p> <p>Percentage forest foliage cover was calculated as the percentage of all LiDAR returns that are 2 m or greater in height. Because foliage and branches cannot be differentiated, then the cover was assumed to include both (FBC). The forest description refers to the fact that only canopy material taller than 2m was sampled, therefore meeting the NFI height definition of forest. The illustration (right) shows returns 2m+ height as the larger black points.</p> <p>Crown Cover was the percentage of the footprint area that was delineated as tree crown. The delineation process uses a canopy density model and extracts a crown edge vector which bounds at least 90% of the canopy LiDAR returns that are 2m + height.</p>	

### 3.7 Summary

This chapter described the research design and methodology that addressed the limitations identified in Chapter 2. A multi-scale hierarchical strategy was described for using LiDAR to link fine scale field data with medium scale data. The strategy was developed in response to national level forest monitoring schemes that utilise a wide range of data, and at a range of scales. Therefore, there was a need to be able to calibrate and validate other data or measurement methodologies at the appropriate scale.

A range of methods were used to derive forest structural attributes at the plot scale, (e.g., height, cover, and growth stage through apparent vertical profiles), which were then compared to field estimates, with results presented in the Chapter 4. Using LiDAR to link consistently between different datasets (e.g., different field measurements, airborne and satellite imagery) at both study sites has allowed for the translation between structural metrics using continuous transfer functions. Methods for improving bare ground fine scale terrain models have been demonstrated, which should allow more precise estimates of tree height to be generated. Certain terrain locations that may cause issues for accurate tree height estimation have been noted, for example steep slopes and cliffs.

Scale theory suggests that an effective way to understand variation in plot scale results (both within the plot, and between plots) was through the use of basic geographic entities. Utilising this concept, a new method to generate structural information at a tree scale (crown and stem entities) from LiDAR data was presented. The Height Scaled Crown Openness Index (HSCOI) uses all canopy returns to calculate the relative penetration of the LiDAR, and output as a 2D raster layer. The HSCOI methods were designed to compliment current canopy height model algorithms, and also represent an advance by using all the LiDAR collected. The HSCOI layers represent high foliage density locations as minima on the surface. Subsequent GIS based hydrological drainage basin and local minima “sink” algorithms were used to generate assumed crown delineations and tree stem location outputs (including sub-canopy trees) at the locations of indicative high foliage density. These outputs were refined through the multi-scale application of spatial analyses using the raw LiDAR (including apparent vertical profiles)

combined with field data derived empirical functions. LiDAR modelled stems and crowns were then attributed with height, cover, and stem diameter values. The HSCOI modelling was further refined to produce component level data (branches and leaf clumps). This facilitates stand-wide reconstruction of the forest at scales fine enough for radar calibration at specific wavelengths, as different wavelengths interact with different tree components.

Methods to investigate the potential impact of assessment scale on reporting forest structure have been presented. These methods allow the comparison of plot estimates of height and cover to be directly compared to stand level estimates using the same data and metrics. This provides an indication of how representative a plot may be with respect to the wider stand or landscape. The methods also allow the assessment of a minimum area for reporting forest, by determining at what scale variation between plot and stand estimates were minimised.

The multi-scale hierarchical strategy using LiDAR has generated structural data that was used to calibrate and validate a number of different medium scale sensors. For example, SLATS Landsat TM derived foliage projective cover was compared with LiDAR foliage-branch cover, crown cover, and stem density. The comparison has also facilitated the investigation of a foliage projective cover-to-crown cover translation function. This function should provide for improved national level data use, as data can be translated without the need for broad categorical classification, thus allowing more sensitivity to change when utilised in monitoring schemes. LiDAR data was used to investigate the extraction of forest stand height and cover from ICESat. A case study was designed to test how terrain and foliage density may impact on the accuracy of the extracted attributes.

The next chapter outlines the results of the methodology with reference to field data and other remotely sensed information. The results of the methodology described here will enable the primary thesis research question to be addressed, and therefore determine how LiDAR can improve forest structure assessment in Australia.



---

## CHAPTER 4. RESULTS

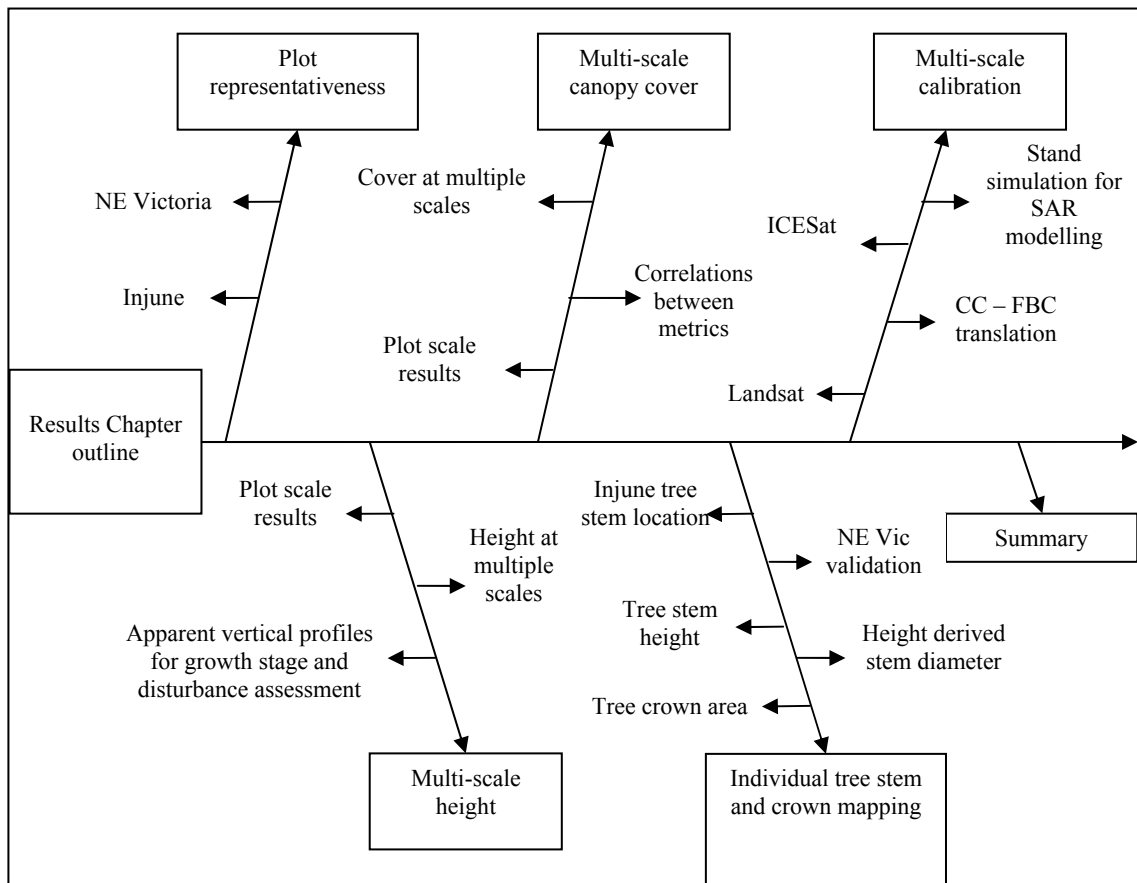
---

### 4.1 Introduction

The preceding chapter outlined the methods utilised in the development of a multi-scale LiDAR strategy to enhance the assessment of Australian forest structure (primarily height and cover), within integrated sampling schemes. This chapter presents the results of this research (Figure 43), focusing specifically on:

- a) Plot scale assessments of height and cover, with comparisons between metrics, datasets, and at a range of different scales;
- b) The representativeness of field plots with respect to landscape estimates using NFI national scale forest data;
- c) The results of the basic geographic entity modelling, at both tree and component scales, for stem location, density, height, and crown area. Above ground biomass is utilised to assess the results of the tree component modelling;
- d) The tree scale results that are used to calibrate other data, including Landsat foliage projective cover, ICESat, and stand reconstructions for SAR simulation modelling. An investigation of different transfer functions for a range of cover metrics is also presented.

The research is focused primarily at the Injune study site, with some initial comparison, validation, and scale specific evaluations undertaken at the NE Victorian site. In this chapter section 4.2 outlines the plot representativeness with respect to the wider landscape. Section 4.3 describes the results of plot and stand scale height analyses, with 4.4 describing the plot and stand scale cover analyses. Tree scale results from the Height Scaled Crown Openness Index are presented in section 4.5, with the multi-scale calibration examples illustrated in section 4.6. The chapter is summarised in section 4.7 (Figure 43).



**Figure 43: Layout of the Results chapter showing the major components of the strategy for using LiDAR to improve forest structure measurement.**

## 4.2 Field Plot Representativeness

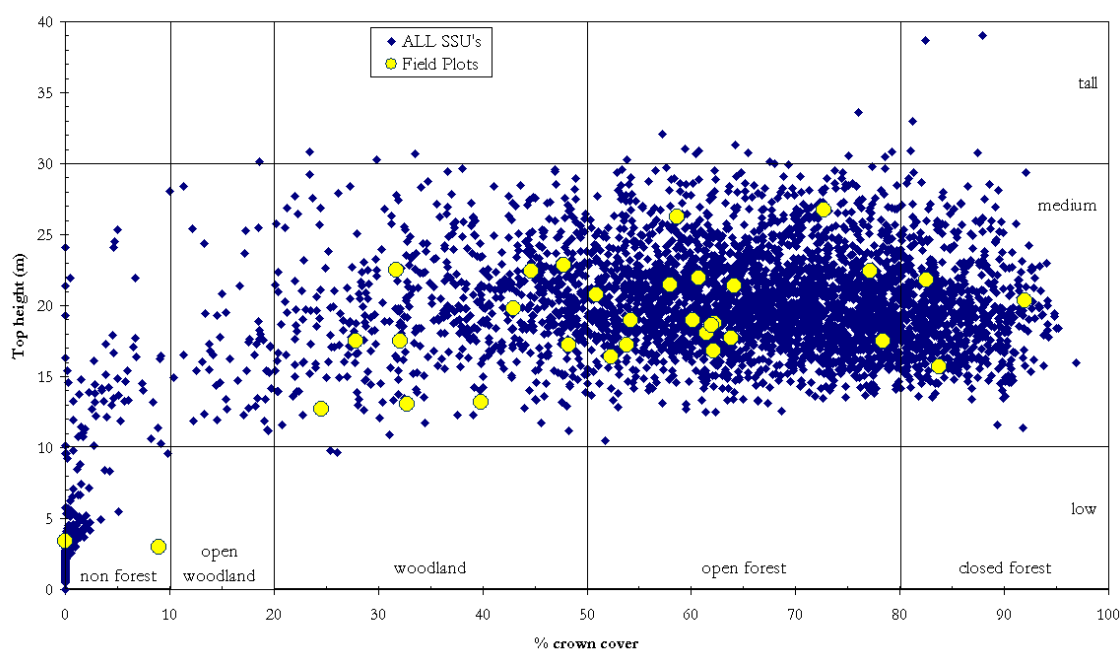
The Injune field plots achieved (i.e. within 5 %) the representativeness aims of the original sampling strategy, when compared to the distribution of forest structure from all 4500 secondary sampling units (Figure 44). Medium open forest is adequately represented by the field plots (4.3 % difference, Table 23); although the plots over and under-represent medium woodland (16.5 %), and medium closed forest (-6.8 %) respectively (Table 23). Non forest (including open woodland) is under-estimated (-4.7%) although the focus of the sampling strategy was on forested sites (as described in Chapter 3). Height comparisons with NFI data indicate that the different datasets broadly agree (i.e. within 5 %), but with some under-estimation of non forest by the LiDAR estimate at both plot and landscape sample scales (Table 23). Cover comparisons with NFI data indicate major differences between woodland and open cover categories. Were the classifications swapped, then the difference between the 4500

LiDAR secondary sampling units and NFI data estimates would be less than 10%, except for closed forest (~16 %). In NE Victoria, the field plots were considered broadly representative (within 10%) for non forest and woodland when compared to the NFI data, although the field plot LiDAR under -estimated tall and open forest, whilst over-estimated medium and closed forest (Table 24).

**Table 23: Representativeness of Injune forest structure sampling, comparing LiDAR from 4500 SSUs across the landscape with LiDAR from field plots (in parentheses), by NFI class.**

NFI Height class	NFI Cover class				Total %*	NFI 2003 (%)*
	Non forest %	Woodland %	Open %	Closed %		
Tall %	0 (0)	0.1 (0)	0.3 (0)	0.1 (0)	0.5 (0)	0
Medium %	2.4 (0)	14.8 (31.3)	57.4 (53.1)	16.2 (9.4)	90.9 (93.8)	86.6
Low %	5.0 (6.3)	0 (0)	0 (0)	0 (0)	5.1 (6.3)	1.6
Non Forest %	3.6 (0)	0 (0)	0 (0)	0 (0)	3.6 (0)	11.7
Total (%)*	11.0 (6.3)	15.0 (31.3)	57.7 (53.1)	16.3 (9.4)		100
NFI 2003 (%)*	11.7	68.2	20	0		

\* Totals may not sum to 100% exactly due to rounding.



**Figure 44: Comparison of the LiDAR structural (height and cover) range of field plots and all SSU's**

**Table 24: Representativeness of NE Victorian forest structure sampling, comparing continental NFI data with field plot LiDAR (in parentheses).**

NFI Height class	NFI Cover class				Total %
	Non forest %	Woodland %	Open %	Closed %	
Tall	0 (0)	0.6 (0)	13.8 (0)	0 (10.3)	14.4 (10.3)
Medium	0 (0)	2.0 (2.6)	18.3 (15.4)	0 (15.4)	20.3 (33.3)
Low	0 (0)	0.1 (0)	0.2 (0)	0 (0)	0.2 (0)
Non Forest	63.2 (56.4)	0 (0)	0 (0)	0 (0)	63.2 (56.4)
Total	63.2 (56.4)	2.7 (2.6)	32.3 (15.4)	0 (25.6)	100

\* Plantations (1.9%) from NFI study area data included in total, but removed from table for clarity

### 4.3 Multi-Scale Height Results

This section presents forest height estimates (maximum height, predominant height) at plot, stand, and landscapes scales. Comparisons are made between field-measured and LiDAR derived height metrics, and LiDAR measures only based on swath scale data (for stands) or an aggregation of plot or stand scale assessment units for stand and landscape scales respectively. The evaluation also considers assessments of growth stage and disturbance evaluations from apparent vertical profiles. Individual values per plot are presented in Appendix A - Table 56 for Injune, and Appendix A – Table 57 for NE Victoria.

#### 4.3.1 Plot scale height results

##### *Maximum canopy height*

At the both the plot and overstorey tree level at Injune, LiDAR was found to be a very robust method of accurately determining maximum height, with initial comparisons indicating strong relationships between field and LiDAR estimates (Table 25, Figure 45). For 100 manually selected overstorey trees that were well separated and taken from a range of field plots, an  $r^2$  value of 0.91 was observed (Tickle *et al.*, 2006).

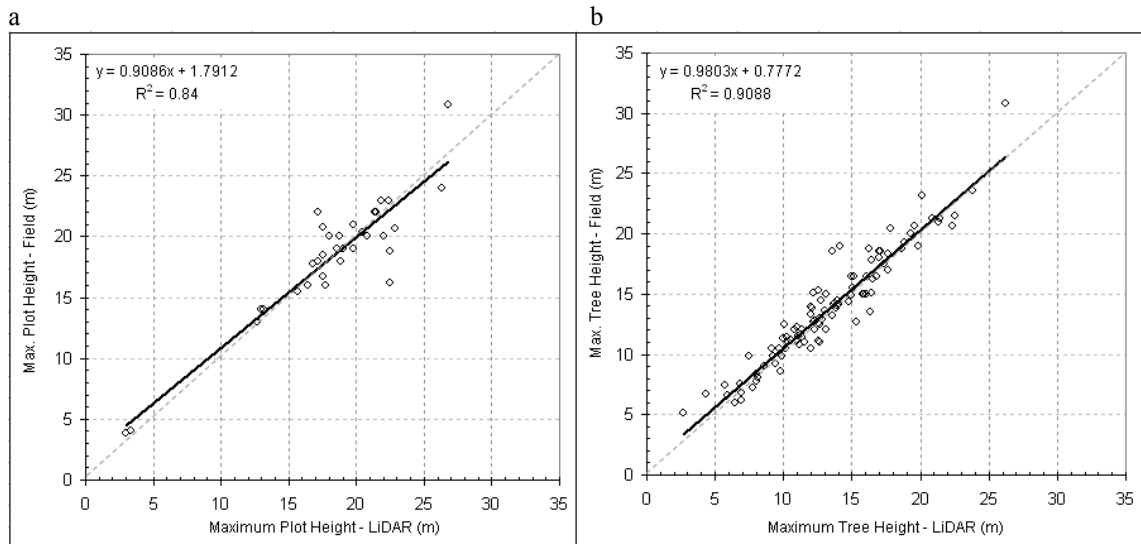
**Table 25: Maximum height comparison between field and LiDAR for Injune and NE Victoria plots**

Description	n	R <sup>2</sup>	RSE	function <sup>a</sup>	P-value
Injune selected overstorey trees <sup>b</sup>	100	0.91	1.38	$Y = 0.9803x + 0.7772$	0
Injune field plots	33	0.84	2.05	$Y = 0.9086x + 1.7912$	$7.15e^{-14}$
NE Victorian field plots	22	0.76	3.75	$Y = 0.7204x + 4.9137$	$1.052e^{-7}$
NE Victorian transect areas	21	0.68	5.49	$Y = 0.7528x - 0.3480$	$4.762e^{-6}$

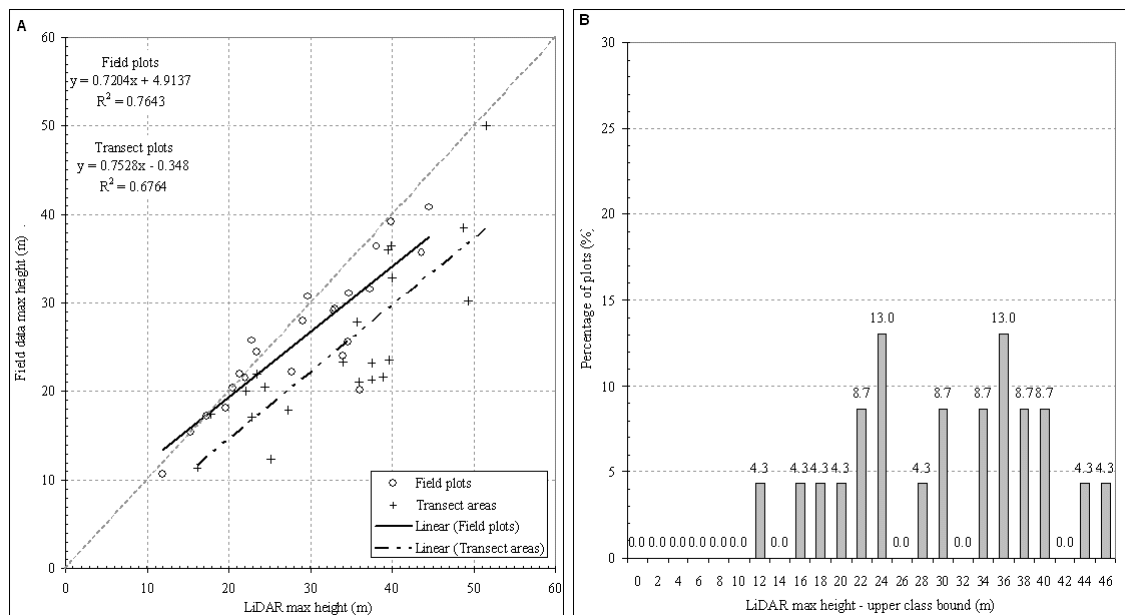
<sup>a</sup> –  $y$  = field data,  $x$  = LiDAR value

<sup>b</sup> – from Tickle *et al.*, (2006)

The field and LiDAR comparison of top height per plot (circle), and transect area (cross) for all NE Victorian field plots indicates that, generally, the plot data has good agreement ( $r^2 = 0.76$ ) between the field and LiDAR data (Table 25, Figure 46a). There are a few plots where the LiDAR maximum height is greater than height recorded in the field data (by up to 15 m), with this most evident in plots where individual trees were taller than 30 m. The sampling transects for the wider one hectare area have greater variability when compared to the LiDAR retrieved heights for the same area.



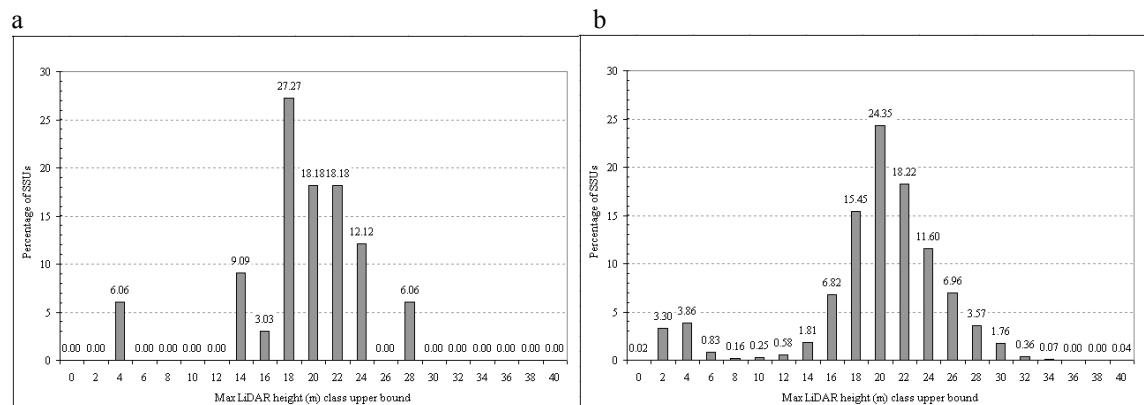
**Figure 45: Comparison of maximum height between field and LiDAR at Injune for; (a) field plots; and (b) individual tree height for 100 manually selected, isolated overstorey trees**



**Figure 46: Comparisons field and LiDAR for NE Victorian plots for; a) max plot height for field plot and transect areas; and b) frequency distribution of maximum LiDAR height.**

The distribution of maximum height for NE Victorian plots (Figure 46b), and at plot and landscape scales for Injune (Figure 47), are normally distributed overall, with a slight skew to taller forest in NE Victoria. At Injune there is a slight skew to forests with lower height with most associated with regeneration following clearance. As both distributions appear similar, (e.g., in terms of the mean value), it is argued that the height estimates from the field data are broadly representative of the wider landscape sample, at least in terms of maximum stand

height. The plot mean was 18.27 m ( $\delta = 5.09$ , range = 3.0 – 26.8 m,  $n = 33$ ), with that of all SSUs being 18.62 m ( $\delta = 5.97$ , range = 0.0 – 39.02 m,  $n = 4500$ ).



**Figure 47: Frequency distribution of LiDAR maximum height at Injune for: (a) field plots; and (b) all 4500 SSUs.**

### *Predominant canopy height*

Simple linear correlations between the field and LiDAR estimates of predominant height for both study sites (Figure 48a, Figure 49a, Table 26), suggested a good correspondence overall, but which declined in the taller and more structurally varied forests ( $> 30$  m). For NE Victoria, using the 5 tallest trees within the field plot (50 trees  $\text{ha}^{-1}$ ) generated the strongest correspondence with the LiDAR cell samples ( $r^2 = 0.71$ , Table 26). The distribution of LiDAR derived predominant height indicates a mostly normal form, with most sites around the 26 - 30 m height range (Figure 48b, Figure 49b).

At Injune, comparisons of predominant height showed that the field sampling rates had correspondence values with LiDAR heights (10 m cells) ranging from  $r^2$  of 0.84 to 0.91 (for 100 and 50 trees  $\text{ha}^{-1}$  respectively, Figure 48a, Table 26). A field sampling rate of 50 trees  $\text{ha}^{-1}$  had less variation than 100 trees  $\text{ha}^{-1}$  across the data range, and a slope value close to one, but a consistent offset or bias was observed, with LiDAR recording approximately 2 m lower height across the observed range. The field sampling rate of 100 trees  $\text{ha}^{-1}$  had greater variation across the data range, although the line of best fit was closer to the 1:1 line, with a low cover plot influencing the slope value. Frequency distributions of predominant height from field plots (Figure 48b) and all 4500 SSUs (Figure 50) shared a similar mode values and shape of the distribution for shorter forests, although the distribution from 4500 secondary sampling units

did record a proportion of taller forest (20-32 m) that was not observed in the field plot distribution.

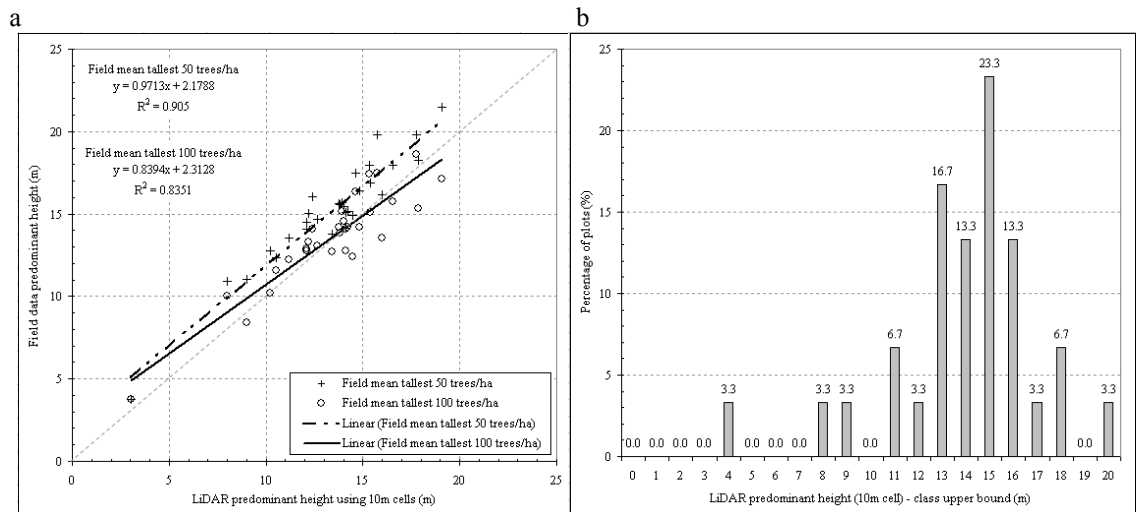


Figure 48: Injune field plot predominant height (10m cells) for: (a) from field data and LiDAR at different sampling rates, and (b) frequency distribution of LiDAR heights.

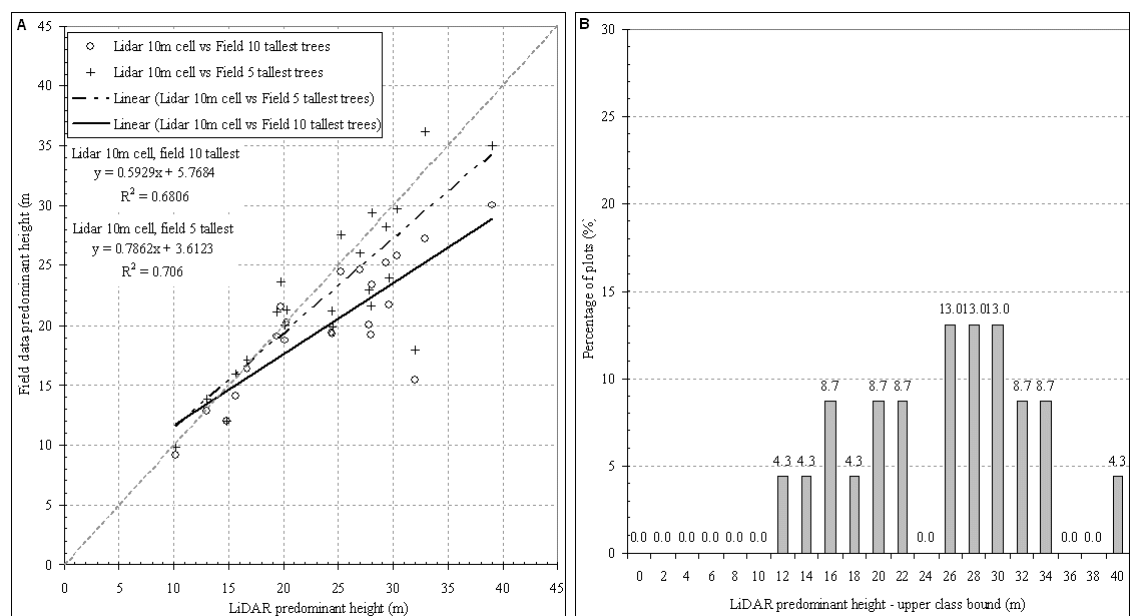
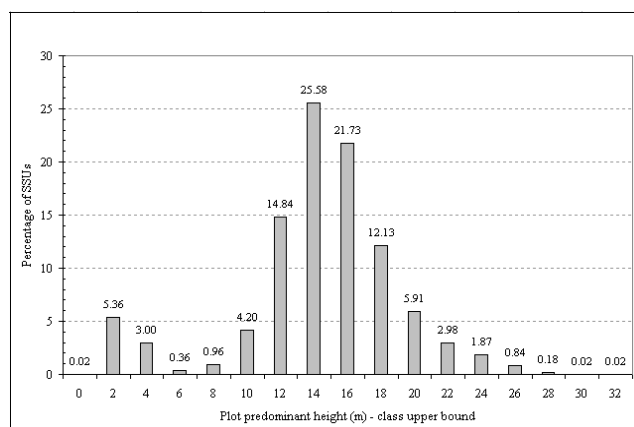


Figure 49: NE Victoria field plot predominant height (10m cells) for: (a) from field data and LiDAR at different sampling rates, and (b) frequency distribution of LiDAR heights.



**Figure 50: Frequency distributions for predominant height at Injune for 4500 SSUs derived from transfer function using 90<sup>th</sup> percentile LiDAR height.**

**Table 26: Comparisons of predominant height: field and LiDAR for Injune and NE Victoria plots**

Description	n	R <sup>2</sup>	RSE	Function <sup>a</sup>	P-value
<i>NE Victorian plots</i>					
Field 50 trees ha <sup>-1</sup> - LiDAR 10m cell	22	0.71	3.79	Y = 0.7862x + 3.6123	9.929e <sup>-7</sup>
Field 100 trees ha <sup>-1</sup> - LiDAR 10m cell	22	0.68	3.03	Y = 0.5929x + 5.7684	2.311e <sup>-6</sup>
<i>Injune plots</i>					
Field 50 trees ha <sup>-1</sup> - LiDAR 10m cell	31	0.91	0.984	Y = 0.9688x + 2.2129	1.11e <sup>16</sup>
Field 100 trees ha <sup>-1</sup> - LiDAR 10m cell	31	0.84	1.19	Y = 0.8447x + 2.2536	1.793e <sup>13</sup>

<sup>a</sup> – y = field data, x = LiDAR value

### 4.3.2 LiDAR height results with different assessment areas

This section compares NE Victorian results at the plot, transect area, and wider stand scales for both predominant and maximum height. Then a continuous assessment from plot to stand is made using LiDAR predominant height, for both study sites.

#### *Multi-scale variation of LiDAR height in NE Victoria*

For NE Victoria, a close correspondence between field plot area and transect area height estimates and the wider stand (LiDAR swath width), for both maximum and predominant height was observed (Figure 51, Table 27). Investigation of the individual plots also identified a range of scale effects for difference ecozones (Figure 110 - Appendix A). Overall, there was large

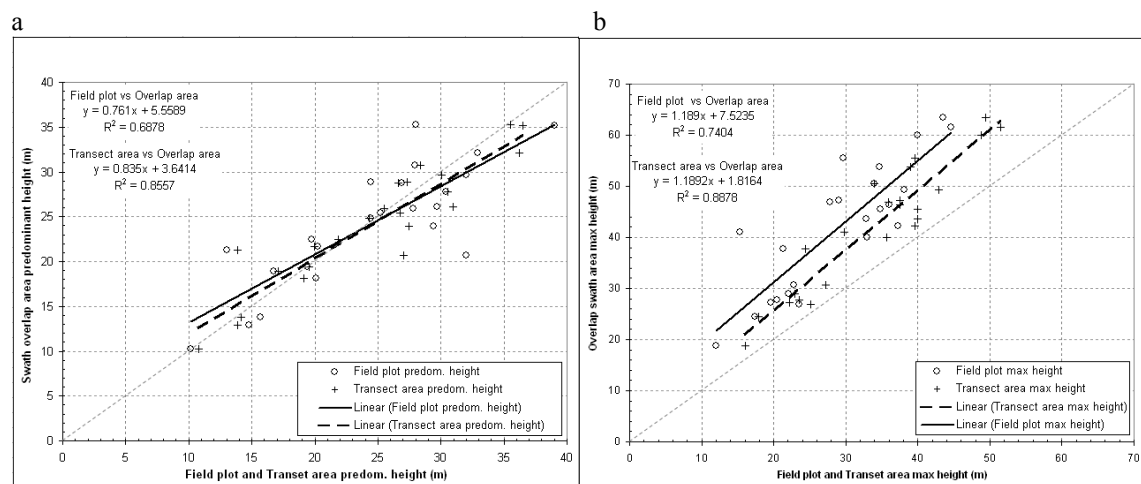


variation in predominant height at scales less than 1 ha, when compared with the wider stand estimate (Figure 52). At assessment areas greater than 1 or 2 hectares, variation in predominant height is small, compared with the stand estimate. Across all sites, the mean predominant height difference between 0.1 ha (field plot) and 20 ha (stand) scales was -1.45 m (range -10.16 to 4.56 m,  $\delta = 3.70\text{m}$ ).

**Table 27: LiDAR height comparisons at a range of assessment area scales for NE Victoria**

Description	n	R <sup>2</sup>	RSE	function <sup>a</sup>	P-value
Max height - overlap area vs field plot	23	0.74	6.60	$Y = 1.1890x + 7.5235$	1.396e-7
Max height - overlap area vs transect area	23	0.89	4.34	$Y = 1.1892x + 1.8164$	1.929e-11
Predom height - overlap area vs field plot	23	0.69	3.84	$Y = 0.7610x + 5.5589$	9.994e-7
Predom height - overlap area vs transect area	23	0.86	2.61	$Y = 0.8350x + 3.6414$	2.748e-10

<sup>a</sup> y = overlap area, x = field plot or transect area. Overlap area is the LiDAR swath width (nominally 400 x 400 m).



**Figure 51: Representativeness test for field plot (~0.09 ha) and transect area (~1 ha) versus swath overlap area (~25ha) for LiDAR (a) predominant height, and (b) maximum height, in NE Victoria.**

The results of the field or transect plot random location test show that the difference in the predominant height is minimal, on average (e.g., less than 0.5 m, with a range up to 2.0 m) (Figure 53, and Figure 111 (Appendix A) for individual plots). This holds for both 30 random field plots, and 30 random transect plots, when compared to the wider 20 ha stand estimates. Further testing would reveal how many random samples are required before the stand estimate varies significantly from the stand area result. If forest type reporting were to rely on just one field plot estimate per location, the mean differences between plot and wider stand per ecozone were +5 m (Floodplain), +0.1 m (Foothills), -0.5 m (Montane), -1 m (Subalpine) respectively.

For woodlands in the Foothills ecozone, the same predominant height ( $\pm 4$  m) is derived regardless of the size or number of samples that were used, or even data source (i.e. field is as good as LiDAR). The Floodplain, Montane and Subalpine environments are more variable however, with mid-slopes and ridge-tops having small differences in height (2 - 3 m) with changing sample size and number. In contrast, stream gully bottoms and water course locations tend to show height differences of 5 - 7 m on average (with a maximum of approximately 15 m), depending on the number of samples and, to a lesser extent, plot size (Figure 111 - Appendix A).

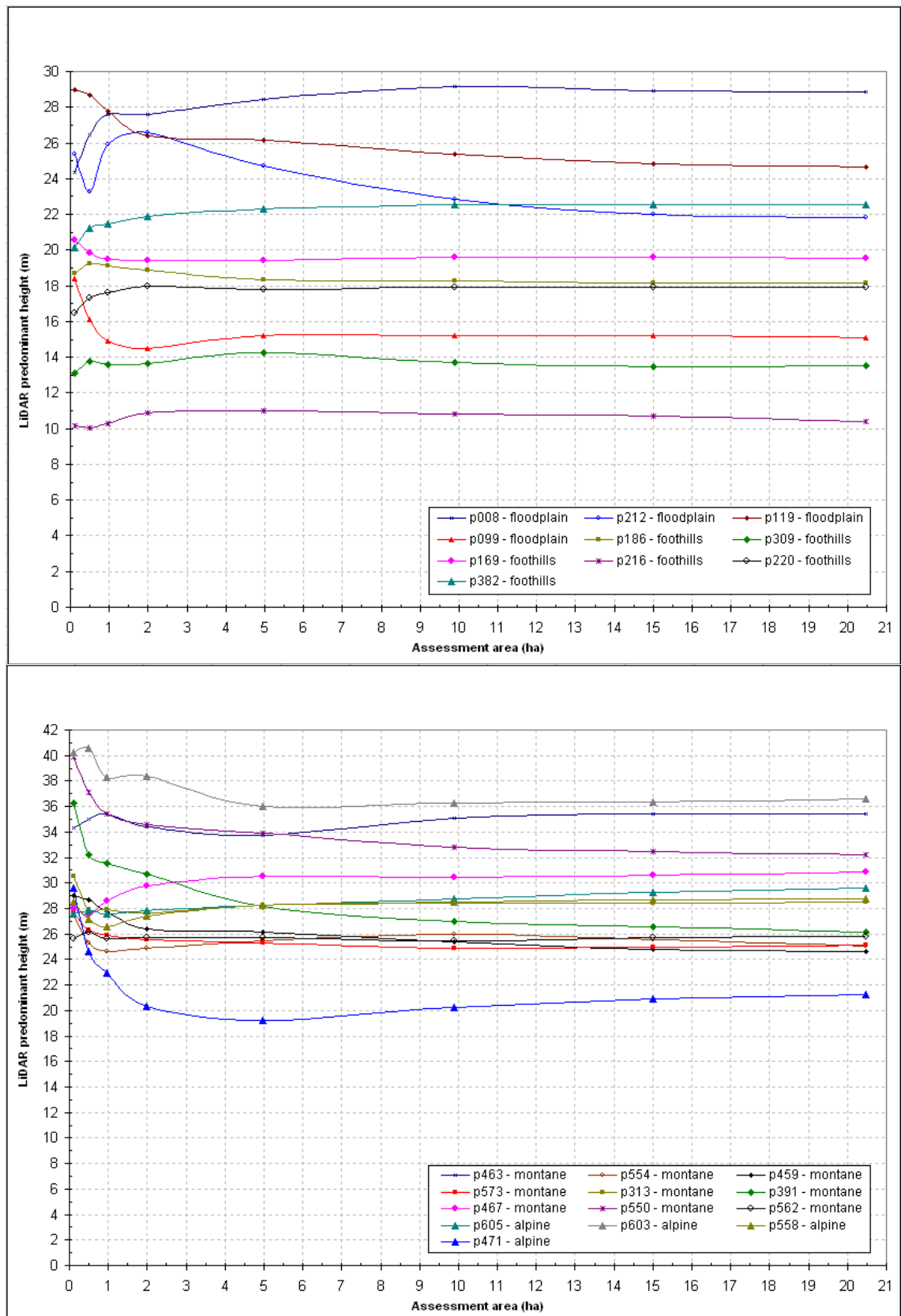
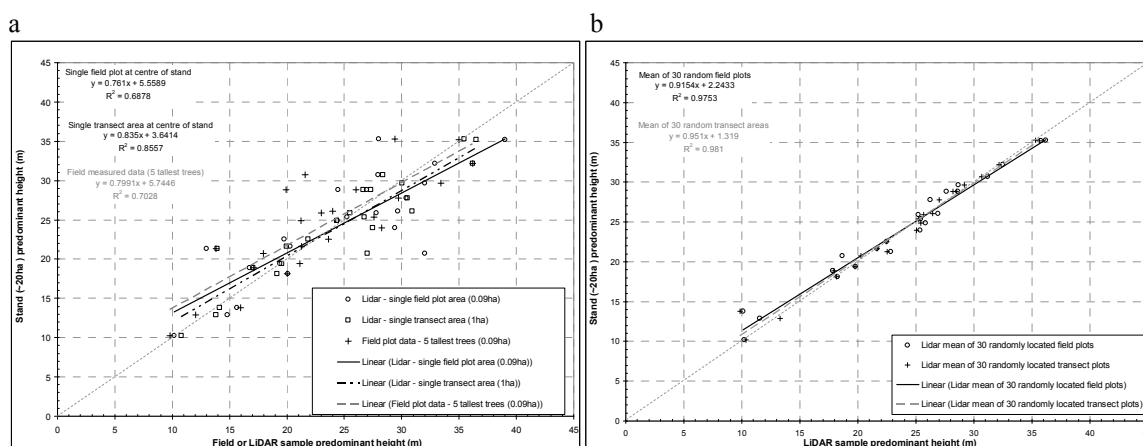


Figure 52: LiDAR predominant height assessment at a range of spatial scales for NE Victorian sites where field plots are located.



**Figure 53: Comparison of sampling strategies for estimating stand (~20ha) predominant height for field plots in NE Victoria using (a) single locations (field or LiDAR); and (b) multiple samples within stand.**

The results presented previously indicate that for any one plot the variation observed due to scale or sampling method may be enough to influence national reporting. However, as sampling schemes such as a CFMF generally report at broad (e.g., ecozone) scales, assessment of the results at this level was undertaken (Table 28), and using LiDAR predominant height with a 10m cell as the assessment unit.

**Table 28: Summary statistics for predominant height at a range of assessment scales, per NE Victorian ecozone**

Ecozone	Assessment area Height Statistic	0.09ha	0.09ha	1 ha	~20 ha
		Field plot-field	Field plot-LiDAR	Transect area	Overlap area
Floodplain	Mean Predominant	20.52	25.38	23.98	21.82
	Mean Std Deviation	6.92	5.40	6.51	7.80
Foothills	Mean Predominant	17.29	16.82	17.03	17.01
	Mean Std Deviation	2.56	1.93	2.55	2.85
Montane	Mean Predominant	26.00	27.40	28.67	27.75
	Mean Std Deviation	7.05	4.77	4.59	5.83
Subsubalpine	Mean Predominant	27.06	26.32	25.69	28.43
	Mean Std Deviation	6.83	2.68	5.32	7.59

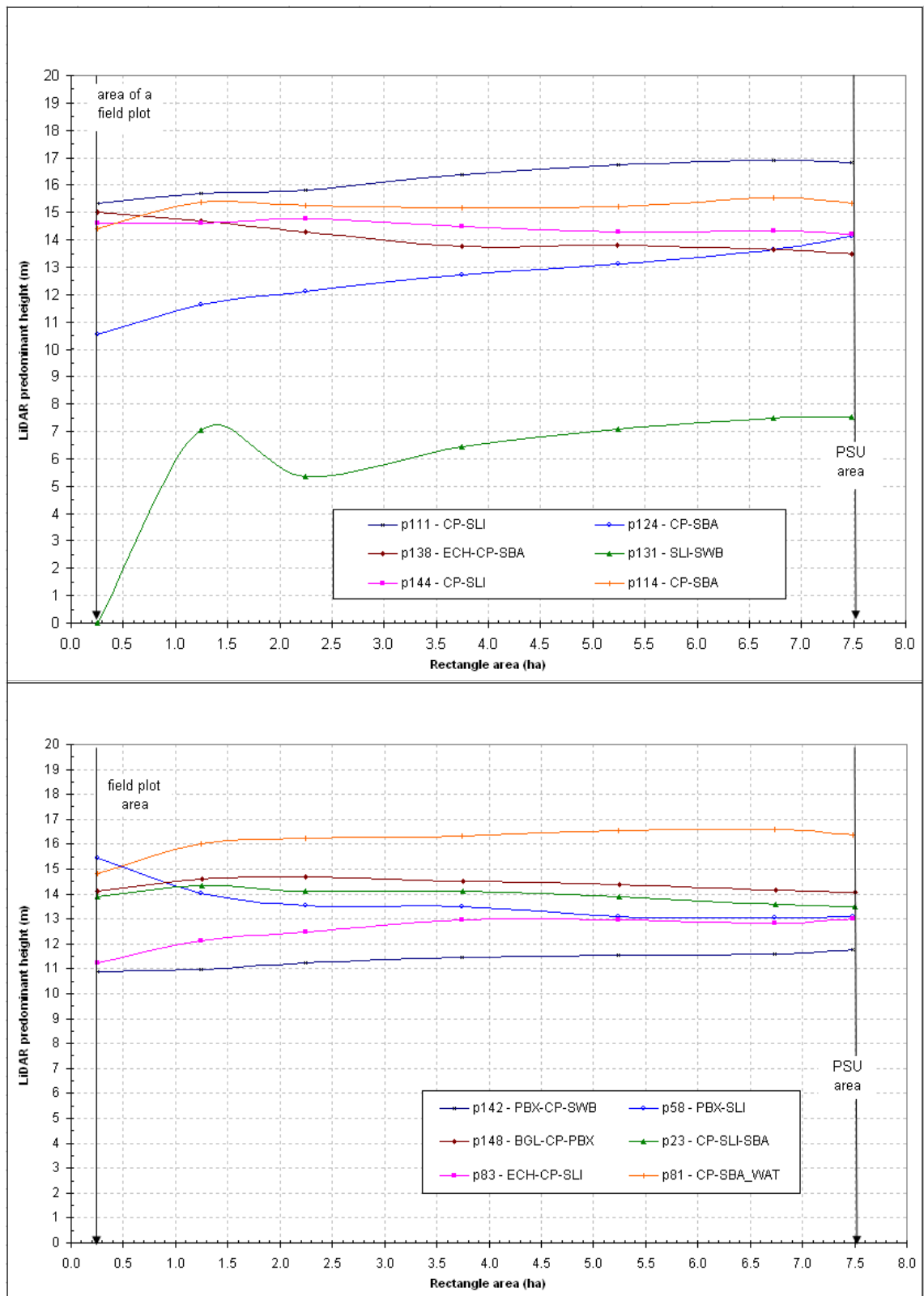
Scale impacts are evident in the Floodplain ecozone, where a trend of declining predominant height with an increasing assessment area was observed. The remaining ecozones showed a slight trend for increasing predominant height, on average, with larger assessment areas. However, the differences between assessment areas for mean predominant height were small compared to the actual height recorded (between 1 - 7%). The standard deviation of heights also increased for all the ecozones with an increasing assessment area (Table 28). This

---

indicates that there is greater variation in the heights identified in plots with larger assessment areas.

### ***Multi-scale variation of LiDAR height at Injune***

There was little difference in predominant height between the centre secondary sampling unit (0.25 ha) and the primary sampling unit area (7.5 ha), for 12 primary sampling units at Injune (Figure 54). The mean difference across the primary sampling units was 1.08 m (range -2.38 – 7.51 m,  $\delta = 2.57$  m), with the primary sampling unit recording the taller height. Whilst some primary sampling units tended to have taller forest at the primary sampling unit scale (often in the order of 2 - 4 m) when compared to secondary sampling units, this was balanced by other primary sampling units recording lower heights of the same magnitude across assessment scales. It was observed that the initial starting location for the assessment could influence the height at fine scales. For example, primary sampling unit 131 had larger areas of non forest, and the first secondary sampling unit occurred on a patch of non-forest. Once the full primary sampling unit area had been assessed, a more complete understanding of the predominant height (and variation) of the forest found at that location was gained.



**Figure 54: LiDAR predominant height assessment at a range of spatial scales for 12 PSUs at Injune. Dominant species codes are given in Chapter 3.**

### 4.3.3 Apparent vertical profiles

This section examines the comparison of growth stage assessed using field data and LiDAR apparent vertical profiles, for an initial test site using a single field plot at Injune, and then subsequently across a range of plots at both the Injune and NE Victorian sites. Assessments are made of a range of forest structural combinations that could be related to different growth stage and potential disturbance combinations (e.g., from fire), based on the shape of the apparent vertical profile. Finally, vertical profiles are used to quantify growth stage and disturbance across a range of scales, from tree to landscape, at Injune.

#### *Simulating apparent vertical profiles*

For test plot p124-19, the field data 3D parameterisation matrix had 2,367 cells (1 m<sup>2</sup>) with 27 x 1 m height levels, resulting in 63,909 voxels (m<sup>3</sup>). A direct comparison between field data and LiDAR revealed a reasonable correspondence between the two datasets when using a two dimensional crown map (Table 29). The comparison showed that 76% of the field simulated matrix cells also containing LiDAR, although these were not necessarily at the same height above ground, as indicated by the relatively low count of voxels that contained both LiDAR and simulated field data.

**Table 29: Summary of matrix results for the field plot area.**

Attribute	No. matrix cells	No. matrix voxels
Field modelled crown elements	557	1944
LiDAR return elements	981	1302
LiDAR and field elements with same vertical column (cell)	426	
Both field and LiDAR canopy elements within same voxel		175

Comparisons between field and LiDAR profiles for all 31 field plots (Figure 55, and Table 59 - Appendix A) show that there was little difference between the two sources of data overall. Two example plots were selected from the accuracy assessment results (Table 3 – Appendix A) to illustrate the range of accuracy observed (Figure 56). For the example plots, p142-02 has similar profiles between field and LiDAR modelling (Figure 55a), and a correspondingly good correlation between the percentages of foliage cubes at each height interval (Figure 56a). However, p81-11 has the opposite case, where major differences in the

profile at certain heights, including the top-height (Figure 55b), result in a poor correlation (Figure 56b). Overall for this plot, the respective shapes of the profiles are similar, but offset due to field measurement differences.

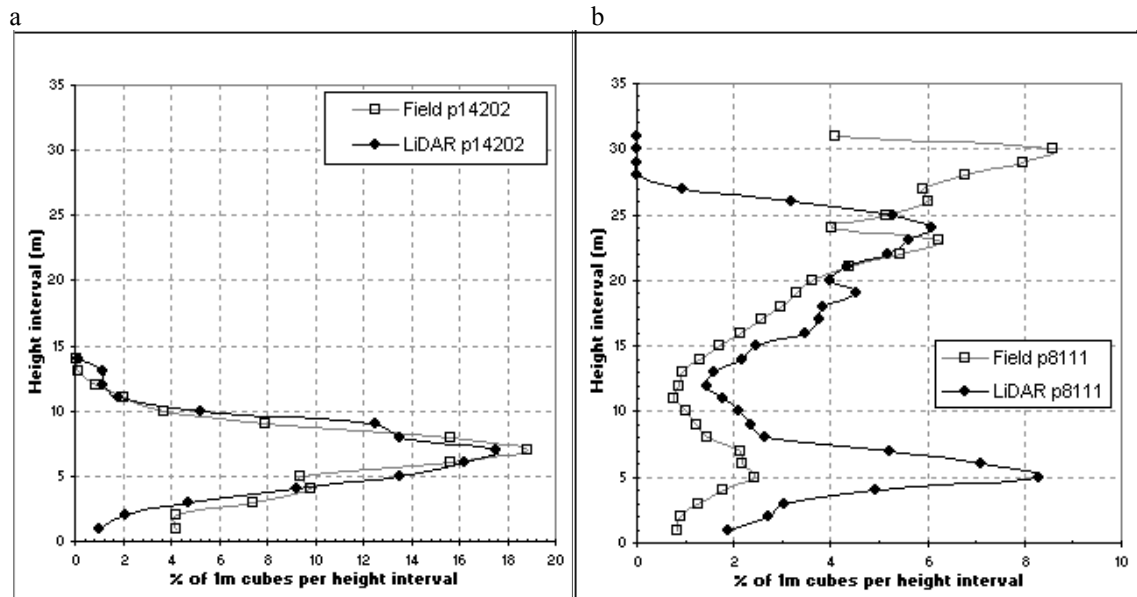


Figure 55: Comparisons between apparent vertical profile from LiDAR and field cubic modelling for matches that are: (a) good (p142-02), and (b) not as good (p81-11).

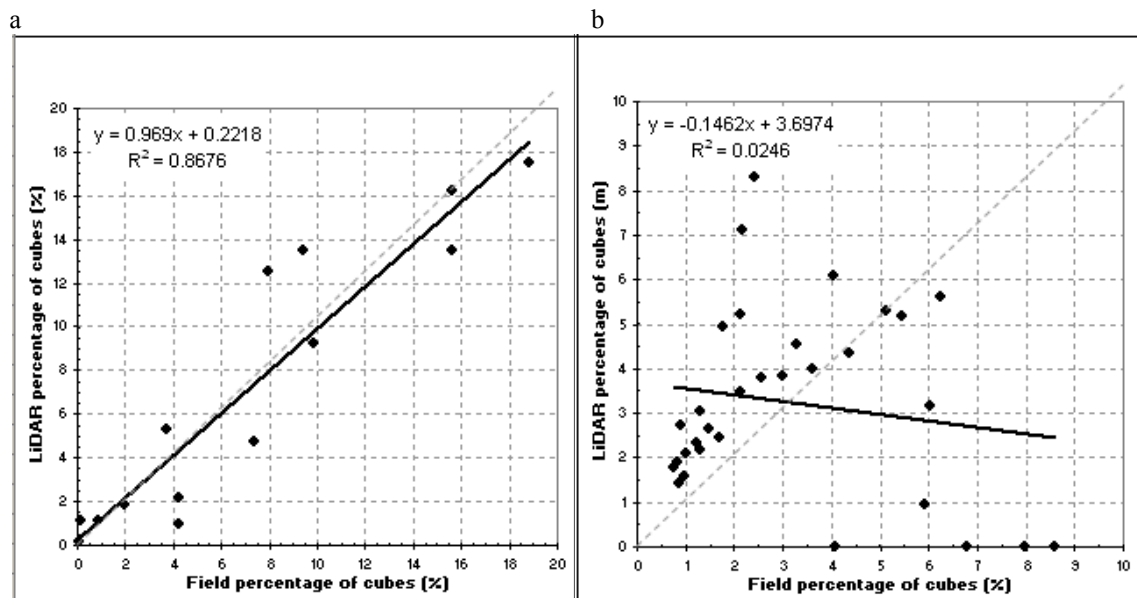


Figure 56: Correlation of percentage of cubes at each 1m height interval, with LiDAR and field apparent vertical profiles for matches that are; (a) good (p142-02), and (b) not as good (p81-11).

The results of the Kolmogorov-Smirnov test for selected plots show that most had good comparisons (high P-values), thus highlighting the overall similarity between the two apparent vertical profiles (Table 58 - Appendix A). A number of plots had lower P-values for the



Kolmogorov-Smirnov test, indicating some difference between the field and LiDAR apparent vertical profiles. The four plots with the lowest P-values (i.e. closest to potentially having a significant difference in the height distributions) also had a range of maximum height differences between the field and LiDAR data. LiDAR was found to be higher than field data in secondary sampling units 114-12 (9 m), 83-12 (2 m), 111-12 (3 m), and 114-04 (8 m) (Table 58 - Appendix A).

### ***Growth stage and disturbance assessment using profiles***

Field data were summarised with a range of structural and floristic attributes (Figure 57) for secondary sampling unit 124-19, to assist with the interpretation of the vertical profiles modelled from field and LiDAR data (Figure 58). The field data summary outlines tree growth stage and species by relative percentage of basal area, and stocking per  $D_{130}$  class. Plot growth stage could be interpreted as complex with an overstorey canopy of large crowns and secondary stratum of trees with more restricted crowns reflecting multiple successional phases (Florence, 1996).

*Eucalyptus* and *Angophora* species occurred throughout the  $D_{130}$  class and growth stage range, and had a mean tree height of 9.1 m ( $\delta = 7.6$  m, range 2.5 – 24.0 m). The taller heights of these trees would associate them with the upper bulge (between 15-20 m height) in the apparent vertical profile. Four distinct cohort age groups were evident with these most likely relating to major disturbance and regeneration episodes in the past. The *Eucalyptus* and *Angophora* had relative few stems (1 - 3 stems per  $D_{130}$  class above 25cm), indicating that they have been on this site for possibly hundreds of years and may have self-thinned to a woodland dynamic equilibrium.

*Acacia* species constitute 67% of all stems, but only 6% of stems were greater than 10 cm  $D_{130}$ , and the mean tree height was 1.1m ( $\delta = 1.5$  m, range 0.5 – 12.3 m). The majority of stems greater than 10cm  $D_{130}$  (77 %) were *Callitris*, with all *Callitris* measuring less than 20 cm  $D_{130}$ . The mean tree height was 7.4 m ( $\delta = 3.1$ m, range 2.7 – 14.0 m), and there stands were associated with the developing growth stage, which is also evident as the large bulge (at

approximately 8 m height) in the apparent vertical profile (Figure 58). Therefore, they would be relatively recent recruits to the plot, possibly as a result of past logging and fire suppression; given this genus is fire intolerant when young.

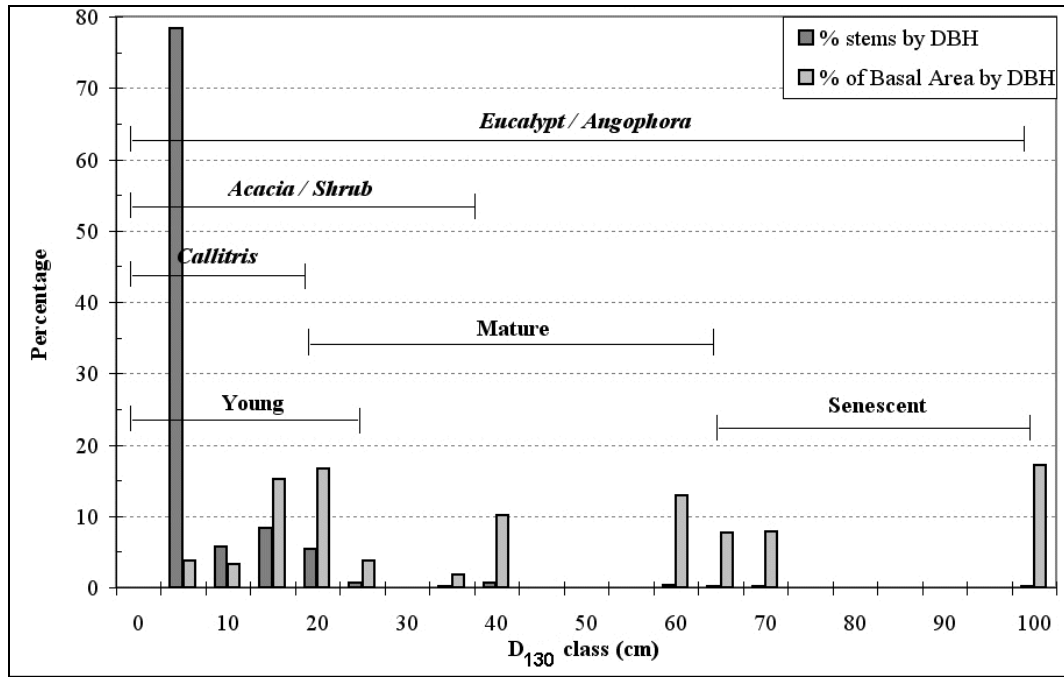


Figure 57: Field data summary for SSU 124-19, illustrating tree growth stage and genus distribution by stem diameter (total Basal Area = 4.30m<sup>2</sup>) and stocking ( $n = 603$ ).

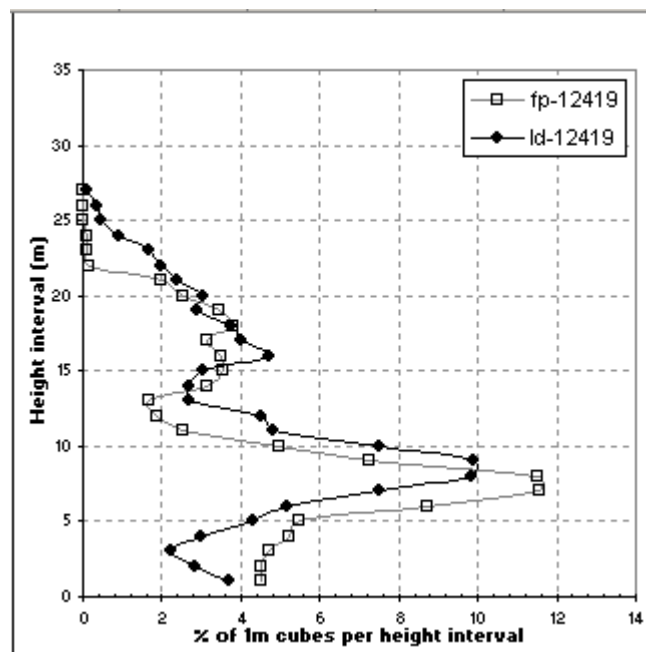


Figure 58: Apparent vertical profiles from LiDAR (black) and field (grey) cubic modelling for SSU 124-19.

---

With the examples of indicative apparent vertical profiles per EMC class, the vertical profile x-axis represents the percentage of vegetation returns; and the y-axis the height interval (m) (Figure 59). The LiDAR profiles appear to match the descriptions for the EMC or SFRI classes, and the photographic illustrations.

Whilst the field plots were not classed into disturbance categories, it was noted from field visits that some of the plots that were burnt in the 2003 fires had a range of fire intensity impacts, mainly related to the amount of understorey remaining after the fire. Some plots have no understorey and quite high trunk scorch marks, while other have less obvious trunk scorching, and some understorey remaining. These qualitative assessments that are evident in photographs can also be inferred from the LiDAR vertical profiles, in terms of the presence or absence of LiDAR returns from understorey strata. An example provides a qualitative assessment of how disturbance might be assessed using the LiDAR (Figure 60). Visual examination of photographs from the field indicate that plot 558 (Figure 60b) was much more severely burnt than plot 562 (Figure 60a).

Extending the growth stage and disturbance analyses, it may also be possible to develop a successional sequence using the apparent vertical profiles (Figure 61). A range of physical attributes for three field plots from the NE Victoria study is used to show the similarity between the plots, apart from the time since last recorded fire (Table 30). All three plots are dominated by mature *E. radiata*, (according to SFRI assessment) and have a mean annual rainfall between 1100 - 1300 mm/year, and are found in gully locations near watercourses. Plot 313 was partially burnt in the 2003 fires, with the severity of fire in the other plots unknown. All sites were logged in a similar manner, using either single tree selection or group selection, between 1983 and 1989. Therefore it could be assumed that the major structural differences observed in the profiles are as a result of the time since the last recorded fire.


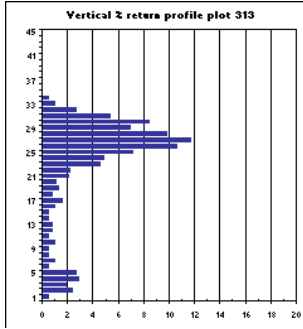

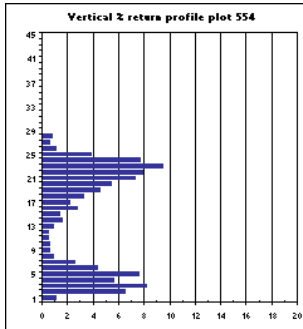

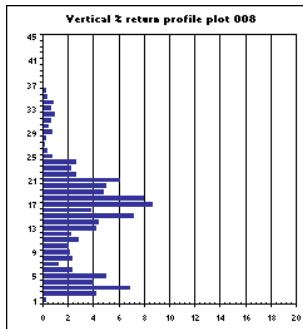

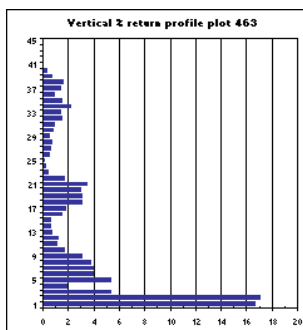

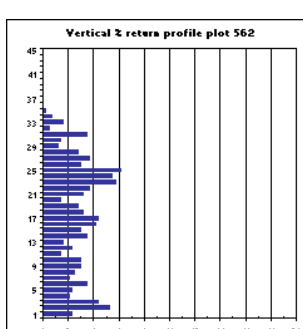
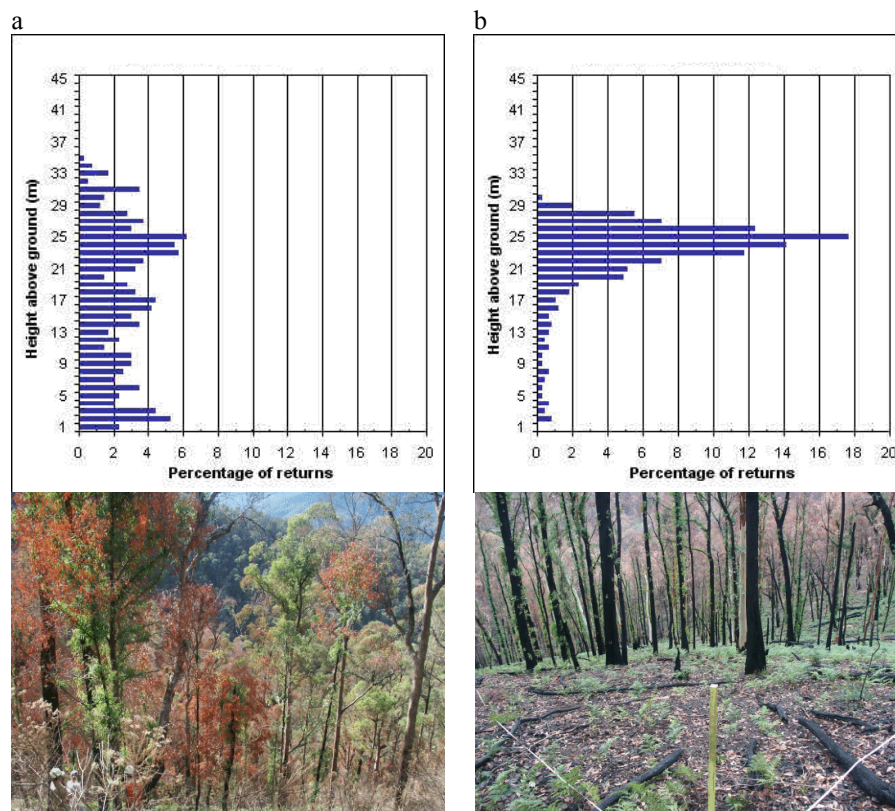
Class	Growth stage	Field plot photo	Example LiDAR profile
1	<p>Dominant in over-mature trees with trace regeneration/regrowth.</p> <p>SFRI – late mature. (Plot 313)</p>		
2	<p>Mainly dominant with mature trees with some shorter regrowth.</p> <p>SFRI- mature. (Plot 554)</p>		
3	<p>Mainly dominant with regrowth with some taller mature trees.</p> <p>SFRI – early mature (Plot 8)</p>		
4	<p>Dominant in regeneration/regrowth with trace mature/over-mature (Plot 463)</p>		
5	<p>SFRI unevenaged - no clear eucalypt age class dominance (Plot 562)</p>		

Figure 59: Growth stage example using indicative LiDAR vertical profiles from NE Victoria. For the LiDAR profiles the x-axis is percentage of canopy returns, y-axis is height above ground (m).



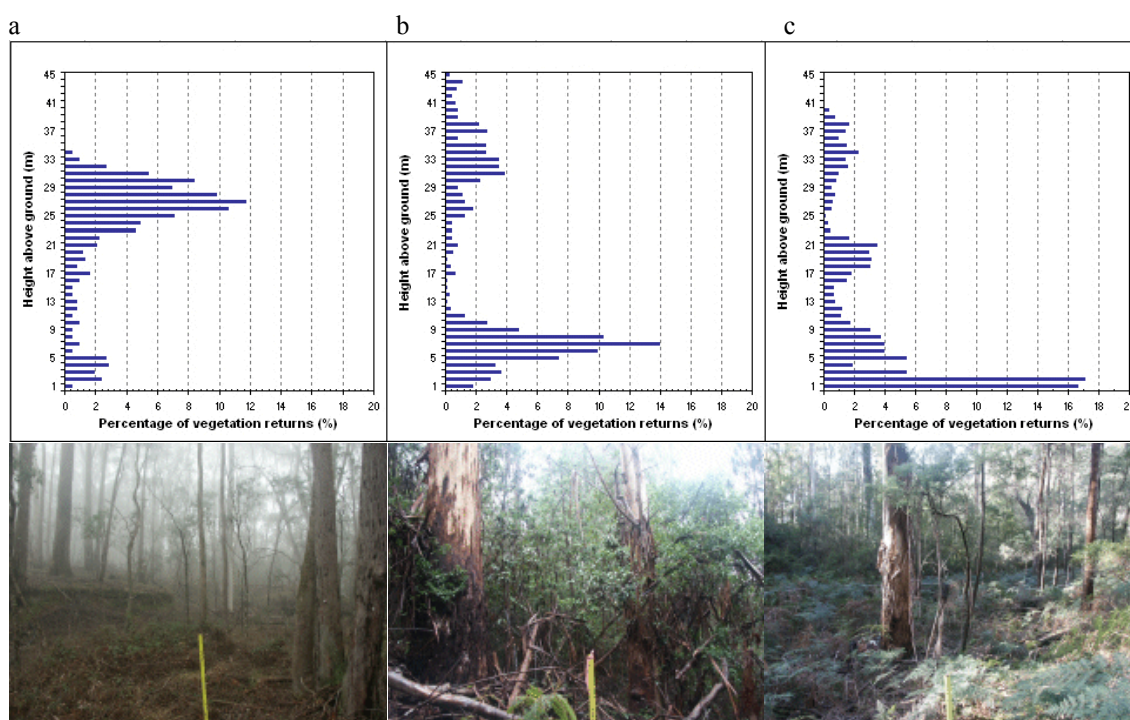
**Figure 60: LiDAR apparent vertical profile showing the potential difference in fire intensity between two high country plots on steep slopes. (a) plot 562, less intensity fire impact, with understorey and lower canopy still present. (b) plot 558, intense fire impact, no understorey or lower canopy left and scorched crowns.**

If this is the case, then a progression of understorey top height could be inferred from the profiles. In this illustration, it is possible that very little understorey or midstorey has recovered in the few months since the 2003 fires, with the small amount evident in the LiDAR profile resulting from an unburnt portion of the field plot. Post fire recovery after 12 years seems to produce an understorey at around 10 m, with very little midstorey. After 64 years without fire, multiple strata occur, with a 20 m midstorey and a 10 m understorey in this case.

**Table 30: Plot descriptions for three plots illustrating growth progression with time since fire.**

Attribute	Plot 313	Plot 550	Plot 463
Soils	Clay/loam (chromosol)	Light clay (dermosol)	Light clay (dermosol)
Elevation (m asl)	689	906	460
Aspect (degrees)	41	170	45
Slope (degrees)	3	17	1
Plot basal area (m <sup>2</sup> /ha)	25.4	34.2	19.2
Number of stems*	28	32	17
Year of last fire	2003	1991	1939
Year of last logging	1986	1989	1983

\* stems 10cm+ D<sub>130</sub>



**Figure 61: Comparison of LiDAR apparent vertical profiles and plot photos for plots in NE Victorian *E. radiata* forests, illustrating a potential understory fire recovery sequence, based on the last recorded fire within; (a) 1 year (p313), (b) 12 years ago (p550), and (c) 64 years ago (p463).**

As the LiDAR had been collected and processed over the landscape at Injune, the growth stage and disturbance analyses using apparent vertical profiles could then be extended to the landscape scale. The utilisation of LiDAR analysis results at a range of scales for the Injune data is illustrated using 7 panels (Figure 62). Panels 1-5 illustrate LiDAR apparent vertical profiles at the different assessment scales. Panel 6 spatially represents the data (height above ground in  $1 \text{ m}^2$  pixels) shown in the first three vertical profiles – single tree, secondary sampling unit (in this case, field plot p81-11) and primary sampling unit 81. Panel 7 shows the location of the primary sampling unit within Transect 9, and then this transect within the study area as a whole. It can be seen that the vertical profiles in panels 1 and 2 are quite similar. As the tree shown in panel 1 is quite large, with a crown diameter of around 20 m, this tree takes up nearly half the plot. Two distinct strata are evident (understorey 1-9 m tall) with the foliage being most dense at around 5 m. The expansive crowns of the mature *Angophora* trees are evident, dominating the overstorey, which is most dense at 24 m.

At stand (panels 2-3) and landscape (panels 4-5) scales, it is evident that the rest of the stand is composed of trees not as tall as the field plot, with crowns most dense at around 11 m. Examination of the profile of Transect 9 (panel 4), which spans 35 km of ground, it can be seen that a large proportion of the LiDAR has interacted with vegetation at between 3 – 5 m. This is likely a result of the transect traversing a large area cleared in 1997, and which now has significant amounts of regrowth. This pattern is reflected to a lesser extent in the study area profile (panel 5), where approximately 10% of the area has been cleared in the last 10 years. Most of the trees in this region appear to be around 10-13 m tall, with very few near 30 m tall. This would indicate that secondary sampling unit 81-11 could be an outlier in terms of tree height, when compared to the rest of the study area.

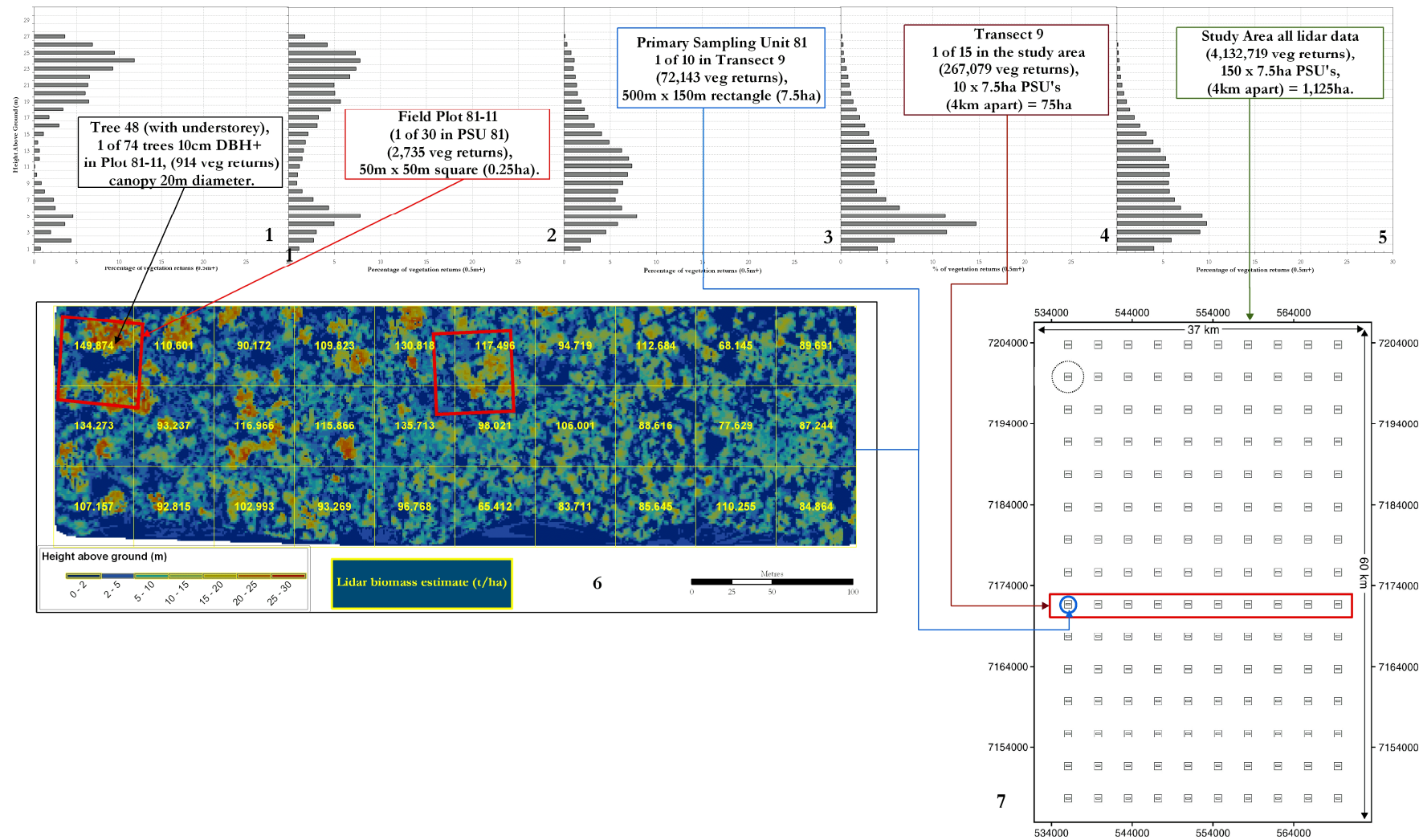


Figure 62: Assessment of stand structure using apparent vertical profiles at a range of scales, for the Injune study area



---

## 4.4 Multi-scale Canopy Cover results

There are three main parts to achieving the cover objective. As the primary reporting metric for the NFI is crown cover, then an assessment of the most accurate measurement of crown cover from a range of datasets (e.g., field, API, LiDAR) is required. Comparisons with other cover metrics (FPC) are required as this is used by wall-to-wall sensors such as the Landsat TM. Additionally, linkages between Landsat-derived foliage projective cover and LiDAR derived foliage measures such as foliage-branch cover are investigated to allow for calibration between these data. Finally, issues of scale are investigated to establish what impacts different assessment areas might have on cover results and reporting. The scale analyses will be used to determine whether a minimum area for reporting forest consistently across scales can be identified.

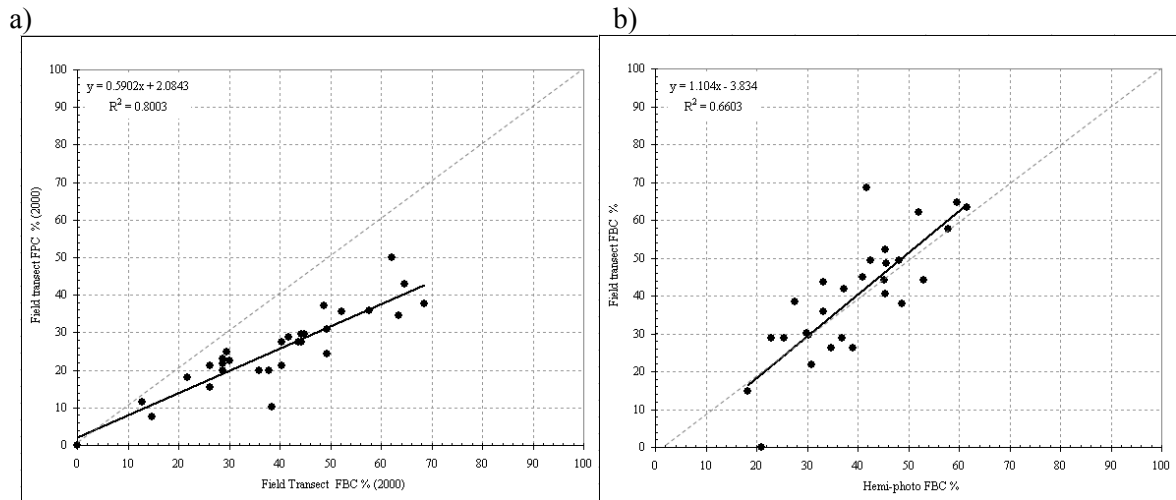
The following section is structured as follows. The estimates of cover for each scale of data (e.g., field, airborne, satellite) are compared against those obtained in the field plots. Similarities or obvious differences between metrics will be highlighted. Comparisons are then made between all data and metrics, across all measurement scales, to gain a better understanding of the interaction between measurement types and scales. Selected graphs showing key correlations are provided, with full comparison graphs found in Appendix A (Figure 114 for Injune and Figure 115 for NE Victoria). Finally, the LiDAR foliage-branch cover metric is used to assess cover at a range of scales, from tree to stand.

### 4.4.1 Plot scale cover results

#### *Comparisons between cover using field data*

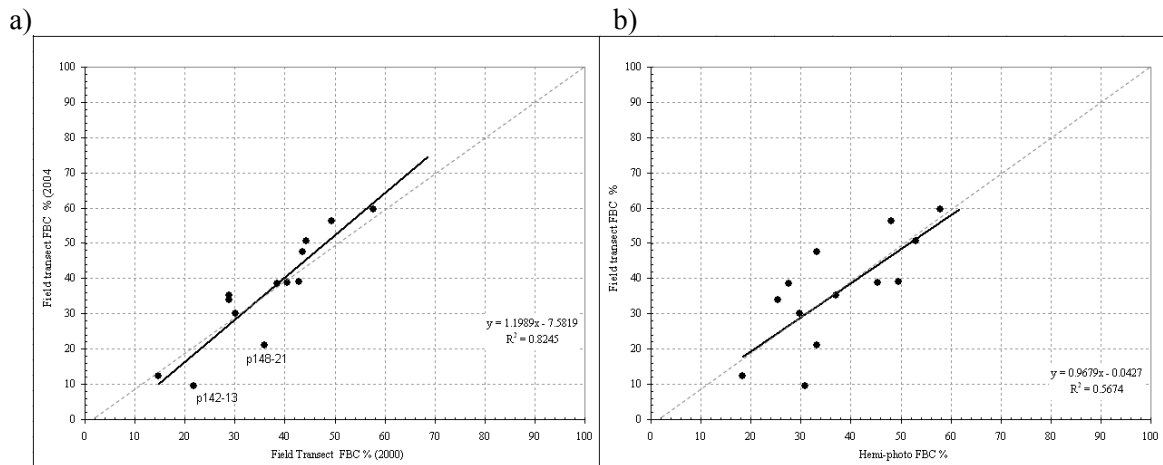
For Injune, the three primary field measurements of plot cover (foliage projective cover, foliage-branch cover and crown cover) utilise transects for foliage projective cover and foliage-branch cover, hemispherical photos for foliage-branch cover, and tree-maps for crown cover. In NE Victoria, hemispherical photos and tree maps are used. Individual plot data results are given in Appendix A - Table 60 for Injune and Appendix A - Table 61 for NE Victoria. Using field transect

data, the difference between foliage projective cover and foliage-branch cover measurements was assessed (Figure 63a), where it was observed that with increasing cover, the branch component of cover increased more than the foliage only component. A good correspondence between field transect foliage-branch cover from 2000 and hemispherical photos from 2004 (Figure 63b) was observed.

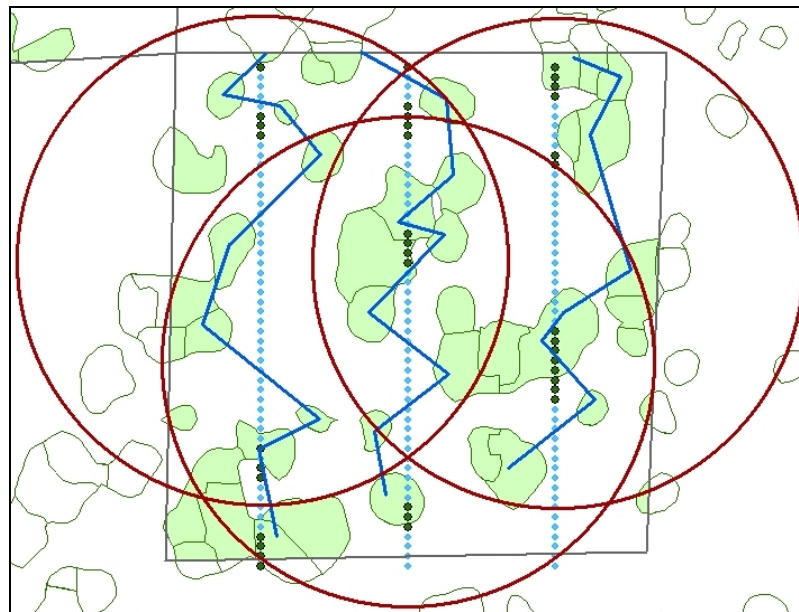


**Figure 63: Injune field data comparisons for transect FFC versus transect FBC (left), and transect FBC (2000) versus field hemi-photo FBC (2004) (right).**

Potential temporal change is assessed by comparing field transect measurements from 2000 and 2004 (Figure 64a). Measurement method differences were compared using foliage-branch cover from transects and hemispherical photo from 2004 (Figure 64b). An example of the estimated view extent of hemispherical photos and transects is provided (Figure 65). There was little change in field-transect foliage-branch cover overall ( $r^2 = 0.83$ ,  $RSE = 6.75$ ,  $p\text{-value} < 0.001$ ,  $n = 13$ ; Figure 64a), although the cover of two sites reduced (by 12.2 % and 14.8 %) over the four years.



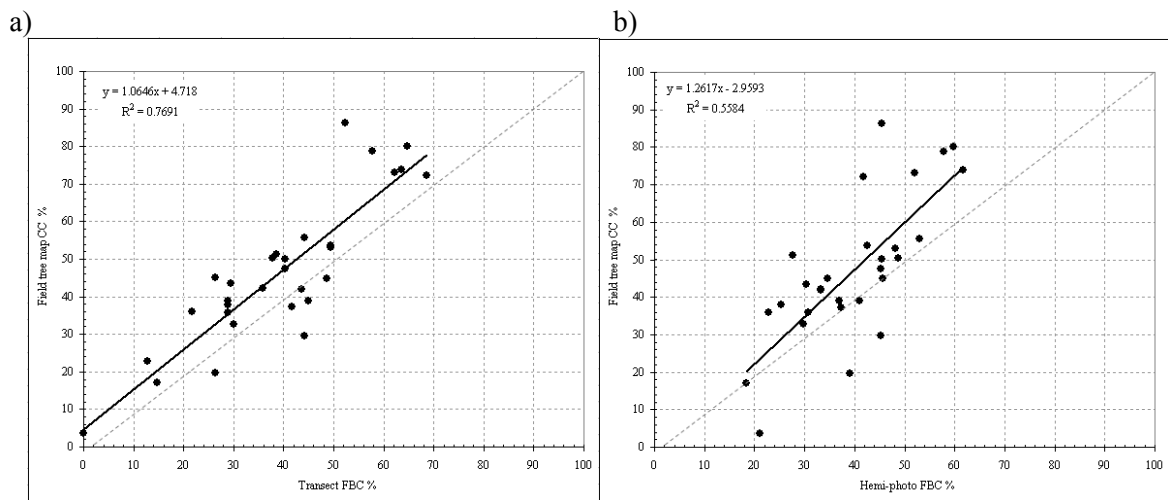
**Figure 64: Comparison of FBC field plot measurements: a) transects in 2000 and 2004; and b) transects and hemispherical photo in 2004.**



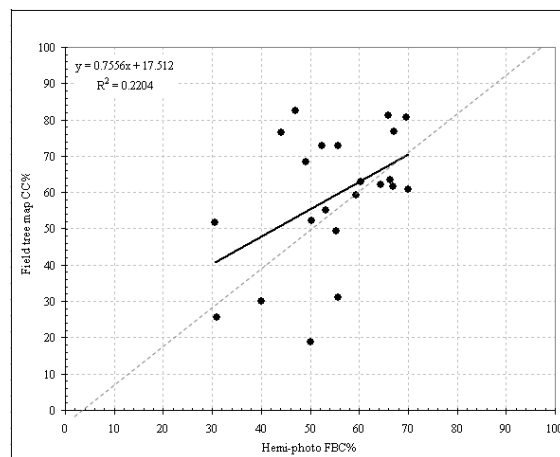
**Figure 65: Estimated hemispherical photo view extent, based on calibration results for p142-13. HSCOI crown delineations are shown for reference. The field plot boundaries and transects are approximately 50m long**

For the field plot transect versus hemi-photo comparison using data solely from 2004 ( $r^2 = 0.57$ ,  $RSE = 10.60$ ,  $p\text{-value} = 0.003$ ,  $n = 13$ ; Figure 64b), a similar range of scatter was observed as that observed in the comparison between 2000 and 2004. The fewer plots sampled in 2004 may make the results less conclusive, compared to those collected in 2000. Comparisons were made between field tree-map crown cover and transects foliage-branch cover (Figure 66a), and with

hemispherical photos (Figure 66b) for Injune. A consistent offset of approximately 8.5% is evident, with foliage-branch cover lower than tree-map crown cover. A number of plots had large differences between hemispherical photo foliage-branch cover and tree-map crown cover ( $r^2 = 0.56$ ), when compared to the transect foliage-branch cover comparison with crown cover. The NE Victorian plots had a variable relationship between field tree-map crown cover and hemispherical photo foliage-branch cover ( $r^2 = 0.22$ , RSE = 16.76, p-value 0.028, Figure 67).



**Figure 66: Comparison of field tree-map CC measurements: a) with transect FBC; and b) with hemispherical-photo FBC.**



**Figure 67: NE Victorian plot tree-map CC correspondence with hemispherical photo FBC.**

### ***Crown cover comparison between LiDAR and photography***

Comparisons were made between API crown cover (mid-point of class) and LiDAR crown cover for Injune primary sampling units (Figure 68). When LiDAR crown cover estimate falls within the API crown cover range (denoted as a green box - Figure 68), such as with API class 4, then there is confidence that the crown cover interpretation has generated estimates that are close to the LiDAR value. However, API results for class 2 and 3 (woodland and open forest) tend to be an underestimate when compared to the LiDAR crown cover.

A summary of the comparison between individual API polygons, associated with 12 primary sampling units, and LiDAR crown cover utilised the mean and range of LiDAR crown cover and the API class mid-point and range (Table 31 and Figure 69). LiDAR were only available within the primary sampling unit whereas the API polygon could extend up to the width of the aerial photograph stereo area (~ 600 x 600 m). Approximately 45 % of the polygons assessed had mean LiDAR crown cover values that occurred within the equivalent API interpreted crown cover class.

**Table 31: Comparison of relative accuracy of CC estimates between API and LiDAR CC, across different LiDAR sampling ranges of the API polygon.**

<b>Category for area of polygon sampled by LiDAR (%)</b>	<b>Count of polygons with LiDAR CC value within same API class</b>	<b>Total API polygons in class</b>	<b>Percentage of polygons with LiDAR in API class</b>
0-10%	1	7	14.3%
11-20%	10	14	71.4%
21-50%	5	11	45.5%
51-80%	2	8	25.0%
<b>Total polygons</b>	<b>18</b>	<b>40</b>	<b>45%</b>

A further 13 / 40 (32.5 %) had LiDAR crown cover estimates within 10% of the API class boundary. The majority of estimates with a match between API and LiDAR crown cover occurred with a LiDAR sample of 11-20% of the area of the API polygon. A comparison was made between overstorey crown cover from SFRI API data with LiDAR crown cover for NE Victoria (Figure 70). The crown cover comparison is more variable and poorer with respect to Injune. Most field plots or transect areas have the LiDAR crown cover outside the API crown cover class range.

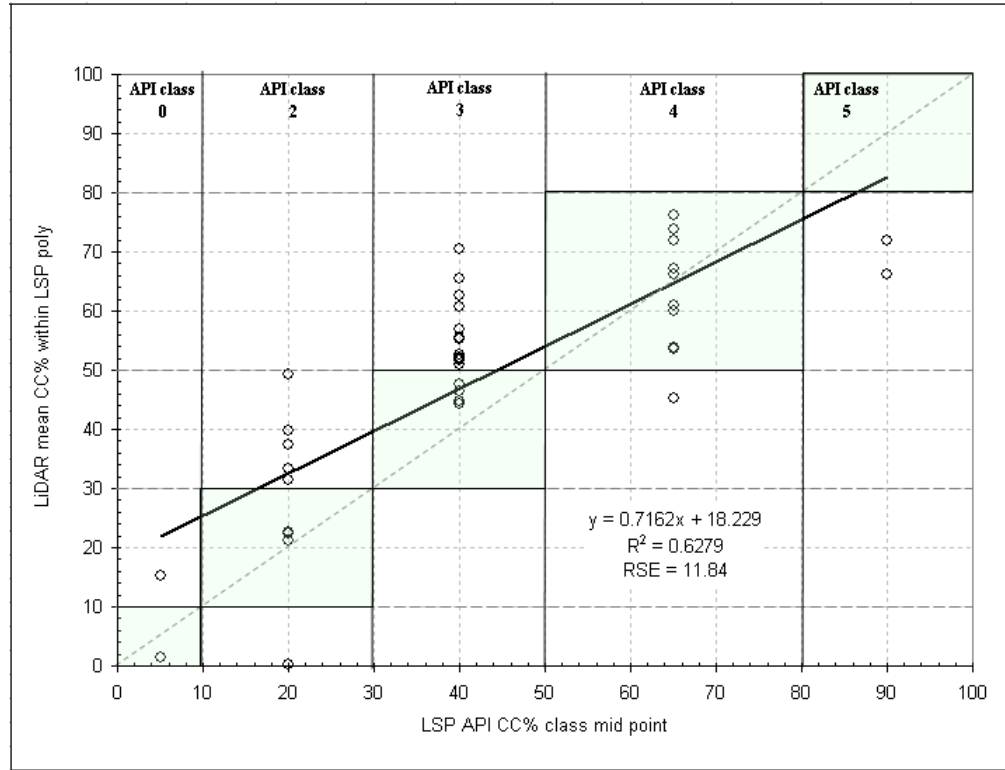


Figure 68: Injune API CC (mid-point of class) correspondence with the LiDAR CC sample within the API polygon.

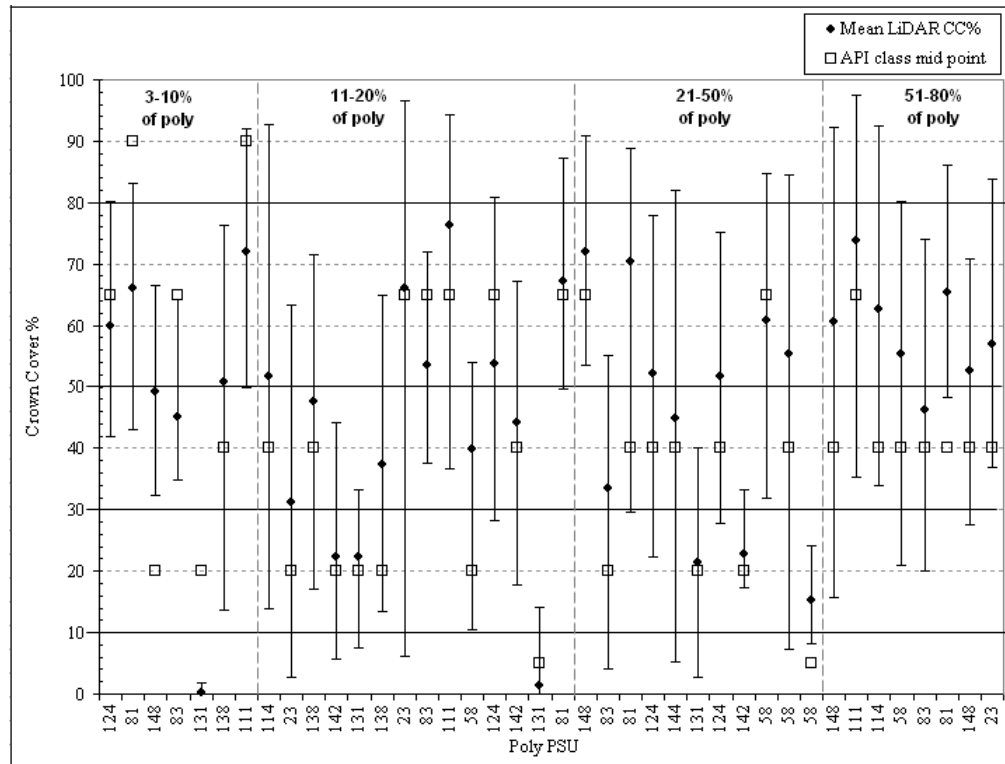
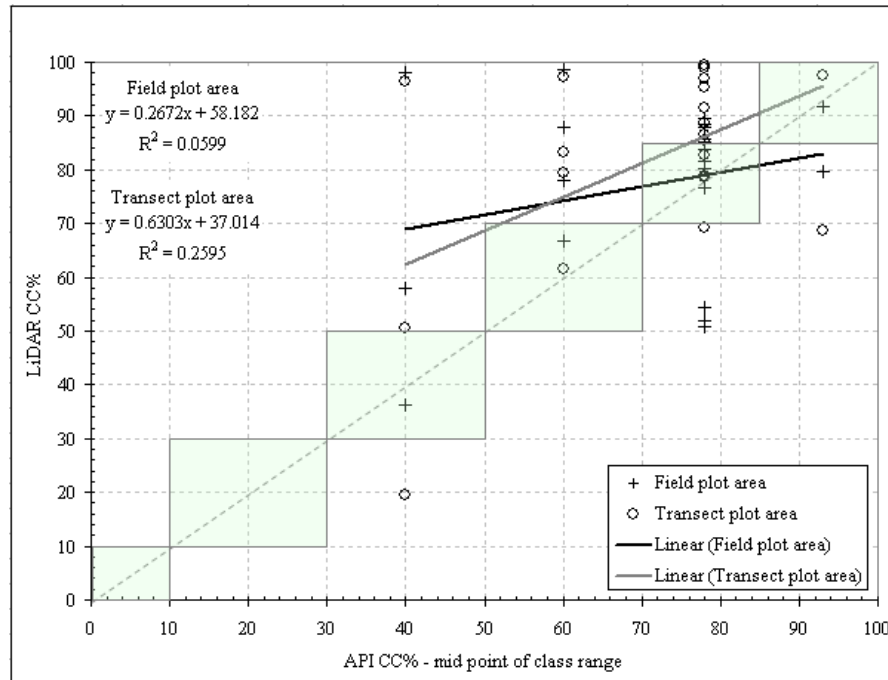


Figure 69: Comparison of individual API polygon CC (mid-point of class) and LiDAR CC (mean, min and max) based on 25m cells within the PSU. Individual polygon IDs have been removed for clarity.



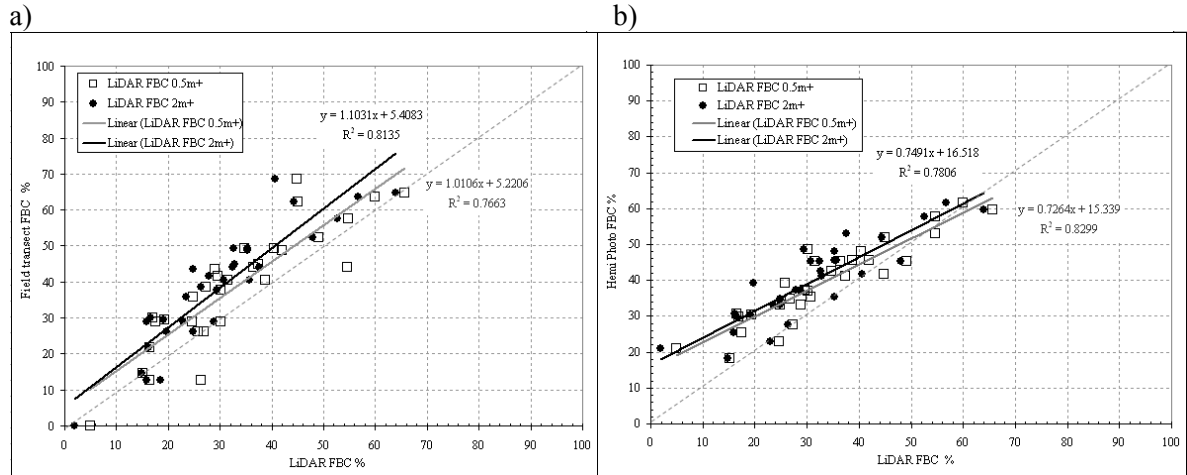
**Figure 70: NE Victorian API CC (mid-point of class) correspondence with the LiDAR CC field plot and transect area sample within the API polygon.**

### *LiDAR foliage-branch cover comparisons with field data*

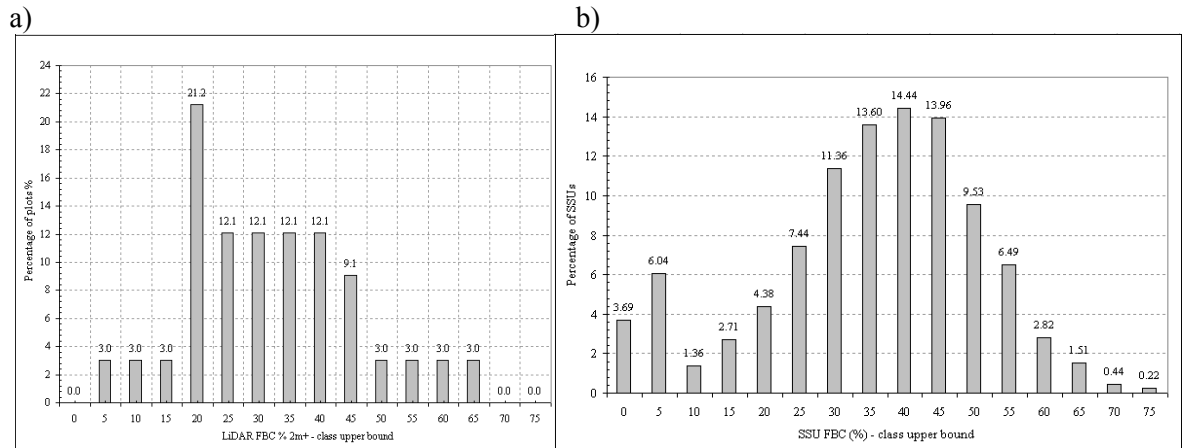
Comparisons between LiDAR foliage-branch cover at both  $> 0.5$  m and  $> 2$  m height thresholds, with field transects (Figure 71a) and hemispherical-photos (Figure 71b) have close correspondences, with  $r^2$  values ranging from 0.77 - 0.83. When compared to field transects, the LiDAR  $> 2$  m threshold has a slightly better  $r^2$  (less variation), but the  $> 0.5$  m threshold selection has a best-fit line closer to the 1:1 line. With hemispherical photo foliage-branch cover, both selections have very similar best-fit lines, when compared to the 1:1 line. Estimates of LiDAR foliage-branch cover were  $\sim 5 - 10\%$  (depending on height threshold) lower on average than those from field transects. Foliage-branch cover estimates generated from hemispherical photographs were similar to LiDAR foliage-branch cover (almost 1:1 correspondence) in plots where cover  $> 40\%$ .

The representativeness of the field plot sample is assessed through comparison of distributions of LiDAR foliage-branch cover across the field plots (Figure 72a), and across all 4500 secondary sampling units in the Injune study area (Figure 72b). The comparison indicates a skew to

the left in the field plots distribution, whereas the study area sample has a more normal distribution, with the majority of values in the 35 - 45 % range. The mean and median LiDAR foliage-branch cover values for the field plots are 29 % and 27.9 % respectively, with the landscape sample mean and median being 33 % and 34.9 % respectively.



**Figure 71: Comparisons of LiDAR FBC at 0.5 and 2 m height thresholds, with a) field transect FBC; and b) FBC derived from hemispherical-photographs.**



**Figure 72: LiDAR FBC distribution from a) Injune field plots; and b) 4500 SSUs across study area.**

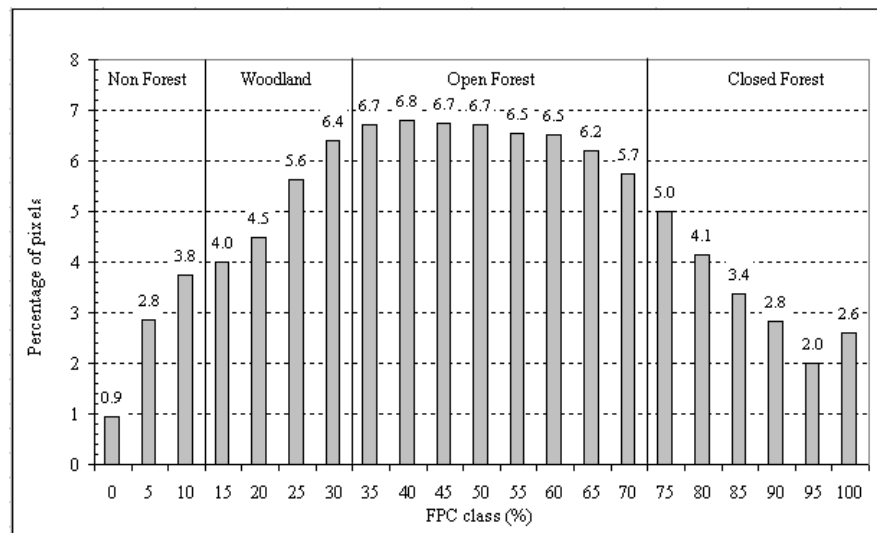


### *SLATS foliage projective cover comparison with LiDAR cover*

Estimates of foliage projective cover across the Injune study area for 2000 (Figure 112 - Appendix A) were generated from Landsat sensor data by the Queensland SLATS program. A summary distribution comparing SLATS foliage projective cover (Figure 73) against LiDAR crown cover and foliage-branch cover using all 150 primary sampling units and converted to National Forest Inventory cover classes, is provided in Table 32. The mean SLATS foliage projective cover value for the study area was 47 % (range 0-100 %,  $\delta = 25$  %), which is higher than the primary sampling unit foliage-branch cover sample mean (as described in the previous section). For each of the National Forest Inventory cover classes, both LiDAR primary sampling unit samples and SLATS foliage projective cover have similar estimates, with the LiDAR crown cover estimates having a closer match (i.e. within  $\pm 5.6$  %) to SLATS. The largest difference is for closed forest between LiDAR foliage-branch cover and SLATS.

**Table 32: Comparison of NFI forest cover class distribution across the Injune landscape using SLATS FPC for study area, and LiDAR PSU sample (1,125ha) for FBC and CC.**

NFI Cover class	LiDAR PSU sample CC estimate (%)	LiDAR PSU sample FBC estimate (%)	SLATS study area FPC estimate (%)
1 – Non forest	11.1	11.1	7.5
2 – Woodland	15.0	25.9	20.5
3 – Open Forest	57.6	62.8	52.0
4 – Closed Forest	16.3	0.2	20.0



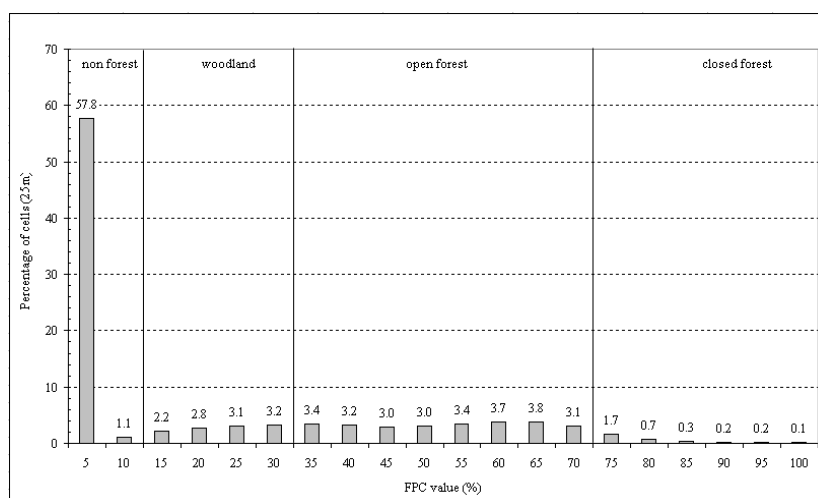
**Figure 73: SLATS Landsat derived FPC distribution for the Injune study area (220,000ha). NFI forest classes are shown.**

In NE Victoria, based on SLATS foliage projective cover data, forest occupies 41.2 % of the area, and non-forest 58.8 % (Figure 74; Figure 113 - Appendix A). Using National Forest Inventory forest classes, comparisons were made at the 20 km systematic sampling sites (field plot and transect area) using hemispherical photos, LiDAR foliage-branch cover and National Forest Inventory data, with the study area estimate using SLATS foliage projective cover and National Forest Inventory data (Table 33). The 20 km grid sample indicates that forest occurs in approximately 42.4 % of the study area (within the Landsat ETM images), which is very close to the SLATS estimate. Overall the forest-non forest split is close (within 10 %) across the different datasets and landscape samples. SLATS foliage projective cover records a lower proportion Open forest (and a correspondingly larger woodland estimate), with the largest disparity found with plot scale comparisons, for both LiDAR and hemi-photo foliage-branch cover.

**Table 33: NE Victotian SLATS FPC for study area compared to LiDAR and hemi-photo data in field plot and transect areas, using percentage of 20km systematic samples in each NFI forest class.**

NFI Cover class	1 – Non forest	2 – Woodland	3 – Open Forest	4 – Closed Forest
Hemi-photo field plot sample (%)	57.6	0.0	42.4	0.0
LiDAR field plot sample (%)	57.6	0.0	39.4	3.0
Hemi-photo transect area sample (%)	57.6	0.0	39.4	3.0
LiDAR transect area sample (%)	57.6	3.0	33.3	6.1
NFI data transect area sample (%) <sup>1</sup>	63.7	3.0	33.3	0.0
NFI study area (%) <sup>2</sup>	65.1	2.7	32.2	0.0
SLATS study area (%)	58.8	11.3	26.7	3.2

<sup>1</sup> NFI data is reported at 100m pixels, therefore field plot and transect area estimates are the same. <sup>2</sup> – Note this NFI estimate is for the entire study area, so open forest in mountains may be over-represented.



**Figure 74: SLATS Landsat derived FPC distribution for the NE Victoria study area. NFI forest classes are shown.**

---

### *Correlations between cover metrics and data sources*

All cover estimates have some potential bias in either the sampling, coverage of the assessment area, or measurement method. Therefore, what is defined as the best estimate varies depending on the data being compared. To explore the relationships between cover metrics and data combinations, data were aggregated into matrix correlation tables for both Injune (Table 34) and NE Victoria (Table 35) (see also Figure 114 and Figure 115 – Appendix A). Data was sourced from field plot transects and tree-maps, hemispherical photos, LiDAR, CASI hyperspectral data, Landsat TM foliage projective cover, and API. Not all the datasets used at Injune were available for NE Victoria. Based on the P-value, all correlations in the Injune data were significantly linear at the 0.05 level, although a number in NE Victoria were not significantly linear at 0.05 (Table 36).

Generally for Injune, LiDAR foliage-branch cover had strong relationships across almost all the other datasets (Table 34). LiDAR derived crown cover had better correlations with other data compared to the canopy height model estimates, though the difference between the two models is minor, as they are strongly correlated with each other ( $r^2 = 0.86$ ; Table 34). For NE Victoria generally the comparisons were much less robust than those found at Injune, with many having a very poor correspondence (Table 35). The best LiDAR foliage-branch cover correlation was with hemispherical-photo foliage-branch cover ( $r^2 = 0.71$ ; Table 35), followed by Landsat foliage projective cover ( $r^2 = 0.59$ ; Table 35).

These tables are useful to determine the likely results when translating between cover data. For example, if only hemispherical photos and Landsat foliage projective cover data were available for one site, and there was a need to make comparisons with other sites that only had LiDAR or field transect measurements, then the table could be used to indicate the level of correlation and potential bias between data and metrics. In this case, hemispherical photo foliage-branch cover has a good correspondence with LiDAR foliage-branch cover ( $r^2 = 0.80$ , slope = 1.05; Table 34), whereas the correlation with foliage-branch cover from field transects is more variable ( $r^2 = 0.66$ , slope = 1.10; Table 34).

Table 34: Matrix of correlations for cover metrics across a range of datasets and measurement scales, for the Injune field plots \*

		X									
		Field transect FPC	Field transect FBC	Field hemi-photo FBC	Field tree map CC	LiDAR FBC (2m <sup>+</sup> )	LiDAR CC (2m <sup>+</sup> ) - HSCOI	LiDAR CC (2m <sup>+</sup> ) - CHM	CASI CC	Landsat FPC	API CC class mid point
Y	Field transect FPC	*	$y=0.5902x+2.0843$ $r^2=0.80$ RSE = 4.84	$y=0.6919x-1.8503$ $r^2=0.57$ RSE = 6.99	$y=0.4227x+5.587$ $r^2=0.61$ RSE = 6.81	$y=0.6418x+5.7556$ $r^2=0.66$ RSE = 6.28	$y=0.5651x-0.3867$ $r^2=0.79$ RSE = 5.0	$y=0.5111x-3.2059$ $r^2=0.76$ RSE = 5.27	$y=0.4584x+1.6946$ $r^2=0.71$ RSE = 6.0	$y=0.8304x-7.7536$ $r^2=0.73$ RSE = 6.57	$y=0.4085x+9.4929$ $r^2=0.41$ RSE = 8.3
	Field transect FBC	$y=1.3559x+5.0031$ $r^2=0.80$ RSE = 7.33	*	$y=1.104x-3.834$ $r^2=0.66$ RSE = 9.26	$y=0.7225x+5.6418$ $r^2=0.77$ RSE = 7.89	$y=1.0755x+6.5814$ $r^2=0.81$ RSE = 7.13	$y=0.9097x-2.0253$ $r^2=0.89$ RSE = 5.49	$y=0.8371x-7.3597$ $r^2=0.89$ RSE = 5.42	$y=0.7206x+2.0422$ $r^2=0.75$ RSE = 8.3	$y=1.3339x-13.7854$ $r^2=0.71$ RSE = 8.85	$y=0.728x+11.1732$ $r^2=0.57$ RSE = 10.77
	Field hemi-photo FBC	$y=0.8277x+18.5398$ $r^2=0.57$ RSE = 7.65	$y=0.5981x+15.8151$ $r^2=0.66$ RSE = 6.82	*	$y=0.4426x+18.8876$ $r^2=0.56$ RSE = 7.77	$y=0.756x+16.5694$ $r^2=0.80$ RSE = 5.29	$y=0.5566x+14.3031$ $r^2=0.65$ RSE = 6.97	$y=0.5373x+9.4835$ $r^2=0.70$ RSE = 6.39	$y=0.5071x+13.4023$ $r^2=0.73$ RSE = 6.14	$y=0.9618x+1.4261$ $r^2=0.74$ RSE = 5.92	$y=0.4736x+21.2693$ $r^2=0.47$ RSE = 8.51
	Field tree map CC	$y=1.4309x+10.3619$ $r^2=0.61$ RSE = 12.52	$y=1.0646x+4.718$ $r^2=0.77$ RSE = 9.57	$y=1.2617x-2.9593$ $r^2=0.56$ RSE = 13.13	*	$y=1.2991x+7.0488$ $r^2=0.80$ RSE = 8.84	$y=1.0377x-0.5787$ $r^2=0.78$ RSE = 9.25	$y=0.9717x-7.594$ $r^2=0.82$ RSE = 8.58	$y=0.8126x+4.568$ $r^2=0.65$ RSE = 11.99	$y=1.5098x-13.5022$ $r^2=0.62$ RSE = 12.34	$y=0.8048x+15.4628$ $r^2=0.47$ RSE = 14.47
	LiDAR FBC (2m <sup>+</sup> )	$y=1.0341x+4.2479$ $r^2=0.66$ RSE = 7.97	$y=0.7543x+0.7595$ $r^2=0.81$ RSE = 5.97	$y=1.0527x-11.1677$ $r^2=0.80$ RSE = 6.24	$y=0.6184x+1.6068$ $r^2=0.80$ RSE = 6.10	*	$y=0.7477x-3.5553$ $r^2=0.86$ RSE = 5.22	$y=0.6907x-8.0879$ $r^2=0.87$ RSE = 5.05	$y=0.6214x-1.5775$ $r^2=0.81$ RSE = 6.16	$y=1.1737x-16.2751$ $r^2=0.78$ RSE = 6.41	$y=0.5983x+7.2921$ $r^2=0.55$ RSE = 9.23
	LiDAR CC (2m <sup>+</sup> ) - HSCOI	$y=1.3933x+10.1783$ $r^2=0.79$ RSE = 7.84	$y=0.9764x+7.044$ $r^2=0.89$ RSE = 5.59	$y=1.1587x-0.1244$ $r^2=0.65$ RSE = 10.06	$y=0.7559x+10.2076$ $r^2=0.78$ RSE = 7.89	$y=1.1442x+10.6155$ $r^2=0.86$ RSE = 6.46	*	$y=0.8633x-2.6972$ $r^2=0.88$ RSE = 5.82	$y=0.7565x+6.2952$ $r^2=0.77$ RSE = 8.24	$y=1.4019x-10.3488$ $r^2=0.73$ RSE = 8.84	$y=0.7464x+16.5793$ $r^2=0.56$ RSE = 11.3
	LiDAR CC (2m <sup>+</sup> ) - CHM	$y=1.4927x+17.9715$ $r^2=0.76$ RSE = 9.01	$y=1.0642x-13.9005$ $r^2=0.89$ RSE = 6.11	$y=1.311x+4.2466$ $r^2=0.70$ RSE = 9.93	$y=0.8383x+16.6787$ $r^2=0.82$ RSE = 7.97	$y=1.252x+17.6469$ $r^2=0.87$ RSE = 6.80	$y=1.0226x+9.2787$ $r^2=0.88$ RSE = 6.34	*	$y=0.8139x+13.5710$ $r^2=0.76$ RSE = 9.34	$y=1.512x-4.4161$ $r^2=0.72$ RSE = 9.85	$y=0.7992x+24.8477$ $r^2=0.54$ RSE = 12.55
	CASI CC	$y=1.5386x+12.6376$ $r^2=0.71$ RSE = 10.92	$y=1.0448x+10.6485$ $r^2=0.75$ RSE = 10.0	$y=1.4429x-5.2390$ $r^2=0.73$ RSE = 10.35	$y=0.7998x+14.4563$ $r^2=0.65$ RSE = 11.9	$y=1.2949x+12.1458$ $r^2=0.81$ RSE = 8.89	$y=1.0218x+5.3099$ $r^2=0.77$ RSE = 9.58	$y=0.9271x+0.1165$ $r^2=0.76$ RSE = 9.96	*	$y=1.8037x-20.1732$ $r^2=0.89$ RSE = 6.69	$y=0.7814x+21.1419$ $r^2=0.43$ RSE = 15.13
	Landsat FPC <sup>a</sup>	$y=0.7603x+20.5313$ $r^2=0.73$ RSE = 6.29	$y=0.5316x+18.8681$ $r^2=0.71$ RSE = 5.59	$y=0.7735x+9.1137$ $r^2=0.74$ RSE = 5.31	$y=0.4084x+20.7390$ $r^2=0.62$ RSE = 6.42	$y=0.6669x+19.48$ $r^2=0.78$ RSE = 4.83	$y=0.5206x+16.1164$ $r^2=0.73$ RSE = 5.39	$y=0.474x+13.3456$ $r^2=0.72$ RSE = 5.52	$y=0.4930x+14.3619$ $r^2=0.89$ RSE = 3.5	*	$y=0.4224x+23.4434$ $r^2=0.48$ RSE = 7.46
	API CC class mid point <sup>b</sup>	$y=1.0089x+13.0544$ $r^2=0.41$ RSE = 13.05	$y=0.7826x+7.8216$ $r^2=0.57$ RSE = 11.16	$y=0.9938x-0.4193$ $r^2=0.47$ RSE = 12.33	$y=0.5872x+11.2249$ $r^2=0.47$ RSE = 12.36	$y=0.9172x+10.6835$ $r^2=0.55$ RSE = 11.43	$y=0.7477x+4.6169$ $r^2=0.56$ RSE = 11.31	$y=0.6759x+0.9089$ $r^2=0.54$ RSE = 11.54	$y=0.5549x+10.4365$ $r^2=0.43$ RSE = 12.75	$y=1.1395x-6.7474$ $r^2=0.48$ RSE = 12.25	*

a – Landsat FPC value for plot uses mean of 5 pixels

b – For the LSP API, only Landsat is a complete comparison within the polygon - all other datasets are a sample.

P-values for all comparisons were significantly less than 0.01. The mean P-value was  $7.22e^{-6}$ , standard deviation =  $2.48e^{-5}$ , range  $5.33e^{-15}$  –  $1.31e^{-4}$ .

\* For comparisons that do not include CASI or hemispherical photos  $n = 30$ . Where CASI or hemi-photos are compared to the other data,  $n = 29$ . Where CASI and hemi-photos are compared against each other,  $n = 28$ .

**Table 35: Matrix of correlations for cover metrics across a range of datasets and measurement scales, for the NE Victorian field plots**

	X					
	Field hemi-photo FBC	Field tree map CC	LiDAR FBC (2m+)	LiDAR CC (2m+) - HSCOI	Landsat FPC	API CC class mid-point
Field hemi-photo FBC	x	$y=0.2917x + 37.6015$ $r^2 = 0.22$ RSE = 10.42	$y=0.7864x + 7.1867$ $r^2 = 0.71$ RSE = 6.31	$y=0.5076x + 15.6266$ $r^2 = 0.55$ RSE = 7.92	$y=0.8377x + 13.8103$ $r^2 = 0.80$ RSE = 4.80	$y=0.2049x + 40.2527$ $r^2 = 0.08$ RSE = 11.35
Field tree map CC	$y=0.7556x + 17.5120$ $r^2 = 0.22$ RSE = 16.76	x	$y=0.6126x + 21.8292$ $r^2 = 0.17$ RSE = 17.33	$y=0.6084x + 11.9781$ $r^2 = 0.30$ RSE = 15.84	$y=0.4320x + 36.8720$ $r^2 = 0.06$ RSE = 19.19	$y=0.4262x + 28.6825$ $r^2 = 0.13$ RSE = 17.76
LiDAR FBC (2m+)	$y=0.9079x + 10.7857$ $r^2 = 0.71$ RSE = 6.78	$y=0.2730x + 44.4420$ $r^2 = 0.17$ RSE = 11.57	x	$y=0.5336x + 19.3657$ $r^2 = 0.53$ RSE = 8.73	$y=0.6249x + 28.1129$ $r^2 = 0.59$ RSE = 6.08	$y=0.2286x + 44.3127$ $r^2 = 0.08$ RSE = 12.15
LiDAR CC (2m+) <sup>b</sup>	$y=1.0810x + 17.9153$ $r^2 = 0.55$ RSE = 11.56	$y=0.5001x + 47.6758$ $r^2 = 0.30$ RSE = 14.36	$y=0.9842x + 17.5683$ $r^2 = 0.53$ RSE = 11.86	x	$y=0.7485x + 39.4733$ $r^2 = 0.27$ RSE = 14.25	$y=0.2672x + 58.1821$ $r^2 = 0.06$ RSE = 16.69
Landsat FPC <sup>a</sup>	$y=0.9572x - 4.2470$ $r^2 = 0.80$ RSE = 5.13	$y=0.1462x + 37.0314$ $r^2 = 0.06$ RSE = 11.16	$y=0.9354x - 7.4855$ $r^2 = 0.59$ RSE = 7.43	$y=0.3586x + 18.9718$ $r^2 = 0.27$ RSE = 9.86	x	$y=0.3159x + 22.6596$ $r^2 = 0.16$ RSE = 10.59
API CC class mid point	$y=0.3660x + 50.8569$ $r^2 = 0.08$ RSE = 15.16	$y=0.2939x + 53.5968$ $r^2 = 0.13$ RSE = 14.75	$y=0.3537x + 49.5000$ $r^2 = 0.08$ RSE = 15.12	$y=0.2242x + 53.6157$ $r^2 = 0.06$ RSE = 15.29	$y=0.4974x + 49.0894$ $r^2 = 0.16$ RSE = 13.29	x

a) – Landsat FPC value for plot uses mean of 5 pixels, and uses uncalibrated Landsat FPC data. b) – Derived from HSCOI modelling.

**Table 36: Matrix of P-values for cover metric correlations across a range of datasets and measurement scales, for the NE Victorian field plots**

	Field hemi-photo FBC	Field tree map CC	LiDAR FBC	LiDAR HSCOI CC -	Landsat FPC
Field tree map CC	0.02751	x			
LiDAR FBC (2m+)	7.51e-07	0.0588	x		
LiDAR HSCOI CC (2m+)	0.00008047	0.007789	0.0001365	x	
Landsat FPC	5.14e-07	0.3144	0.0002197	0.02763	x
API CC class mid point	0.2175	0.1061	0.1996	0.2722	0.1034

### ***Crown separation method test results***

Crown separation comparisons with field and LiDAR data indicate a close match between the crown separation crown cover (zig-zag method) and other crown cover data for p142-13, with a maximum difference between the crown cover estimates of 7.3% (Table 37). The crown separation crown cover for p81-16 has greater differences with the other crown cover data (up to 40.5 %; Table 37). Both plots have the LiDAR crown cover estimate closer (compared to tree-map crown cover) to the crown separation crown cover estimate, with differences of 3.1 % and 16.8 % for p142-13 and p81-16 respectively. Both plots have LiDAR and hemispherical photo foliage-branch cover values similar to the crown separation crown cover. A LiDAR HSCOI derived tree stem is found in close vicinity to a field mapped stem in most cases (Figure 75 for p142-13; Figure 76 for p81-16), with the HSCOI stem accuracy table found in section 4.5.1.

**Table 37: Crown separation test comparison for p142-13 and p81-16.**

<b>Cover or measurement Metric</b>	<b>Transect 1</b>	<b>Transect 2</b>	<b>Transect 3</b>	<b>Plot Total</b>
<i>P142-13</i>				
Number of trees used	8	8	8	24
Total plot trees 5cm+ D <sub>130</sub> (>10cm D <sub>130</sub> )				63 (43)
Zig Zag mean field crown diameter (m)	4.3	5.2	5.3	4.9
Zig Zag mean LiDAR crown diameter (m)	4.4	5.2	5.0	4.9
Zig Zag mean dist. to next crown (m)	4.2	3.5	2.3	3.3
Zig-Zag CC %	20.2	28.7	39.4	28.6
LiDAR CC %				31.7
Field tree map CC %				35.9
Field Transect FBC %	19.2	21.2	25.0	21.8
Photo FBC % <sup>a</sup>	27.7	35.0	29.5	30.7
LiDAR FBC (2m+) %	(west-30m)	(cntr-20m)	(east-30m)	16.2
<i>P81-16</i>				
Number of trees used	14	10	9	33
Total plot trees 5cm+ D <sub>130</sub> (>10cm D <sub>130</sub> )				117 (67)
Zig Zag mean field crown diameter (m)	4.7	5.3	8.0	5.8
Zig Zag mean LiDAR crown diameter (m)	4.1	4.7	7.3	5.2
Zig Zag mean dist. to next crown (m)	1.7	2.1	2.0	1.9
Zig-Zag CC %	43.5	41.5	51.9	45.8
LiDAR CC %				62.6
Field tree map CC %				86.3
Field Transect FBC %	51.9	44.2	59.6	51.9
Photo FBC % <sup>a,b</sup>		45.4		45.4
LiDAR FBC %		(cntr-20m)		48.0

<sup>a</sup> Hemispherical photos used are from the distance along transects from start of transect (southern edge of plot) as indicated in table (see also Figure 75).

<sup>b</sup> Only 1 photo was processed for this plot.

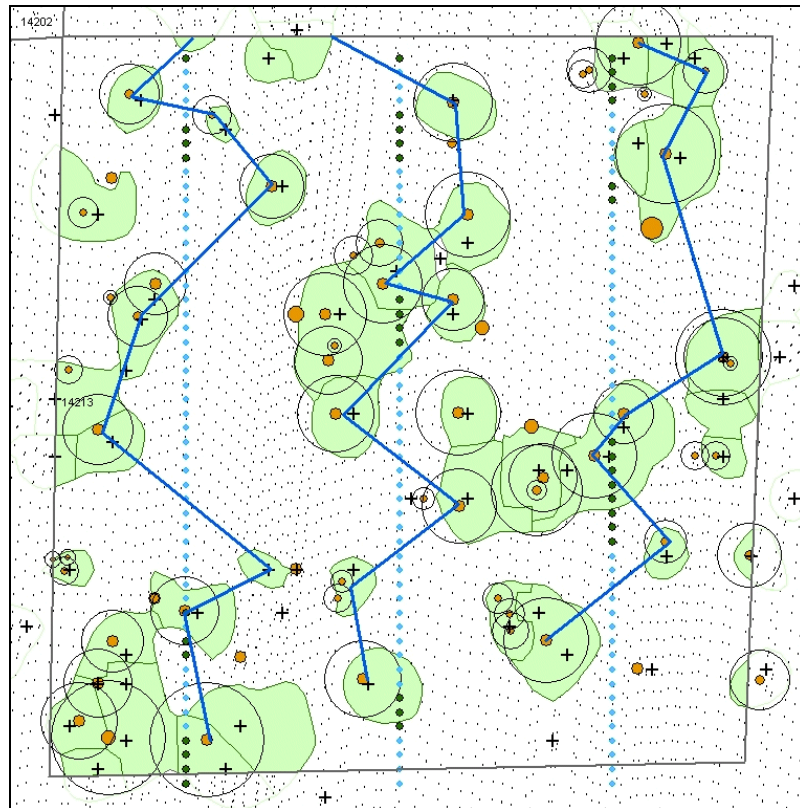


Figure 75: Crown separation transect method for p142-13. Field mapped stems are solid orange circles (proportional to  $D_{130}$ ) and open circles (proportional to mean crown radius). LiDAR point sampling density (grey) and HSCOI crown delineations (green) are shown. Field plot boundaries and transects are 50m long.

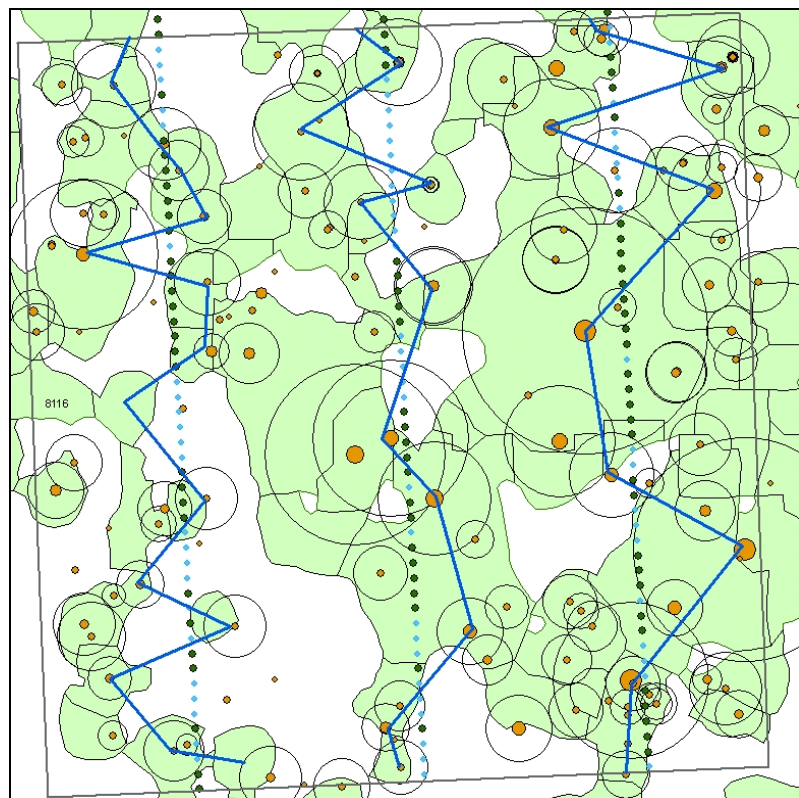


Figure 76: Crown separation transect method for p81-16. Map elements are described in the Figure 75 caption. Field plot boundaries and transects are 50m long.

The LiDAR apparent vertical profiles and illustrative photographs (Figure 77) indicate the vertical structure of the different plots, highlighting the difference in understorey presence, and in the range of foliage heights, which could be factors in the results presented in Table 37. The apparent vertical profile for p142-13 shows the plot has a single dominant overstorey stratum, and is shorter in maximum (14 m) and predominant height (12 m) than p81-16 (23 m and 18 m respectively). From other results the stem density is low (252 stems ha<sup>-1</sup> D<sub>130</sub> ≥ 5 cm), and the trees are well separated, thus making it easier to estimate crown cover, especially as the zig-zag transect trees account for 38 % of all trees measured in the field, and up to 56 % of the potential overstorey trees (i.e. those with D<sub>130</sub> > 10 cm).

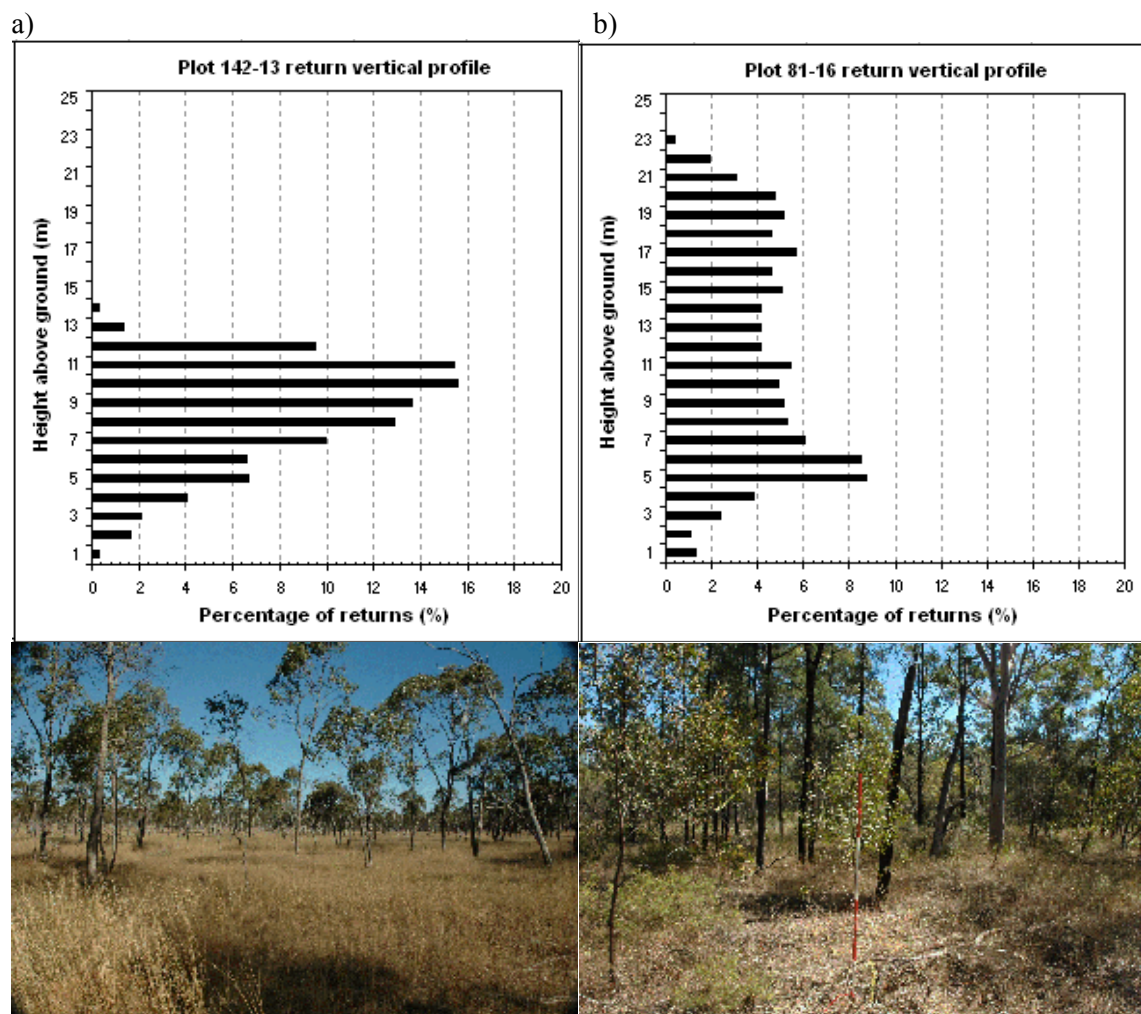


Figure 77: Apparent vertical profiles for p142-13 (a) and p81-16 (b), highlight different vertical foliage characteristics, which may contribute to the different cover results observed.



Conversely, the zig-zag crown cover estimate for p81-16 is much lower than the other crown cover estimates, and this may be a function of the stem density ( $460 \text{ stems ha}^{-1} D_{130} \geq 5 \text{ cm}$ ) being almost double that found in p142-13. Additionally the zig-zag transect trees account for a lower proportion of all trees (28 %), and of potential overstorey trees (49 %).

#### 4.4.2 Forest cover assessment at a range of scales

Multi-scale foliage-branch cover comparison between LiDAR and hemispherical photos was undertaken using NE Victoria plots at two field measurement scales: field plot and transect areas (Figure 78, Figure 79, and Table 38). All three comparisons were quite similar, with the best between LiDAR ( $> 2 \text{ m}$  height threshold) at the transect area scale (i.e. 1 ha) and the field plot centre photo (Table 38). The trial of multi-sensor and multi-scale assessment of foliage-branch cover at a single location (plot 220) (Figure 80), indicated that the woody area from SPOT5 HRV and LiDAR agree at the 2.5 m pixel scale. With the AGO Landsat layer used, a 50 % internal pixel coverage has the closest match to the LiDAR foliage-branch cover estimate. The hemispherical photo foliage-branch cover estimate was within the range of the other datasets used.

Results of the investigation of how the foliage-branch cover estimates changed with an increasing circular assessment area were generated for the following ecozones: Floodplain (Figure 81), Foothills (Figure 82), Subalpine (Figure 83), Montane (Figure 84), and for Injune (Figure 85). The results of the NE Victorian analyses, averaged by ecozone, illustrate the potential effect of scale, with large mean foliage-branch cover variation ( $> 10 \%$ ) observed for floodplains, but less mean variation ( $< 10 \%$ ) for other locations (Table 39).

**Table 38: FBC comparison between field plot and transect area combinations for NE Victoria.**

FBC% parameters (y vs x)	$r^2$	RSE	function	p-value	n
Field plot LiDAR vs field plot photo	0.71	6.78	$y = 0.9079x + 10.786$	$7.507e^{-7}$	22
Transect area LiDAR vs transect photos <sup>a</sup>	0.65	8.93	$y = 0.9605x + 8.1235$	$5.426e^{-6}$	22
Transect area LiDAR vs field plot photo	0.74	7.75	$y = 1.1045x + 1.2794$	$2.995e^{-7}$	22

<sup>a</sup> – mean of five photos

**Table 39: Summary of LiDAR FBC at different scales, averaged per NE Victorian ecozone.**

Reference size	field plot	transect area		LiDAR swath			
Circle area (ha)	0.07	0.8	3.1	12.6			
Radius Distance (m)	15	50	100	200	<sup>1</sup> Diff (plot-swath)		
Ecozone Cover						# plots	
Floodplain	<sup>2</sup> FBC %	55.4	55.8	44.1	40.0	15.4	4
	<sup>3</sup> SD %	2.5	4.6	9.8	14.2		
Foothills	FBC %	54.9	51.8	49.9	46.0	8.9	6
	SD %	12.4	17.3	18.3	18.9		
Montane	FBC %	71.8	72.2	69.5	68.0	3.8	9
	SD %	15.1	11.5	11.4	11.1		
Subalpine	FBC %	73.9	69.8	68.7	67.3	6.7	3
	SD %	9.7	3.6	4.6	1.8		
Region Mean		64.0	62.4	58.1	55.3	8.7	22

<sup>1</sup> – Difference between the field plot cover estimate and swath (stand) cover estimate

<sup>2</sup> - Mean Foliage Branch Cover percent

<sup>3</sup> - Mean Standard Deviation

A more detailed assessment of the results indicates that field plot area (0.09 ha) foliage-branch cover estimates are 5-10% higher on average, than with larger assessment areas, with some sites having a difference as large as 35 %. There was a general shift to lower foliage-branch cover across all plots as the assessment scale increases in area. Floodplain stands have the greatest variability as assessment area increases, while Montane and Subalpine stands have little variability, with woodlands in the Foothill zone showing moderate variability, depending on landscape context. For Injune, the results are much more consistent across all locations, with the wider primary sampling unit foliage-branch cover estimate generally within  $\pm 5$  % of the field plot (0.25 ha) foliage-branch cover estimate.

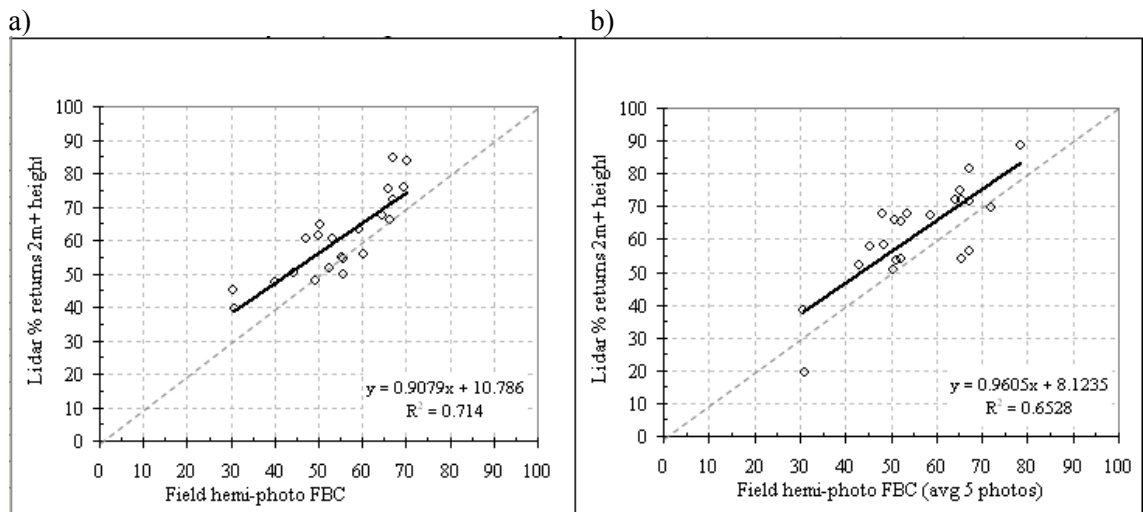


Figure 78: Comparison of FBC from LiDAR and hemispherical photos, in a) field plot area; and b) transect area.

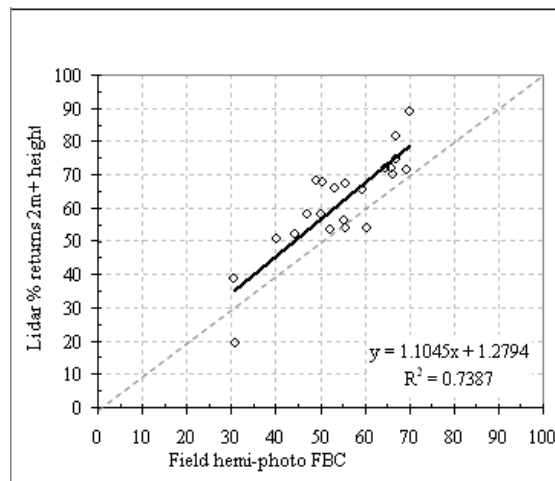


Figure 79: Comparison of FBC from LiDAR in transect area and field plot hemispherical-photo.

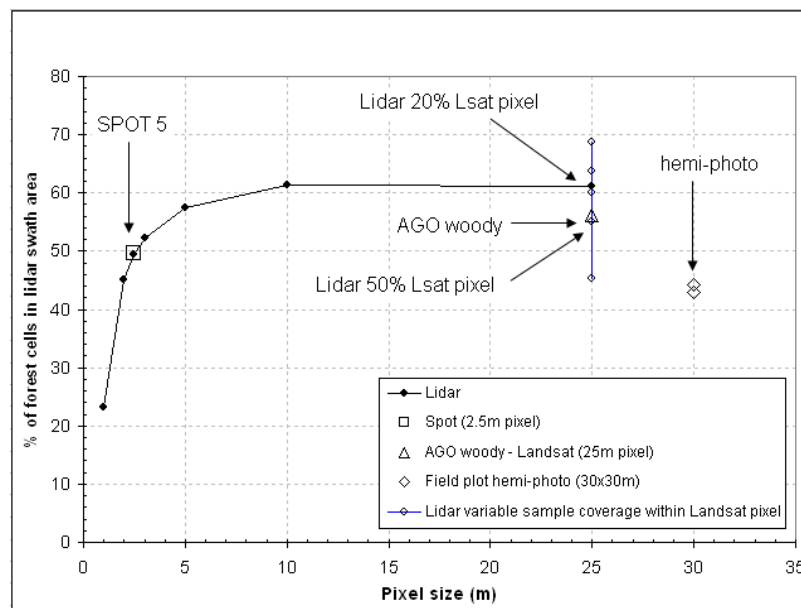


Figure 80: Comparison of FBC for different data and pixel sizes, within the LiDAR swath for NE Victorian plot 220.

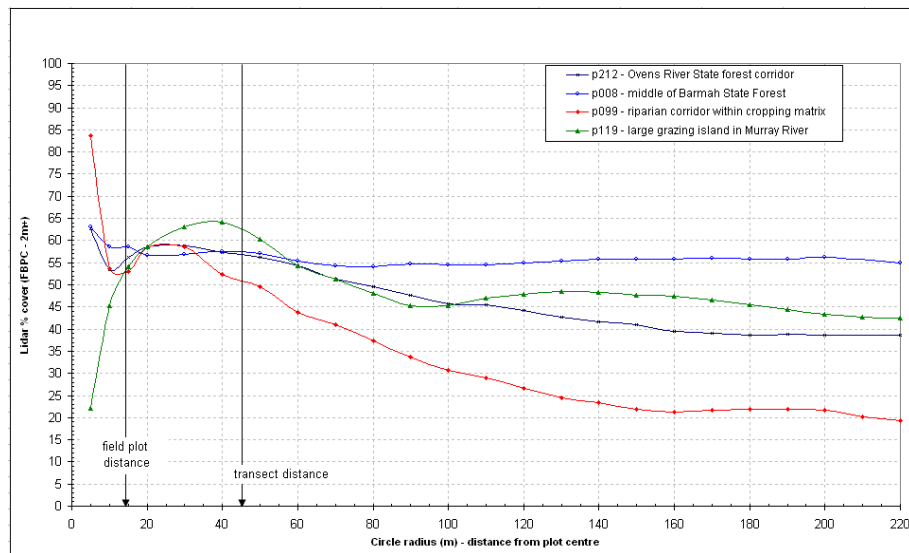


Figure 81: LiDAR FBC at plot locations with increasing assessment area, for Floodplain ecozone.

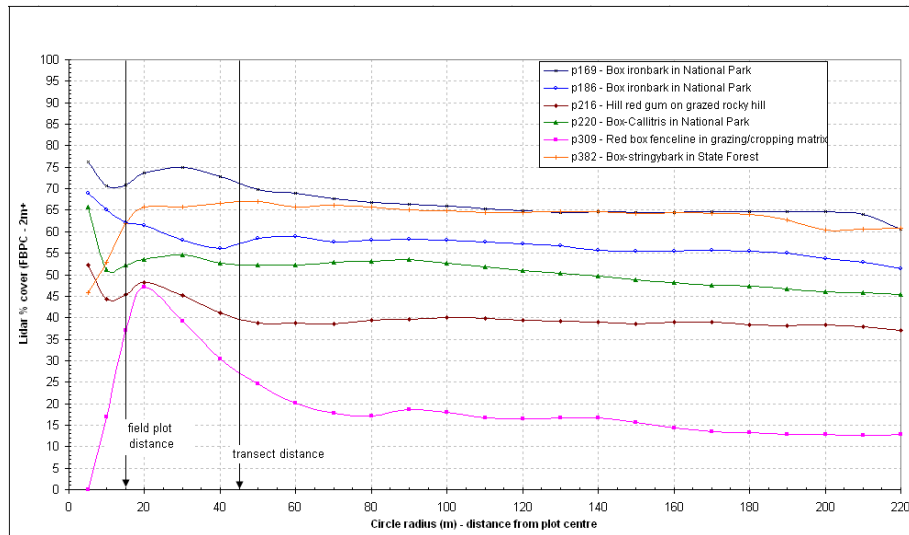


Figure 82: LiDAR FBC at plot locations with increasing assessment area, for Foothills ecozone.

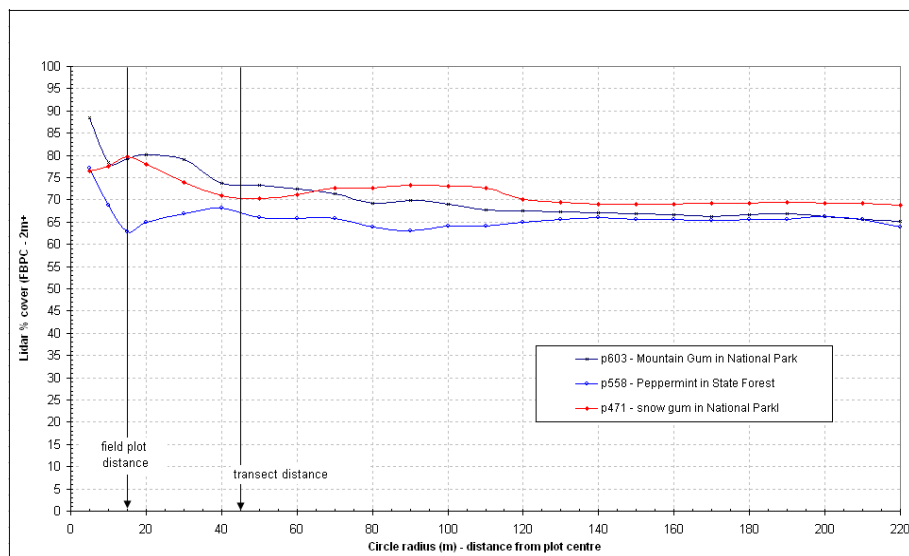
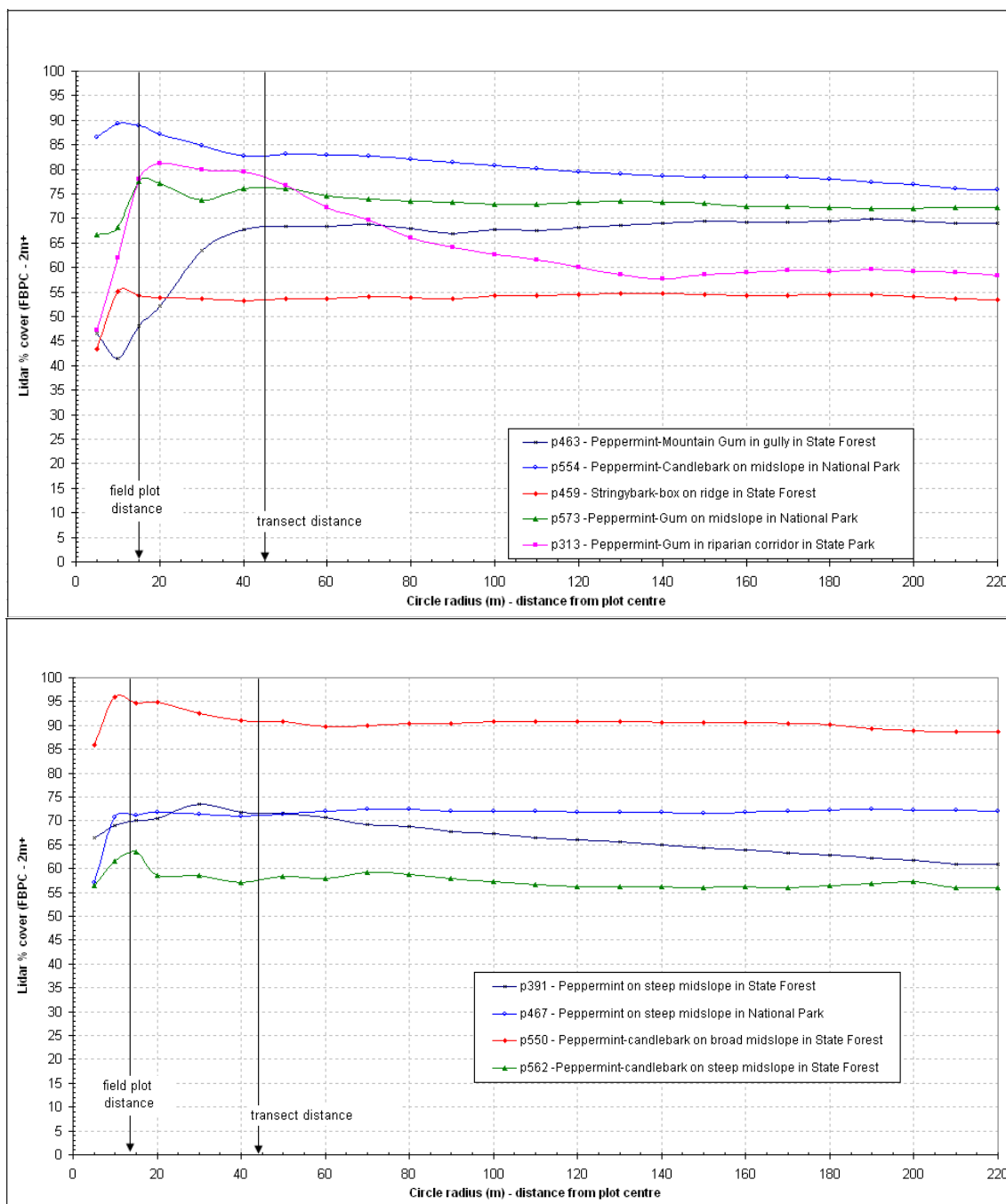


Figure 83: LiDAR FBC at plot locations with increasing assessment area, for Subalpine ecozone



**Figure 84: LiDAR FBC at plot locations with increasing assessment area, for the NE Victorian Montane ecozone.**

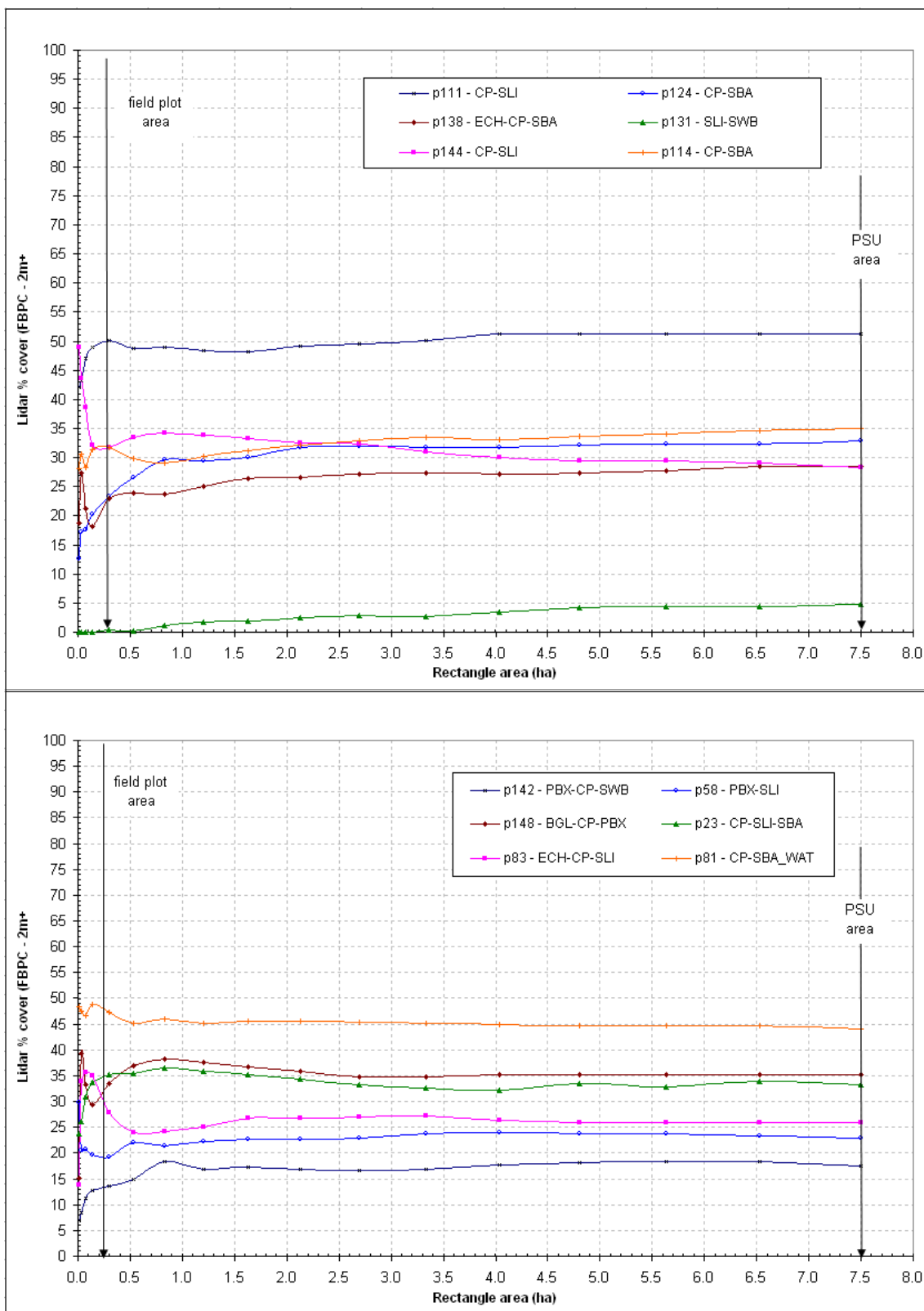


Figure 85: LiDAR FBC at plot locations with increasing assessment area for Injune.

## 4.5 Tree Scale Stem and Crown Delineation Results

This section outlines the results of the tree scale basic geographic entity modelling using the Height Scaled Crown Openness Index (HSCOI). These entities will be used subsequently as part of the case studies presented in the following section, to provide evidence that the multi-scale LiDAR strategy to link field data with remote sensing is valid and robust. This in turn will help to address the primary research question, and determine how LiDAR can improve the assessment of forest structure. Evaluation covers tree level location and plot level stem density, and the spatial arrangement of stems based on Ripley's  $L$ -function nearest neighbour analysis. Crown cover comparisons were presented in the previous section. Both individual tree height and predominant stem height comparisons are made with field data, along with an assessment of  $D_{130}$ , as estimated using empirical functions with tree height. Further validation of the methodology for plot stem density is provided for a range of forest types within northeast Victoria, a proportion of which were structurally similar to those observed at Injune. The majority of the results for this section are fully described in Lee and Lucas (2007), in Appendix C.

### 4.5.1 Tree stem density and location

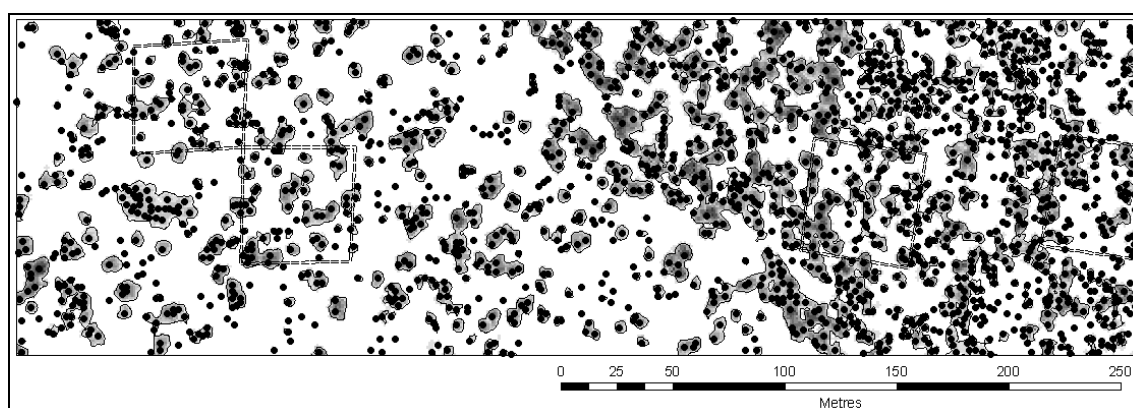
#### *Stem mapping at Injune*

Maps of stem locations, together with crown boundaries, were generated using HSCOI layers for each of 12 primary sampling units (see example in Figure 86). Stem density estimates from 30 plots contained within the 12 primary sampling units were compared with those generated using the HSCOI for the equivalent area and a close correspondence was observed across the stem density range (Table 40). However, for higher densities ( $n > 700$  stems  $\text{ha}^{-1}$ ), a larger number of field stems with  $D_{130} < 10$  cm were not identified using the HSCOI. To evaluate the success of tree location, one field plot from each of the 12 primary sampling units was selected, with the addition of all four field plots associated with primary sampling unit 142,

as these had been assessed previously for another study (Lucas *et al.*, 2006c). HSCOI mapped trees were matched manually to those identified in the field, with the process considering similarities primarily in location, but also height,  $D_{130}$  and estimated crown area.

**Table 40: Tree stem density per plot correspondence for Injune and NE Victoria from HSCOI modelling**

y (Field)	x (LiDAR)	$r^2$	RSE	$n$	Function	P-value
Injune Stem count - all	Stem count (HSCOI)	0.82	133 stems $\text{ha}^{-1}$	30	$y = 1.539x - 142.63$	$3.774e^{-12}$
NE Victoria stem count - all	Stem count (HSCOI)	0.19	152 stems $\text{ha}^{-1}$	22	$y = 0.513x + 73.55$	0.04469
NE Victoria stem count – good match	Stem count (HSCOI)	0.55	62 stems $\text{ha}^{-1}$	7	$y = 0.6756x + 180.74$	0.05681
NE Victoria stem count – poor match	Stem count (HSCOI)	0.67	74 stems $\text{ha}^{-1}$	15	$y = 0.6547x - 90.78$	0.000183

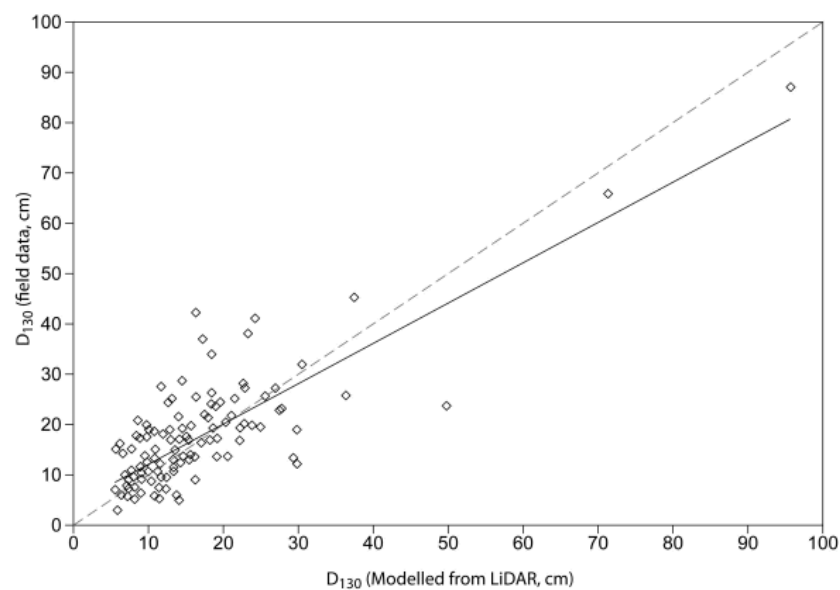


**Figure 86: Crown/clusters and stem locations identified using the HSCOI surface generated for PSU 142. Darker areas in the  $\text{HSCOI}_{\text{stand}}$  surface indicate crowns that are taller and contain a greater density of canopy elements. Internal squares are SSU field plot locations numbered (from left to right) as 02, 13, 18 and 20.**



### *Tree scale stem diameter derived from height*

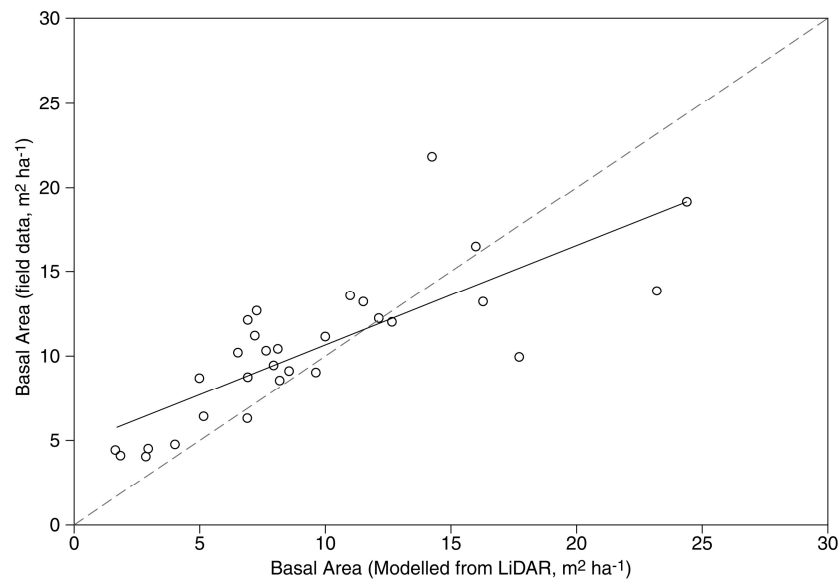
The comparison of  $D_{130}$  between field data and that estimated using LiDAR height and empirical functions was similar to the field tree height-to- $D_{130}$  validation result ( $r^2 = 0.65$ , RSE = 6.89 cm,  $n = 119$ , P-value = 0, regression function  $y = 0.7933x + 4.3875$ ) (Figure 87). Some scatter was observed for trees with 20 - 30 cm  $D_{130}$ , which was attributed to height errors as described in section 4.6.4, although the mean difference between LiDAR and field was -1 cm (LiDAR diameter less than field). The two large-diameter stems may also influence the comparison unduly, and if removed then the correlation would be less than currently observed. Whilst scatter in the correlation is evident, approximately 61 % of the validation set of HSCOI mapped stems had a  $D_{130}$  estimate within 5 cm of the field estimate, and 87 % were within 10 cm of the  $D_{130}$  estimate.



**Figure 87: Correspondence between field-measured  $D_{130}$ , and height derived  $D_{130}$  from HSCOI derived stems.**

The basal area estimated from  $D_{130}$  measurements of field trees and HSCOI stems was also compared for 30 field plots (Figure 88), with the relationship showing that the variability observed at the tree level also occurred at the plot level ( $r^2 = 0.61$ , RSE = 2.69  $\text{m}^2 \text{ha}^{-1}$ ,  $n = 30$ ). At the plot level, the comparison for plots with a basal area of up to 10  $\text{m}^2 \text{ha}^{-1}$  ( $n = 13$ ) had a mean difference between field and LiDAR of -1.3  $\text{m}^2 \text{ha}^{-1}$  ( $\delta = 1.22$ , min = -3.66, max = 0.61) with LiDAR recording the lower basal area estimate. For plots with basal area > 10  $\text{m}^2 \text{ha}^{-1}$  ( $n =$

17) the relationship was much more variable, with a mean difference of  $-0.62 \text{ m}^2 \text{ ha}^{-1}$  ( $\delta = 4.65$ ,  $\text{min} = -7.49$ ,  $\text{max} = 9.4$ ).



**Figure 88: Correspondence between plot-level basal area, for stems measured in the field and estimated from LiDAR HSCOI modelling.**

#### 4.5.2 Tree crown delineation results

Of the 119 randomly selected trees from across all Injune field plots, 90 were selected for validation of the individual crown delineation methods. These trees were generally (though not exclusively) in the overstorey, and the mix of mainly overstorey and some sub-canopy trees allowed an objective assessment of the crown delineation methods. This also allowed an indication of the feasibility of mapping crowns in the sub-canopy (in addition to stems) to be made. Six different types of comparison between field and LiDAR crowns were identified in the validation set (Table 41). The summary results outline the mean area of each aggregated class and statistics of the difference between field and LiDAR crown area estimates (Table 42). Specific examples from different field plots (Table 43) are used to inform the summary and correspondence between the two sets of data (Figure 89). The LiDAR derived crowns which were not found within clusters (i.e. dominant, single and isolated - Table 41) had a close correspondence with the associated field stems on average, with crown area differences in the order of  $\pm 4 \text{ m}^2$  (Table 42).

**Table 41: Description of LiDAR crown delineation validation classification types.**

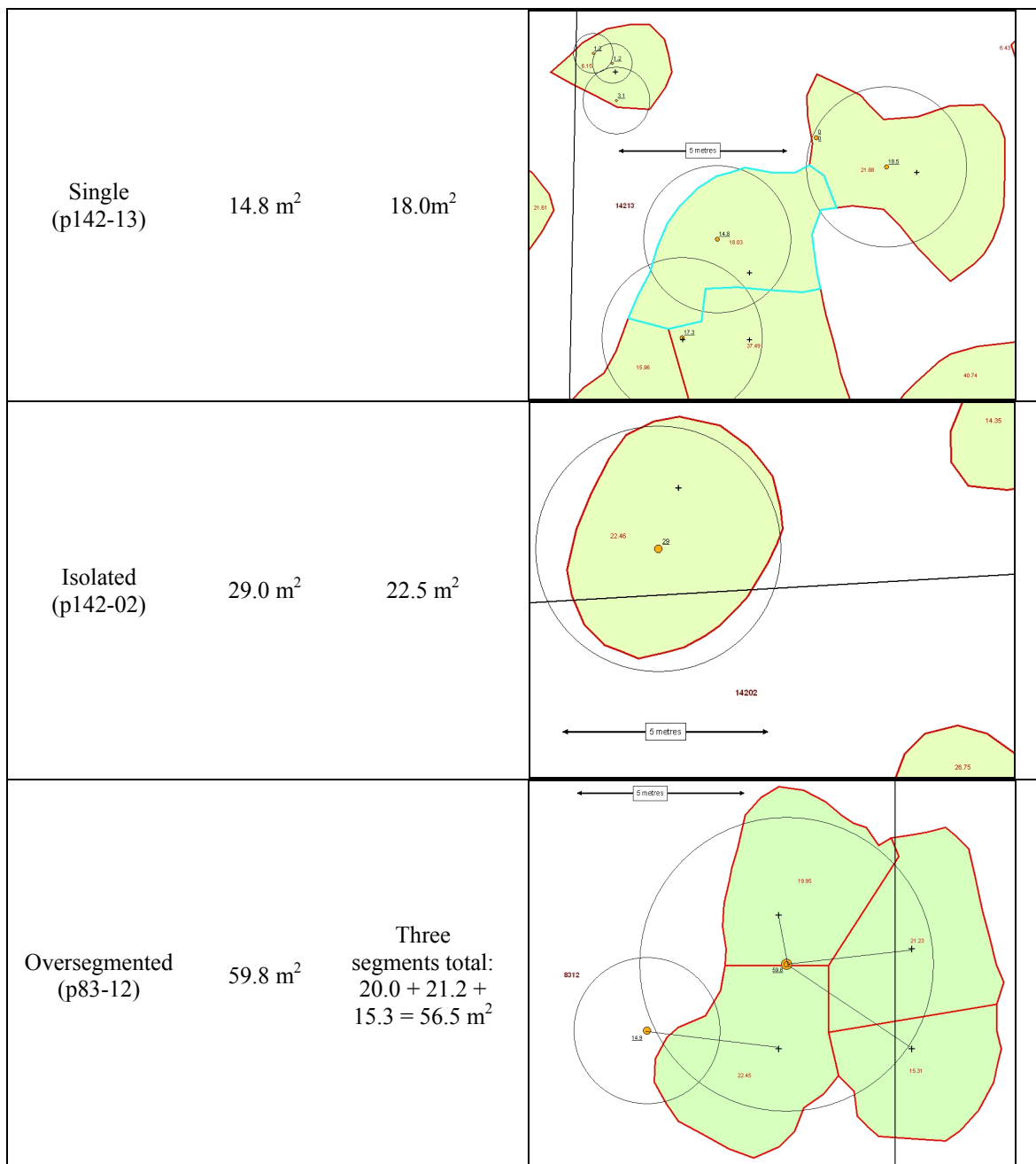
Type	Description	No. of sample crowns	%
Cluster	LiDAR crown encompasses a number of field stems of generally similar size. Segment includes interlocking crowns in overstorey and/or with sub-canopy stems underneath overstorey crowns. HSCOI mapped stem count may be similar to field stem count.	50	55.6%
Segment <sub>1m</sub>	Match between field crown and HSCOI segment <sub>1m</sub> polygon, but merged with adjacent polygons in final segmentation. This usually occurs when a sub-dominant stem is adjacent to a larger crown or where there are many smaller crowns in close proximity.	5	5.6%
Dominant	One or two field stem(s) are the dominant stems within a cluster polygon, with the final LiDAR segment and field crowns generally equivalent. Additional field stems occur in the sub-canopy, and can be identified with HSCOI stems and/or segment <sub>1m</sub> polygons.	10	11.1%
Single	A field stem is related to a single HSCOI stem, within a LiDAR delineated crown, but which are adjacent to other crowns. Generally this type occurs when interlocking crowns are present within a larger stand of trees	17	18.9%
Isolated	Field stem is related to a single HSCOI stem within a LiDAR crown that is isolated from other trees	6	6.7%
Oversegmented	The LiDAR crown delineation for a single field stem was over segmented into a number of polygons (i.e. segments <sub>1m</sub> not merged to larger crown). This generally occurs when a field tree varies greatly from the height to crown area function (e.g., tree has a much larger crown for its height), or has a number of large and distinct branch clumps	2	2.2%
Total		90	100%

**Table 42: Summary of crown delineation validation comparison of 90 trees aggregated by type.**

Crown type	Cluster / segment <sub>1m</sub>	Dominant	Single	Isolated
Field crowns mean area (m <sup>2</sup> )	13.0	53.0	15.3	16.4
Field standard deviation (m <sup>2</sup> )	10.5	119.7	11.7	7.3
Field range (min-max) (m <sup>2</sup> )	0.4 - 53.4	5.7 - 393.2	1.5 - 50.0	9.0 - 29.2
LiDAR crowns mean area (m <sup>2</sup> )	40.5	52.2	18.5	12.6
LiDAR standard deviation (m <sup>2</sup> )	25.9	100.1	16.0	5.6
LiDAR range (min-max) (m <sup>2</sup> )	2.9 - 177.8	9.0 - 336.8	4.2 - 73.0	6.2 - 22.5
Mean difference (m <sup>2</sup> )	27.4	-0.9	3.2	-3.8
Standard dev. of difference (m <sup>2</sup> )	27.5	20.1	7.0	4.6
Smallest - largest error range - (m <sup>2</sup> )	-2.1 - 173.3	3.3 - -56.4	0.1 - 23.0	0.3 - -10.7
Min - Max difference range (m <sup>2</sup> )	-25.7 - 173.3	-56.4 - 12.2	-8.3 - 23.0	-10.7 - 1.9

**Table 43: Examples of LiDAR crown delineation classification types found in the validation.**

Type (field plot)	Field crown area (m <sup>2</sup> )	LiDAR crown area (m <sup>2</sup> )	Figure <sup>a</sup>
Cluster (p142-13)	Total crown area from the 4 stems = 31.5 m <sup>2</sup>	23.8 m <sup>2</sup>	
Segment <sub>1m</sub> (p23-16)	Smaller tree = 15.8 m <sup>2</sup>  Larger tree = 54.1 m <sup>2</sup>	Smaller tree = 22.2 m <sup>2</sup>  Larger tree = 48.3 m <sup>2</sup>	
Dominant (p81-11)	393.2 m <sup>2</sup>	336.8 m <sup>2</sup>	



a – Legend for figures:

thick light blue line - LiDAR crown type being illustrated when adjacent to other crown polygons

thick red line - LiDAR crown when not adjacent to other crown polygons

thin dark blue line - HSCOI segments\_1m polygons

red text- LiDAR polygon crown area

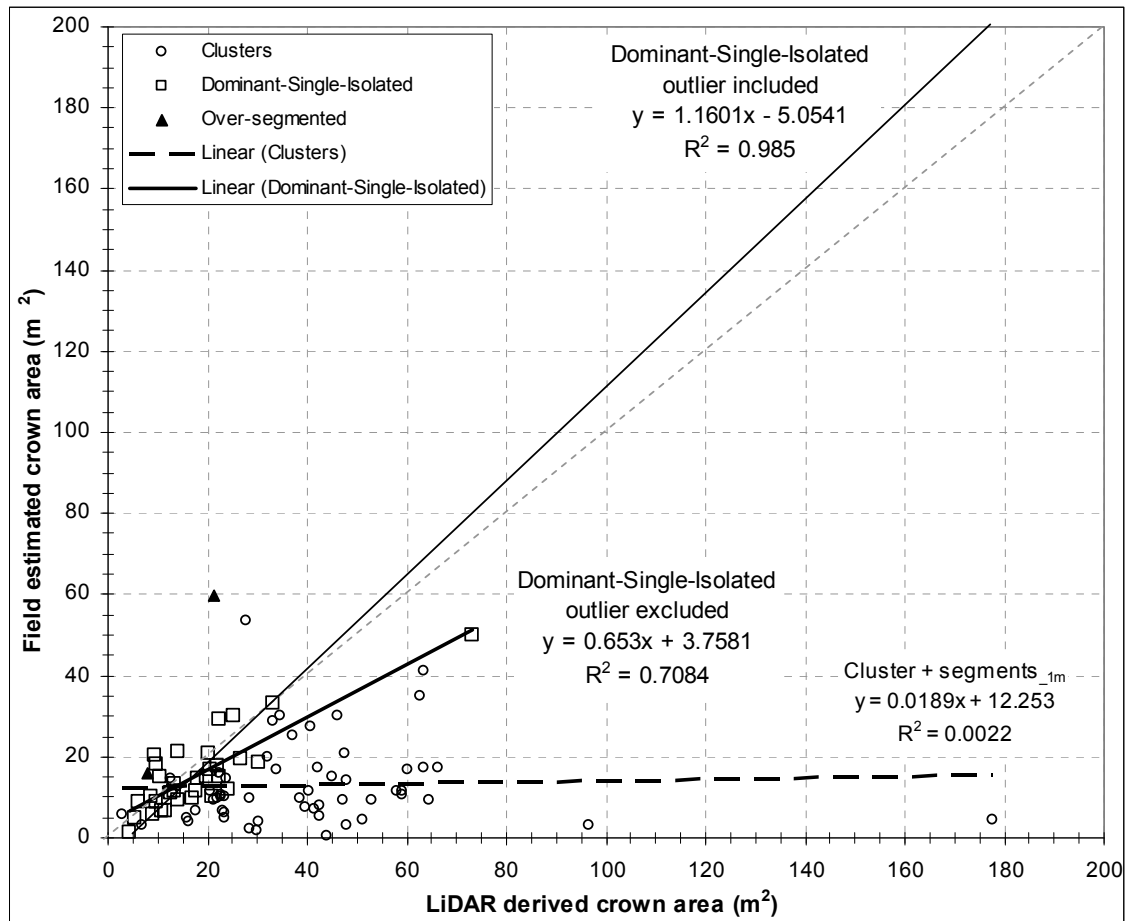
black underlined text - estimated field crown area

solid orange circles - field stems proportional to  $D_{130}$ ,

open black circles- field stems proportional to crown radius (mean of crown north-south and east-west measurements)

The correlation result for all crowns not found within a cluster present an  $r^2$  of 0.99 (RSE = 8.4 m<sup>2</sup>, P-value = 0,  $n = 32$ , Figure 89). With the large crown outlier (field = 393 m<sup>2</sup> and HSCOI segment = 337 m<sup>2</sup>) removed, the  $r^2$  decreases to 0.71 (RSE 5.4 m<sup>2</sup>, P-value = 3.055e<sup>-9</sup>,  $n = 31$ , Figure 89). The correlation (large outlier removed) may be a more realistic assessment of the crown mapping accuracy, within the limits of the sample used and available

field data. It should be noted that there is a good correlation (along the 1:1 line) between LiDAR and field estimates up to around 40 m<sup>2</sup>, but that a second outlier crown (a LiDAR estimated area of 75m<sup>2</sup>) still influences the correlation.



**Figure 89: Correlation between field estimated crown area and area derived from LiDAR HSCOI crown delineations, aggregated into broad class types.**

The genus probability modelling for the segments<sub>1m</sub>, used the 90 randomly selected trees (and associated segments) from all field plots, as described previously. The overall accuracy is 52 % across all delineated crown types (Table 44), though 80 % of dominant and 65 % of single assessed segments had a correct genus probability assigned. Approximately 30 % ( $n = 27$ ) of the validation set were correctly modelled at both 1 m and 5 m scales, with the majority of these being a *Eucalypt-Angophora* genus (Table 44). Approximately 44 % ( $n = 40$ ) were correct at the segment<sub>1m</sub> scale, even though the final genus allocation may have changed the initial assessment. A changed final allocation only occurred for 9 % ( $n = 8$ ) of the validation set (Table 44). The main sources of error were *Eucalypt-Angophora* examples having a

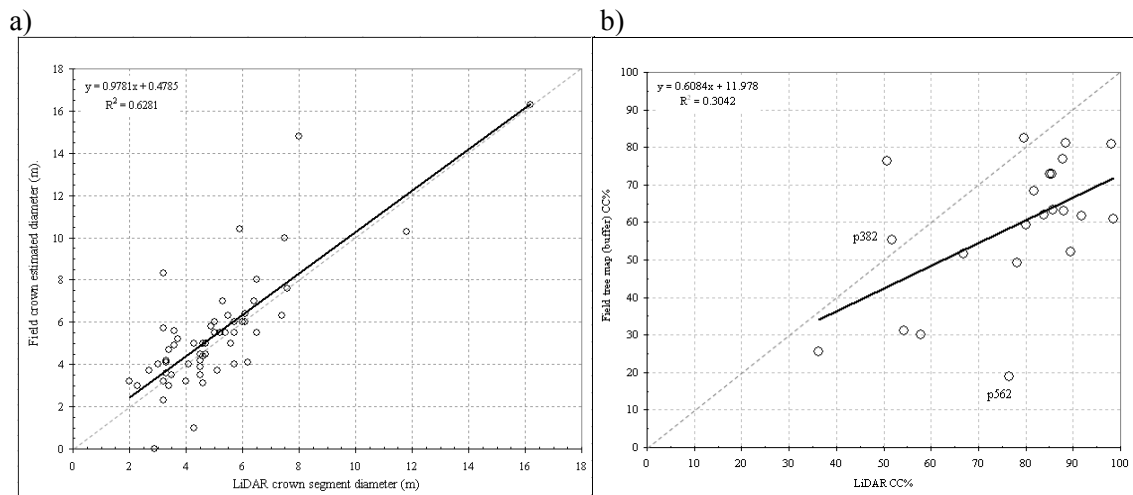
*Callitris* form, for example with young or regenerating stems, or where *Callitris* types occurred within clusters with interlocking crowns, thus (as identified previously) making it difficult to resolve individual crowns.

**Table 44: Genus probably modelling accuracy assessment by delineation type, using 90 randomly selected trees**

Genus score <sup>1</sup>	Cluster	Segment-1m	Dominant	Isolated	Single	Over segmented	Total
1111	1		3		3	1	8
1122	5	1			2		8
1212	1						1
1222	15	1	1		2		19
2111	5	1	1	5	2	1	15
2122	9		1		5		15
2212	3		1		1		5
2222	11	2	3	1	2		19
Total	50	5	10	6	17	2	90
Correct %	24 48%	2 40%	8 80%	1 17%	11 65%	1 50%	47 52%

1 – Four digit code as follows: 1 = *Callitris-Acacia*. 2 = *Eucalypt-Angophora*. 1<sup>st</sup> position = field data, 2<sup>nd</sup> position = segment\_1m estimate. 3<sup>rd</sup> position = segment\_5m estimate. 4<sup>th</sup> position = final allocation after multi-scale assessment. Correct is where 1<sup>st</sup> and 4<sup>th</sup> positions are equal.

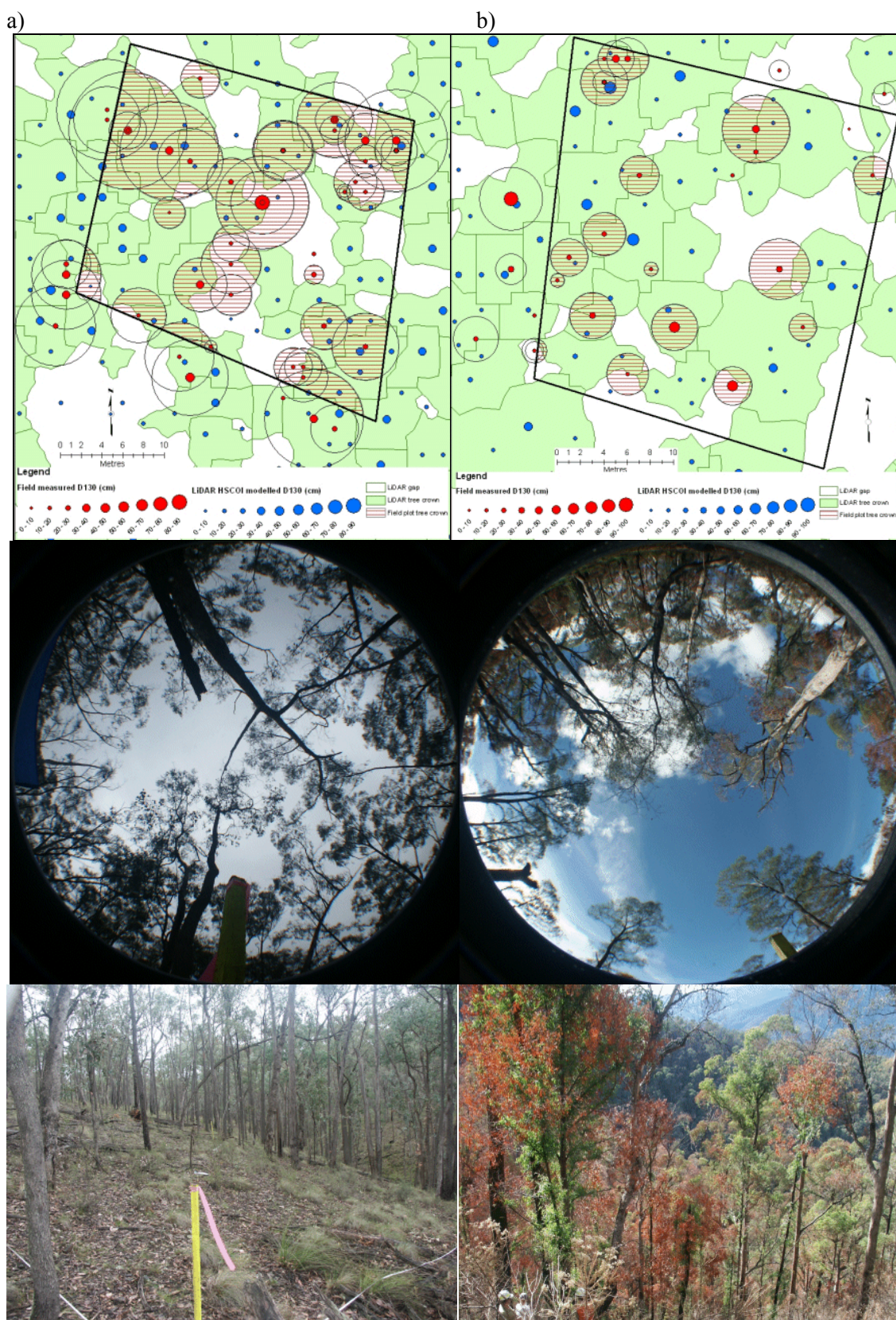
Comparisons were also made between LiDAR crown diameter and field data using the trees from the crown separation trial (Section 4.2.3). The correspondence was  $r^2 = 0.63$  (RSE 1.71 m, P-value =  $2.056e^{-013}$ ,  $n = 57$ , Figure 90a), with a good match between the line-of-best fit and the 1:1 line. This indicates that LiDAR and field crown diameter measurements were equivalent, on average, for the trees assessed. For comparison with Figure 89, the largest crown (~16 m diameter) would equate to a crown area of approximately 200 m<sup>2</sup>, assuming a circular shape. Most crowns have an area between 3 m<sup>2</sup> and 50 m<sup>2</sup>, which is the same range for the crowns used in Figure 89.



**Figure 90: Comparison of crown diameter for; a) field and HSCOI trees from plots 142-13 and 81-16, and b) NE Victorian plot CC comparison between field tree-map buffer and HSCOI crowns.**

For NE Victoria, the LiDAR individual crown delineation comparison with field tree-map data (generated using a circular buffer from the mean of the crown diameter) had a poor correspondence (Figure 90b and Table 40). The field estimated plot crown cover data was generally less than that of the LiDAR plot crown cover, in the order of 10 - 40%. However the P-value was significant, indicating a general linear trend overall. As examples of the NE Victorian application, contrast the plot (p382) with a good correspondence between LiDAR and field tree map for stem density and crown cover (Figure 91a), with a plot (p562) with poor correspondence between the data (Figure 91b).





**Figure 91: NE Victorian LiDAR crown delineation examples and associated field plot centre photos. (a) Plot 382 with a good match between plot level crown cover and stem density; and (b) Plot 562 with a poor match for plot level crown cover and stem density.**

---

## 4.6 Multi-Scale Calibration Results

This section presents results from the LiDAR calibration examples for a range of height and cover metrics, undertaken at a range of scales. Specifically, transfer functions are developed that can translate between foliage and crown cover, thus allowing a consistent comparison and reporting of crown cover. Estimates of crown cover, foliage-branch cover and stem density derived from LiDAR are used to calibrate Landsat data at the pixel scale to minimise any inherent issues associated with differences in scale (e.g., with field data collected at different plot sizes). Estimates of crown cover and foliage-branch cover are compared to those derived from ICESat data, to establish which metrics might be retrieved and the level of confidence expected. The relative accuracy of the LiDAR tree and component modelling used for the SAR simulations is assessed, with reference to the field plot data from primary sampling unit 142.

### 4.6.1 Landsat pixel scale LiDAR cover calibration

Correlations between Landsat derived foliage projective cover and structural metrics derived from LiDAR (Table 45), using 25 x 25 m pixels include foliage-branch cover (Figure 92) crown cover (Figure 93), and stem density (Figure 94, Figure 95). Overall there is a good correspondence between Landsat TM foliage projective cover and LiDAR foliage-branch cover and crown cover with foliage-branch cover having the stronger relationship. Both LiDAR foliage-branch cover and crown cover correspondences are slightly less than what was observed at the field plot level, as reported previously. Stem density can be readily estimated using either Landsat foliage projective cover, or LiDAR derived cover estimates, with LiDAR foliage-branch cover at the 0.5 m height threshold giving the better result.

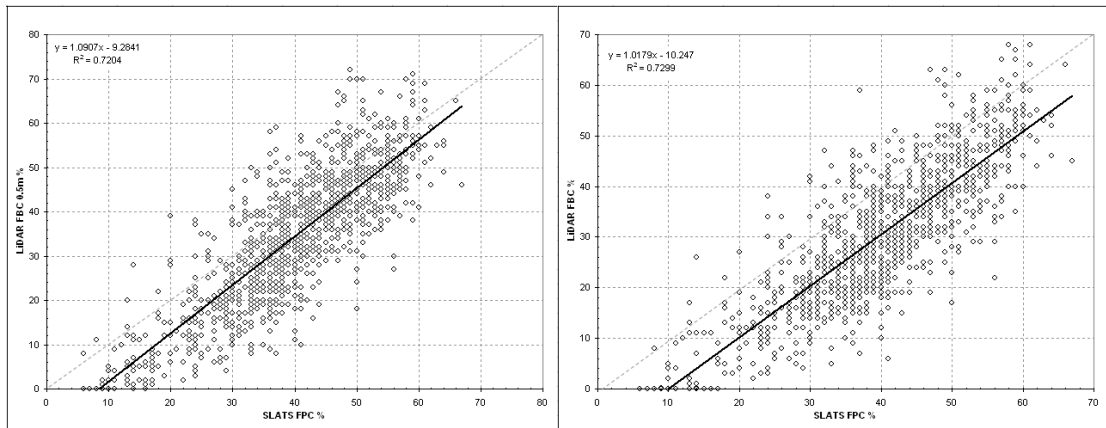


Figure 92: Comparisons of SLATS FPC and LiDAR FBC at 0.5m (left) and 2m (right) thresholds.

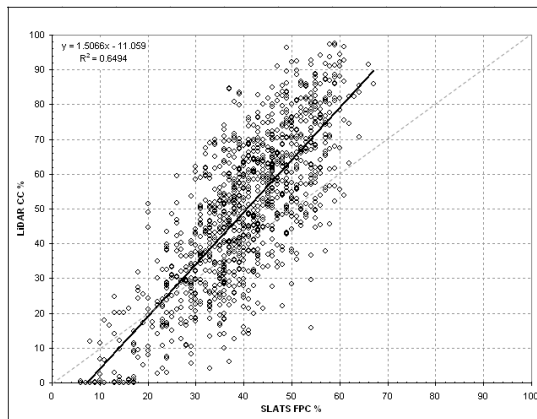


Figure 93: Comparison of SLATS FPC and LiDAR CC.

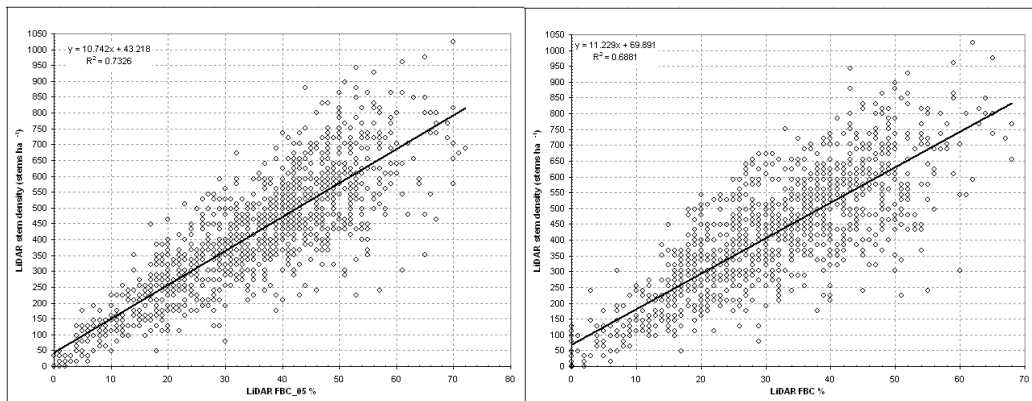


Figure 94: Comparisons of LiDAR stem density and FBC at 0.5m (left) and 2m (right) thresholds.

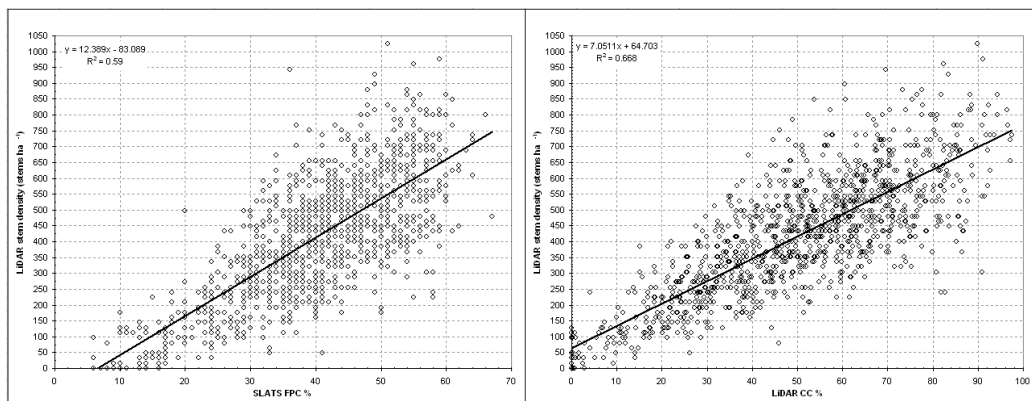


Figure 95: Comparisons of LiDAR stem density and Landsat FPC (left), and LiDAR CC (right).

**Table 45: SLATS FPC comparisons with LiDAR derived cover and stem density metrics for Injune**

Description	n	R <sup>2</sup>	RSE	Function <sup>a</sup>	P-value
LiDAR FBC% (2m+) vs FPC	1161	0.73	7.62	$Y = 1.0179x - 10.2468$	0
LiDAR FBC% (0.5m+) vs FPC	1161	0.72	8.36	$Y = 1.0907x - 9.2841$	0
LiDAR CC% (2m+) vs FPC	1161	0.65	13.62	$Y = 1.5066x - 11.0591$	0
LiDAR stem density ha <sup>-1</sup> vs FPC	1161	0.59	127.1	$Y = 12.3889x - 83.0886$	0
LiDAR stem density ha <sup>-1</sup> vs CC% (2m+)	1161	0.67	114.4	$Y = 7.0511x + 64.7034$	0
LiDAR stem density ha <sup>-1</sup> vs FBC%(0.5m+)	1161	0.73	102.6	$Y = 10.7423x + 43.2175$	0
LiDAR stem density ha <sup>-1</sup> vs FBC%(2m+)	1161	0.69	110.8	$Y = 11.2293x + 69.8910$	0

<sup>a</sup> y = LiDAR metric, x = SLATS FPC, unless otherwise indicated.

#### 4.6.2 Crown and foliage cover translation function

The development of a function to translate between foliage-branch cover or foliage projective cover and crown cover involved comparing LiDAR crown cover with LiDAR foliage-branch cover, and with Landsat foliage projective cover (Table 46). Landsat pixel (25 m) sized sample areas within 12 PSUs (that contain field data) were utilised to initially compare foliage projective cover and LiDAR crown cover (see Figure 93 previously). Calibration of Landsat foliage projective cover first required the selection of cells with foliage projective cover < crown cover (Figure 96). The derivation of the translation function then used regression of 80% of randomly selected cells (Figure 97). Finally, validation of the regression function used the remaining 20% of randomly selected cells (Figure 98).

**Table 46: LiDAR CC comparisons with SLATS FPC and LiDAR FBC, for Injune and NE Victoria.**

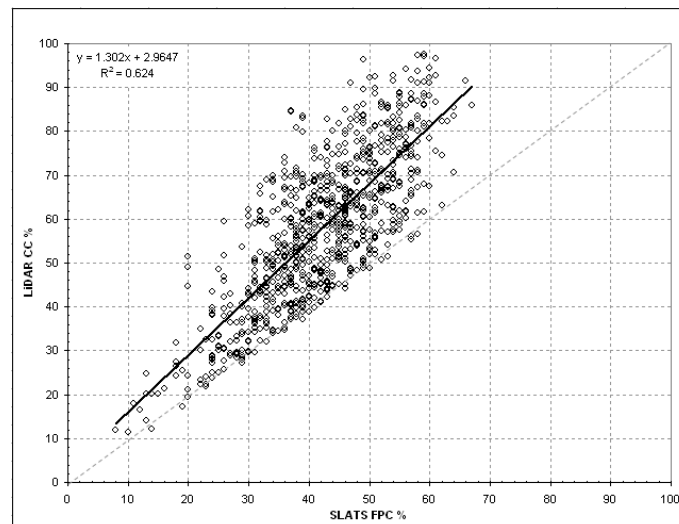
Description	n	R <sup>2</sup>	RSE	Function <sup>a</sup>	P-value
LiDAR CC% (2m+) vs FPC	1161	0.65	13.62	$Y = 1.5066x - 11.0591$	0
LiDAR CC% (2m+) vs FPC <sup>b</sup> (all calib cells)	855	0.62	10.38	$Y = 1.302x + 2.9647$	0
LiDAR CC% (2m+) vs FPC <sup>b</sup> (80% cells)	683	0.63	10.47	$Y = 1.298x + 3.5609$	0
LiDAR CC% (2m+) vs FPC <sup>b</sup> (20% cells)	172	0.63	9.88	$Y = 1.0255x - 3.6281$	0
LiDAR CC% (2m+) vs LiDAR FBC (2m+) <sup>c</sup>	1161	0.80	10.35	$Y = 1.4014x + 6.4695$	0
LiDAR CC% (2m+) vs LiDAR FBC (2m+) – 14 outliers	1147	0.83	9.6	$Y = 1.4278x + 6.1073$	0
LiDAR CC% (2m+) vs LiDAR FBC (2m+) <sup>d</sup>	128	0.86	11.1	$Y = 1.3205x + 8.3506$	0

<sup>a</sup> y = LiDAR metric, x = SLATS FPC, unless otherwise indicated.

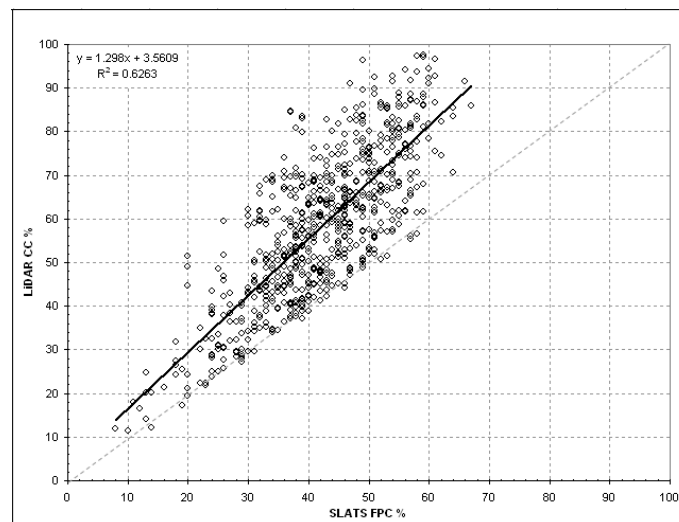
<sup>b</sup> – Cells (25 x 25 m) where CC > FPC only.

<sup>c</sup> – Using Landsat assessment cells (25 x 25 m) across the Injune PSU's

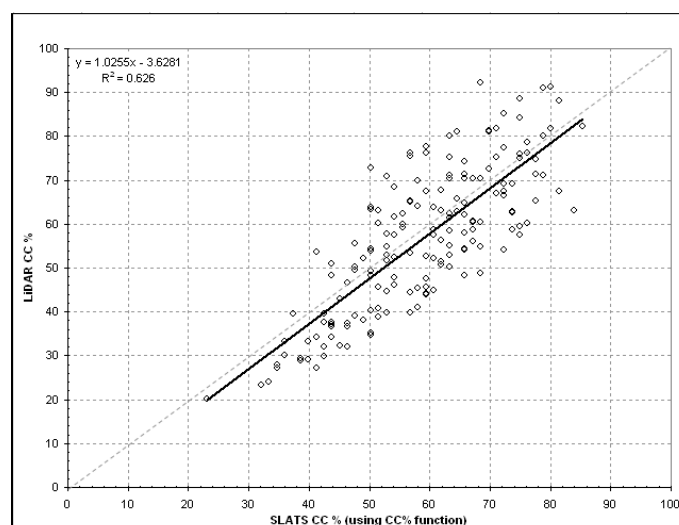
<sup>d</sup> – Using field plots from Injune and NE Victoria, and ICESat footprints from NE Victoria



**Figure 96: Comparison between LiDAR CC and SLATS FPC within 12 PSU's using all 25 m cells where  $CC \geq FPC$  ( $n = 855$ ).**



**Figure 97: Derivation of translation function between SLATS FPC and LiDAR CC within 12 PSU's, using 80% of 25 m cells where  $CC \geq FPC$  ( $n = 683$ ).**



**Figure 98: Validation of translation function between SLATS FPC and LiDAR CC within 12 PSU's, using 20% of 25 m cells ( $n = 172$ ) where  $CC \geq FPC$ .**

---

Based on the Landsat foliage projective cover calibration and validation results (Table 46, Figure 98), a generalised translation function is suggested (primarily for environments similar to Injune) where  $CC = 1.3 \times FPC$ .

The 25 m pixels in the 12 Injune primary sampling units were also used to compare LiDAR foliage-branch cover to LiDAR crown cover (Figure 99), with a good correspondence observed (Table 46). To assess the potential impact of scale on a foliage-branch cover translation function, LiDAR data from field plots at both Injune and NE Victoria were combined with LiDAR from NE Victorian ICESAT footprint areas (Figure 100) (see also Section 4.6.3 for ICESat results). The existing class boundaries for foliage projective cover to crown cover translation as published by the NFI are indicated as red arrows (Figure 100).

Foliage-branch cover is assumed to be equivalent to FPC as the NFI has not published a translation between foliage-branch cover and FPC. Using the LiDAR foliage-branch cover to crown cover comparison data from a range of sources (Table 46) and forcing the intercept through zero, a generalised translation function is suggested, where  $CC = 1.5 \times FBC$ . The difference in crown cover translation factors for foliage-branch cover and FPC could be attributed to the conceptual difference between measurements, which will be discussed in the next chapter.

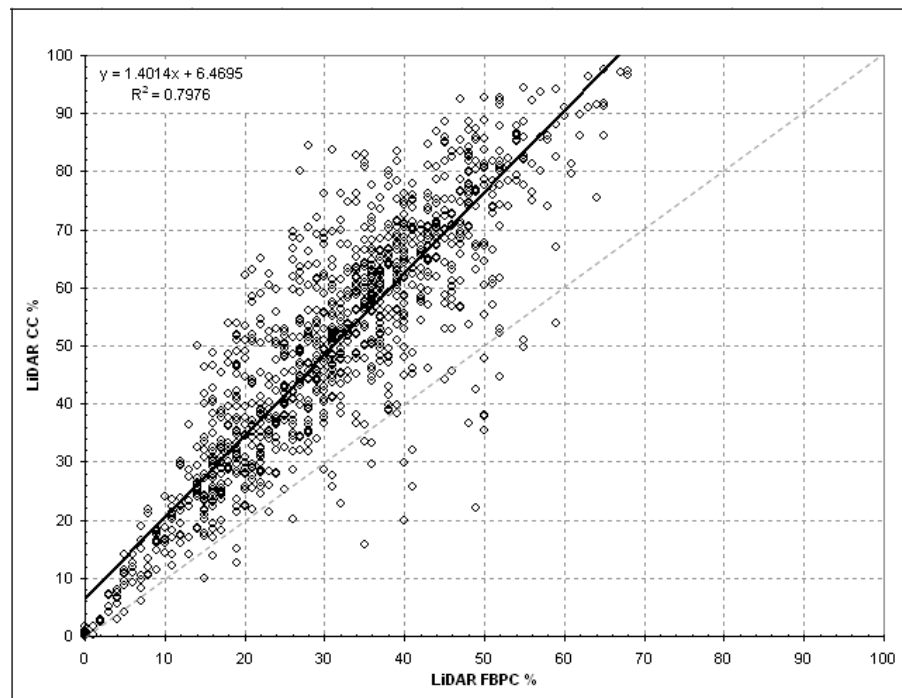


Figure 99: Comparison between LiDAR CC and FBC within 1161 x 25 m pixel sized areas from 12 PSU's.

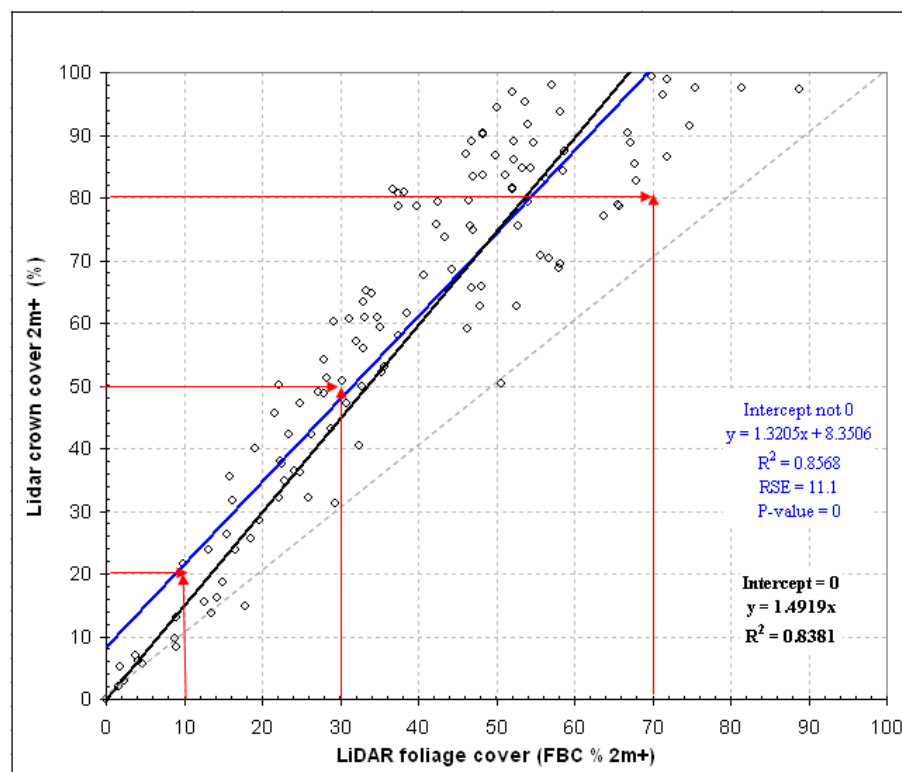


Figure 100: Comparison between LiDAR CC and FBC for Injune SSU's (50 m), NE Victorian field plots (30 m), and selected ICESat footprints from NE Victoria (50 - 100m). Red arrows indicate current NFI CC-FPC translation thresholds.

### 4.6.3 ICESAT case study calibration using LiDAR height and cover

A case study is presented to assess the potential effects of slope, terrain position and vegetation density on the extracted ICESat attributes. The case study highlights several issues that combine to cause difficulties for attribute extraction and calibration. The footprints were all imaged in October 2003, resulting in the same footprint size and processing, but with differing terrain and vegetation at the three footprint locations (Figure 101 and Figure 102).

The case study has identified that ICESat can extract attributes for height and cover that are similar to the LiDAR derived estimates; however there are issues with the consistency of the extraction. For vegetation height, the riparian footprint has a close correspondence was observed for both ICESat 'Fit\_ht' with LiDAR maximum height (~ 1 m difference), and ICESat 'centroid\_ht' with LiDAR predominant height (~ 2 m difference).

For forest cover estimation, the ridge-top footprint correctly estimates foliage-branch cover, whereas the riparian footprint correctly estimates crown cover. At both of these locations the intra-crown foliage density (including branches) is approximately 60 % (i.e. foliage-branch cover / crown cover), with remainder being “gap”, so the inter-crown density (i.e. crown cover or foliage-branch cover) is the primary factor in determining the cover value reported by ICESat. In the case study example the riparian stand has a higher LiDAR foliage-branch cover (43 %), and the ICESat value extracted is closer to LiDAR crown cover (~70 %), whereas the ridge-top LiDAR foliage-branch cover is lower (28 %), with the corresponding ICESat cover value being similar to LiDAR foliage-branch cover.

The mid-slope ICESat footprint cover estimate is much higher than either LiDAR foliage-branch cover or crown cover, with the combination of steeper slope (up to 13°) and lack of tree cover (LiDAR crown cover = 8 %) as potential factors in the difference observed. For vegetation height, the riparian footprint a close correspondence was observed for both ICESat 'Fit\_ht' with LiDAR maximum height (~ 1 m difference), and ICESat 'centroid\_ht' with LiDAR predominant height (~ 2 m difference). This contrasts with the mid-slope and ridge top footprints, which recorded poorer height correspondences overall (differences in excess of 5 m).



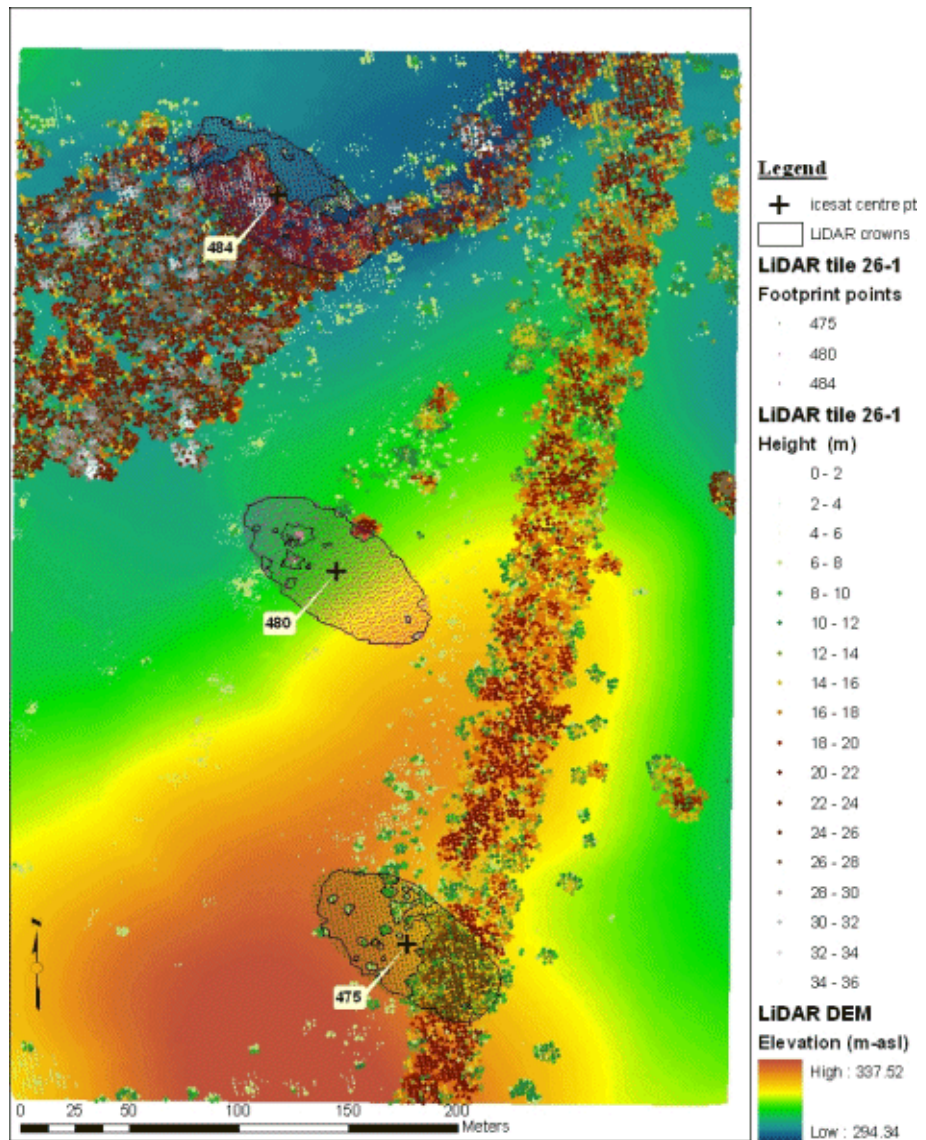


Figure 101: Airborne LiDAR from three ICESat footprints from ALS tile 26 displayed on a 1 m LiDAR derived DEM.

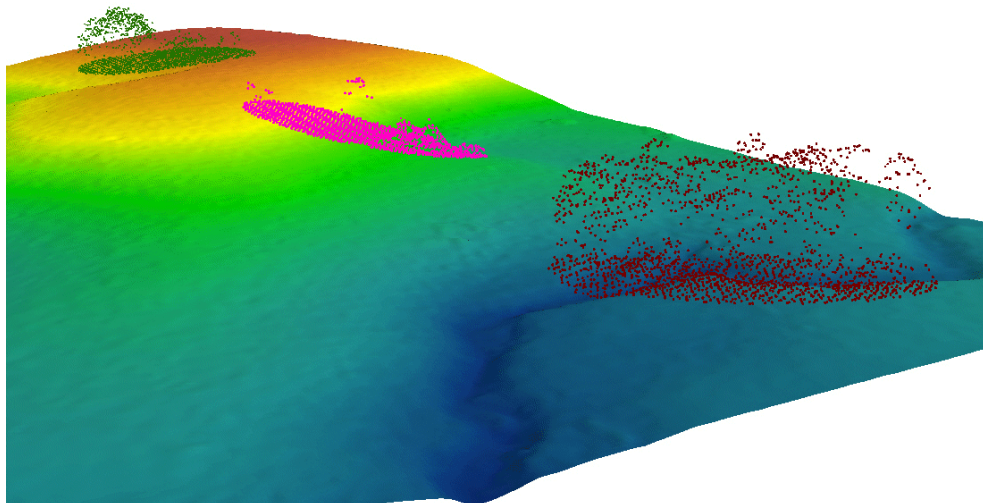


Figure 102: Perspective view of LiDAR within ICESat footprint areas. See Figure 101 for legend.

The exception was for mid-slope ICESat ‘Fit\_ht’ and LiDAR maximum height, where the difference was < 1 m. The poorer correspondences observed for height and cover in the mid-slope and ridge top footprints were attributed to a combination of higher slopes and relatively sparse vegetation within the respective footprints (Table 47, Table 48, and Table 49).

**Table 47: LiDAR and ICESat attributes from the riparian strip footprint f (ICE-id = 484)**

Attribute	LiDAR	ICESat	Comment
Vegetation foliage cover (%)	45.68		The ICESat cover value is close to the LiDAR crown cover value. There is a greater amount of vegetation present in the riparian strip.
Forest foliage cover (%)	43.39		
Forest crown cover (%)	73.66	78.8	
Elevation range (m) <sup>1</sup>	36.51	49.80	ICESat ‘veg height’ exceeds LiDAR by 13 m.
Max vegetation height (m)	34.80	33.87	Fit height is very close to max tree height
Predominant height (m) <sup>3</sup>	22.92	25.01	Centroid height is close to mean height
Mean slope(degrees)	4.93		Slope is relatively flat with steeper river bank sections only accounting for a small proportion.
Absolute slope (degrees)	4.73		

Icesat attributes ~<sup>1</sup>“veg\_height”, <sup>2</sup>“fit\_height”, <sup>3</sup>“centroid\_height”

**Table 48: LiDAR and ICESat attributes from the mid-slope footprint (ICE-id = 480)**

Attribute	LiDAR	ICESat	Comment
Vegetation foliage cover (%)	15.54	60.8	ICESat cover is too high. The steeper slope and shorter vegetation could cause ‘ground’ portions of footprint pulse to be classed as foliage.
Forest foliage cover (%)	8.95		
Forest crown cover (%)	8.22		
Elevation range (m) <sup>1</sup>	27.82	42.10	ICESat ‘veg height’ exceeds LiDAR by 14 m.
Max vegetation height (m) <sup>2</sup>	22.01	21.10	Fit height is very close to max tree height
Predominant height (m) <sup>3</sup>	5.52	13.25	Centroid height exceeds LiDAR by 8 m
Mean slope(degrees)	5.94		While mean slope is relatively flat the absolute slope may be an issue for cover and mean height.
Absolute slope (degrees)	13.04		

Icesat attributes ~<sup>1</sup>“veg\_height”, <sup>2</sup>“fit\_height”, <sup>3</sup>“centroid\_height”

**Table 49: LiDAR and ICESat attributes from the ridge top footprint (ICE-id = 475)**

Attribute	LiDAR	ICESat	Comment
Vegetation foliage cover (%)	33.82	31.7	The ICESat value is close to the LiDAR foliage cover value. The vegetation is sparser on the ridge top, compared to riparian strip.
Forest foliage cover (%)	28.36		
Forest crown cover (%)	51.21		
Elevation range (m) <sup>1</sup>	28.95	55.30	ICESat ‘veg height’ is too high by 26 m.
Max vegetation height (m) <sup>2</sup>	24.87	13.60	Fit height is too low by 11 m
Predominant height (m) <sup>3</sup>	14.51	9.54	Centroid height is too low by 5 m
Mean slope(degrees)	5.54		The mean slope is similar to footprint ID 480 but there is a slightly higher absolute slope.
Absolute slope (degrees)	8.74		

Icesat attributes ~<sup>1</sup>“veg\_height”, <sup>2</sup>“fit\_height”, <sup>3</sup>“centroid\_height”

#### 4.6.4 Stand reconstruction results using tree components

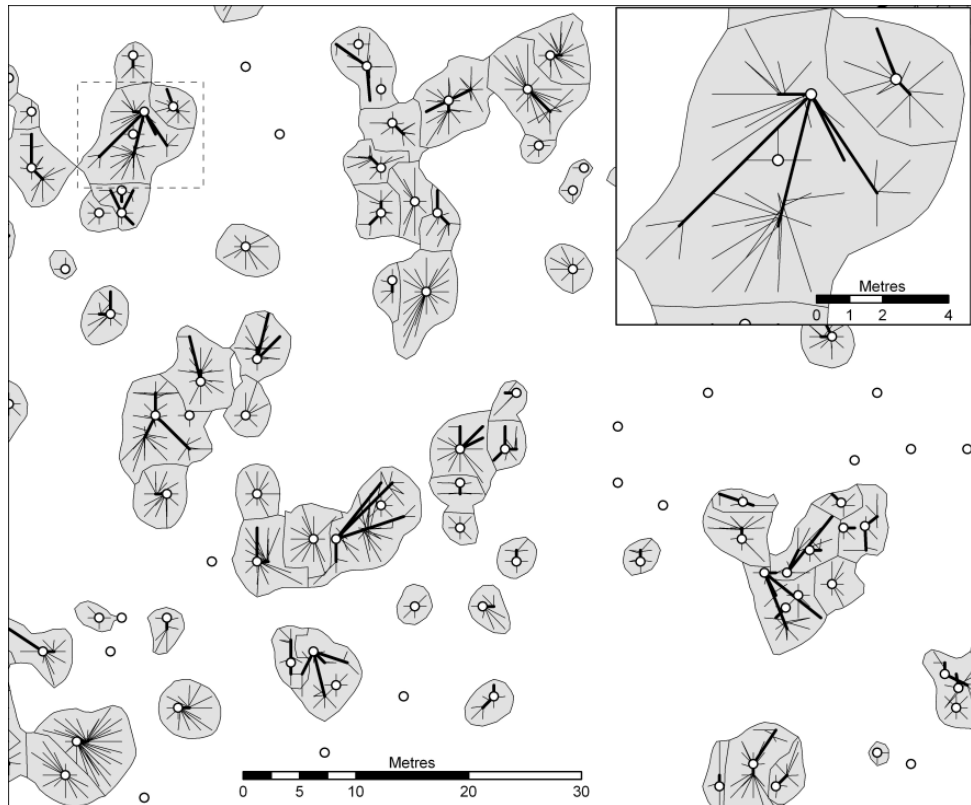
The inputs generated from the LiDAR modelled data for primary sampling unit 142 were used to reconstruct the stand within the Defence Science and Technology Organisation (DSTO) simulation environment. The success of the actual SAR simulation is outlined in Lucas *et al.*, (2006c) (Appendix C). The relative accuracy of the LiDAR stand modelling is described with reference to the field data using structural and biomass comparisons. Assuming that the four field plots in the primary sampling unit were a representative sample of the primary sampling unit, comparison with plot-based measurements indicated a good level of agreement across the different structural attributes (Table 50). Therefore, there is confidence in the identification and attribution of stems across the primary sampling unit, as they are within 15 % of mean field plot data estimates for stem density and within 12 % for stem attributes, and the range of values observed is very similar (Table 50).

**Table 50: Comparison of structural attributes between field data (4 plots) and LiDAR stand modelling for PSU 142**

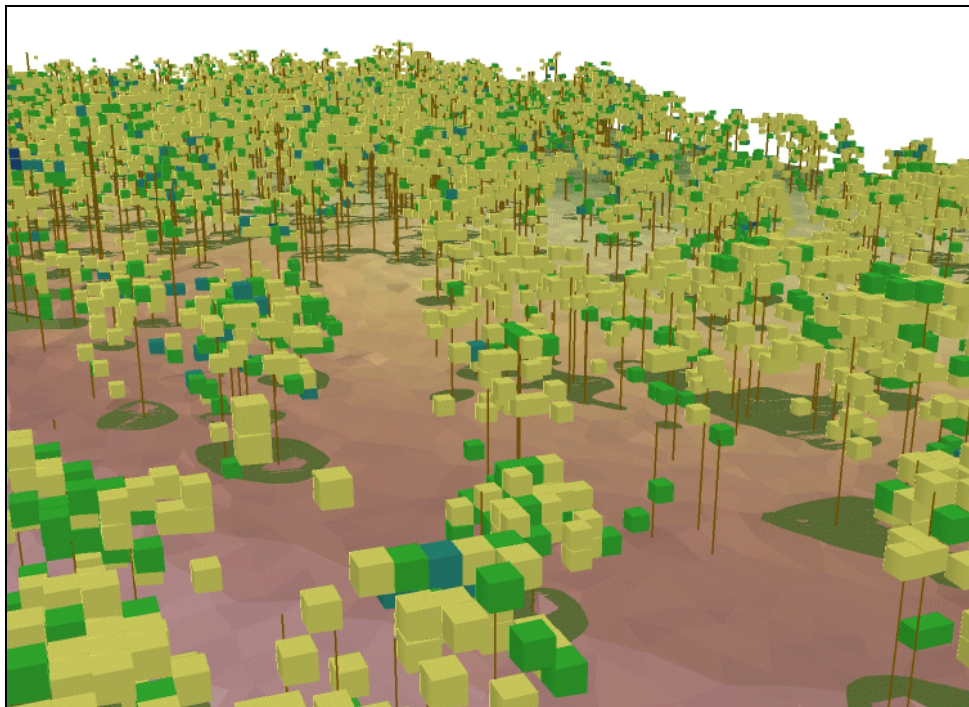
Attribute	Count	Mean	Standard deviation	Range (min-max)
Total branches in PSU	20 295			
Primary branches in PSU	3,616			
Branch length		2.9 m	1.9 m	0.01 – 14.8 m
Branch start radius		0.02 m	0.008 m	0.0001 – 0.075 m
Canopy voxels > 1 m height	21,709	28.0 %		
Mean field plot FBC <sup>a</sup>	4	29.9 %	6.83	21.8 – 38.5 %
LiDAR HSCOI stems in PSU	1,872	250 stems ha <sup>-1</sup>		
Field live stems D <sub>130</sub> ≥ 5 cm	277	277 stems ha <sup>-1</sup>	58 stems ha <sup>-1</sup>	212 - 348 stems ha <sup>-1</sup>
LiDAR stem top height		9.6 m	3.8 m	0.20 – 20.2 m
Field stem top height		8.8 m	1.6 m	2.5 – 18.0 m
LiDAR stem D <sub>130</sub>		17.3 cm	6.7 cm	1.0 – 35.4 cm
Field stem D <sub>130</sub> ≥ 5 cm		15.5 cm	4.2 cm	5.0 – 38.8 cm

<sup>a</sup> using field transects

An example of the modelling uses a portion of primary sampling unit 142 to illustrate the primary and secondary branch distributions (Figure 103), and a 3D view showing tree stems, crowns, and voxels that contain LiDAR returns (Figure 104). These representations are considered realistic, with the primary branches associated with single trees emanating in all directions with those of adjoining objects trending toward the outer edge of the crown. The reconstruction was also evaluated by visualizing the simulated stand using software specifically developed for this by DSTO. This allowed errors relating to branch locations, dimensions, and orientations to be identified.



**Figure 103: Sample of mapped tree stems, crowns, and primary (thicker lines) and secondary (thinner lines) branch distributions in PSU 142 derived from the LiDAR data. Inset extent is marked as a dashed box.**



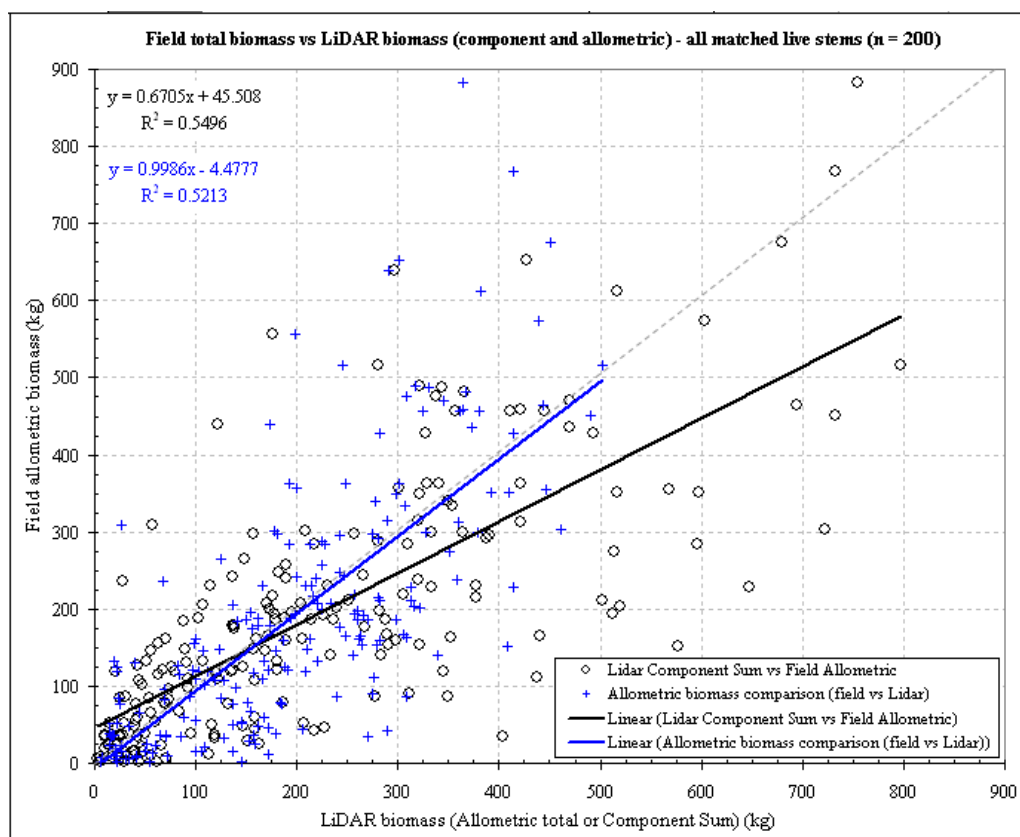
**Figure 104: Perspective view of a portion of PSU 142 showing mapped tree stems, crowns, and voxels derived from the LiDAR analyses. The view extent of Figure 103 is in the foreground.**



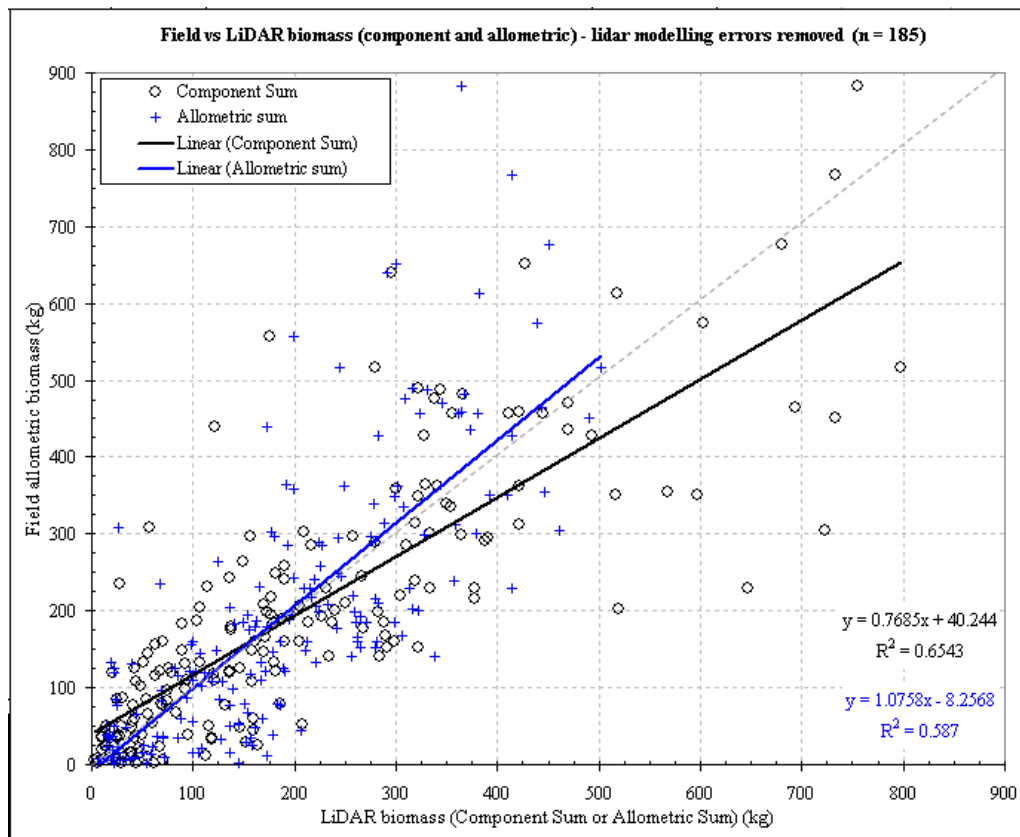
**Figure 105: (a) *E. populnea*-dominated forest at PSU\_142. (b) Graphical output of part of the reconstructed canopy from the DSTO radar simulation (Lucas *et al.*, 2006c).**

The final reconstruction of the forest sampled within primary sampling unit 142 (Figure 105) was considered to be a valid representation of the distribution of trees and elements (i.e., leaves, primary, and secondary and terminal branches and trunks), both visually and quantitatively. Component biomass was developed in primary sampling unit 142, and used to assess the relative accuracy of the LiDAR component modelling for calibration of the SAR simulation. The data from the four field plots was used to validate the results. From the four field plots, 200 live field stems were a direct match to a HSCOI stem, which subsequently were used for validation. Two LiDAR biomass estimates were compared: a) from species-specific allometrics applied to HSCOI stems using  $D_{130}$  derived from height; and b) from species-specific wood density multiplied by the wood or leaf volume from stems, branches, and canopy voxels. A summary of the three biomass estimates (field, and the two LiDAR) is provided in Table 51.

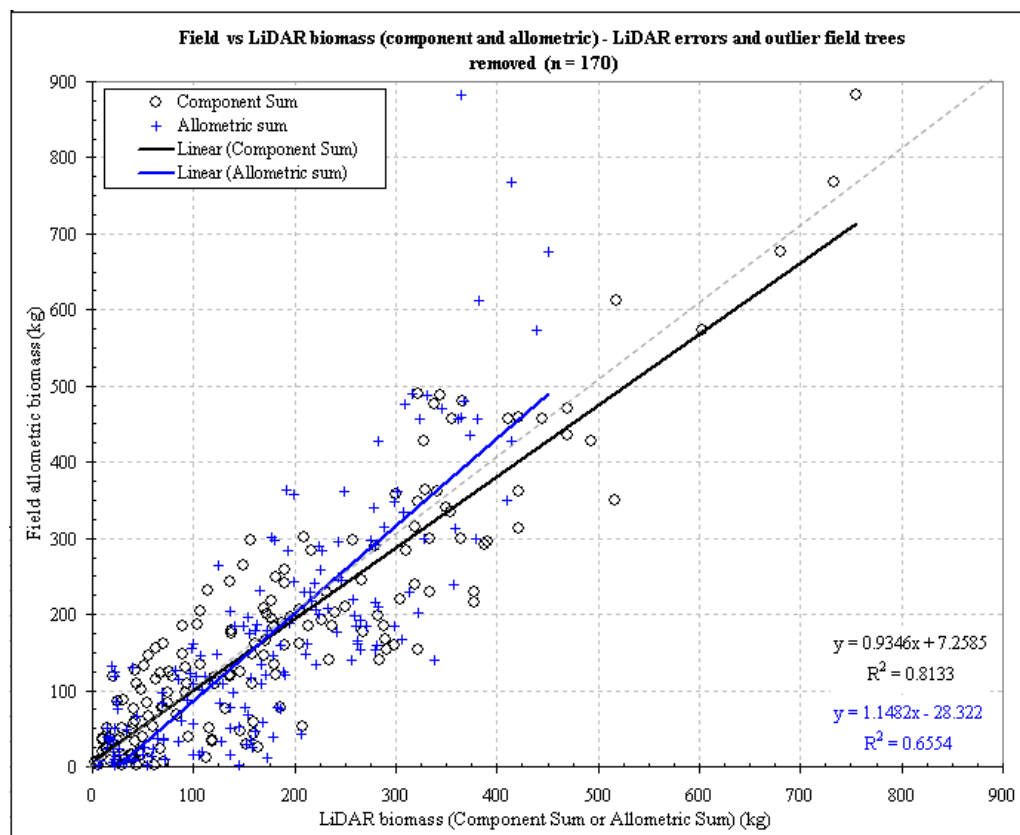
The data were divided into three sets to provide an indication of the strengths and weaknesses of the component modelling: (a) all assessed stems ( $n = 200$ ) (Figure 106); (b) assessed stems minus outlier stems that had LiDAR modelling errors ( $n = 185$ ) (Figure 107); and (c) assessed stems minus LiDAR modelling error stems, and LiDAR stems associated with field trees whose actual  $D_{130}$  differed greatly from that predicted using the height-to- $D_{130}$  function ( $n = 170$ ) (Figure 108). With outliers progressively removed from the comparison sets of (b) and (c), as expected the biomass correspondence between LiDAR and field biomass increased respectively (Table 52), though there were greater improvements from the LiDAR component modelling. Comparison between the two LiDAR biomass estimation methods resulted in a close correspondence (Figure 109 and Table 52), though there was some bias in the slope of the best fit line for stems with biomass  $> 400 \text{ Mg ha}^{-1}$ , where increasing component biomass is observed.



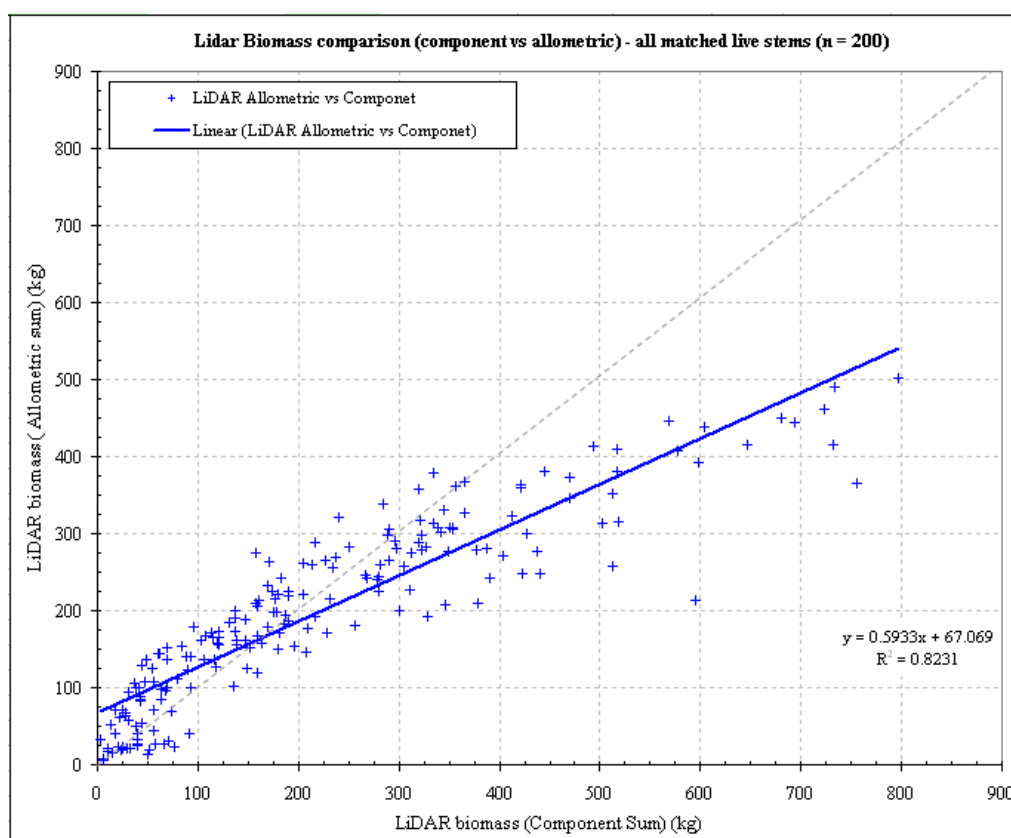
**Figure 106: Injune correspondence between field data and LiDAR allometric and component estimated biomass – all assessed stems ( $n = 200$ )**



**Figure 107: Injune correspondence between field data and LiDAR allometric and component estimated biomass – LiDAR modelling outlier stems removed (n = 185)**



**Figure 108: Injune correspondence between field data and LiDAR allometric and component estimated biomass – LiDAR modelling and highly different field outlier stems removed (n = 170)**



**Figure 109: Injune correspondence between LiDAR allometric and LiDAR component estimated biomass – all assessed stems ( $n = 200$ )**

**Table 51: Summary of biomass estimates for PSU 142 plots from field, LiDAR stem allometric, and LiDAR component sources.**

Attribute	Field plot				
	P142-02	P142-13	P142-18	P142-20	Total
<i>Field trees</i>					
Count of matched and assessed stems per plot	50	49	44	57	200
Total plot biomass ( $\text{Mg ha}^{-1}$ )	26.1	31.5	56.2	39.2	153.1
Mean field tree biomass (Kg)	130.5	160.7	319.5	172.1	191.4
Standard dev. tree biomass (Kg)	97.8	105.0	179.6	191.6	165.0
Tree Biomass range (min-max) (Kg)	5.2 – 475.5	10.0 – 363.4	24.4 – 882.7	2.1 – 766.9	2.1 – 882.7
<i>LiDAR allometric biomass</i>					
Total plot biomass ( $\text{Mg ha}^{-1}$ )	25.4	36.8	52.0	42.8	156.9
Mean field tree biomass (Kg)	126.9	187.6	295.3	187.6	196.1
Standard deviation tree biomass (Kg)	75.9	73.1	101.0	144.7	119.3
Tree biomass range (min-max) (Kg)	15.3 – 308.3	40.8 – 316.0	67.5 – 461.1	5.4 – 502.4	5.4 – 502.4
<i>LiDAR component biomass</i>					
Total biomass (+ hollows) ( $\text{Mg ha}^{-1}$ )	24.0	40.7	63.5	45.8	174.0
Mean field tree biomass (Kg)	120.2	207.5	361.0	200.8	217.5
Standard deviation tree biomass (Kg)	96.9	140.1	189.7	201.4	182.4
Tree biomass range (min-max) (Kg)	14.3 – 438.1	13.3 – 595.6	28.4 – 755.2	3.6 – 796.8	3.6 – 796.8



**Table 52: Summary of biomass functions using field data and LiDAR stem and components**

<b>Biomass comparison description</b>	<b><i>n</i></b>	<b><math>R^2</math></b>	<b>RSE<sup>b</sup></b>	<b>Function<sup>a</sup></b>	<b>P-value</b>
Field allometric vs LiDAR component sum – all matched stems	200	0.55	111.0	$Y = 0.6705x + 45.5079$	0
Field allometric vs LiDAR stem allometric – all matched stems	200	0.52	114.4	$Y = 0.9986x - 4.4777$	0
Field allometric vs LiDAR component sum – minus LiDAR model outliers	185	0.65	99.9	$Y = 0.7685x + 40.2437$	0
Field allometric vs LiDAR stem allometric – minus LiDAR model outliers	185	0.59	109.2	$Y = 1.0758x - 8.2568$	0
Field allometric vs LiDAR component sum – minus LiDAR + field outliers	170	0.81	68.3	$Y = 0.9346x + 7.2585$	0
Field allometric vs LiDAR stem allometric – minus LiDAR + field outliers	170	0.66	92.9	$Y = 1.1482x - 28.3217$	0
LiDAR stem allometric vs LiDAR component sum – all matched stems	200	0.82	50.3	$Y = 0.5933x + 67.0691$	0

<sup>a</sup> y = field allometric stem, x = LiDAR component or LiDAR allometric stem. <sup>b</sup> values in Mg ha<sup>-1</sup>

## 4.7 Summary

This chapter described the results of the research design and methodology, and demonstrated that LiDAR can improve the assessment of forest structure in Australia. The application of a multi-scale hierarchical research design strategy has enabled a wide range of forest structure assessments to be made. For example, good correlations have been observed between height and cover metrics at the plot scale, for both study sites. The Injune site had the best comparisons between field and LiDAR, with greater variability found in NE Victoria due to differences in field measurement and more complex forests. Errors in the comparisons have been quantified, and will be discussed further in the next Chapter. A translation matrix of continuous transfer functions for cover related structural metrics has highlighted the range of results that are generated from different datasets. LiDAR collected within integrated sampling schemes has allowed the landscape variability to be quantified at fine scales, and the representativeness of the field plot sample to be tested. This has shown that, in general, the plots are representative, but that there is some bias towards woodland cover at the Injune site.

The multi-scale assessments of structure have shown that different estimates can occur between plot sized areas and the wider stands in heterogeneous environments, such as floodplain riparian zones. The multi-scale analyses have also identified that one hectare is an efficient minimum area for reporting forest, for some purposes. In general there is higher variability in the structural attribute comparison between plot and stand at sizes less than 1 ha, with little variation at sizes larger than 1 ha. In some cases with heterogeneous forest environments, a different national level cover class can be reported for the same location, depending on whether a plot or stand-scale assessment is made. More sites are required however, for a statistically robust conclusion to be made across all ecozones.

The generation of basic geographic entities (e.g., trees) through the Height Scaled Crown Openness Index modelling was feasible and practical. The model outputs were validated to acceptable levels of accuracy for a range of forest structural attributes using field data. For example, good results for stem density (up to 700 stems ha<sup>-1</sup>), crown cover, individual stem height, and plot predominant stem height are observed. More variability is observed in

---

correlations with individual crown area and stem diameter. Correlation variability was attributed partly to natural variability in field data derived empirical transfer functions. Also factored into the variability were limitations in field measurements of some structural attributes, and issues with the LiDAR modelling not accurately representing some complex forest types.

The wide range of case studies presented has shown the utility of LiDAR as an effective calibration and validation tool. Field cover measurement methods and theory were validated using the LiDAR crown delineation and stem data. Correlations between Landsat TM derived foliage projective cover and LiDAR crown cover, stem density, and basal area show that foliage projective cover could be used for national level structural assessment and modelling, after further calibration in other forest types. A multi-scale foliage projective cover to crown cover translation function was developed, which allows for effective translation between continuous values from a range of datasets.

The ICESat calibration case study has shown that structural attributes extracted from ICESat can be compared to those derived from airborne LiDAR. However, the ICESat attribute extraction appears to be dependant on the density of the forest and terrain slope within the footprint, thus making the extraction inconsistent between structural metrics. More ICESat sites are required for conclusive statements. The stand reconstruction using LiDAR modelled tree components has produced reasonable results, with both the biomass comparisons and actual SAR simulations derived from the modelled data showing promise. Variability in the component modelling was identified as a combination of the modelling assumptions and limitations, mainly due to LiDAR vertical foliage sampling issues, natural variability in the field data empirical transfer functions relating to stem diameter from height, and measurements of tree branches.

The next chapter discusses the implications of the results presented in this chapter. This will enable the primary thesis research question to be addressed, and thus make conclusions on the usefulness of LiDAR for improving forest structure assessment in Australia.

## CHAPTER 5. DISCUSSION

### 5.1 Introduction

This chapter discusses the theoretical and practical implications of using LiDAR to improve the assessment of forest structure in Australia. A review of the literature in Chapter 2 revealed a number of research gaps or limitations in current or proposed national monitoring of forest structure. Specifically, better understanding of how different datasets report forest across a range of structural metrics is required, and the potential impacts of scale on forest data reporting need clarification (Table 53). In this chapter Section 5.2 discusses how forest structure assessment was improved using airborne LiDAR. Section 5.3 outlines the practical implications of the research, its limitations, and recommendations for future research effort.

**Table 53: Major knowledge limitations for LiDAR utilisation in multi-scale sampling schemes**

<b>Knowledge limitation</b>	<b>Extent to which it has been addressed prior to thesis</b>
<i>Plot scale assessments</i>	
Relationships between structural metrics when using different datasets across a range of Australian forest types.	Most studies limited to field data and single sensor at a location.
<i>Tree scale modelling</i>	
Algorithms for crown delineation and stem mapping, including sub-canopy, in Australian forests	Few, if any, LiDAR crown delineation routines published for Australian forests. Most Australian crown delineation methods use fine spatial resolution hyperspectral or aerial photo data. Few, if any, published stem mapping routines.
The use of basic geographical entities within a hierarchical multi-scale framework to investigate effects of scale on forest reporting from different datasets.	Early studies investigated scale effects for medium scale imagery (AVHRR, Landsat MSS, TM, SPOT). Studies have used circles in simulations, rather than explicitly mapped realistic tree crowns or crown components scaled to different sensor sizes or shapes.
<i>Multi scale assessments and calibration</i>	
A continuous transfer function between FPC, FBC and CC for report forest from a range of data sources (e.g., Landsat).	Field data translation relies on subjective interpretation of crown openness, which is less suited to automated remote sensing. Only very broad categories published by NFI, and not a continuous function. Queensland SLATS investigating translation functions, but have only published FPC to basal area function.
Development and use of a minimum area to define forest	AGO utilises 0.2 ha, which is slightly less than 4 Landsat pixels. FAO uses 0.5 ha, whilst the Marrakech rules for the Kyoto Protocol use a range from 0.05-1.0 ha. NFI is currently investigating this issue.
Calibration of ICESat data for height and cover sampling across Australia.	Unpublished pilot studies only.
SAR simulation modelling utilising LiDAR derived 3D tree components across stands.	Not previously done in Australia, limited development internationally.

## **5.2 Improving the Assessment of Forest Structure using LiDAR**

This overview section discusses the improvements that can be undertaken to forest structure assessment when using LiDAR, and is divided into 5 sections. An overview of the application of the multi-scale strategy is given in Section 5.2.1. The extent to which LiDAR provided enhancement for forest height assessment is given in Section 5.2.2, and for forest cover in Section 5.2.3. The results of the tree scale modelling using the Height Scaled Crown Openness Index are discussed in Section 5.2.4. The outcomes of the multi-scale LiDAR calibration and application to medium scale data are given Section 5.2.5.

### **5.2.1 Improving forest structure measurement using LiDAR**

A key component in determining the utility of LiDAR is the development of a multi-scale hierarchical research design strategy that used LiDAR to link fine scale field measurements with medium scale remotely sensed data. Chapter 4 demonstrates successful development of such a strategy, with a number of important results generated. The strategy allowed for fine scale height measurements over larger areas than could be undertaken with field data or API, and the representativeness of the field plot sample to be tested. This has demonstrated that, in general, the plots were representative but that there is some bias towards woodland cover at the Injune site.

In Chapter 3, a number of assumptions were postulated about the advantages and disadvantages of using a three-level hierarchical modelling strategy. When examining these assumptions with respect to the research findings, it was found that the assumptions were all generally valid. The plot scale (hierarchical Level +1) computational process was indeed rapid. For example, the whole 1,100 ha of LiDAR at Injune was processed for height, cover and apparent vertical profiles within 1 hour. The calibration with field data illustrated that the LiDAR plot estimates of height and cover metrics can be measured to the same accuracy as current methods, for both study sites. The magnitude and bias of differences when compared to field data were similar to that published in the literature. The research has improved forest

---

structure measurement by achieving a greater understanding of how a range different forest cover data sources interrelate at the plot scale. This has facilitated the development of new transfer functions that allow prediction of cover metrics from a wide variety of data and for the forest types found within the study sites. Plot boundary location issues were found to affect maximum height estimates through the inclusion of LiDAR from tree canopies originating from stems outside the plot. Importantly, this did not impact on predominant height or cover estimates in an obvious way.

Additionally, there were no apparent impacts of different footprints sizes (7.5 cm in Queensland, 22 cm in NE Victoria) on the forest attributes extracted from the LiDAR. Given a similar post-spacing, it may have been assumed that a smaller footprint may give cover and/or height results that are slightly less than those from slightly larger footprint sensors, as the returns may travel through more canopy gaps than reflect off foliage material. However the comparison with field data showed that the Queensland study site (with a smaller footprint) generally had a greater correlation, as opposed to the sites from NE Victoria. Based on the findings of this study, it is likely that other factors, such as forest type/structure and field measurement error, give rise to greater variability in comparisons with field data, than footprint size.

The assumption that it might be hard to explain inter-plot variability when using just mean forest structural values was validated for a number of plots that recorded similar height and cover values, but had quite different structures when examined at the tree scale. However, one assumed disadvantage in this respect did not eventuate. When plot scale assessments of the apparent vertical profiles were used in conjunction with the mean plot values, then differentiation of plots with similar mean structural values was possible. In addition, the investigations of apparent vertical profiles in forest types that have not been examined before provides a new contribution to forest structure assessment in Australia. The vertical profiles provided unique insight into different forest growth stage and disturbance assessments, and appeared to reflect accurately (though subjectively) the prevailing conditions on the plot. More sites are required however, before quantitative and objective growth stage assessments can be

---

routinely made. Modeling of field data to produce equivalent apparent vertical profiles resulted in good correlation across most plots assessed, with differences mainly attributed to potential error in the field measurement of tree heights. These results reflect investigations made in other forest types presented in the literature, and advance the research and application of LiDAR for height assessment across the landscape, for example when investigating potential scale impacts on forest reporting, or calibrating ICESat data for continental application.

At the tree scale (hierarchical Level 0), generation of basic geographic entities through the Height Scaled Crown Openness Index modelling was successful. Most of the assumed advantages were found to be true, including the ability to examine within plot variability, and up-scaling tree entities for calibration of other data at a range of scales. However, the assumption on reasonably quick computational processing was found not to be the case. It did take longer than expected to process some of the more complex forest stands, especially when there was a high number of smaller stems identified. This was attributed largely to the extra processing required to determine if the additional stems were either from the understorey or were large tree branch clusters. In some cases, complex stands could take a few days to map and attribute (though, as with most computations, this was influenced by hardware memory configurations). The disadvantages with tree scale modelling were all identified, especially in relation to field GPS locations and individual tree measurements. This issue is likely to be common to most calibration studies where field data are collected for a variety of purposes, rather than exclusively for LiDAR calibration at a tree scale.

The multi-scale strategy has facilitated the use of a range of forest structural metrics, including delineated crowns and modelled stems, to examine relationships with structural measures from other medium scale data. For example, LiDAR derived crown cover and stem density was compared to Landsat TM derived foliage projective cover for each pixel, resulting in a comparison sample of over one thousand pixels from 12 primary sampling units at Injune. Robust relationships were observed, the range of variability in the landscape was quantified, and locations of apparent error were identified, such as where the medium scale data may be recording non-forest (shrub/grass) foliage as well as forest. The major advantage of this is that

---

it provides a statistical rigour not available when just using field measured plots, combined with the fact that it is very difficult to align field data with Landsat pixels. The use of basic geographic entities means that almost any relevant scale can be tested (up to the limit of the LiDAR data). For example a future research option could be the examination of the influence of foliage outside the pixel on the foliage cover estimates.

New contributions to national forest assessment using LiDAR were made with the investigation of a function to translate between foliage projective cover to crown cover, and structural comparisons with ICESat data. The foliage projective cover-to-crown cover function provides a valuable first step in being able to objectively translate between continuous cover variable datasets, thus increasing the sensitivity for monitoring subtle forest change at continental scales. These functions also assist in the calibration of other data to determine suitability for application in national forest monitoring, for example with ICESat data. The ICESat case study example found that reliable estimates of forest attributes could be extracted, but that this is not consistent across different environments (e.g., due to combinations of slope, cover and height). Therefore further research is required to better define the thresholds where ICESat does not produce reliable results. Whilst the results presented in this thesis would tend to indicate that ICESat may be unsuited to continental application for national reporting, there is ongoing national and international effort into improving the calibration across a greater range of forested environments, which may yet provide a significant data source for national forest monitoring.

At the component scale (hierarchical Level -1), much greater detail could be modelled, which successfully fed into SAR simulation models. With the stand scale reconstruction using tree component entities, the SAR simulations derived from the LiDAR outputs closely resembled that of the actual AIRSAR data (Lucas *et al.*, 2006c). Given the complexity of the forests, the results generated gave confidence that the approach to forest reconstruction from the LiDAR data was a realistic representation both visually and quantitatively. Variability in the component modelling was identified as a combination of the modelling assumptions and limitations, mainly due to LiDAR vertical foliage sampling issues and natural variability in the



---

field data empirical transfer functions relating field measurements of stem diameter to height, as well as measurements of tree branches. The assumptions on the disadvantages of processing at this scale were borne out however, with some stands taking up to a week to process, largely because of the large number of individual components to be mapped. Effective validation at the scale of modelling was also found to be an issue requiring further research (or more detailed field work).

Another key finding with respect to the utilisation of LiDAR in a multi-scale strategy is that measurement scale can affect the structural values reported for some heterogeneous forests (e.g., woodland and open forests on floodplains). In these forests, the MAUP is evident, resulting in different height and cover estimates when different assessment areas are utilised. This has implications for national level forest reporting if remotely sensed data collected at different scales are utilised (e.g., LiDAR, API, ICESat and MODIS). Additionally, it was noted that an assessment scale of one hectare is an appropriate size for sampling the predominant height and foliage-branch cover of the wider stand. Plot sizes smaller than this tend to have greater variation when compared to the wider stand assessment, though the magnitude of the impact is dependent on the structural heterogeneity of the forest. These results confirm the findings published in the current literature, and advance the utility of LiDAR in Australian forests and woodlands for forest structure estimation.

The previous section has provided an overview of the successful multi-scale LiDAR modelling strategy. The next sections discuss issues with the individual structural elements that were generated from the LiDAR strategy. These include height, cover, apparent vertical profiles, stand and landscape multi-scale sampling, and tree scale modelling with respect to stem density and crown delineation. The outcomes of the case studies are discussed for Landsat TM structural comparisons, cover transfer functions, ICESat calibration and stand reconstruction using tree component scale modelling for SAR simulation.

### 5.2.2 Improving forest height assessment using LiDAR

To determine the utility of LiDAR to improve forest height measurements, comparisons were made between LiDAR and other data, to identify how well LiDAR assessments of forest height matched estimates from field data. This allowed assessment of the relative accuracy of LiDAR for measuring the metric of interest. Then the potential impact of scale was assessed, to facilitate the derivation of a minimum area for reporting, the representativeness of field plots with respect to the wider stand, and to provide guidance on what medium scale sensors with different assessment scales may report as forest.

#### *Maximum canopy height*

At Injune, the mean difference between LiDAR and field-based measurements for the field plots was 0.12 m, with LiDAR recording a slightly lower value. The mean difference for the 100 isolated trees used in Tickle *et al.*, (2006) was 0.5 m, again with the LiDAR recording the lower height. These results confirm previous results (e.g., Lim *et al.*, 2003b; Gaveau and Hill, 2003), and other LiDAR measurements in Australian forests, where differences were in the order of 1.6 – 3 m (Goodwin *et al.*, 2006), with LiDAR recording lower values. However the apparent bias for the forests at Injune is much less than that reported for other forests, and this could be related to the Injune forests being generally shorter with more open canopies, and dominated by species with a broad upper crown form (Jacobs, 1955), thus being easier to measure from both the ground and with LiDAR.

For NE Victoria, there is good agreement between the field and LiDAR plot data, with a mean difference of 3 m but with field data recording the lower mean value, which contrasts with published findings. In these Floodplain and Montane locations, the forests are denser and taller (reaching heights of 70 m and above), with an average LiDAR maximum height of 36 m, and the mean difference with field data of 7 m. As all field plots had LiDAR that was able to penetrate the vegetation to the ground, this allowed reasonably accurate DEM generation, and therefore there is confidence in the LiDAR height above ground estimates.

For the plots with a field data top height data lower by more than two metres compared to the LiDAR (10/22 or 45 %), it is likely that the field observations were not always able to identify the highest point of the tree. Additionally, it was noted that different observers gave estimates that varied by several meters (Zhou *et al.*, 1998). Errors in field estimates compared to LiDAR are noted by Lim *et al.*, (2003a) and Todd *et al.*, (2003).

Another source of error was when the tallest LiDAR return recorded for the plot was not actually from any of the trees measured in the field data, but from taller trees outside the plot with canopies that spread across the boundary. This effect was noticed in plots from both study sites. When using field plots of an arbitrary shape, the boundary is a practical requirement for efficient field measurement (McDonald *et al.*, 1998), although has primarily been designed to measure tree stems (e.g., in a forestry context) (West, 2004). However, there is a conceptual difference with airborne LiDAR measurements, as it primarily interacts with overstorey crown foliage. Therefore when making automated ‘plot’ comparisons with LiDAR within a GIS, especially in heterogeneous forests, there may be a need to reflect the relative importance of tree crowns, and modify the plot boundary to an irregular form. This would provide a better match to the crown extent of the field measured trees, and exclude the crown area from unmeasured trees whose stems are external to the plot. To be effective, this would require crown delineation and stem mapping (Hyypä *et al.*, 2001; Bunting and Lucas, 2006; Lee and Lucas, 2007).

### ***Predominant canopy height***

For Injune, the comparison between LiDAR derived plot canopy predominant height (using 10 m cells) and field measurements (with a sampling rate of 50 trees ha<sup>-1</sup>) resulted in a mean underestimate of approximately two metres by the LiDAR. When using a field-sampling rate of 100 trees ha<sup>-1</sup>, there was almost no bias, but greater variability in the correlation. In NE Victoria the best comparison was between the 5 tallest trees (~50 trees ha<sup>-1</sup>) and the LiDAR predominant height (a mean difference of 1.4 m), with LiDAR recording slightly greater heights. This may be related to the observation that the mean crown diameter across all NE

---

Victorian plots for the 5 tallest trees per plot was 10 m. When compared by ecozone, field plot and LiDAR data agree to within 1.5 m for Foothills, Montane and Subalpine zones, but there was a 5 m difference for Floodplains. It should be noted that only four field plots were assessed in the Floodplain ecozone, so additional plots would be required before conclusive statements could be made.

The magnitude of difference in predominant heights from both study sites confirms existing literature (e.g., Magnussen, and Boudewyn, 1998; Suarez *et al.*, 2005), and results observed in similar environments (e.g., Lovell *et al.*, 2003; Goodwin *et al.*, 2006). However, the NE Victorian plots were contrary to the literature in that there was a tendency towards higher LiDAR values rather than lower, when compared to field data. A possible explanation for this is the conceptual difference between canopy and stem predominant height. When comparing the actual number of height observations per plot, field data has  $n = 5$  for, and LiDAR up to  $n = 9$  (i.e. 10 m cells within a 30 x 30 m plot). Therefore, any shorter trees will have a larger influence on the field estimate, reducing the plot height value. Conversely, with LiDAR estimates the inclusion of cells from tree crown shoulders, which all tend to record similar heights due to mature eucalypt flat-topped crown form (Boland *et al.*, 1992), will increase the mean plot height. As with maximum height, it may be that the LiDAR is giving a more precise estimate of the overall canopy height (Lim *et al.*, 2003a), however further simulation modelling, such as that undertaken by Lovell, *et al.*, (2005), and Goodwin *et al.*, (2007), would be required to better understand LiDAR-tree crown interactions in eucalypt dominated forests. The need for an improved distinction between predominant canopy and predominant stem height for national level reporting is a logical conclusion of these results, with the metric to report dependent on the final use of the data (e.g., stem volume versus LAI modelling) (Means *et al.*, 1999).

For Injune, landscape height comparisons between National Forest Inventory data and the different datasets broadly agree, but with some apparent underestimation of non-forest by the LiDAR estimate. The distribution graphs comparing height metrics from field plots against the 4500 secondary sampling units also support a representative sample. Where

underestimation occurs, it is likely that the LiDAR is identifying trees taller than the forest threshold of 2 m, yet the cover in the secondary sampling unit is below the forest density threshold, so the unit is classed as non-forest. The total non-forest estimate from LiDAR is very close (within 1%) to the National Forest Inventory estimate. For NE Victoria, the height comparisons of the field plot sample against landscape-wide National Forest Inventory data broadly agree. The plot LiDAR records slightly less tall forest, and a greater proportion of medium forest, than the National Forest Inventory data.

### ***Apparent Vertical Profiles***

Apparent vertical profiles were assessed to determine their utility for describing different forest types and growth stage configurations. For Injune plots, LiDAR apparent vertical profiles were compared with those simulated using field data in a 1 m<sup>3</sup> reference matrix. With the initial test plot (p124-19), more 2D cells recorded LiDAR returns than field data simulated canopy elements, possibly indicating that there were additional canopy elements not recorded in the field measurements (i.e. small shrub elements, or irregularly shaped crowns). However, more 3D voxels were tagged with field canopy elements than with LiDAR returns, indicating that LiDAR was occluded from the lower portions of the simulated crowns and trunk voxels, confirming the findings in the literature (e.g., Harding *et al.*, 2001; Lovell *et al.*, 2003; Todd *et al.*, 2003; Chasmer *et al.*, 2006b). Alternatively, this could indicate that the crown simulations were too dense, and that the openness factor applied was too low. Investigation of individual trees in hemi-photos would be required to confirm this hypothesis (e.g., Brown *et al.*, 2002).

Some bias was evident in the LiDAR apparent vertical profiles when compared to simulated field plot data for all 31 Injune plots (Table 59 - Appendix A), a result also observed in simulations developed by Holmgren *et al.*, (2003), and Goodwin *et al.*, (2007). However, in contrast to the findings in the literature, the bias was less, which suggests that the LiDAR profiles are providing an adequate representation of overstorey and understorey distributions in the more open canopy woodland environments of Queensland. The Injune profiles also

compare well against existing vertical foliage profiles for this environment (e.g., Walker *et al.*, 1986). Where differences occur, these often result from a mismatch between field and LiDAR estimates of tree top height, such as (as noted previously) when taller canopies from trees outside the plot overhang the plot area. Additionally, error in the comparison could result from the simulation of field data, with foliage cover not being representative for plots containing short regrowth with a high stem density. With these structural conditions, there is a likely overestimation of the number of canopy cubes in the understorey. Improving the simulation, for example, by reducing the matrix spatial resolution to  $0.5 \text{ m}^3$  and improving the spatial accuracy of field tree locations and crown dimensions (including small stems), are future research options. Additionally, the use of terrestrial laser scanning combined with more sophisticated analyses of profiles and simulations would assist better representing the lower canopy layers (e.g., Lovell, *et al.*, 2003; Chasmer *et al.*, 2006b; Goodwin *et al.*, 2007).

Investigation of LiDAR vertical profiles from different forest types and growth stages in the NE Victorian field plots provide illustrative evidence of the match with both plot photo assessments and field data. The different growth stage interpretations show similar form and complexity in vertical structure as that found in the literature (e.g., Walker *et al.*, 1986; Lefsky *et al.*, 1999; Parker and Russ, 2004, Kao *et al.*, 2005).

However, the interpretation accuracy is still largely subjective and (as described previously) further research is required to develop simple and efficient quantitative assessments of growth stage from small footprint LiDAR vertical profiles. For example, this could include delineating potential strata breaks using mathematical descriptors such as a Fisher-Jenks “natural breaks” or “optimal classification” type algorithm (Fisher, 1958; Jenks, 1977), as described in Slocum (1999), or Weibull functions (Lovell *et al.*, 2003) if the general form is appropriate (i.e. not multi-modal). Coops *et al.*, (2007) fitted multiple Weibull functions to clearly defined overstorey and understorey strata from LiDAR profiles, and were able to quantify the relative amounts of foliage per strata, and crown area dominance per strata. There may be some uncertainty in these applications when no obvious strata breaks occur, especially for automated processing. Structural descriptors derived from strata analyses could be then be

---

linked to stem density and the ecological maturity classes (as in Eyre *et al.*, 2000) derived from field data, or used to assist with habitat complexity measurements and modelling, especially in relation to recovery following fire (e.g., Coops and Catling, 2000).

Issues for growth stage assessment using LiDAR profiles could occur with recent disturbance. Based on the results, this was demonstrated to modify the profile signature, with the amount of difference dependent on the magnitude of the disturbance. Documenting more LiDAR profiles in forests at a range of growth stages and disturbance regimes is required to advance the use of LiDAR profiles for these assessments. For example, with disturbance assessments in NE Victoria, it appears that a fire severity index could be developed when using the apparent vertical profiles, as part of forest structure measures to support wildfire management (e.g., Riano *et al.*, 2003; Morsdorf *et al.*, 2004; Andersen *et al.*, 2005).

From the plots burnt in the 2003 fires, plot 558 appears to have been more severely burnt, based on the lack of understorey and scorched trunks and canopy, with this reflected in the LiDAR profile by a lack of returns below 10 m. Plot 562 retains a relatively even distribution of vegetation returns at all height levels in the LiDAR profile, and the plot photos show that some understorey remains, with a few scorched trees and canopy. The difficulty with disturbance assessment using structural descriptors is that plots that have a burnt understorey have a similar profile signature to an unburnt plot with a short grassy (e.g., grazed) understorey (e.g., compare p119 in Appendix B). In an automated process at the landscape scale, additional optically derived image information on burn intensity or condition would be needed to fully exploit LiDAR profiles for disturbance assessment. It may be possible to use the near-infrared intensity of the LiDAR return (e.g., Moffiet *et al.*, 2005) to show a difference between non-burnt green leaves, and scorched or dead brown leaves. Since the intensity values were uncalibrated for the LiDAR data available (Lovell *et al.*, 2003), this was not investigated further.

---

***Maximum stand height at a range of assessment scales***

At Injune, the field plots consistently recorded lower LiDAR maximum heights when compared to the wider 7.5 ha stand (primary sampling unit), in the order of 2.5 m on average (difference range  $-7.6$  to  $0$  m,  $\delta$  2.14 m). Only one field plot (out of the 29 plots in 12 primary sampling units assessed) recorded the same maximum height as the wider primary sampling unit. There was no clear trend of forest types recording greater or lesser differences, with the primary sampling units with the tallest forest recording both the highest and lowest difference between estimates. With between 1 – 4 plots per primary sampling unit, the plot sample is 3 to 13% of the primary sampling unit, which should be statistically sufficient (Scott, 1998). It may be that the primary sampling units of the Injune forest environment are quite heterogeneous for maximum height, thus implying that the secondary sampling unit sampling is not enough to capture the variability found in the wider stand area. It should be noted that the field plots were designed to be representative of the landscape, rather than the specific primary sampling unit in which they were found (Tickle, *et al.*, 2006). However, it is logical to assume that, generally, a plot should be similar in structure to its immediate surroundings (after Tobler, 1970; Jupp *et al.*, 1989). With 75% of primary sampling units having a difference of 3 m or less, this could be considered the typical bias that would be present in this forest type, when using the type of sampling strategy described in Chapter 3.

In NE Victoria, both field plot and transect assessment areas consistently underestimated the maximum height with respect to the wider stand (~16 ha). Field plots recorded lower heights by around 6.5 m on average in shorter forests ( $< 30$  m), and 15.3 m on average in taller forests (an overall mean difference for all plots of 13 m). Sampling a stand using a one-hectare assessment area reduces the apparent mean bias to 4.4 m for shorter forests, and 9.6 m for taller forests (overall mean difference of 8.2 m).

The mean difference between the field tree measurements along the NE Victorian transects and the whole transect area (90 m x 90 m) was 8.7 m (field lower than wider area). The mean difference was 10.3 m and 4.5 m for taller and shorter respectively. It is likely that longer transects, or transects used in a different configuration (e.g., parallel transects like those



used at Injune), may be required to achieve better results. These results indicate that there are often taller trees in the wider area and that it is difficult to consistently report maximum height for the wider stand when using field plots or transects as described in Chapter 3.

### ***Predominant Height at a range of assessment scales***

At Injune across the 12 primary sampling units assessed, there is little difference in predominant height between the centre secondary sampling unit (0.25 ha) and the primary sampling unit area (7.5 ha), with the wider stand recording the higher mean value (~ 1 meter). When using a one hectare sized assessment area within the primary sampling unit, the comparison with the full primary sampling unit height has a 0.2 m difference (the full stand was taller). This indicates a relatively homogeneous structure when using predominant stand height. As would be expected, there is greater variability where clearing or heavy grazing has occurred within a primary sampling unit, and forest regeneration is present.

In NE Victoria, stand predominant height can be estimated to acceptable levels of accuracy (i.e. within 10%) using plot and transect areas, though, as expected, more structurally heterogeneous environments (e.g., floodplain riparian areas) are more difficult to predict. Across all sites, the mean predominant height difference between 0.1 ha (field plot) and 20 ha (stand) scales is -1.45 m (range -10.16 to 4.56 m,  $\delta = 3.70$  m). When using a one-hectare assessment scale, the mean difference from the wider stand is -0.4 m (range -6.3 to 7.4 m,  $\delta = 2.8$  m). This indicates that field and 1 ha plot sized areas tend to record slightly taller forest than the wider stand, which is in contrast to the maximum height results. These results confirm the literature for similar forest types and scaling methodology (Jupp *et al.*, 1989; Lovell *et al.*, 2003), though tabular results were not provided in Lovell *et al.*, (2003) so the magnitude of the confirmation cannot be given. With the random location test, the average difference in the predominant height between 30 random field plots and 30 random transect plots, with the wider 20 ha stand is minimal across all plots assessed (i.e. less than 0.5 m, with a range up to 2.0 m). This result therefore complies with basic statistical theory, in that with an adequate number of

---

samples, the actual size of the sampling unit does not impact on the overall stand estimate (Thompson, 2002).

### ***National Forest Inventory Reporting***

Both Floodplain and Foothill sites within the NE Victorian study area remain within the National Forest Inventory medium height class at all assessment scales, when using predominant height. However, in the taller Montane and Subalpine forests some locations would change between the medium and tall height classes if different assessment areas were used. Here two plots went from tall to medium forest with an increasing assessment scale, and one plot had the opposite trend. A further two plots were within 40 cm of the 30 m height threshold at either the plot or stand scales. Injune predominant height results show minimal difference at a range of scales, and that this would not impact on the National Forest Inventory height class that would be reported for the primary sampling unit location. The overall impact of these results would depend on the sampling density of plots within ecozones (Scott, 1998), and assumes that results are comparable between different data sources or measurement methods.

### **5.2.3 Improving forest cover assessment using LiDAR**

In this section the relative accuracy of utilising LiDAR for measuring forest cover is discussed with respect to comparisons with field and other remotely sensed data. As with the height assessments, the potential impact of assessment scale was investigated. This is intended to help guide decisions on working towards a useful reporting area (or minimum mapping unit equivalent), and whether field plot areas are representative of the wider stand in which they occur. This section considered four main components: how the different field measured datasets compare against each other; how the LiDAR estimates compare to field measurements; how LiDAR compared to CASI and API polygon estimates; and how LiDAR and field compared to Landsat TM derived data.

---

### ***Field data comparisons***

For the Injune, the three field datasets available for comparison with LiDAR and other remotely sensed data were field transects (foliage projective cover and foliage-branch cover), hemispherical photos (foliage-branch cover), and tree map data (crown cover). There was some variation between transect and hemispherical photo estimates of foliage-branch cover, resulting from two potential sources of error. First, the four-year time difference between data, though temporal change was found to be minimal (apart from two plots) when transect measurement from both years were compared. Second, the two methods were sampling a different area and volume within the plot, with the variation observed indicating that either the transect measurements did not sample the plot area as well as hemispherical photographs (especially in more heterogeneous forests), and/or the hemispherical photos were observing additional canopy elements both inside and potentially outside the plot. Overall though, the line of best fit for the relationship followed the 1:1 line, which could indicate that the two methods give comparable foliage-branch cover results on average. A future research option is to undertake more detailed processing of the hemispherical photos, to better match the sampled area between transects and photos, which may improve the correlation between these data.

The hemispherical photos were considered to be a robust estimate of foliage-branch cover within the plot, with the cover calibration results corresponding with those found in the literature (Lim *et al.*, 2003a; Lovell *et al.*, 2003; Riano *et al.*, 2004). Calibration assessment of the subjective assessment for a foliage discrimination threshold followed established methods (e.g., Frazer *et al.*, 2001; Cescatti, 2007). The assessment of the effective view area with respect to the plot, which, when using a radius of 50 m, was significantly greater than the 15 - 25 m radius utilised in Hanssen and Solberg, (2007), and it was noted by Riano *et al.*, (2004), that an effective radius was equal to the tree height. The different forest types (eucalypt vs conifer), may have influenced the calibration, with eucalypt forests being much more open, with larger gaps between trees, resulting in more foliage being viewable at greater distances and hence the use of larger assessment areas by this study.

It should be noted that the photo processing methods used in this research were not as sophisticated as those used in dedicated hemispherical photographic studies, which tend to primarily focus on Leaf Area Index or similar foliar measures. The primary focus for using photography in this research was to investigate if simple and rapid digital hemispherical photography collection could be utilised to provide foliage-branch cover estimates that are similar to those generated from traditional field transect and LiDAR data. Whilst this was successfully achieved with respect to the aims of the research, further processing of the hemispherical photography would be useful to account for: leaf clumping (Walter *et al.*, 2003), slope in the assessment of cover in heterogeneous forests (Walter and Torquebiau, 2000), and for tree stems, larger branches, and different gap fractions (Macfarlane *et al.*, 2007). These additional analyses may improve the correlations with other data. The photography also provides a permanent record that can be subsequently analysed using different techniques (Coops *et al.*, 2004), for example measuring individual crown area (e.g., Brown *et al.*, 2000) and then comparing to LiDAR derived crown dimension estimates.

When predicting field crown cover from field foliage-branch cover, the transect measurements have a good relationship, with a mean bias (as expected) towards crown cover of 7.4 %. The relationship between field crown cover and hemispherical photos was more variable, and the mean difference was 8.4 %. With both comparisons, conceptually it should not be possible to have a foliage-branch cover value greater than crown cover, if crown cover using opaque crowns is assumed (McDonald *et al.*, 1998). However foliage-branch cover > crown cover was observed for a number of plots from both transects and hemispherical photos, and was most likely from additional foliage elements recorded from trees (i.e. irregular shaped crowns poorly represented with two measurements) or shrubs not mapped during the plot survey.

### ***LiDAR cover comparisons with field and CASI***

For LiDAR foliage-branch cover and crown cover, comparisons with field data at both study sites generally resulted in very good relationships, with  $r^2$  values ranging from 0.78 to

0.82 for equivalent cover metric comparisons. The results are in the same range as those found in the literature (Lim *et al.*, 2003a; Jensen *et al.*, 2006), and magnitude for forest types similar to the NE Victorian locations (e.g., Lovell *et al.*, 2003; Goodwin *et al.*, 2006), with residual standard errors all less than 10%. LiDAR and CASI crown cover results agreed with each other, reflecting the similar scales of assessment. LiDAR crown cover had the stronger correlation with field crown cover, compared to CASI crown cover.

Variation in the crown cover comparison between LiDAR and CASI was attributed to the assumptions and methodology used for the respective crown delineations (e.g., Bunting and Lucas, 2006; Lee and Lucas, 2007), and error in the spatial registration of the two datasets, both to each other and to field tree-map data. Additionally, it was considered that the lower accuracy of field stem locations, especially for very small stems, combined with field-mapped crowns being measured only in the north-south and east-west directions, would influence the correlation results. Whilst the field crown measurements facilitated a rapid survey and estimate of crown area based on an ellipse (McDonald *et al.*, 1998), the irregular shape of many mature eucalypts meant that field estimates were less representative when compared to the LiDAR crown delineation. To resolve crown estimation issues, more detailed measurements would be required, although the cost effectiveness of improving the (already good) accuracy would need to be balanced against the cost of more time spent in the field (Means *et al.*, 2000). Because of the higher LiDAR sampling rate per crown compared to actual field measurements, the LiDAR results were considered to give the better (i.e. more precise) estimate of crown cover (Lim *et al.*, 2003a).

The results observed in the crown separation (zig-zag transect) trial confirm those in the literature (e.g., Walker *et al.*, 1988; Penridge and Walker, 1988; McDonald *et al.*, 1998). The success observed with p142-13 is a consequence of the structural similarity to the forests used to initially develop the method. The presence of the understorey and consistent foliage presence all the way up the vertical profile for p81-16 (see Figure 77), combined with a higher stem density, would appear to make the cover estimates more variable from the difference sources. Therefore there is a need to address the disparity between LiDAR crown cover (with a 2 m

threshold) compared to the zig-zag transect which favours dominant overstorey trees. This could be resolved by a second zig-zag transect measurement for the understorey, which is added to the first to generate total plot crown cover, as indicated in McDonald *et al.*, (1998). However, the limitation with the current field and LiDAR data is that there is no clear indication of which trees are in the overstorey or understorey, and therefore which trees should be chosen for the respective transects. The LiDAR vertical profile gives an indication of a potential stratum break (e.g., possibly at around 12 m), which could be used to define a threshold for tree allocation to strata.

Whilst the NE Victorian plots had a poor correlation between LiDAR and field tree-map crown cover, overall the relationship is significantly linear. The poor result is likely to be from the field survey recording stems with  $D_{130} > 10$  cm, whereas the other datasets would be observing foliage from all stems and understorey greater than one metre height. Other factors such as recent disturbance (e.g., fire) and site conditions (e.g., steep slopes) could make field estimation of tall crowns more difficult (Lim *et al.*, 2003a), and so contribute to the observed differences. For example, the outlier plot p562 (see Figure 67) occurs on a steep slope and was burnt in the 2003 fires, resulting in field estimated crown dimensions that do not match the extent of the LiDAR returns from the crowns.

### ***LiDAR to API comparisons***

Given the arbitrary nature of API cover class thresholds, and the difficulty of assigning a class near a threshold, the results generated in the comparison of LiDAR crown cover estimates at Injune are encouraging. It is initially concluded that fine scale API and LiDAR crown cover estimates can be cross-validated to some extent (i.e. within the limits of interpretation scale and classification methods), for the woodland and open forest environments found at the Injune study site. However, a lack of samples across all polygon classes combined with the issue of comparing continuous data (LiDAR) with categorical data (API), limits the ability to make more definitive statements.

Based on the Injune research findings, there is no major link between the percentage sample of API polygon by LiDAR and the correlation between the two cover estimates. This is not surprising, given an interpreted polygon is, in theory, supposed to be a relative homogeneous area of similar cover, at the scale of assessment (Fensham and Fairfax, 2002). Therefore, any reasonably sized sample of the polygon (by LiDAR for example) should produce a similar cover value (Thompson, 2002). Comparison results could also be affected by the LiDAR sample not being randomly distributed within the API polygon, and with potential for spatial autocorrelation in the 25 m sized assessment units, as they are arranged in a contiguous 7.5 ha block (Tickle *et al.*, 2006). API polygons with 10-20% LiDAR coverage had the greatest number of observations, which could have influenced the improvement in the results observed.

The increased variability observed in the NE Victorian LiDAR and API comparison reflects the relative data sources, interpretative methods and assumptions, and therefore limitations with both sets of data. The SFRI crown cover estimate was for dominant eucalypt overstorey, and does not consider any understorey, whereas the LiDAR considers all canopy foliage above 2 m height. These conceptual differences are reflected in the results; the LiDAR estimates were consistently greater than the API. Applying a height threshold to the LiDAR for the dominant overstorey would be one way to better compare the two datasets. However, if there are no clear indications of the height of the upper stratum, then this could be difficult to implement or automate consistently. Using individual crowns and spatially determining (in 3D) the dominant overstorey crowns would address this issue. To achieve this accurately using the HSOCI strategy, the current crown delineation methodology would need further calibration for it to be more accurate across the range of forest structures found in NE Victoria.

Future research options are generally focused on integrating or fusing LiDAR and high spatial resolution data such as aerial photography, such that the strengths of each data are utilised: LiDAR for structure, spectral for floristics (e.g., McCombs *et al.*, 2003). Analyses are now also progressing from interpreted polygons of relatively homogeneous floristics and structure, which were the practical operational limit of API (Stone, 1998; Fensham and Fairfax, 2002), to tree level estimates of the ancillary variable of interest. However, it is still important

---

to be able to translate between past and current API derived data and newly acquired LiDAR, as the historical archive of aerial photography provides a valuable (and often unique) record from which to monitor change (e.g., St-Onge *et al.*, 2004). For example, major discrepancies in estimates of temporal biomass change from independent ground plots versus API were found by Fensham *et al.*, (2007). The authors concluded that the discrepancies were a result of scale effects on the API calibration with ground reference data, combined with uncertainties in the landscape representativeness of the two independent estimates. Therefore, utilising explicit crown delineations in API calibration that can be up-scaled as required, as highlighted in this thesis, can provide a powerful tool to quantify error between different measurements.

### ***LiDAR to Landsat TM comparisons***

At Injune, LiDAR foliage-branch cover has a very good relationship with Landsat TM foliage projective cover across the assessed field plots. This relationship is even more robust than that found between field foliage projective cover (or foliage-branch cover) and Landsat TM foliage projective cover, with the hemi-photo foliage-branch cover relationship slightly better than the field transect relationships. SLATS field transect methodology has subsequently been updated (as described in the methods chapter) and now differs from the original three transect layout (Lucas *et al.*, 2006b). The updated transect method improved the correlation with Landsat TM foliage projective cover for six test transects measured during the 2004 survey (mean difference of +5.4 % with parallel transects, and -2.1 % difference with star transects). Conceptually, it is noteworthy that both LiDAR and hemispherical photo foliage-branch cover are have a better correlation to Landsat TM foliage projective cover, compared with the field transect data foliage projective cover. This may indicate that, at a plot scale, the more comprehensive sampling by LiDAR and hemispherical photography, as compared to the three parallel transects, more closely matches the imaging of cover within a Landsat TM pixel. Also, based on the findings described above and depending upon the tree canopy structure, field branch observations should perhaps be considered as foliage observations when used for remote sensing calibration. Based on the results, LiDAR could easily supplement field transects for



calibrating Landsat TM foliage projective cover, and even replace field survey in more inaccessible locations where cost and safety issues make field survey difficult (Tickle *et al.*, 2006).

### ***Landscape sampling***

At Injune, the field plot sampling strategy was designed to be broadly representative of the landscape (Tickle *et al.*, 2006). However, even though the shapes of the LiDAR and SLATS cover distribution graphs (for plot and landscape scales) were broadly similar, there were obvious differences in the mean values. For example, the mean Landsat TM foliage projective cover value is 47 %, whereas the mean LiDAR foliage-branch cover is 29 % (field plots) and 33 % (4500 secondary sampling units) respectively. The difference in mean values indicates some bias towards woodland from LiDAR in the field plots, but less so in the 4500 LiDAR sample, where a mode value of 40% is shared with Landsat TM cover. A number of factors may interact to produce the results observed. First, there is the difference between cover metrics, as demonstrated in the Landsat calibration case study, with SLATS foliage projective cover consistently reporting values approximately 10 % higher than LiDAR foliage-branch cover values. Second, the SLATS cover distribution is very broad, with similar frequency values across the cover range, and which includes more values from denser / closed forest. In contrast, the LiDAR landscape sample has a definite peak to the distribution, with fewer secondary sampling units having denser or closed forest. Additionally, there is the influence of the non-forest secondary sampling units on the LiDAR distribution, which would shift the mean value towards the woodland density.

When compared to National Forest Inventory cover data, there is a large discrepancy between the woodland and open forest class comparisons. It appears that there was a definitional change to the supplied source data, as the LiDAR assessment indicates that the forest is dominated by an open forest density, rather than woodland as demonstrated by the current National Forest Inventory data. Another issue with the National Forest Inventory application of forest class definitions is with closed forest. At Injune, the 4500 secondary

sampling units identified 16 % of the area as closed forest, but the data available from the National Forest Inventory at the time did not record any of this density, due to the class being reserved for rainforest only, and any forest that has a density greater than 80 % is included in the open forest class. As of the 2003 State of the Forests report, a closed eucalypt class has been populated with data by the NFI, where this information was available (National Forest Inventory, 2003).

For NE Victoria the field plot data were broadly representative (within 10 %) for non-forest and woodland when compared to the National Forest Inventory data, however the field plots appear to under-estimate open forest and over-estimate closed forest. The 20 km grid node intersections are broadly representative of the study landscape at a forest-non forest level, with the field plot locations giving results within 10% cover of the landscape wide estimates. With only 17 plots, there are issues with the statistical robustness of the sample with respect to the wider landscape (Scott, 1998). LiDAR cover assessment may differ from the National Forest Inventory data (derived mainly from API) derived due to differences in mapping scale, interpretive methods, and measurement assumptions, definitions or thresholds. For example, the discrepancy observed is partly due to the National Forest Inventory data not recognising closed forest for non-rainforest types (as mentioned previously). Also, examining more LiDAR data within the continuous transects across the landscape would go some way to address potential issues with the sampling. Completing the Landsat TM foliage projective cover calibration process to reduce the overestimate of “forest” from high reflectance irrigated pastures would improve the comparisons between foliage projective cover and current National Forest Inventory data at the landscape scale.

### ***Multi-scale sampling and reporting of cover***

In NE Victoria there is a good comparison of foliage-branch cover between hemispherical photography and LiDAR at both field plot and transect scales, and the results confirm the calibration presented in Chapter 3, with the best correlation from a single photo at field plot centre against the transect area LiDAR. This result means that when using

---

hemispherical photography, cover estimates are most appropriate for an area of approximately one hectare, depending on the density of the forest. For plots smaller than this, the photo estimate of cover may be more variable when compared to other data, which is constrained to the field plot area, especially in heterogeneous forest stands.

For the multi-scale trial at NE Victorian plot 220, an internal Landsat TM pixel coverage of 50 % AGO woody cover produced the strongest correlation with LiDAR crown cover. The crown cover per pixel analysis contrasts to the 20 % crown cover threshold to determine forest as claimed by the AGO (Furby, 2002). Later versions of the AGO woody and density layers are supposed to be more sensitive to lower cover in woodland environments, so this discrepancy may have been partially resolved (e.g., Caccetta and Furby, 2004; Chia *et al.*, 2006). However the updated data was not available for comparison with LiDAR derived crown cover estimates.

For the multi-scale cover assessment using all field plot locations across both study sites, and aggregated by ecozone, there are a number of notable results. First, Floodplain stands have the greatest variability as assessment area increases, while Montane and Subalpine stands have little variability, with Foothill woodlands showing moderate variability, depending on landscape context (e.g., riparian or fence-line strips have high variability, contiguous woodland has low variability). These results reflect the natural patch-gap stochastic complexity, or lack thereof, for the different environments. The results have also demonstrated that reporting cover at a one-hectare scale is the most effective when representing the wider stand. Effectiveness is based on the observation that there is little additional predictive ability gained with larger assessment sizes, yet areas smaller than one hectare can be highly variable, compared to the stand estimate. These results confirm the conclusion reached through simulation modelling for patchy forests and woodlands by Jupp *et al.*, (1989), where it was found that plot sizes up to 100 m in diameter may be required for consistent cover estimation between pixels.

Across both study sites, for most plot locations there would be no impact on the National Forest Inventory cover class reported when using different assessment scales. However for 5 / 22 sites in NE Victoria, and 2 / 12 sites at Injune there is a difference in

National Forest Inventory cover class between plot scale and stand scale cover estimates. The impact of this on final reporting of cover within a sampling scheme would depend on the total number of plots that were affected in this way, as a proportion of the total plots within the broad reporting ecozone (Williams, 2001). If it is assumed that the proportion of plots affected by scale at the two study sites is representative for the majority of Australia's forests, then it could be expected that approximately 20% of plots within a continental sampling scheme will potentially give different cover estimates (in terms of a National Forest Inventory cover class) at different assessment scales (e.g., from different sensors), for the same forest stand.

#### **5.2.4 Assessment of the Height Scaled Crown Openness Index (HSCOI)**

An ideal calibration dataset would not be limited to any one pixel size or assessment area (e.g., field plot), thus making it effectively sensor independent for calibration purposes. To achieve this, basic geographic entities (such as trees, or tree components) are required. Therefore a LiDAR derived basic geographic entity calibration dataset was developed, and the application of the LiDAR derived basic entity data to provide enhanced calibration of structural attributes was investigated. This section discusses the accuracy assessment of the tree and component scale modelling outputs by comparing tree stem density, location, height,  $D_{130}$  and crown area with field plot data.

##### ***HSCOI derived stem density***

The HSCOI is a new multi-spatial resolution method developed to generate tree scale basic geographic entities. The information derived from the modelling can then be rescaled as required to enhance the retrieval, mapping, and reporting of key forest structural attributes, and calibration of other data. The HSCOI modelling strategy utilises small footprint discrete return LiDAR data, in semi-automated algorithms that integrate height and cover parameters to generate accurate tree assessments, and sought to compliment existing CHM based methods (e.g., Chasmer *et al.*, 2004; Popescu, and Zhao, 2007). At Injune, the HSCOI facilitated the

location of tree stems associated with both the overstorey and sub-canopy strata, and differentiation of individual crowns and/or crown clusters.

At a plot scale the stem density results had a mean standard error of approximately 100 stems  $\text{ha}^{-1}$ , and a mean stem density prediction accuracy of approximately 81 % (for stems  $D_{130} \geq 5$  cm). The accuracies achieved (see also Lee and Lucas, 2007) are of the same magnitude as found in comparable LiDAR stem mapping studies (Persson *et al.*, 2002; Maltomo *et al.*, 2004). Stem density retrieval accuracy was lower in stands with higher stem density and/or those with a complex mixture of stems in overstorey and understorey strata; conclusions also made in Rowell *et al.*, (2006). The lower accuracy was attributed to the inability of the one metre spatial resolution model to resolve all stems in higher density clusters, and/or when overtopped by larger individuals. Further improvements are achievable with refinements of the method to better model LiDAR penetration (e.g., Goodwin *et al.*, 2007). Height variation in suppressed individuals could be improved through additional field sampling (Florence, 1996). Higher density LiDAR data could also be trialled (Brandtberg *et al.*, 2003), especially for more complex mixtures of overstorey and sub-canopy stems.

When the Injune calibrated HSCOI model was applied to the NE Victorian plots, the overall stem density correlation was relatively weak. Two distinct clusters of plots were identified in the correlation: those that had a good match (32 % of plots) between field and HSCOI stem count (i.e. difference < 10 stems per plot), and those with a poorer match (i.e. mean difference approximately 25 stems per plot, or  $\sim 275$  stems  $\text{ha}^{-1}$ ). The poor correlation was primarily a result of the different forest structures found in the NE Victorian environments, namely taller forests, multiple strata, and larger crowns (Lee and Lucas, 2007). The stem density prediction bias for plots with a poor match was reasonably consistent across the observed stem density range, suggesting that greater accuracy is achievable with further region-specific (e.g., soils, slope, elevation) forest structure calibration.

### ***HSCOI derived stem height and diameter***

Prediction of tree top height and diameter using the HSCOI modelling was found to improve the results compared to more traditional CHM focused methods. This was largely due to the use of all the LiDAR returns, especially those found below the top of the canopy, which are ignored in most CHM methods. The accuracies achieved for individual tree height and diameter generated from automated analyses are comparable to those found in the literature (Naesset and Okland, 2002; Morsdorf *et al.*, 2004), even though most studies usually only report correlation results for dominant overstorey stems, and not usually with sub-canopy stems. There are still a number of calibration issues to resolve, for example smaller diameter sub-canopy stems were more difficult to correctly identify the top height, especially when occurring beneath larger crowns. Difficulties with the estimation of smaller trees are common in similar studies (e.g., Clark *et al.*, 2004; Suárez *et al.*, 2005). Based on the validation sample, and for the forest types found at Injune, the accuracies achieved with the individual tree location and attribution results show that the research objective for the generation and attribution of tree scale basic entities was achieved.

### ***HSCOI crown delineation***

A HSCOI surface can be used to map and attribute the forested area, and delineation of individual crowns or clusters within the mapped area. Two primary tree genus forms (i.e. either decurrent or excurrent; Lucas *et al.*, 2004) are identified for each crown segment using structural measures derived from the apparent vertical profiles and HSCOI layers; methods similar to that used by Ishii *et al.*, (2004) and Chen *et al.*, (2006) as part of their respective crown delineation modelling. An overall accuracy of 52 % for the genus probability assessment may not be much better than chance, but it was comparable with another investigative study undertaken the study site Moffiet *et al.*, (2005), whom also found similar limitations on species/genus accuracy. It should be noted that 70 % of dominant and single crown delineations were correctly classified, which is comparable to results reported in the literature (e.g., Tormä, 2000; Holmgren and Persson, 2004), however Holmgren and Persson (2004) had LiDAR at

twice the sampling rate and in less complex forests, which would assist in a better representation of the crown structure, and therefore likely genus. The height-to-crown area functions gave similar results for tree heights less than 15 m, with a 9 m<sup>2</sup> difference observed for crown area at 15 m height (i.e. *Callitris* = 15.2 m<sup>2</sup>, *Eucalypt* = 24.1 m<sup>2</sup>), or equivalent to a crown diameter of 3.4 m. Therefore, as 88 % of those incorrectly classed had a height less than 15 m, in almost all cases either the correct genus was used, or the expected crown area estimated for the observed height was similar to what would have been calculated had the correct genus probability been assigned.

The individual crown delineations for dominant overstorey crowns proved to be generally accurate when compared to field data, with an  $r^2$  in the order 0.63 – 71 across the different crown types identified. The mean difference in estimated crown area between LiDAR *dominant* (including *single* and *isolated* crowns) crowns and field estimates was less than 4 m<sup>2</sup>, for the validation sample. The crown area results are comparable to those found in the literature for similar LiDAR based studies (e.g., Leckie *et al.*, 2003; Popescu *et al.*, 2003). Additionally, the individual crowns were spatially comparable to those generated from high-spatial resolution hyperspectral data collected in the same primary sampling units, with both sharing similar accuracies when compared to field data (Bunting and Lucas, 2006).

Variation in the correlation is a combination of factors. One factor is the error in the estimation of crown diameter from field data, resulting in less accurate area estimates for more irregularly shaped crowns or those found within clusters. Also, there was some uncertainty in the GPS locations of the field data stems, potentially causing a mismatch between the LiDAR crown/stem and most likely field stem. The mismatch could then influence the correlation especially when using semi-automated processes, as noted in Popescu, and Zhao, (2007). Conversely, where crowns overlap horizontally, but are in separate strata, the LiDAR crown delineation for the sub-dominant tree will underestimate diameter and area compared to field estimates. Under estimation occurs when the taller or dominant crown area ‘occupies’ a portion of the sub-canopy crown area, when represented in a 2D GIS vector model (Popescu *et al.*, 2003). When this occurs with many trees, the *cluster* crown type is generated, which is

---

generally made up of small crown sizes and/or interlocking crowns. With *clusters*, the HSCOI modelling is not able to resolve individual crowns at the finer scale. However, within the HSCOI crown clusters it was observed that the HSCOI stem mapping does correctly identify (to within a few stems) the main stems in most cases (within the validation set). Where a one-to-one comparison between a LiDAR crown cluster and field stem may have produced large differences, this was substantially reduced in many cases if the total crown area of all field stems within the LiDAR segment were compared, as also noted in Morsdorf *et al.*, (2004).

Unlike some other crown delineation methods (generally optical image based), the LiDAR HSCOI strategy can identify crowns across a wide range of crown cover densities, and gaps between crowns were not misclassified as potential crowns (e.g., Culvenor, 2002). The ability to use height thresholds to automatically separate tree crown segments from non-crown areas is a significant advantage of LiDAR over other optical data (Hyypä *et al.*, 2001; Leckie *et al.*, 2003). However, the best results were obtained when both high spatial resolution optical (especially hyperspectral) and LiDAR data were integrated (see Lucas *et al.*, 2008 – Appendix C), and the relative strengths of each sensor are utilised (e.g., LiDAR for structure, spectral for floristics). The strengths of integration have also been demonstrated in a number of studies (e.g., Coops *et al.*, 2004; Hill and Thomson, 2005). One future research option to improve the crown mapping accuracy of sub-canopy trees would be to establish a multi-scale hierarchy of delineated crowns, where the same crown sub-segments could be used to generate different final tree crowns, depending on whether the tree occurs in the upper or lower stratum. Separate overstorey and understorey crown maps could then be generated. The use of different strata heights (if present) retrieved from a LiDAR apparent vertical profile from the tree or tree cluster would also facilitate this option. Further discussion on the HSCOI modelling and crown cover results is given in Lee and Lucas (2007) (Appendix C).



### 5.2.5 Calibration case study examples using LiDAR

This section discusses how generating basic geographic entities enhanced the multi-scale calibration of other data. The main type of calibration undertaken was to rescaled LiDAR derived basic entities to match the sensor spatial resolution for; a) Landsat TM cover, and including the development of a foliage to crown cover translation function, b) ICESat height and cover data, and c) stand reconstruction for input into SAR simulations.

#### *Landsat TM calibration using LiDAR structural output*

LiDAR foliage-branch cover is a close match to SLATS foliage projective cover, though there is some scatter in the relationship, arising from the heterogeneous landscape and different sensing parameters and scales. There is an approximate 10% bias in the relationship between foliage projective cover and LiDAR foliage-branch cover when using a 2 m “forest” threshold. The bias is much less evident when using the 0.5 m threshold for LiDAR foliage-branch cover, especially at the denser end of the cover range. This would tend to confirm the AGO proposition that SLATS foliage projective cover measures all tree/shrub canopy foliage, rather than “forest” foliage as would be the case if a 2 m height threshold were to be strictly applied (AGO, 2003). It should be noted that SLATS do not claim to measure exclusively “forest” at 2 m and above, and have different working definitions of forest to those used by the National Forest Inventory (QDNRM, 2003). Also, SLATS are currently investigating using SAR to improve discrimination of regrowth in response to these issues (Lucas *et al.*, 2006b). As the AGO also predominantly rely on Landsat TM imagery, it could be said that the apparent bias noted in this study could also present in the AGO estimates of “woody”. This is due to height information not being explicitly accounted for from Landsat TM data alone (Donoghue and Watt, 2006), even with temporal analyses combined with growth modelling (Richards and Brack, 2004). There is a less robust relationship (i.e. more variability across the observed cover range) between Landsat TM derived foliage projective cover and LiDAR crown cover. Therefore, when using crown cover as the reporting metric (e.g., Furby 2002), there is more

potential error within any one pixel than if the foliage projective cover (or even foliage-branch cover) metric is used.

Stem density can be estimated from cover information with reasonable accuracy, with best results achieved when using LiDAR foliage-branch cover with a 0.5 m height threshold. This is due to the 5 cm +  $D_{130}$  threshold used for the stem density assessment, as small trees and shrubs would also be accounted for. Based on the modelled HSCOI stems, basal area per pixel was calculated and compared to Landsat TM foliage projective cover, with the resulting correlation (Figure 5 – Appendix A) providing additional independent confirmation of the results published by the SLATS program (QDNRM, 2005; Lucas *et al.*, 2006b).

### ***Foliage-branch cover-to-crown cover translation function***

The results of the investigation into the development of a generalised translation function suggest that, as a quick rule-of-thumb, crown cover = 1.5 x foliage-branch cover (or 1.3 x foliage projective cover). Improvements to the functions would include using a sigmoid shape to better account for potential saturation of crown cover near 100% whilst foliage or foliage-branch cover still increases (P. Scarth, *pers. comm.*). However, it is noted that the apparent saturation of crown cover at higher foliage-branch cover does not appear in the Injune data when using 25 m sized assessment areas. In this case, it appears that almost 100% crown cover results in less than 70% foliage-branch cover. This may reflect the quite open canopy foliage habit and form of the semi-arid forests found at Injune. The difference in scaling factors is small between foliage-branch cover and foliage projective cover, indicating that either: the forests at Injune (primarily) have sparse canopies, such that foliage or foliage-branch cover estimates are generally similar; and/or that Landsat TM foliage projective cover estimates are in fact quite similar to LiDAR foliage-branch cover estimates. This could imply that, when compared with Landsat TM SLATS derived foliage cover, there is little difference between the foliage and foliage-branch cover metrics. The field data results in the matrix of cover correlations table across the different field estimates supports this hypothesis. Further development of the foliage projective cover to crown cover translation function, especially for

forests that are different from those found at Injune (e.g., rainforest) is recommended, to broaden the applicability of the function.

When examining the crown cover to foliage-branch cover relationship, it was noted that there were a number of pixels with a logical consistency issue where foliage or foliage-branch cover was greater than crown cover. Examination of these pixel areas showed that the inconsistency was caused by two conditions. Either the pixel area had some portion with LiDAR returns missing due to irregularities in the helicopter flight path, or the return density was much less than what was found in other pixels. In the outlier pixels, the return density was up to 1/3<sup>rd</sup> of the overall mean density on average, where the mean standard density was equal to 1 return per 0.54 m<sup>2</sup>, whereas the low-density pixels had a mean of 1 return per 1.25 m<sup>2</sup>. Across the Injune field plots, the mean return density was 1 return per 0.57 m<sup>2</sup>, with a range of 1 return per 0.30 m<sup>2</sup> to 0.99 m<sup>2</sup>, and for NE Victoria it was 1 return per 0.59 m<sup>2</sup>, with a range of 1 return per 0.35 m<sup>2</sup> to 0.95 m<sup>2</sup> (see also Table 65 and Table 66 – Appendix A). The plot return density for forest canopy foliage (2 m + height) was 1 return per 1.86 m<sup>2</sup> at Injune, and 1 return per 1.37 m<sup>2</sup> in NE Victoria. When plot return density was compared to error in height or canopy cover estimates between LiDAR and field data at both study sites, there was no clear trend for a lower return density producing more variable results. Greater variability with lower return density certainly occurred in some plots (as with the Landsat TM pixel sizes assessments), but variability in the comparison also occurred in high return density plots. These results support most of the findings of Thomas *et al.*, (2006) and Goodwin *et al.*, (2006).

### ***ICESat calibration for continental monitoring***

Whilst initial comparisons between ICESat and LiDAR structural metrics were variable, ICESat did appear to extract reasonable estimates when compared to the LiDAR, with an apparent threshold of improved accuracy when foliage-branch cover was higher than 30%. The differences observed in the case study were comparable (in terms of RSE for height) with those found in other pilot studies (e.g., Harding and Carabajal, 2005; Lefsky *et al.*, 2005a; Sun *et al.*, 2008), although more comparison sites are required to generate proper correlations (see Lee *et*

*al.*, 2006). The case study also highlighted the utility of small footprint discrete airborne LiDAR, because the point data could be clipped to any size required (within the swath width). This allowed elliptical shapes of various sizes to be extracted and compared explicitly with the modelled waveform footprint: no other calibration data can do this as precisely. Once the ellipses area generated, crown delineations can be clipped to the modelled footprints, and so within footprint analyses of height, foliage and crown cover estimates can be easily made. This methodology is an advance on the current literature for small scale calibration case studies.

Further research is required to address the range of issues identified in the case study example presented, which is needed before reliable continental application can be undertaken. One option is to use a modelled ICESat footprint area that is half the size used in the case study. The intensity of the waveform is greatest at the centre of the footprint, and potentially quite low at the edges (as illustrated in Harding and Carabajal, 2005). Therefore it would be expected that the sensitivity of the waveform vegetation response would be greatest in the centre portion of the footprint (Lefsky *et al.*, 2005a). By halving the major axis value, a smaller footprint size could be simulated in the airborne LiDAR, and attributes extracted and compared. This may result in improved correlation for height and cover in some cases (e.g., areas with sparse vegetation and on steeper slopes, Harding and Carabajal, 2005). Second, further investigation and refinement of foliage projective cover and three height metrics currently extracted from the waveform. There is a need to better understand how terrain and vegetation structure interact with the waveform response, and what is the most appropriate value to extract (which may not be the metrics currently used). Also, the impact of smoke, high cloud, haze, and fog/mist on the ICESat response needs to be considered, especially in riparian areas, where these conditions may occur more frequently. Hazy conditions may result in greater scattering of the laser pulse, so resulting in less sensitivity to the vegetation, and incorrect assessment of height and cover.

### ***Stand reconstruction modelling for SAR simulation***

As described in Lucas *et al.*, (2006c) (Appendix C), a recognized limitation of previous studies aimed at SAR backscatter modelling using 3D coherent simulations was the reliance on

field data for parameterization. However, the reliance on field plots has resulted in a less complete representation across the stand of the spatial variability in the distribution of tree components (stems, branches, leaves etc.) of varying sizes and orientations in either 2D or 3D. Furthermore, such data have often proved inadequate for providing sufficient validation for model outputs. By calibrating the fine spatial resolution data (LiDAR, CASI, LSP) using field data relating to their size (volume), geometry and dielectric properties (including those from destructive harvesting measurements), a more realistic representation of the forest stand and the ground surface was constructed. This in turn has allowed a better explanation of the variation observed within simulated and actual SAR data. Such research has and continues to be undertaken independently by the co-authors (Lucas and Williams).

The LiDAR tree component biomass results indicate that the modelled distributions and dimensions of components were reasonable, given the implicit assumptions. Examination of the stems with poor correlation ( $n = 30$ ) identified a number of issues, summarised in Table 54. First, the height allocation to subcanopy stems was incorrect, largely because the influence of the overstorey canopy resulted in a large disparity between  $D_{130}$  and therefore allometric biomass estimates. In a few cases, the dimensions of the modelled branches (in terms of either length or radius) were too great, which generated a disproportionately large estimate of branch biomass. Some stems located in the field were of a size and form that was outside of the mean predictive functions used for deriving  $D_{130}$  and  $D_{30}$  as described in the Methods chapter. In these cases, the stems had a much larger  $D_{30}$  for the equivalent  $D_{130}$  based on the prediction model, or stems were shorter than average for the predicted  $D_{130}$ .

The reconstruction of the 3D structure of the forest through integration of field, LiDAR and CASI/LSP data is itself a new approach to forest characterization. By seeking to parameterize the coherent SAR model, new techniques were developed for locating tree trunks based on the HSCOI, retrieving height and stem diameters of sub-canopy trees, and delineating tree crowns in complex forest environments (Lee and Lucas, 2007).

The stem and crown products have provided for improved mapping of total and component (leaf, branch and trunk) biomass through integration of LiDAR, CASI and LSP, and

defining leaf and terminal branch distributions based on LiDAR voxels (Lucas *et al.*, 2008). Anomalously bright regions in the initial SAR simulations also provided useful feedback allowing modifications to the LiDAR modelling of stems and branches to be targeted, especially where forest structures found outside the field plot locations were encountered (Lucas *et al.*, 2006c).

**Table 54: Description of different types of LiDAR and field error with stand reconstruction using component modelling, for SAR simulation.**

Broad type	Error / Issue description	No. of trees
LiDAR tree height error	The height allocation to these sub-canopy stems needs further refinement, with an average height overestimate of 5.7m observed (as compared to field data). This then causes the $D_{130}$ and biomass to be overestimated.	11
LiDAR branch modelling error	The error appears to be a result of branches being too large for these sub-canopy stems. This is caused by the trunk being at one end of cluster, and some branches extending out to the other edge of the cluster, with an average length of 8 m. The branches also join near base of trunk, so a branch can be around 52 kg on average. A potential solution would be to restrict number of branches to a stem, and have them join higher up the stem.	4
Field tree volume estimates	Stems are within a cluster. It appears that the modelled trunk volume is larger than it might actually be in the field. The $D_{130}$ and height values between field stem and HSCOI stem are close.	6
Field $D_{130}$ to height relationship	Four of the stems were dominant within the cluster, and they appeared to be shorter trees with a relatively large $D_{130}$ . The height and $D_{130}$ observed in field data were well outside the general predictive function. Height comparisons between field and LiDAR were within 1 m. The mean difference between field $D_{130}$ and the empirically derived $D_{130}$ were 12.9cm (field had larger $D_{130}$ ). One stem was the opposite – the field measured $D_{130}$ was smaller than the predicted value from the height empirical function.	5
Field $D_{30}$ to $D_{130}$ relationship	Three of the 4 stems in this category were found to have larger $D_{30}$ values than what the prediction was from the empirical function with $D_{130}$ . The mean difference was 10.8cm, with the field estimate being higher. One stem was the opposite – the field measured $D_{30}$ was smaller than the predicted value from the $D_{130}$ empirical function.	4

This process has already led to improvements in the SAR simulations and highlights the synergies that are possible when integrating data from a range of sources and across scales. As an extensive LiDAR dataset is available for a range of forests near Injune, future research options are available to further develop the automated algorithms, SAR simulations, and validation of outputs.

---

## 5.3 Practical Implications, Limitations and Recommendations

### 5.3.1 Practical implications

There are a number of practical implications with the successful outcomes of the multi-scale hierarchical strategy. LiDAR was demonstrated to be a very useful dataset for improving the assessment of forest structure, by providing a unique, spatially accurate, extensive (compared to field plots) and precise tool for estimating a range of forest structural attributes at multiple scales.

Ideally LiDAR, utilised within a multi-scale hierarchical framework, would form part of any continental forest sampling or monitoring strategy as a strategic rather than operational tool. Strategic application would limit the impact of high initial cost of data collection, especially if collection could be part of a ‘standing order’ with data providers who would gather data over key sites during transit for normal operations. The strategic application could be optimised by developing a nationally consistent set (or library) of LiDAR “signatures” for key attributes across a wide range of environments, and perhaps seamless integration with aerial photography (ideally hyperspectral) collected at the same time/platform as the LiDAR. A model based sampling strategy would be an efficient way to determining the key sites across the country. The key strategic monitoring sites would then be flown with LiDAR to establish baselines for the regression models. For example, the NFI in its CFMF design report (Wood, *et al.*, 2006) indicate that sites could be re-flown with LiDAR every 15 or 20 years. It is assumed that this allows sufficient time for significant growth (how ever this is defined ecologically) to occur, and which would allow the identification, quantitative description, and monitoring of subtle change (both horizontal and vertical) at fine scales over areas larger than a field plot. The strategy would also have the advantage of spreading the high collection cost over a longer time period.

The research presented in this thesis has shown that LiDAR can be a very useful tool for forest assessment at a range of scales. One of the major impediments to the operational implementation of LiDAR for forest assessments is the perceived high cost of data collection,

---

storage and processing software requirements (often compounded by a lack of commercially available forest analysis specific software). As an example, the supply of data that was utilised by this research was \$53 ha<sup>-1</sup> in Queensland (~A\$40,000 for one week of flying and ~2Gb of data), and \$1.50 ha<sup>-1</sup> in Victoria (i.e., ~A\$90,000 for two days flying (plus transit) and supply of 90 Gb of data; Wood, *et al.*, (2006)). The major initial cost component of data acquisition is aircraft deployment, especially if standby costs are included. Data storage costs these days are generally minimal compared to the overall project value; however software development (time and staff) and hardware costs are usually internalised within the organisation(s). It is beyond the scope of this thesis to enter into a detailed cost/benefit analysis for LiDAR use; though a summary of the major benefits is outlined below. A detailed cost breakdown of LiDAR usage for forest assessment is provided in Rombouts, (2007), and comparison with other data sources in Wood, *et al.*, (2006).

Whilst the initial cost of data acquisition may appear high, if the range of data that can be supplied and applications it can be used for are properly accounted for, then costs have been shown to be readily recouped (Rombouts, 2007). Major benefits of LiDAR usage for forest assessment include (Rombouts, 2007):

- the information can be used for strategic as well as operational planning, and highlight areas where costs could be reduced, such as with down-stream cost savings as a result of better decision making (i.e. cost-loss analysis);
- can reduce costs per hectare (e.g., timber harvesting or national monitoring) owing to improved topographic, road and stream network maps, better stand delineation and inventory, thus improving the accuracy of resource estimates compared to conventional methods;
- significantly reduced time spent collecting data in the field; and
- when applied in a monitoring scheme can utilise dynamic rather than static stand boundaries increasing the ability to track change and update resource estimates.



The use of LiDAR within a multi-scale strategy also provides efficient methods for understanding how scale may impact on local to regional estimation of forest attributes. The results indicate that scale must be explicitly defined in reporting, as different values can be obtained for height and cover metrics at different assessment scales, for some heterogeneous forests. As the proposed Continental Forest Monitoring Framework seeks to utilise multi-scale strategies, then the effect of scale from different data sources on summary results and inferences about trends needs to be further investigated for each broad reporting unit (e.g., ecozone).

Unlike Landsat TM data, ICESat laser data does not provide complete coverage of structural information across the continent. If appropriate calibration for the range of forest types and environments across Australia can be developed using LiDAR (for example), then it may be possible to generate a large sample (> 1 million points) that is consistently collected across the continent. The continental sample could then provide statistical and tabular information on the forest height distribution per ecozone, for the life of the sensor. This would also overcome some of the current limitations with relying on a compilation approach from the States and Territories, where data was collected, interpreted, and classified in a variety of ways. Additionally, the continental sample would present an opportunity to update the existing mapped forest polygons (e.g., from the National Vegetation Information System) with more accurate height information. Alternatively, suitably calibrated ICESAT data could help refine current process models to better predict tree height based on environment, species, cover and disturbance history (Coops *et al.*, 1998; Turner *et al* 2004; Brack *et al.*, 2006). The outputs of the process models could then be combined with existing National Forest Inventory data to improve national forest height mapping, and feed into the national carbon accounting system.

### **5.3.2 Limitations and recommendations for future research**

In the course of developing a multi-scale hierarchical strategy to determine how LiDAR can improve the assessment of forest structure, a number of research limitations were identified. These can be categorised into four general topics: field data limitations, LiDAR data limitations, modelling limitations, and calibration strategy limitations. Overall, rather than detracting from

---

the research findings, the limitations identified here represent opportunities for model enhancements and future research avenues.

Field data limitations are those where the measurements taken in the field had uncertainty because of the measurement method, recording device, or operator error. When field calibration data have greater than expected uncertainty, it can be difficult to identify where or why error has occurred in the remotely sensed data source. In this research, uncertainty in field estimates was noted for stem location because of issues associated with poor GPS signals under canopy, in steep terrain and different times of day. Tree measurement method limitations for LiDAR calibration purposes included not being able to identify the actual top of the tree, variation in estimates between observers, not recording all stems within a plot due to time constraints or sample design, and poor estimation of crown dimensions, especially for irregular crowns. It is recommended that field measurements of individual tree crowns be taken along the longest and shortest axes with the longest axis angle from north also recorded, if they are to be compared with LiDAR results. Other issues were not sampling all major forest types across the landscape, and natural variability in structural empirical transfer functions such as between height and stem diameter. Finally, plot shape and plot sampling techniques (e.g., transects or hemispherical photos) need further research to determine the actual spatial extent they represent with respect to the overstorey canopy, when compared to fine scale remotely sensed data such as LiDAR.

LiDAR data limitations are those related to the data and its collection. Whilst it may not always be practical or affordable, collecting data at higher sampling densities would overcome some of the limitations identified in the literature and by this thesis. When higher sampling densities were collected, tree crowns were easier to identify, and greater definition of the sub-canopy was achieved (and less evidence of sensor lag issues; e.g., Lovell *et al.*, 2003). Aiming for consistent data collection is also recommended, though often difficult to achieve in practise. For example, the effects of wind and/or steep terrain on aircraft height above ground were noted, and resulted in varying sampling density within short distances. This can introduce unintended variability into correlations when comparing extracted structural attributes with field

---

data. Further research and more calibration sites are needed to validate the current assumptions when using LiDAR profiles for growth stage and disturbance assessment, and to allow accurate interpretation for a wider range of forest types and environmental, site, and disturbance conditions.

The primary LiDAR modelling limitation is the need for a complex set of processes to be able to model structurally complex forest environments, and therefore accurately attribute tree entities. This can lead to results that are specific to a site or region, which leads to limited applicability in new areas (as observed in the NE Victorian application). The proof-of-concept component modelling showed promise, but does need further improvements so the SAR simulations and biomass estimates can achieve better validation with field data. However, to do this it is likely that more detailed field measurements and/or terrestrial LiDAR is required. A future research option to enhance the Height Scaled Crown Openness Index (in addition to higher LiDAR return densities) is the use of time-sequential data, so that greater detail on the actual penetration ability for LiDAR pulses can be calculated, rather than just inferred. Finding ways to reduce the inherent variability of field derived empirical functions is also recommended. This could involve further stratification into different forest types based on environment or genus.

There are a number of limitations with the calibration strategy with respect to national application. Both the cover transfer functions and impacts of assessment scale modelling need further calibration across a wider range of forest types (e.g., tropical and temperate rainforests), and across environmental, ecotonal, and disturbance (e.g., fire intensity) gradients before they can be applicable across the continent. Similarly, a greater number of ICESat footprints across a wider range of forest types are needed, including the development of calibration functions and determination of waveform response thresholds to terrain and forest structure. It is recommended that additional data, both LiDAR where available (e.g., process all the NE Victorian data), and other data (e.g., MODIS, SPOT5) be compared at the appropriate scales, to increase the range of data available for national monitoring schemes.

## CHAPTER 6. CONCLUSION

---

### 6.1 Thesis Conclusion

This thesis posed the seemingly simple question ‘how can LiDAR improve the assessment of Australian forest structure?’ From the research presented, the simple answer is ‘by deriving tree scale entities within a multi-scale calibration strategy’. However, when consideration is given to what is meant by the terms ‘improve’, ‘forest structure assessment’, and ‘scale’, the actual answer is more complex.

When considering ‘improvements’ to forest structure assessment using LiDAR, results can be generated for structural metrics with a similar accuracy as current methods but over larger areas, or generate better results by highlighting limitations in field calibration estimates. Alternatively, new measures can be generated that produce the information required for national scale inventory. Examples of all three ‘improvements’ to the assessment of forest have been presented in this thesis. These include accurate estimates of crown and foliage-branch cover, and predominant height at plot, stand and landscape scales. The use of individual crown delineations and stem mapping has improved the validation of field estimates and calibration of medium scale data such as Landsat TM, ICESat and radar. Finally, the use of apparent vertical profiles across different forest types provides new insight into the assessment of stand growth stage and disturbance history. Whilst good results have been demonstrated across most metrics, a number of limitations have been identified; such as in the collection of field data to support LiDAR calibration, the LiDAR data sampling of the forest volume, modelling assumptions and complexity, and the representativeness of calibration strategy across different forest types. These limitations provide opportunities for further research to improve the assessment of forest structure using LiDAR.

‘Forest structure’ is a broad term, which can encompass a wide range of metrics and be valid at a range of scales. Essentially forest structure is a measure of density; that is, the density of tree stems within a unit area, the density of crown branches and foliage originating from those stems, and the density of foliage at different heights throughout the forest volume.

---

Structural measurements can range in ‘scale’ from an individual leaf, the branches and stems that make up a single tree, through to groups of trees, to stands, forest landscapes, and ultimately, forested biomes across continents. Therefore the ability to be able to measure forest ‘structure’ across a range of scales, and importantly, understand how metrics are related between scales and datasets (through continuous transfer functions), provides a significant contribution to national forest inventory and monitoring. By utilising a hierarchal multi-scale strategy to address the primary research question and objectives, this thesis has demonstrated that small footprint LiDAR can improve the assessment of forest structure at a range of scales, from tree components up to landscape elements. Few other remotely sensed datasets can provide information on the same range of structural metrics (i.e. height, cover, and stem density) and across the range of scales that are increasingly required for sustainable forest management, national reporting and environmental research.

The multi-scale strategy and modelling developed in this thesis was found to perform best in forests and woodlands of medium height ( $\leq 30$  m) with a canopy cover up to 80 %, reducing in accuracy in taller forests or those with multiple strata. Whilst open forest and woodland formations of medium height are typical to almost 90 % of Australia’s forests, further evaluation of the tree-scale modelling is required at other sites to better represent the range of forest types and structural forms found in Australia. The multi-scale modelling techniques developed in this research have contributed to the NFI Continental Forest Monitoring Framework pilot project and its potential application across Australia, (e.g., by providing the LiDAR chapter in Wood *et al.*, 2006). For example, the results provide guidance on the most cost effective use of remotely sensed data across a range of scales, and especially for areas where field plot visits are impractical or too expensive. Scale effects have been identified in woodlands and heterogeneous forests, for example in riparian floodplains. The suggestion of an empirically derived one hectare minimum forest area for reporting, progresses the NFI research in this area. The research presented in this thesis therefore offers support to Australian State and Federal Government commitments to national and international forest monitoring and reporting agreements.

---

## REFERENCES

---

- Addink, E. A., de Jong, S. M. and Pebesma, E. J. (2007) The Importance of Scale in Object-based Mapping of Vegetation Parameters with Hyperspectral Imagery. *Photogrammetric Engineering and Remote Sensing*, 73, 905-913.
- Allen, T. F. H. and Starr, T. B. (1982) *Hierarchy: Perspectives for Ecological Complexity*. University of Chicago Press, Chicago, USA. 310p.
- Andersen, H.-E., McGaughey, R. J. and Reutebuch, S. E. (2005) Estimating forest canopy fuel parameters using LIDAR data. *Remote Sensing of Environment*, 94, 441-449.
- Atkinson, P. M. and Curran, P. J. (1995) Defining an optimal size of support for remote sensing investigations. *IEEE Transactions on Geoscience and Remote Sensing*, 33, 768-776.
- Atkinson, P. M. and Tate, N. J. (2000) Spatial Scale Problems and Geostatistical Solutions: A Review. *The Professional Geographer*, 52, 607-623.
- AUSLIG (1990) *Atlas of Australian Resources: Volume 6: Vegetation*. Canberra, Australia. Commonwealth of Australia. 64p.
- Australian Greenhouse Office (AGO) (2003) Comparison of the objectives and methods for the remote sensing of changes in woody vegetation (SLATS) and change in forest cover (NCAS). Technical Note. Canberra, Australia. Australian Greenhouse Office. 25p.
- Australian Greenhouse Office (AGO) (2005) *Greenhouse gas emissions from land use change in Australia: Results of the National Carbon Accounting System 1988-2003*. Canberra, Australia. Australian Greenhouse Office. 42p.
- Baccini, A., Friedl, M. A., Woodcock, C. E. and Zhu, Z. (2007) Scaling Field Data to Calibrate and Validate Moderate Spatial Resolution Remote Sensing Models. *Photogrammetric Engineering and Remote Sensing*, 73, 945-954.
- Barlow, B. A. (1994) Phytogeography of the Australian region. IN Groves, R. H. (Ed.) *Australian Vegetation*. Second edition. Cambridge, UK. Cambridge University Press. 562p.
- Biggs, P. H., Wood, G. B., Schreuder, H. T. and Brink, G. E. (1985) Comparison of point-model based and point-Poisson sampling for timber inventory in jarrah forest. *Australian Forest Resources*, 15, 481-493.
- Boland, D. J., Brooker, M. I. H., Chippendale, G. M., Hall, N., Hyland, B. P. M., Johnston, R. D., Kleinig, D. A. and Turner, J. D. (1992) *Forest Trees of Australia*. Melbourne, Australia. CSIRO Publishing. 687p.
- Brack, C.L. (2000) State of Knowledge Report for IUFRO Unit 6.15.00 Improving education and further education in forestry. *Proceedings IUFRO World Conference*, Malaysia. p15.

- Brack, C. L. (2004) Projecting native forest inventory estimates from public to private tenures. *Australian Forestry*, 67, 230 - 235.
- Brack, C. L., Richards, G. and Waterworth, R. (2006) Integrated and comprehensive estimation of greenhouse gas emissions from land systems. *Sustainability Science*, 1, 91-106.
- Brack, C. L. (2007) National forest inventories and biodiversity monitoring in Australia. *Plant Biosystems - An International Journal Dealing with all Aspects of Plant Biology*, 141, 104 - 112.
- Brandtberg, T., Warner, T. A., Landenberger, R. E. and McGraw, J. B. (2003) Detection and analysis of individual leaf-off tree crowns in small footprint, high sampling density lidar data from the eastern deciduous forest in North America. *Remote Sensing of Environment*, 85, 290-303.
- Brogaard, S. and Olafsdóttir, R. (1997) Ground-truths or ground-lies? Environmental sampling for remote sensing application exemplified by vegetation cover data. *Lund Electronic Reports in Physical Geography I*, URL (<http://www.natgeo.lu.se/Publikationer/Lerpg/l/Article.htm>) (Accessed January 2008).
- Brown, P. L., Doley, D. and Keenan, R. J. (2000) Estimating tree crown dimensions using digital analysis of vertical photographs. *Agricultural and Forest Meteorology*, 100, 199-212.
- Brown, S. (2002) Measuring carbon in forests: current status and future challenges. *Environmental Pollution*, 116, 363-372.
- Bunting, P. J. and Lucas, R. M. (2006) The delineation of tree crowns in Australian mixed species forests using hyperspectral Compact Airborne Spectrographic Imager (CASI) data. *Remote Sensing of Environment*, 101, 230-248.
- Burnett, C. and Blaschke, T. (2003) A multi-scale segmentation/object relationship modelling methodology for landscape analysis. *Ecological Modelling*, 168, 233-249.
- Bureau of Meteorology (2004) URL: <http://www.bom.gov.au> (Accessed April 2004).
- Burrows, W. H., Henry, B. K., Back, P. V., Hoffmann, M. B., Tait, L. J., Anderson, E. R., Menke, N., Danaher, T., Carter, J. O. and McKeon, G. M. (2002) Growth and carbon stock change in eucalypt woodlands in northeast Australia: ecological and greenhouse sink implications. *Global Change Biology*, 8, 769-784.
- Caccetta, P. A. and Furby, S. L. (2004) Monitoring Sparse Perennial Vegetation Cover. *Proceedings of the 12th Australasian Remote Sensing and Photogrammetry Conference*, Fremantle, Western Australia, Australia. 18-22 October.
- Casa, R. and Jones, H. G. (2005) LAI retrieval from multi-angular image classification and inversion of a ray tracing model. *Remote Sensing of Environment*, 98, 414-428.
- Cescatti, A. (2007) Indirect estimates of canopy gap fraction based on the linear conversion of hemispherical photographs: Methodology and comparison with standard thresholding techniques. *Agricultural and Forest Meteorology*, 143, 1-12.

- 
- Chasmer, L., Hopkinson, C. and Treitz, P. (2004) Assessing the three-dimensional frequency distribution of airborne and ground based LiDAR data for red pine and mixed deciduous forest plots. *International Archive of Photogrammetry, Remote Sensing and Spatial Information Sciences*, 36, 66-69.
- Chasmer, L., Hopkinson, C., Smith, B. and Treitz, P. (2006a) Examining the Influence of Changing Laser Pulse Repetition Frequencies on Conifer Forest Canopy Returns. *Photogrammetric Engineering and Remote Sensing*, 72, 1359-1367.
- Chasmer, L., Hopkinson, C. and Treitz, P. (2006b) Investigating Laser Pulse Penetration through a Conifer Canopy by Integrating Airborne and Terrestrial Lidar. *Canadian Journal of Remote Sensing*, 32, 116-125.
- Chen, X., Vierling, L., Rowell, E. and DeFelice, T. (2004) Using LiDAR and effective LAI data to evaluate IKONOS and Landsat 7 ETM+ vegetation cover estimates in a ponderosa pine forest. *Remote Sensing of Environment*, 91, 14-26.
- Chen, Q., Baldocchi, D., Gong, P. and Kelly, M. (2006) Isolating individual trees in a savanna woodland using small footprint lidar data. *Photogrammetric Engineering and Remote Sensing*, 72, 923-932.
- Chia, J., Zhu, M., Caccetta, P. A. and Wallace, J. F. (2006), Derivation of a Perennial Vegetation Density Map for the Australian Continent. *The 13th Australasian Remote Sensing and Photogrammetry Conference Proceedings*, Canberra, Australia, 20-24 November.
- Cihlar, J. (2000) Land cover mapping of large areas from satellites: status and research priorities. *International Journal of Remote Sensing*, 21, 1093-1114.
- Clark, M. L., Clark, D. B. and Roberts, D. A. (2004) Small-footprint lidar estimation of sub-canopy elevation and tree height in a tropical rain forest landscape. *Remote Sensing of Environment*, 91, 68-89.
- Cohen W.B., Goward S.N. (2004) Landsat's Role in Ecological Applications of Remote Sensing. *BioScience* 54 (6), 535-545.
- Combal, B., Isaka, H. and Trotter, C. (2000) Extending a Turbid Medium BRDF Model to Allow Sloping Terrain with a Vertical Plant Stand. *IEEE Transactions on Geoscience and Remote Sensing*, 38, 798-810.
- Commonwealth of Australia (1997) *Australia's First Approximation Report for the Montreal Process*. Bureau of Rural Sciences, Canberra, Australia. 104p.
- Cooke, R. U. and Harris, D. (1970) Remote sensing of the terrestrial environment. Principles and Progress. *Trans. of the Institute of British Geographers*, 50, 1-23.
- Coomes, D. A., Allen, R. B., Scott, N. A., Goulding, C. and Beets, P., (2002) Designing systems to monitor carbon stocks in forests and shrublands. *Forest Ecology and Management*, 164, 89-108.



- Cooperative Research Centre for Greenhouse Accounting (CRCGA) (2006) Injune Collaborative Project <http://www.greenhouse.crc.org.au/injune/> (accessed Jan 2008)
- Coops, N. C., Waring, R. H. and Landsberg, J. J. (1998) Assessing forest productivity in Australia and New Zealand using a physiologically-based model driven with averaged monthly weather data and satellite-derived estimates of canopy photosynthetic capacity. *Forest Ecology and Management*, 104, 113-127.
- Coops, N. C. and Catling, P. C. (2000) Estimating forest habitat complexity in relation to time since fire. *Austral Ecology*, 25, 344-351.
- Coops, N. C., Wulder, M., Culvenor, D. S. and St-Onge, B. (2004) Comparison of forest attributes extracted from fine spatial resolution multi-spectral and lidar data. *Canadian Journal of Remote Sensing*, 30 (6), 855-866.
- Coops, N. C., Hilker, T., Wulder, M., St-Onge, B., Newnham, G., Siggins, A. and Trofymow, J. (2007) Estimating canopy structure of Douglas-fir forest stands from discrete-return LiDAR. *Trees - Structure and Function*, 21, 295-310.
- Culvenor, D. S. (2002) TIDA: an algorithm for the delineation of tree crowns in high spatial resolution remotely sensed imagery. *Computers and GeoSciences-UK*, 28, 33-44.
- Culvenor D.S. (2003). Extracting Individual Tree Information. In: *Remote Sensing of Forest Environments: Concepts and Case Studies* (M. A. Wulder and S. E. Franklin, eds.), pp. 255-277. Kluwer Academic Press.
- Curran, P. J. and Williamson, H. D. (1985) The accuracy of ground data used in remote-sensing investigations. *International Journal of Remote Sensing*, 6, 1637 - 1651.
- Curran, P. J. and Williamson, H. D. (1986) Sample size for ground and remotely sensed data. *Remote Sensing of Environment*, 20, 31-41.
- de Jong, J.J.M.; Klaassen, W.; Kuiper, P.J.C. (2002) Monitoring of rain water storage in forests with satellite radar., *IEEE Transactions on Geoscience and Remote Sensing*, 40 (2), 338-347.
- Dean, C., Roxburgh, S., and Mackey, B.G. (2004) Forecasting landscape-level carbon sequestration using gridded, spatially adjusted tree growth. *Forest Ecology and Management*, 194, 109-129.
- Dobson, M. C., Ulaby, F. T., Pierce, L. E., Sharik, T. L., Bergen, K. M., Kellndorfer, J., Kendra, J. R., Li, E., Lin, Y. C., Nashashibi, A., Sarabandi, K. and Siqueira, P. (1995) Estimation of forest biophysical characteristics in northern Michigan with SIR-C/X-SAR. *IEEE Transactions on Geoscience and Remote Sensing*, 33, 8877-8895.
- Donoghue, D. N. M. (2000) Remote sensing: sensors and applications. *Progress in Physical Geography*, 24, 407-414.
- Donoghue, D. N. M. and Watt, P. J. (2006) Using LiDAR to compare forest height estimates from IKONOS and Landsat ETM+ data in Sitka spruce plantation forests. *International Journal of Remote Sensing*, 27, 2161-2175.

- 
- Drake, J. B., Dubayah, R., Knox, R., Clark, D. B., and Blair, J. B. (2002) Sensitivity of large-footprint LiDAR to canopy structure and biomass in a neo-tropical rainforest, *Remote Sensing of Environment*, 81:378-392
- Department of Sustainability and Environment (DSE) Victoria, (2003). Spatial data supplied for forest fire burnt extent from layers SFRIMap02, Fire100\_1939 and LasBurnt100.
- Dungan, J. L. (2001) Scaling up and scaling down: The relevance of the support effect on remote sensing of vegetation. IN N. Tate, P. A. (Ed.) *Modelling Scale in Geographical Information Science*. Wiley and Sons. 308p.
- Durden, S. L., Zebker, H. A. and van Zyl, J. J. (1989) Modeling and observation of forest radar polarization signatures. *IEEE Transactions on Geoscience and Remote Sensing*, 27, 290-301.
- Environmental Systems Research Institute (2006) Arc/Info Online Documentation. Redlands, CA.
- Executive Steering Committee for Australian Vegetation Information (ESCAVI) (2003) *Australian Vegetation Attribute Manual*, Version 6.0. Department of Environment and Heritage, Canberra.. 144p.
- Eyre, T. J., Jermyn, D. and Kelly, A. L. (2000) Forest condition and habitat assessment in Queensland. Version 2. *Standards for Forest Assessment Technical Report 01/00*. Brisbane, Forest Ecosystem Research and Assessment - Department of Natural Resources. Brisbane, Queensland. 62p.
- Fang, H. and Liang, S. (2005) A hybrid inversion method for mapping leaf area index from MODIS data: experiments and application to broadleaf and needleleaf canopies. *Remote Sensing of Environment*, 94, 405-424.
- Fensham, R. J. and Fairfax, R. J. (2002) Aerial photography for assessing vegetation change: a review of applications and the relevance of findings for Australian vegetation history. *Australian Journal of Botany*, 50, 415-429.
- Fensham, R. J., Bray, S. G. and Fairfax, R. J. (2007) Evaluation of aerial photography for predicting trends in structural attributes of Australian woodland including comparison with ground-based monitoring data. *Journal of Environmental Management*, 83, 392-401.
- Finnish Forest Association, (2008) <http://www.forest.fi/smyforest/foresteng.nsf> (accessed 10-10-08)
- Fisher, J. I., Mustard, J. F. and Vadeboncoeur, M. A. (2006) Green leaf phenology at Landsat resolution: Scaling from the field to the satellite. *Remote Sensing of Environment*, 100, 265-279.
- Fisher, W. D. (1958) On Grouping for Maximum Homogeneity. *Journal of the American Statistical Association* 53, 789-798.
- Florence, R. G. (1996) *Ecology and Silviculture of eucalypt forests*, CSIRO Australia. 413p.

- 
- Food and Agriculture Organisation (FAO) (1998) Forest Resources Assessment 2000: Terms and definitions. *FRA Working Paper 1*. Rome, Italy.
- Forest Ecosystem Research and Assessment (FERA) 1998, Old growth forest in South East Queensland. *Forest Ecosystem Research and Assessment Technical Report 1998/01*, DNRQ980145, Department of Natural Resources, Brisbane.
- Forman, R.T.T. (1995) *Land Mosaics: The Ecology of Landscapes and Regions*. Cambridge University Press, Cambridge, UK. 635p.
- Fotheringham, A. S. (1989) Scale-independent spatial analysis. IN Goodchild, M. and Gopal, S. (Eds.) *Accuracy of Spatial Databases*. Taylor and Francis. 290p.
- Fotheringham, A. S., Brunson, C. and Charlton, M. (2000) *Quantitative Geography: Perspectives on spatial data analysis*, London, Sage publications. 270p.
- Frazer, G. W., Canham, C. D. and Lertzman, K. P. (1999) Gap Light Analyzer (GLA), Version 2.0: Imaging Software to Extract Canopy Structure and Gap Light Transmission Indices from True-color Fisheye Photographs, *Users Manual and Program Documentation*. Simon Fraser University / Institute of Ecosystem Studies, Burnaby, BC; Millbrook, NY. 36p.
- Frazer, G. W., Fournier, R. A., Trofymow, J. A. and Hall, R. J. (2001) A comparison of digital and film fisheye photography for analysis of forest canopy structure and gap light transmission. *Agricultural and Forest Meteorology*, 109, 249-263.
- Furby, S. L. (2002) Land cover change: specification for remote sensing analysis. *NCAS Technical Report 9*, Canberra, Australian Greenhouse Office. 401p.
- Gao, F., Masek, J., Schwaller, M. and Hall, F. (2006) On the blending of the Landsat and MODIS surface reflectance: predicting daily Landsat surface reflectance. *IEEE Transactions on Geoscience and Remote Sensing*, 44, 2207-2218.
- Gastellu-Etchegorry, J. P., Demarez, V., Pinel, V. and Zagolski, V. (1996) Modeling radiative transfer in heterogeneous 3D vegetation. *Remote Sensing Environment*, 58, 131-156.
- Gaveau, D. L. A. and Hill, R. A. (2003) Quantifying canopy height underestimation by laser pulse penetration in small-footprint airborne laser scanning data. *Canadian Journal of Remote Sensing*, 29, 650-657.
- Gehlke, C. E. and Biehl, K. (1934) Certain Effects of Grouping Upon the Size of the Correlation Coefficient in Census Tract Material. *Journal of the American Statistical Association Supplement*, 29, 169-170.
- Gobakken, T. and Naesset, E. (2005) Weibull and percentile models for LiDAR-based estimation of basal area distribution. *Scandinavian Journal of Forest Research*, 20, 490-502.
- Goodwin, N. R., Coops, N. C. and Culvenor, D. S. (2006) Assessment of forest structure with airborne LiDAR and the effects of platform altitude. *Remote Sensing of Environment*, 103, 140-152.

- 
- Goodwin, N. R., Coops, N. C. and Culvenor, D. S. (2007) Development of a simulation model to predict LiDAR interception in forested environments. *Remote Sensing of Environment*, 111, 481-492.
- Gougeon, F. A. and Leckie, D. G. (2006) The Individual Tree Crown Approach Applied to Ikonos Images of a Coniferous Plantation Area. *Photogrammetric Engineering and Remote Sensing*, 72, 1287-1297.
- Haining, R. (1990) *Spatial data analysis in the social and environmental sciences*, Cambridge, Cambridge University Press. 409p.
- Hall, S. A., Burke, I. C., Box, D. O., Kaufmann, M. R. and Stoker, J. M. (2005) Estimating stand structure using discrete-return LiDAR: an example from low density, fire prone ponderosa pine forests. *Forest Ecology and Management*, 208, 189-209.
- Hamilton, F. and Brack, C. L. (1999) Stand volume estimates from modelling inventory data. *Australian Forestry*, 62(4), 360-367
- Hanssen, K. H. and Solberg, S. (2007) Assessment of defoliation during a pine sawfly outbreak: Calibration of airborne laser scanning data with hemispherical photography. *Forest Ecology and Management*, 250, 9-16.
- Harding, D. J., Lefsky, M. A., Parker, G. G. and Blair, J. B. (2001) Laser altimeter canopy height profiles - Methods and validation for closed-canopy, broadleaf forests. *Remote Sensing of Environment*, 76, 283-297.
- Harding, D. J. and Carabajal, C. C. (2005) ICESat waveform measurements of within-footprint topographic relief and vegetation vertical structure. *Geophysical Research Letters*, 32, L21S10.
- Hay, G. J., Niernann, K. O. and Goodenough, D. G. (1997) Spatial thresholds, image-objects, and upscaling: A multiscale evaluation. *Remote Sensing of Environment*, 62, 1-19.
- Hay, G. J., Marceau, D. J., Dubé, P. and Bouchard, A. (2001) A Multiscale Framework for Landscape Analysis: Object-Specific Analysis and Upscaling. *Landscape Ecology*, 16, 471-490.
- Hay, G. J., Castilla, G., Wulder, M. and Ruiz, J. R. (2005) An automated object-based approach for the multiscale image segmentation of forest scenes. *International Journal of Applied Earth Observation*, 7, 339-359.
- Henry, B. K., Danaher, T., McKeon, G. M. and Burrows, W. H. (2002) A review of the potential role of greenhouse gas abatement in native vegetation management in Queensland's rangelands. *Rangeland Journal* 24, 112-132.
- Hill, M. J., Senarath, U., Lee, A. C., Zeppel, M., Nightingale, J. M., Williams, R. J. and McVicar, T. R. (2006) Assessment of the MODIS LAI product for Australian ecosystems. *Remote Sensing of Environment*, 101, 495-518.

- Hill, R. A. and Thomson, A. G. (2005) Mapping woodland species composition and structure using airborne spectral and LiDAR data. *International Journal of Remote Sensing*, 26, 3763-3779.
- Hnatiuk, R., Tickle, P., Wood, M. S. and Howell, C. (2003) Defining Australian forests. *Australian Forestry*, 66, 176-183.
- Hodgson, M. E. and Bresnahan, P. (2004) Accuracy of airborne LiDAR-derived elevation: empirical assessment and error budget. *Photogrammetric Engineering and Remote Sensing*, 70, 331-339.
- Holmgren, J., Nilsson, M. and Olsson, H. (2003) Estimation of tree height and stem volume on plots-using airborne laser scanning. *Forest Science*, 49, 419-428.
- Holmgren, J. and Jonsson, T. (2004) Large scale airborne laser scanning of forest resources in Sweden. *International Archive of Photogrammetry, Remote Sensing and Spatial Information Sciences*, 36, 157-160.
- Holmgren, J. and Persson, A. (2004) Identifying species of individual trees using airborne laser scanner. *Remote Sensing of Environment*, 90, 415-423.
- Hopkinson, C. (2007) The influence of flying altitude and beam divergence on canopy penetration and laser pulse return distribution characteristics. *Canadian Journal of Remote Sensing*, 33, 312-324.
- Hudak, A. T., Lefsky, M. A., Cohen, W. B., Berterretche M. (2002) Integration of LiDAR and Landsat ETM+ data for estimating and mapping forest canopy height. *Remote Sensing of Environment*, 82, 397-416
- Hyde, P., Dubayah, R., Walker, W., Blair, J. B., Hofton, M. and Hunsaker, C. (2006) Mapping forest structure for wildlife habitat analysis using multi-sensor (LiDAR, SAR/InSAR, ETM+, Quickbird) synergy. *Remote Sensing of Environment*, 102, 63-73.
- Hyypä, J., Hyypä, H., Inkinen, M., Engdahl, M., Linko, S. and Zhu, Y.-H. (2000) Accuracy comparison of various remote sensing data sources in the retrieval of forest stand attributes. *Forest Ecology and Management*, 128, 109-120.
- Hyypä, J., Kelle, O., Lehtikoinen, M. and Inkinen, M. (2001) A segmentation-based method to retrieve stem volume estimates from 3-D tree height models produced by laser scanners. *IEEE Transactions on Geoscience and Remote Sensing*, 39, 969-975.
- Imhoff, M. L. (1992) Theoretical analysis of the effect of forest structure on synthetic aperture radar backscatter and the remote sensing of biomass. *IEEE Transactions on Geoscience and Remote Sensing*, 33, 341-352.
- Ishii, H. T., Tanabe, S.-i. and Hiura, T. (2004) Exploring the Relationships Among Canopy Structure, Stand Productivity, and Biodiversity of Temperate Forest Ecosystems. *Forest Science*, 50, 342-355.
- Jack, S. B. and Long, J. N. (1991) Analysis of stand density effects on canopy structure: a conceptual approach. *Trees - Structure and Function*, 5, 44-49.

- Jacobs, M. R. (1955). Growth habits of eucalypts. Canberra: Forestry and Timber Bureau.
- Jelinski, D. E. and Wu, J. (1996) The modifiable areal unit problem and implications for landscape ecology. *Landscape Ecology*, 11, 129-140.
- Jenks, G. F. (1977) Optimal Data Classification for Choropleth Maps. *Occasional Paper No.2*. Department of Geography, University of Kansas.
- Jensen, J. L. R., Humes, K. S., Conner, T., Williams, C. J. and DeGroot, J. (2006) Estimation of biophysical characteristics for highly variable mixed-conifer stands using small-footprint lidar. *Canadian Journal of Forest Research*, 36, 1129-1138.
- Jenson, S. K. and J. O. Domingue, (1988), Extracting Topographic Structure from Digital Elevation Data for Geographic Information System Analysis, *Photogrammetric Engineering and Remote Sensing*, 54 (11): 1593-1600.
- Jerez, M., Dean, T. J., Cao, Q. V. and Roberts, S. D. (2005) Describing Leaf Area Distribution in Loblolly Pine Trees with Johnson's SB Function. *Forest Science*, 51, 93-101 (9).
- Jones, K. L. (2000) Aerial photography interpretation for the Injune Remote Sensing Sampling Strategy. *Forest Ecosystem Research and Assessment Technical Report, vol. 00129*. Brisbane, Queensland Department of Natural Resources. 15p.
- Ju, J., Gopal, S. and Kolaczyk, E. D. (2005) On the choice of spatial and categorical scale in remote sensing land cover classification. *Remote Sensing of Environment*, 96, 62-77.
- Jupp, D. L. B., Strahler, A. H. and Woodcock, C. E. (1989) Autocorrelation and regularization in digital images. II. Simple image models. *IEEE Transactions on Geoscience and Remote Sensing*, 27, 247-258.
- Jupp, D. L. B. and Walker, J. (1996) Detecting structural and growth changes in woodlands and forests: The challenge for remote sensing and the role of geo-optical modelling. IN Gholz, H. L., Nakane, K. and Shimoda, H. (Eds.) *The use of remote sensing in the modeling of forest productivity*. Kluwer Academic Publishers, Dordrecht, The Netherlands. p75-108.
- Kao, D. L., Kramer, M. G., Love, A. L., Dungan, J. L. and Pang, A. T. (2005) Visualizing Distributions from Multi-Return Lidar Data to Understand Forest Structure. *The Cartographic Journal*, 42, 35-47 (13).
- Koestler, A. (1967) *The Ghost in the Machine*. Random House, New York, USA. 384p.
- Koetz, B., Sun, G., Morsdorf, F., Ranson, K. J., Kneubuhler, M., Itten, K. and Allgower, B. (2007) Fusion of imaging spectrometer and LIDAR data over combined radiative transfer models for forest canopy characterization. *Remote Sensing of Environment*, 106, 449-459.
- Koch, B., Heyder, U. and Weinacker, H. (2006) Detection of Individual Tree Crowns in Airborne Lidar Data. *Photogrammetric Engineering and Remote Sensing*, 72, 357-364.

- Koukoulas, S. and Blackburn, G. A. (2005) Mapping individual tree location, height and species in broadleaved deciduous forest using airborne LIDAR and multi-spectral remotely sensed data. *International Journal of Remote Sensing*, 26, 431-455.
- Leckie, D. G., Gougeon, F. A., Hill, D., Quinn, R., Armstrong, L. and Shreenan, R. (2003) Combined high-density LiDAR and multispectral imagery for individual tree crown analysis. *Canadian Journal of Remote Sensing*, 29, 633-649.
- Leckie, D.G., Gougeon, F. A., Tinis, S., Nelson, T., Burnet, C. N., and Paradine, D. (2005) Automated tree recognition in old growth conifer stands with high resolution digital imagery. *Remote Sensing of Environment*, 94, 311-326.
- Lee, A., Chikumbo, O., Davey, S. and Tickle, P. K. (2001) Enhanced visualisation capability for forest management optimization results. IN Ghassemi, F., Post, D., Sivapalan, M. and Vertessy, R. (Eds.) *Proceedings International Congress on Modelling and Simulation*. Canberra, Australia, December.
- Lee, A. C., Norman, P., Wood, M. and Davey, S. (2003) Utilising integrated sampling strategies for regional and continental forest monitoring through criteria and indicators. IN Mason, E. and Perley, C. (Eds.) *Proceedings of Joint Australia and New Zealand Institute of Forestry Conference*, Queenstown, New Zealand, New Zealand Institute of Forestry.
- Lee, A. C., Lucas, R. M. and Brack, C. L. (2004) Quantifying vertical forest stand structure using small footprint LiDAR to assess potential stand dynamics. *International Archive of Photogrammetry, Remote Sensing and Spatial Information Sciences*, 36, 213-217.
- Lee, A. C., Scarth, P. and Gerrand, A. (2006) ICESat and airborne LiDAR calibration pilot project. BRS internal technical report, Bureau of Rural Sciences, Canberra, Australia. 49p.
- Lee, A. C. and Lucas, R. M. (2007) A LiDAR-derived Canopy Density Model for Tree Stem and Crown Mapping in Australian Forests. *Remote Sensing of Environment*, 111, 493-518.
- Lefsky, M. A., Harding, D. J., Cohen, W. B., Parker, G. and Shugart, H. H. (1999) Surface LiDAR remote sensing of basal area and biomass in deciduous forests of eastern Maryland, USA. *Remote Sensing of Environment*, 67, 83-98.
- Lefsky, M. A., Harding, D. J., Keller, M., Cohen, W. B., Carabajal, C. C., Del Bom Espirito-Santo, F., Hunter, M. O., de Oliveira, R. J. and de Camargo, P. B. (2005a) Estimates of forest canopy height and aboveground biomass using ICESat. *Geophysical Research Letters*, 32, L22S02.
- Lefsky, M. A., Turner, D. P., Guzy, M. and Cohen, W. B. (2005b) Combining LiDAR estimates of aboveground biomass and Landsat estimates of stand age for spatially extensive validation of modeled forest productivity. *Remote Sensing of Environment*, 95, 549-558.

- Le Toan, T., Quegan, Q., Woodward, I., Lomas, M., Delbart, N., and Picard G. (2004), Relating Radar Remote Sensing of Biomass To Modelling Of Forest Carbon Budgets. *Climatic Change*, 67(2), 379-402.
- Li, X. and Strahler, A. H. (1985) Geometric-optical modeling of a conifer forest canopy. *IEEE Transactions on Geoscience and Remote Sensing*, 23, 705-721.
- Li, X., Strahler, A. H. and Woodcock, C. E. (1995) A hybrid geometric optical-radiative transfer approach for modeling albedo and directional reflectance of discontinuous canopies. *IEEE Transactions on Geoscience and Remote Sensing*, 33, 466-480.
- Liang, P., Moghaddam, M., Pierce, L. E. and Lucas, R. M. (2005) Radar Backscattering Model for Multilayer Mixed-Species Forests. *IEEE Transactions on Geoscience and Remote Sensing*, 43, 2612-2626.
- Lim, K., Treitz, P., Baldwin, K., Morrison, I. and Green, J. (2003a) Lidar remote sensing of biophysical properties of tolerant northern hardwood forests. *Canadian Journal of Remote Sensing*, 29, 658-678.
- Lim K., Treitz P., Wulder M., St-Onge B., Flood M. (2003b) LiDAR remote sensing of forest structure. *Progress in Physical Geography*, 27(1) 88-106.
- Lim, K. and Treitz, P. (2004) Estimation of above ground forest biomass from airborne discrete return laser scanner data using canopy-based quantile estimators. *Scandinavian Journal of Forest Research*, 19, 558-570.
- Lovell, J. L., Jupp, D. L. B., Culvenor, D. S. and Coops, N. C. (2003) Using airborne and ground-based ranging LiDAR to measure canopy structure in Australian forests. *Canadian Journal of Remote Sensing*, 29, 607-622.
- Lovell, J. L., Jupp, D. L. B., Newnham, G. J., Coops, N. C. and Culvenor, D. S. (2005) Simulation study for finding optimal lidar acquisition parameters for forest height retrieval. *Forest Ecology and Management*, 214, 398-412.
- Lu, H., Raupach, M.R., McVicar, T.R. and Barrett, D.J. (2003) Decomposition of vegetation cover into woody and herbaceous components using AVHRR NDVI time series. *Remote Sensing of Environment*, 86, 1-18.
- Lucas, R.M., Milne, A.K., Cronin, N., Witte, C., Denham, R (2000) The Potential of Synthetic Aperture Radar (SAR) Data for Quantifying the Above Ground Biomass of Australia's Woodlands. *Rangeland Journal*, 22, 124-140.
- Lucas, R. M., Moghaddam, M. and Cronin, N. (2004) Microwave scattering from mixed species woodlands, central Queensland, Australia. *IEEE Transactions on Geoscience and Remote Sensing*, 42, 2142-2159
- Lucas, R. M., Cronin, N., Lee, A. C., Moghaddam, M., Witte, C. and Tickle, P. K. (2006a) Empirical relationships between AIRSAR backscatter and LiDAR-derived forest biomass, Queensland, Australia. *Remote Sensing of Environment*, 100, 407-425.



- Lucas, R. M., Cronin, N., Moghaddam, M., Lee, A. C., Armston, J., Bunting, P. J. and Witte, C. (2006b) Integration of radar and Landsat-derived foliage projected cover for woody regrowth mapping, Queensland, Australia. *Remote Sensing of Environment*, 100, 388-406.
- Lucas, R. M., Lee, A. C. and Williams, M. L. (2006c) Enhancing SAR simulations using LiDAR for understanding the relations between forest structure and SAR imagery. *IEEE Transactions on Geoscience and Remote Sensing*, 44, 2736-2754.
- Lucas, R. M., Accad, A., Randall, L. and Bunting, P. J. (2007) Assessing Human Impacts on Australian Forests through Integration of Airborne/Spaceborne Remote Sensing Data. IN Laforzezza R., C. J., Sanesi G. and Crow T. (Ed.) *Patterns and Processes in Forest landscapes: Multiple Use and Sustainable management - Part III Landscape-scale indicators and projection models*. 426 p. Springer publications.
- Lucas, R.M., Bunting, P.J., Paterson, M. and Chisholm, L. (2008) Classification of Australian forest communities using aerial photography, CASI and HyMap data. *Remote Sensing of Environment*. 112, 2088-2103.
- Lucas, R. M., Lee, A. C., and Bunting, P.J. (2008) Retrieving forest biomass through integration of CASI and LiDAR data: *International Journal of Remote Sensing*, 29 (5), 1553-1577.
- Lund, H. G. (1998) A comparison of multipurpose resource inventories throughout the world. *EFI Working Paper 14*. Torikatu, Finland, European Forestry Institute. 46p.
- Lund, H. G. (2002) When Is a Forest Not a Forest? *Journal of Forestry*, 100, 21-28.
- Macfarlane, C., Hoffman, M., Eamus, D., Kerp, N., Higginson, S., McMurtrie, R. and Adams, M. (2007) Estimation of leaf area index in eucalypt forest using digital photography. *Agricultural and Forest Meteorology*, 143, 176-188.
- Magnussen, S. and Boudewyn, P. (1998) Derivations of stand heights from airborne laser scanner data with canopy-based quantile estimators. *Canadian Journal of Forest Research*, 28, 1016-1031.
- Maltamo, M., Eerikainen, K., Pitkanen, J., Hyyppä, J. and Vehmas, M. (2004) Estimation of timber volume and stem density based on scanning laser altimetry and expected tree size distribution functions. *Remote Sensing of Environment*, 90, 319-330.
- Marceau, D. J. (1999) The scale issue in social and natural sciences. *Canadian Journal of Remote Sensing*, 25, 347-356.
- McCloy, K. R. (2006) *Resource Management Information systems: remote sensing, GIS and modeling*, Boca Raton, Florida, CRC Press, Taylor and Francis Group. 616p.
- McCombs, J. W., Roberts, S. D. and Evans, D. L. (2003) Influence of fusing lidar and multispectral imagery on remotely sensed estimates of stand density and mean tree height in a managed loblolly pine plantation. *Forest Science*, 49, 457-466.

- 
- McDonald, R.C., Isbell, J.G., Speight, J.G., Walker, J. and Hopkins, M.S. (1998) *Australian Soil and Land Survey Field Handbook*. Second edition. Commonwealth Dept of Primary Industries and Energy and CSIRO. 190 p.
- McRoberts, R. E. and Tomppo, E. O. (2007) Remote sensing support for national forest inventories. *Remote Sensing of Environment*, 110, 412-419.
- Means, J. E., Acker, S. A., Harding, D. J., Blair, J. B., Lefsky, M. A., Cohen, W. B., Harmon, M. E. and McKee, W. A. (1999) Use of large-footprint scanning airborne lidar to estimate forest stand characteristics in the Western Cascades of Oregon. *Remote Sensing of Environment*, 67, 298-308.
- Means, J. E., Acker, S. A., Fitt, B. J., Renslow, M., Emerson, L. and Hendrix, C. J. (2000) Predicting forest stand characteristics with airborne scanning LiDAR. *Photogrammetric Engineering and Remote Sensing*, 66, 1367-1371.
- Mitchell, T. L. (1846) *Journal of an expedition into the interior of tropical Australia*. Adelaide, Australia University of Adelaide Library. 269p.
- Miura, T., Huete, A. and Yoshioka, H. (2006) An empirical investigation of cross-sensor relationships of NDVI and red/near-infrared reflectance using EO-1 Hyperion data. *Remote Sensing of Environment*, 100, 223-236.
- Moffiet, T., Mengersen, K., Witte, C., King, R. and Denham, R. (2005) Airborne laser scanning: Exploratory data analysis indicates potential variables for classification of individual trees or forest stands according to species. *ISPRS Journal of Photogrammetry and Remote Sensing*, 59, 289-309.
- Morsdorf, F., Meier, E., Kotz, B., Itten, K. I., Dobbertin, M. and Allgower, B. (2004) LIDAR-based geometric reconstruction of boreal type forest stands at single tree level for forest and wildland fire management. *Remote Sensing of Environment*, 92, 353-362.
- Næsset, E. (2002) Predicting forest stand characteristics with airborne scanning laser using a practical two-stage procedure and field data. *Remote Sensing of Environment* 80 88-99
- Naeset, E. and Okland, T. (2002) Estimating tree height and tree crown properties using airborne scanning laser in a boreal nature reserve. *Remote Sensing of Environment*, 79, 105-115.
- National Aeronautics and Space Administration (NASA) (2008) Landsat project homepage. <http://landsat.usgs.gov/index.php>. (Accessed January 2008).
- National Forest Inventory (1998) *Australia's State of the Forests Report, 1998*. Canberra, Australia. Bureau of Rural Sciences. 190p.
- National Forest Inventory (2003) *Australia's State of the Forests Report, 2003*. Canberra, Australia. Bureau of Rural Sciences. 382p.
- National Land and Water Resources Audit (NLWRA) (2001) *Australian native vegetation assessment*. Canberra, Australia. Department of Environment and Heritage. 332p.
- Natural Resources Canada, (2007) <http://cfs.nrcan.gc.ca/subsite/eosd> (accessed 10-10-2008).

- Nelson, R. (1997) Modelling forest canopy heights: the effects of canopy shape. *Remote Sensing of Environment* 60, 327-334.
- Nelson, R., Valenti, M. A., Short, A. and Keller, C. (2003) A multiple resource inventory of Delaware using airborne laser data. *Bioscience*, 53, 981-992.
- Nelson, R., Short, A., and Valenti, M. (2004) Measuring biomass and carbon in Delaware using an airborne profiling LIDAR. *Scandinavian Journal of Forest Research*, 19, 500-511.
- Norman, P., Wood, M. and Lee, A. C. (2003) *A Continental Forest Monitoring Framework for Australia - Background, concept and rationale*. Canberra, Australia. National Forest Inventory, Bureau of Rural Sciences. 40p.
- O'Neill, R. V., DeAngelis, D. L., Waide, J. B., and Allen, T. F. H. (1986). *A Hierarchical Concept of Ecosystems*. Princeton University Press, Princeton, USA. 253p
- Openshaw, S. (1984) *The modifiable areal unit problem*, Norwich, UK. Geobooks. 41p.
- Parker, G. G. and Russ, M. E. (2004) The canopy surface and stand development: assessing forest canopy structure and complexity with near-surface altimetry. *Forest Ecology and Management*, 189, 307-315.
- Patenaude, G., Milne, R. and Dawson, T. P. (2005) Synthesis of remote sensing approaches for forest carbon estimation: reporting to the Kyoto Protocol. *Environmental Science and Policy*, 8, 161-178.
- Peel, D. R., Pitman, A. J., Hughes, L. A., Narisma, G. T. and Pielke, S. R. A. (2005) The impact of realistic biophysical parameters for eucalypts on the simulation of the January climate of Australia. *Environmental Modelling and Software*, 20, 595-612.
- Penridge, L. K. and Walker, J. (1988) The crown-gap ratio (C) and crown cover: Derivation and simulation study. *Austral Ecology*, 13, 109-120.
- Persson, A., Holmgren, J. and Soderman, U. (2002) Detecting and measuring individual trees using an airborne laser scanner. *Photogrammetric Engineering and Remote Sensing*, 68, 925-932.
- Popescu, S. C., Wynne, R. H. and Nelson, R. F. (2003) Measuring individual tree crown diameter with lidar and assessing its influence on estimating forest volume and biomass. *Canadian Journal of Remote Sensing*, 29, 564-577.
- Popescu, S. C. and Wynne, R. H. (2004) Seeing the trees in the forest: using LiDAR and multispectral data fusion with local filtering and variable window size for estimating tree height. *Photogrammetric Engineering and Remote Sensing*, 70, 589-604.
- Popescu, S. C. and Zhao, K. (2007) A voxel-based lidar method for estimating crown base height for deciduous and pine trees. *Remote Sensing of Environment*, (In Press) (doi:10.1016/j.rse.2007.06.011).
- Pouliot, D. A., King, D. J., Bell, F. W. and Pitt, D. G. (2002) Automated tree crown detection and delineation in high-resolution digital camera imagery of coniferous forest regeneration. *Remote Sensing of Environment*, 82, 322-334.

- Pouliot, D. A., King, D. J. and Pitt, D. G. (2005) Development and evaluation of an automated tree detection–delineation algorithm for monitoring regenerating coniferous forests. *Canadian Journal of Forest Research*, 35, 2332-2345.
- Queensland Department of Natural Resources and Mines (QDNRM) (2003) *The Statewide Landcover and Trees Study (SLATS) - 2003 Report*. Brisbane, Australia. Queensland government. 92p.
- Queensland Department of Natural Resources and Mines (2005) *Land cover change in Queensland 2001-2003, incorporating 2001-2002 and 2002-2003 change periods. A Statewide Landcover and Trees Study (SLAT)*. Brisbane, Australia. Queensland government. 93p.
- Ranson, K. J., Sun, G., Kovacs, K. and Kharuk, V. I. (2004) Use of ICESat GLAS data for forest disturbance studies in central Siberia. *Proceedings International Geoscience And Remote Sensing Symposium (IGARSS)*. Anchorage, Alaska, USA. 20-24 September.
- Research Working Group 2 (1999) Code of Forest Mensuration Practise: A guide to good tree measurement practise in Australia and New Zealand. G.B. Wood, B.J. Turner, and C.L. Brack (eds). <http://sres.anu.edu.au/associated/mensuration/rwg2/code/3-4-2.htm> (Accessed January 2008).
- Resource Assessment Commission (RAC)(1992) *Forest and Timber Inquiry Final Report*, Canberra, Commonwealth of Australia. 79p.
- Reutebuch, S. E., Andersen, H.-E. and McGaughey, R. J. (2005) Light Detection and Ranging (LIDAR): An Emerging Tool for Multiple Resource Inventory. *Journal of Forestry*, 103, 286-292.
- Riano, D., Meier, E., Allgower, B., Chuvieco, E. and Ustin, S. L. (2003) Modeling airborne laser scanning data for the spatial generation of critical forest parameters in fire behavior modeling. *Remote Sensing of Environment*, 86, 177-186.
- Riano, D., Valladares, F., Condes, S. and Chuvieco, E. (2004) Estimation of leaf area index and covered ground from airborne laser scanner (LiDAR) in two contrasting forests. *Agricultural and Forest Meteorology*, 124, 269-275.
- Richards, G. P. (ed.) (2002) Biomass estimation: Approaches for assessment of stocks and stock change. *National Carbon Accounting System Technical Report No. 27*. Canberra, Australia. Australian Greenhouse Office. 140p.
- Richards, G. P. and Brack, C. L. (2004) A continental biomass stock and stock change estimation approach for Australia. *Australian Forestry*, 67, 284-288.
- Richards, G. P. and Evans, D. M. W. (2004) Development of a carbon accounting model (FullCAM Vers. 1.0) for the Australian continent. *Australian Forestry*, 67, 284-288
- Richards, T., Gallego, J. and Achard, F. (2000) Sampling for forest cover change assessment at the pan-tropical scale. *International Journal of Remote Sensing*, 21, 1473-1490.

- 
- Robinson, W. S. (1950) Ecological correlations and the behaviour of individuals. *American Sociological Review*, 15, 351-357.
- Rombouts, J. (2007) Application of airborne LiDAR in forestry in North America and Scandinavia. 2006 Gottstein Fellowship Report. J.W. Gottstein Memorial Trust Fund, Clayton South, Victoria, Australia. 45p.
- Rowell, E., Seielstad, C., Vierling, L., Queen, L. and Shepperd, W. (2006) Using Laser Altimetry-based Segmentation to Refine Automated Tree Identification in Managed Forests of the Black Hills, South Dakota. *Photogrammetric Engineering and Remote Sensing*, 72, 1379-1388.
- Scarth, P. and Phinn, S. R. (2000) Determining forest structural attributes using an inverted geometric-optical model in mixed eucalypt forests, Southeast Queensland, Australia. *Remote Sensing of Environment*, 71, 141-157.
- Scarth, P., Phinn, S. R. and McAlpine, C. (2001) Integrating high and moderate spatial resolution image data to estimate forest age structure. *Canadian Journal of Remote Sensing*, 27, 129-142.
- Schreuder, H. T., Gregoire, T. G. and Wood, G. B. (1993) *Sampling methods for multi-resource forest inventory*, New York, USA, John Wiley and Sons. 464p.
- Scott, C. T. (1998) Sampling methods for estimating change in forest resources. *Ecological Applications*, 8, 228-233.
- Simon, H. A. (1962) The architecture of complexity. *Proceedings of the American Philosophical Society*, 106, 467-482.
- Simon, H. A. (1973) The organization of complex systems. In H. H. Pattee (ed.), *Hierarchy Theory: The Challenge of Complex Systems*, pp. 1-27. George Braziller, New York, USA.
- Skidmore, A. K. and Turner, B. J. (1987) Remotely sensed digital data in forestry: a review. *Australian Forestry*, 50, 40-53.
- Slocum, T. A. (1999) *Thematic cartography and visualization*. New Jersey, USA, Prentice-Hall, Inc. 293p.
- Smith, J. A. and Goltz, S. M. (1994) Updated thermal model using simplified short-wave radiosity calculations. *Remote Sensing of Environment*, 47, 167-175.
- Smith, W. B. (2002) Forest inventory and analysis: A national inventory and monitoring program. *Environmental Pollution*, 116, S233-S242.
- Solberg, S., Naesset, E. and Bollandsas, O. M. (2006) Single Tree Segmentation Using Airborne Laser Scanner Data in a Structurally Heterogeneous Spruce Forest. *Photogrammetric Engineering and Remote Sensing*, 72, 1369 - 1378.
- Specht, R. L. (1970) Vegetation. In Leeper, G. W. (Ed.) *The Australian Environment*. Fourth edition. Melbourne, Australia. CSIRO-Melbourne University Press. pp 44-67.

- 
- Specht, R. L. and Specht, A. (1999) *Australian Plant Communities: Dynamics of structure, growth and biodiversity*, Melbourne, Oxford University Press. 491p.
- Strahler, A. H., Woodcock, C. E. and Smith, J. A. (1986) On the nature of models in remote sensing. *Remote Sensing of Environment*, 20, 121-139.
- Stone, M.G. (1998) Forest-type mapping by photo-interpretation: A multi-purpose base for Tasmania's forest management. *Tasforests* 10, 15-32.
- Stone, C., Coops, N. C. and Culvenor, D. S. (2000) Conceptual development of a eucalypt canopy condition index using high resolution spatial and spectral remote sensing imagery. *Journal of Sustainable Forestry*, 11, 23-45.
- St-Onge, B., Jumelet, J., Cobello, M. and Véga, C. (2004) Measuring individual tree height using a combination of stereophotogrammetry and lidar. *Canadian Journal of Forest Research*, 34, 2122-2130.
- Suarez, J. C., Ontiveros, C., Smith, S. and Snape, S. (2005) Use of airborne LiDAR and aerial photography in the estimation of individual tree heights in forestry. *Computers and Geosciences*, 31, 253-262.
- Sun, G., Ranson, K. J. and Kharuk, V. I. (2002) Radiometric slope correction for forest biomass estimation from SAR data in the Western Sayani Mountains, Siberia. *Remote Sensing of Environment*, 79, 279-287.
- Sun, G., Ranson, K. J., Kimes, D. S., Blair, J. B. and Kovacs, K. (2008) Forest vertical structure from GLAS: An evaluation using LVIS and SRTM data. *Remote Sensing of Environment*, 112, 107-117.
- Thackway, R. and Cresswell, I. D. (1995) *An Interim Biogeographic Regionalisation for Australia: a framework for establishing the national system of reserves, Version 4.0* Canberra, Australia. Australian Nature Conservation Agency.
- Thackway, R., Lee, A. C., Donohue, R., Keenan, R. J. and Wood, M. (2007) Vegetation information for improved natural resource management in Australia. *Landscape and Urban Planning*, 79, 127-136.
- Thomas, V., Treitz, P., McCaughey, J. H. and Morrison, I. (2006) Mapping stand-level forest biophysical variables for a mixedwood boreal forest using lidar: an examination of scanning density. *Canadian Journal of Forest Research*, 36, 34-47.
- Thompson, S. K. (2002) *Sampling*, New York, Wiley. 367p.
- Tickle, P. K., Lee, A. C., Lucas, R. M., Austin, J. and Witte, C. (2006) Quantifying Australian forest floristics and structure using small footprint LiDAR and large scale aerial photography. *Forest Ecology and Management*, 223, 379-394.
- Tobler, W.R. (1970) A computer movie simulating urban growth in the Detroit region. *Economic Geography*, 46, 234-240.

- Todd, K. W., Csillag, F. and Atkinson, P. M. (2003) Three-dimensional mapping of light transmittance and foliage distribution using LiDAR. *Canadian Journal of Remote Sensing*, 29, 544–555.
- Tormä, M., (2000). Estimation of tree species proportions of forest stands using laser scanning. *International Archives of Photogrammetry and Remote Sensing ISPRS Congress Symposium July 16–23, Amsterdam*, pp. 1524– 1531. Volume XXXIII.
- Townend, J. (2002) *Practical Statistics for Environmental and Biological Scientists*. John Wiley and Sons, Ltd. Chichester, UK. 286p.
- Turner, D. P., Ollinger, S. V. and Kimball, J. S. (2004) Integrating Remote Sensing and Ecosystem Process Models for Landscape- to Regional-Scale Analysis of the Carbon Cycle. *BioScience*, 54, 573-584.
- Turner, M.G. and R. H. Gardner (eds.). (1991) *Quantitative Methods in Landscape Ecology. the analysis and interpretation of landscape heterogeneity*. Springer-Verlag, New York, NY, USA. 536p.
- Van Genderen, J. L., Lock, B. F. and Vass, P. A. (1978) Remote Sensing: Statistical Testing of Thematic Map Accuracy. *Remote Sensing of Environment*, 7, 3-14.
- Victorian Department of Natural Resources and Environment (VicDNRE) (2002) Quick Reference Guide to SFRImap Data. Melbourne, Australia. Victorian Department of Natural Resources and Environment.
- Visvalingam, M. (1991) Areal Units and the Linking of Data: some conceptual issues. IN Worrall, L. (Ed.) *Spatial Analysis and Spatial Policy Using Geographic Information Systems*. London, Belhaven Press, pp12-37.
- Walker, J., Jupp, D. L. B., Penridge, L. and Tian, G. (1986) Interpretation of vegetation structure in Landsat MSS Imagery: A case study in disturbed semi-arid eucalypt woodlands. Part 1. Field Data Analysis. *Journal of Environmental Management*, 23, 19-33.
- Walker, J., Penridge, L., (1987) FOL-PROF: A fortran-77 package for the generation of foliage profiles. *Part 1 User Manual. Technical Memorandum 87/9*. Canberra, Australia. CSIRO. 27p.
- Walker, J., Crapper, P. and Penridge, L. (1988) The crown-gap ratio (C) and crown cover: The field study. *Australian Journal of Ecology* 13, 101-108.
- Walker, J., Bullen, F., and Williams, B.G. (1993) Eco-hydrological changes in the Murray-Darling Basin. I. The number of trees cleared over two centuries. *Journal of Applied Ecology*, 30, 265-273
- Walter, J.-M. N. and Torquebiau, E. F. (2000) The computation of forest leaf area index on slope using fish-eye sensors. *Comptes Rendus de l'Academie des Sciences - Series III - Sciences de la Vie*, 323, 801-813.

- 
- Walter, J.-M. N., Fournier, R. A., Soudani, K. and Meyer, E. (2003) Integrating clumping effects in forest canopy structure: an assessment through hemispherical photographs. *Canadian Journal of Remote Sensing*, 29 (3), 388-410.
- Wardell-Johnson, G. W., Williams, J. E., Hill, K. D. and Cumming, R. (1997) Evolutionary biogeography and contemporary distribution of eucalypts. IN Williams, J. E. and Woinarski, J. (Eds.) *Eucalypt ecology: individuals to ecosystems*, pp 92-128. Cambridge University Press, Cambridge.
- Weller, D., Denham, R., Witte, C., Mackie, C. and Smith, D. (2003) Assessment and monitoring of foliage projected cover and canopy height across native vegetation in Queensland, Australia, using laser profiler data. *Canadian Journal of Remote Sensing*, 29, 578-591.
- West, P. W. (2004) *Tree and Forest Measurement*, Berlin, Springer-Verlag. 167p.
- Williams, M. S. (2001) Comparison of Estimation Techniques for a Forest Inventory in which Double Sampling for Stratification Is Used. *Forest Science*, 47, 563-576.
- Wood, G. B. and Schreuder, H. T. (1986) Implementing point-poisson and point-model based sampling in forest inventory. *Forest Ecology and Management*, 14, 141-156.
- Wood, M., Keightley, E. K., Lee, A. C. and Norman, P. (2006) *Continental Forest Monitoring Framework, Technical Report - Design and Pilot Study*. Canberra, Australia. National Forest Inventory, Bureau of Rural Sciences. 178p.
- Woodcock, C. E. and Strahler, A. H. (1987) The factor of scale in remote sensing. *Remote Sensing of Environment*, 21, 311-332.
- Wu, J. (1999) Hierarchy and scaling: Extrapolating information along a scaling ladder. *Canadian Journal of Remote Sensing*, 25, 367-380.
- Wu, J. and Qi, Y. (2000) Dealing with scale in landscape analysis: An overview. *Geographic Information Sciences*, 6, 1-5.
- Wu, J. (2004) Effects of changing scale on landscape pattern analysis: scaling relations. *Landscape Ecology*, 19, 125-138.
- Wulder, M. (1998) Optical remote-sensing techniques for the assessment of forest inventory and biophysical parameters. *Progress in Physical Geography*, 22, 449-476.
- Wulder, M., Niemann, K. O. and Goodenough, D. G. (2000) Local maximum filtering for the extraction of tree locations and basal area from high spatial resolution imagery. *Remote Sensing of Environment*, 73, 103-114.
- Wulder, M. and Seemann, D. (2003) Forest inventory height update through the integration of lidar data with segmented Landsat imagery. *Canadian Journal of Remote Sensing*, 29, 536-543.
- Wulder, M., Kurz, W. and Gillis, M. (2004) National level forest monitoring and modeling in Canada. *Progress in Planning*, 61, 365-381.



- Wulder, M., White, J. C., Goward, S. N., Masek, J. G., Irons, J. R., Herold, M., Cohen, W. B., Loveland, T. R., and Woodcock, C. E. (2008) Landsat continuity: Issues and opportunities for land cover monitoring. *Remote Sensing of Environment*, 112 (3), 955-969.
- Zhou, Q., Robson, M. and Pilesjo, P. (1998) On the ground estimation of vegetation cover in Australian rangelands. *International Journal of Remote Sensing*, 19, 1815-1820.

## APPENDIX A

### Ancillary Results

Appendix A contains a range of Tables and Figures which support the results presented in Chapter 4.

**Table 55: Species name and API codes for Injune trees**

Code	Scientific name	Common Name
BGL	<i>Acacia harpophylla</i>	Brigalow
BLH	<i>Casuarina cristata</i>	Belah
BRI	<i>Eucalyptus fibrosa</i> spp. <i>fibrosa</i>	Broad-leaved red ironbark
BOK	<i>Allocasuarina luehmanni</i>	Bull oak
CP-	<i>Callitris glaucophylla</i>	White cypress pine
ECH	<i>Eucalyptus dealbata</i> var <i>chlorodata</i>	Tumbledown red gum or Baradine gum
FMP	<i>Callitris preissii</i>	Family pine
GTI	<i>Eucalyptus decorticans</i>	Gum top ironbark
NRI	<i>Eucalyptus crebra</i>	Narrow-leaved red ironbark
PBX	<i>Eucalyptus populnea</i>	Poplar box
RBA	<i>Angophora floribunda</i>	Rough barked apple
SBA	<i>Angophora leiocarpa</i>	Smooth barked apples
SLI	<i>Eucalyptus melanaphloia</i>	Silver-leaved ironbark
SWB	<i>Eremophila mitchelli</i>	Sandalwood box
WIL	<i>Gejeira parviflora</i>	Wilga

**Table 56: Injune field plot height results from field and LiDAR data for max and predominant height, and at different measurement scales.**

Plot ID	Field Max ht (m)	LiDAR max ht (m)	Field mean tallest – 50 trees ha <sup>-1</sup> (m)	Field mean tallest – 100 trees ha <sup>-1</sup> (m)	LiDAR predom. Ht - 10m cells ~ 100 trees ha <sup>-1</sup> (m)	LiDAR HSCOI stem mean tallest - 50 trees ha <sup>-1</sup> (m)	API height range (m)
23-15	16.7	17.52	15.13	14.22	14.23	15.91	12-30
23-16	19.0	18.61	15.59	13.83	13.82	16.20	12-30
23-20	20.7	22.86	14.94	12.43	14.49	17.75	12-30
23-24	22.0	21.48	19.81	17.49	15.76	19.79	12-30
58-24	19.0	19.8	16.08	14.08	12.40	16.92	12-30
58-29	22.0	17.2	16.08	14.59	14.04	15.53	12-30
59-27	4.0	3.4	3.74	3.74	3.04	- <sup>1</sup>	0
81-11	30.8	26.75	21.48	17.11	19.09	23.35	12-30
81-16	23.0	22.41	17.97	15.74	16.57	18.57	12-30
83-12	18.5	17.50	12.31	10.23	10.23	13.23	12-30
83-20	20.0	20.80	15.64	14.18	13.76	16.75	12-30
111-12	20.4	20.38	17.46	16.36	14.61	17.29	12-30
111-18	23.0	21.80	19.73	18.61	17.78	19.57	12-30
114-04	20.0	18.80	18.29	17.40	15.33	16.42	12-30
114-12	16.2	22.50	14.15	12.76	14.10	14.203	12-30
124-06	18.0	18.90	16.20	15.18	13.93	15.45	<12
124-19	24.0	26.30	18.23	15.36	17.85	18.47	30+
131-18	13.0	12.69	11.06	8.42	8.99	11.34	12-30
138-16	20.0	18.00	15.02	13.30	12.17	15.41	12-30
138-21	17.8	16.83	14.52	12.78	12.11	14.64	12-30

---

142-02	20.8	13.03	10.93	10.00	7.99	10.33	12-30
142-13	14.0	13.22	12.35	11.56	10.52	12.27	12-30
142-18	14.0	16.38	15.11	14.08	14.10	15.27	12-30
142-20	16.0	17.19	14.68	13.09	12.66	14.74	12-30
144-13	18.0	21.61	16.86	15.10	15.37	17.95	12-30
144-19	22.0	22.50	14.07	12.88	12.11	14.32	12-30
148-01	18.8	15.70	13.55	12.26	11.19	13.91	12-30
148-16	15.5	21.97	16.15	13.56	15.99	17.31	12-30
148-21	20.0	18.98	16.38	14.20	14.84	15.75	12-30
148-29	19.0	17.74	13.76	12.70	13.43	15.32	12-30

Notes to table headings: 1)Due to the small number of returns above 2m height observed in this regrowth plot, no stems were generated from the HSCOI modelling.

Table 57: NE Victorian field plot height results across a range of datasets and measurement scales. All values are in metres.

Plot ID <sup>1</sup>	Field plot field max	Field plot LiDAR Max	Field plot field predom (5 tallest)	Field plot LiDAR predom (50 trees ha <sup>-1</sup> )	Field plot LiDAR predom (100 trees ha <sup>-1</sup> )	Transect field max <sup>2</sup>	Transect LiDAR max	Transect field predom (5 tallest)	Transect LiDAR predom (50 trees ha <sup>-1</sup> )	Transect LiDAR predom (100 trees ha <sup>-1</sup> )	SFRI class max API height <sup>3</sup>	NFI height class
008	20.20	36.08	19.92	26.26	24.45	21.4	37.49	17.70	29.26	27.30	22.0 - 27.9	Medium
212	31.50	37.21	17.94	34.69	32.00	36.0	39.58	21.60	28.86	27.01	28.0 - 33.9	Tall
119	29.30	33.02	28.26	30.58	29.40	29.3	35.64	25.50	28.61	27.48	-	Medium
099	20.40	20.45	15.94	13.60	15.67	22.0	23.51	16.70	15.12	14.13	-	Non forest
186	21.60	22.09	20.02	20.46	20.09	21.6	22.91	17.10	19.74	19.13	-	Medium
309	17.30	17.41	12.02	13.74	14.81	17.5	17.87	13.40	13.00	13.84	-	Non forest
169	24.50	23.50	21.14	19.69	19.39	24.5	25.13	18.50	20.46	19.53	-	Medium
216	10.60	12.00	9.78	10.92	10.15	11.4	16.12	7.60	11.65	10.79	-	Medium
220	18.10	19.61	17.12	16.77	16.72	20.0	22.21	15.50	17.69	17.07	-	Medium
382	25.80	22.84	23.64	20.75	19.76	25.8	27.25	19.20	22.59	21.82	-	Medium
463	39.20	39.92	29.40	32.62	28.02	39.2	48.75	25.50	38.03	35.48	28.0 - 33.9	Tall
554	22.30	27.83	21.20	23.75	24.41	22.3	35.90	19.80	25.72	24.33	-	Tall
459	22.00	21.28	21.30	20.26	20.27	22.0	24.40	18.50	20.62	19.99	-	Medium
573	30.80	29.73	27.60	27.23	25.24	30.8	39.58	18.30	28.24	26.74	-	Medium
313	31.10	34.78	29.70	31.47	30.40	36.5	39.91	26.40	31.49	30.53	-	Tall
391	29.10	32.85	24.00	29.31	29.68	32.9	40.03	21.60	32.29	30.94	22.0 - 27.9	Medium
467	25.60	34.64	21.60	28.50	27.93	25.6	38.92	19.00	29.71	28.37	34.0 - 39.9	Tall
550	40.80	44.60	36.20	33.93	32.91	50.0	51.46	27.10	38.67	36.20	34.0 - 39.9	Tall
562	24.00	34.01	23.00	27.39	27.78	24.0	34.01	18.00	27.33	25.48	15.0 - 21.9	Medium

---

6054	36.40	38.13	33.40	32.75	32.01	36.4	42.91	23.10	31.42	30.02	34.0 - 39.9	Tall
603	35.70	43.58	35.00	39.54	39.02	35.7	49.38	27.00	37.67	36.53	34.0 - 39.9	Tall
558	28.00	29.06	26.00	27.83	26.93	28.0	37.46	21.80	27.68	26.64	-	Medium
471	15.40	15.33	13.82	13.38	13.00	15.4	29.80	13.82	14.61	13.90	-	Low

Notes to table headings: 1) Plots are ranked (lowest to highest) by elevation. 2) Maximum height of all plot trees and trees found on transects. 3) SFRI overstorey heights only measured within State Forest managed areas. 4) Field and LiDAR data are not co-incident for plot 605, so comparisons cannot be made between these data. LiDAR, SFRI, and NFI are coincident for p605.

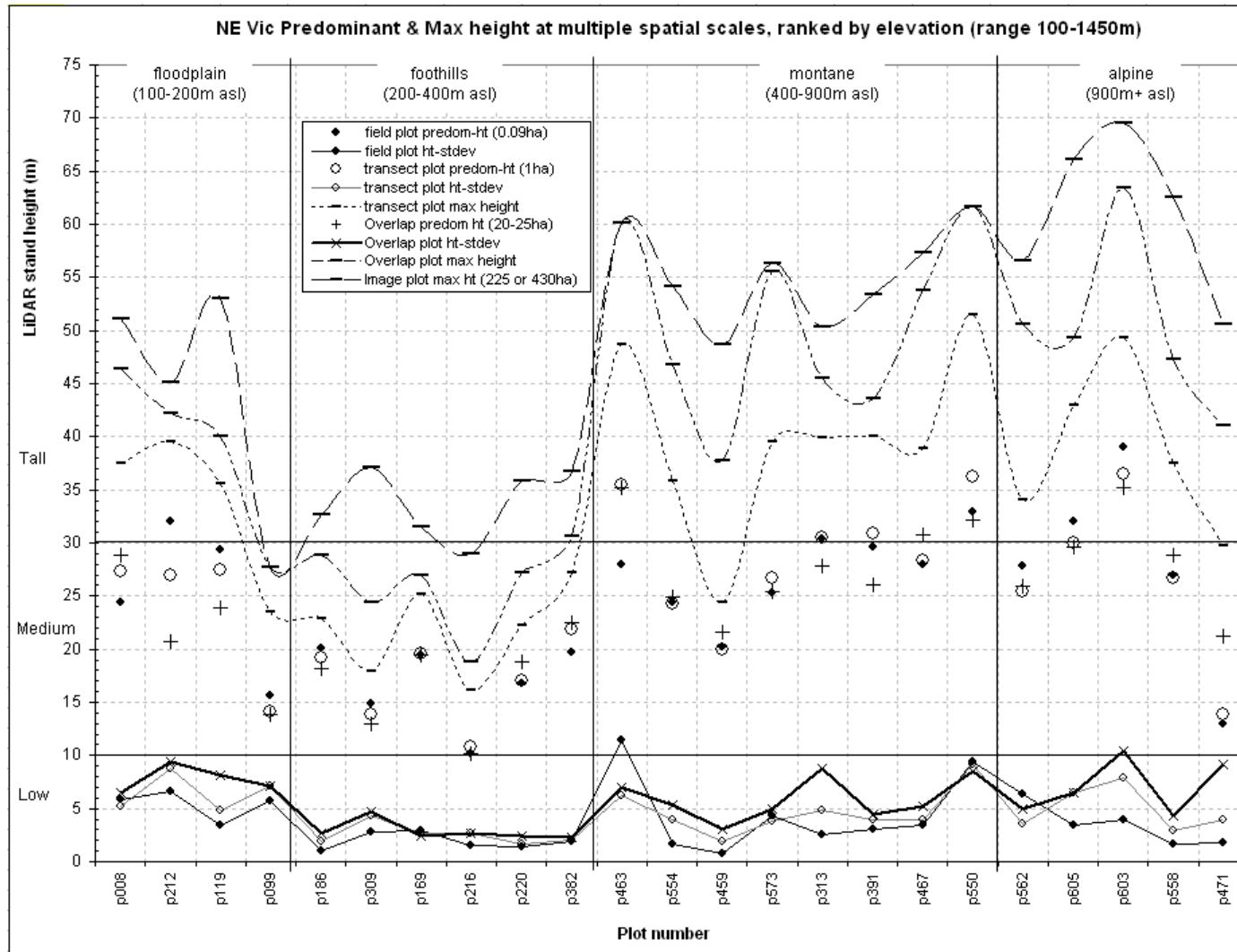


Figure 110: Summary of predominant and max height for each CFMF field plot, by ecozone.

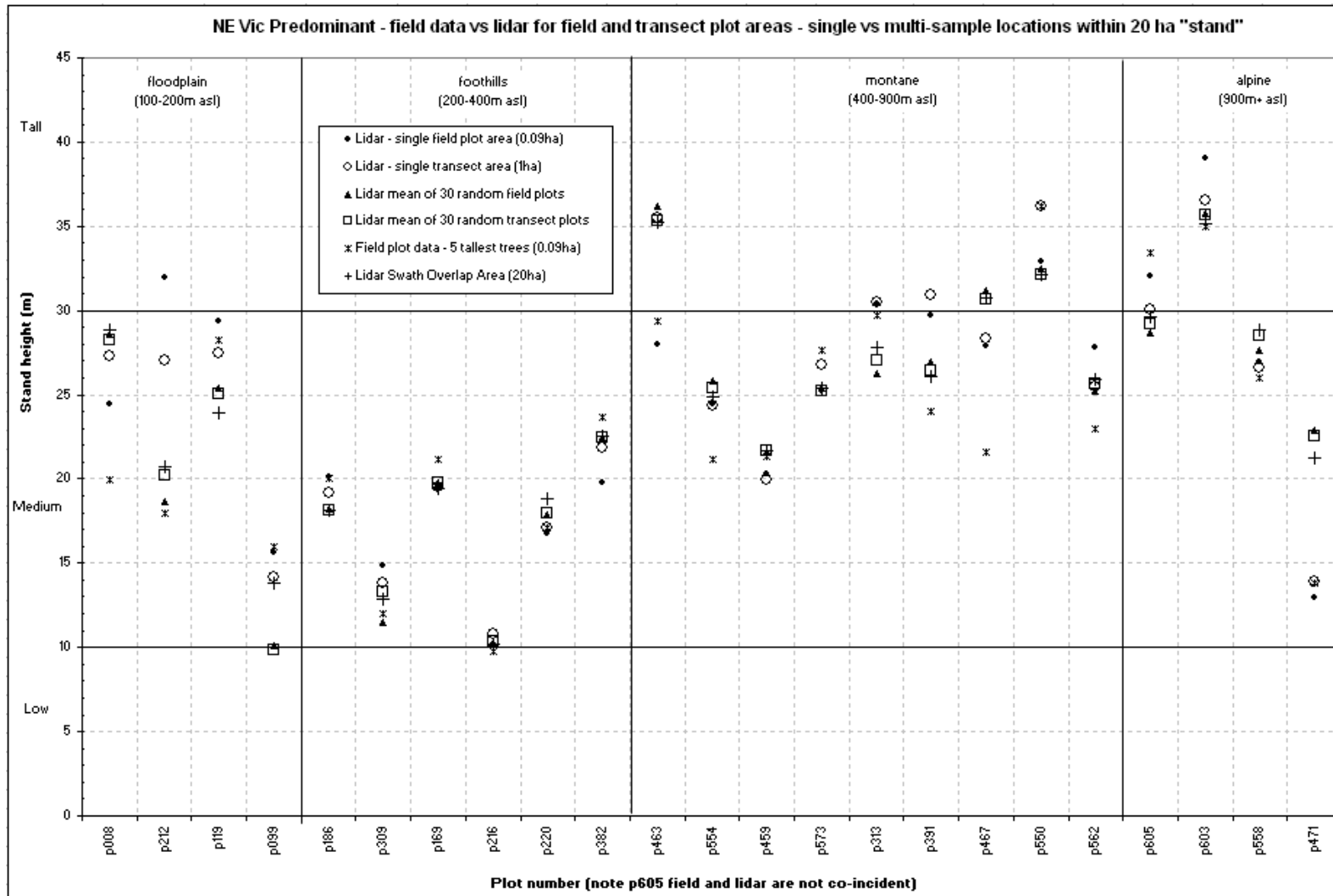


Figure 111: Comparison of stand sampling strategies for estimating stand (~20ha) predominant height by ecozone.



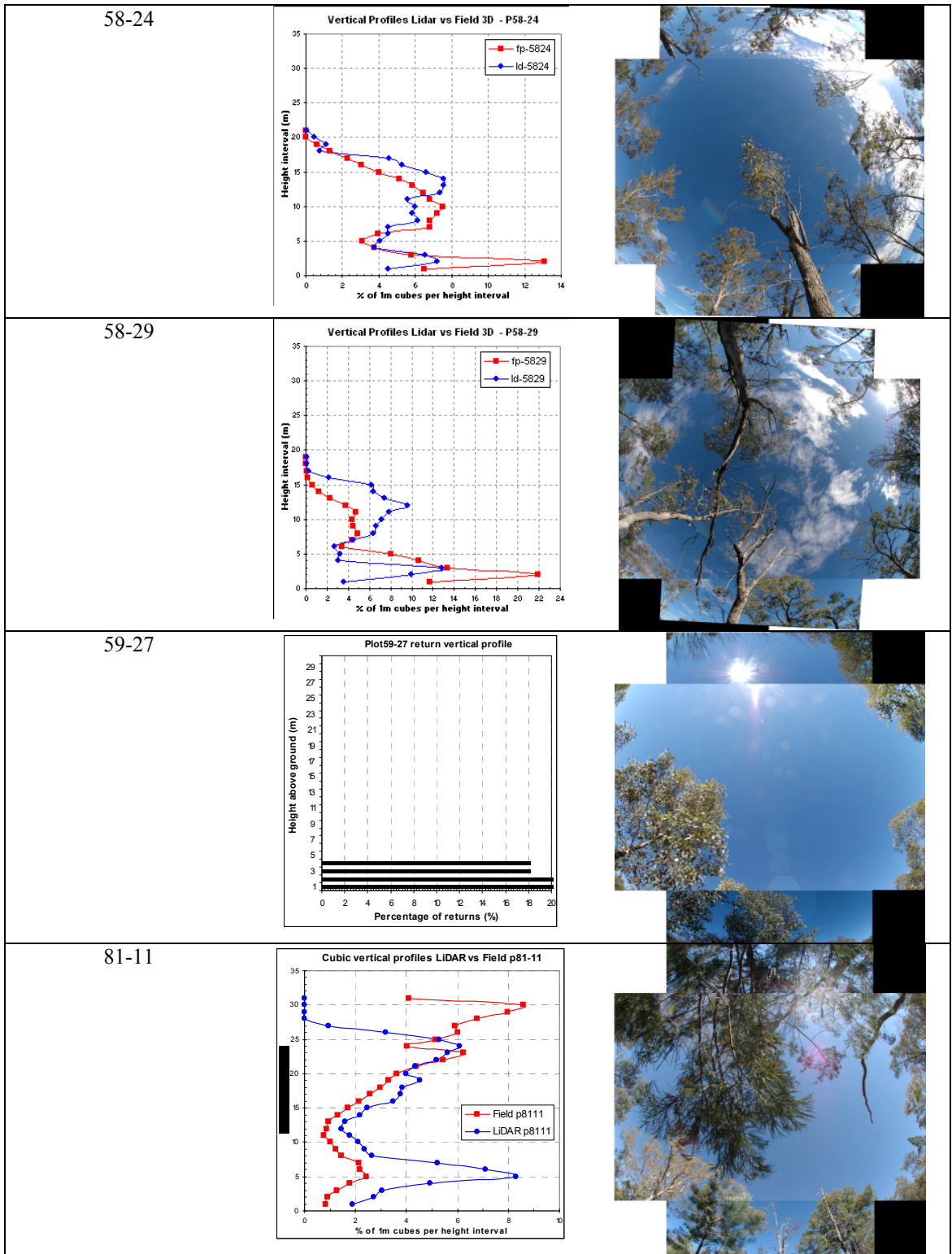
**Table 58: Results from correlation and Kolmogorov-Smirnov test comparisons between LiDAR and field cubic modeling derived apparent vertical profiles for Injune.**

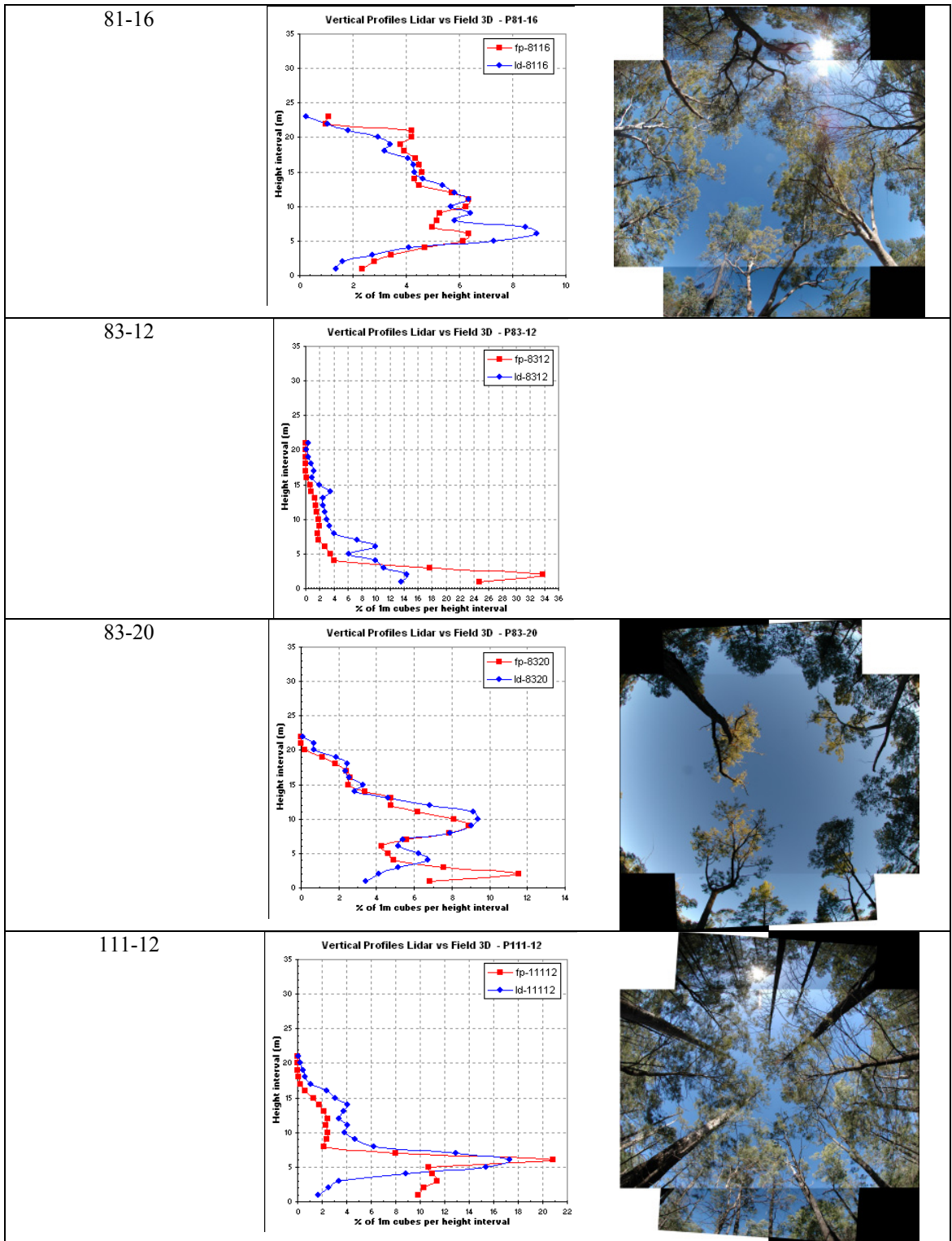
Kolmogorov-Smirnov test			Correlation comparison at each height interval			
Plot	KS <sup>a</sup> statistic	p-value	r <sup>2</sup>	RSE	p-value	function <sup>b</sup>
p11112	0.3333	0.1963	0.54	3.39	0.00010	y= 0.6400x + 1.7143
p11118	0.1923	0.7327	0.32	2.91	0.00300	y= 0.5919x + 1.5668
p11404	0.2857	0.2053	0.40	2.25	0.00030	y= 0.3587x + 2.2902
p11412	0.3600	0.0779	0.70	1.42	2.266e <sup>7</sup>	y= 0.4128x + 2.3487
p12406	0.2857	0.3650	0.12	2.78	0.13050	y= 0.1715x + 3.9451
p12419	0.1852	0.7537	0.68	1.50	1.207e <sup>7</sup>	y= 0.6584x + 1.2651
p13816	0.3000	0.3356	0.14	3.41	0.09965	y= 0.2448x + 3.7758
p13821	0.1667	0.9715	0.61	2.71	0.00010	y= 0.7546x + 1.3631
p14202	0.1429	0.9996	0.87	2.41	1.29e <sup>6</sup>	y= 0.9690x + 0.2218
p14218	0.1765	0.9631	0.56	3.29	0.00060	y= 0.7613x + 1.4043
p14220	0.1667	0.9715	0.44	2.34	0.00280	y= 0.5777x + 2.3460
p14413	0.2727	0.3937	0.22	2.59	0.02720	y= 0.7672x + 1.0583
p14419	0.2609	0.4218	0.58	2.27	0.00002	y= 0.6102x + 1.6949
p5824	0.2381	0.6028	0.59	1.56	0.00005	y= 0.5864x + 1.9697
p5829	0.2632	0.5379	0.26	3.14	0.02565	y= 0.3173x + 3.5938
p8111	0.1613	0.8235	0.03	2.13	0.40000	y=-0.1462x + 3.6974
p8116	0.2174	0.6601	0.76	1.17	6.251e <sup>8</sup>	y= 1.3673x - 1.5970
p8312	0.3810	0.0948	0.70	2.53	2.422e <sup>6</sup>	y= 0.4135x + 2.7931
p8320	0.0909	1.0000	0.55	1.93	0.00007	y= 0.6746x + 1.4791

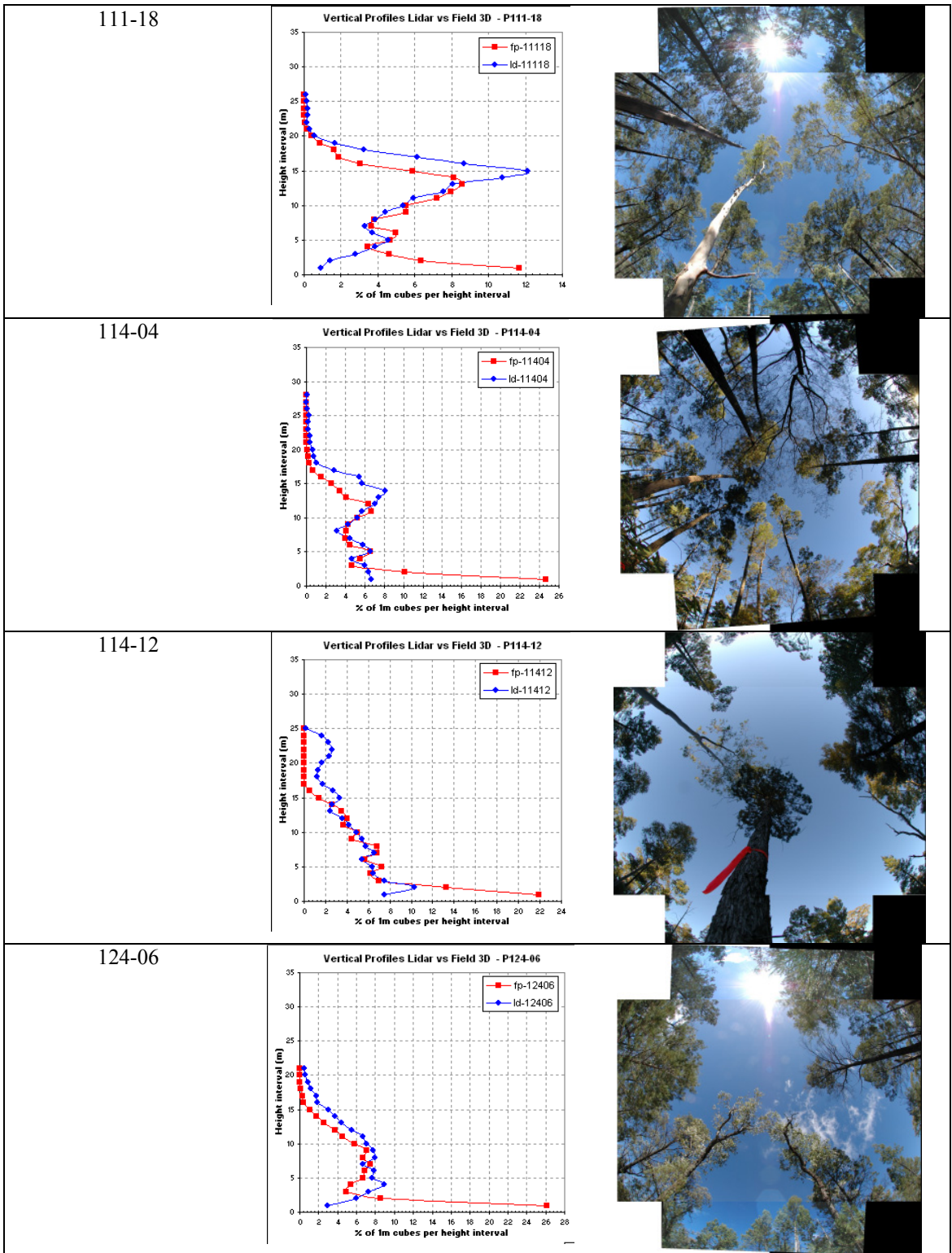
<sup>a</sup>Kolmogorov-Smirnov test statistic, <sup>b</sup>y= LiDAR value of percentage cubes per height interval, x = field value

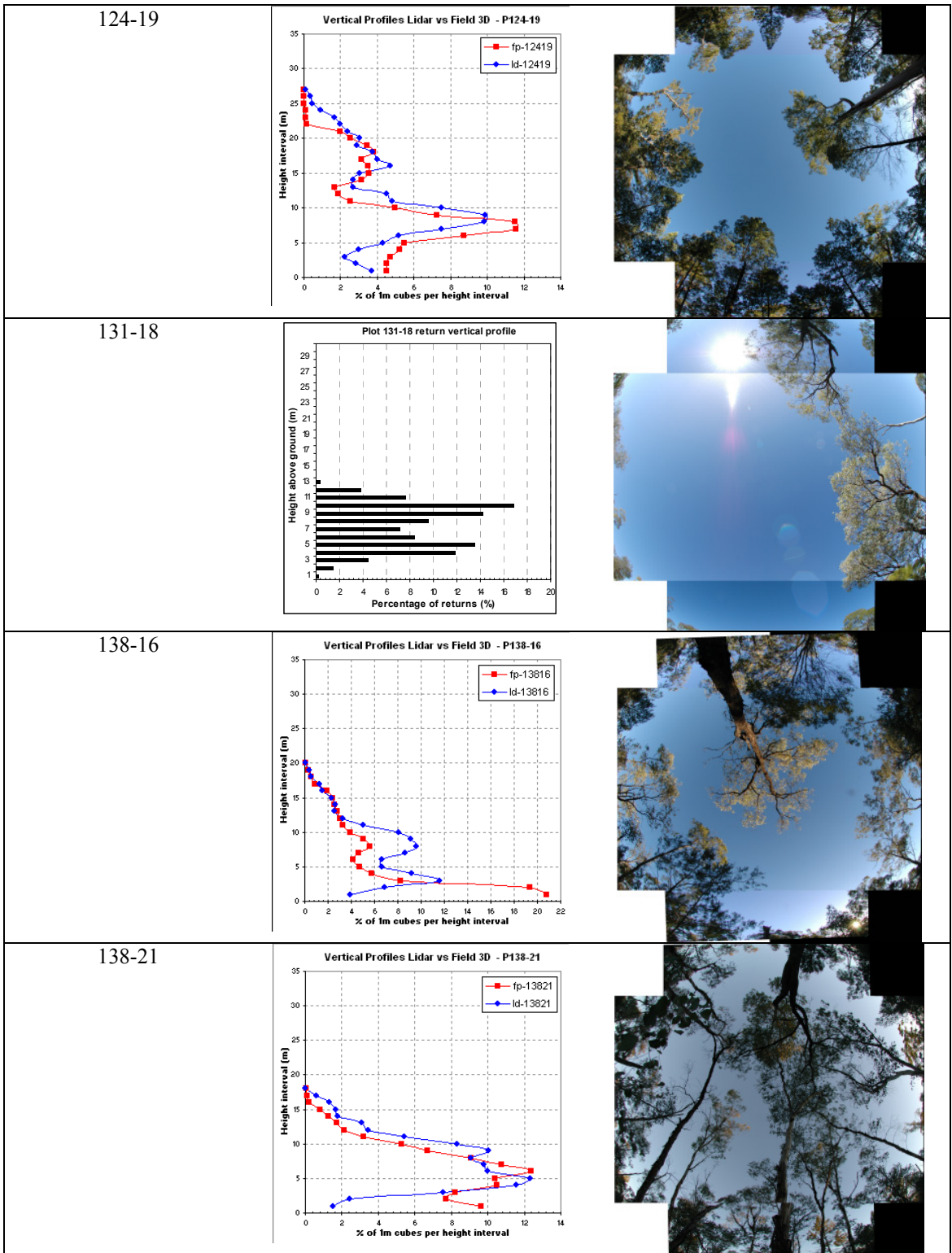
**Table 59: Injune field plots apparent vertical profiles using modelled field data (red) and LiDAR returns (blue), and plot centre hemispherical photo.**

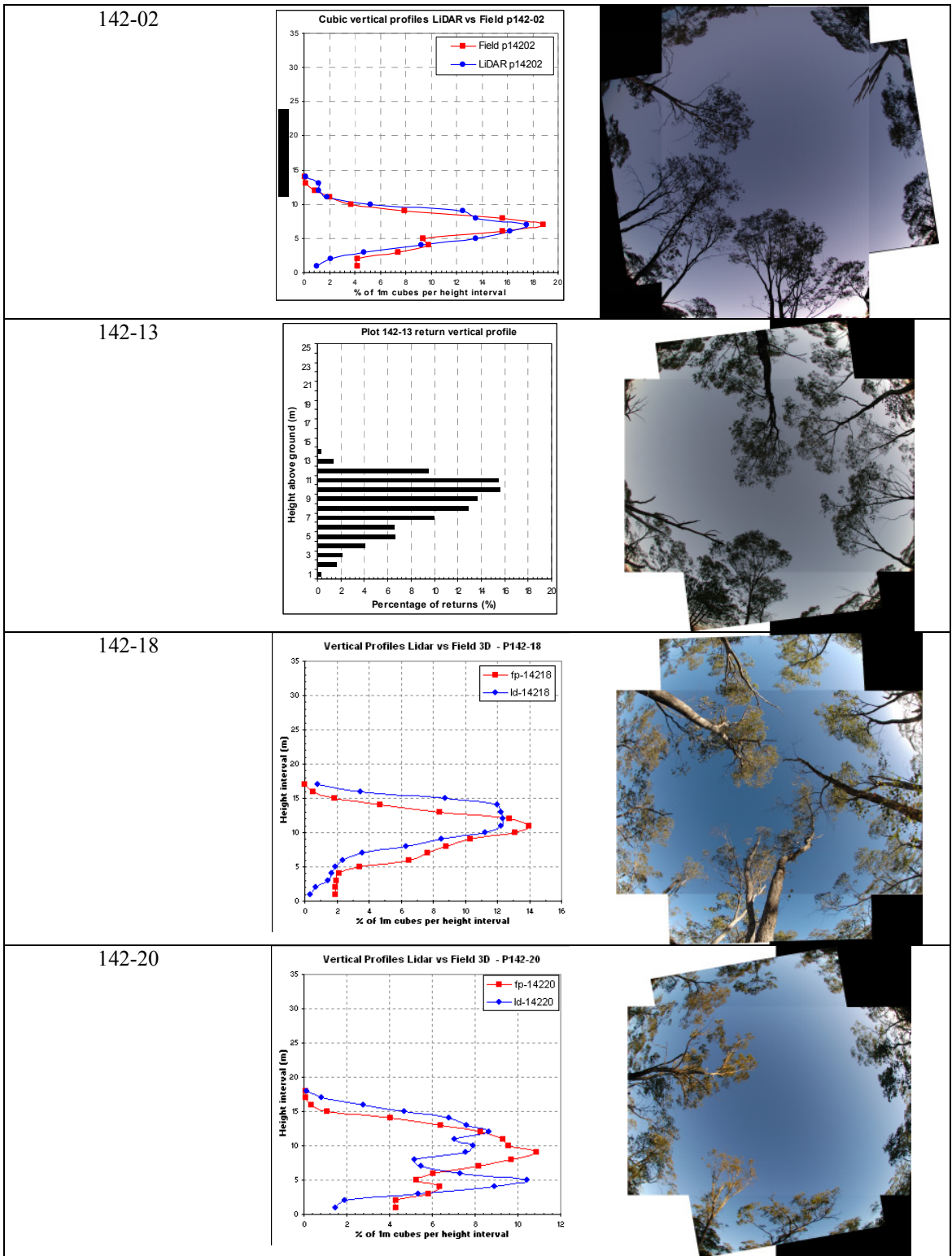
Plot	LiDAR and Field vertical profile	Plot centre hemi-photo
23-15		
23-16		
23-20		
23-24		

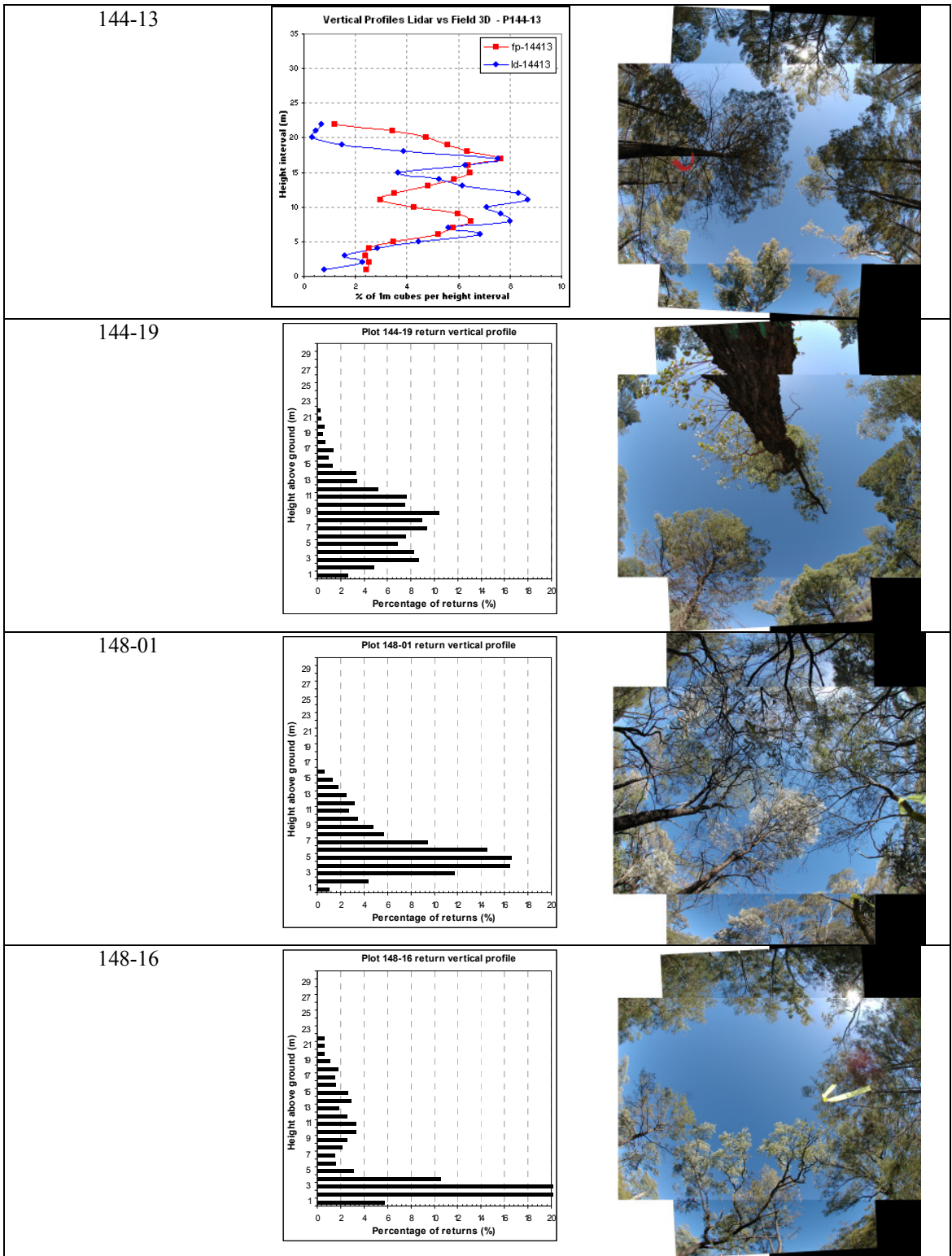






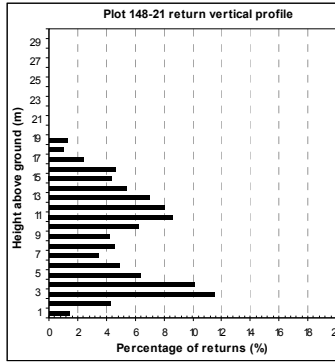




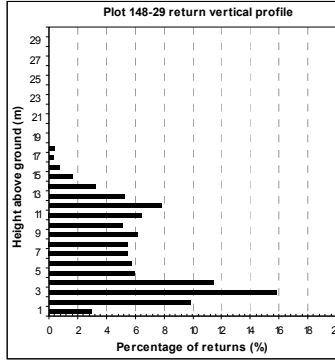




148-21



148-29



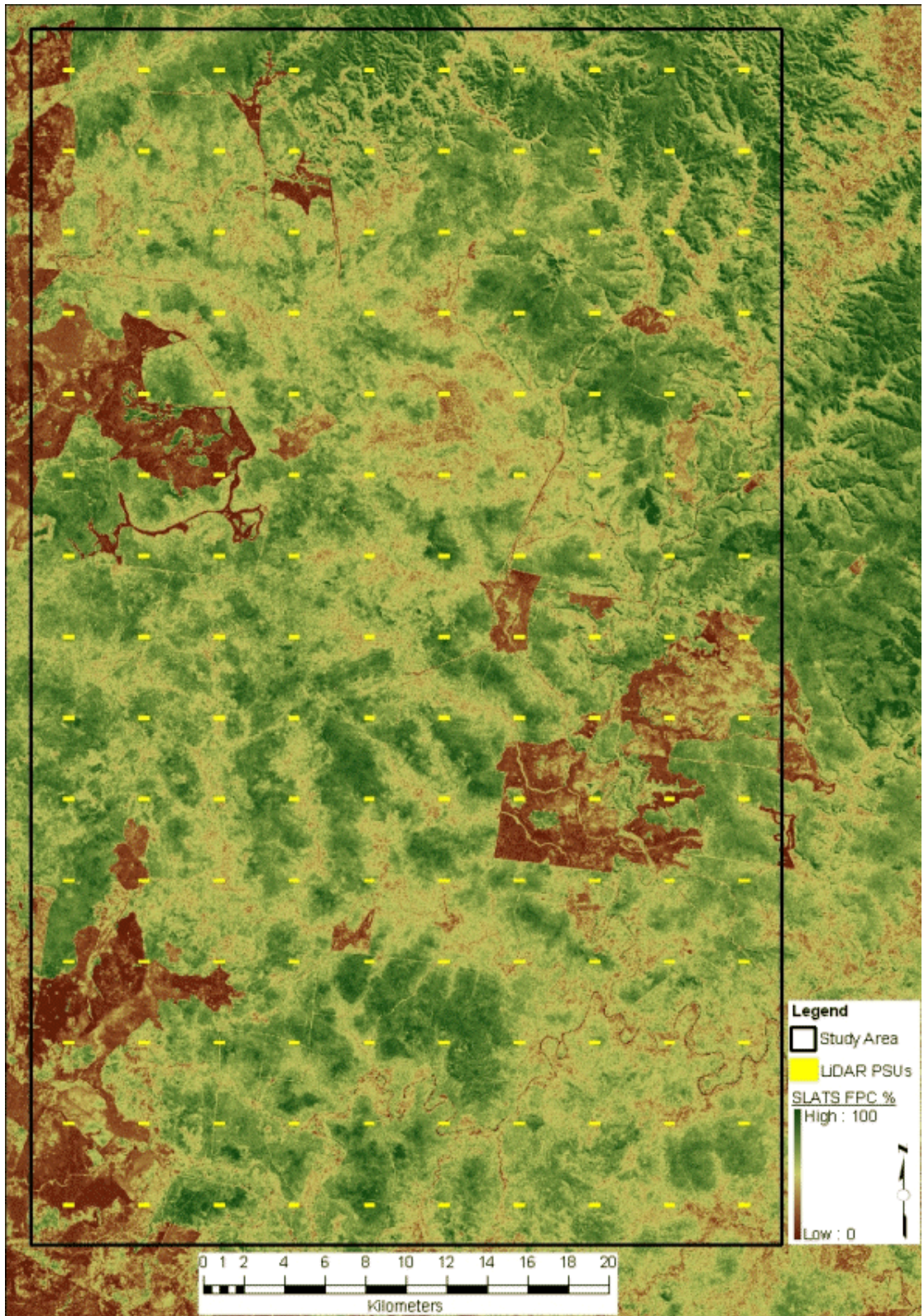


Figure 112: SLATS Landsat FPC (2000) spatial distribution at the Injune study site.

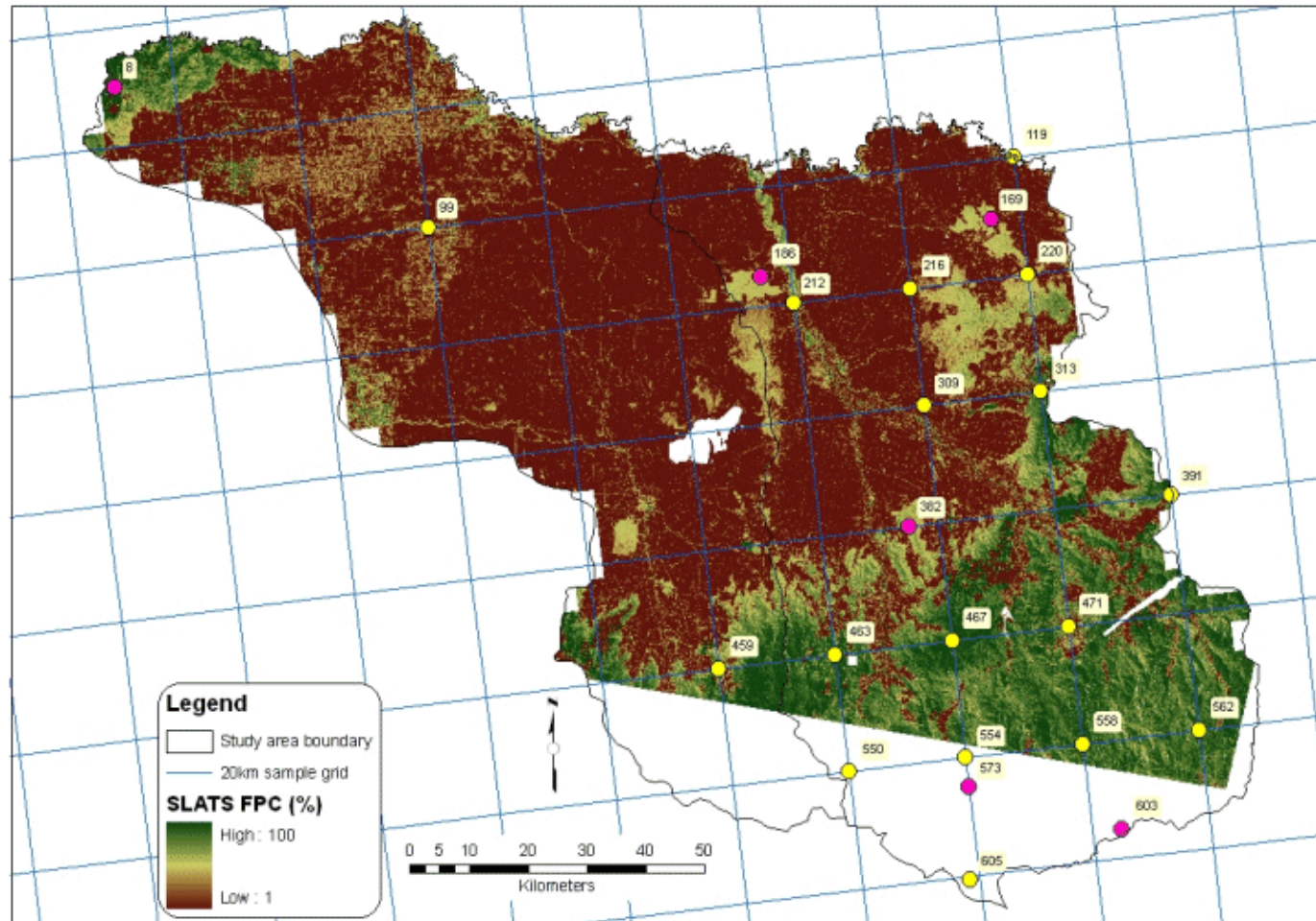


Figure 113: NE Victorian SLATS FPC (uncalibrated) from two Landsat scenes. Systematic field plots are yellow, additional calibration plots are pink.

**Table 60: Injune field plot percentage cover results across a range of datasets, cover metrics, and measurement scales.**

Plot ID	Field FPC	Field FBC	Field FBC (2004)	Photo FBC (2004)	Tree map CC (>5cm)	LiDAR FBC 0.5m+	LiDAR FBC 2m+	HSCOI CC	CHM CC	CASI CC	API CC range mid-point	Landsat FPC
23-15	37.82	68.6	n/a	41.78	72.17	44.82	40.63	67.56	78.38	76.29	65	48.8
23-16	28.85	41.7	n/a	37.25	37.20	29.60	27.85	48.66	61.94	55.65	20	40.6
23-20	23.08	28.8	n/a	22.86	35.87	24.60	22.97	34.93	47.78	39.59	20	32.4
23-24	37.18	48.7	n/a	45.67	44.94	41.93	35.22	59.41	58.01	62.68	40	50.4
58-24	21.79	28.8	33.97	25.35	37.93	17.54	15.90	35.53	42.95	35.38	20	31.8
58-29	27.56	43.6	47.44	33.24	41.97	28.94	24.87	47.17	53.85	45.82	40	38.6
59-27	0	0	n/a	21.06	3.54	5.00	1.82	5.13	13.00	24.00	5	27.0
81-11	35.90	57.7	59.6	57.82	78.79	54.74	52.62	62.68	72.74	82.45	40	55.6
81-16	35.48	51.9	n/a	45.4	86.33	49.14	47.97	62.63	77.17	82.40	40	52.2
83-12	11.54	12.8	n/a	n/a	22.81	26.29	18.53	25.60	32.10	29.06	20	34.0
83-20	19.87	28.8	35.3	36.98	38.90	30.16	28.80	43.20	50.89	45.39	65	35.4
111-12	42.95	64.7	n/a	59.69	80.10	65.69	63.85	77.07	91.99	83.56	65	60.6
111-18	50.00	62.2	n/a	52.00	73.10	45.02	44.37	68.52	82.49	79.46	65	54.0
114-04	27.56	44.2	n/a	45.26	29.64	36.49	32.46	40.46	62.21	68.42	40	44.2
114-12	21.15	26.3	n/a	39.10	19.69	25.73	19.69	28.58	31.77	45.53	40	38.6
124-06	21.15	40.4	n/a	45.52	50.07	38.66	35.70	52.93	60.19	60.64	40	42.2
124-19	24.36	49.4	n/a	42.59	53.65	34.67	32.71	49.85	58.62	60.77	65	50.4
131-18	7.69	14.7	12.42	18.32	17.16	15.14	14.88	18.64	24.53	23.53	20	22.4
138-16	29.49	44.9	n/a	41.04	38.93	37.43	32.91	56.02	61.49	44.38	40	35
138-21	27.56	40.4	60.9	45.35	47.50	31.52	30.81	47.28	62.14	54.83	40	40.4

142-02	22.40	30.0	30.1	29.84	32.71	16.95	16.57	23.76	32.74	25.45	20	20.6
142-13	17.95	21.8	9.62	30.8	35.89	16.48	16.16	31.70	39.88	35.44	20	25.6
142-18	25.00	29.5	n/a	30.38	43.43	19.36	19.15	40.03	52.29	30.71	40	29.6
142-20	10.26	38.0	38.5	27.64	51.24	27.25	26.34	42.21	48.22	32.15	40	33.8
144-13	19.87	37.8	n/a	48.75	50.36	30.11	29.33	31.16	64.11	41.00	40	40.4
144-19	15.38	26.3	n/a	34.67	45.00	26.85	24.84	36.13	44.62	32.57	40	31.4
148-01	34.62	63.5	76.3	61.63	73.81	59.94	56.67	70.29	83.80	74.04	65	48.2
148-16	29.49	44.2	50.6	53.01	55.59	54.58	37.53	57.98	60.68	77.08	40	49.4
148-21	19.87	35.9	n/a	33.22	42.14	24.86	23.44	42.19	54.19	n/a	20	35.2
148-29	30.77	49.4	56.41	48.14	52.98	40.41	35.23	52.22	63.79	51.74	40	42.4

Notes to table headings: 1) Field is field transects. 2) Photo FBC is from hemispherical photos. 3) LiDAR FBC is the percentage of returns above threshold height. 4) HSCOI CC is crown cover from LiDAR HSCOI modelling. 5) CHM CC is crown cover from canopy height modelling. 6) CASI CC (1 m pixels) data were supplied from Bunting and Lucas, (2006). 7) API CC mid point is from the aerial photography crown cover class mid-point of the range. 8) Landsat FPC was supplied from SLATS analyses, using a 2000 baseline product. 9) All data measured in 2000 unless otherwise indicated. 10) n/a indicated data was not collected for the field plot.

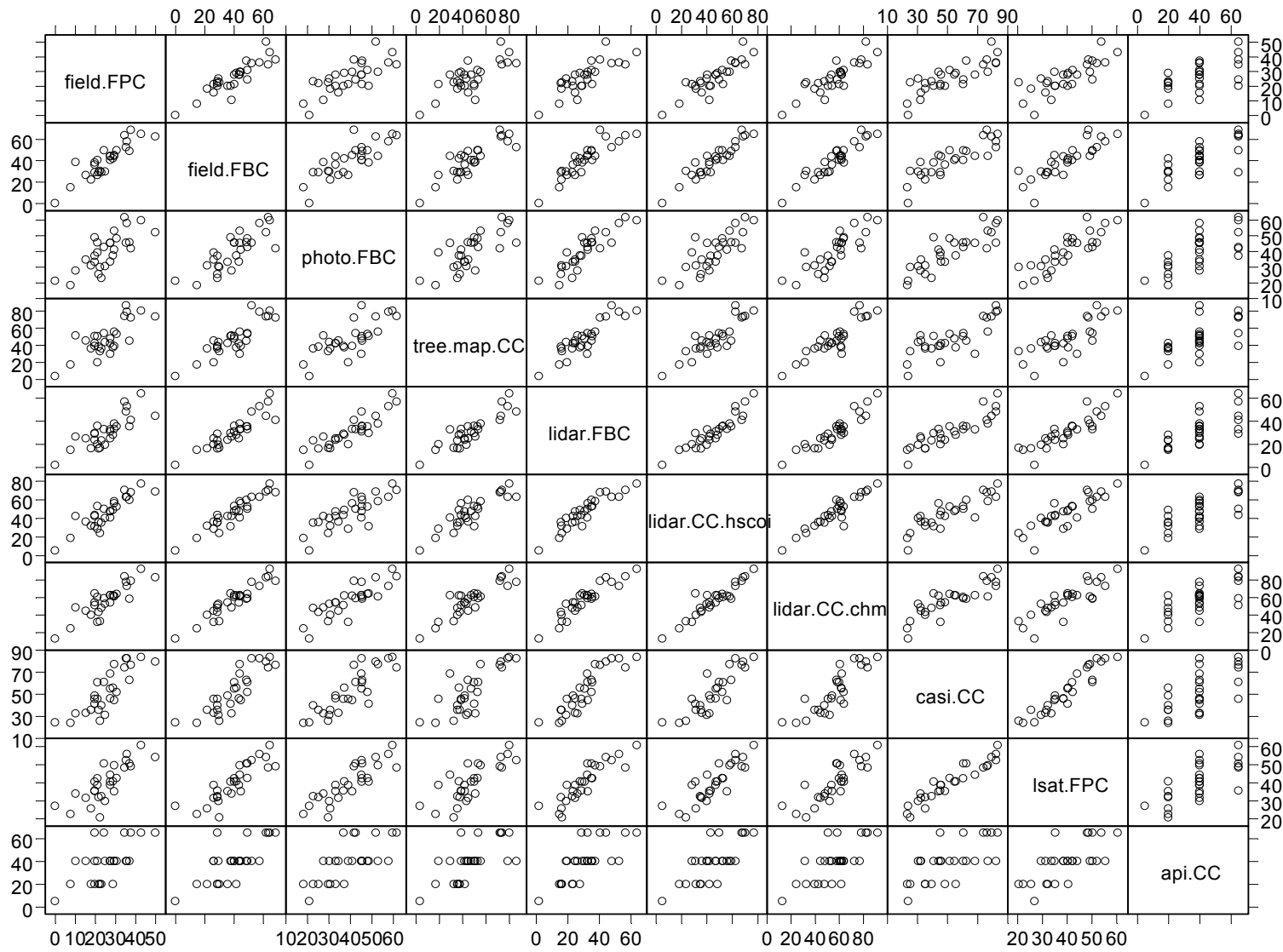
**Table 61: NE Victorian field plot percentage cover results across a range of datasets, cover metrics, and measurement scales. All values in percentage cover.**

Plot ID1, 4	Field plot Tree map CC (>10cm)	Field plot Photo FBC	Transect Photo FBC	Field plot LiDAR FBC 2m+	Transect LiDAR FBC 2m+	Field plot HSCOI CC (2m+)	Transect HSCOI CC (2m+)	NFI data cover class	SFRI API CC range	Landsat FPC2
008*	72.80	55.62	52.20	54.59	54.1	85.10	91.60	Open	70-84	39.00
212	62.91	60.36	65.51	55.73	54.1	88.00	79.39	Open	50-69	46.50
119	49.30	55.27	67.09	54.98	56.2	78.10	83.16	Woodland	-	52.50
099	30.15	40.11	50.59	47.47	50.6	57.90	50.43	Non forest	-	35.75
186*	82.51	47.04	45.50	60.40	58.0	79.70	68.73	Open	85-100	38.25
309	25.62	30.99	31.04	39.35	19.3	36.30	19.48	Non forest	-	27.67
169*	68.39	49.22	53.70	48.00	68.0	81.70	82.72	Open	70-84	40.00
216	51.65	30.58	30.80	44.92	38.6	66.80	61.54	Open	50-69	26.50
220	76.43	44.18	42.93	50.37	52.1	50.80	96.86	Open	70-84	40.00
382*	55.21	53.22	51.02	60.52	65.7	51.80	78.62	Open	70-84	38.50
463	31.09	55.69	58.85	49.74	67.3	54.30	88.78	Open	70-84	53.00
554	61.64	67.01	67.20	84.86	81.4	91.80	97.42	Open	85-100	-
459	72.80	52.40	51.08	51.42	53.6	85.60	95.24	Open	70-84	40.25
573*	76.85	67.17	65.24	71.88	74.8	87.80	91.50	Open	70-84	-
313	81.17	66.04	64.02	75.18	72.0	88.50	86.54	Open	70-84	63.50
391	63.32	66.42	72.07	65.83	69.9	85.80	99.35	Open	70-84	64.00
467	62.03	64.44	65.47	67.43	72.0	83.90	98.89	Open	70-84	63.00
550	60.78	70.04	78.62	83.64	88.8	98.50	97.37	Open	50-69	-
562	18.85	50.13	48.55	61.55	58.2	76.60	69.33	Open	70-84	42.67

---

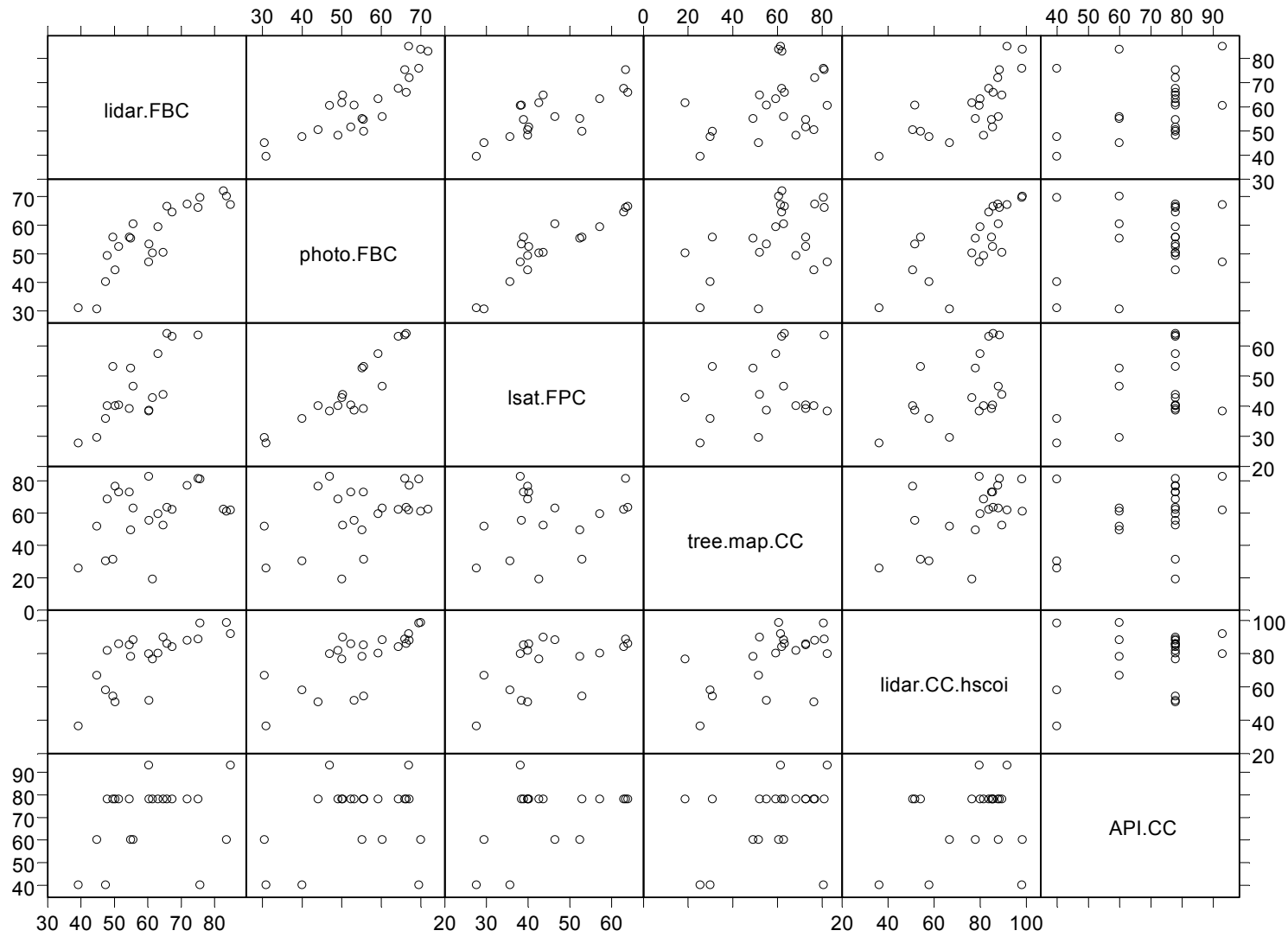
6053	62.17	71.89	77.09	82.75	78.74	-	-	Open	70-84	-
603*	80.78	69.57	67.24	75.72	71.4	98.20	96.38	Woodland	30-49	-
558	59.38	59.32	52.21	63.18	65.6	80.10	78.85	Open	70-84	57.25
471	52.23	50.37	48.10	64.70	67.7	89.60	85.45	Open	70-84	43.75

Notes to table headings: 1) Plots are ranked (lowest to highest) by elevation. 2) Landsat FPC estimate is uncalibrated for NE Victorian environments; plots without values were outside available images. 3) Field and LiDAR data are not co-incident for plot 605, so comparisons cannot be made. HSCOI CC modelling was not undertaken. 4) Plots marked with \* are remote sensing calibration plots.



**Figure 114: Injune cover matrix graphs. All scales are percent cover.**





**Figure 115: NE Victoria cover matrix graphs. All scales are percent cover.**

Table 62: Crown Separation ratio calculation test for p142-13

Transect	Tree No	Field Crown Diameter (m)	LiDAR Segment diameter (m)	Distance to next crown edge (m)	Transect estimated CC%	Field transect FBC%	Photo FBC%*
1	3	8	6.5	4.8			
1	5	5	4.7	1.9			
1	9	0	2.9	9.9			
1	10	5	4.3	2.0			
1	11	4	5.7	7.5			
1	17	5	4.6	2.6			
1	506	3	2.3	3.2			
1	16	4	4.1	2.0			west-30m
Mean	n = 8	4.3	4.4	4.2	20.2	19.2	27.7
2	23	5.5	5.4	2.8			
2	507	3.5	3.5	6.4			
2	29	5.5	5.7	6.1			
2	22	5.5	5.2	2.0			
2	33	4.5	4.7	0.0			
2	19	5.5	6.5	0.5			
2	34	6	5.7	3.2			
2	36	5.5	5.0	7.0			cntr-20m
Mean	n = 8	5.2	5.2	3.5	28.7	21.2	35.0
3	24	6	6.1	5.4			
3	44	3	3.4	2.6			
3	27	6	5.0	-1.0			
3	43	4	3.0	2.5			
3	42	7	5.3	7.8			
3	40	7	6.4	0.5			
3	39	3.5	4.5	0.5			
3	38	6	6.0	0.0			east-30m
Mean	n = 8	5.3	5.0	2.3	39.4	25.0	29.5
Plot Mean	n = 24	4.9	4.9	3.3	28.6	21.8	30.7

\* Hemispherical photos used are from the distance along transects from start of transect (southern edge of plot) as indicated in table (see also **Figure 75**).

**Table 63: Crown Separation ratio calculation test for p81-16**

Transect	Tree No	Field diameter (m)	LiDAR diameter (m)	Distance to next crown edge (m)	Transect CC% estimate	Transect FBC% estimate	Hemi-photo FBC%*
1	26	4.2	4.5	1			
1	24	4.1	6.2	2.1			
1	2	3.1	4.6	4.1			
1	22	8.3	3.2	2.7			
1	7	3.2	2	2.7			
1	21	4.2	3.3	4			
1	10	3.9	4.5	1			
1	28	2.3	3.2	0.5			
1	32	4.4	4.6	2			
1	16	10	7.5	3.6			
1	33	3.6	3.3	0			
1	34	4.1	3.3	0			
1	35	4.7	3.4	0			
1	36	5.6	3.6	0			
Mean	n = 14	4.7	4.1	1.7	43.5	51.9	
2	55	3.7	2.7	0			
2	54	3.2	4	3.9			
2	59	4.5	4.5	3			
2	50	7.6	7.6	-2			
2	49	10.4	5.9	6			
2	45	5.2	3.7	3.5			
2	41	4.9	3.6	1			
2	73	1	4.3	3.3			
2	39	6.4	6.1	2			
2	74	5.8	4.9	0			
Mean	n = 10	5.3	4.7	2.1	41.5	44.2	45.4
3	115	3.2	3.2	6			
3	51	10.3	11.8	-3			
3	96	14.8	8	2.5			
3	63	5.7	3.2	-2.3			
3	64	16.3	16.2	0			
3	83	6.3	5.5	4.2			
3	70	6.3	7.4	5.5			
3	79	5	5.6	4.7			
3	76	3.7	5.1	0			
Mean	n = 9	8.0	7.3	2.0	51.9	59.6	
Plot Mean	n = 33	5.8	5.2	1.9	45.8	51.9	45.4

\* Photo used if from centre transect and 30m from start of transect (southern edge of plot).

**Table 64: Slope and intercept significance values for calibration and validation functions**

Description	Function	Slope SE	Slope P-value	Intercept SE	Intercept P-value
Landsat pixel comparisons in 12 PSUs					
LiDAR CC vs LiDAR FBC in 1161 25 m cells	$Y = 1.4014x + 6.4695$	0.0207	0	0.6922	0
LiDAR CC vs SLATS FPC in 855 25 m cells	$Y = 1.302x + 2.9647$	0.0346	0	1.5069	0.0495
LiDAR CC vs SLATS FPC calibration (683 cells - 80%)	$Y = 1.298x + 3.5609$	0.0384	0	1.6708	0.0334
LiDAR CC vs SLATS FPC validation (172 cells - 20%)	$Y = 1.0255x - 3.6281$	0.0608	0	3.6692	0.3242
PSU 142 stem and component biomass comparisons					
Field allometric vs LiDAR component sum – all matched stems	$Y = 0.6705x + 45.508$	0.0431	0	12.2317	0.0003
Field allometric vs LiDAR stem allometric – all matched stems	$Y = 0.9986x - 4.4777$	0.068	0	15.6	0.7744
Field allometric vs LiDAR component sum – minus LiDAR model outliers	$Y = 0.7685x + 40.244$	0.0413	0	11.1238	0.0004
Field allometric vs LiDAR stem allometric – minus LiDAR model outliers	$Y = 1.0758x - 8.2568$	0.0667	0	14.98	0.5822
Field allometric vs LiDAR component sum – minus LiDAR + field outliers	$Y = 0.9346x + 7.2585$	0.0345	0	8.1587	0.3749
Field allometric vs LiDAR stem allometric – minus LiDAR + field outliers	$Y = 1.1482x - 28.322$	0.0642	0	13.4868	0.0372
LiDAR stem allometric vs LiDAR component sum – all matched stems	$Y = 0.5933x + 67.069$	0.0195	0	5.5426	0
LiDAR to field data comparisons – Injune					
Plot Field stem pred. Ht vs Stem pred. Ht (HSCOI)	$y = 0.8049x + 2.7633$	0.0389	0	0.6199	0.0001
Plot Field stem pred. Ht vs Stem pred. Ht (CHM)	$y = 0.7137x + 3.8844$	0.0458	0	0.7519	0
Plot Field stem pred. Ht vs canopy pred. Ht (HSCOI)	$y = 0.9712x + 2.1795$	0.0594	0	0.8189	0.0127
Field stem Ht vs LiDAR stem Ht (CHM)	$y = 0.5868x + 3.6323$	0.0641	0	0.8144	0
Field stem Ht vs LiDAR stem Ht (HSCOI/CHM)	$y = 0.8237x + 1.8197$	0.0486	0	0.5569	0.0014
Field stem Ht vs LiDAR stem Ht (CHM) - outliers	$y = 0.9391x + 0.2727$	0.0466	0	0.5514	0.622
Field stem Ht vs LiDAR stem Ht (HSCOI/CHM) - outliers	$y = 0.8797x + 0.9877$	0.0408	0	0.4728	0.039
Field stem count vs LiDAR stem count	$y = 1.539x - 142.63$	0.1361	0	57.6225	0.0194
Field 50 trees ha-1- LiDAR 10m cell	$Y = 0.9688x + 2.2129$	0.0557	0	0.7751	0.0079
Field 100 trees ha-1- LiDAR 10m cell	$Y = 0.8447x + 2.2536$	0.0673	0	0.9377	0.0229
Field max height vs LiDAR	$Y = 0.9086x + 1.7912$	0.0712	0	1.3498	0.1942

max height (field plots)					
Field D130 vs LiDAR D130	$Y = 0.7933x + 4.3875$	0.0544	0	1.0923	0.0001
Field FPC vs LiDAR FBC	$y = 0.6418x + 5.7556$	0.0863	0	2.8585	0.0538
Field FBC vs LiDAR FBC	$y = 1.1285x + 4.057$	0.0942	0	3.0633	0.195
Field photo FBC vs LiDAR FBC	$y = 0.7617x + 16.5086$	0.0711	0	2.3791	0
Field tree map CC vs LiDAR CC (HSCOI)	$y = 1.0377x - 0.5787$	0.1028	0	4.9559	0.9079
LiDAR to field data comparisons – NE Victoria					
Field plot photo FBC vs field plot LiDAR FBC	$y = 0.7864x + 7.1867$	0.1113	0	6.8689	0.3079
Transect area photos FBC vs transect LiDAR FBC	$y = 0.6796x + 13.8757$	0.1108	0	7.0323	0.0625
Transect area LiDAR FBC vs field plot photo FBC	$y = 1.1045x + 1.2794$	0.1469	0	8.2142	0.8778
Field max height vs LiDAR max height (field plots)	$Y = 0.7204x + 4.9137$	0.0895	0	2.6911	0.0828
Max.htPredom. Ht - Field 50 trees ha-1- LiDAR 10m cell	$Y = 0.7862x + 3.6123$	0.1134	0	2.84	0.218
Predom. Ht - Field 100 trees ha-1- LiDAR 10m cell	$Y = 0.5929x + 5.7684$	0.0908	0	2.2737	0.0196
Field stem count vs LiDAR stem count (NE Victoria)	$y = 0.513x + 73.55$	0.2396	0.0447	130.5565	0.5794

**Table 65: LiDAR return density at different height thresholds for Injune plots.**

<b>PLOT ID</b>	<b>Plot Area (m<sup>2</sup>)</b>	<b>All Returns</b>	<b>All returns density (m<sup>2</sup>/ret)<sup>a</sup></b>	<b>Ground returns</b>	<b>Ground return density<sup>a</sup></b>	<b>Canopy returns 0.5m+</b>	<b>Canopy returns 2m+</b>	<b>Canopy 2m+ return density<sup>a</sup></b>
23-15	2,568	4,041	0.64	2,230	1.15	1811	1642	1.56
23-16	2,604	3,760	0.69	2,647	0.98	1113	1047	2.49
23-20	2,428	3,622	0.67	2,731	0.89	891	832	2.92
23-24	2,402	3,489	0.69	2,026	1.19	1463	1229	1.95
58-24	2,401	4,195	0.57	3,459	0.69	736	667	3.60
58-29	2,370	6,051	0.39	4,300	0.55	1751	1505	1.57
59-27	100	220	0.45	209	0.48	11	4	25.00
59-28	100	156	0.64	108	0.93	48	8	12.50
81-8	1,544	2,906	0.53	1,653	0.93	1253	1221	1.26
81-11	2,615	4,996	0.52	2,261	1.16	2735	2629	0.99
81-16	2,403	4,699	0.51	2,390	1.01	2309	2254	1.07
83-12	2,496	4,759	0.52	3,508	0.71	1251	882	2.83
83-20	2,456	4,393	0.56	3,068	0.80	1325	1265	1.94
111-12	2,756	5,406	0.51	1,855	1.49	3551	3452	0.80
111-18	2,465	5,335	0.46	2,933	0.84	2402	2367	1.04
114-04	2,501	3,130	0.80	1,988	1.26	1142	1016	2.46
114-12	2,411	4,750	0.51	3,528	0.68	1222	935	2.58
124-06	2,507	4,392	0.57	2,694	0.93	1698	1568	1.60
124-19	2,371	6,887	0.34	4,499	0.53	2388	2253	1.05
131-18	2,602	8,704	0.30	7,386	0.35	1318	1295	2.01
138-16	2,501	4,643	0.54	2,905	0.86	1738	1528	1.64
138-21	2,483	5,212	0.48	3,569	0.70	1643	1606	1.55
142-02	2,399	7,724	0.31	6,415	0.37	1309	1280	1.87
142-13	2,549	6,886	0.37	5,751	0.44	1135	1113	2.29
142-18	2,528	6,313	0.40	5,091	0.50	1222	1209	2.09
142-20	2,535	3,948	0.64	2,872	0.88	1076	1040	2.44
144-13	2,439	2,458	0.99	1,718	1.42	740	721	3.38
144-19	2,527	6,593	0.38	4,823	0.52	1770	1638	1.54
148-01	2,548	5,027	0.51	2,014	1.27	3013	2849	0.89
148-16	2,342	4,146	0.56	1,883	1.24	2263	1556	1.51
148-21	2,420	6,186	0.39	4,648	0.52	1538	1450	1.67
148-29	2,608	6,390	0.41	3,808	0.68	2582	2251	1.16
mean	2,037	3,637	0.57	2,353	0.88	1,284	1,168	3.77

a – return density is the nominal area spacing per single return (on average). Therefore a density value of 0.57 is 1 return per 0.57 m<sup>2</sup>

Table 66: LiDAR return density at different height thresholds for NE Victorian plots.

PLOT ID	Plot Area (m <sup>2</sup> )	All Returns	All returns density (m <sup>2</sup> /ret) <sup>a</sup>	Ground returns	Ground return density <sup>a</sup>	Canopy returns 0.5m+	Canopy returns 2m+	Canopy 2m+ return density <sup>a</sup>
8	943	2,369	0.40	1,374	0.69	995	950	0.99
99	943	994	0.95	662	1.42	332	314	3.00
119	853	2,083	0.41	1,204	0.71	879	866	0.99
169	898	1,273	0.71	645	1.39	628	616	1.46
186	876	1,183	0.74	747	1.17	436	419	2.09
212	990	2,737	0.36	1,405	0.70	1,332	1,262	0.78
216	886	2,345	0.38	1,379	0.64	966	819	1.08
220	914	3,568	0.26	2,034	0.45	1,534	1,471	0.62
309	904	1,062	0.85	806	1.12	256	256	3.53
313	874	1,311	0.67	639	1.37	672	653	1.34
382	795	1,048	0.76	680	1.17	368	363	2.19
391	1,143	2,828	0.40	782	1.46	2,046	1,690	0.68
459	897	2,582	0.35	1,339	0.67	1,243	1,082	0.83
463	873	2,368	0.37	864	1.01	1,504	992	0.88
467	905	2,381	0.38	614	1.47	1,767	1,410	0.64
471	855	1,080	0.79	410	2.08	670	609	1.40
550	907	1,295	0.70	124	7.32	1,171	1,115	0.81
554	1,009	1,396	0.72	333	3.03	1,063	972	1.04
558	890	1,313	0.68	775	1.15	538	534	1.67
562	818	1,000	0.82	566	1.45	434	398	2.06
573	736	876	0.84	310	2.37	566	487	1.51
603	909	2,580	0.35	922	0.99	1,658	1,596	0.57
mean	901	1803	0.59	846	1.54	957	858	1.37

a – return density is the nominal area spacing per single return (on average). Therefore a density value of 0.59 is 1 return per 0.59 m<sup>2</sup>

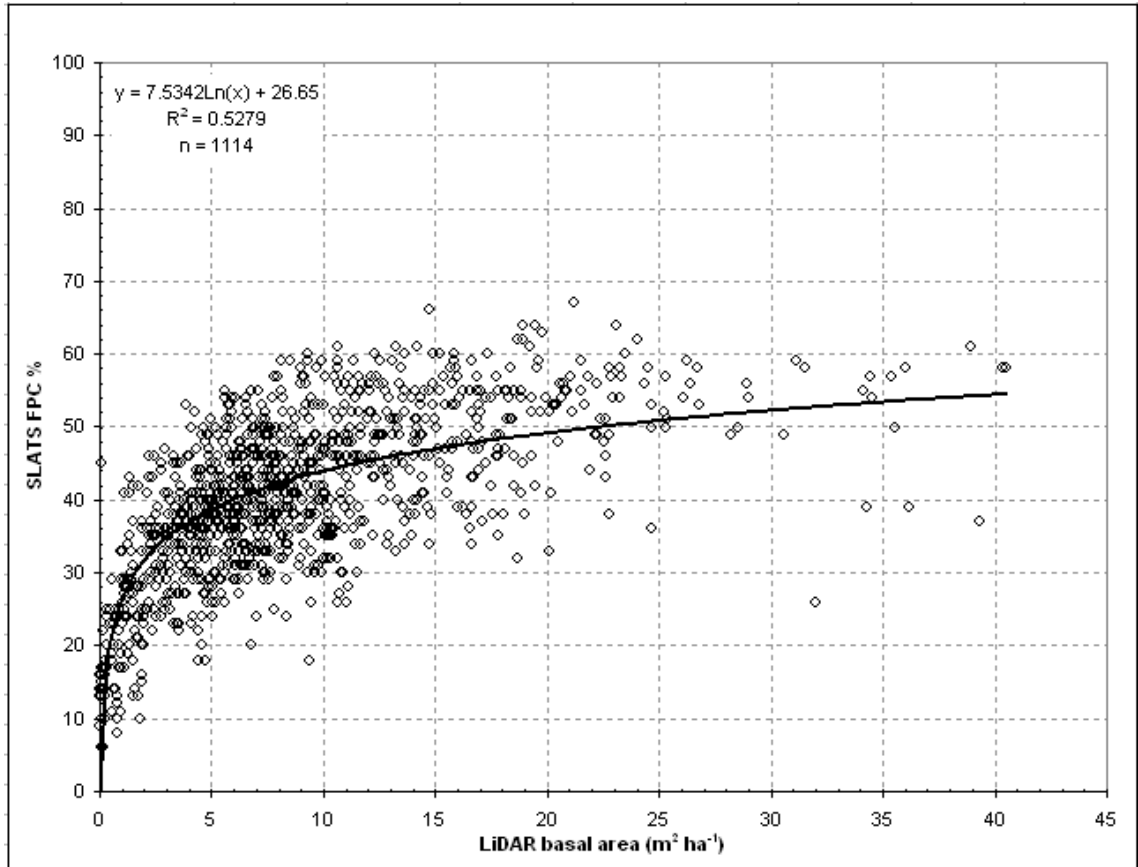


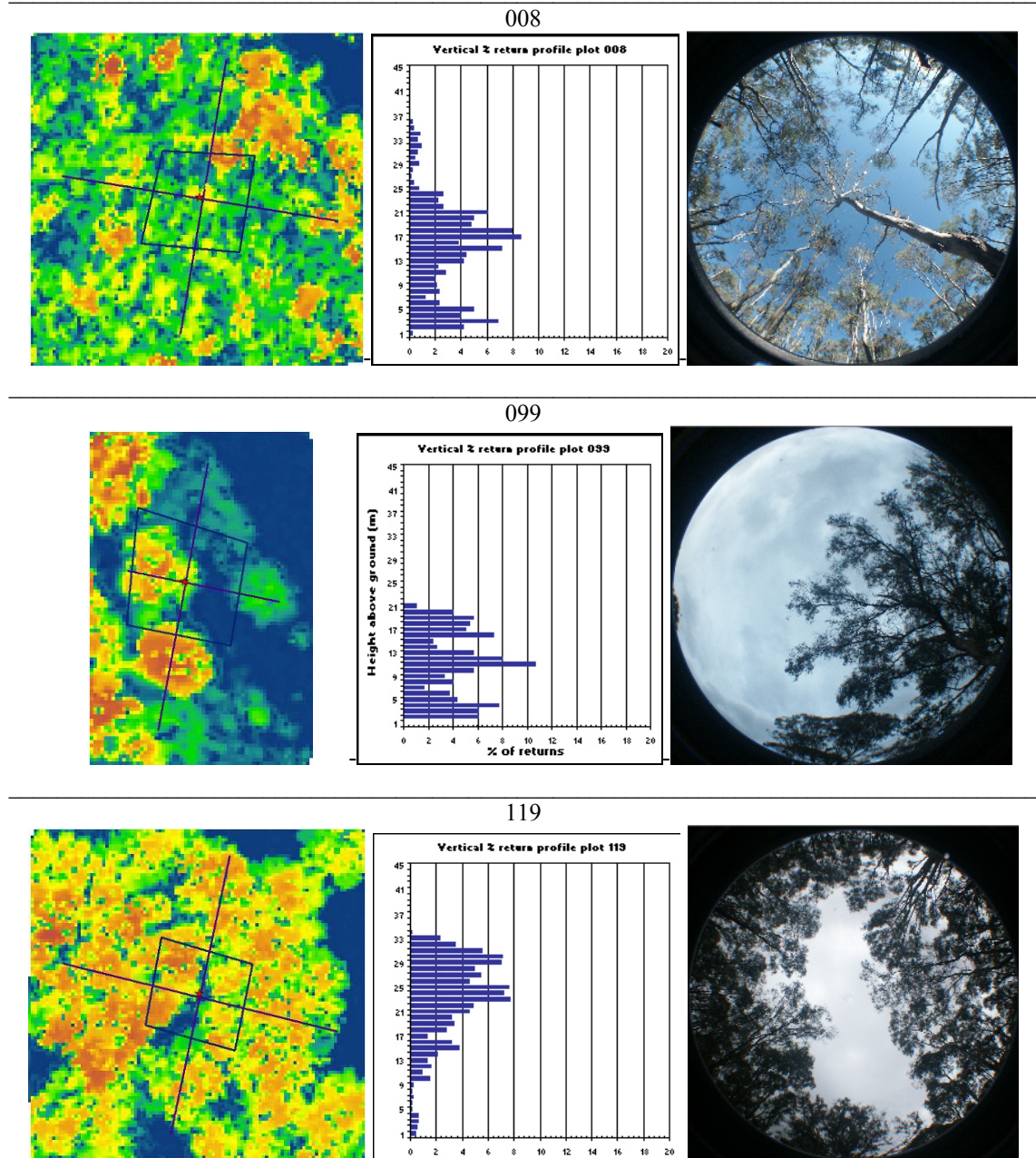
Figure 116: LiDAR derived tree stem basal area (per pixel) versus SLATS FPC, for 1114 Landsat pixels in 12 PSUs at Injune.



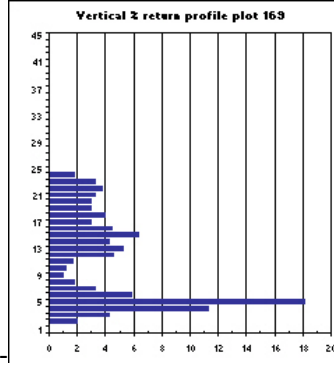
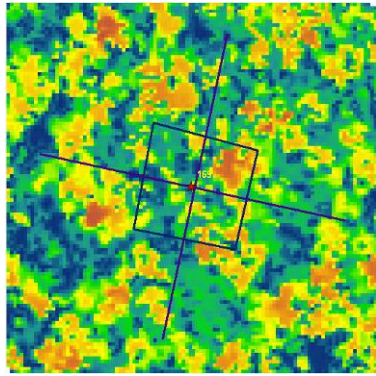
## APPENDIX B

### Plot data illustrations for NE Victoria.

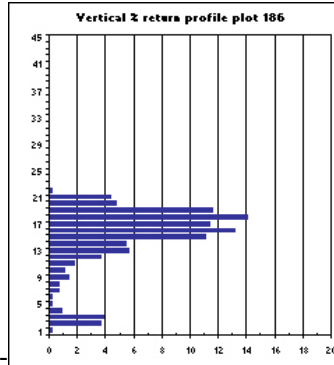
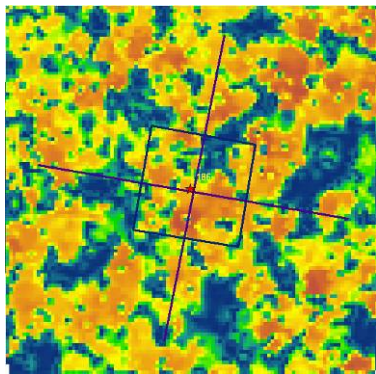
**Table 67: NE Victorian field plot data (left to right) - LiDAR CHM surfaces, LiDAR apparent vertical profiles, and plot centre hemispherical photos. With CHM surfaces dark blue is ground, red-brown is tallest canopy. Refer to LiDAR profile for respective heights (m).**



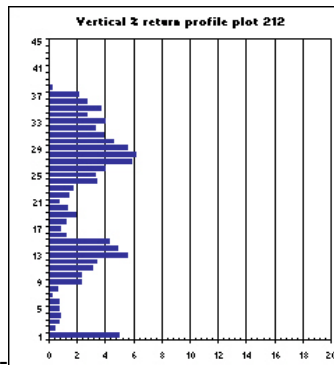
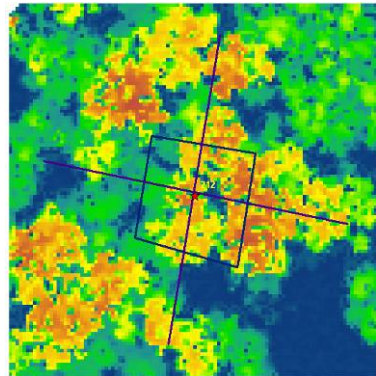
169



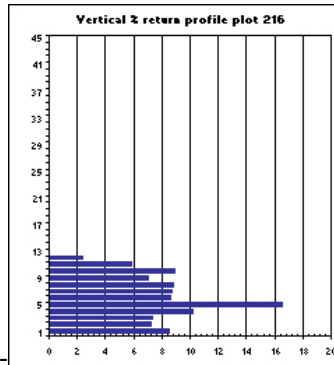
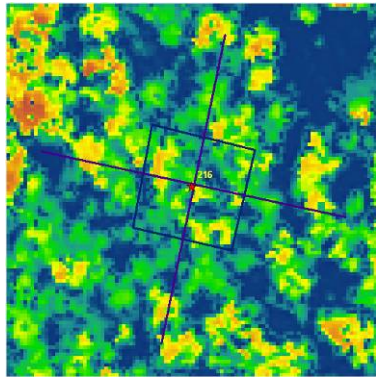
186



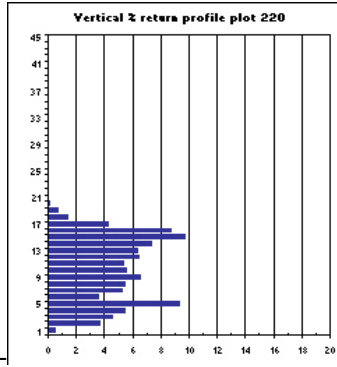
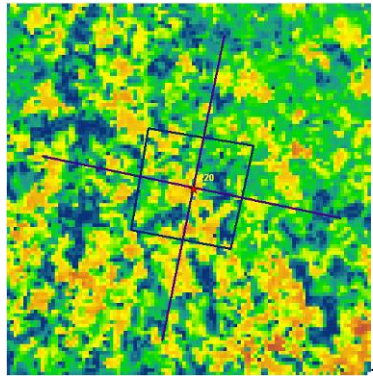
212



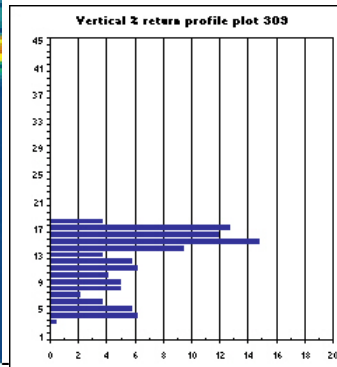
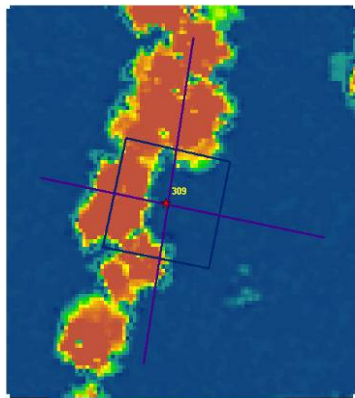
216



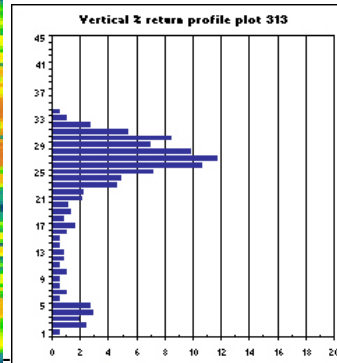
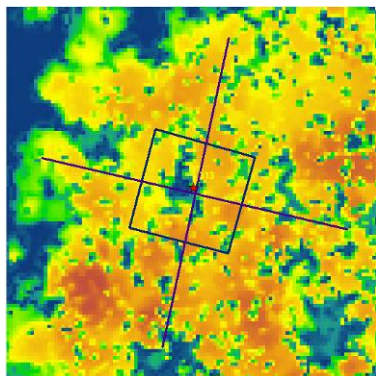
220



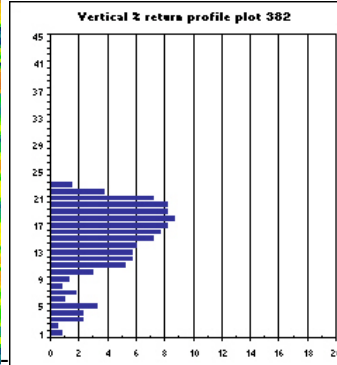
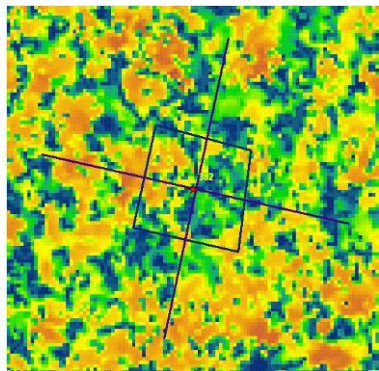
309



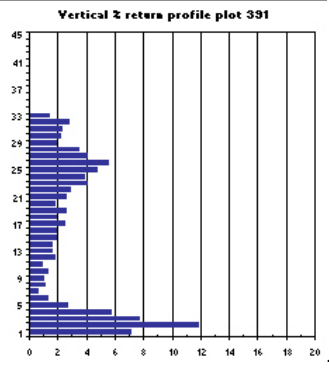
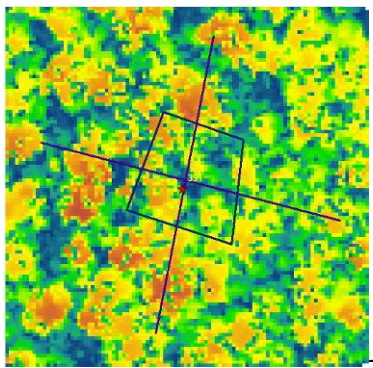
313



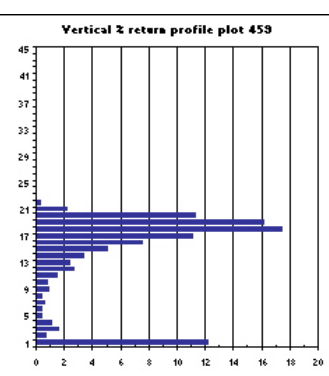
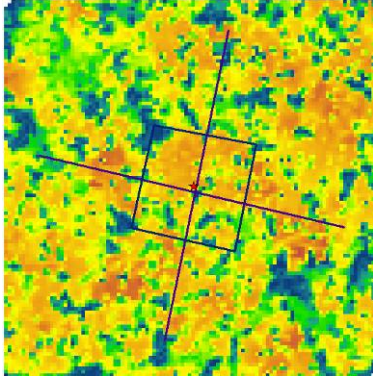
382



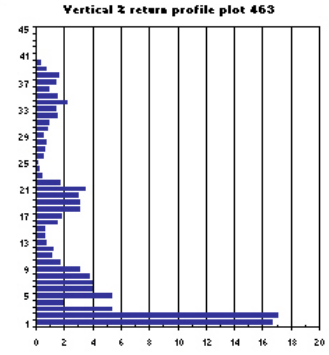
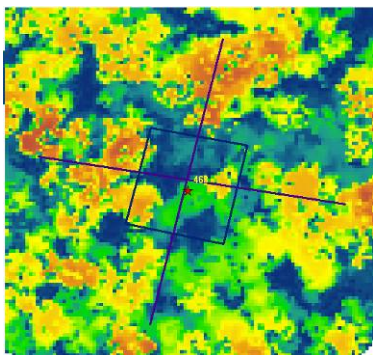
391



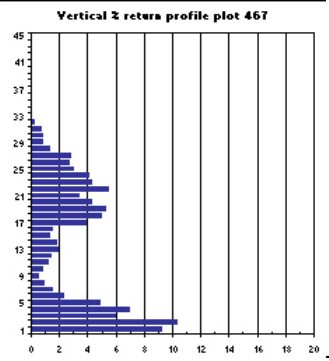
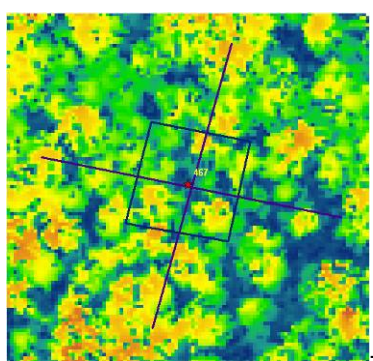
459



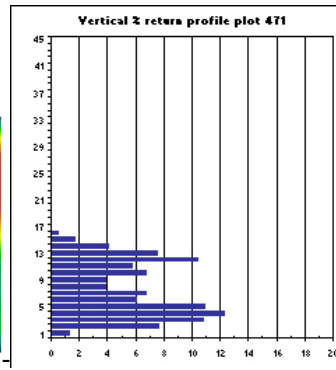
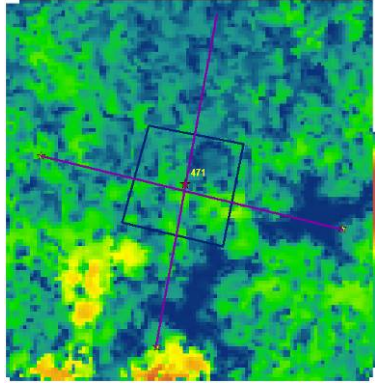
463



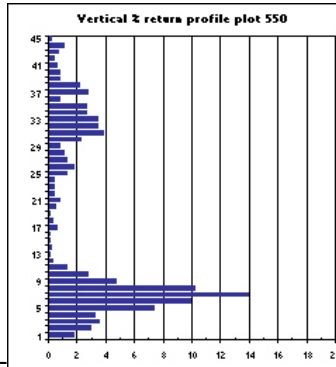
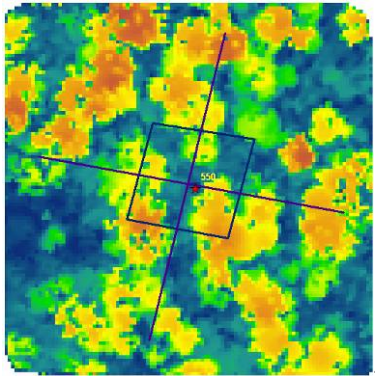
467



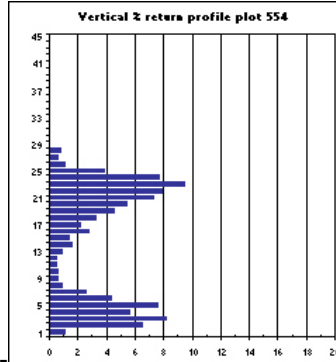
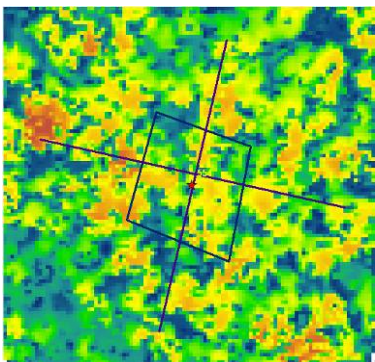
471



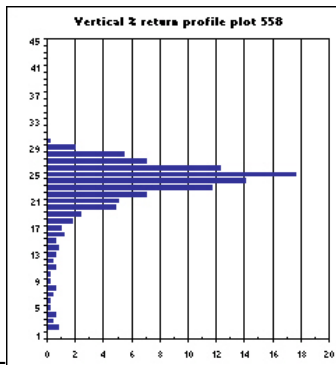
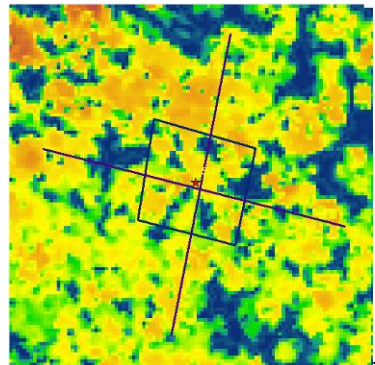
550



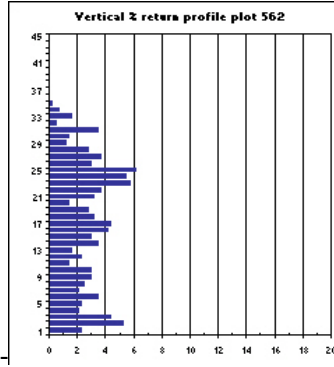
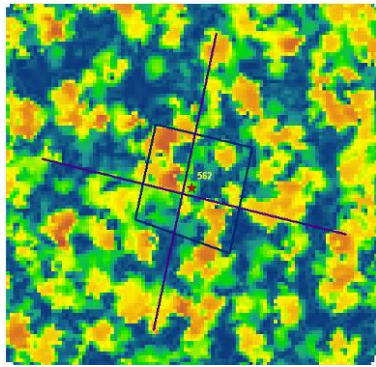
554



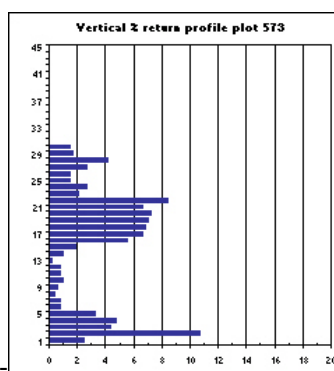
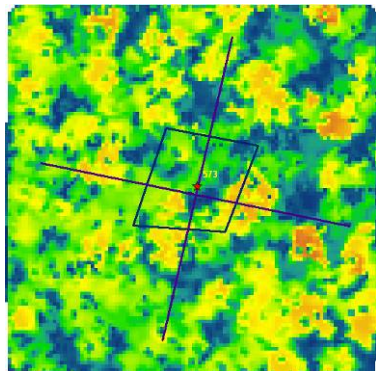
558



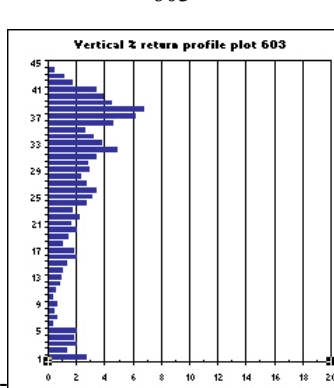
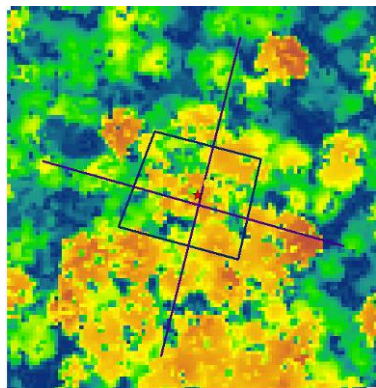
562



573



603



## APPENDIX C

---

### List of Published Papers

List of published papers that appear in this appendix:

- Lee, A., Chikumbo, O., Davey, S. and Tickle, P. K. (2001) Enhanced visualisation capability for forest management optimization results. IN Ghassemi, F., Post, D., Sivapalan, M. and Vertessy, R. (Eds.) *Proceedings International Congress on Modelling and Simulation*. Canberra, Australia, December 2001.
- Lee, A., Lucas, R. and Brack, C. (2004) Quantifying vertical forest stand structure using small footprint LiDAR to assess potential stand dynamics. *International Archive of Photogrammetry, Remote Sensing and Spatial Information Sciences*, 36, 213-217.
- Tickle, P. K., Lee, A., Lucas, R. M., Austin, J. and Witte, C. (2006) Quantifying Australian forest floristics and structure using small footprint LiDAR and large scale aerial photography. *Forest Ecology and Management*, 223, 379-394.
- Lucas, R. M., Lee, A. C. and Williams, M. L. (2006) Enhancing SAR simulations using LiDAR for understanding the relations between forest structure and SAR imagery. *IEEE Transactions on GeoScience and Remote Sensing*, 44, 2736-2754.
- Lee, A. C. and Lucas, R. M. (2007) A LiDAR-derived Canopy Density Model for Tree Stem and Crown Mapping in Australian Forests. *Remote Sensing of Environment*, 111, 493-518.
- Lucas, R. M., Lee, A. C., and Bunting, P.J. (2008) Retrieving forest biomass through integration of CASI and LiDAR data: *International Journal of Remote Sensing* (in press)

## Statement of Author Contribution to Published Papers

In the majority of my thesis I have sought to not replicate the text of published papers where I have been primary or second author. This is to reduce duplication and the overall length of the thesis, and because the published work has already been peer reviewed. Where components of the thesis have been replicated (for example, study area and field data description), this has been included as it is of direct relevance to the results and discussion chapters. Where I have relied on text from the papers where other co-authors have contributed methodology, data or results, this is clearly stated in the text. For example, in Chapter 1, I clearly state that the sampling designs are the product of existing research projects, and my research seeks to use the results of the projects, with any descriptions of the project experimental design (e.g. landscape sampling strategy) provided to allow discussion of the relative strengths of the design based on the results I have generated.

The following table provides a detailed description of the different contributions I have made in each of the published papers that I have included in this Appendix, and from which I refer to in my thesis.



<b>Paper and Authors</b>	<b>Conception</b>	<b>Experimental Design</b>	<b>Methods</b>	<b>Analysis</b>	<b>Writing</b>
Enhanced Visualisation Capability for Forest Management Optimisation Results (2001) A. Lee, O. Chikumbo, S Davey, P. K. Tickle.	Alex Lee developed the conceptual basis for comparing a range of LiDAR visualisation methods and assessment of utility.  The other authors developed the idea to apply the methods to the visualisation of forest management optimisation modelling results	Alex Lee was the primary developer of the comparison of the different visualisation methods, particularly with respect to LiDAR visualisation products.  The other authors provided input into how they might be utilised in forest management scenarios.	Alex Lee undertook all the methods for LiDAR visualisation.  R.M. Lucas and P K. Tickle, as part of the Injune collaborative project, primarily undertook the SVS modelling.	Alex Lee did the primary analysis and visual assessment.	Alex Lee did the first draft. This was substantially edited by O. Chikumbo. All authors provided subsequent input to final paper.
Quantifying vertical forest stand using small footprint LiDAR to assess potential stand dynamics. (2004) A. Lee, R. Lucas, C. Brack	Alex Lee developed the idea to integrate LiDAR and field information within a 3D voxel matrix, based on the application of voxels in the literature.  R M. Lucas provided input on the requirements for 3D SAR simulation modelling and associated concepts from the literature.	Alex Lee primarily developed the experimental design, with iterative input from co-authors, especially to refine some components.	Alex Lee undertook all the methods.	All analysis was undertaken by Alex Lee	Alex Lee did the first draft. Both co-authors contributed to edit, reduce and improve the text. Co-authors also provided input for background information, and broad application of results (e.g. carbon sequestration).
Quantifying Australian forest floristics and structure using small footprint LiDAR and large scale aerial photography	The conceptual design for the Injune collaborative project was developed by a range of people, with the landscape sampling and	The integrated sampling strategy was primarily developed by P. K. Tickle, R. M. Lucas and C. Witte	The statistical assessment of the sampling strategy was undertaken primarily by P. K. Tickle and R. M. Lucas. The LiDAR	Analysis of results was undertaken by all authors. Alex Lee and J. Austin compiled and tabulated the different results, as well as	R. M. Lucas and Alex Lee wrote the initial drafts. The other authors then contributed to edits and revision. R. M. Lucas and

<p>(2006) P.K. Tickle, A. Lee, R.M. Lucas, J. Austin, C. Witte</p>	<p>integration of LiDAR and aerial photography developed by P. K. Tickle.</p>	<p>Alex Lee provided primary input to LiDAR processing and reporting methodologies.</p>	<p>methodologies (including integration with aerial photography results) were primarily undertaken by Alex Lee, and by J. Austin at the direction of Alex Lee. The aerial photography was initially interpreted by the Queensland govt team headed by C. Witte.</p>	<p>initial analyses. The other authors subsequently interpreted the results in the context of the aims of the paper. P K. Tickle and R. M. Lucas primarily undertook the statistical assessments.</p>	<p>Alex Lee undertook the final edits and revision.</p>
<p>Enhanced simulation of Radar backscatter from forests using LiDAR and optical Data (2006) R. M. Lucas, A. C. Lee, M. L. Williams</p>	<p>R. M. Lucas primarily developed the idea (in consultation with co-authors) to integrate LiDAR derived forest stand representations with SAR simulation models.</p>	<p>M. L. Williams developed the SAR simulation models. Alex Lee developed the LiDAR derived forest stand representations. R.M. Lucas assisted with the integration of field data within the LiDAR modelling, and to link the forest representations to the SAR simulation models.</p>	<p>Alex Lee undertook all the LiDAR related methods. The other authors undertook the SAR related methods. The LiDAR branch models were cross-validated after processing through SAR simulation. Where anomalous results were observed in the modelled SAR image, the LiDAR branch models were checked and updated if found to be outside field data estimates.</p>	<p>Analysis and interpretation of LiDAR derived forest simulation was primarily done by Alex Lee, with consultation of other authors. The SAR components of the analysis and interpretation were undertaken by the other two authors.</p>	<p>Authors wrote their own sections based on their relative expertise (e.g. Alex Lee wrote the LiDAR related sections). All authors contributed equally to final editing and review.</p>
<p>A LiDAR-derived canopy density model for tree stem and crown mapping in Australian forests (2007) A. C. Lee, R. M. Lucas</p>	<p>Building on the concepts developed in the 2004 paper, and 2006 SAR simulation paper, Alex Lee was the primary driver to further refine the LiDAR canopy density modelling, to include individual crown</p>	<p>Alex Lee primarily developed the experimental design.</p>	<p>Alex Lee undertook all the methods.</p>	<p>Alex Lee undertook all the analysis. R M. Lucas assisted in the interpretation of point density comparison statistics.</p>	<p>Alex Lee wrote the majority of the paper. Significant editorial input was provided by R. M. Lucas, mainly to reduce the length of the paper.</p>

	delineation and stem mapping applications.				
Retrieving Forest Biomass through Integration of CASI and LiDAR data (2008) R. M. Lucas, A. C. Lee, P. J. Bunting	R.M. Lucas primarily developed the concept of integrating CASI and LiDAR, in consultation with the co-authors.	Alex Lee undertook all LiDAR related research design, based on the 2007 LiDAR paper. The other authors did the hyperspectral research design.	Alex Lee undertook all the LiDAR related methods. The other authors implemented the hyperspectral related methodology. All authors contributed equally to the integration methodology.	All authors contributed equally to the integration analyses, with particular emphasis on their area of expertise (e.g. Alex Lee for LiDAR, other authors for hyperspectral, all authors for biomass).	Each author wrote the section relating to their expertise (e.g. Alex Lee for LiDAR section). All authors contributed to editing and final revision.

# Enhanced Visualisation Capability for Forest Management Optimisation Results

A. Lee<sup>a</sup>, O. Chikumbo,<sup>b</sup> S Davey<sup>a</sup>, and P. K. Tickle.<sup>c</sup>

<sup>a</sup>*Bureau of Rural Sciences, PO Box E11, Kingston, ACT, 2604 Australia. (Alex.Lee@brs.gov.au, Stuart.Davey@brs.gov.au)*

<sup>b</sup>*The Swedish University of Agricultural Sciences, Department of Forest Resource Management and Geomatics, Umeå S-901 83, Sweden. (Oliver.Chikumbo@resgeom.slu.se)*

<sup>c</sup>*Geospatial Systems, Raytheon Australia Pty Ltd, 15 National Circuit, Barton ACT 2600 Australia (ptickle@raytheon.com.au)*

**Abstract:** Despite the adoption of heuristic search algorithms for optimising large-scale spatial harvesting mainly constrained for socio-economic and environmental concerns, visualisation of landscape outcomes is still in the domain of 2-D GIS maps. Issues on visual impact due to harvesting, or forest structure for habitat niches, may not necessarily become obvious from a basic 2-D GIS map, making 3-D visualisation highly desirable. This paper looks at the potential use of airborne scanning lidar for visualisation that can be used to view modelled spatial harvesting scenarios from optimisation models and thus provide decision-makers with a capability to qualitatively improve on any optimisation scenario. Two case studies are looked at in this paper, to verify the visualisation capabilities of airborne scanning lidar.

**Keywords:** Airborne scanning lidar, Spatial harvesting, 3-D visualisation

## 1. INTRODUCTION

In the last ten to fifteen years, forest analysts have made progress in modelling the forest ecosystem in tandem with the changing views and concerns raised by the public, governments and other private bodies in regards to the sustainability of forest management practices. Not only are forests managed for timber, but also for a myriad other entities that in themselves contribute equally in defining the complete forest ecosystem. Today we talk of ‘ecosystem management’, a terminology widely used in the United States, or ‘sustainable forest management’, which all mean the utilisation of forest resources in a manner that would not lead to depletion of any of the components that makeup the ecosystem in question. Such a situation would cripple the forest ecosystem in such a way that it loses its capability to self-repair in the event of anthropogenic or natural disturbances.

In terms of modelling the forest ecosystem, there has been a gradual shift from basic wood or timber models integrated with linear programming for scheduling harvesting over a prescribed time horizon, to more complex ways of accounting for spatial harvesting such that non-timber values are catered for. Because of the limitations of linear

programming in its inability to solve problems of 0-1 integer type (combinatorial) for resolving land use or management action of neighbouring land parcels, other linear programming variants have been put to test, however, fraught with size problems. Mixed-integer linear programming comes to mind and handles these kinds of problems well, but only for small problems. Also when constraints are tight, the problem can be difficult to formulate, making the search hard to find an optimal solution. The Boise Cascade Corporation has tackled the problem in another way by linking a linear programming formulation, using FORPLAN [Barber and Rodman, 1990] and a GIS package, ARC/INFO [ESRI, 2001] to produce an application called Spatial Feasibility Test (SFT). A linear programming formulation is resolved using FORPLAN and the solution is ‘disaggregated’ by a process that attempts to resolve adjacency violations of neighbouring polygon stands [Carroll et al., 1995]. The method is interactive, and FORPLAN is run many a time and at each run altering the constraints until such a time when the spatial constraints are satisfied. Given that SFT is deterministic and depends on the order of the list of polygon stands, each FORPLAN solution is tested against different lists, making the process time-consuming.

A quicker way to resolve these problems has been the use of heuristic search algorithms that are well known for their robustness in resolving large-scale combinatorial problems, although they are much harder to verify optimality. Since they are to be applied in situations where direct methods (such as linear programming) or enumerative methods (such as dynamic programming for exhaustive search) are difficult to apply, the goal becomes one of finding a solution that will improve the status quo rather than striving for optimality [Goldberg, 1989]. Some recent work has shown that heuristic search algorithms are now being applied although it will take years of monitoring the outcomes of implemented strategies derived from these models, to see whether they are indeed improving the status quo [Chikumbo et al., 2000; Lockwood and Moore, 1993; Van Deusen, 1999].

To aid spatial modelling, visualisation is an important part of this kind of modelling. Most of the work so far has been to link optimisation results to GIS layers such that the overall spatial impact can be seen. For example, the new FORPLAN version, SPECTRUM, can now be linked seamlessly to a GIS visualisation capability called SPECTRAVISION, which is an ESRI ArcView extension [Chikumbo et al., 1999]. That means at each time step in the optimisation, one can visualise the area extent that is harvested. Although this is quite essential, it is still inadequate for visualising forest stand structures which help to inform on habitat quality for fauna, identifying impact on recreational areas, visual impact of the forests and so on. The basic 2-D GIS maps would not suffice here, and 'enhanced 3-D visualisation' will go a long way in satisfying our needs.

This paper explores the capability of enhanced 3-D visualisation using airborne scanning lidar, as a potential tool for visualising optimisation results, such that further improvements are made to the spatial solution by qualitative means. This may also aid in reformulation of an optimisation problem. These days, forest analysts perform 3-D visualisation in commercial GIS packages by draping remotely sensed images over digital elevation models (DEMs). The information gleaned from this is only good for assessing visual impact from a myriad of forest management practices. However, the ability to visualise stand structure that would be invaluable for assessing animal habitat areas and enhance visual impact is not realised, as more information is required for this level of assessment. A more realistic representation of many elements within the 3-D landscape, for example trees and forests, becomes

essential, hence the combination of remotely sensed data and the airborne scanning lidar.

## 2. STUDY AREAS AND DATA CAPTURE

Two study areas were considered here, in the states of Queensland and New South Wales (NSW) of Australia. The primary study area covers 220,000 hectares of private and public land near Injune in central Queensland. Due to past and present agricultural and forestry management practices a wide range of regeneration and degradation stages exist, creating woodland communities that vary structurally. An associated study site covers two coastal forest compartments totalling nearly 400 hectares in the southern Hunter Region, New South Wales. Here State Forests of NSW have established a series of research sites located in native regrowth forest and hardwood plantation production forests with complex structural heterogeneity.

Airborne scanning lidar data were captured at the Injune and Hunter study sites on the week starting August 24<sup>th</sup> 2000 and May 28<sup>th</sup> 2001, respectively. Specific detail of the data capture can be found in Tickle et al., [2001]. Data were provided as ASCII text files, pre-processed into ground and vegetation returns, with an average sampling interval of <1m. At Injune, field data were gathered in 33 ground plots of 0.25ha. Within each plot, each tree over 10cm in diameter at breast height (DBH) was located and mapped, including various structural (canopy and trunk) components.

## 3. METHOD

Since the GIS programs store their information in databases, an optimisation solution can be integrated in a database, showing when, where and how much timber will be harvested, which areas will be preserved for fauna and flora conservation and so on. This information may then be displayed like a movie over a time-series in a GIS program as in SPECTRAVISION [Chikumbo et al., 1999], making it possible for the user to study the spatial effects of the solution in a visual manner. Combining this with a DEM and airborne scanning lidar would provide an enhanced 3-D visualisation, that would lead to an improved understanding of optimisation results, with the added advantage of further refining the solution qualitatively, such that it better suits the wildlife and visual impact issues.

The data preparation process for the enhanced 3-D visualisation is described below, based on the two study areas. This process basically involved visualising the lidar and other remotely sensed data, by using a combination of tools that included

ESRI ArcView, ARC/INFO, ArcGIS [ESRI 2000], ERDAS Imagine [ERDAS 2001] and ENVI & IDL products [Research Systems, 2001]. The DEMs used in the visualisation were generated in an involved way, that was automated by using a scripting language called AML in ARC/INFO and the steps in the process were as follows:

- The raw ASCII data (lidar) were converted to point data and first and last ground returns combined;
- A ground TIN (Triangulated Irregular Network) was generated with a 2m proximal tolerance;
- For each vegetation point, a height above the ground TIN surface was calculated. Ground points were assigned a height-above-ground value of zero;
- First return vegetation data were combined with ground data, and a combined TIN canopy/ground surface created with a 1m proximal tolerance; and
- Bare earth and canopy TINs were converted to 1m raster DEMs for analysis with other raster datasets. Vector contours were derived from raster DEMs.

During testing of the routines the TINs were visually checked to confirm correct classification of ground and vegetation returns. Estimates of canopy cover were generated by calculating the proportion of vegetation to ground hits within a specified cell size, and height range. ARC/INFO topogrid analysis routines were tested in the Hunter study area and they seemed to produce smoother terrain models, however quantitative assessment of the different processing methods is still to be carried out.

#### 4. RESULTS AND DISCUSSION

Visualisation of spatial harvesting results from an optimisation problem maybe carried out at different scales depending on the information requirements of the analyst. Issues on harvesting block sizes of a management area within specified upper and lower limits for each successive period over a planning horizon, can be visualised using 2-D maps. However, issues on access and stand structure are better handled using enhanced 3-D visualisation. This section describes visualisation at different scales using data from the two study areas, Injune and the Hunter Region.

The three scales are as follows;

- Tree level,
- Stand level (group of trees),
- Compartment level (group of stands).

#### 4.1 Tree Level Scale

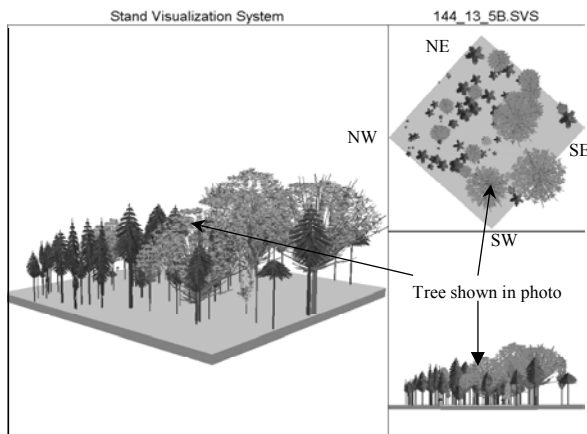
An initial attempt was made to visualise at one time-step, tree species, which would represent simulated harvested area, from a typical spatial harvesting optimisation problem. Stand Visualisation Software package (SVS), developed by the US Forest Service [McGaughly, 1997] was used to reconstruct field plot data for 3-D visualisation and assessment. Opportunities to identify and correct errors were realised, allowing for better interpretation of how the various sensors reported different canopy components and relative stand densities of the study plots. A lesson learnt here was that if we are to interpret spatial harvesting solutions in 3-D visualisation, carefully measured training areas from stands that have been previously prescribed similar management strategies, would be invaluable. Such information would then make it possible to simulate 3-D visualisation for the rest of the management area in question.



**Figure 1:** Digital photo of actual field plot portrayed in Figure 2. The view is from south-west looking north-east.

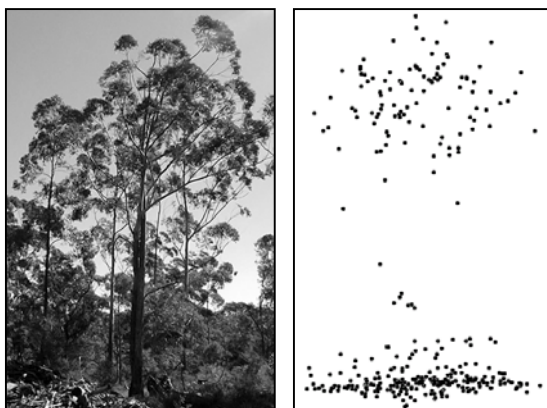
While SVS is useful for visualising stand-based data, it does not provide true representation of the Australian woodland forest. This is because the program was developed to cater for the coniferous forest in North America. However, with realistic tree location coordinates, it provides excellent relative positioning and density visualisation albeit not spatially linked to a coordinate system that enables integration with other GIS or remotely sensed data. Figure 1 illustrates one of the field plot sites at Injune. Each tree was visualised in SVS and this is shown in Figure 2.

It is obvious that the visualisation of the irregular nature of eucalypt canopies is not well represented in SVS. Adaptation of the tree models may rectify the problem, but it would be time-consuming. The outputs from SVS would also need to be changed such that they can be exported to other programs. The value of this approach was therefore limited.



**Figure 2:** 3-dimensional stand reconstruction of field plot data using SVS. The perspective view in the main window is from the south-west to the north-east (as per photo view).

Another option was to use ArcView 3D Analyst combined with lidar data. Lidar data were visualised using colour, which allowed us to differentiate first and last returns. Figure 3 illustrates the result of this visualisation, and compares the lidar return cloud with the actual tree as seen in the field (Hunter study site).



**Figure 3:** Single tree visualisation using lidar data and digital photo of same tree in the field.

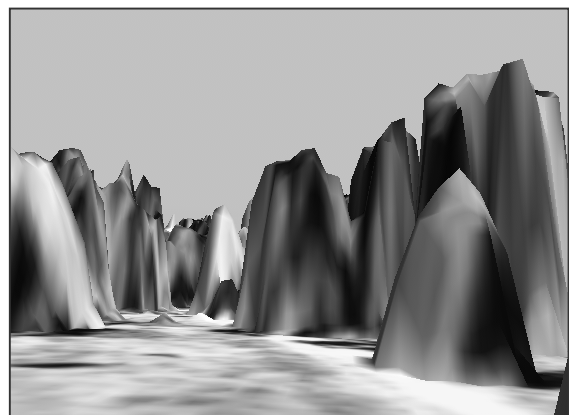
Lidar returns had been provided as pre-processed vegetation and ground returns. Further inspection of the returns, while out in the field, allowed differentiation of various canopy structural components. Pulses coded as vegetation first return corresponded to the outer canopy and some internal branches. Ground first returns corresponded to trunk, understorey vegetation, and some base ground points respectively. Vegetation last return pulses identified trunk and major internal branches, whereas ground last returns were generally all base ground points. Overall SVS proved better for quick initial assessments of tree density, species location, and general form based on height, due to the stylised nature of the tree output. However, ArcView allowed greater understanding of the actual tree form using lidar

data, as well as its position with respect to other trees in the stand and the surrounding terrain. Problems arose using this method in heavily stocked stands where many interlocking branches prevented individual tree recognition.

## 4.2 Stand Level Scale

While improving field data can provide significant enhancement to models, it is costly and time-consuming. Using stand based data we can extrapolate over much larger areas, and so realise more of the spatial variability that is not evident at the tree level scale. Using a sampling strategy combining lidar with other remotely sensed data such as interpreted aerial photography or high resolution hyperspectral data, we can enhance stand measurements of height, canopy cover, species composition, growth stage, disturbance and so on.

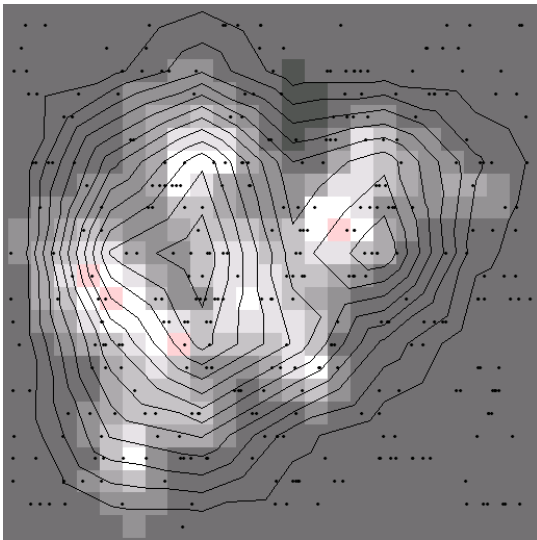
An example of stand-based improvements through lidar, as well as visualisation of the results is illustrated in Figure 4, which demonstrates the combined ground with canopy model, with a 1:4000 aerial photo draped over it.



**Figure 4:** Lidar derived canopy and terrain model (1m resolution) with draped 1:4000 aerial photo.

Realistic location and spatial extent of tree canopies are achieved, but not accurate representation of canopy form or volume. As with most GIS based visualisation packages, photo-realistic effects are limited by the resolution of draped data, especially the terrain when viewed closely. Using lidar data, improvements were made in representing the range of tree and stand forms found in forests and woodlands. However, a number of significant issues still exist in the application of terrain surface models for lidar data analysis at the stand level scale. With the 1-2m proximal tolerance used, we observed that approximately a third of all lidar returns were utilised in TIN or DEM generation. This was due to a large number of returns and redundancies in the significance of returns for representation of a

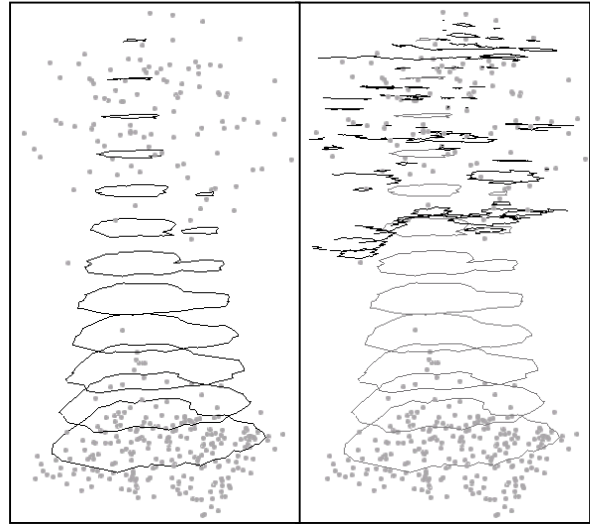
surface. Note that many of these returns were from internal canopy hits and were not required for outer canopy edge volume rendering. A more serious issue was the loss of returns from under a canopy that resulted in a tree model resembling a blanket draped over a tree as seen in Figure 4. Figure 5 illustrates an extreme example of this process for a single tree in the Hunter study region (see Figure 3). The lighter areas of the grid represented high points in the canopy, and gaps in the canopy were clearly identified. Lidar returns, from which the grid was derived, are shown as black points. The contours derived from the grid were at 2m intervals for clarity. In planimetric view the contours adequately described the shape and extent of the canopy, and showed two distinct portions to the canopy.



**Figure 5:** Canopy contours derived from 0.5m interpolated grid (background).

When the contours are displayed in 3-D (as illustrated in Figure 6, left), it became clear that they did not represent the correct shape of the canopy when compared to the lidar cloud. The contours representing the extent of the canopy were not at their correct heights. As the DEM is being generated, ground returns have more influence on the final cell height that is calculated for the edge of the canopy. As a result of this height averaging, the cells at the outer edge of the canopy are assigned the relative height of between 1-5m, depending on the shape. Trees and stands are therefore “grown” from the ground up such that a generalised conical shape is created. When these virtual trees are displayed in 3-D, the canopy does not assume the spherical or irregular ellipsoidal shape of the eucalypt trees. Canopy models developed in this way tend to be dominated by spikes, where the high (but sometimes not the highest) parts of the canopy exert the greatest influence. It was observed that

this effect occurred in both TIN and raster derived elevation models. We then conducted an analysis that used raw point data at 2m height intervals and created a stacked set of surfaces within the canopy. Contours were generated from these surfaces, and were stacked in 3-D to give a better representation of canopy shape (see Figure 6, right). These stacked contours are only viewed in 3-D as established cartographic rules would be violated due to multiple contours crossing in a planimetric view.



**Figure 6:** Left - Canopy contours from Figure 5 shown in 3-D, with the lidar return cloud. Right - Potential canopy contours (in black) derived from surfaces generated at 2m intervals.

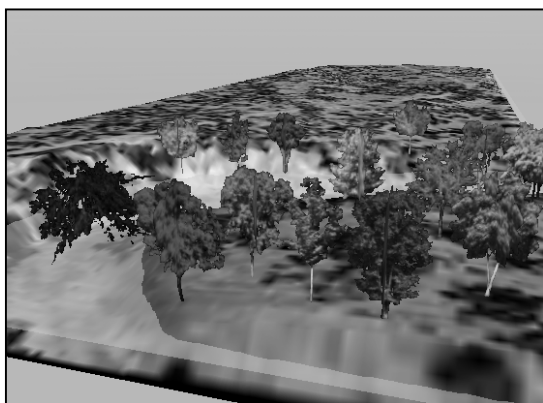
A visual assessment of the tree indicated that an ellipsoid shape best described the canopy. Canopy volume was then calculated using actual crown dimensions in the  $x$ ,  $y$  and  $z$  planes. This was then compared to the volume derived from the TIN surface for the same tree. It was found that the TIN volume was 40% of the ellipsoid volume, indicating that current canopy DEM's may not be adequate for volume calculations, and therefore biomass estimates. Existing biomass calculations are often constrained when using tree height due to trees expanding in canopy width rather than height after a certain age. Canopy volume would then allow improved biomass estimates at the stand level scale as both tree height and canopy width would be used. We will be using Research Systems IDL to further refine the results of volume visualisations, thereby improving our canopy volume calculations and ultimately, biomass estimates.

#### 4.3 Compartment Level Scale

Accurate tree and stand-based parameters improve the quality of empirical models and subsequently harvested volume estimates. Existing 2-D map or



satellite images draped over simple terrain DEMs may prove inadequate to convince the public and/or experts that all spatial requirements for non-timber values are being met. At compartment level broad vegetation types are investigated using a tool such as ERDAS Imagine Virtual GIS. Imagine is noted for providing virtual tree models that have been created from digital photos of real trees. These tree models can be manually placed, or used with point or attribute polygon layers to populate a scene for more realistic density visualisations. These models are general in nature and do not convey the variety of forms observed in the study areas. Individual models can be scaled with respect to height, width and depth, but accurate portrayal of non-standard canopy dimensions cannot be done. Therefore, current landscapes that use points or polygons for automatically populating forests with trees will have tree species of the same dimensions. This does not reflect typical woodlands and forests in Australia. Figure 4 illustrates an example of virtual trees in a lidar derived DEM, and shows the few Australian virtual trees that are currently available.



**Figure 7:** Lidar derived ground terrain model with virtual trees arbitrarily placed.

These species are not indicative of the species found at the study sites. Height and shape of virtual trees are less than what's observed in reality.

## 5. CONCLUSION

This current work has demonstrated the potential of visualising stand structure (for optimisation results of spatial harvesting), information that is invaluable in determining viable animal habitat and visual impact. There are, however, hurdles still to be overcome, given that visualisation tools are not yet seamlessly linked with mainstream GIS software. Also computer programs such as BRYCE, by Corel Corporation will assist in designing tree forms that represent each species and environment, rather than the pre-generated tree forms in visualisation programs.

## 6. REFERENCES

- Barber, K.H. and S.A. Rodman, FORPLAN: the marvellous toy, *Journal of Forestry* 88: 26-30, 1990.
- Carroll, B., V. Landrum, and L. Pious, Timber Harvest Scheduling With Adjacency Constraints: Using ArcInfo To Make FORPLAN Realistic, ESRI User Conference, <http://www.esri.com/library/userconf/proc95/to300/p299.html>, 1995.
- Chikumbo, O., R.H. Bradbury, and S. Davey. Large-scale ecosystem management as a complex systems problem: multi-objective optimisation with spatial constraints. In: *Applied Complexity-From Neural Nets to Managed Landscapes*. S. Halloy and T. Williams (eds), New Zealand Institute for Crop & Food Research Ltd, Christchurch, New Zealand. p124-155, 2000.
- Chikumbo, O., D. Bush and S. Davey, Trial of SPECTRUM and SPECTRAVISION as additional tools for scheduling timber harvesting in the Eden Management Area, *Australian Forestry* 62(2): 139-147, 1999.
- ERDAS, Information on ERDAS Imagine Virtual GIS, located at <http://www.erdas.com>, 2001.
- ESRI, Information on ArcView 3-D Analyst and ArcGIS 8.1, <http://www.esri.com/>, 2001.
- Golberg, D.E. *Genetic Algorithms in Search Optimisation and Machine Learning*, University of Alabama. Addison Wesley Longman, Inc., 1989.
- Lockwood, C. and T. Moore, Harvest scheduling with spatial constraints: a simulated annealing approach, *Canadian Journal of Forest Research*, 23:468-478, 1993.
- McGaughly, R.J., Techniques for visualizing the appearance of timber harvest operations. In *Forest operation for sustainable forests and health economies*. 20<sup>th</sup> Annual meeting of the Council for Forest Engineering, Rapid City, SD. 10p, 1997.
- Research Systems, Information on ENVI & IDL located at <http://www.rsinc.com/products>, 2001.
- Tickle, P. K., C. Witte, A. Lee, R.M. Lucas, K. Jones, and J. Austin, Use of Airborne Scanning Lidar and Large-scale Photography within a Strategic Forest Inventory and Monitoring Framework Proceedings IEEE Int. Geoscience and Remote Sensing Symposium, University of New South Wales, Australia, 2001.
- Van Deusen, P. C., Multiple solution harvest scheduling, *Silva Fennica*, 33(3): 207-216, 1999.

# QUANTIFYING VERTICAL FOREST STAND STRUCTURE USING SMALL FOOTPRINT LIDAR TO ASSESS POTENTIAL STAND DYNAMICS.

A. Lee<sup>a,\*</sup>, R. Lucas<sup>b</sup>, C. Brack<sup>a</sup>

<sup>a</sup>School of Resources, Environment and Society, Australian National University, Canberra, ACT 0200, Australia

<sup>a</sup>Cooperative Research Centre for Greenhouse Accounting GPO Box 475, Canberra, ACT, Australia  
alex.lee@anu.edu.au, cris.brack@anu.edu.au

<sup>b</sup>Institute of Geography and Earth Sciences, The University of Wales, Penglais Campus, Aberystwyth, Ceredigion, SY23 3DB, UK.  
email: rml@aber.ac.uk

**KEY WORDS:** LiDAR, apparent vertical profiles, 3D modelling, forest stand dynamics

## ABSTRACT:

The vertical distribution of plant elements (e.g., foliage and wood) within a forest can yield important information on stand structure, dynamics and growth stage but such information is often difficult to acquire across landscapes using traditional methods of field survey and aerial photograph interpretation. Recent advances in airborne laser scanning (ALS), however, have facilitated rapid assessment of stand height and cover to levels of accuracy considered acceptable for forest inventory and management. A few studies have extended this analysis to the descriptions of growth stage and retrieval of biomass, particularly in complex forest environments. However, current research has raised issues as to how well the vertical profile can be represented and whether the relative amounts of over and understorey can be quantified accurately. Focusing on subtropical open forests and woodlands, in central Queensland, Australia, this paper provides a better insight into how small footprint Light Detection and Ranging (LiDAR) sensor data can be used to create apparent vertical profiles to describe aspects of vertical stand structure (e.g., overstorey/understorey) and also infer broad successional or growth stages. Such profiles were integrated with field measurements within a common reference matrix (based on 1 m cubes), thereby providing spatially explicit tree/crown maps in three dimensions and allowing validation of those generated from LiDAR. Such interpretations, as well as enhancing forest information retrieval, were considered important in the interpretation of other forms of remote sensing data, including radar and optical data. The conceptual basis for this integration method is outlined with an example utilising one field plot, and the role this method might play in quantifying stand dynamics and carbon sequestration is discussed.

## 1. INTRODUCTION

As a signatory to international agreements that include the United Nations Framework Convention on Climate Change (UNFCCC), the Kyoto Protocol and the Montreal Process, Australia is increasingly obliged to provide spatial and temporal information on ecosystem biomass, structure and community composition. Such information is particularly necessary for regional assessments of biological diversity and forest condition, supporting sustainable utilisation of ecosystems, and calculating greenhouse gas emissions associated with land use change and forestry (Burrows, *et al.*, 2002). In natural forests and woodlands, or those where a diversity of management practices are imposed, traditional point measurements of structure, biomass and species composition are difficult to extrapolate to the landscape because of the inherent complexity of the system. Such variability arises from natural disturbance; different processes of regeneration, and management practices occurring at a range of spatial and temporal scales. The difficulty in quantifying this inherent variability leads, therefore, to uncertainties in local to regional extrapolations of, for example, species diversity and carbon balances. The integration of remote sensing data, acquired by either airborne or spaceborne platforms, however provides a more appropriate mechanism for extrapolation as data of varying spatial and temporal resolution and information content can be combined.

In recent years, the integration of LiDAR with other forms of remote sensing data has attracted attention as the resulting accuracy of structural attributes (e.g., height, crown cover) are considered to be equivalent or greater than those obtained on

the ground. Furthermore, such data provides a unique perspective on the vertical as well as the horizontal distribution of plant elements and hence the structure, dynamics and growth stage of forest stands. Already, results of landscape-wide estimates of forest biomass generated through integration of LiDAR have been used to parameterise models of carbon partitioning (e.g., Hurtt *et al.*, 2004). LiDAR collected within a sampling framework has also been used to assist the calibration and validation of radar wave scattering models, thereby allowing a better understanding of microwave interaction with plant elements, and facilitating inversion of such models for quantitative mapping of forest structure and biomass (Lucas *et al.*, 2004).

Despite these advances, there is still a need to better understand how the LiDAR beam interacts with vegetation structural components and whether key structural attributes can be derived consistently and to acceptable accuracy levels. Such research is essential as studies, (e.g., Lovell *et al.*, 2003) have raised issues as to whether apparent vertical profiles are truly representative of forest structure. Specifically, such data may not be reflecting the actual vertical distribution of foliage as they may not penetrate to the understorey, particularly where canopy cover is dense, and may over-represent the dominance and closure of the overstorey. The return profile is also affected by the openness of tree crowns and canopies (which varies within and between species), differences in leafing and branching structures and also the number of strata within the vertical profile.

### 1.1 Conceptual basis for a common reference matrix

The broad aim of the study was to reproduce the 3D structure of the forest as required by some radar simulation models (e.g., Sun and Ranson, 1995) for parameterisation in the third dimension. Airborne Synthetic Aperture Radar (AIRSAR) data were acquired over the study area (see section 2.1) at the same time as the LiDAR, and parameterisation of 2D models utilising the concepts outlined in Durden *et al.*, (1989) has already been undertaken (Lucas *et al.*, 2004). The progression to 3D representations of forest structure from LiDAR was the next step, building on the concepts outlined by Sun and Ranson, (1995) and Lexer and Honninger, (2001), as illustrated in Figure 1. Specifically, the study aimed to a) reconstruct the canopy based on voxels (i.e., volumetric pixels) of varying dimension (e.g., 0.5, 1, 2 m<sup>3</sup>) with the view to ultimately populating these with quantitative estimates of structural or biomass attributes (e.g., foliage density, branch size, leaf angle distributions, moisture contents) and b) derive ground parameters (e.g., slope and surface roughness) from the LiDAR ground returns. Such attributes can then be used subsequently as input to models such as that described by Sun *et al.* (2002), which simulate microwave interaction and attenuation through the canopy. Through this process, a better understanding of microwave interaction with stand elements can be obtained, thereby refining the understanding and interpretation of the SAR response in complex environments. The results presented in this paper illustrate the representations of the canopy at 1 m<sup>3</sup> as this resolution was considered optimal with respect to the average lidar return density.

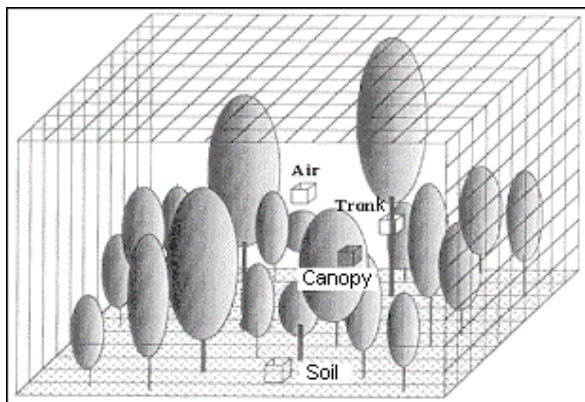


Figure. 1. Conceptual modelling framework for a 3D representation of a forest (after Sun & Ranson, 1995).

This paper presents a subset of the main project aims as outlined previously. Specifically, a conceptual method is presented that validates LiDAR derived apparent vertical profiles by integrating field and LiDAR data within a common reference matrix. This provides a spatially explicit and variable resolution three-dimensional (3D) map of LiDAR returns which can be used to give a better representation of their distribution and the relationship with the actual location of plant elements. Such maps allow better quantitative retrieval of forest structural properties (e.g., foliage, branch and trunk distributions) and hence facilitate the parameterisation of radar and potentially bi-directional reflectance (BRF) models that function in the third dimension. The use of profiles generated from LiDAR data for determining the growth stage of forest stands and hence carbon sequestration potential is described and compared with field

data, in order to investigate if the concepts outlined in Harding *et al.*, (2001) using full waveform large footprint LiDAR could also be undertaken with small footprint LiDAR.

## 2. METHODS

### 1.2 Study Area and Data Sources

The study was undertaken over a 220,000 hectare (ha) area containing diverse multi-aged woodlands and open forests located near Injune, central Queensland, Australia. The project design utilised a systematic sampling scheme with 150 Primary Sampling Units (PSUs), arranged on a 4km grid over the 37 x 60km study area. Each PSU was 500 by 150 metres (7.5 ha), where one metre resolution first/last return airborne LiDAR (footprint size 0.09m) was collected. PSUs were subdivided into 30 50 x 50 m Secondary Sampling Units (SSUs) numbered consecutively from 1 to 30. AIRSAR data were acquired across the entire study area. Detailed field surveys were undertaken in 31 square (0.25 ha) ground plots where complete tree maps were generated. These plots were selected using a stratified random field-sampling scheme within 13 selected PSU's, which sampled across broad community and structural types. Core attributes collected included species composition, forest structure, growth stage, biomass, disturbance, and land use. Tree map locations are derived from  $\pm 1$  metre GPS recording of plot corners and then a laser rangefinder distance and bearing to tree from the corner coordinate. A more detailed description of the sampling methods can be found in Tickle *et al.*, (2001) and Lucas *et al.* (2004). At the site, the mean annual rainfall is approximately 630 mm per year and the mean annual maximum temperature is 27°C (Bureau of Meteorology, 2004).

### 1.3 Parameterisation of the common reference matrix

Parameterisation of a common cubic reference matrix can be undertaken for a range of forest types, but this paper provides an example by focusing on a plot in mixed species forest (referred to as SSU 124\_19) dominated by white cypress pine (CP-) (*Callitris glaucophylla*), smooth barked apple (SBA) (*Angophora costata*, spp *leiocarpa*), various *Eucalyptus* species, and wattle (*Acacia* species), with a range of growth stages from regrowth to medium height (up to 30m). This forest had established on flat terrain with sandy soils. The plot was contained within an area of State Forest tenure that had been managed for selective native forest timber production (*Callitris*), as well as low intensity beef grazing. The last recorded logging event in the area was 20 years ago, and fire has been actively suppressed for 50-100 years.

To generate the 3D representation from the LiDAR data and to integrate available field measurements in a common reference matrix, the following method was applied. This simulation method follows the general concepts developed for the FOL-PROF programs as described in Walker & Penridge, (1987).

1. A reference matrix was generated with a 1m<sup>2</sup> fishnet ESRI ArcInfo polygon layer to cover the maximum geographical extent of field and LiDAR data.
2. Database items were added to the layer for each one-metre height interval, up to the tallest height recorded in the plot (either from field or LiDAR data). This created 'virtual' voxels (for this analysis, a voxel is defined as the combination of cell (XY) and a respective height interval database item (Z)) of 1m<sup>3</sup> for the plot volume.

3. The LiDAR point layer was intersected with the matrix layer, and both the height above ground and intensity values for each return were recorded in the corresponding voxel in the matrix. Where multiple returns occurred within one voxel, then the maximum height, mean intensity and number of returns were recorded.
4. The field data tree map layer was intersected with the matrix layer. Those cells that contained the tree point became 'trunk' cells, and were coded thus for all height intervals up to the canopy base height in the database.
5. Crown dimensions (diameter in north-south and east-west directions, canopy depth), species and growth stage were extracted from the tree map layer (i.e., field data), and the whole crown was modelled on a 1m<sup>3</sup> basis. An elliptical shape was assumed in the horizontal plane, and shape assumptions in the vertical plane were based on species and growth stage. Here three major shapes were used – the cubic expression of an ellipse (generic crown), a pyramid (conifer or young eucalypt), and an inverted pyramid (senescent eucalypt).
6. A canopy openness factor was then applied to crowns larger than 5 metres in diameter. Here, records were removed randomly from the database until the appropriate openness percentage for that particular crown had been achieved. Crown openness was based on published records for selected species in the literature and through hemispherical photograph interpretation.

Apparent vertical foliage profiles of field simulated and LiDAR data were generated by summarising the number of voxels that were coded with canopy elements per one metre height interval, as a proportion of all canopy voxels in the plot volume. This allowed any obvious strata breaks to be quantified and validated against existing vertical foliage profiles for this environment, as shown in Walker, *et al.*, (1986).

### 3. RESULTS AND DISCUSSION

#### 1.4 Integrating Field Simulation and LiDAR Data

Within the plot matrix there were 2,367 cells with 27 (1m) height levels, resulting in 63,909 virtual voxels (1m<sup>3</sup>). The results of the simulated field data, as visualised 3D in ESRI's ArcScene software, are shown in Figure 2. Note that for clarity this image shows the simulation without the canopy openness factor applied.

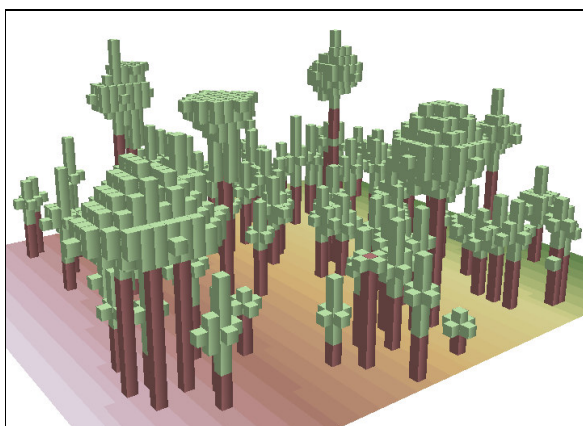


Figure 2. 'Cubic' 3D modelling and visualisation of field tree data from mixed *Callitris* and *Angophora* forests.

Table 1 summarises the direct comparison between field data and LiDAR on a cubic metre basis. Overall there was good correspondence between the two datasets in terms of a two dimensional crown map, with 76% of the field simulated matrix cells also containing LiDAR, although these were not necessarily at the same height above ground. More cells recorded LiDAR returns than field data simulated canopy elements, possibly indicating that there were additional canopy elements not recorded in the field measurements (i.e. small shrub elements). However, more voxels were tagged with field canopy elements than with LiDAR returns, which could indicate that the LiDAR is being occluded from the lower portions of the simulated crowns and trunk voxels. Individual tree comparisons would be required to provide a more conclusive validation.

Attribute	No. Matrix cells	No. Matrix voxels
Field modelled crown elements	557	1,944
LiDAR return elements	981	1,302
Both LiDAR and field elements within the same vertical column (cell)	426	
Both field and LiDAR canopy elements within same voxel		175

Table 1. Summary of matrix results for the field plot area.

Additional mismatch error could result from north-south and east-west dimensions, as measured in the field, not correlating with the longest axis of the crown. The modelled crown may not, therefore, reflect the true shape (or the shape as indicated by LiDAR data), especially with very uneven crowns (as is typical of *Angophora* and *Eucalyptus* species). Preliminary comparisons of crown shapes derived from the LiDAR crown delineations versus the simulated field data ellipses have shown this to be a significant issue. Additionally the field data tree map and LiDAR may not line up correctly due to discrepancies in the field-based measurement of tree trunk relative to crown location and also due to GPS and rangefinder error.

Comparisons between field and LiDAR profiles for SSU 124\_19 (Figure 3) show that there was little difference between the two, potentially indicating that, for the less dense woodlands and open forests of Queensland, the LiDAR profiles are providing an adequate representation of overstorey and understorey distributions. This analysis is being undertaken on all 31 field plots in order to verify if this conclusion is supported across a range of forest structures. A number of issues were identified when comparing the two profiles. First, a discrepancy of approximately 2 metres exists between the two estimates of maximum top-height, with LiDAR recording taller tree height which most likely results from the inability to identify correctly and measure accurately the top of the tree in the field. Second, field and LiDAR curves diverge significantly at around 22 metres, which suggest that the field crown shapes in the simulation are not creating sufficient canopy elements to match the LiDAR strikes recorded. Testing an inverted pyramid shape for tall overstorey crowns so that proportionally more canopy elements are found closer to the top heights as opposed to the centre of the crown could resolve this issue. Third, there appears to be a 1 metre offset on average between LiDAR and field profiles, with the LiDAR recording the taller value. This could indicate that field measures are underestimated, especially where the density of stems is high

(~600 stems within the 50 x 50m plot), and the measurement of the correct top height and/or canopy base is more difficult. Conversely, this could indicate that the lidar is only striking the upper portions of crowns, and so over-representing their taller portions, which then results in a curve with an apparent taller canopy.

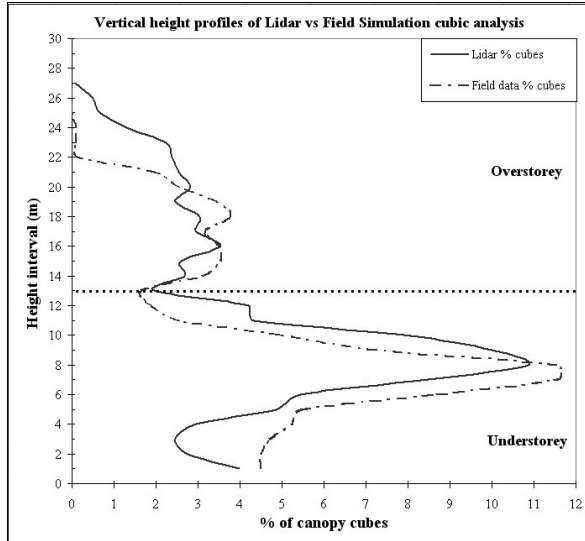


Figure. 3. Comparison of apparent vertical profiles generated from the common 3D reference grid, for LiDAR and field simulated data.

Fourth, the difference in lower understorey curves between 2-5 metres could indicate that not many LiDAR returns are penetrating the dense understorey, and therefore the amount of vegetation is potentially under-represented. Conversely, the 1m<sup>2</sup> size of all field-modelled trunks (regardless of actual size) could be over-representing the amount of vegetation potentially available for the LiDAR to strike. Understorey measurements (i.e., stems 1-5cm diameter at breast height (DBH)) were only sampled in four 5 x 5 metre subplots within the field plot, and scaled up subsequently to the full extent of the plot prior to simulation. Therefore, the presence of a significant understorey component could change the relative distribution of LiDAR percentage cover throughout the vertical profile with respect to field-simulated data. This could introduce some error in very heterogeneous sites, where the samples do not reflect the wider plot. The subplot sampling resulted in a mean stem count of 18 per subplot, with a standard deviation of 9 stems, and a Coefficient of Variation of 50%, indicating that this plot is heterogeneous for stems 1 - 5cm DBH. Checking the simulations against photographs of the plots would also assist in reducing this potential error.

Crown shape has been shown to be important for assessing the interaction between LiDAR and tree crowns (e.g. Nelson, 1997), and this was also identified during the algorithm development phase, where it was observed that crown shape and openness had a significant influence on how field and LiDAR profiles compared. The consistent application of crown shape is being explored through assessment of photographs of field plot trees.

### 1.5 Assessing Stand Dynamics and Carbon

Figure 4 presents a summary of the field data for SSU 124\_19, outlining tree growth stage and species by relative percentage of basal area and stocking per DBH class. Plot growth stage could be interpreted as complex with an overstorey canopy of large crowns reflecting, multiple successional phases (based on Florence, 1996). *Eucalyptus* and *Angophora* species occurred throughout the DBH class and growth stage range, and have a mean tree height of 9.1 m (Standard deviation, SD, of 7.6m, range 2.5 – 24.0 m). Four distinct cohort age groups were evident with these most likely relating to major disturbance and regeneration episodes in the past. However, these species have relative few stems (only 1 - 3 stems per DBH class above 25cm), indicating that they have been on this site for possibly hundreds of years and have self-thinned to a woodland climatic equilibrium. *Acacia* species constitute 67% of all stems, but only 6% of stems greater than 10cm DBH, and have a mean tree height of 1.1m (SD 1.5 m, range 0.5 – 12.3 m). *Callitris* has the majority of stems greater than 10cm DBH (77 %) but they are all less than 20cm DBH and, with a mean tree height of 7.4 m (SD 3.1m, range 2.7 – 14.0 m), and are identified with the developing growth stage. Therefore, they would be relatively recent recruits to the plot, possibly as a result of past logging and fire suppression, given this genus is fire intolerant when young.

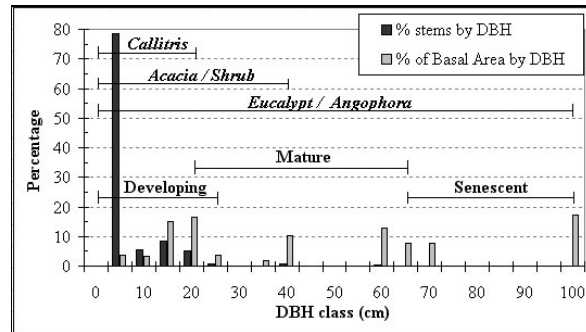


Figure. 4. Field data summary illustrating tree growth stage and genus distribution by basal area (total BA = 4.30m<sup>2</sup>) and stocking (n = 603).

In terms of inferring potential stand growth stage and therefore carbon sequestration potential from the vertical profiles, a number of elements can be related to the field data. A distinct strata break between understorey and overstorey could be inferred at 13 metres, which broadly corresponds to the previously described plot growth stage. There are 13 stems with a top height greater than 13 metres (2 % of all stems), but these stems account for 55 % of the total basal area, so the strata break is reasonable. The dominant understorey proportion visible in the curve would indicate a dense understorey layer that is capturing a significant number of returns (75 % of non ground returns are <14 m). Further lidar analyses indicate this is from many small crowned stems, rather than a few stems with dense and wider crowns, which again reflects the field data. The less dominant overstorey (in terms of cover) is likely to be quite open as evident by the relatively few voxels with canopy elements, compared to the understorey. Also, comparisons between this plot and other field and lidar plots indicate that the tallest trees in this plot are near the maximum height for this environment. Based on this stand structure, carbon sequestration potential is likely to reduce from

the current stock of 143 Mg ha<sup>-1</sup>, as the few large senescent individuals are anticipated to die eventually and the growth of the other larger DBH cohorts is likely to be slow. There is potential for increased sequestration from the large number of CP-regrowth stems present. However in this environment they can 'lock-up' and remain small for long periods of time (decades) unless disturbance (e.g. fire) leads to thinning of individuals.

#### 4. CONCLUSION

To date LiDAR has mainly been used to produce maps of the two-dimensional height and cover of forests. In this study, we have shown that by distributing LiDAR returns within a voxel matrix, and simulating actual vertical and horizontal foliage distributions, a 3D representation of forest structure can be generated. As each voxel can be populated with information on plant structural elements (e.g., foliage density), these representations can be used as input to models of microwave or radiation interaction with forests, thereby facilitating better interpretation of their radar response or even bi-directional reflectance, as recorded by airborne or spaceborne remote sensing instruments. Voxels (1 m<sup>3</sup>) within the matrix were found to correspond to simulated crown elements and were summed per one metre height interval, producing vertical foliage profiles similar to those generated with LIDAR for the same forests. The vertical strata identified in the LiDAR profiles appeared to match qualitative assessments of disturbance history and quantitative field measures. However there is a requirement for adequate field and ancillary data to effectively calibrate and validate the analyses. The methods investigated in this paper provide insight into the utilisation of small footprint LIDAR for determining potential stand structural dynamics (e.g., forest structure, biomass, potential growth stage, types of disturbance and succession stage), and further research is underway to improve the consistency of forest attribute estimates across a wider range of structural and environmental types.

#### REFERENCES

- Bureau of Meteorology, 2004. [http://www.bom.gov.au/climate/map/annual\\_rainfall/](http://www.bom.gov.au/climate/map/annual_rainfall/) (accessed 02 Aug. 2004).
- Burrows, W. H.; Henry, B. K.; Back, P. V.; Hoffmann, M. B.; Tait, L. J.; Anderson, E. R.; Menke, N.; Danaher, T.; Carter, J. O.; McKeon, G. M., 2002. Growth and carbon stock change in eucalypt woodlands in north-east Australia: ecological and greenhouse sink implications. *Global Change Biology*, 8(8), pp. 769-784.
- Durden, S. L., Zebker, H. A., van Zyl, J. J., 1989. Modeling and observation of forest radar polarization signatures. *IEEE Trans. Geoscience Remote Sensing*, 27(3), pp. 290-301.
- Florence, R.G., 1996 *Ecology and silviculture of Eucalypt forests*. CSIRO Australia.
- Harding, D.J., Lefsky, M.A., Parker, G.G., Blair, J.B., 2001 Laser altimeter canopy height profiles: Methods and validation for closed canopy, broadleaf forests. *Remote Sensing of Environment*, 76(3), pp. 283- 297.
- Hurt, G. C., Dubayah, R., Drake, J., Moorcroft, P. R., Pacala, S. W., Blair, J. B., Fearon, M. G., 2004. Beyond potential vegetation: combining LIDAR data and a height-structured

model for carbon studies. *Ecological Applications*, 14(3), pp. 873-883.

Lexer, M., Honninger, K., 2001. A modified 3D-patch model for spatially explicit simulation of vegetation composition in heterogeneous landscapes. *Forest Ecology and Management* 144(1-3), pp. 43-65.

Lovell, J. L., Jupp, D. L. B., Culvenor, D. S., Coops, N. C., 2003. Using airborne and ground-based ranging LiDAR to measure canopy structure in Australian forests. *Canadian Journal of Remote Sensing*, 29(5), pp.607-622.

Lucas, R.M., Moghaddam, M., Cronin, N., 2004. Microwave scattering from mixed species woodlands, central Queensland, Australia. *IEEE Transactions on Geoscience and Remote Sensing*, (in press).

Nelson, R., 1997. Modelling forest canopy heights: the effects of canopy shape. *Remote Sensing of Environment* 60(3), pp. 327-334.

Sun, G., Ranson, K. J., 1995. A three-dimensional radar backscatter model of forest canopies. *IEEE Transactions on Geoscience and Remote Sensing*, 33(2), pp. 372-382.

Sun, G., Ranson, K.J., and Kharuk, V.I., 2002. Radiometric slope correction for forest biomass estimation from SAR data in the Western Sayani Mountains, Siberia. *Remote Sensing of Environment*, 79(2-3), pp. 279-287.

Tickle, P. K., Lee, A., Austin, J., Witte, C., Lucas, R.M., 2001 Estimating the biomass and structural attributes of Australian forests and woodlands using LiDAR and large-scale photography. In *Proceedings International Geoscience And Remote Sensing Symposium July 2001*, Sydney, Australia, Vol III, pp. 1000-1003

Walker, J., Jupp, D. Penridge, L., Tian, G., 1986. Interpretation of vegetation structure in Landsat MSS Imagery: A case study in disturbed semi-arid eucalypt woodlands. Part 1. Field Data Analysis. *Journal of Environmental Management* 23, pp. 19-33.

Walker, J., Penridge, L., 1987. FOL-PROF: A fortran-77 package for the generation of foliage profiles. Part 1 User Manual. *CSIRO Technical Memorandum 87/9*, Canberra.

#### ACKNOWLEDGEMENTS

The authors would like to acknowledge the support provided by the Australian Research Council, under their SPIRIT program, the Cooperative Research Centre for Greenhouse Accounting, and the Australian Commonwealth Department of Agriculture, Fisheries and Forestry. We would also like to thank Kerstin Jones, Robert Denham, Norm Good, and the staff of UNSW, QDNRM, BRS, QUT and QDPI Tropical Beef Centre.

# Quantifying Australian forest floristics and structure using small footprint LiDAR and large scale aerial photography

P.K. Tickle<sup>a,1</sup>, A. Lee<sup>b</sup>, R.M. Lucas<sup>c,\*</sup>, J. Austin<sup>b</sup>, C. Witte<sup>d,2</sup>

<sup>a</sup> Geoscience Australia GPO Box 738, Canberra, ACT 2601, Australia

<sup>b</sup> School of Resources, Science and Society, The Australian National University & CRC Greenhouse Accounting, Canberra, ACT 0200, Australia

<sup>c</sup> Institute of Geography and Earth Sciences, The University of Wales, Aberystwyth, Penglais Campus, Aberystwyth, Ceredigion SY23 3DB, United Kingdom

<sup>d</sup> Forest Ecosystem Research and Assessment, Queensland Department of Natural Resources and Mines, Resource Sciences Centre, 80 Meiers Road, Indooroopilly, Qld 4068, Australia

Received 26 August 2005; received in revised form 30 November 2005; accepted 30 November 2005

## Abstract

Light detection and ranging (LiDAR) data and large scale (1:4000) photography (LSP) were investigated for their potential to quantify the floristics and structure of mixed species forests near Injune, central east Queensland, and to scale these up to the region for purposes of baseline assessment and on-going monitoring. For a 220,000 hectare (ha) area, LiDAR and LSP were acquired over 150 500 m × 150 m (7.5 ha) primary sampling units (PSUs) located on a ~4 km systematic grid. Based on LSP interpretation, 292 species combinations were observed, although forests were dominated or co-dominated primarily by *Callitris glaucophylla*, *Eucalyptus melanaphloia*, *Eucalyptus populnea* and *Angophora Leiocarpa*. Comparisons with species distributions mapped using LSP and in the field suggested a 79% correspondence for dominant species. Robust relationships were observed between LiDAR and field measurements of individual tree ( $r^2 = 0.91$ , S.E. = 1.34 m,  $n = 100$ ) and stand ( $r^2 = 0.84$ , S.E. = 2.07 m,  $n = 32$ ) height. LiDAR-derived estimates of plot level foliage/branch projected cover (FBPC), defined by the percentage of returns >2 m, compared well ( $r^2$  of 0.74, S.E. = 8.1%,  $n = 29$ ) with estimates based on field transects. When translated to foliage projected cover (FPC), a close correspondence with field measurements ( $r^2 = 0.62$ , S.E. = 6.2%,  $n = 29$ ) was observed. Using these relationships, floristics and both height and FPC distributions were estimated for forests contained with the PSU grid and extrapolated to the study area. Comparisons with National Forest Inventory (NFI), National Vegetation Information System (NVIS) and Queensland Herbarium data suggested that sampling using LSP and LiDAR aggregated to the landscape provided similar estimates at the broad level but allowed access to a permanent and more detailed record. Observed differences were attributed to different scales of data acquisition and mapping. The cost of survey was also reduced compared to more traditional methods. The method outlined in the paper has relevance to national forest monitoring initiatives, such as the Continental Forest Monitoring Framework currently being evaluated in Australia.

© 2005 Elsevier B.V. All rights reserved.

**Keywords:** Forests; LiDAR; Aerial photography; Floristics; Structure; Monitoring; Australia

## 1. Introduction

As a signatory to international agreements, including the United Nations Framework Convention on Climate Change (UNFCCC) and the Montreal Process for sustainable forest

management, Australia is increasingly required to provide accurate and quantitative information on the species/community composition (herein referred to as floristics), structure and condition of its forests through time (MPIG, 2001; Barrett et al., 2001). In addition, such information is required by governments, industry, private landholders and the public to detect trends in commercial, biodiversity and greenhouse values (NFI, 1998, 2003; AGO, 2000; Henry et al., 2002), assess the performance of management practices and public policies, guide sustainable development and forecast the future condition of these ecosystems (NFI, 2003). However, undertaking such assessments within Australia represents a significant challenge for two main

\* Corresponding author. Tel.: +44 1970 622612; fax: +44 1970 622659.

E-mail addresses: Phil.Tickle@ga.gov.au (P.K. Tickle), Alex.Lee@anu.edu.au (A. Lee), rml@aber.ac.uk (R.M. Lucas), Christian.Witte@dnr.qld.gov.au (C. Witte).

<sup>1</sup> Tel.: +61 2 62499111.

<sup>2</sup> Tel.: +61 7 38969832.

reasons. First, Australia has an estimated 164 million hectares (ha) of native forests, which are distributed largely around the outer margins of the continent. Second, around 70% of these forests are under private management and less than 10% are in commercial public forest estates (NFI, 2003). In the areas under private management, the information available on structure and condition is especially limited (MPIG, 2001). The development of efficient and cost-effective methods for retrieving this essential information is therefore critical if international obligations are to be better fulfilled and the sustainable development and conservation of forest resources optimised.

The overall objective of this research, therefore, was to evaluate whether large scale (1:4000) stereo aerial photography (herein referred to as LSP) and/or small footprint light detection and ranging (LiDAR) data could be used as tools, either singularly or in combination, for routinely sampling, describing and quantitatively assessing the floristics and structure of these forests. Focusing on areas of agricultural land and mixed species forests in central Queensland, which were considered typical of those occurring across large areas of Australia, the study aimed specifically to evaluate whether: (a) floristics could be described through air photograph interpretation (API) of LSP, (b) measures of structure (e.g., height and canopy cover) could be estimated from LiDAR data, (c) the resulting quantitative estimates of each could be extrapolated to the landscape with levels of reliability comparable to or better than those currently available and (d) data from these sensors combined offered a viable and cost-effective alternative or supplement to methods used currently for on-going regional assessment and monitoring of forests.

## 2. Background

Although LSP has been used as a basic forest inventory tool for some time (e.g., Spencer, 1992), the integration of LSP and LiDAR data has only been possible in the past few years due to advances in sensor design and data acquisition and processing. The following sections therefore provide a brief overview of these two systems and their use in Australia.

### 2.1. Airborne scanning LiDAR

LiDAR is an active remote sensing technique that directs a near infrared (NIR) laser pulse downwards towards the Earth's surface (Lefsky et al., 2002). This pulse reflects from objects (e.g., tree canopies, buildings and the ground), and is then received by the sensor. The time-delay between pulse transmission and receipt is related directly to distance and hence height, density and areal proportions of objects can be retrieved. The intensity of the return (which has no units) provides information on the pseudo NIR reflectance characteristics of the objects (Wehr and Lohr, 1999; Suárez et al., 2005).

Airborne scanning LiDAR is currently experiencing rapid commercial growth, with small footprint LiDAR being used increasingly for terrain mapping, powerline surveys and vegetation classification (Dowling and Accad, 2003). The number of commercial companies operating LiDAR has

increased substantially in recent years, as has the sophistication of instruments. In a period of only 5 years, the industry standard has advanced from systems emitting 5000 pulses per second and measuring a single return to those emitting between 25,000 and 75,000 pulses per second, and measuring up to five returns, with some recording the intensity of each return (Moffet et al., 2005). In most systems, the laser beam is emitted through a rotating mirror, which creates a zigzag swath of laser returns either side of the aircraft.

Depending upon flying height, the footprint size may vary from 0.1 to 5.0 m and the interval between laser returns may range from 0.25 to 5 m. With the aid of real-time global positioning systems (GPS) and sophisticated inertial navigation systems (INS) that compensate for aircraft pitch, yaw and roll, most LiDAR are now capable of achieving absolute spatial accuracies of  $<\pm 1$  m in the  $x$  and  $y$  directions and  $<0.25$  m in the  $z$  direction (i.e., elevation). For forest assessment purposes, such accuracies now makes it possible to "image" individual tree crowns, and to locate the same trees on the ground using, for example, hand-held GPS.

Over the last 15 years, the use of small footprint airborne LiDAR for retrieving ground surface and vegetation parameters have been demonstrated (as examples, see Nelson et al., 1984, 1988; Aldred and Bonner, 1985; Nilsson, 1994; Naesset, 1997; Magnussen and Boudewyn, 1998; Means et al., 1999; Weller et al., 2001; Lovell et al., 2003; Riaño et al., 2004). This work has now matured to the state where direct estimates of structural variables (e.g., tree heights and canopy cover) routinely achieve  $r^2$  values approaching or exceeding 0.90 (e.g., Suárez et al., 2005). Hyypä et al. (2001) demonstrated that LiDAR could provide more precise stand-based estimates than conventional field-based inventory.

### 2.2. Large scale photography

LSP has long been recognised as a valuable tool for forest inventory, improving the efficiency of ground sampling through improved stratification and plot selection and bridging the gap between ground measurements and other forms of remotely sensed data using multi-phase and multi-stage techniques (Spencer and Hall, 1988). Although LSP has been operational for many years (Spencer and Hall, 1988; Spencer, 1992; Nielson, 1997; Pitt et al., 1997; Spencer and Czaplowski, 1997), its application in Australia has been limited, with the notable exception of a comprehensive inventory of two million hectares of forest in western Australia (Spencer, 1992). This inventory demonstrated that large area inventories could be undertaken at one-tenth of the cost of traditional ground surveys. The reasons for the lack of adoption include the perceived high cost of data capture, film processing, labour cost (for parallax-based measurement of stand variables), establishment of ground control and the requirement of specialised medium format camera systems (often mounted on helicopters). However, with the advent of image motion compensation, specialised aerial films, INS and real-time differential GPS, LSP can now be captured from fixed-wing aircraft (using large format aerial cameras) by the mainstream aerial survey and photogrammetry industry.



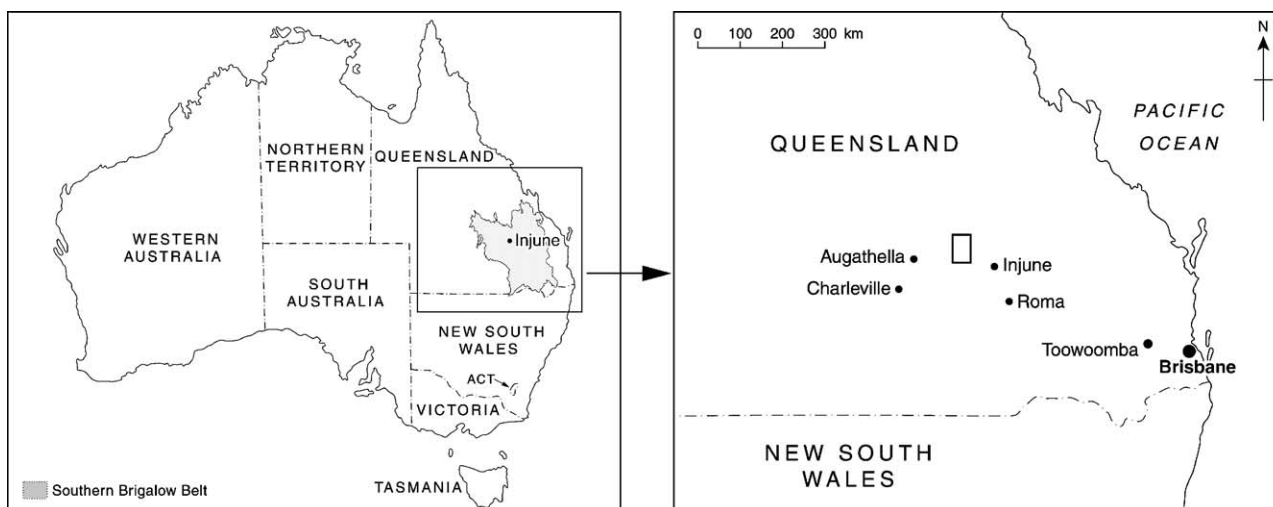


Fig. 1. The location of the 37 km × 60 km study area, central east Queensland.

### 3. Study area

To evaluate the use of both LSP and LiDAR for quantifying the floristics and structure of forests, an area of 37 km × 60 km (222,000 ha) of private and public land near Injune, central Queensland (Lat 25°32'S, Long 147°32'E), was selected (Fig. 1). The study area was chosen, as the forests are typical to those of much of Australia<sup>1</sup> in terms of floristics and structure. Furthermore, a wide range of regeneration and degradation stages exist, due primarily to past and present agricultural and forestry management practices, creating forest communities that are structurally diverse (Lucas et al., 2004, 2006). The forests near Injune have also been the focus of extensive clearance, particularly in the late 1990s and the early 2000s, and have contributed to the significant losses of carbon associated with vegetation clearance in Australia (Barrett et al., 2001; Burrows et al., 2002; Henry et al., 2002).

The study area was located within the Southern Brigalow Belt (SBB) biogeographic region, and contained a diverse range of forest communities (Queensland Department of Natural Resources (QDNR, 2000)). Based on 1:250,000 broad vegetation mapping (Montreal Process Implementation Group (MPIG, 2001)) and 1:100,000 scale land cover mapping from aerial photography and Landsat TM, the forest communities were dominated by White Cypress Pine (*Callitris glaucophylla*, herein referred to as CP-), Poplar Box (*Eucalyptus populnea*, PBX), Silver Leaved Ironbark (*E. melanophloia*, SLI), Smooth Barked Apple (*Angophora leiocarpa*, SBA) and/or Brigalow (*Acacia harpophylla*, BGL). Common understorey genera included Sandalwood Box (*Eremophila mitchellii*, SWB) and Wilga

(*Geijera parviflora*, WIL). In the north of the area, the terrain was hilly and dissected by small gorges in places, and ranged from 400 to 1000 m above sea level (ASL). In the centre and south, undulating hills, plateaux and plains at approximately 200–400 m ASL occurred. The mean annual rainfall was approximately 630 mm year<sup>-1</sup> and the mean annual maximum temperature was 27 °C (Bureau of Meteorology, 2004).

### 4. Image and field data collection

The acquisition of image and field data was undertaken in four main stages (Table 1). In stage I, a systematic sampling scheme (Schreuder et al., 1993) was implemented to guide the acquisition of LSP (stage II) and LiDAR data (stage III). Following collection and initial interpretation of these data, forest inventory data were collected from selected areas (stage IV). The majority of the fieldwork was carried out during the period of LiDAR data acquisition and within 1-month of the LSP data acquisition, thereby minimising any seasonal effects and the likely impacts of anthropogenic land cover change at the field sites. The following sections describe these four stages.

#### 4.1. Stage I: sample design

The sampling framework for the collection of the LiDAR and LSP data was implemented to allow comparison with estimates generated using wall-to-wall mapping undertaken as part of other studies (QDNR, 2000) and also to provide operational experience in the implementation of sampling frameworks that may be adopted in future regional and national inventory programs (e.g., the National Forest Inventory (NFI)). A systematic sampling scheme was selected, as knowledge of the floristics and structure of the forests was too limited to allow application of efficient stratified sampling methods. The state of the forests had also changed rapidly over recent years, largely because of extensive clearance of vegetation within the area, thereby preventing the use of historical spatial layers for stratification.

<sup>1</sup> Within Australia, forest is defined as all woody vegetation with a top height equal or greater than 2 m above the ground and a crown cover ≥20%. Woodlands are defined as supporting 20–50% crown cover (equivalent to 10–30% FPC), and open forests as 51–80% crown cover (equivalent to 30–70% FPC; NFI, 1998). Woodland formations such as those found in the study area are representative of over 70% of Australia's forests (Montreal Process Implementation Group (MPIG, 2001)).

Table 1  
Main stages in the acquisition, processing and analysis of field and remote sensing data

Stage	Task	Purpose
Sampling and data acquisition		
I	Sample design	To select appropriate field sample locations
II	LSP capture and pre-stratification	To allow description of the species/community composition
III	LiDAR capture	To facilitate retrieval of structural attributes (height, crown, foliage and/or branch cover)
IV	Field sampling	To provide ground truth for interpretation of LSP and LiDAR and validation of products
Post-processing		
V	Georeferencing of LSP to LiDAR	To allow overlay of API vector information
VI	Generation of LiDAR height surfaces	Calculation of a bare earth DEM and vegetation height
Data analysis		
VII	Classification of forest communities based on LSP interpretation	To determine spatial distributions of dominant, co-dominant and sub-dominant species
VIII	Tree height, FBPC, FPC and canopy cover retrieval from LiDAR	To provide individual tree and stand level estimates

Based on these considerations, the systematic sampling scheme for the 37 km × 60 km study area allowed the acquisition of LSP pairs across a grid containing 150 (10 columns and 15 rows) points located 3.7 km × 4 km apart in the east–west and north–south directions, respectively (Fig. 2). The acquisition of LSP was planned such that the 800 m × 800 m (64 ha) area (herein referred to as a primary photo plot or PPP) was centred on each of the 150 grid points. For each PPP and within the 60% stereo overlap area of the LSP, a 500 m × 150 m (7.5 ha) primary sampling unit (PSU) was established. Each of the 150 PSUs was then subdivided into 30 systematically numbered secondary sampling units (SSU) which were 50 m × 50 m (0.25 ha) in area. Using this scheme, data could be analysed and summarised for each of the 150 PPPs and PSUs (4500 SSUs) that represented 5.3% (3.9% for only the stereo area) and 0.5% of the 222,000 ha study area, respectively.

4.2. Stage II: LSP capture

For each of the 150 PPPs, and using pre-defined coordinates, 1:4000 stereo colour aerial photographs (in negative format) were acquired on the 11th July 2000 by QASCO Surveys Pty. Ltd. on behalf of the Queensland Department of Natural Resources and Mines (QDNR&M) Landcare Centre. Photographs were taken using an RC20 large format photographic camera from late morning to mid afternoon. The effective swath width was 920 m and, for each photo principle point, GPS coordinates were recorded to within a nominal precision of ±20 m absolute location. As 150 PSUs were sampled, 300 frames of photographs were obtained.

4.3. Stage III: LiDAR data capture

Airborne scanning LiDAR data were captured over a 1-week period commencing August 24th 2000 using an Optech 1020

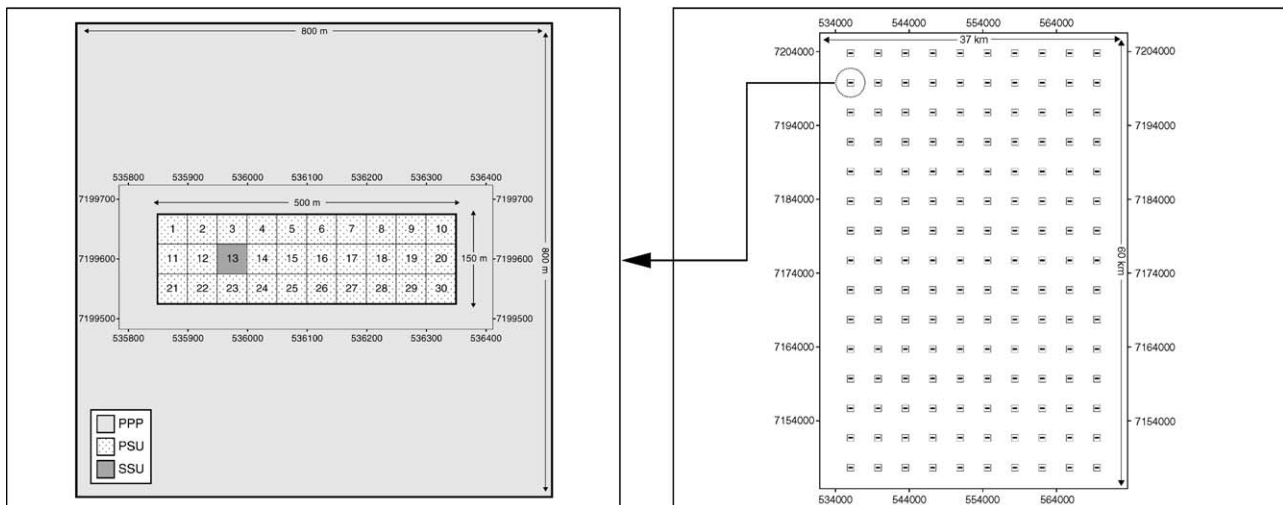


Fig. 2. Layout of the PPP, PSU and SSU grid.

scanning LiDAR mounted in a Bell Jet Ranger helicopter. The Optech 1020 measured 5000 first and last returns and the intensity of each return per second. The LiDAR operated within the NIR spectrum with a beam divergence of 0.3 mrad, a footprint of approximately 7.5 cm and an average sampling interval of <1 m. Data were acquired flying in an east–west direction (and centred on each PSU row), at a nominal altitude of 250 m and a swath width of approximately 200 m. A GPS base station was established for all flights. With full differential GPS corrections, in addition to pitch, yaw and roll compensation from an INS, coordinates were guaranteed to an absolute accuracy of <1 m in the  $x$  and  $y$  directions and <0.15 m in the  $z$  direction.

#### 4.4. Stage IV: field sampling

Field inventory data were collected during August 2000. The collection of field data over the same period as the remote sensing data acquisition was considered necessary to limit the impact of changes in seasonal foliage cover or land cover (associated with disturbance by fire or clearing) on the subsequent development of relationships with remotely sensed data.

Prior to acquisition of the field data, a 100 m × 100 m dot grid was overlain onto the overlap area of each of the 150 hardcopy LSP stereo pairs and used to estimate the proportions of land use, land cover and forest types as well as forest height and cover, disturbance regimes and vehicular access (Jones, 2000). The LSP code allocations were then used to stratify and identify suitable locations for field sampling on the assumption that the vegetation types contained within the 150 PSUs were representative of the proportions across the entire study area. For the purposes of stratification, and based on the vegetation assessment, the API codes were classified into four woodland types: Acacia or sparse vegetation (containing species such as BGL, SWB, *Casuarina cristata*, *Allocasuarina luehmanni*); Callitris (e.g., CP-, *C. preissii*); Eucalypt Ironbark (e.g., SLI, *E. decorticans*, *E. fibrosa* spp. *Fibrosa* and *E. crebra*) and Eucalypt other/Angophora (e.g., PBX, *E. dealbata*, SBA and *Angophora floribunda*). The Eucalypt class was split as the various Ironbark species were seen to contribute a significant proportion of the mapped landscape. Each forest type was then ranked into three (low, medium and high) potential and relative structure/biomass classes, based on structural information obtained from API (Jones, 2000) and a biomass map generated previously using Japanese Earth Resources Satellite (JERS-1) Synthetic Aperture Radar (SAR) data (Lucas et al., 2000), thereby producing 12 vegetation strata. The number of field plots sampled ( $N_s$ ) was then allocated based on the area of each of the 12 strata ( $A_s$ ) as a proportion of the total area occupied by the PSUs (where  $A_t = 1125$  ha) such that:

$$N_s = \frac{nA_s}{A_t} \quad (1)$$

where  $n$  represented the number of SSUs available for sampling based on criteria relating to road access, travel times and safety issues. Each of the PSUs (and their contained SSUs) was

necessarily scored according to whether road and subsequent foot access was possible, as determined primarily from the LSP interpretation. Landsat-7 Enhanced Thematic Mapper (ETM+) data were also used to identify roads outside of the LSP, thereby assisting assessment of the quality of road access. Knowing that travel times and safety issues would restrict field inventory to 2–4 SSUs per day using 2 field crews of 5 staff, 13 PSUs were selected that contained the necessary strata and met access criteria. Within these, 34 SSUs were sampled across the 12 strata (in proportion to their area within the 150 PSUs). Within each of the 13 PSUs where field measurement took place, SSUs used for field data collection were selected at random from the 390 possible SSUs and according to API-defined classes prior to arriving at the site. Plot coordinates were also calculated and entered into a GPS navigation system to ease location in the field. The final plot allocations per strata are shown in Table 2.

Once located, a 50 m × 50 m square plot, aligned in a north–south direction, was established using GPS survey and laser range finding equipment. Tapes of 50 m length were then laid out to produce a 10 m × 10 m grid to guide the subsequent location of trees for measurement. For three additional SSUs identified as non-forest but containing regenerating vegetation, species and structural measures were conducted in five 10 m × 10 m plots contained within the selected SSU. Within each plot, the location of all trees >10 cm in diameter (at 130 cm above ground level) was recorded digitally by placing reflectors at each of the plot corners and then using either a GEOSCAN or CENTURION Laser Rangefinder to record the distance and angle from each tree to the nearest visible reflector. Using this approach, the Universal Transverse Mercator (UTM) coordinates of all trees were calculated. Trees 5–10 cm in diameter were located by reading the  $x$  and  $y$  distances (in cm) from 50 m tapes placed perpendicularly (at 10 m intervals) across the entire plot. The cover and height of trees and shrubs <5 cm in diameter was estimated within five 10 m × 10 m sub-plots, with the centres of four located at a distance of 10 m from each of the corners and a fifth located at the centre of the plot. Within each plot, each tree was identified to species level and key measurements recorded included trunk diameter (cm, at both 30 and 130 cm) and height (m) to the top of the tree. Transects were established within the field plot to estimate vegetation cover and consisted of three 50 m tapes laid out in the north–south direction at 10, 25 and 40 m, moving eastward from the south–west corner. Along each transect the presence or absence of canopy material was recorded at 1 m intervals. The

Table 2

Allocation of sampled SSUs to each of 12 strata described by floristics and biomass, giving a total of 34

	Above ground biomass (mg ha <sup>-1</sup> )		
	Low (<50; $n = 10$ )	Medium (50–100; $n = 10$ )	High (>150; $n = 14$ )
Acacia (1)	1	0	0
Callitris (12)	2	3	7
Ironbark (12)	3	3	6
Eucalypt other (9)	4	4	1

recording method, after Specht (1970), uses a plastic tube which is attached to a 2 m length rod and contains an internal cross-hair. A mirror situated at the base of the tube at an angle of 45° then enables the operator to record the presence or absence of green leaves or wood (trunk or branches) in the canopy vertically above. Foliage/branch projected cover (FBPC) and foliage projected cover (FPC) is then calculated as the sum of foliage and/or branch records as a proportion of the total. For the purposes of this study, FBPC relates to the amount of light that would reach the ground, and is the percentage of the plot area occupied by the vertical projection of foliage and branches, while FPC only considers light interception by green foliage (McDonald et al., 1998).

## 5. Post-processing of field and remote sensing

Following collection, the inventory data were analysed primarily to determine the species composition of the forests, so that the API could be better evaluated, and to generate tree and stand level estimates of height and cover that could be regressed against LiDAR data. For this purpose, further stages of LSP (stage V) and LiDAR data (stage VI) processing were necessary (Table 1).

### 5.1. Stage V: georeferencing of LSP to LiDAR

Following hard copy production of the LSP, photo prints were scanned at 600 dpi. Initial rectification was undertaken using the known locations of the principle points and camera parameters. Comparisons with the LiDAR data confirmed that the photo products were generally accurate to  $\pm 20$  m without

additional registration. The spatial accuracy of the LSP was refined further by collecting ground control points (GCPs) from the LiDAR data. This generally resulted in root mean square (rms) errors of  $< \pm 2$  m within the LiDAR strips, enabling the LSP to be georeferenced with the LiDAR data. Following registration of the LSP, floristic and structural mapping interpreted from the photographs (Jones, 2000; Fig. 3) was also scanned, vectorised and rectified using the same transformation as the digital imagery, to allow GIS overlays over the LiDAR data (3).

### 5.2. Stage VI: generation of LiDAR height surfaces

Each LiDAR strip was subset to encompass only the areas corresponding to the PSUs. A bare-earth Digital Elevation Model (DEM) was then generated for each PSU using both the first and last return pre-classified “ground” LiDAR data, such that all measurements of vegetation height were based upon a reliable ground reference. Both first and last returns were used as in some cases (e.g., bare ground), only one return (i.e., first) was recorded. The DEM was generated for each LiDAR strip by creating a triangular irregular network (TIN) based on a 1 m proximal tolerance. The resultant TIN was then checked visually to confirm correct classification of ground returns and then transformed into a 1 m grid using quintic interpolation methods such that irregularities in the surface, resulting from the high density of first and last returns used, could be smoothed out. The final DEM was checked visually against the LSP to ensure all vegetation was removed and potential mis-registration between LiDAR and LSP was accounted for. Given that ground surface features  $< 20$  cm high were easily

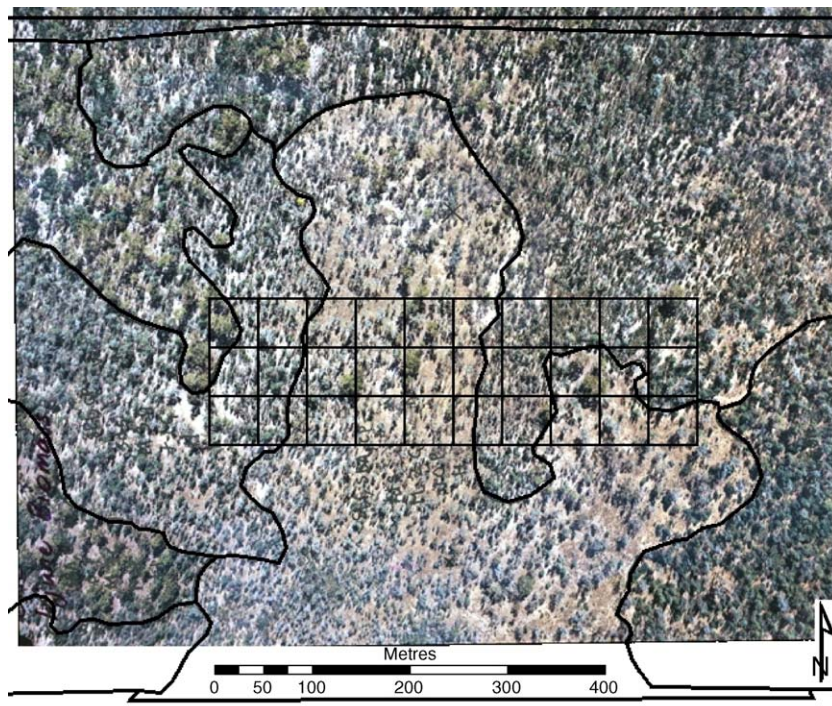


Fig. 3. True colour 1:4000 stereo aerial photograph of PSU 138 overlain with the 500 m  $\times$  150 m PSU boundary, contained SSUs (50 m  $\times$  50 m) and polygon vectors associated with different forest communities (based on species composition and cover), as mapped through aerial photography interpretation (API).

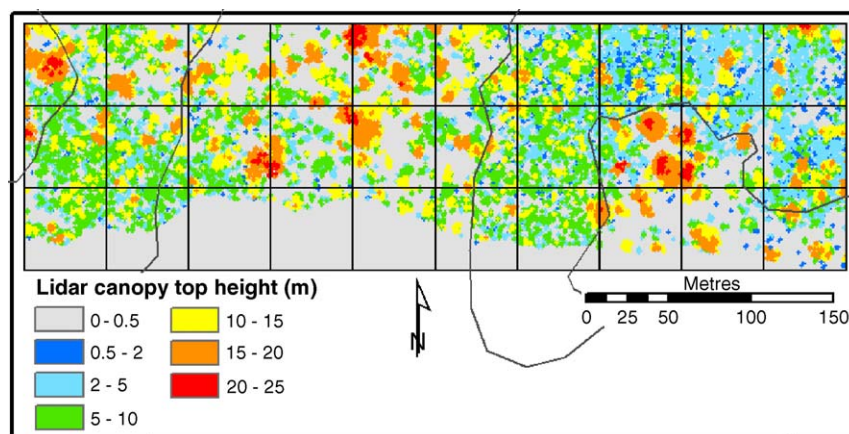


Fig. 4. LiDAR data representing tree crown heights acquired over PSU 138 and rasterised to a 1 m spatial resolution grid.

discernable, the relative elevation accuracy of the final DEM was considered to be  $<1$  m. The height above ground of each LiDAR vegetation return was then calculated as the elevation difference between the ground DEM and the vegetation return. Canopy surfaces were interpolated using a TIN from all vegetation returns, and this was converted subsequently to a  $1 \text{ m}^2$  grid (Fig. 4) for further analysis.

## 6. Data analysis

To provide summary information on the forests, their floristic composition was described using LSP (stage VII) whilst estimates of tree and stand height and cover were retrieved from LiDAR data (stage VIII).

### 6.1. Stage VII: classification of forest communities

Based on API, polygons interpreted from the LSP were allocated between one and three dominant tree species which, herein, are referred to as D1–D3. However, it should be recognised that D2 and D3 could be co-dominant or sub-dominant (e.g., common in the understorey). This resulted in 292 unique combinations of species code sequences (e.g., CP-SLI or PBXSLISWB) throughout the study area. For reporting clarity, these 292 species combinations were aggregated into five broad genus groups based on the dominant species: *Acacia*, *Callitris*, *Eucalypt Ironbark*, *Eucalypt other* and *Angophora*. Areas of non-forest were also distinguished. *Angophora* was identified as a separate class as the distribution of this species is poorly documented in regional datasets, particularly as these species are often mixed with other genera.

### 6.2. Stage VIII: tree height and cover retrieval

More than 2300 individual trees with diameters  $>10$  cm (at 130 cm) were measured for diameter and height in the field. From this pool, the heights of  $\sim 100$  clearly identifiable trees were extracted from the LiDAR data. Adjustments were required in some cases, as the centres of many tree crowns (particularly *Eucalyptus* species) did not correspond to the

locations of the trunks. Field and LiDAR measurements of height were then compared. At the plot level, relationships were also established between field-based estimates of FBPC and FPC, which represented the percentage of the SSU occupied by the vertical projection of foliage and branches (Carnahan, 1990) and foliage (excluding branches), respectively. Both FBPC and FPC were compared against the number (for each SSU) of (a) actual vegetation LiDAR returns with a height  $>2$  m above ground level and (b) interpolated vegetation cells (based on a  $1 \text{ m}^2$  pixel grid) as a proportion of all cells to determine whether stand level estimates of both cover attributes could be retrieved. Crown cover (CC) was also estimated through interpretation of the LSP, and considered the area occupied by the whole crowns (which are considered opaque), with respect to the polygon area.

## 7. Results: tree and stand level estimates

Based on the analysis outlined above, the use of both LSP and LIDAR for tree and stand level assessment, in terms of floristics, tree height and canopy cover was evaluated.

### 7.1. Species/community composition from LSP

The discrimination of species from LSP required skills in API with knowledge of the appearance (in terms of colour and texture) of different species. Although individual trees were not mapped or identified by the interpreter, and so a tree-by-tree comparison was not possible, a close correspondence ( $24/34 = 70.5\%$ ) between the dominant species within the field plot SSUs and that assigned by the API was observed (Table 3). Forests dominated by *Callitris* species were identified in all cases. SSUs identified through API as non-forest typically contained remnant trees and regrowth stands of BGL but also non-forest, and hence the API classification was deemed correct in this case, increasing the overall correspondence to 79%. API identified 40 and 17.6% of D2 and D3 genera correctly. However, all SSUs inventoried in the field contained the same species identified as D1–D3 through API. Therefore, although the exact order of dominance differed, the species

Table 3  
Count of field plots classified through API vs. tree basal area estimates, for D1–D3 species

API	Based on field (basal area) data					
	Non-forest	Acacia	Angophora	Callitris	Eucalypt other	Eucalypt Ironbark
<b>D1 = dominant</b>						
Non-forest		3				
Acacia		1				
Angophora			3			
Callitris			2	9	1	
Eucalypt other			1		7	1
Eucalypt Ironbark					2	4
Total						34
<b>D2 = co-dominant</b>						
Non-forest						
Acacia		2		4	2	
Angophora			2		1	
Callitris				3	2	
Eucalypt other		4		1	2	3
Eucalypt Ironbark			1			3
Total						30
<b>D3 = co- or sub-dominant</b>						
Non-forest						
Acacia				2		
Angophora		1			1	1
Callitris				1		2
Eucalypt other		2		1	3	
Eucalypt Ironbark		1		1	1	
Total						17

composition was correctly identified in the majority of cases. Such a strong correspondence gave confidence in the subsequent classification of dominant species and communities within each of the 4500 SSUs.

### 7.2. Tree and stand height estimates from LiDAR

A close correspondence ( $r^2 = 0.91$ , S.E. = 1.34 m,  $n = 100$ ) between tree heights derived from both field measurements and LiDAR data was observed (Fig. 5a). The comparison suggested, however, that the height was more reliably estimated for trees with more hemispherical crowns (e.g., Eucalypt and Angophora species) compared to those that were more pointed (i.e., Callitris species). The estimates of height, both from the field and LiDAR measurements, were within largely  $\pm 1$  m of each other, although discrepancies as high as 4 m were observed, which suggested some over-estimation by field measurement or under-estimation from LiDAR. The height estimates provided by the LiDAR were, however, considered to be more reliable for several reasons. First, height measurements were obtained from a greater area of the canopy and therefore the highest point of the canopy could be located objectively. This is particularly significant as the interpretation of the highest point of the tree from the ground varies with the observer and can lead to errors of the order observed between LiDAR and field measurements. Second, the field-based height measurements were often considered to contain errors as the highest point of the tree was not always visible. Even so, a disadvantage of the LiDAR

was that the wind effects on the crown might lead to minor errors. For the stand, a close correspondence between the maximum ( $r^2 = 0.84$ , S.E. = 2.07 m,  $n = 32$ ) height (excluding non-forest) estimated from the field and LiDAR data was observed (Fig. 5b).

### 7.3. Foliage cover estimates from LSP and LiDAR

From LSP, CC was interpreted and also categorised into four forest cover classes: 10–30, 30–50, 50–70 and 70–100%, and a non-forest class (<10%). All classes were observed, but the majority of cover was from 30 to 70%, which equates to open forests under the Carnahan (1990) classification (Specht and Specht, 1999). A close relationship between field-based measurements of FBPC and FPC was observed (Fig. 5c) which indicated that, on average, FPC was 67.7% (range 50–92%) of FBPC. In general, the percentage of leaf material was lower within forests with a greater proportion of Angophoras and Eucalypt other and was greater within those containing Callitris, Ironbarks and Acacia.

On average, there were approximately 5000 LiDAR point measurements in total per 0.25 ha field plot, with an average of 1700 vegetation returns from objects greater than 0.5 m in height. In comparison, there were only up to 150 canopy measurements from the three 50 m transects per SSU. Exploratory data analysis was undertaken to identify which field measures were most closely explained by the LiDAR vegetation returns. In this analysis, 29 of the 34 field plots were

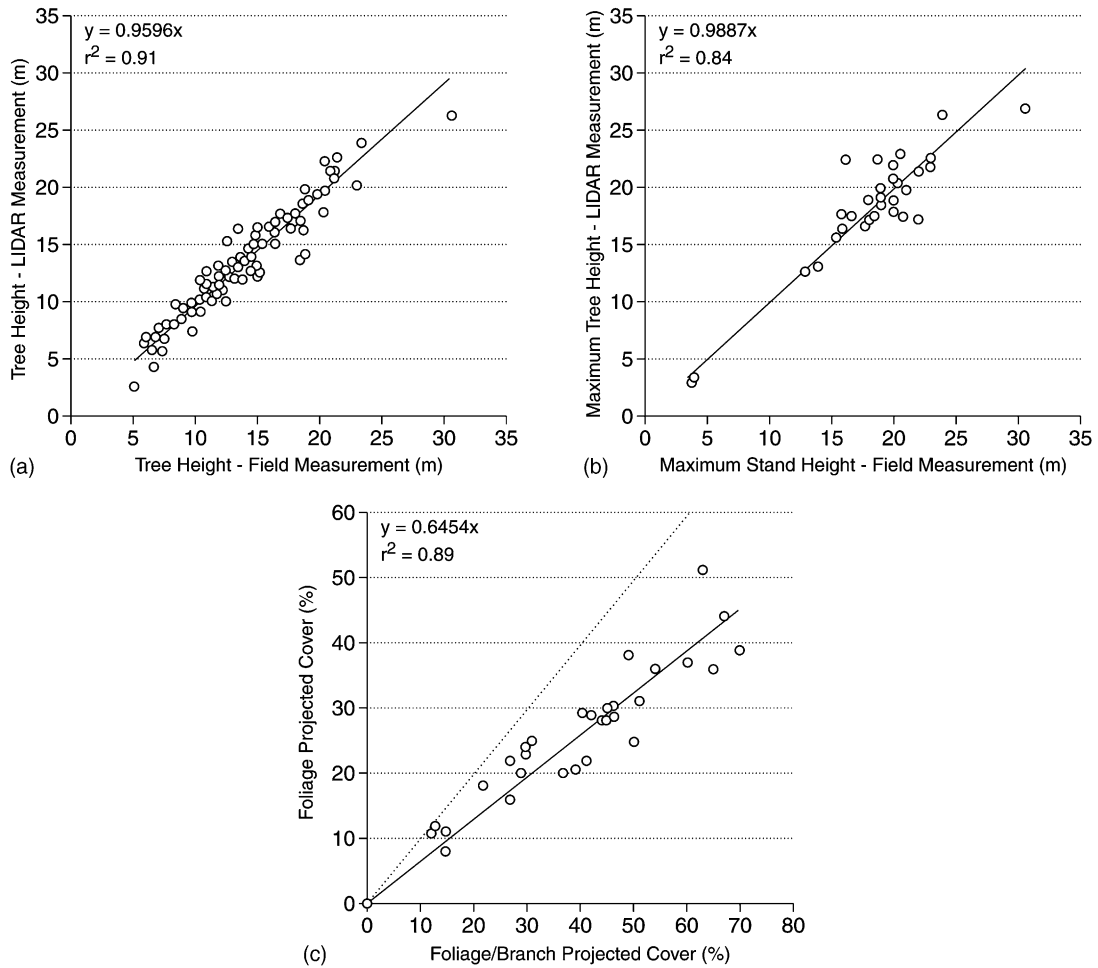


Fig. 5. Relationships between (a) individual tree height and (b) maximum stand height (based on SSUs), as estimated in the field and from LiDAR, and (c) field-based assessments of FBPC and FPC (with 1:1 line in grey).

compared, as field measurements were not obtained for plot 142\_02, and plot 138\_28 was missing significant LiDAR data as a result of errors in data acquisition caused primarily by adverse wind conditions. Three plots were located in sparsely vegetated short regrowth areas and were not therefore included. For those plots with partial loss of LiDAR data, transects were clipped to the extent of the available LiDAR data. The strongest relationship between LiDAR data and field estimates was that between field FBPC and LiDAR returns 2 m height and above (Table 4;  $r^2 = 0.74$ , S.E. = 8.1%,  $n = 29$ ). In order to compare LiDAR derived cover estimates with existing regional scale data, which was based on FPC field calibration alone, a relationship between field FBPC and FPC was necessarily applied to the LiDAR vegetation returns, as the LiDAR is

responsive to both leaves and branches. This relationship suggested a good correspondence ( $r^2 = 0.89$ , S.E. = 4.0%,  $n = 29$ ) between these parameters. The LiDAR-predicted estimates of FPC, when plotted against the field-estimates of FPC, suggested that this cover measure could be estimated with a reasonable degree of certainty ( $r^2 = 0.62$ , S.E. = 6.2%,  $n = 29$ ; Fig. 6), particularly given the disparity between respective number of measures per method, and also the measurement coverage within the plot (field = ~3% of plot; LiDAR = 100% of plot). The lower outlier identified in Fig. 6 was associated with an SSU in which one of the three field transects passed through a particularly open section, suggesting that the ground measurements were not adequately capturing the variability within the plot. The upper outlier was associated with a SSU

Table 4  
Relationships between FC and FPC and the proportion (x) of LiDAR vegetation returns ( $\geq 2$  m)

Cover descriptor	$r^2$	Adjusted $r^2$	S.E. (%)	$n$	Equations
Field FBPC vs. LiDAR veg returns	0.74	0.73	8.1	29	$Y = 1.09x + 6.24$
Field FPC vs. field FBPC	0.89	0.88	4.0	29	$Y = 0.6454x + 3.23$
Field FPC vs. LiDAR FPC (returns)	0.62	0.61	6.2	29	$Y = 1.08x + 3.46$

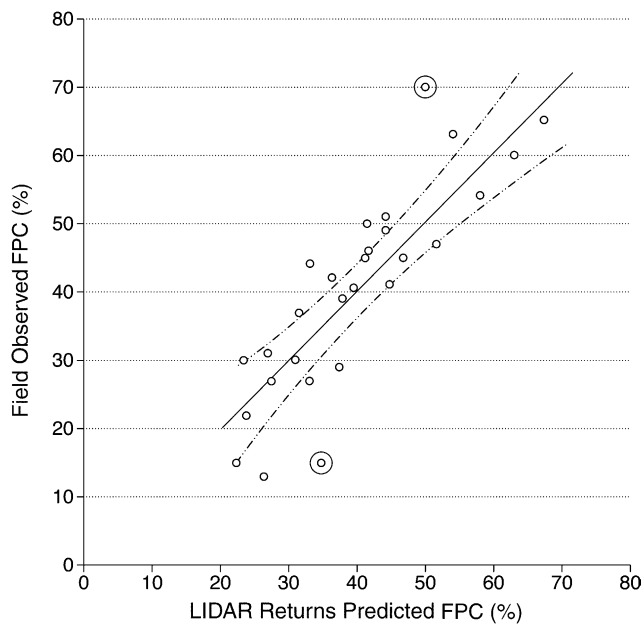


Fig. 6. Estimates of LiDAR predicted FPC vs. actual field estimates. Outliers associated with open ground or less dense LiDAR returns are circled. Dashed lines indicate 95% confidence intervals.

with high cover, but poor LiDAR coverage (2 m spacing) compared to other SSU's, as a result of adverse wind conditions. With these plots removed, the strength of the relationship increased further ( $r^2 = 0.68$ , S.E. = 4.9%,  $n = 27$ ). The various relationship values for field to LiDAR cover conversions are summarised in Table 4.

## 8. Scaling up to the landscape

On the basis of the plot level relationships established with LSP (floristics) and LiDAR (height and canopy cover), predictions of mean attribute values and distributions at both the PSU (150 predictions) and SSU (4500 predictions) level for the entire 220,000 ha study area were generated. The following sections present a summary of the extrapolations and then compare the sampled distributions with the mapped distributions based on datasets currently used by both the Queensland and Federal Governments.

Table 5  
Comparison of dominant genus groups as sampled from the 4500 SSUs and mapped using Queensland Herbarium data for the SSUs and also the region

Data source	Percentage area of dominant genus group					
	Acacia	Callitris	Eucalypt Ironbark	Eucalypt other <sup>c</sup>	Angophora	Non-forest
Field plots (7.75 ha) <sup>a</sup>	8.8	30.3	15.7	30.3	15.1	–
API-PSU (1125 ha)	3.1	35.6	24.3	16.1	10.9	10.0
API-PPP (8713 ha)	2.8	36.8	25.2	15.1	9.5	10.7
Qld Herbarium (PSU area)	0.0	18.8	54.5	4.6	12.4	9.7
Qld Herbarium (PPP area)	0.3	17.5	54.5	5.4	12.7	9.7
Qld Herbarium (study area)	1.1	18.6	51.9 <sup>b</sup>	6.8	11.0	10.7

<sup>a</sup> Percentage based on basal area (for trees 10 cm DBH+) and not crown area.

<sup>b</sup> 28% could also be included in the "Eucalypt other" class.

<sup>c</sup> Includes unknown species in the field plot and LSP data.

### 8.1. Species distributions

The floristic composition was established by summarising the occurrence of species associations within the 4500 SSUs. Approximately 70% of the D1 species were represented by CP-, SLI, SBA and Eucalypt species, with CP- being the most common. Only 10% of the study area was non-forest. Within the remaining 20%, species such as *Eucalyptus dealbata* (TDG), *E. fibrosa* sp. *Fibrosa* (BRI) and *E. decorticans* (GTI) were commonplace. Of the D2 species, SLI, EUS, CP- and SBA continued to account for the majority (55%), with the remaining co-dominant including GTI, TDG and PBX. D3 species were absent from 35% of the PSUs and, where they did occur, these were dominated by *Eucalyptus* species (particularly SLI), although a diversity of other species were present. Such species, many of which are understorey, included BGL and SWB. Species associations were commonplace. Based on the presence of D1 and D2 species (e.g., PBXSWB, which represents an association of PBX and SWB), CP-SLI formed the most extensive association although CP-SBA, SBA-CP- and SLI-CP- were common. However, these associations (together within non-forest) represented only 31% of all associations. Other associations, including SLI-EUS and CP-EUS, dominated within 61% of the PSUs with non-forest occurring in the remainder.

Within the existing regional datasets (i.e., 1:250,000 broad vegetation mapping; MPIG, 2001) and 1:100,000 scale land cover mapping based on Landsat TM, the equivalent detail at a species level was not available. Therefore, species information for the SSUs were extracted from Queensland Herbarium data and based primarily on the dominant species according to the main categories of Acacia, Callitris, Eucalypt/Ironbark, Eucalypt (other), Angophora and non-forest. It should be noted that the regional datasets were also generated partially from the Herbarium data, but the final aggregation classes were too broad for our needs. The distribution of species/communities within the study area, as sampled using the field plots, the PSUs and also the PPPs, was then compared (Table 5). Areas of Angophora and non-forest mapped using the Herbarium data (for the PPPs and PSUs) were similar to those mapped using API. The mapped area of Acacia was far lower within the Herbarium data, although this may have been attributed to the extensive clearance



of woodlands and subsequent regrowth of *Acacia* in the period between the Herbarium (1995) and the LSP survey (2000). The area of *Callitris* were under-estimated (by ~50%) by the Herbarium and a greater area of *Eucalypt*/*Ironbark* was mapped compared to just *Eucalypt* and other genera. The combined area of Herbarium-mapped forests with *Eucalypt* dominance was, however, greater (by about 20%) compared to the 2000 survey. The relative proportion of Herbarium classes within the area of the PSUs and PPPs, was similar to that observed across the entire study area, suggesting that the proportion of species observed in the LSP for the PSUs and PPPs should be representative of the area as a whole.

The discrepancies observed between the two surveys were attributed partly to the differing scales of the datasets rather than to the different approaches to mapping (i.e., wall-to-wall mapping and systematic sampling). Specifically, the Herbarium classifications were generated from a combination of Landsat sensor data with API of 1:80,000 scale photography and some field survey, and hence less detail was able to be resolved. Also, the Herbarium classifications were designed for describing community mosaics, so that the relative dominance of species in any one polygon may not match a field survey plot in that same polygon; however, the overall landscape composition will be robust. The differences in the extent of *Callitris* are of concern, however, as these are spectrally most distinct from other communities within the Landsat sensor data. The analysis suggests that the LSP API provided a good estimate of the extent of dominant species within the study area and also a better identification of the composition of the communities.

8.2. Height and FPC distributions

A comparison of height estimates for the 13 PSUs with those estimated through the NFI (2003; Table 6) indicated a general correspondence between classes but demonstrated the greater

detail that could be obtained using LiDAR (as only two height categories were stated by the NFI). Within Australia, forests are defined as being >2 m in height and supporting a canopy cover of ≥20% and, within this vegetation type, woodland, open forest and closed forest are regarded as having an FPC between 10 and 30%, 30 and 70% and greater than 70%, respectively (Carnahan, 1990; Specht and Specht, 1999). These broad categories were therefore used to summarise the spatial distribution of FPC (and also height), as estimated using the regression equations with LiDAR outlined above, across the 4500 SSUs (Table 7).

Heights, in this case, were defined as the maximum height within each SSU, as estimated using LiDAR, whilst FPC was defined as the total FPC of the SSU. Based on the FPC classes, approximately 10% of the area represented by the SSUs was defined as non-forest, whilst 17.7 and 72.2% were defined as woodland and open forest, respectively. Within the non-forest areas, the maximum height of vegetation was <9 m (for approximately 85% of the class) with greater heights associated with large and relatively isolated trees (e.g., remnant within paddocks). Within the woodlands and also the open forests, the maximum height of the trees was distributed relatively evenly between the 10–19 and 20–29 m classes. Few PSUs with trees 30–39 m tall were observed.

The distribution of height by genus group (Table 8) suggested that different height classes were dominated by different genera, namely *Acacias* (2–9 m), *Callitris* and *Eucalyptus* (10–19 m), *Callitris* (30%, 20–29 m) and *Callitris*/*Angophoras* (30–39 m). Within the 20–29 m height class, *Callitris* predominated (36.5% of the category) but *Eucalypt*/*Ironbark*, *Eucalypt*/other and *Angophora* occurred in moderate (~20%) and roughly equal proportions.

LiDAR FPC estimates were also generated for each of the 4500 SSUs. The distribution of FPC by community (Table 9) suggested that within the non-forest category (i.e., FPC < 10%), *Acacia* was more abundant, with BGL dominating. Within woodlands, all other genus types were equally represented. However, within the open forest, *Callitris* and *Eucalypt* other/*Ironbark* represented over 70% of the dominant genera occurring.

Estimates of forest cover by type (based on either API or LiDAR) for the area were compared subsequently against prior estimates generated by the State Land Cover And Trees Survey (SLATS) land cover change analysis (1991/1999; QDNR,

Table 6  
Estimates of the maximum and range (top 10%) of heights as estimated using LiDAR and by the NFI (2003)

PSU	LiDAR height		NFI (2003) height
	Maximum <sup>a</sup> (m)	Range <sup>b</sup> (top 10%, m)	Range (m)
114	30	16–30	11–30
124	29	17–29	11–30
83	29	17–29	11–30
111	29	16–29	11–30
81	27	18–27	11–30
58	25	14–25	11–30
23	24	14–24	11–30
138	23	15–23	11–30
148	23	13–23	11–30
144	24	15–24	0–30
142	20	13–20	0
59	20	11–20	0
131	15	10–15	0

<sup>a</sup> The highest LiDAR return above the ground.

<sup>b</sup> 10% of returns sorted highest to lowest.

Table 7  
Percentage distribution of 4500 SSUs within different height and FPC classes

Height interval (m)	Non-forest (<10%)	Woodland (10–<30%)	Open forest (30–<70%)	Total
<2	3.5	0	<0.1	3.5
2–9	5.0	<0.1	0	5.1
10–19	1.3	9.3	38.2	48.8
20–29	0.2	8.2	33.6	42.1
30–39	0	<0.1	0.4	0.5
Total	10.1	17.7	72.2	100.0

Table 8  
Proportion of different dominant genera within the 4500 SSUs

Height interval <sup>a</sup> (m)	Percentage of SSU's by dominant genus group						Total
	Non-forest	Acacia	Callitris	Eucalypt Ironbark	Eucalypt other	Angophora	
<2	2.64	0.80	0.04	0.0	0.04	0.0	3.53
2–9	4.58	0.36	0.13	0.0	0.02	0.0	5.09
10–19	2.11	1.58	20.04	15.38	8.20	1.53	48.84
20–29	0.64	0.40	15.18	8.82	7.78	9.22	42.04
30–39	0.02	0.0	0.18	0.09	0.07	0.13	0.49
Total	10.0	3.13	35.58	24.29	16.11	10.89	100.0

<sup>a</sup> Max LiDAR height of SSU.

Table 9  
The percentage distribution of FPC by dominant genus group across the 4500 SSUs

FPC	Percentage of SSU's by dominant genus group						Total
	Non-forest	Acacia	Callitris	Eucalypt Ironbark	Eucalypt other	Angophora	
Non-forest (<10%)	8.47	1.22	0.20	0.09	0.09	0.2	10.09
Woodland (10–<30%)	1.31	0.36	3.60	4.13	4.20	4.09	17.69
Open forest (30–70%)	0.22	1.56	31.78	20.07	11.82	6.78	72.22
Total	10.0	3.13	35.58	24.29	16.11	10.89	100

Table 10  
Forest extent estimates (FPC) as a percentage of the 220,000 ha study region based on existing regional mapping compared to those generated using LSP and LiDAR

Data source	Date	Non-forest (% of area)	Woodland (% of area)	Open forest (% of area)
SLATS	1991 <sup>a</sup>	12	17	71
NFI (SOFR)	1997	11	30	60
NVIS <sup>b</sup>	1999	11	70	19
NFI <sup>c</sup> (Montreal reporting)	2000	13	67	20
LSP sample (3.9% of study area) <sup>d</sup>	2000	11 ± 5	43 ± 5	38 ± 5
LIDAR sample (0.5% of study area)	2000	10 ± 2	18 ± 2	72 ± 2

<sup>a</sup> The FPC value (i.e., woodland/open forest) is based on 1991 estimates, whilst the non-forest area is based on 1999 land cover change mapping.

<sup>b</sup> For Queensland, the NVIS is derived from the Herbarium data.

<sup>c</sup> The NFI provides information only on broad vegetation classes (e.g., Callitris, Acacia and Eucalypt) and is a combination of Landsat cover estimates plus regional ecosystem mapping (including Queensland Herbarium data).

<sup>d</sup> Translation of LSP estimate of CC to FPC.

2000), the 1998 State of the Forest Report (SOFR; NFI, 1998), the National Vegetation Information System (NVIS; NLWRA, 2001) and more recent NFI data (through Montreal Process reporting; Commonwealth of Australia, 2002). Of the existing datasets, the area estimates generated through SLATS and NFI (from the State of the Forests Report, SOFR) suggested a lower proportion of woodland compared to open forest (Table 10). NVIS and the NFI were also similar but suggested that the area of woodland far exceeded that of open forest. In all cases, the area of non-forest was relatively similar. The distribution of FPC within the PSUs/SSUs was most similar to that of SLATS (when based on the LiDAR) and the NFI (SOFR), although some variability between samples was observed. The comparison also suggested a discrepancy in the area of non-forest, with a lower amount estimated using the LiDAR data (Lee et al., 2003).

## 9. Discussion

The study has shown that LSP and LiDAR can provide estimates of stand level floristics and structure (e.g., canopy cover) which are more comprehensive, precise and of greater number compared to field measurements alone. Through API and the development of empirical relationships with LiDAR data, regional level estimates can be generated through simple extrapolation. This approach provides options for operational mapping of such attributes. These options are discussed in greater detail in the following sections.

### 9.1. Retrieval of tree and stand level floristics and structure

The identification of tree species and an assessment of their dominance within the community can be achieved through

interpretation of LSP, although the skills of an experienced interpreter are required. As the diversity of D1 species is not high compared to D2 and D3 genera and many are spectrally distinct in the visible wavelengths, reasonable identification can be achieved at this scale. This capability was confirmed by the high correspondence between the API assessment of dominant species and the field observations. However, the classification of the community according to the three levels of dominance appears to be more subjective because the composition of the communities is well described but the relative order of dominance is not.

Previous studies within Australia and also overseas have indicated that the estimates of tree height from LiDAR are likely to be more accurate than field-based measurements under most conditions, largely because of the difficulty in locating the highest part of larger, non-uniform crowns in the field (particularly in closed canopies) and the errors associated with the measuring devices (e.g., rangefinders) themselves (Witte et al., 2000). Even so, variations occur between sites (Lovell et al., 2005) as LiDAR estimates of tree height are affected by sensor configurations as well as crown shape (Nelson, 1997). Correction factors may therefore need to be applied, although this requires additional knowledge on tree form or species distributions. Within woodlands and open forests, however, estimates of tree height are likely to be more reliable compared to closed forest situations because of the greater likelihood of retrieving returns from the underlying ground surface.

Strong relationships were obtained between field-based estimates of both FBPC and FPC and LIDAR, regardless of the forest type. Similar outcomes were reported by Riaño et al. (2004), who demonstrated that LiDAR-derived estimates of canopy cover correlated well with ground estimates of covered ground and leaf area index (LAI,  $\text{m}^2 \text{m}^{-2}$ ) generated using hemispherical photography, although the study indicated that variation with forest type occurred. The retrieval of both parameters from LIDAR was considered more reliable than from field measurements and (in the case of CC) API estimates, largely because of the capacity to quantitatively encompass the spatial distribution of tree crowns and the variability in crown shapes. Furthermore, the estimates from LIDAR can be re-sampled to support the interpretation of other data (e.g., as acquired by Landsat sensors), thereby avoiding the specific design of field-sampling layouts to suit the resolution of the particular data involved.

## 9.2. Regional estimates of floristics and structure

Comparison with Queensland Herbarium data suggested that although the area of non-forest was similar, the areas occupied by forest types differed. In particular, the LSP data suggested that *Callitris* dominated approximately one-third of the forests occurring, whilst the Herbarium data suggested this figure to be less than one-fifth. The Herbarium data also suggested that over 50% of the forests were dominated by *Eucalyptus* species including Ironbark, whereas the LSP data indicated that Ironbarks were less represented or absent in approximately 15% of the forests observed as containing

*Eucalyptus*. The LSP therefore provided a better indication of the species composition of the forests and a more detailed and permanent record. The areas of *Angophora* and non-forest were reasonably similar to those mapped by the Queensland Herbarium, although a greater extent of *Acacia* was noted from the LSP.

Based on the analysis, LSP was considered to be an efficient and reliable sampling tool that also provided a single, consistent source of information on vegetation structure, land use, disturbance regimes and other landscape attributes. The LSP also provided a more robust regional estimate of community composition than existing mapping sources and was also more suited for establishing baselines of community composition and monitoring long-term changes, particularly as a photographic record was provided. In terms of structure, the height (both maximum and range) distributions from LiDAR were considerably more detailed than those available previously (e.g., NFI, 2003) and provided a greater insight into the structure of the forests. For the study area, the greatest heights were typically associated with open forests dominated by *Callitris* and *Angophora*. *Angophoras* are often remnant within the area because of their low commercial value and large individuals with expansive crowns are commonplace. *Callitris* forests are also managed for commercial purposes (Harris et al., 2003) and large trees are therefore typical. *Acacias* generally dominated the lower height classes, particularly as many are in the early stages of regeneration as a result of recent clearance and degradation (Scanlan, 1991; Fensham et al., 1998).

The FPC estimated from LiDAR suggested that the majority of the area could be classified as open forest, with woodlands occupying a relatively small amount. The greatest FPC was associated with *Callitris* and also *Eucalypt Ironbark* forests. Both CP- and SLI, which are typical to these forests, have a high density of foliage compared to many other species and the density of crowns within CP- is also often large (several thousand per hectare). Although being amongst the largest trees, *Angophoras* typically support a lower density of foliage (which is generally orientated vertically) and hence there is some representation of *Angophoras* within the woodland category. Similarly, the *Eucalypt/other* category was associated more with the woodlands. The lower cover estimates from LSP were attributed to the more qualitative assessment compared to when LiDAR data are used.

The FPC estimates from LiDAR for the PSUs corresponded well with those generated by SLATS and to a certain extent with the NFI SOFR. However, the estimates of the proportion of the area allocated to woodland and open forest differed substantially from the NVIS and NFI (Montreal Process reporting) which was attributed largely to differences in mapping techniques and issues of scale.

## 9.3. Operational implications

The study has confirmed that LSP and LIDAR, both singularly or in combination, can provide stand-based and landscape estimates of floristics and structural attributes (e.g., height, FPC) for structurally complex forests that are typical to

large areas of Australia. At the stand level, such estimates are probably at least as accurate as and potentially more precise than ground-based sampling methods and can be implemented at the same cost once initial calibrations with field data are undertaken. As illustration, 4500 0.25 ha estimates of stand height and cover were produced across the 37 km × 60 km area for approximately AU \$120,000 including labour. The same 4500 “plots” would take more than 20 person years to complete and are estimated to cost between AU \$4–6 million using traditional field-based methods. Such methods would also be difficult to implement across the area due to problems of access. Additional analyses are required to estimate how these savings and benefits may translate into national and regional inventory and monitoring programs. However, it is realistic to expect cost savings well in excess of 90% over traditional field-based methods when surveying large areas.

Whilst the potential savings through integration of LSP and LiDAR have been indicated, further savings would be realized through their combined use within an integrated monitoring framework. For baseline surveys of very mixed and heterogeneous forests, LSP is crucial for identifying, for example, land cover, floristics and disturbance, and for assisting with the calibration and validation of LiDAR information. Under many circumstances, LSP alone may seem a “cheaper” option compared to flying both LSP and LiDAR, particularly considering LSP offers the ability to record more than structural attributes. However, the labour costs associated with LSP are effectively fixed, so each subsequent survey will cost approximately the same as the first. LiDAR is significantly different in that the majority of the cost in terms of labour occurs in the early stages of the first survey and automated procedures decrease labour costs as the areas flown and the requirement for monitoring increase. LiDAR also offers the ability to automatically monitor structural attributes (e.g., canopy density or defoliation) relating to, for example, forest condition at a more precise level than LSP. For these reasons, the use of both LSP and LiDAR in an initial baseline survey and the acquisition of LiDAR in subsequent survey would be the most cost-effective option for sample-based inventories. Fully automated procedures could also be used to identify significant areas of change using the LiDAR data.

## 10. Conclusions and recommendations

The research has demonstrated that sampling using LSP and/or LiDAR can provide quantitative assessments of floristics and key structural attributes (height, cover) which can be extrapolated across the landscape. These estimates are comparable to those generated using traditional wall-to-wall mapping approaches although absolute comparison is limited because of the coarser level of detail associated with many existing datasets. This feature highlights then the additional information that can be obtained using the fine spatial resolution datasets. Furthermore, the assessments are based largely on statistical relationships established between remote sensing data and field-based measurements and the procedures are consistent, reproducible and are also cost-effective.

Although the level of detail is greater and the sampling appears to represent the distribution of floristic and structural attributes across the landscape, wall-to-wall mapping is still regarded as essential for certain purposes (e.g., to evaluate the loss of communities associated with land clearing). However, such mapping is actually enhanced considerably by the provision of an extensive fine spatial resolution dataset as acquired during this research.

The study therefore recommends the establishment of an integrated mapping and monitoring framework which has, at its base, sampled acquisition of fine spatial resolution data (namely LiDAR, LSP, videography or even hyperspectral data) supported by a comprehensive and targeted field campaign and same-date acquisition of airborne or spaceborne remote sensing data for scaling purposes. Once established, repeated overflights of all datasets can be used to determine change in floristics and structure and better inform and/or support regional forest and woodland management, obligations to international agreements (e.g., the Montreal Process, International Biodiversity Treaty and the UNFCCC) and national and international opinions on, for example, greenhouse gas emissions and conservation of biodiversity.

Within Australia, a Continental Forest Monitoring Framework (CFMF) has been initiated to provide an integrated, nationally consistent inventory and monitoring program for meeting assessment and reporting requirements (BRS, 2003). For the CFMF, new data integration and analysis techniques are being investigated and evaluated on the basis of cost-effectiveness, ease of application, repeatability, transparency and verification. The outcomes from the CFMF are intended to provide a scientifically robust analysis of status and trends in the extent and condition of forest ecosystems (including the environmental services they provide) in a timely and consistent manner across all tenures. The information will be used to inform and evaluate national policy and regional decisions on trans-boundary issues and to support sub-regional monitoring activities aimed at evaluating management actions (BRS, 2003). The CFMF will be designed with consideration to political, economic and scientific requirements and constraints. This design will take advantage of opportunities presented by recent developments in remote sensing at a range of scales, whilst at the same time retaining the maximum extent of coverage and incorporating new and more efficient data collection techniques as these become available. The design features three interrelated tiers of data collection and is being evaluated in north-east Victoria where a wide range of forest types and environments exist (Lee et al., 2003). The techniques developed in this research are contributing to this CFMF pilot project and it anticipated will form the basis for wider application across Australia.

## Acknowledgements

The authors would like to acknowledge the support provided by the Australian Research Council, under their SPIRT program, the Cooperative Research Centre for Greenhouse Accounting, and Agriculture, Fisheries and Forestry Australia.

We would also like to thank Kerstin Jones, Robert Denham, Norm Good, and the staff of UNSW, QDNR&M, BRS, QUT and QDPI Tropical Beef Centre.

## References

- Aldred, A.H., Bonner, G.M., 1985. Application of Airborne Laser to Forest Surveys, Information Report PI-X-51, Canadian Forestry Service. Petawawa National Forestry Institute, Chalk River, p. 62.
- Australian Greenhouse Office, 2000. National Greenhouse Gas Inventory: Land Use Change and Forestry Sector 1990–1999, Canberra.
- Barrett, D.J., Galbally, I.E., Graetz, R.D., 2001. Quantifying uncertainty in estimates of C-emissions from above-ground biomass due to historic land-use change to cropping in Australia. *Global. Ch. Biol.* 7, 883–902.
- Bureau of Meteorology, 2004. [http://www.bom.gov.au/climate/map/annual\\_rainfall/](http://www.bom.gov.au/climate/map/annual_rainfall/).
- Bureau of Rural Sciences, 2003. A Continental Forest Monitoring Framework for Australia – Background, Concept and Rationale. Department of Agriculture, Fisheries and Forestry, Canberra.
- Burrows, W.H., Henry, B.K., Back, P.V., Hoffmann, M.B., Tait, L.J., Anderson, E.R., Menke, N., Danaher, T., Carter, J.O., McKeon, G.M., 2002. Growth and carbon stock change in eucalypt woodlands in north-east Australia: ecological and greenhouse sink implications. *Global. Ch. Biol.* 8, 1–16.
- Carnahan, J.A., 1990. Vegetation. Atlas of Australian Resources, vol. 6, Third Series. Australian Surveying and Land Information Group. Department of Administrative Services, Canberra, Australia.
- Commonwealth of Australia, 2002. Implementation of Montreal Process Criteria and Indicator Reporting—An operational Demonstration Using Sample-Based Inventory Designs and Commercially Available Remote Sensing Systems. Department of Agriculture Fisheries and Forestry Australia, Canberra, unpublished.
- Dowling, R., Accad, A., 2003. Vegetation classification of the riparian zone along the Brisbane River, Queensland, Australia using light detection and ranging (lidar) data and forward looking digital video. *Can. J. Remote Sens.* 29, 556–563.
- Fensham, R.J., McCosker, J.C., Cox, M.J., 1998. Estimating clearance of Acacia dominated ecosystems in central Queensland using Land-system mapping data. *Aust. J. Bot.* 46, 305–319.
- Harris, M.R., Lamb, D., Erskine, P.D., 2003. An investigation into the possible inhibitory effects of white cypress pine (*Callitris glaucophylla*) litter on the germination and growth of associated ground cover species. *Aust. J. Bot.* 51, 93–102.
- Henry, B.K., Danaher, T., McKeon, G.M., Burrows, W.H., 2002. A review of the potential role of greenhouse gas abatement in native vegetation management in Queensland rangelands. *Rangeland J.* 24, 112–132.
- Hyyppä, J., Olavi, K., Lehtikoinen, M., Inkinen, M., 2001. A segmentation-based method to retrieve stem volume estimates from 3-D tree height models produced by laser scanners. *IEEE Trans. Geosci. Remote Sens.* 39, 969–975.
- Jones, K.L., 2000. Aerial Photography Interpretation for the Injune Remote Sensing Sampling Strategy. Queensland Department of Natural Resources, Brisbane, Forest Ecosystem Research and Assessment Technical Report No. 00129.
- Lee, A., Norman, P., Wood, M., Davey, S., 2003. Utilising integrated sampling strategies for regional and continental forest monitoring through criteria and indicators. In: Mason, E., Perley, C. (Eds.), Proceedings Joint Australia and New Zealand Institute of Forestry Conference, April, Queenstown, New Zealand. New Zealand Institute of Forestry, Christchurch, NZ, pp. 248–259.
- Lefsky, M.A., Cohen, W.B., Parker, G.G., Harding, D.J., 2002. LiDAR remote sensing for ecosystem studies. *Bioscience* 52, 19–30.
- Lovell, J.L., Jupp, D.L.B., Culvenor, D.S., Coops, N.C., 2003. Using airborne and ground-based ranging LiDAR to measure canopy structure in Australian forests. *Can. J. Remote Sens.* 29, 607–622.
- Lovell, J.L., Jupp, D.L.B., Newham, G.J., Coops, N.C., Culvenor, D.S., 2005. Simulation study for finding optimal LiDAR acquisition parameters for forest height retrieval. *Forest Ecol. Manage.* 214, 398–412.
- Lucas, R.M., Milne, A.K., Cronin, N., Witte, C., Denham, R., 2000. The potential of synthetic aperture radar (SAR) for quantifying the biomass of Australia's woodlands. *Rangeland J.* 22, 124–140.
- Lucas, R.M., Moghaddam, M., Cronin, N., 2004. Microwave scattering from mixed species forests, Queensland, Australia. *IEEE Trans. Geosci. Remote Sens.* 42, 2142–2159.
- Lucas, R.M., Cronin, N., Lee, A., Witte, C., Moghaddam, M., 2006. Empirical relationships between AIRSAR backscatter and forest biomass, Queensland, Australia. *Remote Sens. Environ.* 100, 407.
- Magnussen, S., Boudewyn, P., 1998. Derivations of stand heights from airborne laser scanner data with canopy-based quantile estimators. *Can. J. Forest Res.* 28, 1016–1031.
- McDonald, R.C., Isbell, J.G., Speight, J.G., Walker, J., Hopkins, M.S., 1998. Australian Soil and Land Survey Field Handbook, second ed. Commonwealth Department of Primary Industries and Energy & CSIRO, p. 190.
- Means, J.E., Acker, S.A., Harding, D.A., Blair, B.J., Lefsky, M.A., Cohen, W.B., Harmon, M., McKee, W.A., 1999. Use of large footprint scanning airborne LIDAR to estimate forest stand characteristics in the western Cascades of Oregon. *Remote Sens. Environ.* 67, 298–308.
- Moffiet, T., Mengersen, K., Witte, C., King, R., Denham, R., 2005. Airborne laser scanning: exploratory data analysis indicates potential variables for classification of individual trees or stands according to species. *ISPRS J. Photogram. Remote Sens.* 59, 289–309.
- Montreal Process Implementation Group, 2001. Sustainable Forest Management-Criteria and Indicators for Sustainable Management of Australia's Forests: Report on Implementation of Category A Indicators, Canberra, unpublished.
- Naesset, E., 1997. Determination of mean tree height of forest stands using airborne laser scanner data. *ISPRS J. Photogram. Remote Sens.* 52, 49–56.
- National Forest Inventory (NFI), 1998. Australia's State of the Forests Report. Bureau of Rural Sciences, Canberra.
- National Forest Inventory (NFI), 2003. Australia's State of the Forests Report. Bureau of Rural Sciences, Canberra.
- National Land and Water Resources Audit (NLWRA), 2001. Australian Native Vegetation Assessment. National Land and Water Resources Audit, Canberra.
- Nelson, R., 1997. Modelling forest canopy heights: the effects of canopy shape. *Remote Sens. Environ.* 60, 327–334.
- Nelson, R.F., Krabill, W.B., Maclean, G.A., 1984. Determining forest canopy characteristics using airborne laser data. *Remote Sens. Environ.* 15, 201–212.
- Nelson, R.F., Krabill, W.B., Tonelli, J., 1988. Estimating forest biomass and volume using airborne laser data. *Remote Sens. Environ.* 24, 247–267.
- Nielson, U., 1997. Operational resource data collection using large-scale aerial photography. In: Bauer, M., et al. (Eds.), Proceedings of The First North American Symposium on Small Format Aerial Photography, October 14–17, Cloquet, Minnesota, USA. American Society for Photogrammetry and Remote Sensing, Cloquet, pp. 3–47.
- Nilsson, M., 1994. Estimation of Tree Heights and Stand Volume Using Airborne LiDAR System, Report 57. Department of Forest Survey, Swedish University of Agricultural Sciences, Umea, p. 59.
- Pitt, D.G., Wagner, R.G., Hall, R.J., King, D.J., Leckie, D.G., Runesson, U., 1997. Use of remote sensing for forest vegetation management: a problem analysis. *Forestry Chronicle.* 73, 459–477.
- Queensland Department of Natural Resources, 2000. Land Cover Change in Queensland 1997–1999. A Statewide Landcover and Trees Study (SLATS) Report. Queensland Department of Natural Resources, Brisbane.
- Riaño, D., Valladares, B., Condes, S., Chuvieco, E., 2004. Estimation of leaf area index and covered ground from airborne laser scanner (LiDAR) in two contrasting forests. *Agric. Forest Meteorol.* 124, 269–275.
- Scanlan, J.C., 1991. Woody overstorey and herbaceous understorey biomass in Acacia harpophylla (brigalow) woodlands. *Aust. J. Ecol.* 16, 521–529.
- Schreuder, H.T., Gregoire, T.G., Wood, G.B., 1993. Sampling Methods for Multi-Resource Forest Inventory. John Wiley and Sons, New York, p. 446.
- Specht, R.L., 1970. Vegetation. In: Leeper, G.W. (Ed.), The Australian Environment. fourth ed. CSIRO-Melbourne University Press, Melbourne, pp. 44–67.
- Specht, R.L., Specht, A., 1999. Australian Plant Communities. Dynamics of Structure, Growth and Biodiversity. Oxford University Press, Melbourne, Australia.

- Spencer, R.D., 1992. Application of modern inventory techniques in the forests of western Australia. West Australian Department of Conservation and Land Management, Perth, CALM Occasional Paper No 1/92.
- Spencer, R.D., Czaplewski, R.L., 1997. National forest inventory in the USA: an outline of the procedure. *Aust. Forest* 60, 56–66.
- Spencer, R.D., Hall, R.J., 1988. Canadian large-scale aerial photographic systems (LSP). *Photogram. Eng. Remote Sens.* 54, 475–482.
- Suárez, J.C., Ontiveros, C., Smith, S., Snape, S., 2005. Use of airborne LiDAR and aerial photography in the estimation of individual tree heights in forestry. *Comp. Geosci.* 31, 253–262.
- Wehr, A., Lohr, U., 1999. Airborne laser scanning—an introduction and overview. *Photogram. Eng. Remote Sens.* 54, 68–82.
- Weller, D., Witte, C., Mackie, C., Smith, D., Denham, R., 2001. Using airborne laser altimetry to assess and monitor biodiversity. Queensland Department of Natural Resources, Brisbane, Forest Ecosystem Research and Assessment Technical Paper No. 0102.
- Witte, C., Norman, P., Denham, R., Turton, D., Jonas, D., Tickle, P., 2000. Airborne laser scanning—a tool for monitoring and assessing the forests of Australia. In: *Proceedings, 10th Australasian Remote Sensing Conference*, August. Adelaide, Australia. Remote Sensing and Photogrammetry Association of Australasia, Adelaide (CD-ROM).

# Enhanced Simulation of Radar Backscatter From Forests Using LiDAR and Optical Data

Richard M. Lucas, Alex C. Lee, and Mark L. Williams

**Abstract**—Focusing on a forest dominated by Poplar Box (*Eucalyptus populnea*) near Injune in Queensland, Australia, light detection and ranging (LiDAR) and optical remote sensing data are integrated with tree- and stand-level information to parameterize a coherent L-band synthetic aperture radar (SAR) imaging simulation that models microwave penetration and interaction with the canopy, understory, and ground. The approach used LiDAR data to generate a three-dimensional representation of the distribution of tree components (leaves and small branches) by species (based on 1-m<sup>3</sup> voxels) and the ground surface. Tree trunks were mapped across a 7.5-ha forest stand using a LiDAR-derived height-scaled crown openness index. Primary and secondary branches were modeled as tapering cylinders and linked the canopy voxels to the LiDAR trunks. The dimensions of vegetation and soil components and their geometric and dielectric properties required by the model were calibrated with field-based measurements. Visual and numerical comparison between NASA JPL Airborne SAR data and the model simulation suggests the effective modeling of SAR imagery at L-band. The study provides a proof-of-concept approach for integrating LiDAR data in the parameterization of coherent SAR simulation models, and the model presents options for better understanding of the information content of SAR data in real forest situations.

**Index Terms**—Australia, forestry, light detection and ranging (LiDAR), radar, scattering, simulation.

## I. INTRODUCTION

**K**NOWLEDGE of the information content of synthetic aperture radar (SAR) data acquired over forest environments, particularly microwave interaction with different components (i.e., leaves, trunks, and branches), is required to support the retrieval of their biomass, structure, and floristic composition at an operational level. Such knowledge is increasingly important given the successful launch of Japan's Advanced Land Observing Satellite (ALOS) Phased Array L-band SAR (PALSAR) in January 2006 and the proposed deployment of other spaceborne SARs operating at L-band,

C-band (e.g., RADARSAT-2), and X-band (e.g., TerraSAR). Data from these and currently operating SARs are anticipated to play a major future role in global forest characterization, mapping, and monitoring and will be used to support greenhouse accounting, carbon cycle science, biodiversity assessment, resource management, and sustainable utilization of forests.

In gaining such knowledge, a number of approaches can be adopted. These include the use of empirical relationships with structural attributes and biomass [1]–[3]. More sophisticated models use two-dimensional (2-D) layered distributions of tree components of varying sizes, geometries, and dielectric properties [4]–[6] to simulate (and understand) microwave interaction with the forest volume together with the overall backscatter coefficient ( $\sigma^\circ$ ) and the magnitude of contributory mechanisms (e.g., single bounce, volume scattering) [7], [8]. However, in both cases, much of the information used has been derived from field data collected from individual trees and/or stands (e.g., through plot-based survey). Such information is limited, however, as the three-dimensional (3-D) distribution of plant components is not adequately captured. Furthermore, many layered models assume a random but uniform distribution of scattering elements within the forest volume, whereas many forests are much more structurally complex.

An opportunity to provide a more realistic representation of forest volume has arisen with the advent of light detection and ranging (LiDAR) data. These data have been used primarily to retrieve commonly measured forest attributes, namely tree-based estimates of top height and crown dimensions [9]–[11] or stand-based estimates of mean or maximum canopy height [12], basal area [13], canopy cover [14], [15], timber volume [16], and/or biomass [17]. Algorithms have typically been developed through reference to or using empirical relationships with ground data, and their success has been reported by referring to a testing ground data set and utilizing standard statistical descriptors (e.g., the coefficient of variation  $r^2$ ). Most of these studies have been conducted across a range of forested biomes (boreal, temperate, subtropical, and/or tropical) in the U.S. [18], [19], Canada [20], [21], Australasia [22], [23], and Europe [24], [25] and largely by timber companies, government organizations, and the academic scientific community. As with this study, data acquired by discrete return small footprint LiDAR have generally been utilized [26]. This is typically a two-return system (although some systems can retrieve up to five returns), whereby the ground and vegetation returns are separated (into first and last). Depending upon the flying height, the laser footprint size can vary from 0.1 to 5.0 m and the interval of laser returns from 0.25 to 5.0 m [23]. Large-footprint full-waveform LiDAR is also increasingly being used, as these systems facilitate a more comprehensive assessment of the forest canopy volume [15], [19], [26], [27], although they have yet to

Manuscript received October 4, 2005; revised May 16, 2006. This work was supported by the Defence Science and Technology Organisation and in part by the Australian Research Council, the Australian National University, and the Cooperative Research Centre (CRC for Greenhouse Accounting). The Injune Landscape Collaborative Project was supported by the Queensland Department of Natural Resources and Mines, the Bureau of Rural Sciences, the Australian Greenhouse Office, and the CRC for Greenhouse Accounting.

R. M. Lucas is with the Institute of Geography and Earth Sciences, University of Wales, SY23 3DB Aberystwyth, U.K. (e-mail: rml@aber.ac.uk).

A. C. Lee is with the School of Resources, Environment, and Society, Australian National University, Canberra, ACT 0200, Australia, and also with the Cooperative Research Centre for Greenhouse Accounting, Australian National University, Canberra, ACT 0200, Australia (e-mail: Alex.Lee@anu.edu.au).

M. L. Williams was with the Defence Science and Technology Organisation, Edinburgh, SA 5111, Australia. He is now an independent SAR consultant (e-mail: mark.williams@physics.org).

Digital Object Identifier 10.1109/TGRS.2006.881802

become commercially feasible or as widely available as small-footprint systems. When retrieving forest structural attributes, a majority of the studies utilized the LiDAR height information, which has generally been in the form of canopy height surfaces interpolated from point data. However, research is increasingly focusing on alternative measures (e.g., summaries of the vertical distribution of returns) for retrieving forest structural attributes [16], [17], including those that have proved more difficult to quantify [e.g., the density and actual location of trees and the distribution of individual plant components (e.g., leaves, branches) within the forest volume]. It is this information that is also sought by scientists researching the interaction of microwaves with the forest volume and the potential of radar for retrieving forest structural attributes and biomass.

Developments in SAR simulation modeling have occurred alongside those in LiDAR remote sensing, with the former increasingly seeking and utilizing information on the 3-D stratification of forests. For example, Stupis *et al.* [28] used simplified models of *Pinus* (pine) and *Quercus* (oak) species to reconstruct forested terrain and coupled these to a model that both simulated microwave interaction and produced an image. In this case, the forests were not generated using detailed ground truth, and simulations from single polarization channels only were reported. More realistic representations [of *Acer* (maple) trees] were generated in [29] and [30] using fractal models, although only backscatter levels were predicted and the data were not coupled with SAR simulations. A number of researchers have developed SAR simulation models based on cubes or “voxels” of varying dimensions (e.g., [8], [34], and [36]) attributed with input parameters from modeled representations of trees. These SAR imaging calculations determine the attenuation of microwaves during their passage through the forest canopy as a function of the dimensions, orientations, and dielectric constants of the tree components by voxel. As with the 2-D models, they simulate both total and decomposed (i.e., according to the contributions of different scattering mechanisms) SAR backscatter. For example, Praks *et al.* [33] used models of Scots Pine (*Pinus sylvestris*) coupled to backscatter calculations and compared these with actual SAR observations (although a full SAR image calculation was not performed). In [34], similar tree models were used in a very high frequency (VHF; 20–90 MHz) SAR calculation, and image outputs were compared with CARABAS [31] observations; the simulations used for this paper are an extension of this earlier technique. In [35], a model canopy generated from a statistical description of Indonesian rainforest was combined with a full SAR simulation to perform a coherent (phase preserving) InSAR calculation, including a prediction of interferometric coherence. By indicating the potential for the recovery of canopy structure using interferometry, this work highlighted the importance of coherent SAR image prediction. In [32] and [36], a biologically accurate model forest was coupled to a coherent SAR simulation to assess the potential of an algorithm (which relied upon both polarimetry and interferometric coherence) for detecting subcanopy moisture [32] and concealed targets [36]. Despite these advances, no studies have yet utilized LiDAR data to map or model the explicit distribution and size of plant components (leaves, branches, and trunks) within different canopy layers and in three dimensions for input to SAR simulations. Furthermore, in parameterizing the models (e.g., with geometric and

dielectric information), most have used data from external and often historical sources rather than undertaking field sampling (e.g., destructive harvesting of trees for assessing moisture content) at the same time and location at which the SAR data were acquired.

In this study, and focusing on a 7.5-ha forested site in Queensland, central east Australia, we bridge gaps in forest canopy model 3-D representation and SAR simulation by presenting a proof-of-concept methodology that revolves around the construction of a 3-D voxel matrix (1-m<sup>3</sup> resolution). The matrix is intersected with airborne scanning LiDAR data, and voxels containing LiDAR returns are used to model the 3-D distribution of leaf and terminal branches within the forest volume. A LiDAR-derived canopy density surface is used to map potential tree stem locations. An algorithm for delineating individual crowns/clusters of crowns (objects) is then applied to the LiDAR data, and each object is associated with a species type through reference to classifications of hyperspectral Compact Airborne Spectrographic Imager (CASI) data and large-scale (1 : 4000) aerial photography (LSP) acquired over the same forests. Voxels are then associated with individual crown/cluster objects based on criteria of proximity and adjacency and are attributed subsequently with species-specific and field-measured parameters related to the dimensions and geometric and dielectric properties of leaves and terminal branches. Finally, secondary branches of varying dimension and orientation are constructed between individual voxels and primary branches, with the latter constructed between discrete groups of voxels and the LiDAR-mapped stems. The ground surface is also characterized using field observations and classifications undertaken through linear spectral unmixing of CASI data. Using this information, we parameterize a 3-D coherent SAR image simulation model that considers microwave penetration and interaction with canopy and understory components.

The research presented is unique in that it is the first to reconstruct a forest from LiDAR data and use this to perform a coherent SAR image calculation and predict a fully polarimetric single-look complex (SLC) SAR image. Simulations are performed at L-band. The significance of an ability to predict coherent SAR imagery was amply highlighted in [35], where calculations indicated the potential of recovering structural information from InSAR measurements. This potential has recently been demonstrated using the model reported in this paper; here, SAR imagery of the Injune forest was simulated, and tree height was retrieved using PolInSAR techniques [37]. This research also emphasized the importance of the correct prediction of SAR coherence in modeling.

This paper is constructed as follows. Sections II and III provide an overview of the study site and the collected data. Section IV considers the formation and parameterization of the model forest canopy using LiDAR. Section V describes some of the more salient features of the SAR simulation. In Section VI, the fully polarimetric simulation results for a single forest at L-band are illustrated and compared with airborne SAR (AIRSAR) observations of the modeled area at the same frequency. Section VII then evaluates the procedures developed for integrating the LiDAR, CASI, and field data to reconstruct the forest and parameterize the coherent SAR model, the SAR simulation results, and the benefits and implications of the research. The study is summarized and concluded in Section VIII.



## II. SITE DESCRIPTION

The study focused on an area of mixed species forests near Injune in central Queensland, Australia (latitude  $25^{\circ}32'S$ , longitude  $147^{\circ}32'E$ ). In preparation for the acquisition of LSP, LiDAR, and hyperspectral (e.g., CASI) data as well as airborne NASA JPL SAR (AIRSAR), a grid of one hundred fifty  $500 \times 150$  m primary sampling units (PSUs; 10 columns, 15 rows) was established, with each separated in the north–south and east–west directions by approximately 4 km. PSUs were numbered sequentially from top left (1) to bottom right (150), with each subdivided into 30 secondary sampling units (SSUs) that were numbered sequentially from 1 to 30. The study area is described in full in [4] and [23], which include illustrations and descriptions of the PSU/SSU grid and remote sensing data sets acquired.

For this particular study, a  $500 \times 150$  m section (PSU 142) of forest dominated by Poplar Box (*Eucalyptus populnea*) was considered, as data from four  $50 \times 50$  m field plots (SSUs) had been collected at the same time as the remote sensing data. This forest contained relatively sparse cover with a biomass ranging from 43 to  $80 \text{ Mg} \cdot \text{ha}^{-1}$  for the contained SSUs, as calculated by applying species-specific allometric equations [38] to plot measurements of stem diameter. Although *E. populnea* dominated, individuals of other species, including Brigalow (*Acacia harpophylla*), White Cypress Pine (*Callitris glaucophylla*), and Silver-Leaved Ironbark (*E. melanaphloia*), were also present, but none represented more than 5% of individual trees within the four plots. In sections, a 5–6-m-high understory consisting of Sandalwood Box (*Eremophila mitchelli*) occurred. The forests ranged from thinned (typically ring barked) stands, which contained a significant proportion of regenerating individuals (to the west), to more mature stands dominated by trees with larger trunk diameters (up to 45 cm at 130 cm above ground level; to the east). Across the PSU, grazing by stock had occurred.

## III. DATA COLLECTION

### A. Acquisition of LSP, LiDAR, and Hyperspectral Data

For the  $37 \times 60$  km study area, LSPs were acquired in July 2000, which is a month before a field campaign in August 2000. Small-footprint airborne scanning LiDAR data were acquired over a one week period commencing on August 24, 2000, using an Optech 1020 scanning LiDAR mounted in a Bell Jet Ranger Helicopter. The Optech measured 5000 first and last returns and the intensity of each return per second. The LiDAR operated within the near-infrared spectrum with a beam divergence of 0.3 mrad, a footprint of approximately 7.5 cm, and an average sampling interval of  $< 1$  m. Data were acquired flying in an east–west direction (and centered on each PSU row) at a nominal altitude of 250 m and over a swath width of approximately 200 m. A global positioning system (GPS) base station was established for all flights. With full differential GPS corrections in addition to pitch, yaw, and roll compensation from an inertial navigation system (INS), coordinates were provided with an absolute accuracy of  $< 1$  m in the  $x$  and  $y$  directions and  $< 0.15$  m in the  $z$  direction [23].

For PSU 142, a total of 195 446 LiDAR returns were recorded, with 82% and 18% classed as ground and vegetation

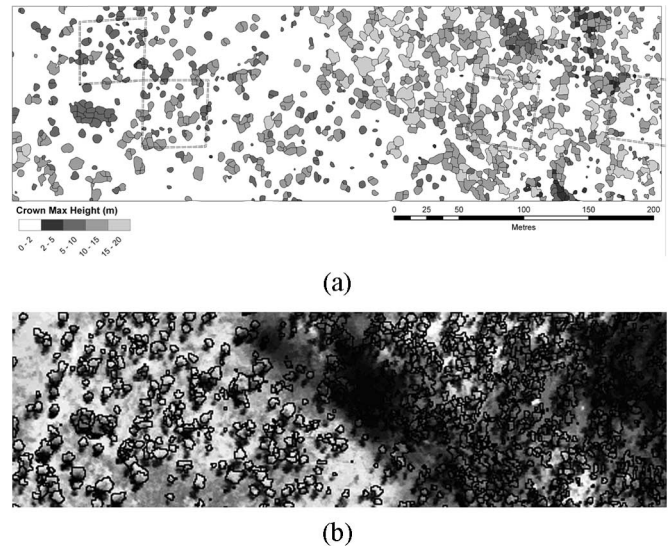


Fig. 1. Study stand of PSU 142. (a) LiDAR-derived crowns and extracted tree heights and the location of the four field plots (boxes). (b) CASI near-infrared reflectance data. In both images, crowns were delineated using the procedures outlined in [43] and [39], respectively.

strikes (i.e., greater than 0.5 m height above ground) respectively. The average number of strikes per 0.25 ha SSU ( $n = 30$ ) within the PSU was 5337 and 1178 for ground and vegetation respectively, which is equivalent to approximately one strike per  $0.4 \text{ m}^2$  on the average. The tallest LiDAR return in the PSU was 20.2 m, with an average maximum height (from the 30 SSUs) of 15.9 m. The LiDAR height data (by crowns/crown clusters) for PSU 142 are shown in Fig. 1(a).

Over a similar time period, 1-m spatial resolution CASI data were acquired on August 29 and September 1, 2000, close to the solar noon and over the same areas as the LiDAR, although the aircraft flew in a north–south direction. Fourteen wavebands of data covering the visible to near-infrared wavelength regions were acquired at a flying height of approximately 500 m. Full calibration of the CASI data was achieved by laying out one black and one white  $4 \times 4$  m calibration tarpaulin of the same material at each of three separate PSUs and at the time of the CASI overpass and simultaneously collecting reflectance measurements from one set using an ASD field spectroradiometer. Empirical line calibration (ELC) was then subsequently employed to generate a calibration file for converting CASI data for all PSUs from units of “at sensor” radiance ( $L$ , in watts per square meter per steradian per micrometer) to surface reflectance (in percent). Further details of the calibration can be found in [39]. An example of the CASI data for PSU 142 is shown in Fig. 1(b). Several hyperspectral HyMap images ( $\sim 1.2$  km swath width and orientated in the north–south direction) were acquired in September 2000 along selected PSU columns and consisted of 128 bands of data at 2.6-m spatial resolution. These data, which were also georeferenced using GPS and INS, provided a landscape view of tree and other land cover distributions and were used subsequently to assist the georegistration of the AIRSAR data.

Four strips of fully polarimetric C-, L-, and P-band AIRSAR data were acquired over the PSU grid on September 3, 2000 [4]. The AIRSAR data were generated by the NASA JPL using the integrated processor version 6.3.1 in compressed Stokes matrix

format. The range and azimuth resolutions were stated as 3.3 and 4.6 m, respectively. Further details of the AIRSAR data and processing can be found in [4]. In previous studies, the AIRSAR data were registered to Landsat sensor data georeferenced through the Queensland government's Statewide Land Cover and Trees Study (SLATS) [40], but here, the registration was fine-tuned by establishing common GCPs between individual trees identified within the HyMap data acquired in the area around and including PSU 142 and P-band HH backscatter data. This AIRSAR channel was selected, as the phase center was considered to be closer to the base of the trunks compared to other frequencies and polarizations.

### B. Forest Inventory and Destructive Harvesting

At the same time as the LiDAR, CASI, and LSP data were acquired, forest inventory data were collected from selected SSUs located within 12 of the 150 PSUs, with four located within PSU 142 [4]. These data consisted of basic forest inventory measurements for each tree, including the following:

- 1) diameter (in centimeters) at 30 and 130 cm [herein referred to as  $D_{30}$  and  $D_{130}$  (which is equivalent to the diameter at breast height), respectively; measured using standard diameter tapes];
- 2) heights (in meters) to the top, canopy base, and the first leafing branch (measured using either a GEOSCAN or CENTURION Laser Rangefinder to within  $\pm 0.5$ –1 m, depending on tree size and form);
- 3) crown dimensions (in meters) in the east–west and north–south directions (measured using 50-m tapes to within  $\sim \pm 1$  m, depending on tree size and form).

Each tree measured was identified to species and associated with a growth stage (e.g., young, mature, senescent) by experienced botanists employed by the Queensland Department of Natural Resources and Mines. Most trees, including those in PSU 142, were photographed from the side (with a scale) using a digital camera. Soil measurements included type (e.g., clay, sand), gravimetric moisture content (in percent), and the dielectric constant [using a time-domain reflectometer (TDR)]. Leaf dimensions (i.e., length, width, and thickness, in millimeters) were also measured in the field using calipers and subsequently in the laboratory using a leaf area meter, from which the mean and variance were calculated.

Following the collection of field data, destructive harvesting of *E. populnea* ( $n = 7$ ) and *E. melanaphloia* ( $n = 5$ ) took place, primarily to assess the validity of existing equations [41] but also to obtain: 1) equations relating tree size (i.e.,  $D_{30}$ ,  $D_{130}$ , height, and crown area) to the biomass of components of differing dimension (e.g., branches of  $< 1$ , 1–4, 4–10, and  $> 10$  cm diameter) and 2) data on the moisture content and amount of leaves, branches, and trunks at the time of the AIRSAR overpass. The procedures for harvesting and for obtaining biomass and moisture content followed those outlined in [41]. The harvesting of *E. populnea* was undertaken within PSU 142. Comprehensive accounts of the methods of field data collection, destructive harvesting, and also the measurement of the dimensions, orientations, and dielectric moisture contents of plant components can be found in [23] and [37].

## IV. MODEL PARAMETERIZATION

### A. Generation of a Digital Terrain Model

A 1-m spatial resolution DTM was generated for PSU 142 to provide information on the ground surface topography and to assign height (above the ground surface) to the LiDAR vegetation returns. Initially, the DTM was constructed by interpolating preclassified first and last ground returns with a 1-m proximal tolerance (where any returns found within 1 m of other returns were excluded) and represented as a triangulated irregular network (TIN) model. However, examination of the resulting surface indicated a certain degree of “noise” and surface variation resulting from on-ground surface features (e.g., logs, grass swards, and shrubs). Therefore, and following other studies (e.g., [11]), a multiscale filtering strategy was employed. Here, the lowest returns (first or last) within local search windows of increasing dimension ( $1 \times 1$  to  $5 \times 5$  m) were selected to generate a bare ground surface, on the assumption that these were more likely to represent the true elevation surface. The most suitable window size for generating the final elevation surface was determined by examining a corresponding elevation standard deviation surface generated using a  $5 \times 5$  search area. Specifically, where low standard deviations in the surface occurred, the lowest returns from the  $3 \times 3$  search area were used, whereas for areas with higher deviation (e.g., water courses), the lowest returns from the smaller search areas were used [9], with the elevation deviation determining the search area used. Subtracting the initial TIN ground model from the final spatially filtered surface produced a difference surface. The surface analysis for PSU 142 indicated that the spatially filtered elevation layer was lower and differed, on the average, by 8 cm (standard deviation  $\delta = 8$  cm, range =  $-0.5$  to 0.5 m), which compared well with other studies (e.g., [42]). The on-ground surface features previously identified were also evident within the difference surface, indicating that spatial filtering of the surface was effective in their removal. Once calculated, the height of woody vegetation was determined as the difference in elevation between the final bare ground surface and the first and last vegetation LiDAR returns. Only returns above 0.5 m were used subsequently for canopy assessment, as those below this height were considered to be from shrubs, tall grass, and larger items of woody debris.

### B. Trunk Location and Tree Crown/Cluster Delineation

To indicate canopy density and potential stem location, the relative penetration of LiDAR pulses through the forest volume was quantified within a  $1\text{-m}^3$  voxel matrix (i.e., a horizontal and vertical spatial resolution of 1 m). This approach is fully described in [43] and is also similar to that adopted in [44]. Within the 3-D matrix, voxels containing canopy LiDAR returns were identified (through intersection), and each was attributed with the tallest recorded height value occurring within the  $1\text{-m}^3$  volume space. A height-scaled crown openness index (HSCOI; expressed as a percentage) was then calculated as

$$\text{HSCOI (in percent)} = \sum_{n=1}^{n_c} \left( \left( \frac{h_{\max} - h_{\text{vox}}}{h_{\max}} \right) \times \frac{1}{n_c} \right) \times 100 \quad (1)$$

where  $h_{\max}$  represents the maximum height over a specified area (see later part of this section), and  $h_{\text{vox}}$  represents the

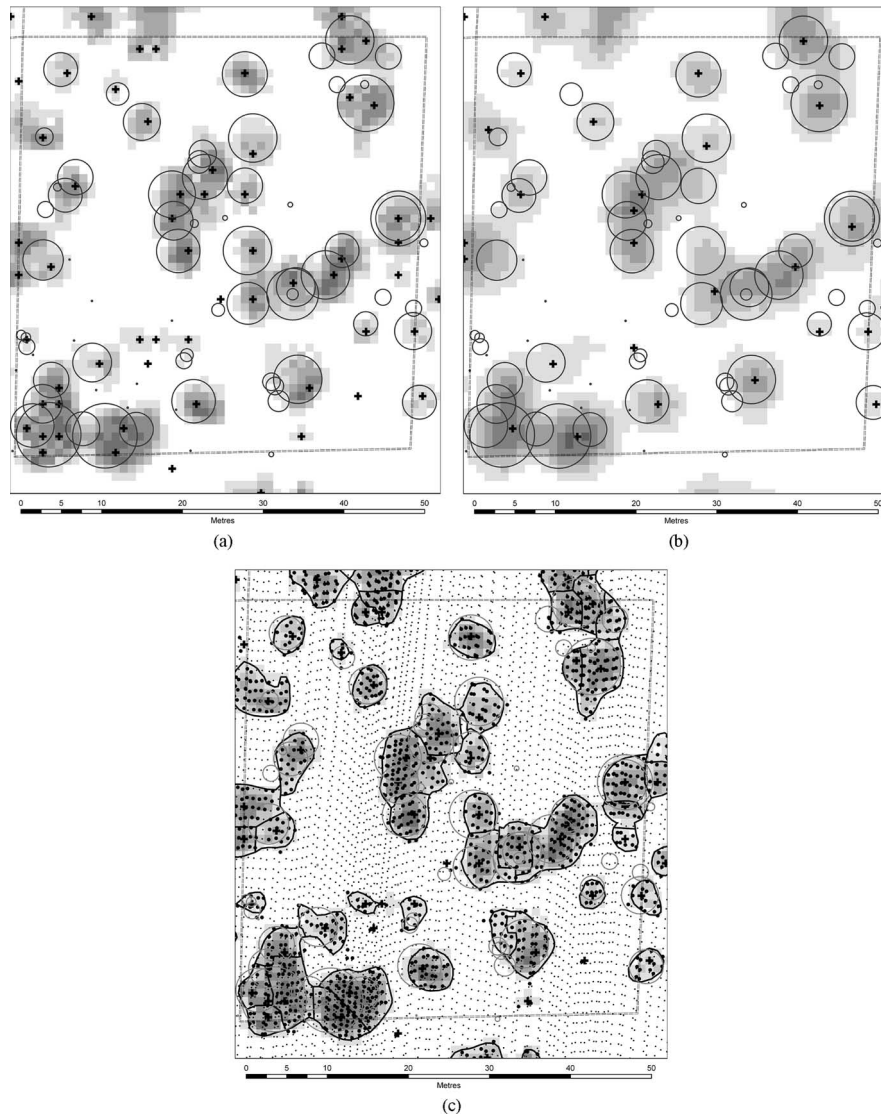


Fig. 2. HSCOI surface and local minima (black crosses) for SSU 142-13. Surfaces are smoothed with a focal-mean function using (a) 1 m circular and (b)  $5 \times 5$  m rectangular kernels. (c) Extent of crowns mapped using a 69% HSCOI contour and raw LiDAR point data (returns  $> 2$  m in height are larger). Darker areas have lower HSCOI values, and tree crowns mapped from the field data are shown as circles.

height of each voxel (within the  $1\text{-m}^2$  vertical column) associated with a LiDAR return. The summation of individual canopy penetration distances (from the top of the canopy) was based on voxel positions within a vertical column of  $1 \times 1 \times n_l$  m, where  $n_l$  represented the number of 1-m height levels within the vertical profile and was determined from the maximum height of the stand. The final HSCOI is a summation of the penetration percentage for all canopy voxels ( $n_c$ ) found within the vertical column such that each voxel contributes equally to the cell result. As a result of the LiDAR sampling density and forest stand structure, between one and five voxels per  $1\text{-m}^2$  column were observed. HSCOI values, which are expressed as a percentage, were outputted as a 2-D raster grid of  $1\text{-m}^2$  spatial resolution. Once generated, the HSCOI layer was smoothed using a  $3 \times 3$  focal mean function, which is defined as a low-pass filter that averages the values of an  $n \times n$  kernel (or focus) and assigns the result to the center cell [45]. Local minima in the HSCOI surface were then identified using the ArcInfo Topogrid function [44], and comparisons between the locations of low points and actual tree locations, including those in the

subcanopy, suggested a close correspondence. Two HSCOI layers were derived to improve stem mapping: one using  $h_{\max}$  extracted from a canopy height surface created using a local low-pass filter ( $3 \times 3$  kernel) and the other using the maximum LiDAR height found in the 7.5-ha PSU. Specifically, the local height kernel surface improved stem identification in dense clusters, while the stand maximum height surface allowed stems in the overstory and understory to be better differentiated. An initial limitation of using the HSCOI minima to locate stems was the practical difficulty in separating stems from branch clusters within the crowns of larger trees (i.e., with an area approximately  $> 100 \text{ m}^2$ ). To overcome this difficulty, HSCOI surfaces were also generated at two different spatial scales. The first was based on a circular kernel of 1 m radius, and minima were associated with small trees [with  $D_{130} > 5$  cm; Fig. 2(a)] as well as the branch clusters of larger trees. A second was generated using a square  $5 \times 5$  m kernel [Fig. 2(b)], and HSCOI minima were predominantly associated with the stem locations of larger trees. HSCOI minima extracted from surfaces of both spatial scales were combined, and where minima identified

using the 1-m-radius kernel occurred within a certain distance of those identified using a  $5 \times 5$  m kernel, these were removed, as they were assumed to be branch clusters. The exclusion distance was based on the expected crown area for a given trunk height, with this relationship derived from field data ( $r^2 = 0.7$ , RMSE = 16.2, and  $n = 249$ ) [43]. A comparison of tree locations mapped using the LiDAR and in the field indicated (for PSU 142) a 92% and 82% correspondence for trees  $> 10$  m in height and  $> 10$  cm in  $D_{130}$ , respectively. Omission errors were associated mainly with trees that were senescent or dead, occurred in a cluster with high stem density, or were small and beneath the canopy of larger overstory trees. Commission errors were found to occur with branches of large trees (as mentioned previously), or occasionally with small shrubs that were not measured in the field.

The retrieval of  $D_{130}$  for the located trees was critical for subsequent application of allometric equations for estimating total and component (e.g., branch) biomass, particularly as this was the independent variable in most of the available allometric equations [38]. Using field data, a significant non-linear relationship was observed between  $D_{130}$  and height [43] ( $r^2 = 0.76$ , RMSE = 6.47 cm, and  $n = 249$ ), which was used to estimate  $D_{130}$  for all LiDAR mapped stems. Determining the true height of subcanopy trees was often problematic, however, as the overstory trees generally intercepted many of the LiDAR pulses, particularly where the canopy (i.e., leaves and branches) were dense. In these cases, their height was necessarily estimated using an empirical function established between the HSCOI value and field-measured height [43] rather than using the canopy height surface alone. A procedure that checked the stem height from the LiDAR canopy height model against that determined using the HSCOI was developed. If the height difference was greater than 20%, then stems were attributed with the HSCOI-derived height. Examination of the PSU 142 field data indicated that, on the average, trees that were overtopped by the crowns of others accounted for 28% of stems  $> 5$  cm  $D_{130}$  and 24% of the basal area.

Tree crowns or clusters were delineated subsequently by generating contours of the HSCOI layer (derived using the stand maximum height and smoothed with a 1-m circular kernel) at 1-m intervals and intersecting these with the original LiDAR point data. An iterative process was then used to identify the HSCOI contour, which contained at least 90% of the original LiDAR returns  $> 2$  m in height [Fig. 2(c)]. Depending upon the structure of the forests, the contour identified to fulfill this criterion varied from 65% to 90% HSCOI value, and for PSU 142, a HSCOI threshold of 69% was selected. The result of this process for PSU 142 indicated an average crown cover per SSU of 30.4% ( $\delta = 12.4\%$ , range: 13.7%–57.8%). Within the defined crown area, individual crown/cluster segments (objects) could be differentiated further by applying hydrological drainage basin delineation routines available within the ArcInfo Hydrological suite to the HSCOI surface [43], [45]. Within larger crowns, objects were often associated with clusters of branches, and additional rules utilizing spatial location, size, and shape, as well as crown attributes such as height and density, were necessary to merge these into a single object [43]. The final map of stem and crown locations generated from the HSCOI layer covering the 7.5-ha PSU is shown in Fig. 3(a).

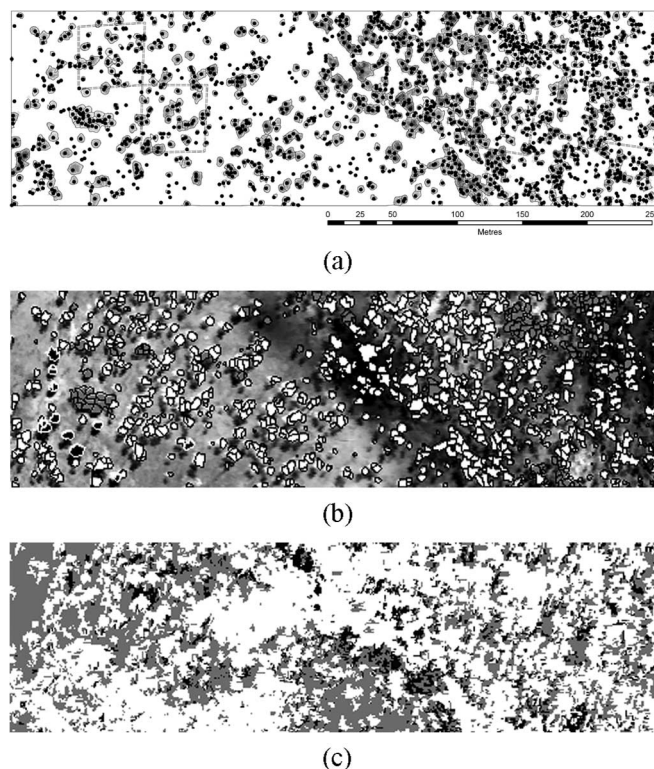


Fig. 3. Data layers generated for PSU 142. (a) LiDAR-derived stem and crown map, with the four field plots shown as squares (numbered from left to right as 02, 13, 18, and 20). (b) Tree species classification generated from CASI data showing *E. populnea* (white), *E. melanaphloia* (black), and *E. mitchelli* (gray). (c) Ground cover class map derived through linear spectral unmixing of CASI data showing bare soil (black), photosynthetic vegetation (ground shrubs and forbs; gray), and NPV (primarily grass; white).

### C. Tree Species Discrimination and Structural Attribution

Maps of crowns by species type were produced by first applying a tree crown delineation procedure to the CASI data [38], which was developed independently within eCognition Expert (based on the Cognition Network Technology [46]). The mean-lit spectra, which are defined by taking the average spectra from pixels that were above the average for the crown as a whole, were then extracted from crowns of known species [47] and used to develop discriminant functions based on a selection of the 14 wavebands. These functions were then used subsequently to classify all remaining crowns to species. The species classification for PSU 142 [Fig. 3(b)] confirmed the dominance of *E. populnea*, and based on ground truth, accuracies in the classification of all species exceeded 80%. A species type was assigned to each LiDAR-delineated crown object by linking and referencing crowns generated from CASI data based on criteria of proximity and area. The extraction of mean-lit spectra from crowns delineated using the LiDAR-derived HSCOI was not undertaken because of slight misregistration with the CASI data, although automated procedures for registering LiDAR and CASI data have been developed subsequently to overcome this limitation [48]. Cloud shadow reduced the reflectance of trees in the central and eastern sections of the CASI scene (see Fig. 1), but the crowns in this area were identified using the LiDAR data and could be associated with species discriminated through visual interpretation of the cloud-free LSP, thereby enabling complete mapping of species within the stand.

Each stem within the LiDAR-delineated crown or cluster objects was then attributed with information on height (from the LiDAR height or HSCOI) and  $D_{130}$  (from the relationship with height however derived). By applying the available species-specific allometric equations [38], [41], [49], which required height or  $D_{130}$  as input, each delineated object was also attributed with an estimate of leaf and branch (including terminal branches of  $< 1$  cm diameter) biomass. The numbers of leaves and terminal branches per tree, which for most trees in this forest were regarded as tertiary, were then estimated by dividing the total dry weights of leaves and terminal branches by the mean weights of individuals, as determined from field measurements and approximations of branch volume (from branch start and end radii and length) and wood density, respectively.

A classification of the ground surface was also undertaken by applying linear spectral unmixing to CASI data for the areas outside of the delineated crowns [50], [51]. The mapped distribution of bare soil, nonphotosynthetic vegetation (NPV; dry grass) and photosynthetic vegetation (shrubs) [Fig. 3(c)] corresponded closely to those observed within the LSP and on the ground. Beneath the crowns, the surface was assumed to be similar to that of the surrounding open areas, although field survey transects suggested that more litter might be expected in these areas.

#### D. Voxel Construction and Association With LiDAR Data

To distribute the leaves and terminal branches associated with each crown/cluster, a 3-D ( $1\text{ m}^3$ ) voxel matrix representing the forest volume was constructed from the LiDAR data [52]. Initially,  $1\text{-m}^2$  fishnets were generated for each 1-m height interval, from the ground surface to the tallest height recorded, and covering the maximum geographical extent ( $500 \times 150 \times 21$  m) of the LiDAR data. For PSU 142, this resulted in a 3-D matrix of 1 575 000 potential  $1\text{-m}^3$  voxels, with each associated with a combination of cell ( $x, y$ ) and height ( $z$ ) coordinates. The LiDAR point height data were then intersected with the voxel matrix such that each voxel that contained LiDAR data was attributed with the height above ground of the LiDAR return. This resulted in a total of 77 647 voxels with LiDAR returns (including ground). Within the 3-D matrix, voxels were associated, through geographical reference, with the nearest HSCOI-derived local minima (stem) and object (i.e., crown/cluster) delineated using the HSCOI surface (Fig. 4). Subsequent steps in the reconstruction replaced the voxel stem with a cylinder form and removed voxels that did not contain LiDAR returns.

#### E. Voxel Parameterization: Leaves and Terminal Branches

For each delineated object, the associated voxels were attributed collectively with structural information. Specifically, leaf dimensions (i.e., width, length, and thickness) were obtained from field measurements of individual leaves (an example for *E. populnea* is given in Table I, but see also [4]). Terminal branches ( $< 1$  cm diameter) were defined as those with a start radius of  $< 0.005$  m (i.e., 0.5 cm) at the base and 0.0005 m (i.e., 1 mm) at the terminus. The lengths of the terminal branches were taken, on the average, as being close to the voxel dimensions and no longer than 1.2 m (to fit within the voxel space) and were distributed with a large standard

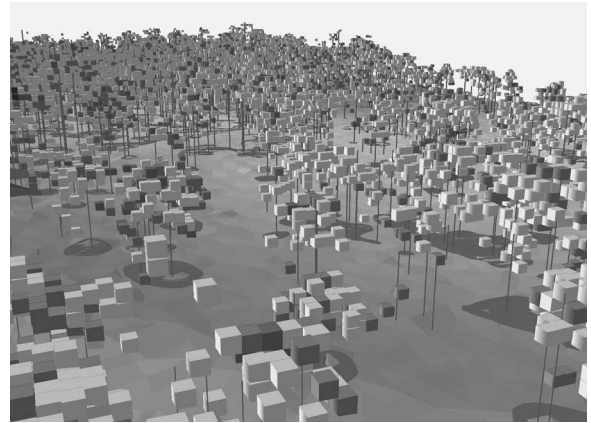


Fig. 4. Tree stem locations and associated voxels for 7.5 ha PSU 142. Branches are modeled subsequently from tree stems to voxel locations; stems are replaced with tapering cylinders scaled according to modeled  $D_{130}$ .

TABLE I  
EXAMPLES OF ATTRIBUTES LINKED TO EACH LiDAR VOXEL  
AND USED AS INPUT TO THE SAR COHERENT MODEL

Voxel Attribute	Value
General	
Species code	1 (i.e., <i>E. populnea</i> )
Crown-ID	23
Voxel ( $x, y, z$ ) coordinates <sup>1,2</sup>	38, 150, 10
No. terminal branches	13
Terminal Branches	
Branch order <sup>3</sup>	2
Length distribution <sup>2</sup>	<sup>5</sup> 0.5, 1.2, 1, 1
Radii distribution <sup>2</sup>	<sup>5</sup> 0.001, 0.005, 0.003, 0.003
Zenith angle distribution (°)	<sup>5</sup> 0.98, 82.56, 32.41, 16.54
Leaves	
Type code	4 (round leaves)
No. per unit Branch length (1 m)	39.38
Dimensions <sup>2</sup>	<sup>4</sup> 0.0656, 0.0616, 0.0003475

<sup>1</sup>PSU coordinates relative to lower left corner (0,0); <sup>2</sup>units in metres

<sup>3</sup>value indicates a join with a secondary branch; <sup>4</sup>width, length and thickness (m)

<sup>5</sup>minimum, maximum, mean and standard deviation.

deviation. The density of leaves and terminal branches was estimated by dividing the total number for the delineated tree by the number of associated voxels and assuming an even distribution. The average number of leaves per branch length (assuming an average of 1 m) was also estimated. The distribution of terminal branch and leaf orientations within voxels was assumed to be uniform. The moisture contents (%) of terminal branches and leaves were determined from the dry/wet weight ratios obtained for each species through on-site destructive harvesting. Voxel descriptions for attributes with a distribution of quantities (e.g., branch length and radii, or leaf orientation) are listed in Table I in the following order: minimum, maximum, mean, and standard deviation.

#### F. Primary and Secondary Branches and Trunks

To approximate the distribution of primary branches, voxels associated with each delineated object were divided into groups based on criteria relating to adjacency, relative height, and polar angle (Fig. 5).

As examples, for trees  $< 15$  m, the voxel above the HSCOI minima (i.e., the trunk location) was associated with the main

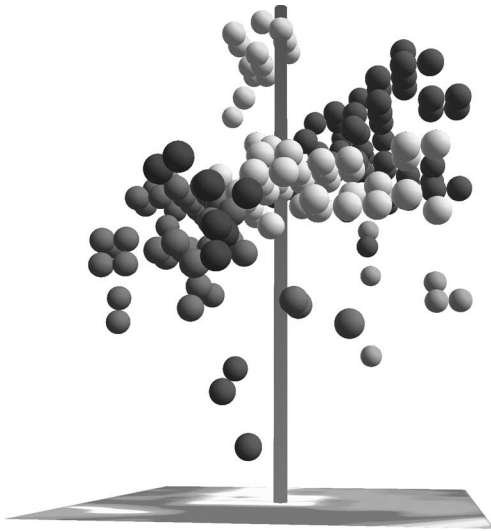


Fig. 5. Groups of voxels associated with branch clusters within an individual tree.

branch extending from the trunk. Voxels immediately adjacent to this upper voxel were associated with branches emanating from the trunk and in the upper part of the crown. All subsequent branch clusters were associated with adjoining groups of voxels (up to nine from a  $3 \times 3 \times 1$  m search kernel in the  $x$ ,  $y$ , and  $z$  directions) identified and assigned by searching, both in distance and azimuth orientation, from the trunk center. For trees  $> 15$  m in height, branch clusters were identified using a search kernel of  $3 \times 3 \times 2$  m (up to 18 voxels per group). The search commenced at the top of the tree and worked progressively downward through the canopy until all voxels had been assigned to a branch group. Search orientations for each new group were selected randomly to minimize bias in grouping. The number of groups (and therefore primary branches) varied, depending upon the height and crown dimensions of trees, with up to seven found within larger individuals.

In addition to the terminal branches ( $< 0.005$  m radii; which were distributed within the voxels), primary and secondary branch distributions were reconstructed for each crown/cluster. The end points of primary branches were associated with the centroid location of the different voxel groups, whereas the start points (i.e., the join with the trunk) were determined using species-specific zenith angle distributions from the vertical. These were established by taking measurements of branch angles from digital photographs of individual field trees (details are given in [4]). In some cases, the estimated join point was too close to the tree base, and this location was then associated with the height where the first leafing branch joined the trunk, as approximated using species-specific relationships with top height. Both measures of height had been recorded during the field campaign (see Section III-B). Secondary branches were constructed subsequently from the base of each voxel within the group associated with each primary branch to positions along the primary branch. These join positions were based on the proportional distance and location of each voxel base to the trunk. Regroupings of voxels and, hence, adjustments to secondary branch origins were necessary to compensate for voxels that were grouped initially with a primary branch cluster but were then considered to be too far away or at an unrealistic angle to be associated. An overview of primary and secondary

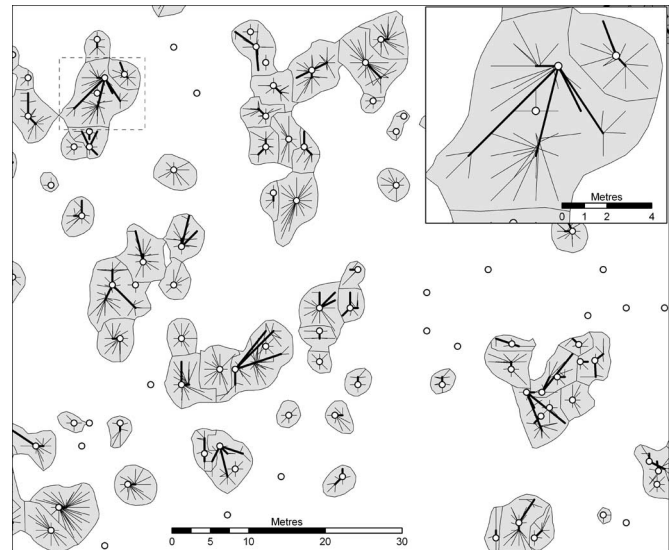


Fig. 6. Sample of mapped tree stems, crowns, and primary (thicker lines) and secondary (thinner lines) branch distributions in PSU 142 derived from the LiDAR data. Inset extent is marked as a dashed box.

branch distributions for part of PSU 142 is given in Fig. 6. This representation is considered realistic, with the primary branches associated with single trees emanating in all directions with those of adjoining objects trending toward the outer edge of the crown.

The length of primary and secondary branches was estimated from their relative positions in 3-D space. Values for the start and end radii of both branch categories were based primarily on trunk and branch diameter data (see Section IV-B) that were recorded as trees were being destructive-harvested as well as during a corresponding study undertaken on the same trees at Injune and also several near Dingo in central east Queensland [53]. This latter study aimed to evaluate the use of randomized branch and importance sampling for quantifying the biomass of *E. populnea* and provided measurements of branch diameters at divisions from the trunk to the top of the tree for  $\sim 15$  trees covering a range of growth stages. From these data, the assumptions that the start radii of each primary branch was one-half of the diameter of the trunk where the primary branch joined and that the start radii of the secondary branch was one-half of the primary branch diameter at the join point were considered reasonable. Given the complex growth structure of *E. populnea* and other tree species, considerable variations in the start and end radii of the branches will occur, particularly as this depends upon the number and different sizes of the branches following division. However, these rules were considered to adequately represent the reduction in radii with branching. The radius of all primary branches at the end point was assigned as 0.01 m (i.e., 2 cm diameter) with any smaller assigned to secondary branches. The end radius of all secondary branches was given as 0.005 m. These divisions, while partly arbitrary, were considered to reflect the progressive division and diminishment of size toward the periphery of the crown. The trunk radius at ground level was calculated using an empirical function with  $D_{130}$ , which was again established with field data and was assumed to decrease progressively (through taper and division) and terminate as a small (tertiary) branch with radius 0.005 m at the base of the uppermost voxel. The moisture content of

all woody material was determined (through destructive harvesting) as 45%, and a mean permittivity of  $12.4 + j3.3$  was assigned.

### G. Stand Validation and Reconstruction

Using the inputs generated from the LiDAR data, the stand associated with PSU 142 was reconstructed. Across the PSU, 20 295 branches were modeled in total, with 3616 (18%) of these being primary. The mean length of all branches (whether primary or secondary) was 2.9 m ( $\delta = 1.9$  m, range = 0.01–14.8 m), and the start radius was 0.02 m ( $\delta = 0.008$  m, range = 0.0001–0.075 m). There were 21 709 canopy voxels utilized across the PSU (i.e., voxels greater than 1 m height above ground). The canopy voxel density across the PSU was 28%, which compared well to the mean-field plot foliage branch projective cover of 29.8%.

Comparison with plot-based measurements of structural attributes indicated a good level of agreement. Specifically, the LiDAR modeling produced 1872 stems across the PSU, giving a mean density of 250 stems per hectare. For the LiDAR stems identified, the mean tree top height was 9.6 m ( $\delta = 3.8$  m, range = 0.20–20.2 m), and the mean  $D_{130}$  was 17.3 cm ( $\delta = 6.7$  cm, range = 1.0–35.4 cm). Assuming that the four field plots in the PSU were a representative sample of the PSU, the field data (live stems with  $D_{130} \geq 5$  cm) indicated a mean stem density of 295 stems per hectare, a mean tree top height of 8.8 m ( $\delta = 1.6$  m, range = 2.5–18.0 m), and a mean  $D_{130}$  of 15.5 cm ( $\delta = 4.2$  cm, range = 5.0–38.8 cm). Therefore, there is confidence in the identification and attribution of stems across the PSU, as they are within 15% of mean-field data estimates for stem density and within 12% for stem attributes, and the range of values observed is very similar.

For stems located using the LiDAR and able to be matched to those identified in the field (i.e., within the four field plots), woody biomass was estimated by multiplying the length and radius (i.e., volume) of each trunk and individual branches by species-specific wood densities (in kilograms dry matter per cubic meter); tapering and hollows within larger trees were both considered. Leaf mass was recalculated by multiplying the assumed number of leaves by species-specific leaf weight. The total component biomass per tree (above-ground) was then calculated as the sum of stem, branch, and leaf biomass. Total tree biomass was also estimated by applying species-specific allometric equations to all located stems, using LiDAR-derived height and/or  $D_{130}$  as input. Comparison of the two biomass estimation methods for each LiDAR stem resulted in a close correspondence in total above-ground biomass ( $r^2 = 0.82$ , RMSE = 50.3 kg, and  $n = 200$ ). This indicated that the modeled distributions and dimensions of components were reasonable, given the implicit assumptions. The component biomass modeled from LiDAR was also compared to that estimated for corresponding field trees by applying species-specific allometric equations to ground measurements, although this was less robust ( $r_2 = 0.52$ , RMSE = 114.4 kg, and  $n = 200$ ) largely because of differences in height and  $D_{130}$  estimated from the LiDAR data. Examination of the stems with poor correspondence ( $n = 30$ ) identified two main issues. First, the height allocation to subcanopy stems was incorrect largely because the influence of the overstory canopy resulted in a

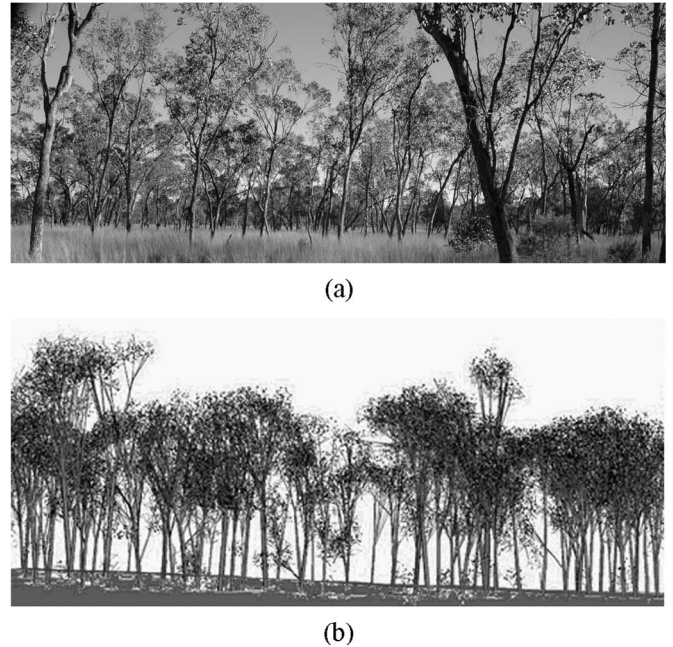


Fig. 7. (a) *E. populnea*-dominated forest at PSU 142. (b) Graphical output of part of the reconstructed canopy from the DSTO radar simulation (ground cover is not shown).

large disparity between  $D_{130}$  and therefore allometric biomass estimates. In a few cases, the dimensions of the modeled branches (in terms of either length or radius) were too great, which generated a disproportionately large estimate of branch biomass. Second, some stems located in the field were of a size and form that was outside of the mean predictive functions used for deriving  $D_{130}$  and  $D_{30}$  as described in Sections IV-C and E. In these cases, the stems had a much larger  $D_{30}$  for the equivalent  $D_{130}$  based on the prediction model, or stems were shorter than average for the predicted  $D_{130}$ . With the 30 outliers removed, and as expected, the biomass correspondence between LiDAR component sum and field stem allometric increased ( $r^2 = 0.81$ , RMSE = 68.3 kg, and  $n = 170$ ).

The reconstruction was also evaluated by visualizing the simulated stand using specifically developed software (Fig. 7), which allowed errors relating to branch locations, dimensions, and orientations to be identified. The final reconstruction of the forest sampled within PSU 142 was considered to be a valid representation of the distribution of trees and elements (i.e., leaves, primary, and secondary and terminal branches and trunks), both visually and quantitatively.

## V. SAR SIMULATION

### A. Mean-Field SAR Simulation

The unique coherent scattering and imaging model developed in [33], [34], and [54] and used successfully to model the SAR response of the Scots Pine (*P. sylvestris*) forest at L-band was adapted for the forests at Injune focusing, in this case, on those associated with PSU 142. No capacity for simulation at C- and P-band data was provided, although this is the subject of further research. The simulation employed a 3-D voxel-based vector wave propagation and scattering model coupled to the recovered forest structure. The model is approximate but

TABLE II  
KEY SOIL INPUT PARAMETERS TO THE SAR COHERENT MODEL

Parameter	Value
Soil permittivity	5.1 + j 0.07(10% moisture)
RMS height (small scale)	0.0055m
RMS height (large scale)	0.038m
Correlation length (small scale)	0.08 m

tractable, since the complexity of the real scene does not permit a full numerical solution to the scattering problem. The simulation produces synthesized, fully coherent, and polarimetric SLC SAR imagery that can be analyzed as real observations.

The simulation models the SAR image as a coherent superposition of focused scattering events, each attributed to an element of the scene much smaller than the SAR system resolution such that the polarimetric pixel value  $\underline{\mathbf{P}}(x, R)$  at cross range  $x$  and slant range  $R$  is described by

$$\underline{\mathbf{P}}(x, R) = \sum_n \underline{\mathbf{F}}_n I(x, R, \mathbf{e}_n) \quad (2)$$

where  $\underline{\mathbf{F}}_n$  is the polarimetric scattering amplitude associated with the scene element, and  $I(x, R, \mathbf{e}_n)$  is the complex system point spread function (impulse response) that depends upon the effective scattering center  $\mathbf{e}_n$ . By accounting correctly for phase in the point spread function, the simulation is made fully coherent. In addition, the SAR image calculation is essentially deterministic, since it is coupled directly to a 3-D model of the scene, and fully polarimetric, since it employs the fully polarimetric scattering amplitudes calculated for scene elements. Since the calculation is based on that detailed in [36], the following focuses largely on adaptations that yield significant differences with previous forest SAR imaging calculations.

The primary difference between the present coherent SAR simulation and that employed in [36] for forests dominated by *P. sylvestris* is in the interface between the radar calculation and the forest input model. Previously, the forest canopy was described using detailed tree architecture models that have been replaced in the current implementation with the voxel description of the model canopy, along with related trunk and branch lists. This means that in the previous model, modeled trees of a certain height were chosen at random to fill locations where it was known that a tree of a certain height existed. The forest model was statistically correct, but not a match for the forest area in detail. In the new approach, the detailed description of each tree at any given location exactly matches the available ground and LiDAR data. In addition, the previous model described tertiary branches explicitly, whereas in this new approach, these are described statistically from which a deterministic realization is generated.

In contrast to [36], the SAR simulations utilized the LiDAR data to produce a digital elevation model (DEM) of the underlying terrain surface and CASI data to classify the ground cover. Text files describing soil parameters for each cover in terms of scattering elements, including local roughness, correlation length, soil type, and permittivity (derived from moisture content) [55], were also provided as input to the simulation (Table II).

As in [36], the forest canopy and understory vegetation were represented by a distribution of discrete, dielectric objects, and scattering by the canopy at L-band was calculated using the mean-field approach pioneered in [21] and [22]. The rationale

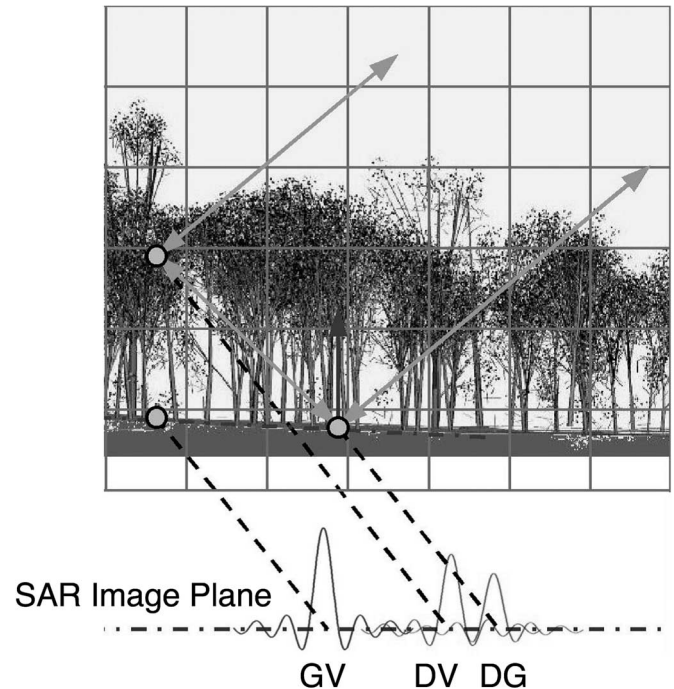


Fig. 8. Illustration of the composition of a simulated SAR image. Scattering events focus on the SAR image plane at the projection of their “effective” scattering center position.

for this approach is described fully in [36]; scattering of the coherent mean wave is focused by the SAR instrument using the phase history of the scattered signal [56], [57]. Coherent phase histories are modeled in the simulation, but the contribution to the image from scattering of the incoherent wave is not modeled directly but can be incorporated in the form of a noise signature.

Three significant classes of scattering event have been included in the calculations, namely: 1) direct–ground (DG); 2) direct–volume (DV); and 3) ground–volume (GV) terms, where

$$\underline{\mathbf{P}}(x, R) = \sum_{\alpha=\text{DG,DV,GV}} \sum_n^{N_\alpha} \underline{\mathbf{F}}_{\alpha n} I(x, R, \mathbf{e}_{\alpha n}). \quad (3)$$

Both forest canopy and understory contribute to DV and GV scattering, whereas GV ground scattering is generally insignificant and was found to be below anticipated noise levels. Each scene element, such as a ground facet, branch segment, leaf, or a section of a blade of grass in the understory, has an effective scattering center  $\mathbf{e}_{\alpha n}$ , where  $\alpha \in \{\text{DG, DV, GV}\}$ , and an associated *in situ* polarimetric scattering amplitude  $\underline{\mathbf{F}}_{\alpha n}$ , which can be calculated using an appropriate model. This effective scattering center is projected as the point of focus of the scattering event in the 2-D SAR image (Fig. 8). For DG and DV terms involving only first-order or direct backscatter, the effective scattering center is simply the center of the scene element. For higher order returns involving multiple reflections, the effective scattering center must be determined from the imaging geometry [36].

### B. Modeling Attenuation

In the mean-field model, locally incident fields are approximated by the mean wave propagating in the canopy. The



forest canopy is inhomogeneous on a scale commensurate with the spatial resolution of the SAR system, and it is desirable to incorporate the effects of canopy inhomogeneity into the simulation. To achieve this, the form of the layered Green's function of the mean wave in a homogeneous medium [58], [59] was employed, but the wavenumber of the mean wave was estimated locally for the aperture used to focus each scattering interaction.

For this purpose, the canopy volume was again subdivided into new subvolumes (voxels) but on a scale determined by the sensor resolution such that, on the whole, each voxel contained a large number of scattering objects. The LiDAR vegetation model was then used to determine the occupancy of each voxel, and the effective permittivity ( $\underline{\epsilon}^{\text{eff}}$ ) of each was calculated using the Foldy–Lax approximation and forward scattering amplitudes [60], [61] such that (e.g., [59])

$$\underline{\epsilon}^{\text{eff}} = \underline{\mathbf{I}} + n_o \frac{4\pi}{k_o^2} \langle \underline{\mathbf{S}}(\mathbf{k}_i, \mathbf{k}_i) \rangle \approx \begin{pmatrix} \epsilon & 0 & 0 \\ 0 & \epsilon & 0 \\ 0 & 0 & \epsilon_z \end{pmatrix}. \quad (4)$$

Vegetation permittivities were determined using the model described in [62] at frequencies employed by the SAR instrument. To remove sensitivity to the choice of permittivity in the model, the vegetation element moisture contents were assumed a normal distribution with a standard deviation of 10% of the mean value for each scattering element of each species. In the model, those voxels in the line of sight of the scattering element contributed to the attenuation of the scattering amplitude of that element as observed by the radar. The contribution to attenuation from each voxel was calculated using the distance traversed in that voxel, and the effective wavenumber of the voxel calculated using (4) and (5) [59].

### C. Focus of GV Terms

Scattering between the ground and elements in the forest volume was modeled in the far field. A mean surface for ground–element interactions was calculated from the DEM close to the scattering element. In practice, this entailed developing a map of “local mean surface” by essentially fitting a local flat plane to points on the DEM and using an area many wavelengths in dimension. The area was sufficiently large to contain the path of the specular point of reflection in the mean plane over the synthetic aperture. At the same time that an estimate of ground surface roughness about the local mean is made, a flat surface was determined over the same area for use in the GV scattering calculation. The extent of the mean flat surface was taken to be sufficiently large to allow the GV interaction to be modeled as the bistatic scattering by the volume element of the specular or coherent field reflected from the (rough) mean surface. By geometrical arguments (see the Appendix), the specular path for any point on the platform trajectory has the same length as the direct path from the point located at the normal projection of the volume element onto the mean plane. Thus, GV interactions appear as direct returns originating close to ground level, although their polarimetric phases differ from those of DV returns as a result of the ground reflection.

### D. Calculation of DG Images

DG contributions were calculated from ground facet elements using a hybrid deterministic/stochastic approach. The ground DEM was divided into tiny flat rough facets, each much smaller than the SAR resolution. The ground was modeled as a homogeneous half-space with dielectric permittivity determined from soil type, moisture content, and frequency following [62].

L-band ground facet RCS values depend on local incidence angle in the small perturbation model (SPM) used in these calculations. The ground facet scattering amplitude is scaled by attenuation matrices determined from line-of-sight visibility through the canopy and averaged over azimuth and frequency as follows:

$$\underline{\mathbf{F}}_{\text{DG}n} = \langle \underline{\gamma}_s \cdot \underline{\mathbf{S}}_{\text{DG}n} \cdot \underline{\gamma}_i \rangle \quad (5)$$

where the angular brackets denote azimuth and frequency averaging,  $\underline{\gamma}_s$  the attenuation suffered over the scattering path,  $\underline{\gamma}_i$  the attenuation suffered over the incident path, and  $\underline{\mathbf{S}}_{\text{DG}n}$  the unattenuated DG scattering amplitude associated with the  $n$ th ground facet.

Our model may be considered as being two scale in the sense that the ground DEM describes the large-scale surface height variation, whereas the facets have local small-scale roughness and correlation length. Since the true realization of surface roughness on any facet was unknown, we used the SPM and local facet orientation to obtain local HH and VV scattering cross sections for the facet. These values were taken to be the means for local fully developed exponential intensity speckle distributions [63]. These distributions were sampled randomly to obtain modeled scattering amplitudes for each ground facet. The sampled HH–VV phase statistics were then incorporated using a supplied coherence model such that ground surface polarimetric entropy was nonzero. Finally, a speckle phase was added using a spatially correlated speckle phase model [36]. The local scattering amplitude was then converted into the global frame for incorporation into the image [60]. By maintaining the correct random number sequence, the deterministic nature of the DG calculation was preserved to the extent that interferometric coherence may be simulated using multiple baselines as demonstrated in [29]. The importance of predicting correctly the interferometric behavior has been amply demonstrated in [37], wherein the present simulation has been used to demonstrate the potential for canopy height recovery by the new PALSAR sensor aboard the recently launched ALOS.

### E. Calculation of DV Images

To calculate direct forest clutter, each vegetation element was addressed, in turn, with scattering amplitudes calculated using the mean-field and appropriate physical scattering models such that

$$\underline{\mathbf{F}}_{\text{DV}n} = \langle \underline{\gamma}_s \cdot \underline{\mathbf{S}}_{\text{DV}n} \cdot \underline{\gamma}_i \rangle. \quad (6)$$

Branch segments were modeled using truncated infinite-cylinder approximations [64]. Scattering by vegetation, which

is typically extremely thin in at least one dimension, was calculated using the generalized Rayleigh–Gans (GRG) approach [65] applied to spheroidal needles, long leaves, and round leaves, depending upon tree species. Ground cover vegetation was modeled using GRG needles, leaves, grass blades [66], or stems, depending upon ground cover class. The dry grass was modeled as random distributions of cylindrical stems to a depth of 0.5 m and a mean volume fraction of 0.05. Low-level photosynthetic vegetation was modeled as a mixture of stems and round leaves to a depth of 0.2 m and a mean volume fraction of 0.02. All quantities used to describe the low-level vegetation were distributed statistically. No calculation of multipath between vegetation elements was performed. However, for correct calculation of cross-polar returns at frequencies higher than L-band, the explicit incorporation of such multiple interactions may be necessary [67].

Leaves and understory elements were too numerous for deterministic calculation, so populations of these were sampled, and their GRG contributions were scaled to preserve estimated  $\sigma^\circ$ . Large samples ensured that fully developed speckle and random samples were preserved to be consistent between simulated observations. This preserved also the deterministic nature of the calculations and ensured correct behavior of interferometric coherence with baseline [67], which will be the subject of future investigations.

#### F. Calculation of GV Images

GV returns were calculated using the bistatic scattering amplitude for scattering of the specularly reflected wave from the rough local mean flat surface. The magnitude of the reflected field vector was moderated by the Rayleigh parameter in the manner described in [34]. To calculate the Rayleigh parameter, the local estimate of the combined (large scale and small scale) roughness at the specular point was used, which was determined for each sampled sensor position and frequency in the averaging process such that the scattering amplitude for a GV interaction may be written as follows:

$$\begin{aligned} \underline{\mathbf{R}}_{GVn} = & \left\langle \underline{\gamma}_s \cdot \underline{\mathbf{S}}_{GVn}(\mathbf{k}_s, \mathbf{k}_r) \cdot \underline{\gamma}_r \cdot \underline{\mathbf{R}}_n(\mathbf{k}_r, \mathbf{k}_i) \cdot \underline{\gamma}_i \right\rangle \\ & + \left\langle \underline{\gamma}_i \cdot \underline{\mathbf{R}}_n(\mathbf{k}_s, -\mathbf{k}_r) \cdot \underline{\gamma}_r \cdot \underline{\mathbf{S}}_{GVn}(-\mathbf{k}_r, \mathbf{k}_i) \cdot \underline{\gamma}_s \right\rangle. \quad (7) \end{aligned}$$

Equation (7) is the sum of two terms, namely: 1) the forward path and 2) the reverse path, which combine in phase (coherently), since they have the same path length. These paths are indicated in Fig. 8. Each scattering path divides into three sections, namely: 1) sensor–ground; 2) GV; and 3) volume–sensor. The attenuations on each path are calculated separately and represented in (7) by the matrices  $\underline{\gamma}_i$ , which denote the attenuation suffered between sensor and specular point on the ground,  $\underline{\gamma}_r$ , which is the attenuation between the ground and volume element, and  $\underline{\gamma}_s$ , which is the attenuation between sensor and vegetation element. In each path,  $\underline{\mathbf{R}}_n$  is a Fresnel reflection matrix, which incorporates the ground roughness effects, representing the effects of the ground on the reflected wave. Finally,  $\underline{\mathbf{S}}_{GVn}$  is a bistatic scattering amplitude of a vegetation element for scattering from the ground to the sensor, or vice versa (here,  $\mathbf{k}_r$  is the reflection of the incident

wave vector  $\mathbf{k}_i$  at the ground, and  $\mathbf{k}_s$  is the scattered wave vector in the direction of the sensor).

The Rayleigh roughness correction [68] can display great sensitivity to surface roughness estimates, particularly at smaller incidence angles. The recorded mean large-scale roughness was 0.038 m, leading to a mean combined roughness of 0.043 m and a subsequent reduction in scattering amplitude of 0.38; this is equivalent to a typical loss in power of 8.3 dB in the GV term as a result of surface roughness.

#### G. Simulation Details

Simulations were conducted at the center wavelength of 0.24 m (L-band) for the reconstructed forests associated with PSU 142. The SAR swath center corresponded to the center of the 500 × 150 m area of the PSU, and as with the AIRSAR, the site was imaged east–west, with a broadside ground range of 9965 m, a height above ground of 7746 m, and an incidence angle (at scene center) of 52.1°. The final SLC image was 228 × 199 pixels (each 0.65625 × 2.5 m in dimension) and corresponded to an area of approximately 150 m (azimuth) × 500 m (ground range). The simulation matched the reported JPL AIRSAR bandwidth of 40 MHz and employed a high azimuth resolution (width at half height power) of 1.6 m. Only the multilooked image was available from JPL for comparison, so the SLC image was multilooked in azimuth by a factor of 9 in accordance with the AIRSAR processing so that the final image resolution was within 3% of that reported by JPL.

With any attempt at simulation, one ultimately encounters the issue of limited ground measurements, and although in this instance, the ground truth campaign was intensive, it was not exhaustive. Thus, some quantities could not be fully quantified, such as the distribution of small branch biomass within voxels, the understory biomass, and the rough ground correlation length, which have necessarily been estimated based upon other studies or experience. For example, the small-scale rough ground correlation length was chosen to reproduce closely the DG returns reported in [4].

## VI. RESULTS

#### A. L-Band Coherent Simulations

The AIRSAR image in Fig. 9(a) may be compared with the multilooked simulation of Fig. 9(b), which itself was derived from the original SLC image displayed in Fig. 9(c). Values of  $\sigma^\circ$  were derived from the simulated imagery and compared favorably with the AIRSAR data (Table III), with the total  $\sigma^\circ$  showing greatest difference at HV polarization. Levels of  $\sigma^\circ$  and the relative contributions of the different scattering mechanisms were within several decibels of those observed in [4], although results in [4] were obtained for one SSU (142-18) and by using a two-layered model only. This can be expected given that the cross-polarized response is typically underestimated in a first-order model of this kind [67]. A greater range of scattering mechanisms was also considered.

Simulated backscatter levels were seen to vary slightly with different imaging geometries and resolutions. This arose primarily from the variation in the DEM-derived ground roughness estimate from different interpolations of the original DEM

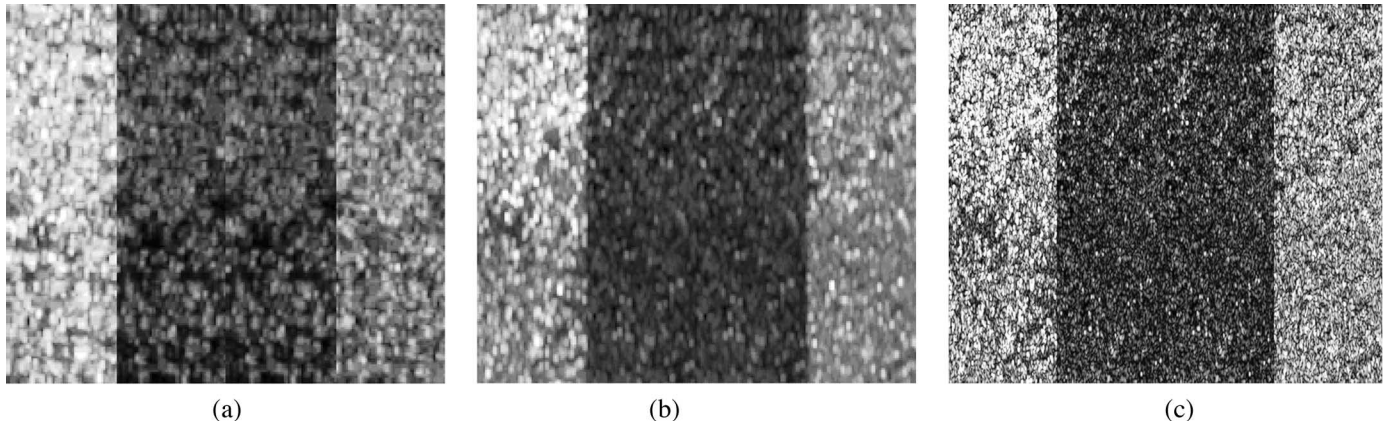


Fig. 9. (a) AIRSAR L-band image. (b) Simulated multilooked L-band image. (c) Simulated L-band SLC image for PSU 142 showing HH-, HV-, VH-, and VV-polarized images from left to right (in each case).

TABLE III  
COMPARISON OF SIMULATED AND ACTUAL  $\sigma^{\circ}$

	HH	VV	HV
DG	-31.4	-26.0	-55.7
DV	-18.2	-18.4	-27.2
GV	-14.3	-25.0	-36.1
Total	-12.7	-17.0	-26.7
AIRSAR	-12.7	-17.4	-22.5

and different realizations of the attenuation voxels. The GV return can be sensitive to estimates of ground roughness, which leads to variations in  $\sigma^{\circ}$ . However, the typical values reported in Table III did not vary by more than a fraction of a decibel when system resolutions and pixel spacings were altered.

The decomposition of the total return into different scattering mechanisms [5] indicated that at HH polarization, GV returns were the most significant and resulted primarily from ground-trunk interactions. The DV component was secondary and resulted largely from scattering by primary branches (i.e., those originating from the stem), whereas DG terms were not significant in this model. At VV polarization, DV returns from primary branches predominated. However, in contrast to the cross-polarization case, the combined contributions of DG and GV were significant in the VV return. This agreed with the results of [4]. Overall VV returns were lower than HH because of the strength of the GV interaction in the HH channel.

Cross-polarization (HV) returns were dominated by the DV response, to which primary branch, groundcover, and voxel contributions were commensurate. As with [4], simulated HV backscatter levels were underestimated by the model, and the second-order volume-volume terms required to correct for this defect [67] will be the subject of future work. The production of imagery is a unique feature of the coherent wave simulation, and the simulated and AIRSAR images were visually comparable, particularly at HH polarization (Fig. 10). Close examination revealed that large-scale features and even individual tree clusters could be matched within the simulated and AIRSAR imagery, which itself suggested that the canopy reconstruction and SAR simulation had been performed to a high degree

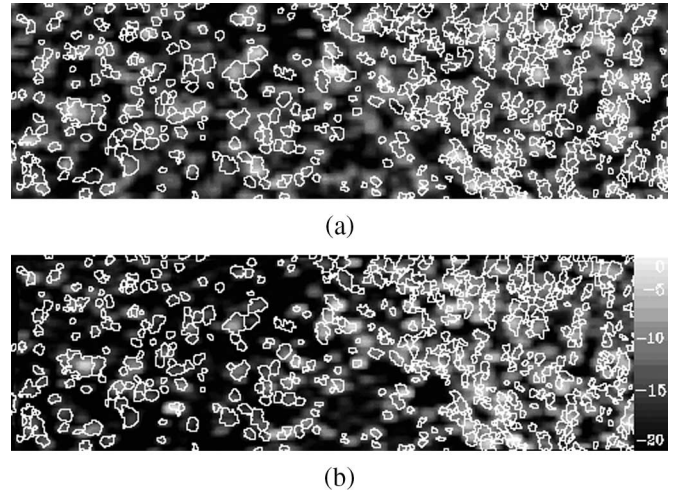


Fig. 10. Comparison of L-band HH images (a) acquired by the AIRSAR and (b) simulated using the coherent wave model.

of fidelity. Brightness in the HH imagery, although greater over the denser forest areas, showed less variation within the AIRSAR image.

## VII. DISCUSSION

### A. Analysis and Integration of LiDAR and Optical Data

A recognized limitation of previous studies aimed at SAR backscatter modeling has been the reliance on field data for parameterization, which has resulted in a less complete representation of the spatial variability in the distribution of tree components (e.g., leaves, branches) of varying sizes and orientations in either 2-D or 3-D. Furthermore, such data have often proved inadequate for providing sufficient validation for model outputs. By integrating LiDAR and field data in this study, a more realistic representation of the forest stand has been constructed, and hence, the variation observed within simulated and also actual SAR data can be better explained. As a large LiDAR data set has been acquired for a range of forests near Injune, options are also now available for further development of the simulations and validation of outputs.

The reconstruction of the 3-D structure of the forest through integration of field, LiDAR, and CASI/LSP data is itself a new approach to forest characterization. By seeking to parameterize the coherent SAR model, new techniques have been developed for locating tree trunks based on the HSCOI canopy density model and retrieving the heights and diameters of subcanopy trees [43]. Tree crown delineation methods in complex forest environments have been advanced using both CASI [39] and LiDAR [43] data, as well as discriminating and mapping common tree species through discriminant classifications. Finally, the new techniques have allowed finer resolution mapping of total and component (i.e., leaf, branch, and trunk) biomass through integration of LiDAR, CASI, and LSP and defining leaf and terminal branch distributions based on LiDAR voxels. The development stage explicitly included a continuous improvement component, whereby intermediate LiDAR-derived component 3-D outputs were run through the SAR simulation process. In some cases, anomalous SAR artifacts were identified (e.g., overly bright pixels in seemingly sparse vegetation). When these were checked in the LiDAR component model, they were found to correspond to branches that were not realistic in terms of length or size. The process of continuous improvement therefore allowed the LiDAR model branch location and size allocation to be improved, which removed the SAR artifacts in the next simulation run. An added advantage of using the continuous improvement approach was that crown locations outside of the field plots could be validated and crown configurations not observed in the field plots could be encompassed in the simulations. This process highlights the synergies that are possible when integrating data from a range of sources and scales.

The SAR simulations closely resembled that of the actual AIRSAR data and gave confidence that the approach to forest reconstruction from the LiDAR data was reasonable across the range of forest structures present in the scene. Considering the complexity of the forests, the reconstruction provided a realistic representation of the forest.

### B. SAR Simulation

The 3-D coherent SAR simulations were based on field (including destructive harvesting) measurements and finer spatial resolution data acquired over a similar time period as the AIRSAR overpass. Therefore, the distribution of foliage and terminal branches (within the voxels), primary and secondary branches, and trunks was considered realistic as was the attribution of these elements and the ground surface with information relating to their size (volume), geometry, and dielectric properties. The ground surface was similarly well characterized. A particular advantage of acquiring data at this time was that much of the uncertainty associated with, for example, tree distributions, vegetation moisture contents, or leaf amount, was reduced.

The unique SAR simulations provided a realistic overview, both visually and numerically, of L-band backscatter from *E. populnea*-dominated forests. Differences in brightness variation across the actual AIRSAR and simulated images indicated, however, that the recovery technique might have overestimated the variation in biomass across PSU 142 or there was loss of dynamic range in the compressed AIRSAR data or both.

These differences in dynamic range are illustrated in Fig. 11, which plots the distributions of normalized pixel amplitudes in the three polarimetric channels at L-band over PSU 142. The difference between simulated and actual data was most noticeable at HH polarization, where the major contribution to the returned power arises from the ground–stem interaction. Examination of the ground roughness map revealed that roughness was not the major cause of variation in the GV term across the simulated image but that the biomass of the stems might contribute significantly.

Other possible sources of loss of dynamic range at L-band include the influence of clutter motion, which leads to loss of focus and a spreading of energy throughout the image, and the incoherent component of the GV interaction [69], both of which have not been included in current calculations. The low HV return predicted by the model is also traceable to the lack of multipath in the DV calculation [67].

### C. Benefits and Implications

In a previous study that focused on these same forests [4], the wave scattering model of [5] was used to understand the interaction of microwaves of different frequency and polarization with vegetation components (i.e., leaf, branch, and trunks). Although the original model assumed scatterers to be distributed in two layers, modifications were made to allow multiple distributions of branch and trunk cylinders within the upper and lower layers, respectively, thereby facilitating a better representation of the multilayered canopy. Despite good simulations, it was considered that the complex structure of the forests could be better represented if layers were allowed to overlap and a tapered trunk model was included. This led to the development of a multilayer canopy scattering model [7] based on the Michigan Microwave Canopy Scattering model (Multi-MIMICS [6]). The use of a 3-D voxel-based coherent vector wave propagation and scattering SAR model [33], [34], [54] to simulate fully coherent and polarimetric SLC SAR imagery from a realistic representation of the distribution of foliage, branch, and trunk elements (and their attributes; as mapped primarily from LiDAR with reference to field data) therefore represents further advancement. The simulations from this model compare well with those of [4] and [7] for the same forest confirming the validity of each. As with these approaches, a better understanding of how both total and component biomass and structural attributes can be retrieved from SAR can potentially be obtained. The model can also be used to assess the extent to which the forest structure can be simplified in order for a realistic interpretation of the SAR backscatter through modeling to be obtained. Future work will focus on the integration of the various approaches such that the modeling of SAR backscatter within this forest environment can be optimized and a greater understanding of how biomass and structural attributes can be retrieved using these data can be obtained.

The focus on L-band SAR simulation is particularly pertinent given that Japan successfully launched the ALOS PALSAR in January 2006 and other sensors operating at this frequency are being planned and proposed. This sensor is anticipated to provide near global coverage of L-band HH and HV data several times per year, and considerable interest has been generated regarding the use of these data for forest

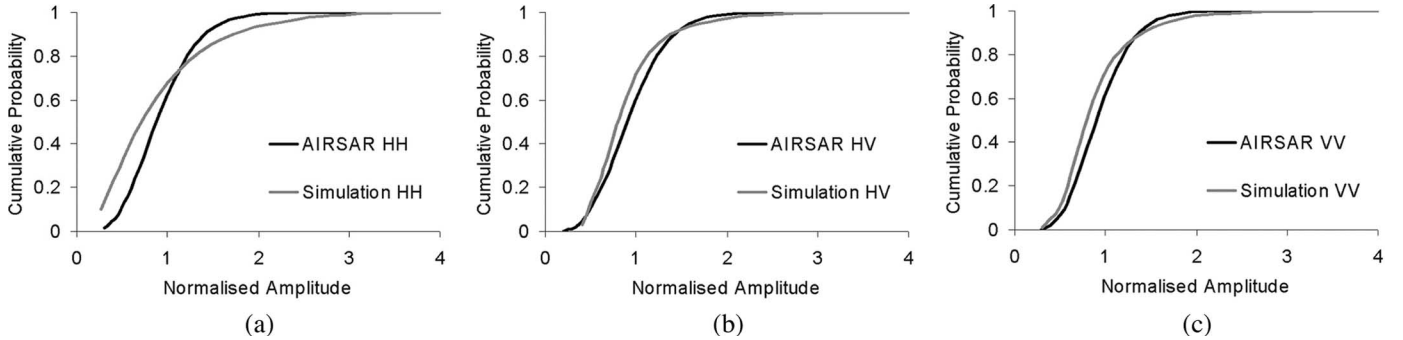


Fig. 11. Distribution of (a) HH, (b) VV, and (c) HV pixel amplitudes in simulated and actual AIRSAR L-band imagery.

assessment, particularly biomass retrieval. The study presented here provides a series of tools that allow the reconstruction of the forest stand and the subsequent simulation of L-band SAR images as well as overall backscatter and contributory mechanisms, which will ultimately be used to support interpretation of these data. The Injune study area is also well suited for such research as a comprehensive data set exists, which includes a substantial quantity of field, LiDAR, CASI, LSP, and AIRSAR data. The integration of these data with coherent SAR models can therefore support efforts in the characterization and mapping of forests in Queensland, as well as across Australia, and presents opportunities for understanding the information content of these data for research and operational purposes.

## VIII. SUMMARY AND CONCLUSION

By integrating LiDAR, CASI, aerial photography, and field data, a 3-D representation of an Australian forest has been constructed and populated with quantitative information related to the size, geometry, and dielectric properties of foliage, branch, and trunk components. Using these same data, a representation of ground surface properties has also been generated. This information has been used as input to a coherent SAR model to simulate SLC images, from which multilooked backscatter data have been retrieved. Comparisons with AIRSAR L-band data indicate a close correspondence in the backscatter and also imagery, particularly at HH and VV polarizations, a realistic representation of the contribution from different scattering mechanisms and comparative results with those obtained in previous studies [4], [7]. As such, the potential of the 3-D coherent SAR simulation model as a tool for further investigating the utility of SAR data for retrieving the biomass and structural attributes of complex mixed species forests typical to large parts of Australia has been demonstrated.

Model simulations have been performed for a forest dominated by *E. populnea* at L-band, and performance in different forests types and at other frequencies will be the subject of future investigations. The validated forest reconstruction and L-band SAR models provide significant opportunities for better understanding the potential of current and forthcoming satellite mission, including the ALOS PALSAR, for retrieving forest structural attributes and biomass. LiDAR data from other PSUs are being processed for further simulation of SAR data, which will be reported in subsequent papers.

## APPENDIX LOCATION OF SURFACE-VOLUME MULTIPATH IN SAR IMAGERY

Consider the following imaging geometry for a small target above a sloping terrain. The SAR platform position

$$\begin{aligned} \mathbf{r} &= x\hat{\mathbf{x}} + \mathbf{r}_0 \\ \mathbf{r}_0 &= y\hat{\mathbf{y}} + H\hat{\mathbf{z}} \end{aligned} \quad (\text{A1})$$

progresses in the  $\hat{\mathbf{x}}$  direction at a constant ground range  $y$  and height  $H$  in the world coordinate system. Let  $\mathbf{T}$  be the projection of the true target position  $\mathbf{t}$  onto the sloping flat terrain with surface normal  $\hat{\mathbf{n}}$ .  $\mathbf{T}$  may be written in terms of unit vectors  $\{\hat{\mathbf{a}}, \hat{\mathbf{b}}\}$  and a ground-plane location  $\mathbf{G}$  as follows:

$$\begin{aligned} \mathbf{T} &= \mathbf{G} + \alpha\hat{\mathbf{a}} + \beta\hat{\mathbf{b}} \\ \hat{\mathbf{a}} \cdot \hat{\mathbf{n}} &= \hat{\mathbf{b}} \cdot \hat{\mathbf{n}} = 0. \end{aligned} \quad (\text{A2})$$

If the target is at a height  $h$  above the sloping terrain in the normal direction, then

$$\mathbf{t} = \mathbf{G} + \alpha\hat{\mathbf{a}} + \beta\hat{\mathbf{b}} + h\hat{\mathbf{n}} \quad (\text{A3})$$

from which it follows that

$$\begin{aligned} \alpha &= (\mathbf{t} \cdot \hat{\mathbf{a}}) - (\mathbf{G} \cdot \hat{\mathbf{a}}) \\ \beta &= (\mathbf{t} \cdot \hat{\mathbf{b}}) - (\mathbf{G} \cdot \hat{\mathbf{b}}) \\ h &= (\mathbf{t} \cdot \hat{\mathbf{n}}) - (\mathbf{G} \cdot \hat{\mathbf{n}}). \end{aligned} \quad (\text{A4})$$

Consider first the range history of the direct return from the true target position, which is written as follows:

$$\begin{aligned} R(x) &= 2|\mathbf{r}(x) - \mathbf{t}| \\ &= 2\sqrt{(x - t_x)^2 + (y - t_y)^2 + (H - t_z)^2}. \end{aligned} \quad (\text{A5})$$

Following SAR processing, this return is focused at azimuth  $x = t_x$  and at range  $R = ((y - t_y)^2 + (H - t_z)^2)^{1/2}$  [12]. The pulse transmitted by the sensor can be modeled as the band-limited weighted sum of harmonic signals. Each harmonic signal is scattered by the rough surface into diffuse and coherent terms. It is assumed that the diffuse scattered term will not appear focused in the SAR image, since it contains phase and

amplitude elements, which vary in an effectively random manner along the synthetic aperture. The coherent term, however, will focus in the SAR image if the phase history for the interaction is similar to that of the direct return from a point scatterer. We show that in the far-field approximation, the phase history of both the term containing a single ground reflection and the term containing a double ground reflection vary in exactly this way and, hence, may be expected to appear focused in SAR images.

The coherent wave scattered from a flat (albeit rough and tilted) half-space is in the specular direction. For the purposes of this paper, the flat surface is taken to be the mean surface about which the real surface height fluctuates, and from which rms height fluctuations may be determined.

The specular reflected wave is then either scattered back to the sensor directly from the target to yield the single-reflection multipath return or first scattered back to the ground and then coherently reflected to the sensor to form the double-reflection multipath return. Thus, we need to determine the path of the specular point for the interactions to understand their eventual focus.

Let the specular point for platform azimuth position  $\mathbf{r}$  be  $\mathbf{S}$ . The total path length of the single-reflection multipath interaction is determined from the far-field geometry. Since reflection is specular,  $\mathbf{r}$ ,  $\mathbf{S}$ , and  $\mathbf{t}$  lie in a plane normal to the terrain, and which therefore contains the projection  $\mathbf{T}$  of the target onto the terrain.

The case of low grazing angle is shown in Fig. 12. With reference to the figure, the single-reflection multipath return contains a path length that is twice the distance from sensor to specular point  $\mathbf{S}$  plus two additional lengths, namely 1) the distance  $D = |\mathbf{S} - \mathbf{t}|$  and 2) the distance  $A = |\mathbf{t} - \mathbf{u}|$ .

Now, let us suppose that there exists a point target at  $\mathbf{T}$ , which contributes a direct return. The path length associated with this supposed scatterer also contains twice the distance from sensor to specular point and an additional term, i.e.,  $2C = 2|\mathbf{T} - \mathbf{q}|$ , where the lines  $\mathbf{T}\mathbf{q}$  and  $\mathbf{S}\mathbf{u}$  are orthogonal. We proceed to show that the additional path lengths are given such that  $D + A = 2C$ , regardless of the position of the sensor. Close examination of Fig. 12 reveals that

$$A = D \sin \gamma \quad (\text{A6})$$

from which it follows that

$$D + A = D(1 + \sin \gamma) \quad (\text{A7})$$

and that

$$\begin{aligned} C &= A + E \\ &= D \sin \gamma + h \sin \theta. \end{aligned} \quad (\text{A8})$$

Using the fact that

$$h = D \sin \theta \quad (\text{A9})$$

we can write for (A8)

$$C = D(\sin \gamma + \sin^2 \theta). \quad (\text{A10})$$

Clearly

$$\gamma = 90 - 2\theta \quad (\text{A11})$$

so that

$$\sin \gamma = \cos 2\theta = \cos^2 \theta - \sin^2 \theta \quad (\text{A12})$$

where

$$\begin{aligned} 2C &= 2D(\cos^2 \theta - \sin^2 \theta + \sin^2 \theta) \\ &= 2D \cos^2 \theta \end{aligned} \quad (\text{A13})$$

and

$$\begin{aligned} D + A &= D(1 + \cos^2 \theta - \sin^2 \theta) \\ &= D(\cos^2 \theta + \sin^2 \theta + \cos^2 \theta - \sin^2 \theta) \\ &= 2D \cos^2 \theta \end{aligned} \quad (\text{A14})$$

and, finally, by comparison of (A13) and (A14)

$$D + A = 2C. \quad (\text{A15})$$

The identity (A15) means that for any position of the platform, the path length of the single-reflection multipath term is equal to that between the sensor and the fixed point, which is the projection of the target position onto the mean plane. This implies that the single-reflection multipath term appears focused in the image at azimuth and range given by

$$x = T_x \quad (\text{A16})$$

$$R = \sqrt{(y - T_y)^2 + (H - T_z)^2} \quad (\text{A17})$$

where  $\mathbf{T} = (T_x, T_y, T_z)$  may be determined using (A2)–(A4), given knowledge of the terrain slope. We note that the single-reflection multipath term has an increase in path length over the direct target return of

$$2E = 2h \sin \theta. \quad (\text{A18})$$

We now move on to consider the other multipath term involving two reflections at the terrain surface. It is apparent from the geometry of Fig. 12 that the double-reflection multipath term incurs an increase in path length over the direct target return of

$$2D - 2A = 4h \sin \theta. \quad (\text{A19})$$

Comparison between (A18) and (A19) leads one to speculate that there exists another fixed point  $\mathbf{T}'$  for which the direct return has the same path length as the double-reflection multipath term. This is indeed the case, and the point is clearly located at a position below the terrain at

$$\begin{aligned} \mathbf{T}' &= \mathbf{T} - h\hat{\mathbf{n}} \\ &= \mathbf{t} - 2h\hat{\mathbf{n}}. \end{aligned} \quad (\text{A20})$$

Since this point is also fixed with respect to the world coordinate system, the double-reflection multipath term must focus at azimuth and range given by

$$x = T'_x \quad (\text{A21})$$

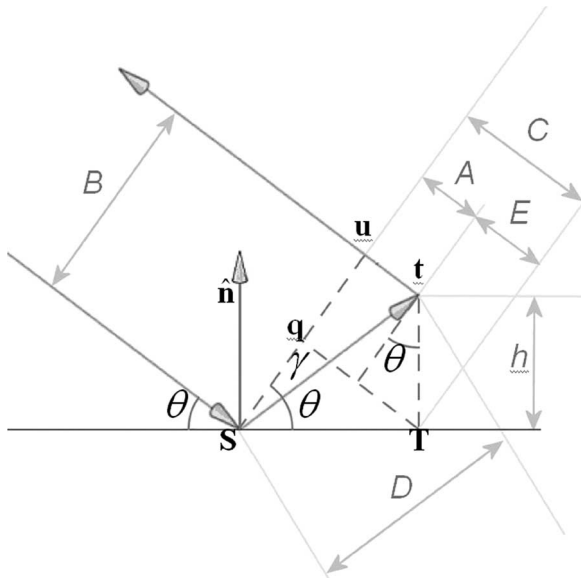


Fig. 12. Geometry for determining the multipath path length.  $T$  is the projection of the target position  $t$  onto the sloping terrain with normal  $\hat{n}$ .

$$R = \sqrt{(y - T'_y)^2 + (H - T'_z)^2}. \quad (\text{A22})$$

Again, this may be found using available knowledge of the terrain.

#### ACKNOWLEDGMENT

The authors would like to thank the Queensland Department of Primary Industries Tropical Beef Centre for assisting with destructive harvesting and the NASA Jet Propulsion Laboratory for acquiring the AIRSAR data. Particular thanks go to T. Milne (University of New South Wales), C. Witte (QDNR&M), P. Bunting (Institute of Geography and Earth Sciences), and M. Moghaddam (University of Michigan) for their assistance in data acquisition and interpretation.

#### REFERENCES

- [1] M. C. Dobson, F. T. Ulaby, T. LeToan, A. Beaudoin, E. S. Kasischke, and N. Christensen, "Dependence of radar backscatter on coniferous forest biomass," *IEEE Trans. Geosci. Remote Sens.*, vol. 30, no. 2, pp. 412–415, Mar. 1992.
- [2] T. Le Toan, S. Quegan, I. Woodward, L. Mark, D. Nicolas, and P. Ghislain, "Relating radar remote sensing of biomass to modeling of forest carbon budgets," *Clim. Change*, vol. 67, no. 2/3, pp. 379–402, Dec. 2004.
- [3] R. M. Lucas, A. K. Milne, N. Cronin, C. Witte, and R. Denham, "The potential of synthetic aperture radar (SAR) data for quantifying the above ground biomass of Australia's woodlands," *Rangeland J.*, vol. 22, no. 1, pp. 124–140, 2000.
- [4] R. M. Lucas, M. Moghaddam, and N. Cronin, "Microwave scattering from mixed species woodlands, central Queensland, Australia," *IEEE Trans. Geosci. Remote Sens.*, vol. 42, no. 10, pp. 2142–2159, Oct. 2004.
- [5] S. L. Durden, H. A. Zebker, and J. J. van Zyl, "Modeling and observation of forest radar polarization signatures," *IEEE Trans. Geosci. Remote Sens.*, vol. 27, no. 3, pp. 290–301, 1989.
- [6] F. T. Ulaby, K. Sarabandi, K. McDonald, M. Whitt, and M. C. Dobson, "Michigan microwave canopy scattering model (MIMICS)," Univ. Michigan, Ann Arbor, MI, Tech. Rep. 022486-T-1, 1988.
- [7] P. Liang, M. Moghaddam, L. E. Pierce, and R. M. Lucas, "Radar backscattering model for multilayer mixed-species forests," *IEEE Trans. Geosci. Remote Sens.*, vol. 43, no. 11, pp. 2612–2626, Nov. 2005.
- [8] G. Sun, K. J. Ranson, and V. I. Kharuk, "Radiometric slope correction for forest biomass estimation from SAR data in the western Sayani Mountains, Siberia," *Remote Sens. Environ.*, vol. 79, no. 2/3, pp. 279–287, 2002.
- [9] D. Leckie, F. Gougeon, D. Hill, R. Quinn, L. Armstrong, and R. Shreenan, "Combined high-density LiDAR and multispectral imagery for individual tree crown analysis," *Can. J. Remote Sens.*, vol. 29, no. 5, pp. 633–649, 2003.
- [10] D. A. Pouliot, D. J. King, and D. G. Pitt, "Development and evaluation of an automated tree detection–delineation algorithm for monitoring regenerating coniferous forests," *Can. J. For. Res.*, vol. 35, no. 10, pp. 2332–2345, Oct. 2005.
- [11] J. C. Suárez, C. Ontiveros, S. Smith, and S. Snape, "Use of airborne LiDAR and aerial photography in the estimation of individual tree heights in forestry," *Comput. Geosci.*, vol. 31, no. 2, pp. 253–262, Mar. 2005.
- [12] J. Holmgren, M. Nilsson, and H. Olsson, "Estimation of tree height and stem volume on plots using airborne laser scanning," *For. Sci.*, vol. 49, no. 3, pp. 419–428, Jun. 2003.
- [13] M. Wulder, K. O. Niemann, and D. G. Goodenough, "Local maximum filtering for the extraction of tree locations and basal area from high spatial resolution imagery," *Remote Sens. Environ.*, vol. 73, no. 1, pp. 103–114, 2000.
- [14] D. Riaño, F. Valladares, S. Condés, and E. Chuvieco, "Estimation of leaf area index and covered ground from airborne laser scanner (LiDAR) in two contrasting forests," *Agricult. For. Meteorol.*, vol. 124, no. 3/4, pp. 269–275, Aug. 2004.
- [15] K. W. Todd, F. Csillag, and P. M. Atkinson, "Three-dimensional mapping of light transmittance and foliage distribution using LiDAR," *Can. J. Remote Sens.*, vol. 29, no. 5, pp. 544–555, 2003.
- [16] M. Maltamo, K. Eerikainen, J. Pitkanen, J. Hyypä, and M. Vehmas, "Estimation of timber volume and stem density based on scanning laser altimetry and expected tree size distribution functions," *Remote Sens. Environ.*, vol. 90, no. 3, pp. 319–330, 2004.
- [17] M. A. Lefsky, A. T. Hudak, M. Guzy, and W. B. Cohen, "Combining LiDAR estimates of biomass and Landsat estimates of stand age for spatially extensive validation of modelled forest productivity," *Remote Sens. Environ.*, vol. 95, no. 4, pp. 549–558, 2005.
- [18] S. A. Hall, I. C. Burke, D. O. Box, M. R. Kaufmann, and J. M. Stoker, "Estimating stand structure using discrete-return LiDAR: An example from low density, fire prone ponderosa pine forests," *For. Ecol. Manag.*, vol. 208, no. 1–3, pp. 189–209, Apr. 2005.
- [19] M. A. Lefsky, D. Harding, W. B. Cohen, and G. G. Parker, "Surface LiDAR remote sensing of basal area and biomass in deciduous forests of eastern Maryland, USA," *Remote Sens. Environ.*, vol. 67, no. 1, pp. 83–98, Jan. 1999.
- [20] K. S. Lim and P. M. Treitz, "Estimation of above ground forest biomass from airborne discrete return laser scanner data using canopy-based quantile estimators," *Scand. J. For. Res.*, vol. 19, no. 6, pp. 558–570, Dec. 2004.
- [21] S. Magnusson and P. Boudewyn, "Derivations of stand heights from airborne laser scanner data with canopy-based quantile estimators," *Can. J. For. Res.*, vol. 28, no. 7, pp. 1016–1031, 1998.
- [22] J. L. Lovell, D. L. B. Jupp, D. Culvenor, and N. C. Coops, "Using airborne and ground-based ranging LiDAR to measure canopy structure in Australian forests," *Can. J. Remote Sens.*, vol. 29, no. 5, pp. 607–622, 2003.
- [23] P. K. Tickle, A. Lee, R. M. Lucas, J. Austin, and C. Witte, "Quantifying Australian forest and woodland structure and biomass using large scale photography and small footprint LiDAR," *For. Ecol. Manag.*, vol. 223, no. 1–3, pp. 379–394, 2006.
- [24] J. Hyypä, O. Kelle, M. Lehtikoinen, and M. Inkinen, "A segmentation-based method to retrieve stem volume estimates from 3-D tree height models produced by laser scanners," *IEEE Trans. Geosci. Remote Sens.*, vol. 39, no. 5, pp. 969–975, May 2001.
- [25] D. L. A. Gaveau and R. A. Hill, "Quantifying canopy height underestimation by laser pulse penetration in small-footprint airborne laser scanning data," *Can. J. Remote Sens.*, vol. 29, no. 5, pp. 650–657, 2003.
- [26] K. Lim, P. Treitz, M. Wulder, B. St-Onge, and M. Flood, "LiDAR remote sensing of forest structure," *Prog. Phys. Geogr.*, vol. 27, no. 1, pp. 88–106, Mar. 2003.
- [27] J. B. Drake, R. O. Dubayah, R. G. Knox, D. B. Clark, and J. B. Blair, "Sensitivity of large-footprint LiDAR to canopy structure and biomass in a neotropical rainforest," *Remote Sens. Environ.*, vol. 81, no. 2/3, pp. 378–392, 2002.
- [28] P. A. Stuopis, J. M. Henson, R. E. Davis, and K. Hall, "The modeling of forested areas for real and synthetic aperture imaging radar simulation," in *Proc Int. Geosci. Remote Sens. Symp.*, Lincoln, NE, 1996, vol. 1, pp. 254–256.
- [29] K. Sarabandi and Y.-C. Lin, "Simulation of interferometric SAR response to deciduous and coniferous forest stands," in *Proc Int. Geosci. Remote Sens. Symp.*, Singapore, 1997, pp. 1887–1889.

- [30] Y.-C. Lin and K. Sarabandi, "A Monte Carlo coherent scattering model for forest canopies using fractal generated trees," *IEEE Trans. Geosci. Remote Sens.*, vol. 37, no. 1, pp. 440–451, Jan. 1999.
- [31] A. Gustavsson, P. O. Frörlind, H. Hellsten, T. Jonsson, B. Larsson, and G. Stenström, "The airborne VHF SAR system CARABAS," in *Proc. Int. Geosci. Remote Sens. Symp.*, Tokyo, Japan, 1993, pp. 558–562.
- [32] S. R. Cloude and M. L. Williams, "Estimating sub-canopy soil-moisture using PolInSAR," in *Proc. ESA Workshop PolInSAR*, Frascati, Italy, Jan. 2005.
- [33] J. Praks, P. Ahtonen, and M. Hallikainen, "Simulation of polarimetric scattering from forest canopy," in *Proc. XXVII URSI/IEEE Conv. Radio Sci.*, Helsinki, Finland, 2002, pp. 96–98.
- [34] M. L. Williams, T. Manninen, S. Kellomaki, V.-P. Ikonen, R. Sievanen, M. Lehtonen, E. Nikinmaa, and T. Vesala, "Modeling the SAR response of pine forest in southern Finland," in *Proc. Int. Geosci. Remote Sens. Symp.*, Toulouse, France, 2003, vol. 2, pp. 1350–1352.
- [35] C. Varenkamp and D. H. Hoekman, "High-resolution InSAR image simulation for forest canopies," *IEEE Trans. Geosci. Remote Sens.*, vol. 40, no. 7, pp. 1648–1655, Jul. 2002.
- [36] S. R. Cloude, D. G. Corr, and M. L. Williams, "Target detection beneath foliage using polarimetric synthetic aperture radar interferometry," *Waves Random Media*, vol. 14, no. 2, pp. S393–S414, Apr. 2004.
- [37] M. L. Williams, R. M. Lucas, A. Lee, and S. R. Cloude, "The potential of new SAR sensors for PolInSAR over Australian forests," in *Proc. EUSAR*, Dresden, Germany, May 2006.
- [38] W. H. Burrows, M. B. Hoffman, J. F. Compton, P. V. Back, and L. J. Tait, "Allometric relationships and community biomass estimates for some dominant eucalyptus in central Queensland woodlands," *Aust. J. Bot.*, vol. 48, no. 6, pp. 707–714, 2000.
- [39] P. Bunting and R. M. Lucas, "The delineation of tree crowns within CASI data of Australian mixed species woodlands," *Remote Sens. Environ.*, vol. 101, no. 2, pp. 230–248, 2006.
- [40] Queensland Department of Natural Resources and Mines, *The Statewide Landcover and Trees Study (SLATS)—2003 Report*, 2003.
- [41] W. H. Burrows, M. B. Hoffman, J. F. Compton, and P. V. Back, "Allometric relationships and community biomass stocks in white cypress pine (*Callitris glaucophylla*) and associated eucalypts of the carnarvon area—South central Queensland," Australian Greenhouse Office, Canberra, Australia, National Carbon Accounting System Tech. Rep. 33, 2001.
- [42] M. E. Hodgson and P. Bresnahan, "Accuracy of airborne LiDAR-derived elevation: Empirical assessment and error budget," *Photogramm. Eng. Remote Sens.*, vol. 70, no. 3, pp. 331–339, Mar. 2004.
- [43] A. C. Lee and R. M. Lucas, "Stand based tree trunk and canopy mapping using multi-layered LiDAR analyses in Australian woodlands," *Remote Sens. Environ.*, 2006, submitted for publication.
- [44] L. Chasmer, C. Hopkinson, and P. Treitz, "Assessing the three-dimensional frequency distribution of airborne and ground based LiDAR data for red pine and mixed deciduous forest plots," *Int. Arch. Photogramm., Remote Sens. Spatial Inf. Sci.*, vol. 36, no. 8/W2, pp. 66–69, 2004.
- [45] Environmental Systems Research Institute (ESRI), *Topogrid Reference Within System Documentation*, 1996.
- [46] Definiens, *eCognition Version 5 Object Oriented Image Analysis User Guide*, 2005, Munich, Germany: Definiens AG.
- [47] D. G. Leckie, F. A. Gougeon, S. Tinis, T. Nelson, C. N. Burnet, and D. Paradine, "Automated tree recognition in old growth conifer stands with high resolution digital imagery," *Remote Sens. Environ.*, vol. 94, no. 3, pp. 311–326, Feb. 2005.
- [48] R. M. Lucas, A. C. Lee, P. J. Bunting, and M. Williams, "Forest reconstruction from LiDAR and CASI data: A case study from Australia," in *Proc. 3D Remote Sens. For.*, Vienna, Australia, Feb. 2006, pp. 13–14.
- [49] G. Harrington, "Estimation of above ground biomass of trees and shrubs in *Eucalyptus populnea* (F. Muell.) woodland by regression of mass on trunk diameter and plant height," *Aust. J. Bot.*, vol. 27, no. 2, pp. 135–143, 1979.
- [50] Y. E. Shimabukuro and J. A. Smith, "The least-squares mixing models to generate fraction images from remote sensing multispectral data," *IEEE Trans. Geosci. Remote Sens.*, vol. 29, no. 1, pp. 16–20, Jan. 1991.
- [51] M. A. Cochrane and C. M. Souza, "Linear mixture model classification of burned forests in the eastern Amazon," *Int. J. Remote Sens.*, vol. 19, no. 17, pp. 3433–3440, Nov. 1998.
- [52] A. C. Lee, R. M. Lucas, and C. Brack, "Quantifying vertical forest stand structure using small footprint LiDAR to assess potential stand dynamics," *Int. Arch. Photogramm., Remote Sens. Spatial Inf. Sci.*, vol. 36, no. 8/W2, pp. 213–217, 2004.
- [53] N. Good, M. Paterson, C. Brack, and K. Mengersen, "Estimating tree component biomass using variable probability sampling methods," *J. Agricult. Biol. Environ. Statist.*, vol. 6, no. 2, pp. 258–267, Jun. 2001.
- [54] M. L. Williams and N. Harris, "Demonstration of reduced false alarm rates using simulated L-band polarimetric SAR imagery of concealed targets," in *Proc. IEEE Int. Conf. Radar*, Adelaide, Australia, 2003, pp. 535–540.
- [55] M. C. Dobson, F. T. Ulaby, M. Hallikainen, and M. El-Rayes, "Microwave dielectric behaviour of wet soil—Part II: Four-component dielectric mixing models," *IEEE Trans. Geosci. Remote Sens.*, vol. GRS-23, no. 1, pp. 35–46, Jan. 1985.
- [56] R. H. Lang, "Electromagnetic scattering from a sparse distribution of lossy dielectric scatterers," *Radio Sci.*, vol. 16, no. 1, pp. 15–30, Jan. 1981.
- [57] R. H. Lang and J. S. Sidhu, "Electromagnetic scattering from a layer of vegetation: A discrete approach," *IEEE Trans. Geosci. Remote Sens.*, vol. GRE-21, no. 1, pp. 62–71, Jan. 1983.
- [58] G. Franceschetti and R. Lanari, *Synthetic Aperture Radar Processing*. Boca Raton, FL: CRC, 1999.
- [59] J. A. Kong, *Electromagnetic Wave Theory*, 2nd ed. New York: Wiley-Interscience, 1990.
- [60] L. Tsang, J. A. Kong, and R. T. Shin, *Theory of Microwave Remote Sensing*. Hoboken, NJ: Wiley, 1985.
- [61] U. Frisch, "Wave propagation in random media," in *Probabilistic Methods in Applied Mathematics*, vol. 1, A. T. Bharucha-Reid, Ed. New York: Academic, 1968.
- [62] F. T. Ulaby and M. A. El-Rayes, "Microwave dielectric spectrum of vegetation—Part II: Dual-dispersion model," *IEEE Trans. Geosci. Remote Sens.*, vol. GRE-25, no. 5, pp. 550–557, Sep. 1987.
- [63] C. Oliver and S. Quegan, *Understanding SAR Images*. Norwood, MA: Artech House, 2000.
- [64] M. A. Karam and A. K. Fung, "Electromagnetic scattering from a layer of finite, randomly oriented, dielectric, circular cylinders over a rough interface with application to vegetation," *Radio Sci.*, vol. 18, no. 7, pp. 557–563, 1983.
- [65] F. T. Ulaby and C. Elachi, *Radar Polarimetry for Geoscience Applications*. Norwood, MA: Artech House, 1990.
- [66] S. S. Saatchi, D. M. LeVine, and R. H. Lang, "A microwave backscattering and emission model for grass canopies," *IEEE Trans. Geosci. Remote Sens.*, vol. 32, no. 1, pp. 177–186, Jan. 1994.
- [67] M. L. Williams and S. Quegan, "Modeling microwave backscatter from discrete random media using a multiple scattering series: Convergence issues," *Waves Random Media*, vol. 7, no. 2, pp. 213–227, 1996.
- [68] J. A. Ogilvy, *Theory of Scattering from Random Rough Surfaces*. Bristol, U.K.: IOP, 1991.
- [69] R. H. Lang, "Scattering from a layer of discrete random medium over a random interface: Application to microwave backscattering from forests," *Waves Random Media*, vol. 14, no. 2, pp. S359–S391, Apr. 2004.



**Richard M. Lucas** received the B.Sc. degree (with first class honors) in biology and geography and the Ph.D. degree in the remote sensing of snow and vegetation using AVHRR and Landsat sensor data from the University of Bristol, Bristol, U.K., in 1986 and 1989, respectively.

He is currently a Reader at the University of Wales, Aberystwyth, U.K., where he is involved primarily in the integration of single-date and time-series SAR and optical (hyperspectral) and LiDAR data for retrieving the biomass, structure, and species/community composition of ecosystems ranging from subtropical woodlands to tropical forests and mangroves. His research has been on the carbon dynamics of these systems and their response to natural and human-induced change. He has authored or coauthored over 100 journal articles, book chapters, and conference papers.





**Alex C. Lee** received the B.Sc. and M.Sc. degrees (with first class honors) in geography from the University of Auckland, Auckland, New Zealand, in 1994 and 1997, respectively. He is currently working toward the Ph.D. degree at the Australian National University, Canberra, Australia, where he is developing algorithms for the utilization of small footprint airborne scanning laser (LiDAR) data for forest structure and biomass assessment in Australia.



**Mark L. Williams** was born in Kent, U.K., in 1961. He received the B.Sc. degree in physics with computing and the Ph.D. degree in physics from the University of Kent, Canterbury, U.K., in 1983 and 1987, respectively.

He has occupied teaching and research positions at the University of Kent, Universiti Brunei Darussalam, the National University of Singapore, and the University of Sheffield, where he first began work in radar remote sensing at SCEOS in 1994. He moved to the Defence Research Agency (formerly the RSRE), Malvern, U.K., in 1996 and worked predominantly on SAR and the theoretical modeling of microwave backscatter. He moved to Australia in 2002, where, until recently, he was employed by the Defence Science and Technology Organisation, Adelaide, Australia. He is now an independent SAR Consultant, and his research interests include the validation and exploitation of combined coherent scattering and SAR imaging models.

# A LiDAR-derived canopy density model for tree stem and crown mapping in Australian forests

Alex C. Lee<sup>a</sup>, Richard M. Lucas<sup>b,\*</sup>

<sup>a</sup> School of Resources, Environment and Society, Australian National University, and CRC Greenhouse Accounting, Canberra, ACT, Australia

<sup>b</sup> Institute of Geography and Earth Sciences, The University of Wales Aberystwyth, Aberystwyth, Ceredigion, SY23 3DB, United Kingdom

Received 12 March 2006; received in revised form 12 April 2007; accepted 14 April 2007

## Abstract

The retrieval of tree and forest structural attributes from Light Detection and Ranging (LiDAR) data has focused largely on utilising canopy height models, but these have proved only partially useful for mapping and attributing stems in complex, multi-layered forests. As a complementary approach, this paper presents a new index, termed the Height-Scaled Crown Openness Index (HSCOI), which provides a quantitative measure of the relative penetration of LiDAR pulses into the canopy. The HSCOI was developed from small footprint discrete return LiDAR data acquired over mixed species woodlands and open forests near Injune, Queensland, Australia, and allowed individual trees to be located (including those in the sub-canopy) and attributed with height using relationships ( $r^2=0.81$ , RMSE=1.85 m,  $n=115$ ; 4 outliers removed) established with field data. A threshold contour of the HSCOI surface that encompassed  $\sim 90\%$  of LiDAR vegetation returns also facilitated mapping of forest areas, delineation of tree crowns and clusters, and estimation of canopy cover. At a stand level, tree density compared well with field measurements ( $r^2=0.82$ , RMSE=133 stems  $\text{ha}^{-1}$ ,  $n=30$ ), with the most consistent results observed for stem densities  $\leq 700$  stems  $\text{ha}^{-1}$ . By combining information extracted from both the HSCOI and the canopy height model, predominant stem height ( $r^2=0.91$ , RMSE=0.77 m,  $n=30$ ), crown cover ( $r^2=0.78$ , RMSE=9.25%,  $n=30$ ), and Foliage & Branch Projective Cover (FBPC;  $r^2=0.89$ , RMSE=5.49%,  $n=30$ ) were estimated to levels sufficient for inventory of woodland and open forest structural types. When the approach was applied to forests in north east Victoria, stem density and crown cover were reliably estimated for forests with a structure similar to those observed in Queensland, but less so for forests of greater height and canopy closure.

© 2007 Elsevier Inc. All rights reserved.

**Keywords:** LiDAR; Forests; Structure; Height; Canopy density; Canopy cover; Queensland; Australia

## 1. Introduction

Stand density (e.g., stems  $\text{ha}^{-1}$ ), basal area ( $\text{m}^2 \text{ha}^{-1}$ ), predominant height (m), and measures of canopy extent, including crown cover, Foliage Projected Cover (FPC, %) and Foliage Branch Projected Cover (FBPC, %) are structural variables that are often used to characterise forests in support of inventory and mapping programs, management strategies and conservation activities (Specht & Specht, 1999). As examples, density by species and size class (e.g., diameter at 130 cm above ground level ( $D_{130}$ ) or top height ( $H$ )) and basal area are fundamental for assessing timber yields and carbon stocks (Florence, 1996), whilst measures of crown cover (CC) are used commonly to assist

quantification of carbon fluxes and understanding of ecosystem function (Parker, 1995; Popescu et al., 2004). In Australia, where this study is focused, thresholds of both CC and  $H$  are used to distinguish forests from other terrestrial vegetation (e.g. Lovell et al., 2003) and both are useful for assessing biodiversity values (Ishii et al., 2004; Turner et al., 2003).

In recent years, the retrieval of forest structural attributes across the landscape has been advanced considerably following the development of remote sensing technology and particularly multiple (discrete) return and full waveform Light Detection and Ranging (LiDAR) (Lim et al., 2003). In earlier studies using LiDAR data, emphasis was placed on retrieving tree or stand  $H$  from canopy height models (CHM) or information on the vertical stratification of foliage and branch elements (e.g., Lovell et al., 2005; Magnussen & Boudewyn, 1998; Todd et al., 2003). However, attention is increasingly turning to the estimation of a

\* Corresponding author.

E-mail address: [rml@aber.ac.uk](mailto:rml@aber.ac.uk) (R.M. Lucas).

greater range of forest attributes as processing methods become more sophisticated. Desirable attributes include tree density (e.g., Holmgren et al., 2003; Leckie et al., 2003), basal area or biomass (e.g., Lefsky et al., 1999, 2005; Lim & Treitz, 2004) and measures of canopy cover (Chen et al., 2005; Riaño et al., 2004). For purposes of retrieving these attributes, measures derived from the LiDAR CHM (maximum, mean or percentiles) and/or the percentage of canopy strikes per unit area or volume have typically been considered. For estimating stem density, for example, several studies have simply counted crowns delineated using the CHM (e.g., Hyypä et al., 2001; Leckie et al., 2003; Suárez et al., 2005) whilst others have used more complex transfer functions based on specific percentiles of the height distribution of canopy LiDAR pulses or mathematical functions (e.g., Weibull or Johnson's SB) that describe apparent vertical profiles (Jerez et al., 2005; Maltamo et al., 2004). Plot and stand level descriptions (e.g., density, mean  $H$  and canopy cover) have been obtained through aggregation of tree level information (e.g., Popescu et al., 2003). However, success in locating and attributing stems occurring in high density young forests or beneath overstorey canopies and integrating these with those of the overstorey trees for stand-based estimation has been limited to only a few studies (e.g., Hyypä et al., 2001; Leckie et al., 2003; Gaveau & Hill, 2003; Suárez et al., 2005).

The majority of studies on forest characterisation have focused on small footprint LiDAR, largely because of the earlier development of this technology but also because of the wider availability of commercial systems in many countries. By contrast, full waveform airborne large footprint systems are still experimental and (at the time of writing) generally not commercially available outside North America, although this limitation is being addressed to some extent by spaceborne LiDAR platforms such as the Geoscience Laser Altimeter System (GLAS) on the current NASA Ice, Cloud, and land Elevation Satellite (ICESat). These and other full waveform LiDAR data (e.g., SLICER and LVIS) are showing considerable promise for forest characterisation. Depending on foliage canopy, they are capable of sampling almost the full canopy profile within each footprint and providing information on the distribution of strata (including the sub-canopy), the canopy volume and other stand attributes (e.g., growth stage) which have proved difficult to obtain with small footprint LiDAR (Harding et al., 2001; Lefsky et al., 1999, 2005; Lim et al., 2003). However, whilst providing stand level descriptions, these systems have proved limited for retrieving tree level information such as the location of individual stems and their associated crowns dimensions. This occurs largely because the diameter of the footprint, which is generally 8–70 m (Lim et al., 2003), presents a lower bound on the horizontal spatial resolution. Also, it is often difficult to relate field scale data or provide absolute measures of the foliage height distribution (Harding et al., 2001). This is in contrast to the small footprint systems within which tree crowns can be readily discerned and information on the vertical profile also obtained. Large footprint systems also generate a full waveform for each footprint, and so large volumes of complex data requiring sophisticated processing are generated. Small footprint systems also generate large

volumes of data but the data themselves are relatively simple (i.e., in terms of spatial location, elevation and intensity) and are more readily available for immediate use and analysis. Even so, the representation of the canopy vertical profile is at a lower resolution and can be biased toward the upper parts of the canopy (Lovell et al., 2003).

A key benefit of all LiDAR systems is that they provide information on the distribution of plant elements in the sub-canopy and, in Australia, this information is sought as it has relevance to managing flora and faunal species and understanding both forest health and condition and the capacity of forests to regenerate (Stone et al., 2000; Todd et al., 2003). Such knowledge is also required for improved carbon accounting of both current and future carbon stocks (Dean et al., 2004), and for risk assessment in relation to fire fuel loads and crown fires (Anderson et al., 2005; Riaño et al., 2003). However, useable algorithms for retrieving information on the sub-canopy of forests in Australia from LiDAR have been difficult to obtain, partly because most have been developed on, and are applicable to, single-layered forests or those that are multi-layered but with a relatively uniform structure. Such structures are common to forests in temperate and boreal regions, which are composed primarily of coniferous (e.g., Hall et al., 2005) and/or broad-leaved (e.g. Patenaude et al., 2005; Wulder & Seemann, 2003) species, and also the tropics (Clark et al., 2004; Drake et al., 2002). Within Australia, the structural characteristics and distribution of plant communities is largely a function of geologic, pedologic and climatic (e.g., rainfall) influences (Peel et al., 2005). Most native forests are more open and comprised of species with architectures that are markedly dissimilar to those found in temperate, boreal and tropical closed forests (Barlow, 1994). The vegetation is mostly woody, sclerophyllous and evergreen, and is characterised by the presence of relatively small, rigid, long lived leaves, which also tend to be vertically orientated in response to the high sun intensity. The dimensions (area and depth) of crowns in the upper canopy are highly variable, ranging from large and expansive (typical to many *Eucalyptus* and *Angophora* species) to small and compact (typical to *Callitris* species). In many cases, both crown types occur in the same stand but often in different strata, and variation in tree height, crown size, shape and density (which is high even within species) occurs as a function of the volume and type of soil that can be exploited for water and nutrients. Crown size is also indicative of the area a plant will influence through, for example, shading and litter deposition (Jupp & Walker, 1997).

These configurations present significant challenges for estimating tree density, basal area and CC when utilising a LiDAR CHM (particularly that generated from small footprint data). Specifically, when locating individual trees within the CHM, many trees that are partially or wholly within the sub-canopy or understorey are not identified (Hyypä et al., 2001), high points in crowns often do not necessarily correspond to the location of the stem (Lee et al., 2001), and multiple high points within a single crown may occur that falsely indicate the presence of several separate trees (Florence, 1996). Estimates of stand-based CC are also often based on arbitrary thresholds of the CHM rather than on measures that better relate to the distribution of foliage and branch elements.

This study relates to mapping at a tree scale, but with particular reference to sub-canopy elements. Ideally, the sub-canopy assessment would be undertaken using full waveform large footprint systems, as confidence in the representative assessment of the vertical elements would be increased. However, in the absence of available systems, the practical solution is to emulate some of the large footprint system attributes using small footprint systems. Algorithms for assessing Australian vegetation structure from LiDAR also need to be tailored to Australian conditions, and particularly consider soils and climate as these factors play a major role in influencing growth form, even within the same species group. For this purpose, we have developed a new structural assessment tool, termed here the Height-Scaled Crown Openness Index (HSCOI). This index, which is calculated from small footprint LiDAR, provides a quantitative measure of the penetration of the LiDAR pulse through the forest canopy and is considered complementary rather than supplementary to the traditional LiDAR CHM-based approaches. The HSCOI was developed primarily to address problems that can arise when utilising CHMs to identify stems in Australian forests. This paper describes the conceptual development of the HSCOI and then evaluates its utility, both alone and in conjunction with the CHM, for:

- a) Locating tree stems and estimating  $H$  within both the overstorey and sub-canopy of multi-layered forests that are common to semi-arid environments (e.g., wooded savannas).
- b) Delineating the extent of the forest canopy and individual or clusters of crown(s) contained within.

The paper also provides a preliminary assessment of the applicability of a HSCOI (developed for a semi-arid forest) to other forested environments in Australia, and the implications and requirements for regional calibration and application. The paper reports the results from initial proof of concept investigations into stem mapping and attribution. The set of

procedures required to meet adequate levels of accuracy are outlined, and are then tested on independent sites in another location. This has been undertaken to highlight additional regional calibration requirements.

## 2. Study areas and data collection

### 2.1. Site descriptions

The study focused on two locations. The primary development and calibration location is an area of open forests and woodlands near Injune (Latitude  $25^{\circ} 36' S$ , Longitude  $147^{\circ} 30' E$ ) in central Queensland, Australia (Fig. 1; Lucas et al., 2006a; Tickle et al., 2006). Within this area, elevation varies from 437 to 850 m and the mean annual rainfall is approximately 635 mm, though variable, with most recorded between December and February (summer). The mean annual maximum temperature is  $27^{\circ} C$  (Bureau of Meteorology, 2004).

The forests are diverse and dominated by several species, with both excurrent (e.g., pines) and decurrent structural forms commonplace (Lucas et al., 2004). White cypress pine (*Callitris glaucophylla*) dominates many stands but this species is also selectively harvested, so large individuals are typically absent. Most *Callitris* trees occur in dense stands comprised of a large number of smaller individuals (up to several trees per  $m^2$ ). *Eucalyptus* species are widespread throughout the area, with Silver-leaved Ironbark (*E. melanaphloia*) and Poplar Box (*E. populnea*) being prevalent. Tumbledown Red Gum (*Eucalyptus dealbata* var *chlorodata*) and Smooth Barked Apple (*Angophora leiocarpa*) occur along the creeks and at scattered locations throughout the landscape, and individual trees often contribute the greater proportion of the stand biomass. Larger individuals of both *Eucalyptus* and *Angophora* species form the upper canopy of many stands, below which several layers of sub-canopy trees of varying densities occur. Brigalow (*Acacia harpophylla*) and understorey shrubs such as Wilga (*Gejeira parviflora*) and Sandalwood Box (*Eremophila*

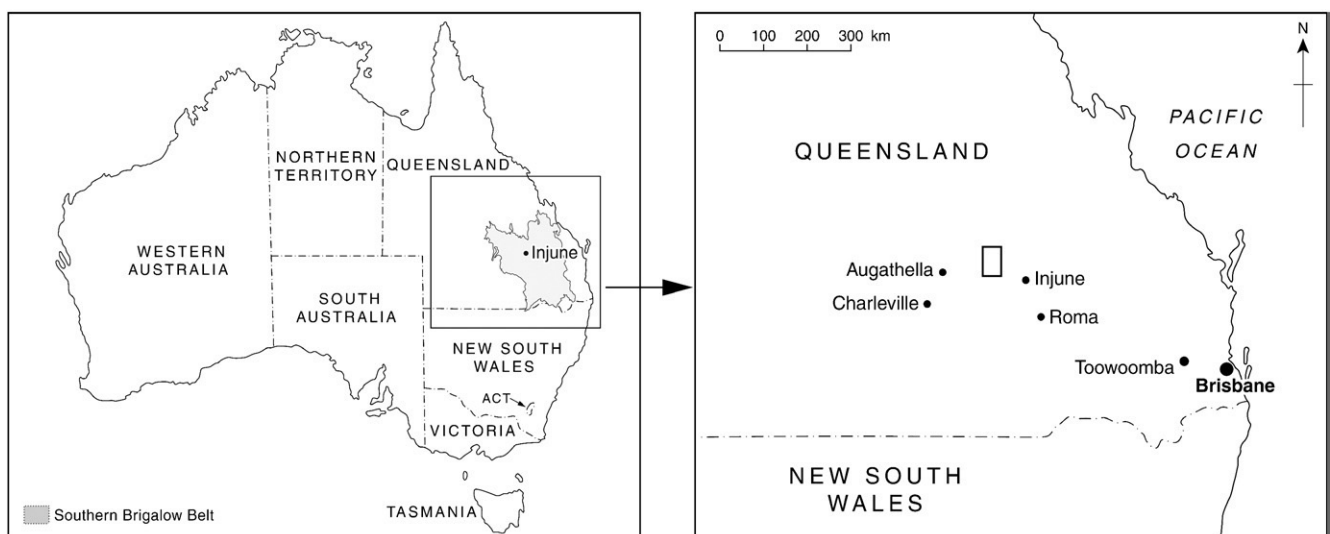


Fig. 1. The location of the Injune study area.

*mitchelli*) are commonplace. Many stands contain a mix of *Acacia*, *Callitris*, *Eucalyptus* and *Angophora* species and a wide range of growth (and therefore structural forms) exist because of the varying impacts of natural fires, droughts, clearing (e.g., pulling, poisoning) and grazing (Tickle et al., 2006).

The secondary study site (utilised for regional validation of the HSCOI) was located in northeast Victoria (Fig. 2). Here, a National Forest Inventory (NFI) Continental Forest Monitoring Framework (CFMF) pilot project was undertaken in 2003–04 to evaluate multi-tier data collection sampling design and attribute measurement approaches (BRS, 2003a). The CFMF was initiated to provide an integrated nationally consistent inventory and monitoring program for meeting assessment and reporting requirements. The pilot region, the Ovens and Broken catchments, covered 1.5 million hectares, and contained a wide range of forest types ranging from high rainfall alpine and montane environments to rolling foothills and semi-arid floodplains. The elevation ranges from around 1900 m in the alpine area to a low of around 100 m above sea level in the floodplains. The mean annual rainfall ranges from 2264 mm yr<sup>-1</sup> to 394 mm yr<sup>-1</sup> from the alpine to the floodplains areas respectively. Forest covers approximately 35% of the area and the remainder is occupied largely by agricultural land. In terms of structure, the forests studied in Queensland and northeast Victoria were considered representative of the majority occurring within Australia.

## 2.2. LiDAR data acquisition

For Queensland, small footprint discrete return LiDAR data was collected using an Optech 1020 system, mounted in a Bell Jet Ranger helicopter with a nominal flying altitude of 250 m and

a swath width of approximately 200 m. The data were captured over a regular grid of 10 × 15 primary sampling units (PSUs) located ~4 km apart in the north–south and east–west directions. Each PSU was 500 × 150 m in the *x* and *y* dimensions respectively, and was further divided into 30 secondary sampling units (SSUs) that were 50 m × 50 m (0.25 ha). The sampling strategy is described in more detail in Lucas et al. (2006a) and Tickle et al. (2006). The acquisition occurred over a one-week period commencing August 24th 2000. The Optech 1020 had a laser repetition rate of 5 kHz, operated at 1047 nm (near infrared spectrum), with a beam divergence of 0.25 mrad, a footprint of approximately 7.5 cm, and an average sampling interval of 1 m. First and last returns and the intensity of each return were acquired flying in an east–west direction (centred on each PSU row).

Within northeast Victoria, LiDAR data were collected using an Optec ALTM 1225 system mounted in a fixed wing aircraft, with a nominal flying height of 1100 m and an average swath width of 400 m. The LiDAR data were acquired over a 20 km regular grid laid out across the two catchments and LiDAR data were flown along a total length of 1485 km and an area of ~59,400 ha. The system supported a laser repetition rate of 25 kHz, with a beam divergence of 0.1 mrad, and a footprint size of 0.24 m. The data averaged a nominal point spacing of 1 m, though some plots were over-flown multiple times at the sampling grid intersections, resulting in a return spacing of 30–50 cm at these locations (BRS, 2006).

At both sites, a Global Positioning System (GPS) base station was established for all flights. With full differential GPS corrections, in addition to pitch, yaw and roll compensation from an inertial navigation system, coordinates were supplied to

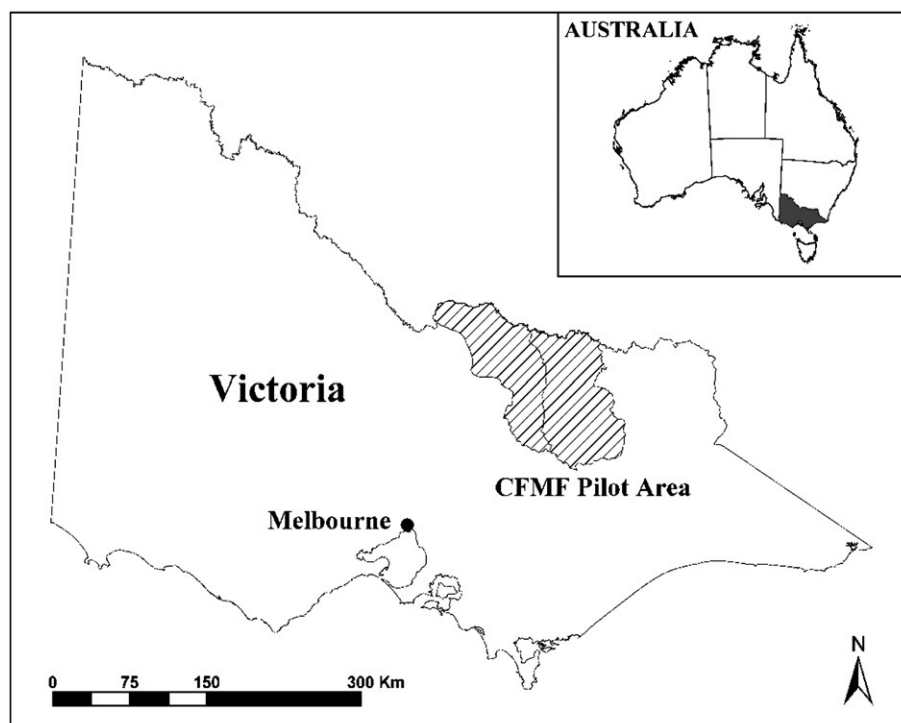


Fig. 2. Location of the CFMF pilot study in northeast Victoria.

an absolute accuracy of <1 m in the  $x$  and  $y$  directions and <0.15 m in the  $z$  direction.

### 2.3. Field data

During August 2000, field data were collected in Queensland from the equivalent of 34 sub-sampling units located within 12 of the 150 PSUs such that the main vegetation types and regeneration stages were represented. For 31 SSUs, field data were collected from 50 × 50 m plots, each of which also contained five 10 × 10 m subplots for recording trees with diameters <5 cm. Within three additional sub-sampling units representing non-forest and re-growth, five 10 × 10 plots rather than one 50 × 50 m plot were established in the centre and along the diagonals 10 m distant from the four corners, largely because of the high density of small trees occurring. Within each plot, stem diameter at 130 cm ( $D_{130}$ ) and 30 cm ( $D_{30}$ ), stem  $H$ , crown dimensions ( $x$ ,  $y$  and  $z$ , representing the east–west and north–south directions and crown depth respectively) as well as the species of each tree were recorded. To map trees and thereby determine stem density, the location of all trees with  $D_{130} \geq 10$  cm was recorded digitally within each plot by placing reflectors at each of the four corners and then using either a GEOSCAN or CENTURION Laser Rangefinder to measure the distance and angle from each tree to the nearest visible reflector. Using this approach, the location of trees in UTM coordinates was calculated. Adjustments were made subsequently to correct for angular errors, which were assisted by differential GPS measurements of plot corners, and a few key trees. Trees with  $D_{130}$  between 5 and 10 cm were located separately by reading the  $x$  and  $y$  distances (in cm) from the 50 m tapes laid out in the plot and assigning each a coordinate relative to that of the south west corner, which was located using differential GPS. Several measures of cover were generated for each plot. CC was calculated as the percentage of the plot that was contained within the vertical projection of the periphery of crowns of trees inside a plot, with crowns considered opaque (McDonald et al., 1998). FBPC, defined as the horizontal percentage cover of leaves and branches, was estimated by applying the sighting tube method (Specht and Specht, 1999) at 1 m intervals across three 50 m north–south transects established within each plot at 10, 25 and 40 m intervals eastwards from the south-west corner. The FBPC method is described in more detail in Tickle et al. (2006). Initial LiDAR plot FBPC estimates were generated by calculating the percentage of all LiDAR returns that were 2 m and above in height.

For northeast Victoria, 22 field plots (30 × 30 m) were measured at forested sites located at the nodes of the 20 km systematic sampling grid. Where forest was not present at these nodes, plots were separate by several 10 s of kilometers. The plot locations were coincident with the LiDAR swaths and, within each, structural attributes similar to those measured within the Injune study area were recorded (e.g., location, species, height, and crown dimensions for every tree with  $D_{130} \geq 10$  cm). The plots were stratified subsequently into three broad ‘ecozone’ categories — montane (including alpine), foothills, and floodplains. These categories were defined from elevation, terrain, soils and vegetation maximum height characteristics (BRS, 2006). Summaries of tree and plot distributions of key attributes (stem density, basal area,

Table 1

Summary of tree and stand attributes based on measurements from 32 × 0.25 ha and 22 × 0.09 ha plots located in forests near Injune Queensland and in northeast Victoria respectively

Attribute	Total/count	Mean	SD	Minimum	Maximum
<i>Injune, Queensland</i>					
Plot Stems per hectare ( $D_{130} \geq 5$ cm)	32	518	444	76	2452
Tree $D_{130}$ (cm)	3771	13.5	9.4	5.0	97.1
Tree height (m)	3771	8.7	3.9	0.3	30.8
Tree crown area (m <sup>2</sup> )	3771	9.6	19.7	0.1	397.4
Plot basal area (m <sup>2</sup> /ha)	32	10.8	4.4	4.0	21.6
Plot crown cover (%)	32	46.5	19.6	3.5	86.3
Plot predominant stem height (m)	32	15.7	2.5	10.9	21.5
Plot Stems per hectare ( $D_{130} \geq 10$ cm)	32	246	362	0	1964
Tree $D_{130}$ (cm)	1813	7.1	0.6	5.0	9.9
Tree height (m)	1813	6.1	1.7	0.3	19.3
Plot basal area (m <sup>2</sup> /ha)	32	1.0	1.6	0.04	8.6
Plot Stems per hectare ( $D_{130} \geq 10$ cm)	32	263	114	100	492
Tree $D_{130}$ (cm)	1958	19.4	9.4	10	97.1
Tree height (m)	1958	11.2	3.8	2.0	30.8
Plot basal area (m <sup>2</sup> /ha)	32	9.7	3.6	3.7	18.2
<i>Northeast Victoria</i>					
Plot Stems per hectare ( $D_{130} \geq 10$ cm)	22	383	221	22	1078
Tree $D_{130}$ (cm)	839	25.9	18.5	9.7	194.8
Tree height (m)	839	13.7	6.7	1.6	40.8
Plot basal area (m <sup>2</sup> /ha)	22	32.2	11.7	14.0	63.6
Plot crown cover (%)	22	81.7	19.0	19.5	99.4
Plot predominant stem height (m)	22	23.0	7.0	9.8	36.2

diameter, height and crown area) are provided in Table 1 and Fig. 3. Note that 2 SSUs in the Queensland data were excluded (i.e.,  $n=32$ ) because these were only partially covered by LiDAR data.

## 3. Data analysis

### 3.1. Data analysis overview and strategy

The analysis of field and LiDAR data was undertaken in several successive stages (Stages I–IX; Table 2). Specifically, the field data were used to a) evaluate the potential of the LiDAR data for identifying stem locations, including those associated with sub-canopy trees, b) support the generation of empirical relationships between LiDAR-derived data (i.e., the CHM and HSCOI) and  $H$  for all identified stems, and c) evaluate the potential of the LiDAR for retrieving stand level estimates of stem density, predominant stem  $H$  and cover (namely CC and FBPC).

#### 3.1.1. Stage I. Calibration and validation strategy

A three-stage calibration and validation strategy was developed to optimise the HSCOI stem and cover mapping process for the semi-arid woodlands and open forests found in the primary study area (i.e., Injune).

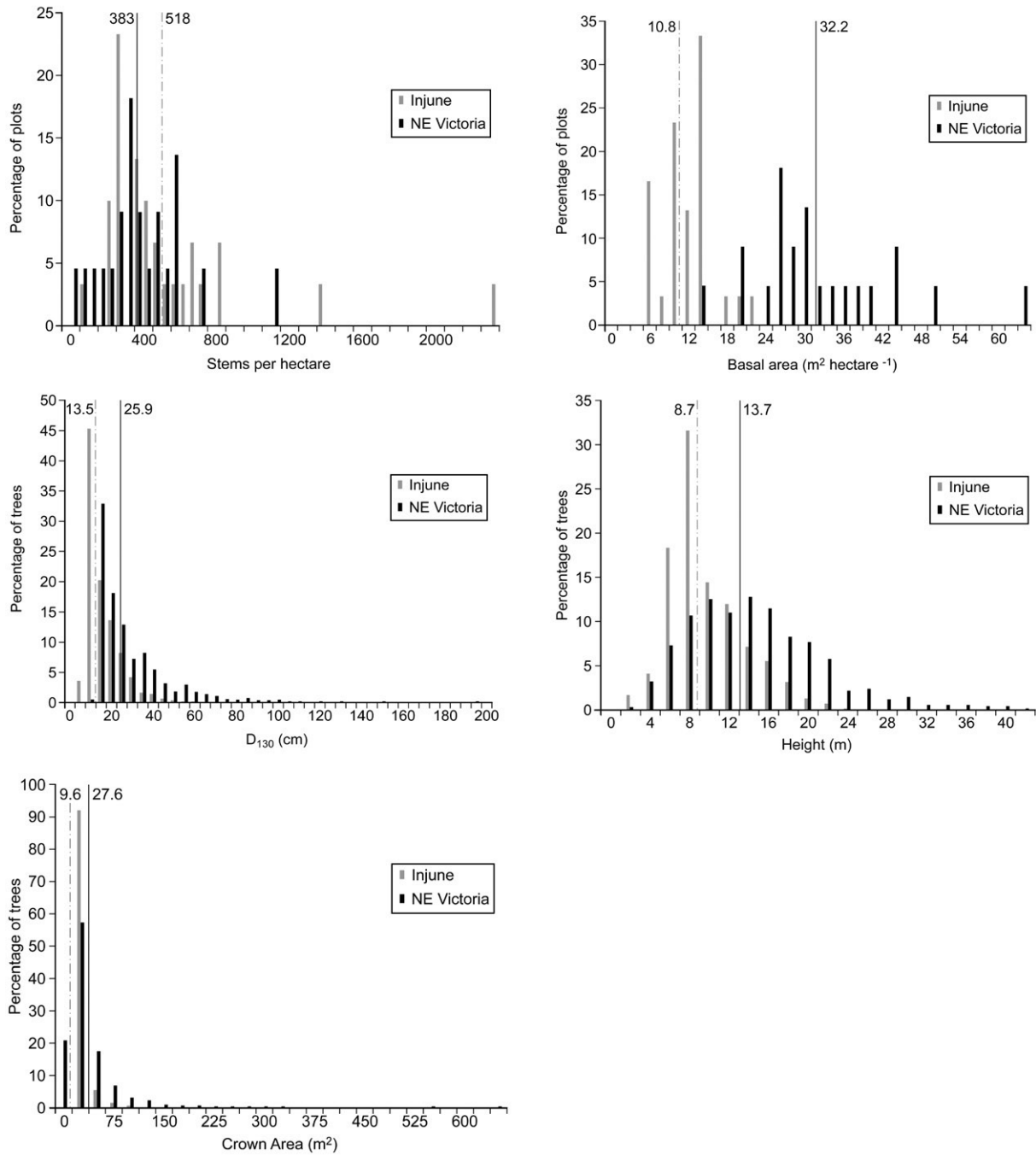


Fig. 3. A summary of stand attributes from field data across  $32 \times 0.25$  ha plots for Queensland and  $22 \times 0.09$  ha plots for northeast Victoria. Mean values are labelled and indicated as dashed (Injune) and solid (NE Victoria) vertical lines respectively.

1. Initially, four field plots (111-18, 81-11, 124-19 and 81-16; referenced by their PSU and SSU number respectively) that spanned the different dominant forest structures observed across three widely separated PSUs were selected. These are shown (circled and labelled) with reference to the other field plots in Fig. 4. The HSCOI was then developed using data from these plots, and the stem extraction and attribution method refined such that consistent results were achieved when compared to field data. These plots were selected for the following reasons:

- The predominant height of the forest stands within the four plots was greater compared to the other plots and

these were expected to support multiple strata and stems in the sub-canopy.

- The plots were located in forests that spanned more than one half of the FBPC range, and were in the upper half of the cover range. Plots with a higher FBPC tended to support more stems and/or larger crowns, which contribute to the difficulties associated with stem mapping.
- The species contained within the plots were typical of those within the study area. Specifically, plot 111-18 contained a mature *Callitris* pine forest, which had tall stems with small crowns, with a few large *Eucalyptus* trees. Plot 81-11

Table 2  
Overview of processing stages in the analysis of field and LiDAR data

Stage	Purpose
I Calibration and validation strategy	To ensure a) a sequence of reliable inputs to models and b) data to test model outputs across a range of forest types and environments.
II Calculation of plot-based stem density, cover, and sub-canopy tree assessment	To provide calibration and validation sets at the plot level and to establish, based on field data, the realism of retrieval.
III Ground and canopy height surfaces	To provide an accurate ground DEM against which to retrieve vegetation heights from LiDAR point data.
IV Conceptual development of the Height-scaled Crown Openness Index (HSCOI)	To conceptualise and demonstrate the steps required for calculation of the HSCOI.
V Calculation of the HSCOI <ul style="list-style-type: none"> <li>•Matrix generation and intersection of LiDAR points.</li> <li>•Calculation of LiDAR penetration.</li> </ul>	
VI Smoothing of the HSCOI and generation of minima	To allow detection of stems regardless of crown dimensions and position in the vertical profile.
VII Stem location using the HSCOI: <ul style="list-style-type: none"> <li>•Stem identification and extraction</li> <li>•Filtering at multiple scales utilising tree crown area and HSCOI thresholds.</li> </ul>	To allow mapping of stems by locating HSCOI minima and refinement of these maps by utilising empirical functions and field-measurements (e.g., height, crown area) for different species.
VIII Crown/cluster area and cover estimation	To identify the forest/non-forest boundary and crowns/crown clusters contained within.
IX Estimation of stem <i>H</i> and plot-scale attributes (including density and predominant height).	To indicate stem size at the tree and stand level, thereby facilitating tree and stand level assessment of growth (successional) stage and estimation of biomass.

contained a stand of mature *Angophora* species with very large crowns and included a *Callitris* midstorey with an *Acacia* understorey. Plot 124-19 supported a senescent *Angophora* forest with a few larger crowns (though smaller than plot 81-11) and a dominant understorey of *Callitris*. Plot 81-16 contained co-dominant *Angophora* and *Callitris* in the upper canopy. The remainder of the validation plots included variations along this continuum; though in some plots different genus combinations were observed.

2. Subsequently, the HSCOI routines were applied to the remaining 26 field plot locations from the 12 PSUs, and comparisons made with field data at these locations. There were between 1 and 4 field plots within these PSUs, which

were widely spaced throughout the study area (separated by 4–50 km). Where multiple field plots occurred within a PSU, the plots were located within different forest structural types. This then provided independent validation across a greater range of forest structural configurations.

3. Finally, the HSCOI routines calibrated against the Injune datasets were applied to field plot locations in northeast Victoria to assess capability for stem density mapping and validation across a wider range of forested environments. This was undertaken to highlight issues that might arise when applying the technique to forests supporting trees and stands of differing structure and to determine what further calibration requirements (e.g., consideration of regional or

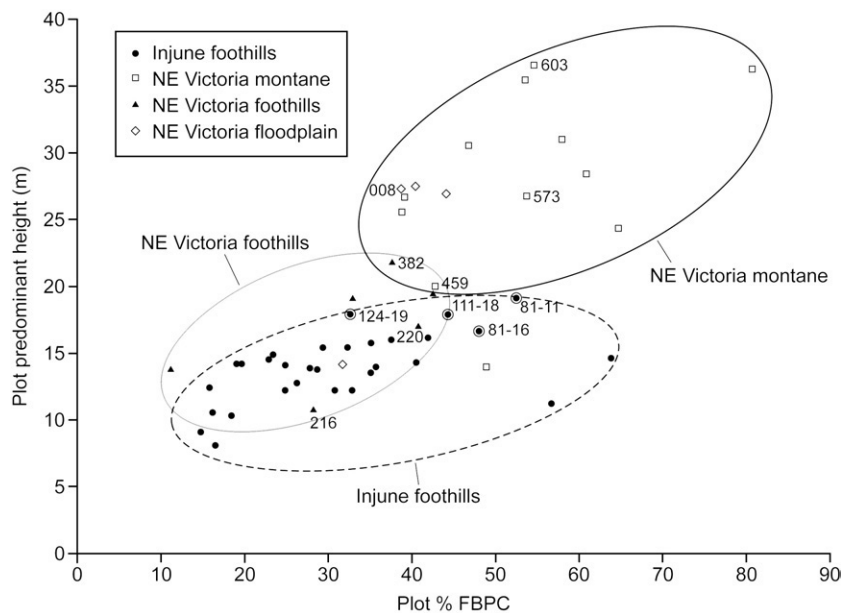


Fig. 4. The distribution of the 32 × 0.25 ha (Queensland) and 22 × 0.09 ha (northeast Victoria) plots within the FBPC and predominant height feature space. Key plots used in development of the HSCOI are indicated (circled and labelled).



environment-specific factors) might be required to broaden the utility of the HSCOI algorithms.

From Fig. 4, the Injune plots were observed to occupy a FBPC range of between 14–64% and a predominant height range of 8–20 m which was largely outside the cover-height envelope associated with the forest plots in northeast Victoria. For this reason, these data were considered suitable for assessing the utility (or otherwise) of the HSCOI algorithms when applied to forests with a structural range outside that used for algorithm development.

### 3.2. Field data processing stages

#### 3.2.1. Stage II. Calculation of plot-based stem density, cover and sub-canopy tree assessment

At the plot level, and using the field data for trees with  $D_{130} \geq 5$  cm, stem density (i.e., the sum of all stems within field plots) and basal area were calculated. Trees with  $D_{130} < 5$  cm were excluded as these were only sampled in subplots within the sub-sampling unit. Both measures were scaled to a per hectare basis. Predominant  $H$  was also calculated as the mean top  $H$  of the 13 tallest trees in the plot area (i.e., 0.25 ha). This measure is a standard descriptor of Australian forests and is usually calculated as the mean top  $H$  of the 50 tallest trees per hectare; though between 40 and 75 trees can be selected (Research Working Group 2, 1999). CC was estimated by summing the crown areas of individual trees with  $D_{130} \geq 5$  cm. FBPC was calculated as the percentage of leaf and branch observations along three 50 m transects within each field plot.

The development of the HSCOI was motivated initially by the requirement to locate stems in the sub-canopy, which could not be achieved using a CHM. As a preliminary investigation, the field data were analysed to evaluate the likely percentage of sub-canopy trees (i.e., overtopped by taller individuals) across a range of stands. For this analysis, three plots were excluded from the initial 34 as they were regrowth plots with vegetation  $< 2$  m height and generally  $D_{130} < 5$  cm, whilst one had significant portions of the plot area missing LiDAR data because of adverse wind conditions at the time of the overflight. For the remaining 30 plots, a circular buffer based upon the crown radius, calculated as half the average crown width in the north–south and east–west directions, was created around the stem location for all trees with  $D_{130} \geq 5$  cm. Starting with the tallest tree, a count was then made of any stems located within the buffered area and with  $H$  shorter than the tree being assessed. No tree was counted more than once. The contribution of sub-canopy stems to the total in terms of, for example, basal area, was also evaluated to establish the importance of including these in stand-based estimates (e.g., for carbon accounting purposes).

### 3.3. LiDAR data processing

#### 3.3.1. Stage III: Ground and canopy height surfaces

An initial Digital Terrain Model (DTM) was constructed by interpolating pre-classified first and last ground returns with a 1 m proximal tolerance (where any returns found within 1 m of

other returns were excluded) and represented as a Triangulated Irregular Network (TIN) model. However, examination of the resulting surface indicated a certain degree of ‘noise’ and surface variation resulting from on-ground surface features (e.g., logs, grass swards and shrubs). Therefore, and following other studies (e.g., Suárez et al., 2005), a multi-scale filtering strategy was employed. Here, the lowest returns (first or last) within local search windows of increasing dimension ( $1 \times 1$  m to  $5 \times 5$  m) were selected to generate a bare ground surface on the assumption that these were more likely to represent the true elevation surface. The most suitable window size for generating the final elevation surface was determined by examining a corresponding elevation standard deviation surface generated using a  $5 \times 5$  search window. Here, flat areas with low deviation in elevation only required ground returns from large search windows (e.g.  $5 \times 5$  m). Where ground elevation was more variable (e.g. around water courses) then returns from smaller windows were used, with the general rule being that the greater the deviation, the smaller the search window.

Subtracting the initial TIN ground model from the final spatially filtered surface produced a difference surface. As an example, the surface analysis for PSU 142 indicated that the spatially filtered elevation layer was lower and differed, on average, by 8 cm (standard deviation ( $\delta$ )=8 cm, range= $-0.5$  to 0.5 m). Similar results were observed within the other PSUs, and these compared well to other studies (e.g., Hodgson & Bresnahan, 2004). The on-ground surface features previously identified were also evident within the difference surface, indicating that spatial filtering of the surface was effective in their removal. Once calculated, the height of woody vegetation was determined as the difference in elevation between the final bare ground surface and the first and last vegetation LiDAR returns. Only returns above 0.5 m were subsequently used for canopy assessment, as those below this height were considered to be from shrubs, tall grass, and larger items of woody debris.

#### 3.3.2. Stage IV. HSCOI conceptual development

Australian forests can be stratified both vertically and horizontally. In the vertical domain, all vegetation has an upper stratum and lower layers may exist whilst in the horizontal domain, variations result from the arrangement (spacing) and density of foliage within any given vertical layer (Jupp & Walker, 1997). In open forests and woodlands, this relationship is often referred to as “gapiness”, in that foliage clumping creates gaps through which light may penetrate to the lower layers (Nilson and Ross, 1997). Conceptually, the HSCOI considers the penetration of the LiDAR pulse through the forest volume and therefore relates to canopy gapiness (or porosity) and also light transmittance. As such, it provides a 3D measure of opacity and can therefore be considered an extension of traditional foliage cover estimates calculated from point observations, most of which are summarised above or below a certain height threshold (typically eye level; McDonald et al., 1998) and transformed to give a 2D projection of canopy extent. The HSCOI also draws upon some of the conceptual aspects surrounding the interpretation and analysis of full waveform large footprint LiDAR, including those presented in the initial

phases of the Canopy Volume Method (CVM; Harding et al., 2001; Lefsky et al., 1999). Comparisons between the HSCOI and CVM are described in Section 5.1. The development of the HSCOI additionally incorporates a multi-scale strategy in both the initial generation stage, and in the subsequent stages of spatial refinement and attribution. This is because the HSCOI is designed to assess both trees and stands of trees, which may occur at a range of sizes. Since the utilisation of multi-scale analyses have been shown to reduce scale effects in spatial analyses, and thus provide enhanced understanding of ecological patterns (Burnett & Blaschke, 2003; Frazer et al., 2005; Hay et al., 1997; Jelinski and Wu, 1996), this strategy has been adopted with the HSCOI.

### 3.3.3. Stage V. Calculation of the HSCOI

To generate the HSCOI, the LiDAR data were processed in a raster format for computational speed and efficiency, with each 1 m height interval represented within the attribute database of the final output 2D raster grid. To quantify the relative penetration of LiDAR pulses through the forest volume, these data were transformed into a three-dimensional (3D) voxel matrix of 1 m<sup>3</sup> spatial resolution (i.e., horizontal and vertical spatial resolution of 1 m); an approach adopted also by Chasmer et al. (2004). The 1 m output spatial resolution reflected the post-spacing of the base LiDAR point data and was commensurate with other acquired datasets, namely the Compact Airborne Spectrographic Imager (CASI; Bunting & Lucas, 2006) and large-scale aerial photography (Tickle et al., 2006). Within this 3D matrix, canopy voxels containing returns were attributed with the tallest recorded LiDAR height value occurring within the voxel space. The HSCOI (expressed as a percentage) can be considered a weighted summation of a proxy variable of the inverse of canopy density (i.e., 1/number of voxels containing returns ( $n_{\text{voxels}}$ ) per 1 m<sup>2</sup> vertical column). The weighting used is the relative height of the voxel ( $\text{voxel}_{\text{ht}}$ ) with respect to a kernel window or stand/PSU, where:

- a) The local maximum height,  $\text{HSCOI}_{\text{local}}$ , uses the maximum height ( $\text{max}_{\text{ht}_{\text{local}}}$ ) in an  $n \times n$  kernel window.

$$\text{HSCOI}_{\text{local}} = \sum_{n=1}^{n_{\text{voxels}}(i)>0} \left( \left( \frac{\text{max}_{\text{ht}_{\text{local}}} - \text{voxel}_{\text{ht}}}{\text{max}_{\text{ht}_{\text{local}}}} \right) * \frac{1}{n_{\text{voxels}}} \right) * 100 \quad (1)$$

- b) The stand maximum height  $\text{HSCOI}_{\text{stand}}$ , uses the maximum height of the stand ( $\text{max}_{\text{ht}_{\text{stand}}}$ ), as represented by a plot/SSU or PSU.

$$\text{HSCOI}_{\text{stand}} = \sum_{n=1}^{n_{\text{voxels}}(i)>0} \left( \left( \frac{\text{max}_{\text{ht}_{\text{stand}}} - \text{voxel}_{\text{ht}}}{\text{max}_{\text{ht}_{\text{stand}}}} \right) * \frac{1}{n_{\text{voxels}}} \right) * 100 \quad (2)$$

where the summation uses only those voxels that contain LiDAR returns. This is achieved with a counter variable ( $i$ ), which counts the LiDAR voxels (containing returns) up to the

maximum number of levels (i.e., maximum height of column). The HSCOI therefore translates point observations from the LiDAR into a measure of relative penetration of LiDAR pulses, by scaling these from the top of the canopy such that 0% indicated no canopy penetration whilst 100% represented full penetration to the ground. As an illustration, if four LiDAR strikes were recorded within a column, then each would contribute 25% of the total  $\text{HSCOI}_{\text{stand}}$  value. If  $\text{max}_{\text{ht}_{\text{stand}}}$  was 25 m and the voxel heights in the column were 0 m (ground), 5 m, 10 m and 25 m, then:

$$\begin{aligned} \text{HSCOI}_{\text{stand}} &= \left[ \left( \frac{25-0}{25} * \frac{1}{4} \right) + \left( \frac{25-5}{25} * \frac{1}{4} \right) + \left( \frac{25-10}{10} * \frac{1}{4} \right) + \left( \frac{25-25}{25} * \frac{1}{4} \right) \right] * 100 \\ &= (0.25 + 0.20 + 0.15 + 0.0) * 100 \\ &= 60\% \text{ HSCOI}_{\text{stand}} \text{ for the 2D output cell} \end{aligned}$$

If  $\text{max}_{\text{ht}_{\text{local}}}$  (e.g., within a  $3 \times 3$  kernel) was 15 m (rather than 25 m) but returns were still recorded at 0 m, 5 m and 10 m, then a  $\text{HSCOI}_{\text{local}}$  of 66% would be calculated. The higher HSCOI therefore indicates a greater likelihood of penetration to the ground surface as a consequence of the relative scarcity of leaves and branches in the canopy. A top of canopy height grid (in 2D), which contained the maximum height found within each square meter column of the 3D matrix, was also generated. This allowed creation of a  $\text{CHM}_{\text{local}}$ , which was required for deriving reliable tree  $H$  and estimating  $\text{max}_{\text{ht}_{\text{local}}}$  within a ( $3 \times 3$ ) kernel area.

The use of both the local kernel and the stand maximum height in the calculation of the HSCOI presented two advantages. First, with  $\text{HSCOI}_{\text{local}}$ , areas of dense vegetation within crown clusters could often be identified regardless of height because of the local nature of the kernel. Second, with  $\text{HSCOI}_{\text{stand}}$ , crown clusters containing a high density of stems with low height (e.g., understorey) were separated from those associated with taller overstorey trees. In this latter case, the heights were closer to the maximum of the plot and hence  $\text{HSCOI}_{\text{stand}}$  values were lower compared to those of shorter sub-canopy trees. As the height range within the larger stand area was generally greater, fewer minima were identified in the understorey clusters.

### 3.3.4. Stage VI: HSCOI smoothing and minima generation

During development of the HSCOI, comparisons with field data suggested that lower HSCOI values were associated with either the locations of stems or clumps of branches contained within larger crowns. To better define local minima that may correspond to stems, this stage had two main phases. First, a range of smoothing kernels of varying size and shape were evaluated in order to determine the optimal configuration for surface generation and subsequent minima extraction. The optimal configuration sought to minimise internal crown gaps/holes in the canopy density surface (i.e., the initial HSCOI layer) that occurred because of branch clumping, the LiDAR sampling rate, and the spatial resolution of the HSCOI matrix. The second phase took the final smoothed layers and passed them through a topographic assessment routine for rapidly

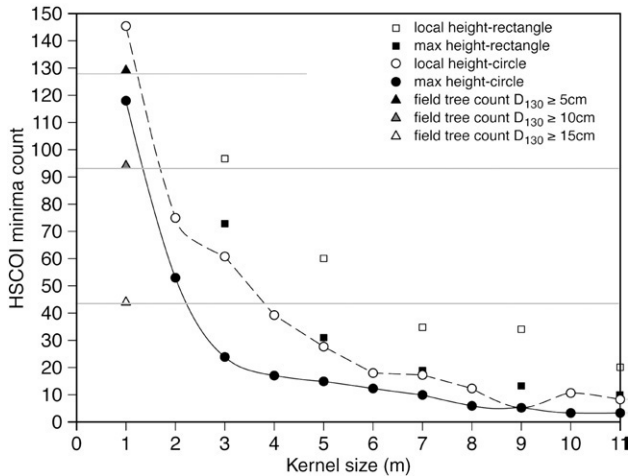


Fig. 5. The comparison between the number of minima produced with different kernel sizes and shapes for test SSU 124-19, and the number of trees of different stem diameter sizes identified in the field.

extracting minima that could be compared against actual stem locations.

Previous research has described the use of multiple kernel sizes and shapes for enhancing individual tree crown identification (e.g. [Wulder et al., 2000](#); [Popescu and Wynne, 2004](#)). Therefore, a range of focal mean smoothing functions were evaluated to identify branches associated with larger crowns and fill internal crown gaps. This step applied kernels of varying shapes (e.g., squares or circles) and sizes (e.g., with pixel side length or radii increasing from 1 to 11 m) to one of the calibration plots (SSU 124\_19) that contained crowns of varying sizes and dimension (Fig. 5). [Pouliot et al. \(2005\)](#) described a similar comparison using fine spatial resolution optical imagery and bright point counting within segmented crowns. The HSCOI process confirmed the findings of [Pouliot et al. \(2005\)](#) in that an increasing kernel size resulted in fewer

minima, with this size effect also found when a range of field data stem counts at different stem diameter size thresholds were assessed (Fig. 5). This indicated a link between kernel spatial resolution and likely tree crown area (i.e., small crowns are not detected with larger kernels because of spatial smoothing).

A circular kernel of 1 m radius (which averaged the centre and four adjacent cells) applied to the stand maximum height surface provided the best initial correspondence for the count of stems with  $D_{130} \geq 5$  cm. By applying to the HSCOI, gaps in the canopy were filled and the crown edges of many trees were clearer in definition, thus corresponding well with those observed in the field (Fig. 6a). When rectangular (square) kernel sizes of 5 m or greater were used, lower values of the HSCOI extended beyond the estimated boundary of the field-measured crowns. However, minima associated with the 5 m rectangular kernel were found to better identify the centre of taller individuals and the dominant trees within clusters compared to other rectangular kernel sizes (e.g.,  $3 \times 3$ ), although many of the smaller trees identified previously using the circular kernel of 1 m radius were not detected (Fig. 6b).

To extract minima from the smoothed HSCOI layers, the ArcInfo Topogrid function ([ESRI, 1996](#)) was used to create interpolated surfaces of  $1 \text{ m}^2$  cell size and corresponding 'sinks' or minima. The locations of these sinks were then compared against the location and number of stems recorded in the field. The resultant smoothed HSCOI surfaces (Fig. 7a) can be considered akin to an inverted CHM, but with a significant difference. In a CHM, the tallest parts of a crown tend to form the apex of the surface (Fig. 7b) whereas with a HSCOI surface, the densest part of the crown forms the minima as the LiDAR pulses have the most difficulty in striking the ground. As the densest part of the crown is typically directly above the stem, the HSCOI minima better represent the stem location. By contrast, the tallest parts of the crown identified using the  $\text{CHM}_{\text{local}}$  are only directly above the stem location for certain

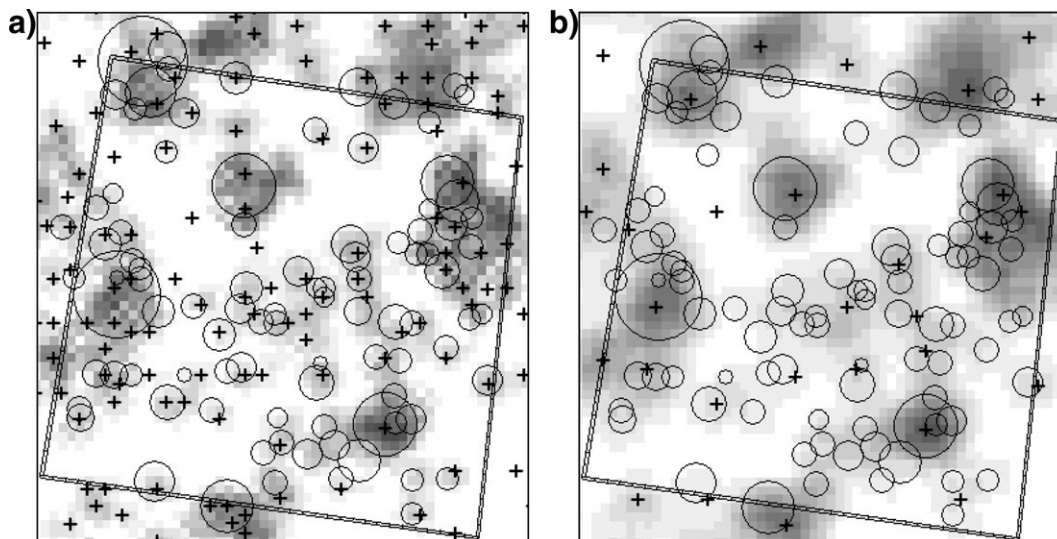


Fig. 6. A  $\text{HSCOI}_{\text{stand}}$  surface (based on plot maximum height) for SSU 124\_19, smoothed with a focal-mean function using a) 1 m circular and, b) a  $5 \times 5$  m rectangular kernels. Darker areas represent lower  $\text{HSCOI}_{\text{stand}}$  values and hence a higher canopy density. Local HSCOI minima are indicated with crosses, whilst tree crowns identified in the field are represented as circles that are proportional to crown radius.

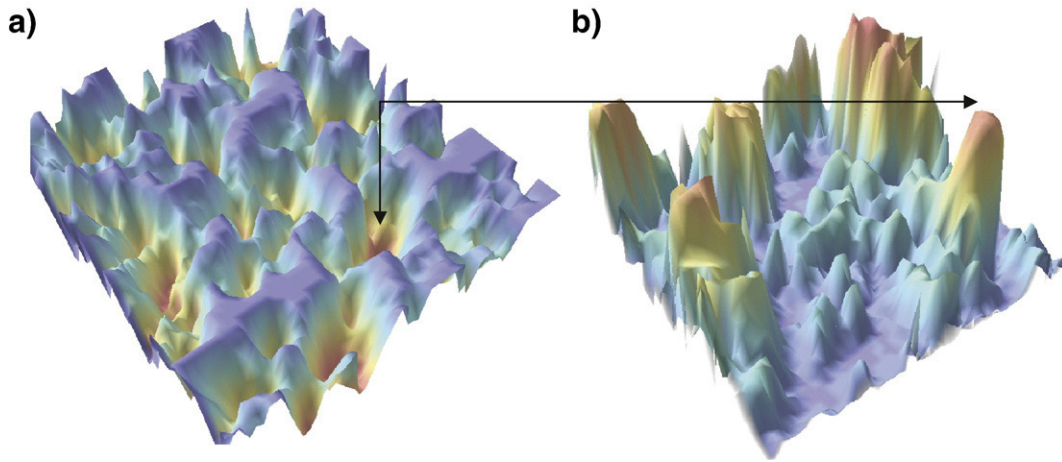


Fig. 7. Comparison of (a) HSCOI<sub>stand</sub> surface and (b) an interpolated CHM calculated for SSU 124-19 (50 m × 50 m). Both images have a spatial resolution of 1 m<sup>2</sup> and dark blue areas represent the ground surface.

structural forms (e.g., *Callitris* pine species with conical shaped crowns) but less so for others (e.g., *Eucalyptus* species with expansive crowns containing multiple high points).

### 3.3.5. Stage VII: Stem location using the HSCOI

As the different HSCOI layers extracted using different parameter combinations contained valuable information for locating stems, so the minima from both HSCOI<sub>local</sub> and HSCOI<sub>stand</sub> surfaces were combined. For example, the combination of both 1 m and 5 m kernel layers allowed smaller individuals adjacent to or beneath the canopies of larger trees to be identified and differentiated. To distinguish these stems from clumps of branches within the crowns of larger individuals, two criteria were used:

- a) Distance from the 5 m kernel minima (main stem) to the 1 m kernel minima (potential branch clump). This criterion was used to determine if the distance of the potential branch clump was within the expected crown area of the main stem. The main stem height was extracted from the CHM<sub>local</sub>, and the crown area was estimated using a function derived from a random selection of field data ( $n=994$ ) where:

$$\text{Crown Area} = 0.6038 * \exp^{0.2458 * \text{height}} \quad (3)$$

Using a validation dataset, the function produced a strong correspondence ( $r^2$  0.70, RMSE=16.2 m<sup>2</sup>,  $n=249$ ) with a slope and intercept of the best-fit line being 1.66 and  $-1.937$  respectively. The assumption behind this criterion was that stems occurring within the expected crown area of the larger stem should be branches rather than sub-canopy stems. Given the slope of the best-fit line, some bias is evident in that the area of the field-measured crowns appears to be around 1.5 times that estimated from LiDAR-derived height. This is likely to be a consequence of natural variation in tree form and the simplified method used to estimate crown area in the field. Although there is uncertainty in the both the field and LiDAR-derived estimates of crown areas, at this

intermediate stage of the processing stream, the relationship is acceptable. However, the function could be refined using data specific to species and the physical environment (e.g., soil type).

- b) A threshold of the HSCOI<sub>stand</sub>, which allowed differentiation of sub-canopy stems from branches of trees with larger stems. If the HSCOI<sub>stand</sub> value was below the threshold, then the minima were associated with a clump of branches and leaves in the upper parts of the crown, otherwise a sub-canopy stem was assumed for values above the threshold. The HSCOI<sub>stand</sub> threshold (HSCOI<sub>stand\_t</sub>), which was determined through analysis of the four calibration plots, was calculated such that:

$$\text{HSCOI}_{\text{stand}_t} = 19.5 * \text{Log}(\text{mt\_HSCOI}_{\text{stand}}) - 11.4 \quad (4)$$

where mt\_HSCOI<sub>stand</sub> represents the HSCOI value of the main stem in the cluster, with HSCOI<sub>stand</sub> values assigned when minima are generated. This threshold was applied because the HSCOI<sub>stand</sub> value is scaled with reference to the tallest tree in the plot, so minima that have HSCOI<sub>stand</sub> values similar to the taller trees are more likely to be branches of these trees.

If the selected stem occurred within the expected crown area of the main stem and the HSCOI<sub>stand</sub> value was less than the HSCOI<sub>stand</sub> threshold, there was greater confidence that the minima represented a branch of the larger tree and was coded accordingly. Otherwise, the minima were considered to be sub-canopy trees (i.e., beneath the overstorey crown) and were retained as such in the final stem map. On this basis, the locations of stems across the PSUs were mapped from the HSCOI minima.

### 3.3.6. Stage VIII: Crown/cluster area and cover

Crown cover is used commonly, often in combination with height, to establish whether a stand of trees can be classified as a forest. As the HSCOI relates to crown openness, this index can be used to delineate crowns or clusters (where clusters are

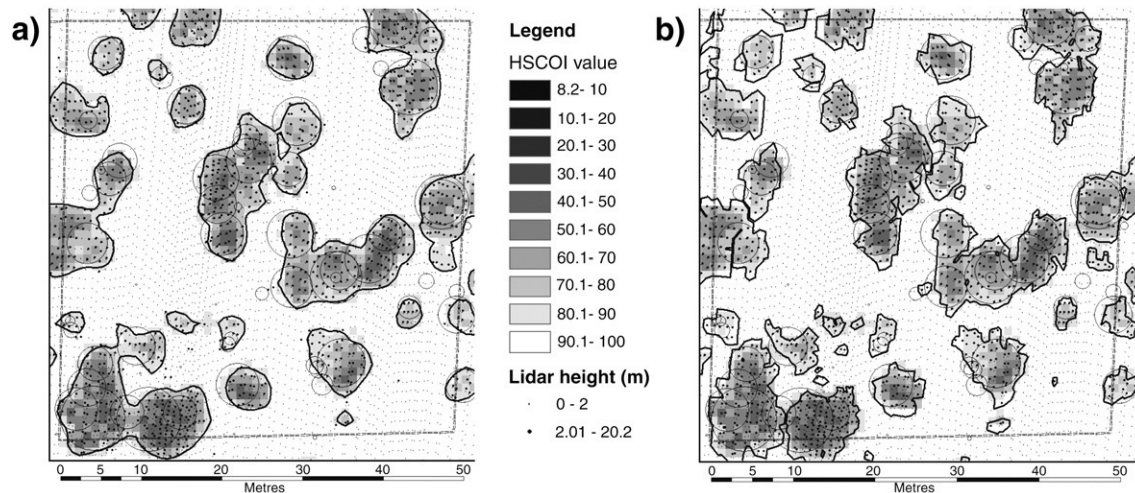


Fig. 8. (a) Crown cluster delineation PSU 142-13, based on the 69% contour (thick black line) from the underlying  $HSCOI_{stand}$  grid, and the distribution of LiDAR returns  $>2$  m in height. Note that 90% of the LiDAR returns are encompassed by the contour. (b) TIN canopy height model 2 m contour for the same plot.

defined as a group of trees with interlocking crowns and/or occurring within the sub-canopy of larger crowns) and hence forest stands. However, when determining the crown edge boundary, and hence a crown/non-crown mask, a number of issues should be considered.

1. As the  $HSCOI_{stand}$  relates to canopy density, and since the layers have been spatially smoothed, an objective threshold is difficult to define as there is no clear indication where the crown boundary may be. Instead, break-lines or density contours may be determined where HSCOI values seem to reach a plateau in the density surface. These, in turn, could equate to the actual maximum crown edge.
2. The edge of the crown is unlikely to be as clearly defined as in high-resolution optical imagery but contours of the  $HSCOI_{stand}$  may well indicate the crown edge. The issue then becomes that of extracting the most appropriate density contour.
3. The original point height data rather than the rasterised  $HSCOI_{stand}$  surface are likely to provide a more realistic representation of where actual crowns occur, although the post-spacing of the LiDAR will determine how well the crowns are discerned.
4. Validation of the best procedure is difficult as field measurements of crown extent often only provide a very basic representation, particularly where crowns are highly variable and irregular in shape.

On this basis, the following method was applied to identify the edges of crowns and subsequently calculate crown cover and the forested area. Contours of  $HSCOI_{stand}$  openness were generated at 1 m intervals and were intersected with the original LiDAR point data. An iterative process was then used to obtain the  $HSCOI_{stand}$  contour that contained at least 90% of the original LiDAR returns  $\geq 2$  m in height. Depending upon the structure of the forests, the contour of the  $HSCOI_{stand}$  providing the optimal crown edge delineation varied from 65 to 90% for the 12 PSUs investigated. For example, the optimal crown edge

contour for PSU 142 was 69% (Figs. 8a and 10). The optimal contour was selected according to the user-defined percentage of returns required. In this study, the 90% value used was considered indicative of the planimetric crown area because higher percentage values resulted in the overestimation of crown area as a consequence of a greatly expanded contour. As the  $HSCOI_{stand}$  contour value represents the maximum crown delineation, so values of  $HSCOI_{stand}$  less than the contour value were considered part of the crown. The count of  $1 \text{ m}^2$  cells with these values was then summed for a defined area (stand/plot/PSU) and expressed as a percentage of the total number of cells to estimate crown cover.

Crown cover estimates were also generated independently using the  $CHM_{local}$  by spatially interpolating LiDAR returns  $\geq 2$  m height and representing these using a Triangular Irregular Network (TIN). The TIN surface was rasterised subsequently to generate a top of canopy surface at  $1 \text{ m}^2$  cell spatial resolution. A 2 m height contour was then extracted from the surface to represent the planimetric crown area (Fig. 8b), as this height threshold conformed to definitions of forest cover (BRS, 2003b). Crown cover, expressed as a percentage, was then calculated as the sum of all cells  $\geq 2$  m height divided by the count of all cells. Crown cover estimates from both the  $HSCOI_{stand}$  and  $CHM_{local}$  analyses were compared against each other, and to field estimates.

### 3.3.7. Stage IX. Calculation of stem H and plot scale attributes

As the forests are structurally complex, several stages were required to attribute mapped stems, including those in the understorey, with an estimate of H. These focused on first deriving H for relatively simple forest structures using the CHM. The attribution approach was then evaluated through investigation, implementation and validation of more advanced procedures where complex forest structures were observed (e.g., when many sub-canopy stems occurred). These more advanced approaches involved, in part, the development of empirical relationships between the HSCOI and H with these varying with environmental and forest structural categories.

Table 3  
Functions used to estimate stem *H* from the HSCOI as a function of environment (soils and land management)

Max height (m)	Function criteria	No. crown-clusters used in function	<i>r</i> <sup>2</sup>	Function equation <sup>a</sup>
<16	Heavy clays in heavily grazed environments	267	0.91	$y = -0.153x + 16.764$
16–20.4	Duplex clays in partially grazed environments	1035	0.79	$y = -0.1842x + 21.39$
20.5–25.4	Clay loam to sandy loam in partially grazed environments	8412	0.83	$y = -0.0003x^3 + 0.0031x^2 - 0.2956x + 25.264$
>25.4	Sandy loam to sand in partially grazed or logged environments	8463	0.82	$y = -0.00004x^3 + 0.0052x^2 - 0.4455x + 31.453$

<sup>a</sup> *y*=tree height, *x*=HSCOI value at stem location.

A consistent and accurate derivation of stem *H* was required to attribute mapped stems with a size parameter that could then be used directly or indirectly (e.g., through a relationship with *D*<sub>130</sub>) as input to allometric equations for biomass estimation. The retrieval of *H* class distributions was also considered beneficial for assessing growth or successional stage and

regenerative capacity. When using LiDAR data, the *H* of the dominant overstorey trees can generally be retrieved using the CHM, but sub-canopy stem *H* is more difficult to obtain because only the upper canopy returns are used in the derivation of the CHM (Hyypya et al., 2001). The HSCOI was therefore of greater utility for retrieving sub-canopy stem *H*, as the

Table 4  
Criteria description for final stem height allocation

Criterion	Criteria conditions		Criteria result	
	Crown/cluster area (m <sup>2</sup> )	Main stem height (m)	Final height=HSCOI height	Final height=CHM height
1	<100	<20	(HSCOI <sub>ht</sub> <sup>1</sup> < (CHM <sub>ht</sub> <sup>2</sup> - 20%))	(HSCOI <sub>ht</sub> ≥ (CHM <sub>ht</sub> - 20%))
2	30–100	≥20	Where $\left( \text{Crown\_Expected}^3 = \left( \sum_{n=1}^{n\_stems} \text{stem\_crown\_area} \right) \times 1.33 \right)$ and If (Crown_Expected > Crown_Actual <sup>4</sup> ) then (Crown_Threshold = 2) else (Crown_Threshold = 1) then, where (HSCOI <sub>ht</sub> < (CHM <sub>ht</sub> - 20%))	(HSCOI <sub>ht</sub> ≥ (CHM <sub>ht</sub> - 20%)) then Final <sub>ht</sub> <sup>5</sup> = $\frac{\text{HSCOI}_{ht}}{\text{Crown\_Threshold}}$
3	>100	≥20	HSCOI <sub>ht</sub> < (CHM <sub>ht</sub> - 20%) then Final <sub>ht</sub> = $\frac{\text{HSCOI}_{ht}}{3}$	HSCOI <sub>ht</sub> ≥ (CHM <sub>ht</sub> - 20%) then Final <sub>ht</sub> = $\frac{\text{CHM}_{ht}}{3}$

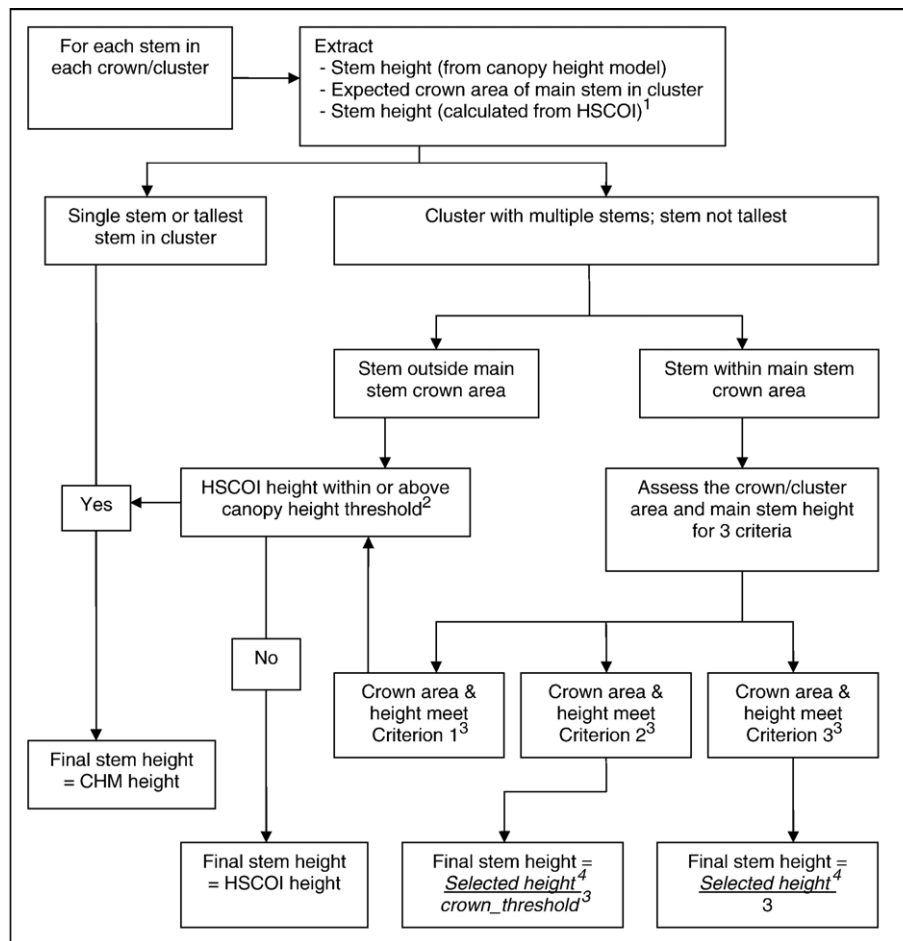
<sup>1</sup>HSCOI<sub>ht</sub>=stem height as calculated from HSCOI value, as described in Table 3 (m); <sup>2</sup>CHM<sub>ht</sub>=stem height as derived from canopy height model (CHM, m); <sup>3</sup>Crown\_Expected=expected crown area (sum of estimated crown area (stem\_crown\_area) for all stems (n\_stems) in cluster multiplied by scale factor) (m<sup>2</sup>); <sup>4</sup>Crown\_Actual=crown or cluster actual area (m<sup>2</sup>), as mapped from the HSCOI contour; <sup>5</sup>Final<sub>ht</sub>=final height allocated to stem (m).

distribution of LiDAR returns within the vertical profile was considered and minima with higher values indicated a greater number of returns from the sub-canopy. Sub-canopy stem  $H$  was subsequently retrieved based on relationships between the HSCOI and field-measured stem height. A limitation of this approach was that the  $HSCOI_{stand}$  values were dependent upon the top height of the forest stand under consideration. These stands varied primarily as a function of environmental conditions, such as soils and land management/disturbance history. For this reason, different relationships between the HSCOI and height were established for four observed height ranges ( $\sim 5$  m intervals) that could be associated with four broad environmental regimes (Table 3).  $HSCOI_{stand}$ -derived  $H$  was then cross-checked against CHM-derived  $H$  and where the estimates differed by  $>20\%$ , stems were attributed with the  $HSCOI_{stand}$ -derived  $H$  on the assumption of an overestimate by the CHM.

Based on analysis of the field data from the four calibration plots, additional refinement of the estimated  $H$  was undertaken, using a range of criteria and functions to specifically account for observed variations in stem height and crown/cluster area

combinations. The variations were considered to partly reflect the internal dynamics of the forest (Table 4; summarised in Fig. 9). For example, where trees were taller and supported a larger crown then a greater height suppression of sub-canopy stems was commonly observed (Florence, 1996). In these instances, the CHM height for sub-canopy stems was found to be too large. Therefore, specific criteria (e.g. 2 and 3) were utilised to reduce sub-canopy stem height according to the likely suppression effect, such that a main stem with a taller overstorey stem  $H$  and large crown resulted in a greater height reduction for associated sub-canopy stems.

At the stand level, structural descriptors retrieved were stem density, predominant stem  $H$  and canopy predominant  $H$ . Stem density (within the area of the field plots) was estimated by simply counting stems, both field and those mapped from the HSCOI. Field and HSCOI predominant stem  $H$  were calculated as the mean of the maximum  $H$  of the tallest 13 stems in the plot area. Canopy predominant  $H$  was calculated as the mean of the maximum LiDAR height for  $10 \times 10$  m ( $100 \text{ m}^2$ ) cells (25 per plot). From the field data, 99% of trees with  $D_{130} \geq 10$  cm supported a crown area  $\leq 100 \text{ m}^2$  and hence few trees would



<sup>1</sup>See Table 3

<sup>2</sup>Canopy height threshold defined as height from canopy height model  $\pm 20\%$ .

<sup>3</sup>See Table 4

<sup>4</sup>"Selected height" refers to height from either the HSCOI or canopy height model as per Table 4.

Fig. 9. Flowchart of steps for final stem height allocation.

Table 5  
Summary of correspondence between forest attributes measured in the field and estimated using LiDAR data for Queensland and NE Victorian sites

y (Field)	x (LiDAR)	$r^2$	RMSE <sup>a</sup>	$N^b$	Function	Ref. <sup>c</sup>
<i>Tree level comparisons</i>						
H	H (CHM)	0.42	3.19 m	119	$y=0.587x+3.63$	1
H	H (HSCOI/CHM)	0.71	2.25 m	119	$y=0.824x+1.82$	2
H	H (CHM) <sup>d</sup>	0.79	1.91 m	110	$y=0.939x+0.27$	3
H	H (HSCOI/CHM) <sup>d</sup>	0.81	1.85 m	115	$y=0.880x+0.99$	4
<i>Plot level comparisons</i>						
Stem count	Stem count (HSCOI)	0.82	133 stems ha <sup>-1</sup>	30	$y=1.539x-142.63$	5
Stem pred. H <sup>e</sup>	Stem pred. H (HSCOI)	0.91	0.77 m	30	$y=0.898x+1.28$	6
Stem pred. H	Stem pred. H (CHM)	0.81	1.11 m	30	$y=0.720x+3.86$	7
Stem pred. H	Canopy pred. H (HSCOI)	0.86	0.94 m	30	$y=0.891x+3.34$	8
CC	CC (HSCOI)	0.78	9.25%	30	$y=1.038x-0.58$	9
CC	CC (CHM)	0.81	8.58%	30	$y=0.972x-7.59$	10
FBPC	CC (HSCOI)	0.89	5.49%	30	$y=0.910x-2.03$	11
NE Victoria stem count	Stem count (HSCOI)	0.19	152 stems ha <sup>-1</sup>	22	$y=0.513x+73.55$	12

<sup>a</sup> Root Mean Square Error.

<sup>b</sup> Number of observations.

<sup>c</sup> Correspondence reference number as listed in text.

<sup>d</sup> Outliers excluded.

<sup>e</sup> Predominant stem height.

have crowns extending beyond this area, though some crowns might be split between cells. Canopy predominant  $H$  was derived to investigate its use as a rapid initial assessment or surrogate for stem predominant  $H$ , as this would not require more complex individual stem mapping and  $H$  attribution.

#### 4. Results

The following sections provide an evaluation of the success in retrieving forest structural attributes in the Injune forests. Evaluation covers tree level location and  $H$ , plot level stem density, canopy cover and predominant height, and the spatial arrangement of stems based on Ripley's  $L$ -function nearest neighbour analysis. Further validation is provided for a range of forest types within northeast Victoria, a proportion of which were structurally similar to those observed at Injune. All comparisons were based on the correspondence with field-based observations, and are summarised and cross referenced in Table 5.

##### 4.1. Stem density per plot, tree location, and spatial arrangement of stems

Maps of stem locations, together with crown boundaries, were generated using HSCOI layers for each of 12 PSUs (see example in Fig. 10). Stem density estimates from 30 plots contained within the 12 PSUs (Tickle et al., 2006) were compared with those generated using the HSCOI for the equivalent area and a close correspondence was observed across the stem density range (Table 5, Ref. 5, Fig. 11). However, for densities  $> \sim 700$  stems ha<sup>-1</sup>, a larger number of field stems with  $D_{130} < 10$  cm were not identified using the HSCOI. This was attributed to the 1 m spatial resolution being too coarse to resolve all stems in higher density clusters, and also to frequent overtopping by larger individuals.

To evaluate the success of tree location, one field plot from each of the 12 PSUs was selected, with the addition of all four field plots associated with PSU 142, as these had been assessed

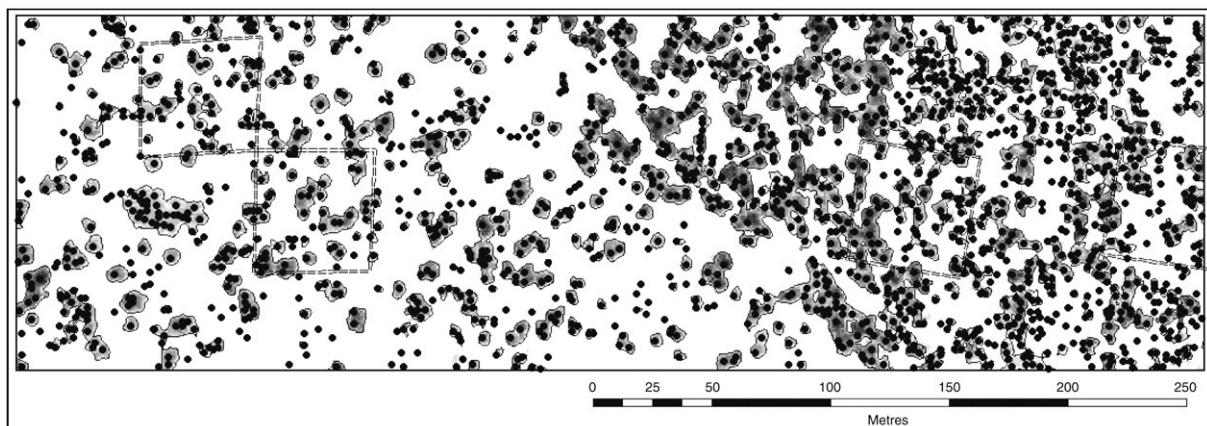


Fig. 10. Crown/clusters and stem locations identified using the HSCOI surface generated for PSU 142. Darker areas in the HSCOI<sub>stand</sub> surface indicate crowns that are taller and contain a greater density of canopy elements. Internal squares are SSU field plot locations numbered (from left to right) as 02, 13, 18 and 20.



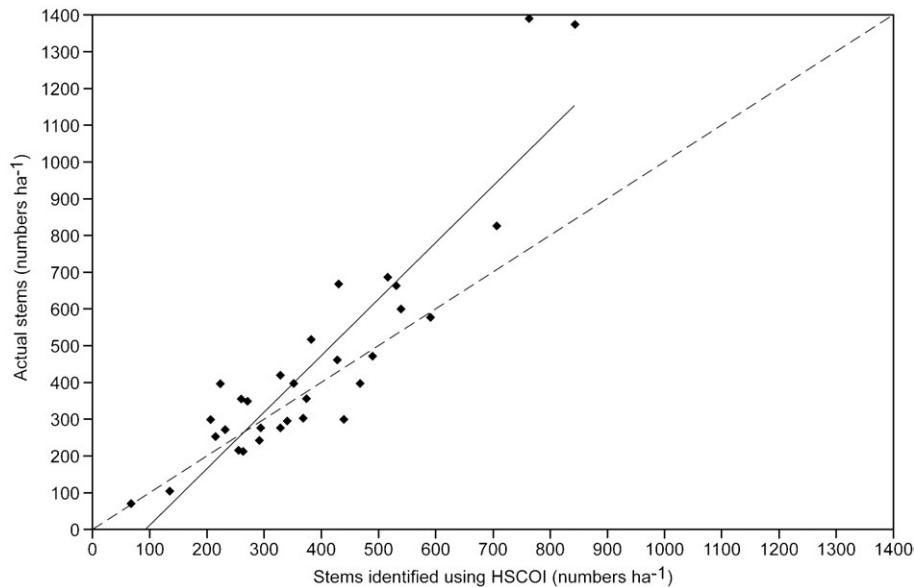


Fig. 11. Correspondence between field stem counts and HSCOI stem count for 30 field plots across a diverse range of forest structural types.

previously for another study (Lucas et al., 2006b). HSCOI mapped trees were matched manually to those identified in the field, with the process considering similarities primarily in location, but also height,  $D_{130}$  and estimated crown area. The validation set contained 50.2% ( $n=1772$ ) of all field trees (with  $D_{130}>5$  cm) measured across the 12 PSUs, and 1226 trees mapped using the HSCOI. As a number of the trees measured in the field supported more than one stem, a total of 1892 individual stems were considered. Validation using all stems within all plots was not undertaken because most of the forest structural formations occurring within the study area were represented by the sample. The commission and omission analysis results are presented in Table 6.

On average across the validation plots ( $n=12$ ), 73% of stems ( $\delta=12.1\%$ ; range 50.8–90.6%) identified using the HSCOI were matched correctly with a stem identified in the field, although this reduced to 70% when multiple stems were considered. Accuracies were greatest (over 90%) when stems were fewer and crowns were larger, more mature and separated from each other. Accuracies lowered to around 50% where the density of stems was higher and where many occurred as understorey trees. Across the plots, a mean of 12% ( $\delta=8.8\%$ ; range 0–27%) of stems identified using the HSCOI were not matched to those identified in the field. This was attributed to incorrect assignment of branch clusters to stems or to shrubs of a smaller size that they were not mapped in the field.

To assess the importance of identifying trees within the smaller size classes, the number of stems within the 5–10 cm  $D_{130}$  range as a proportion of the total (within all 30 field plots) was determined. This size class range comprised a mean of 38.5% ( $\delta=17.8\%$ ; range=0–85%) of all stems ( $D_{130}\geq 5$  cm) across the 30 plots, but only a mean of 8.1% ( $\delta=8.1\%$ ; range=0–39.8%) of the plot basal area. A mean of 28% of stems ( $D_{130}\geq 5$  cm) were overtopped by taller individuals ( $\delta=12\%$ ; range 9–66%) and these constituted a mean of 17% ( $\delta=8\%$ ; range=5–48%) of the plot basal area. These proportions were therefore considered

indicative of the proportion omitted if a CHM alone was used to quantify stem density, and explained some of the error observed with plots containing a high density of stems.

To further assess the ability to locate trees using the HSCOI, second order statistics that described the small-scale spatial correlation structure of point patterns identified from two sources (in this case, field and HSCOI stems) were considered. These include Ripley's  $K$  or  $L$  and the pair-correlation (typically referred to as  $g$ ) functions. Each can describe the characteristics of the point pattern over a range of distance scales, thereby allowing detection of patterns relating to dispersion and aggregation (Wiegand & Moloney, 2004). In this analysis, the bivariate nearest neighbour (NN) distance, which is a component of the Ripley's  $L$ -function, was used to assess the similarities between mapped stem patterns from the HSCOI and field data. The analysis was conducted within Programita (Wiegand et al., 2006) using the 30 Injune plots, with an open circles model and a 0.2 m cell size. All cells within the area were included and, to convey the assumption of a homogeneous pattern, the test model was set to null. For each of the field-mapped stem distributions (pattern 1), the nearest HSCOI mapped stem was identified (pattern 2). A cumulative NN distance distribution was calculated and normalised by the number of stems mapped in the field. The output was the proportion of field stems that were within an NN distance ( $d$ ) of a HSCOI mapped stem. The larger the proportion at smaller distances, the better the spatial arrangement match between the two stem distributions. Stems mapped in the field were considered to be 'truth' and hence the analysis focused on assessing the success in the LiDAR-based mapping. The accumulated univariate distribution of the field stem NN distribution was also calculated to establish whether the spatial scale of the field stem pattern itself might impact on the bivariate NN result.

The NN distance at an arbitrary assessment threshold of 80% accumulated distribution was chosen to represent the univariate and bivariate results for each plot. An NN distance at 80%

Table 6  
Commission and Omission table for selected SSUs within all 12 PSUs with field measurements

PSU-SSU	Field-LiDAR match	Field-LiDAR multi-stem <sup>a</sup> match	LiDAR stems no match (commission)	Field stems no match (omission)	Field multi-stems <sup>a</sup> no match	Total match tree level %	Total match stem level %	LiDAR commission % (total LiDAR)
<i>Plots used for calibration</i>								
81-11	64	3	24	5	2	92.8	94.4	26.4
81-16	89	2	15	26	21	77.4	66.9	14.2
111-18	127	1	12	57	0	69.0	69.6	8.6
124-19	78	0	5	53	0	59.5	59.5	6.0
Mean	90	2	14	35	7	74.7	72.6	13.8
<i>Plots used for validation</i>								
131-18	29	0	5	3	1	90.6	87.9	14.7
58-29	72	0	22	9	0	88.9	88.9	23.4
114-12	61	1	13	10	1	85.9	86.1	17.3
142-18	49	0	18	13	5	79.0	73.1	26.9
142-13	50	1	3	17	7	74.6	68.9	5.6
83-20	72	0	9	26	4	73.5	70.6	11.1
138-16	118	5	8	48	5	71.1	71.9	6.1
144-19	57	0	5	24	10	70.4	62.6	8.1
142-02	52	2	1	24	16	68.4	58.7	1.8
142-20	57	0	14	33	11	63.3	56.4	19.7
23-20	55	1	2	40	4	57.9	56.6	3.4
148-01	180	0	0	174	17	50.8	48.5	0.0
Mean	71	1	8	35	7	72.9	69.2	11.5
All plots total	1210	16	156	562	104			
All plots mean	76	1	10	35	7	73.33	70.04	12.08

This validation sample accounts for 50% of all field-measured stems at the Queensland study site.

<sup>a</sup> Multiple stems are mapped where split occurs below 1.3 m in height, and all extra stems are mapped at same XY location as main stem. Field stem counts include dead stems without foliage and crowns which are difficult to map using LiDAR data.

cumulative distribution indicated that at least 80% of field stems were associated with a LiDAR-mapped stem NN separated by up to distance  $d$ . The mean NN value across all plots was then

calculated for both based on univariate and bivariate analyses. The mean NN distance for the bivariate analysis was 2.6 m ( $\delta=0.6$  m, range 1.9–4.2 m,  $n=30$ ) whereas the univariate mean

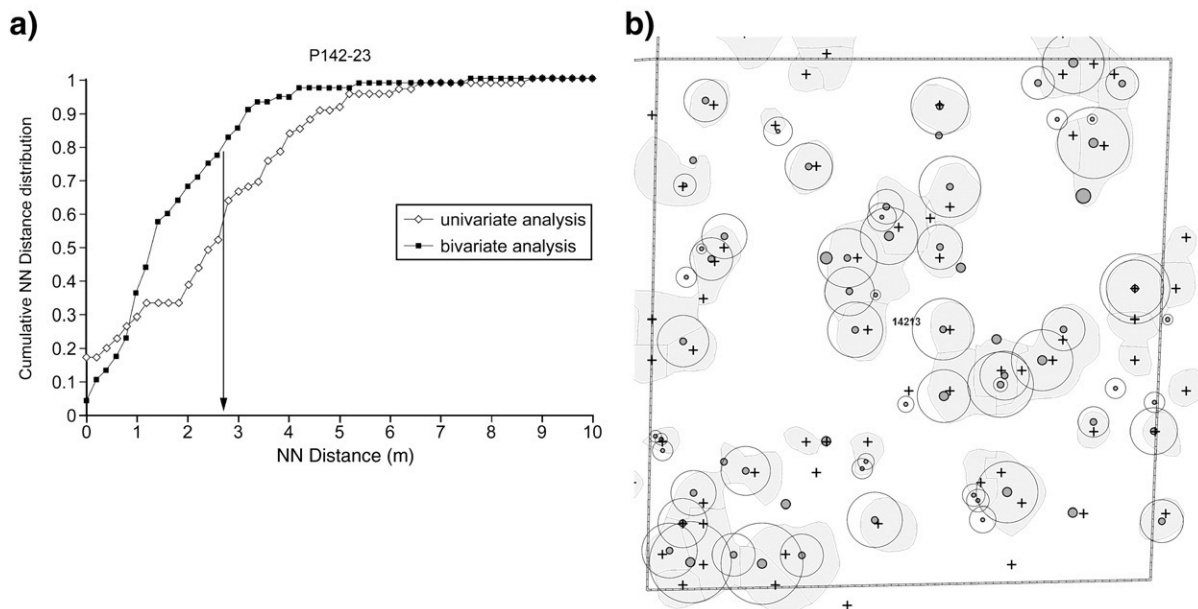


Fig. 12. Example of Ripley's  $L$  univariate and bivariate NN analyses for SSU 142-13, with the associated stem maps generated from field data and the HSCOI. Filled circles represent field stem locations, with the size proportional to  $D_{130}$ . Open circles are proportional to crown radius. Crosses represent HSCOI stems. The field stem density is 252 stems  $ha^{-1}$ .

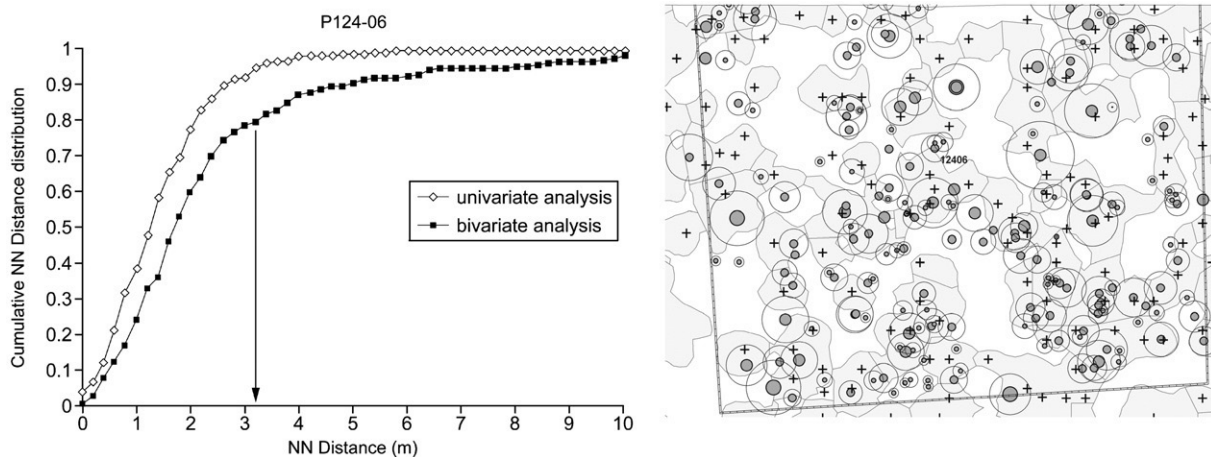


Fig. 13. Example of Ripley's  $L$  univariate and bivariate NN analyses for SSU 124-06, with the associated stem maps generated from field data and the HSCOI. Filled circles represent field stem locations, with the size proportional to  $D_{130}$ . Open circles are proportional to crown radius. Crosses represent HSCOI stems. The field stem density is  $668 \text{ stems ha}^{-1}$ .

NN distance was greater at 3.2 m ( $\delta=1.1 \text{ m}$ , range 1.3–5.8 m,  $n=30$ ). A paired Student's  $t$ -Test generated a  $P$  of 0.001 which indicated a significant difference between the univariate and bivariate NN distances for the 30 plots. This illustrated that the stems mapped using the HSCOI were closer to those mapped in the field than were the field-mapped stems to each other. For 25 of the 30 field plots, the univariate spatial scale did not impact on the bivariate result. An example is shown in Fig. 12, where the bivariate NN and univariate NN distances were 2.7 m and 3.9 m at 80% cumulative distribution respectively. While there is some under-estimation of stems using the HSCOI in Fig. 12 (field stems=75, LiDAR stems=54), attributable largely to not identifying small and dead field stems, the general spatial pattern of larger trees and tree clusters is adequately represented by the HSCOI stem mapping. This then instilled confidence in the HSCOI as a tool for mapping stems in this forested environment.

The opposite case, where the univariate scale pattern may impact on the bivariate result, is illustrated in Fig. 13. Here, the univariate NN distance was lower with respect to the bivariate NN distance. This condition was observed in the remaining 5 of the 30 plots, all of which supported a higher density of stems. When stems with  $D_{130} < 10 \text{ cm}$  were excluded and the NN analyses repeated, the bivariate NN distance was reduced from 3.0 to 2.6 m (range 2.0–3.0 m), whereas the univariate NN distance increased from 2.1 to 3.2 m (range 2.6–4.1 m). This illustrated that the HSCOI mapping was generally successful for locating stems  $> 10 \text{ cm } D_{130}$  even in higher stem density plots.

To provide additional evidence for the HSCOI mapping accuracy, a more detailed Ripley's bivariate analysis was undertaken. Consider the bivariate quantity  $\lambda_2 K_{12}(r)$ , which is the expected number of type 2 points (HSCOI stems) within distance  $r$  of an arbitrary type 1 point (field stem). If spatial mapping errors are not too large, we may expect that a HSCOI mapped stem is always in the neighbourhood of a field-mapped stem. This will produce an attraction into the bivariate point pattern. The more accurate the HSCOI mapping, the stronger is the attraction and the smaller the range of attraction (Wiegand

et al., 2006). To test if both patterns show small-scale attraction, the  $K$ -function of the data can be contrasted to  $K$ -functions derived from Monte Carlo simulations of the null model of independence where one pattern (HSCOI stems) is shifted as a whole by a random vector and wrapped on a torus. This null model maintains the first- and second-order structures of both patterns but breaks its dependence. The theoretical expectation under independence is  $L(r)=0$ . The  $L$ -function was utilised as the test statistic, which is a square-root transformation of the  $K$ -function. The analysis used 99 Monte Carlo simulations of the null model to construct 95% confidence limits, which were the 5th lowest and highest  $L_{12}(r)$  from the Monte Carlo simulations. In order to develop an idea of the overall potential mapping accuracy across all plots, the  $L$ -function ( $r$ ) values and confidence limits were calculated for all 30 plots, and the mean value at each  $d$  generated and plotted (Fig. 14). This shows that there is a strong attraction and it is significant at scales  $r < 7 \text{ m}$ . Thus, LiDAR-mapped stems are significantly more frequent within a distance of 7 m around field-mapped stems. The mean NN distance across the 30 plots utilising 100% of stems was 6.02 m, which supports the bivariate  $L$ -function assessment of 7 m, with both these figures being close to the expected field mapping error when using GPS, tape and compass.

#### 4.2. Height attribution of trees using the HSCOI

The accuracy of stem attribution with a size estimate (e.g., H) using the HSCOI was assessed based on a validation set of 119 trees (with  $D_{130} \geq 5 \text{ cm}$ ), selected randomly from 30 field plots. Up to 4 live trees per plot were utilised, with at least one stem with  $D_{130}$  in the range 5–10 cm included (where present) within each plot to provide an indication of success in mapping and attributing sub-canopy stems. When initial selections were made, 13 of the 119 field trees (10.9%) could not be matched with HSCOI minima, with over half of these occurring in the 5–10 cm  $D_{130}$  size range. If a HSCOI stem could not be linked

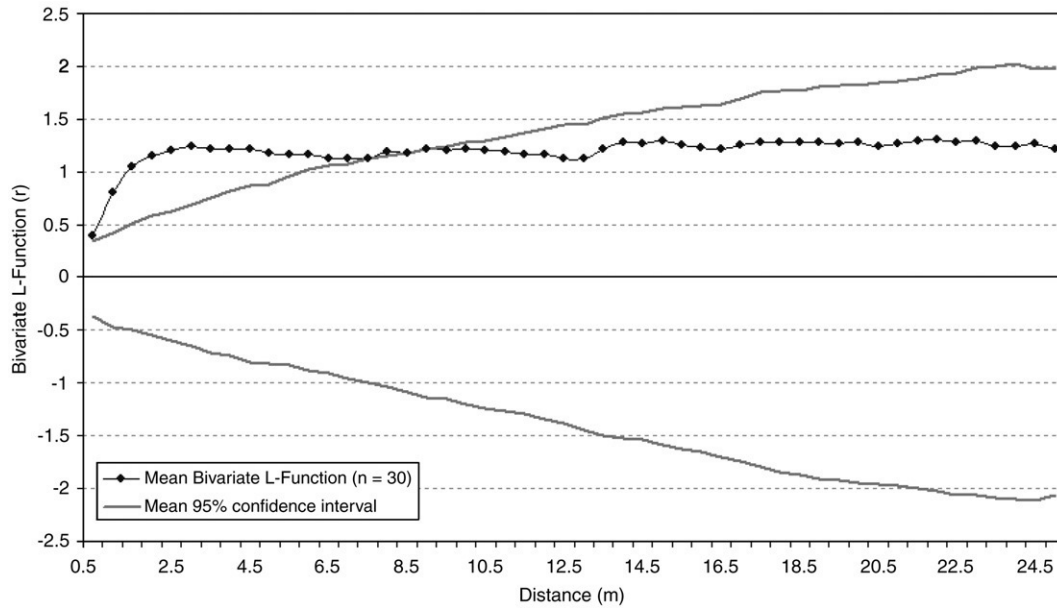


Fig. 14. Ripley's bivariate *L*-function analysis summary, illustrating the mean of spatial stem distribution (field and HSCOI derived) comparison results across 30 field plots.

initially to a field stem, then a new field stem was selected randomly to maintain 119 trees in the validation set. The mean offset distance between stems located in the field and using the HSCOI surface was 2.25 m (Gaussian distribution,  $\delta=1.46$  m; range 0.22–8 m, which was within the standard GPS error of  $\pm 5$ –10 m; Garmin, 2003).

Previous research from this study site (Tickle et al. 2006) reported a close correspondence between *H* measured in the field and from the LiDAR CHM ( $r^2=0.91$ ,  $SE=1.34$  m,  $n=100$ ). However, that analysis only considered trees that were clearly distinguished from others (i.e., occurring in the overstorey or as isolated individuals). By contrast, the 119 trees selected in this study consisted of both overstorey and sub-

canopy stems, and hence when the heights extracted from the CHM were compared initially with the field validation set, the correspondence was reduced significantly (Table 5, Ref. 1). However, the correspondence increased (Table 5, Ref. 2) when *H* was extracted from a combination of the CHM and the HSCOI (utilising methods illustrated in Fig. 9 and Table 3). Comparison with field data identified a few outliers that occurred regardless as to whether the CHM or HSCOI was used for *H* extraction. *H* was overestimated mainly where the CHM was used (Fig. 15, circled at right), but fewer underestimates occurred when the CHM and HSCOI were combined (circled at left in Fig. 15). Removal of these outliers increased the correspondence (as expected) with field *H* for both extraction

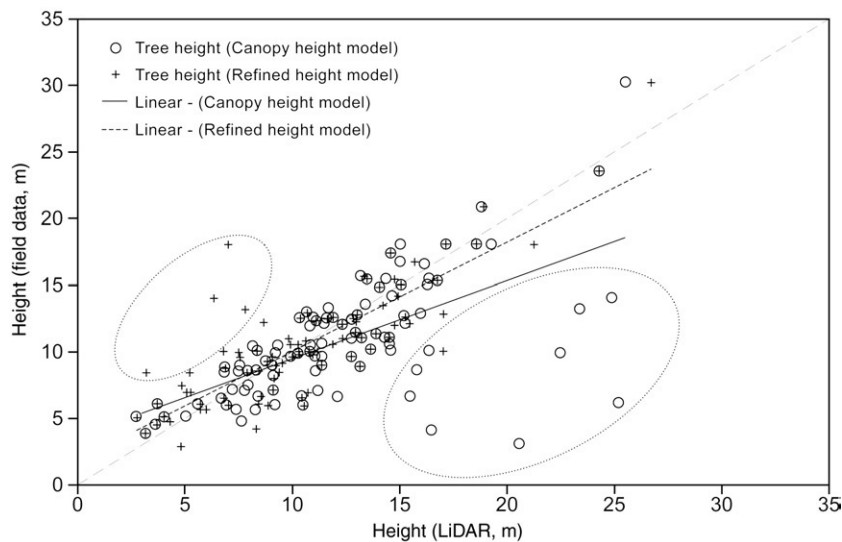


Fig. 15. Correspondence between *H* measured in the field and estimated from (a) the initial CHM, and (b) integrated CHM and HSCOI after application of height refinement methods.

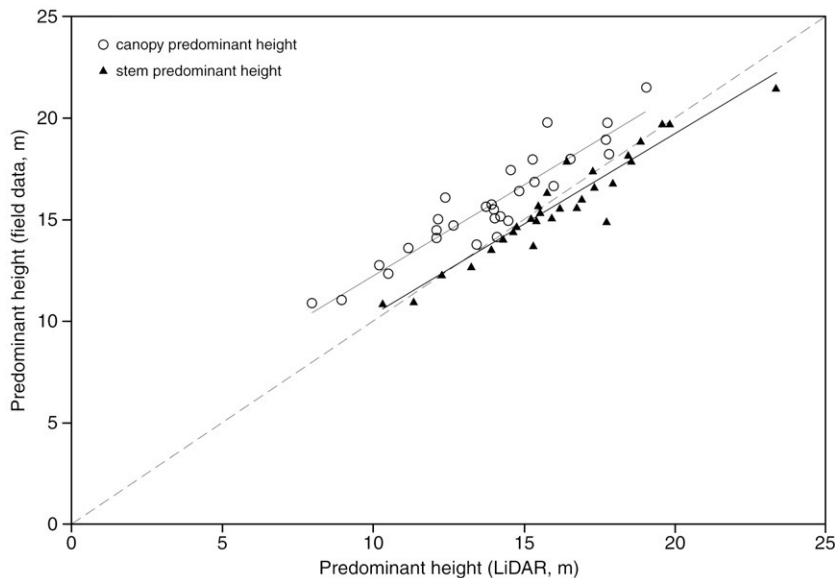


Fig. 16. The correspondence between field and LiDAR-estimated predominant height for 30 field plots, calculated using the average of a) 25  $10 \times 10$  m canopy height model cells associated with each field plot and b) the tallest 13 HSCOI-mapped stems within the 0.25 ha area.

methods (Table 5, Ref. 3 and 4), thus highlighting that improved results are achievable if further model calibration was undertaken. Errors in  $H$  extracted from the CHM model are unlikely to be correctable because sub-canopy stems are not observed. However, with further calibration, the HSCOI is expected to provide better estimation of sub-canopy height as this index can be adapted for different forest environments and crown configurations.

Some variability in  $H$  retrieval at a tree level was evident and expected given the irregular crown shapes of the many trees, particularly those associated with *Eucalyptus* and *Angophora* species. When stem predominant  $H$  derived from the HSCOI was compared to the field estimate (Fig. 16), a very close (almost 1:1) correspondence was observed (Table 5; Ref. 6). However, when derived from the CHM, the correspondence with field data was reduced (Table 5; Ref. 7). Stem predominant  $H$  estimated from either a CHM alone or in combination with the HSCOI was equivalent for plots with an upper canopy height of 18 m or less. However, for plots with taller trees, the assumed overestimation of stem  $H$  for sub-canopy trees from the CHM was more evident in that the slope and intercept of the best-fit line decreased and increased respectively (Table 5). This indicated that the overestimation in stem  $H$  for sub-canopy trees lead to greater error in plot-based predominant  $H$  where taller trees occur. When canopy predominant  $H$  calculated from  $10 \times 10$  m cells was compared to field measurements (Fig. 16), the correspondence was reduced slightly (Table 5, Ref. 8) and an underestimate of approximately 2 m (on average) was observed. This was attributed to the conceptual difference between canopy and stem predominant  $H$ , as the inclusion of parts of crowns that are lower than the tallest point in the calculation reduced the overall mean height. With predominant stem  $H$ , only the height of the top of each stem was used in the calculation and the heights of other parts of the crown (i.e., the crown extent) were ignored.

#### 4.3. Projected cover

A close correspondence between measures of crown cover estimated from field measurements (for stems  $D_{130} \geq 5$  cm) and both the HSCOI surface (Table 5, Ref. 9; Fig. 17a) and the CHM (Table 5, Ref. 10; Fig. 17b) was observed. However, a closer match to the 1:1 correspondence line was observed between field and HSCOI-derived crown cover. Cover estimated from the HSCOI also exhibited a closer relationship with FBPC (Fig. 17a; Table 5; Ref. 11). The CHM method was observed to overestimate crown cover by  $\sim 10\%$ , although scatter in the relationship was similar to that observed in the relationship with HSCOI-derived crown cover.

#### 4.4. Evaluation of HSCOI in different environments

As an independent test, the HSCOI model generated using the Injune data was applied to LiDAR data acquired over three north-east Victorian ecozones, and validated against plot data for stem density only (Table 5, Ref. 12; Fig. 18). As expected, the correspondence in the stem density comparison was relatively weak overall given the structural and environmental differences outlined in Section 3.1 and Figs. 3 and 4. However, two distinct clusters of plots were identified (Fig. 18). Within seven plots (represented as squares), the number of stems counted (mean  $559 \text{ stems ha}^{-1}$ ,  $\delta = 98 \text{ stems ha}^{-1}$ , range 452–748) was within 20% of those observed in the field (differing only by 2–8 stems per plot). The density of the remaining 15 plots was consistently overestimated by more than 20% (by more than 10–39 stems per plot) using the HSCOI model, which suggested potential for refinement of the approach. The forests in these latter plots were highly variable structurally, reflecting the range of forest environments considered, and contained a lower mean density of stems ( $318 \text{ stems ha}^{-1}$ ;  $\delta = 255 \text{ stems ha}^{-1}$ , range 22–1135).

**5. Discussion**

*5.1. Conceptual linkages between HSCOI and waveform LiDAR*

The HSCOI method has sought to emulate aspects of full waveform large footprint LiDAR processing using small footprint data. Conceptual development has drawn on methods presented in the initial phases of the CVM of Lefsky et al. (1999) and Harding et al. (2001). In these studies, a 3D matrix consisting of a 5 × 5 grid of contiguous waveform footprints was used to characterise the 3D geometry of the forest canopy volume. Three main differences between the HSCOI method and the CVM were noted:

a) Using the CVM, gaps were explicitly accounted for and classified, which contrasts to the HSCOI where they are not.

The small footprint LiDAR data used to generate the HSCOI only sampled the vertical and horizontal distribution of canopy elements and can be biased, especially because the LiDAR pulse is preferentially captured by the upper layers of the canopy. Therefore, the absence of LiDAR returns at lower levels cannot be explicitly used to infer a real canopy gap. As a result, the volume calculations for the different canopy classes differ between the CVM and the HSCOI, with the latter limited to voxels that explicitly contain LiDAR returns.

b) The CVM uses 5 × 5 arrays of 10 m footprints whereas the HSCOI is calculated at a 1 m resolution across the LiDAR swath width (nominally 200–400 m). Both CVM and HSCOI share the 1 m vertical bins as part of the 3D matrix but the 1 m horizontal post-spacing of the small-footprint LiDAR allows multiple measurements of individual tree crowns, and facilitates their identification and subsequent

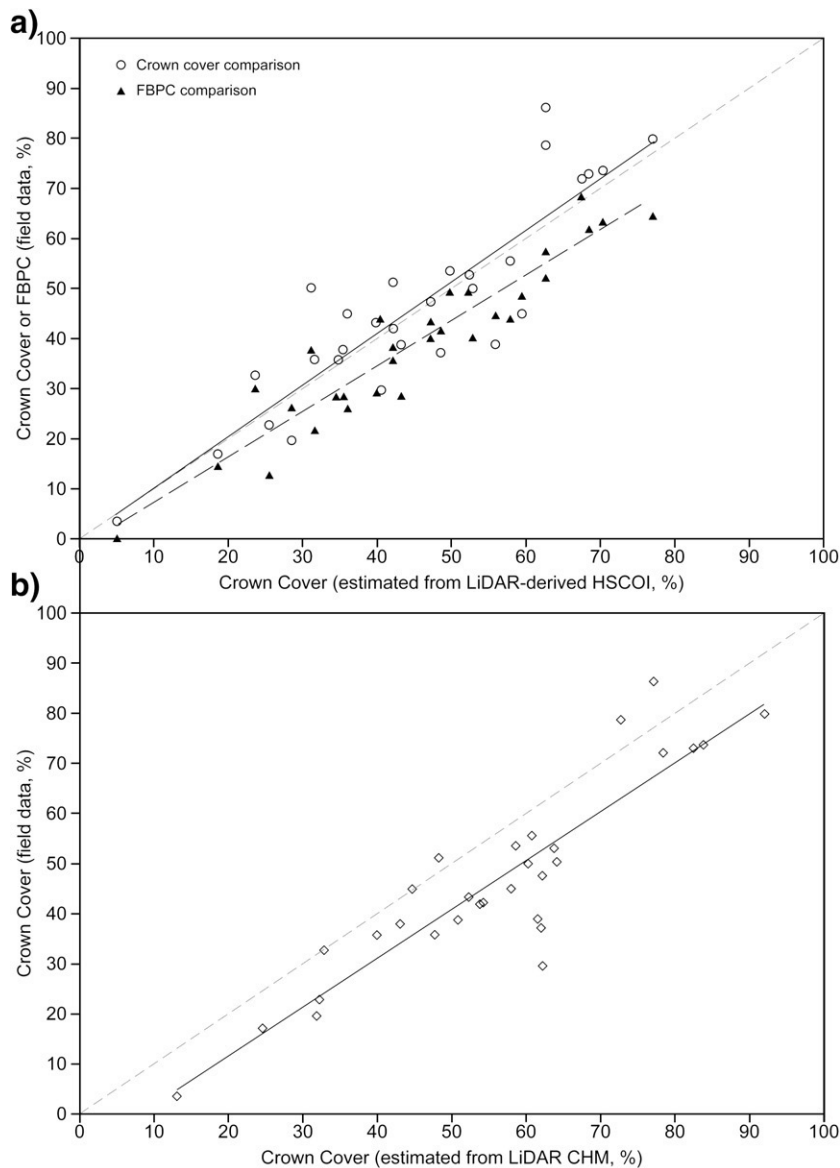


Fig. 17. The correspondence between a) LiDAR HSCOI percent of tree cells (CC %) within plot with field based estimates of CC (open circles) and FBPC (solid black triangles); and b) CC (%) estimated from the CHM and the field data.

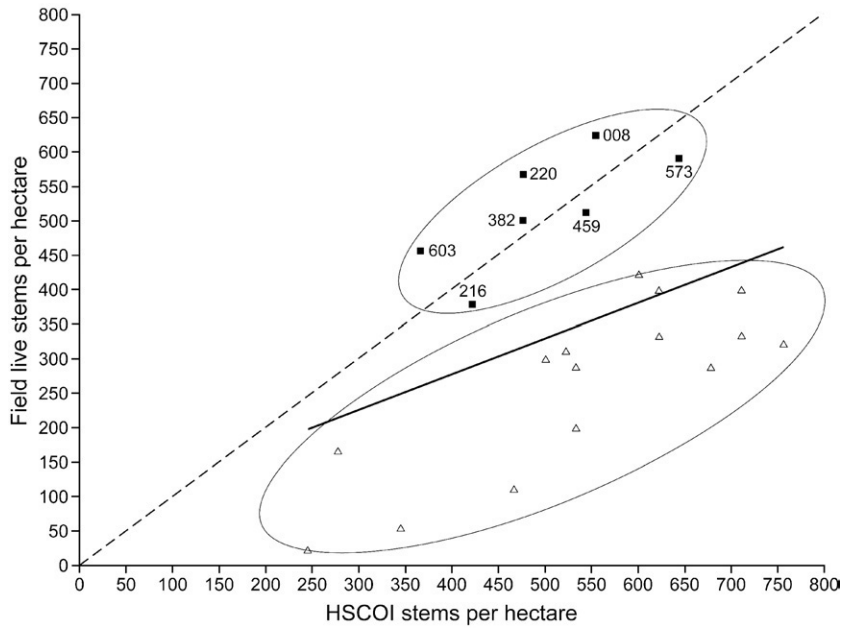


Fig. 18. Independent validation of the HSCOI application results for northeast Victorian plots.

delineation (at least those occurring in the upper canopy). To evaluate how this sampling reflects the overall structure of the forest and therefore how large footprint data might represent Injune forests, tree crowns measured in the field were reconstructed in 3D by generating an ‘artificial’ 1 m<sup>3</sup> voxel matrix in the same manner as that used in the HSCOI

calculation. This process utilised field measurements of stem location and *H*, crown area and depth, and general shape assumptions based on species and growth stage. The percentage of tree canopy voxels per 1 m height interval was then summarised to give apparent vertical profiles, which were then compared to equivalent plot level profiles

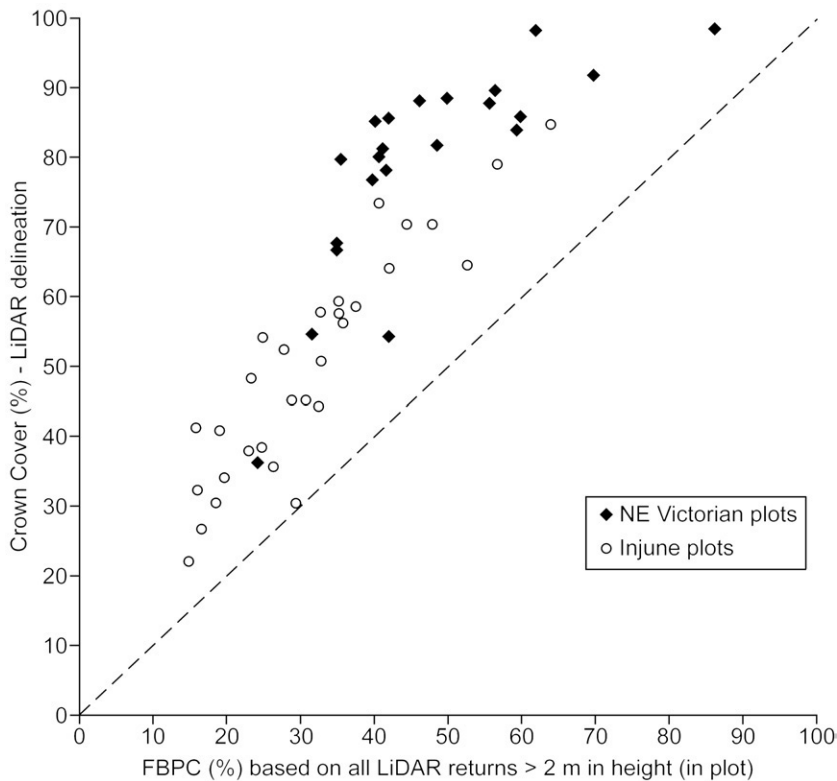


Fig. 19. Comparison of LiDAR-derived plot crown cover (CC) and Foliage Branch Projective Cover (FBPC) for Queensland and northeast Victorian plots.

generated from the LiDAR return data. This comparison suggested a close correspondence in profile shape (for an example figure, see Lee et al., 2004) within the limits of the spatial modelling scale. Acceptable sampling of the vertical canopy profile, particularly for more open canopies, was therefore assumed. Some studies (e.g., Harding et al., 2001; Lovell et al., 2003) have identified potential biases in apparent vertical profiles generated from discrete return data. The approach adopted here suggests that such biases are less evident, though still present, in the more open forests of this structure and form observed at the study site.

- c) The forest canopies found at the study site are likely to differ greatly from those used to initially interpret the full waveform data and methods. In particular, Harding et al. (2001) indicated that open woodlands and stands containing cone-shaped crowns strongly depart from the assumptions of uniformity in terms of random horizontal organisation (no clumping) and the height of the canopy outer surface within the LiDAR footprint. In addition, large footprint canopy height profile bias associated with error in the ground reflectance scaling factor increases with decreasing canopy closure because of greater error introduced in the transformation weighting function (Aber, 1978; MacArthur & Horn, 1969). An error in the scaling factor causes an error in closure that is larger, in an absolute sense, for open canopies compared to canopies with high closure (Harding et al., 2001). As the canopies found at the study site are generally very open, then many of the large footprint processing assumptions relating to canopy uniformity are likely to be violated. The HSCOI has therefore been developed to address differing processing requirements.

### 5.2. Impact of trees that are large crowned, or small, or dead

While senescent and dead trees may have little or no foliage for the LiDAR beam to interact with, returns from the branches (if present) and stem are sufficient to create minima in the HSCOI surface at the location of the stem, particularly where these are isolated from other crowns. However, senescent or dead trees are less able to be located if they occur within clusters or underneath leafy canopies. As an example, only 44% (25/57) of dead trees from four field plots (located within PSU 142; Fig. 10) were located correctly. Improving the identification and attribution of these stems would most likely require LiDAR at higher sampling densities.

Stems with  $D_{130} \leq 10$  cm are also more difficult to map from the HSCOI, particularly as many support a small crown area (often less than 1–2 m<sup>2</sup>), occur in stands of high density (several per m<sup>2</sup>) and/or are often located beneath the canopy of larger trees. In these cases, the HSCOI surface generated at 1 m spatial resolution may be limited in detecting small stems. For example, only 33% (47/144) and 26% of stems with  $D_{130} \leq 10$  cm and  $D_{130} \leq 5$  cm respectively were identified within the four field plots within PSU 142 (Fig. 10). As with senescent stems, the use of finer spatial resolution LiDAR data (e.g.  $\leq 30$  cm post-spacing) for HSCOI calculation would lead to refinements in mapping and attribution of stems occurring in this size range.

Using individual crown delineations combined with apparent vertical profiles to classify crowns into decurrent & excurrent forms (Lucas et al., 2004) could also reduce the negative influence of the large spreading crowns of overstorey trees on the sub-canopy stem  $H$  retrieval. This would allow a more targeted application of crown area/ $H$  functions for stem attribution, especially where sub-canopy stems occur within clusters. Variation in the correspondence between crown cover estimated from the field data and the HSCOI was observed and was most likely a result of inadequate representation by field measurements (in the north–south and east–west directions) of the irregularly shaped crowns of trees of the decurrent form. A greater correspondence would be expected if field measurements were taken along the longest and shortest axes, although this requires measurement of the angle of the longest axes from north. Even so, the estimates of crown cover based on the HSCOI were regarded as representative of the forests considered.

### 5.3. Northeast Victorian HSCOI validation

Two main issues were identified when applying the Injune-calibrated HSCOI model to forests in north-east Victoria. First, most of the plots were outside the calibration range, as identified previously (Fig. 4), in terms of predominant height, crown cover, crown area and foliage density, and the number of strata. Factors such as elevation, soils and rainfall, which influence tree and stand form/structure, also differed. Second, stems in the 5–10 cm  $D_{130}$  range were not mapped in Victoria. As the Injune HSCOI had been calibrated to allow small stems to be identified, an overestimate in the number of stems mapped by the HSCOI was observed in Victoria (Fig. 18). The three plots that were successfully modelled (labelled in Fig. 18 and Fig. 4 as plots 216, 220 and 382) contained woodlands in the Foothills ecozone which were structurally similar to those observed at Injune, partly because they established on similar sandy or sandy loam soils. The three Foothills plots that did not compare as well were located on clay/loam soils. These differences were attributed to variations in soil nutrient availability, as the more productive clay/loam soils could support trees with large spreading crowns even though these were relatively short (up to ~20 m). These plots were also dominated by species that have denser foliage, as compared to the other Foothills sites with sandy soils (Boland et al., 1992). Plots 459 and 573 were Montane zone plots, with a predominant height less than 28 m and FBPC of between 40 and 60 %. These forests were therefore at the lower bounds of the Montane structural envelope and closer to the environmental envelope that encompassed the Injune forest plots. Plot 459 was also situated on a ridge top where the poorer soils and reduced water availability led to a forest structure similar to that observed at Injune. Likewise, the forests represented by plot 603, which was located in the high elevation Montane ecozone, had been burnt in 2003 and the reduced foliage cover and understorey also rendered these structurally similar.

Tree crown area, shape and foliage density may be factors contributing to the successful application of the HSCOI



(Nelson, 1997). The northeast Victorian plots that compared favourably using the current HSCOI calibration had a mean tree crown area that was generally smaller than tree crowns found in the plots where the stem number had been overestimated. From the 22 northeast Victorian plots, the overall mean tree crown area was  $28 \text{ m}^2$  ( $\delta=46 \text{ m}^2$ , range 0–644  $\text{m}^2$ ,  $n=810$ ; Fig. 3). For the seven plots where the Injune calibration was successful, the mean tree crown area was  $24 \text{ m}^2$  ( $\delta=32 \text{ m}^2$ , range 0–277  $\text{m}^2$ ,  $n=350$ ), whereas for the other 15 plots the mean tree crown area was  $30 \text{ m}^2$  ( $\delta=54 \text{ m}^2$ , range 0–644  $\text{m}^2$ ,  $n=460$ ). It seems plausible therefore that the Injune calibration performs best for plots containing trees with smaller crowns (i.e.  $<30 \text{ m}^2$ ) in general. This is highlighted by the fact that the mean crown area for trees  $>10 \text{ cm } D_{130}$  across all 30 Injune plots was  $16 \text{ m}^2$  ( $\delta=25 \text{ m}^2$ , range 0–397  $\text{m}^2$ ,  $n=1960$ ).

This study defines foliage density as the amount of green leaf foliage than occupies a given crown area, and is measured using LiDAR with the FBPC metric. Foliage density can vary widely depending on the genus and species as well as environmental constraints such as water and soil nutrient availability. Where FBPC approaches CC, canopies will tend to be denser with few internal crown gaps. Alternatively, where taller trees occur, this could also indicate the presence of multiple strata with vegetation at lower levels making use of all available light space from gaps (either within or between crowns) higher in the canopy. An increase in foliage density per plot would result in the LiDAR pulse having a lower ability to penetrate the overstorey canopy, which would potentially be detrimental to the retrieval of canopy density and stem locations. Fig. 19 indicates that Victorian forests tend to have greater CC and FBPC when compared forests at Injune. This is likely to lead to the identification of more branch clusters (particularly when combined with the larger tree crowns found in northeast Victoria) and the overestimation of stems observed in Fig. 18. The Injune calibration has not yet accounted for the higher part of the CC and FBPC range. Therefore additional structural formations such as larger crown areas combined with higher cover would need to be included in future HSCOI model development and to more reliably predict stem density in forests where the density of foliage is greater.

#### 5.4. Wider application

The woodland and open forest formations occurring at Injune, and for which the HSCOI was developed, are generally less than 30 m in height, contain 1 or 2 main strata, and a canopy cover of up to 80%. As such, these formations are typical to approximately 90% of Australia's forest estate in terms of structure when classed at the broad National Forest Inventory level; 95% of these forests have a reported height of  $<30 \text{ m}$  (BRS, 2003a). Therefore, the HSCOI should be broadly applicable to Australian forests in other locations that have similar soils, terrain and climate to that found at Injune, and where LiDAR data with adequate or optimal post-spacing are available. The remaining forests can exceed 60 m, contain multiple strata levels and have denser canopies (BRS, 2003a) and therefore the HSCOI might be less effective, as shown by the northeast Victorian validation.

Products from the HSCOI (stems, canopy voxels) have been used to calibrate coarser scale remote sensing data. Firstly, these have been used to generate fine scale descriptions of the distribution of tree components (leaves, branches and stems) for application in three-dimensional coherent SAR imaging simulation. Visual and numerical comparison between actual AIRSAR data and simulated SAR data so far suggests effective modelling of SAR imagery (Lucas et al., 2006b). Secondly, products are currently being used to validate the height and cover extraction routines for ICESat full waveform satellite LiDAR, as part of the NFI CFMF continental monitoring strategy.

## 6. Conclusions

The capacity to locate stems regardless of their position in the forest vertical profile, and attribute these with key common structural descriptors (e.g.,  $H$ ,  $D_{130}$ ) is perhaps of greatest significance for forest inventory. The HSCOI is a new multi-scale measure for enhancing the retrieval, mapping and reporting of key forest structural attributes that utilises small footprint discrete return LiDAR data acquired at 1 m post-spacing. The HSCOI was developed to maximize the amount of information that can be retrieved from scanning LiDAR. As part of the initial proof of concept investigations, algorithms have been written which allow automated integration of HSCOI and CHM measures for forest assessment, and specifically stem mapping and attribution in complex semi-arid forests. With appropriate calibration, the set of procedures has met adequate levels of accuracy for the semi-arid forests found at the primary study site. Independent validation in different locations has highlighted the requirement for additional regional calibration.

For the open forests and woodlands near Injune, and with reference to the northeast Victorian validation site, the HSCOI facilitated the location, density and height of tree stems associated with both the upper and sub-canopy strata, and differentiation of individuals and clusters was successful (i.e. 70–80% accuracy) for stems with  $D_{130} \geq 5 \text{ cm}$ . Spatial arrangement analyses confirmed the accuracy of the stem location, with 80% of field stems having an HSCOI stem within 3 m (on average) across 30 field plots. Success in retrieval was more variable in higher density and structurally complex stands, which in turn required the application of more complex processing routines. Stand-based estimation of predominant stem  $H$ , crown cover and FBPC achieved accuracies in the order of 70–90%, which allowed detailed mapping of the forested areas, and delineation of both individuals and clusters of crowns. Following independent validation in different regions and forested environments, the requirement for additional contextual information for calibration was identified. Data on soils and/or terrain provided additional flexibility for the modelling of complex forests, and especially to cater for regional differences where these attributes have an influence on tree size and architecture.

The HSCOI should not, however, be considered as a replacement for the CHM surface but rather as a complementary tool for assessing forests with highly variable structure.

Traditional CHM strengths include the provision of reasonably accurate upper canopy tree  $H$  measurement, where relationships between measured  $H$  are generally more robust. However, the HSCOI specifically allows additional stems in the dominant overstorey and sub-canopy to be identified and associated with an estimate of  $H$ , either from a CHM or the HSCOI itself. By combining data for individual trees, stand level estimates of predominant  $H$ , and crown cover can also be obtained. While not explicitly reported in this paper, it would be relatively simple process to generate additional structural information such as  $D_{130}$  and basal area through empirical relationships established with  $H$  using field data. The retrieval of structural information using the HSCOI and CHMs has supported the interpretation of other remote sensing data acquired over the Injune study area, and is being used to better quantify the carbon and diversity values of forests at Injune. Even so, whilst applicable to some forests in Australia, further testing of the algorithms are certainly required and recommended for both within the country and overseas. However, the research does currently provide input to Australian State and Federal Government commitments to national forest monitoring initiatives such as the CFMF, and for international reporting agreements (BRS, 2003b; Henry et al., 2002; Patenaude et al., 2005).

## Acknowledgements

The authors would like to acknowledge the support provided by the Australian Research Council (ARC), under their SPIRT program, the Cooperative Research Centre (CRC) for Greenhouse Accounting, and the National Forest Inventory. We would also like to thank the staff of the Australian government Bureau of Rural Sciences (BRS), Queensland Department of Natural Resources and Mines (QDNRM), University of New South Wales (UNSW), Queensland University of Technology (QUT) and the Queensland Department of Primary Industries (QDPI) Tropical Beef Centre. Antony Smith (IGES) is thanked for illustrations. The authors would also like to thank the anonymous reviewers for many constructive comments.

## References

- Aber, J. D. (1978). A method for estimating foliage-height profiles in broad-leaved forest. *Journal of Ecology*, 67, 35–40.
- Anderson, H. E., McGaughey, R. J., & Reutebuch, S. E. (2005). Estimating forest canopy fuel parameters using LiDAR data. *Remote Sensing of Environment*, 94, 441–449.
- Barlow, B. A. (1994). Phytogeography of the Australian region. In R. H. Groves (Ed.), *Australian vegetation*, (2nd ed.). Cambridge, UK: Cambridge University Press. 562 pp.
- Boland, D. J., Brooker, M. I. H., Chippendale, G. M., Hall, N., Hyland, B. P. M., Johnston, R. D., et al. (1992). *Forest trees of Australia*. Canberra: CSIRO Publishing.
- Bunting, P., & Lucas, R. M. (2006). The delineation of tree crowns within CASI data of Australian mixed species woodlands. *Remote Sensing of Environment*, 101, 230–248.
- Bureau of Meteorology (2004). URL: <http://www.bom.gov.au> (Accessed April 2004).
- Bureau of Rural Sciences (2003). *A continental forest monitoring framework for Australia — background, concept and rationale*. Canberra, Australia: Department of Agriculture, Fisheries and Forestry 37 pp.
- Bureau of Rural Sciences (2003). *Australia's forests at a glance*. Canberra, Australia: Department of Agriculture, Fisheries and Forestry 68 pp.
- Bureau of Rural Sciences (2006). *Continental forest monitoring framework, technical report — design and pilot study*. Department of Agriculture, Fisheries and Forestry. Canberra, Australia. 160 pp.
- Burnett, C., & Blaschke, T. (2003). A multi-scale segmentation/object relationship modelling methodology for landscape analysis. *Ecological Modelling*, 168, 233–249.
- Chasmer, L., Hopkinson, C., & Treitz, P. (2004). Assessing the three-dimensional frequency distribution of airborne and ground based LiDAR data for red pine and mixed deciduous forest plots. *International Archive of Photogrammetry, Remote Sensing and Spatial Information Sciences*, 36- 8/ W2, 66–69.
- Chen, X., Vierling, L., Rowell, E., & De Felice, T. (2005). Using LiDAR and effective LAI data to evaluate IKONOS and Landsat 7 ETM+ vegetation cover estimates in a ponderosa pine forest. *Remote Sensing of Environment*, 91, 14–26.
- Clark, M. L., Clark, D. B., & Roberts, D. A. (2004). Small-footprint LiDAR estimation of sub-canopy elevation and tree height in a tropical rain forest landscape. *Remote Sensing of Environment*, 91, 68–89.
- Dean, C., Roxburgh, S., & Mackey, B. G. (2004). Forecasting landscape-level carbon sequestration using gridded, spatially adjusted tree growth. *Forest Ecology and Management*, 194, 109–129.
- Drake, J. B., Dubayah, R. O., Knox, R. G., Clark, D. B., & Blair, J. B. (2002). Sensitivity of large-footprint LiDAR to canopy structure and biomass in a neotropical rainforest. *Remote Sensing of Environment*, 81, 378–392.
- Environmental Systems Research Institute(ESRI) (1996). *Topogrid reference within system documentation*.
- Florence, R. G. (1996). *Ecology and silviculture of eucalypt forests*. Australia: CSIRO Publishing.
- Frazer, G. W., Wulder, M. A., & Niemann, K. O. (2005). Simulation and quantification of the fine-scale spatial pattern and heterogeneity of forest canopy structure: A lacunarity-based method designed for analysis of continuous canopy heights. *Forest Ecology and Management*, 214, 65–90.
- Garmin (2003). *GPS V personal navigator — owners manual and reference guide*. USA: Garmin International Inc.
- Gaveau, D. L. A., & Hill, R. A. (2003). Quantifying canopy height underestimation by laser pulse penetration in small-footprint airborne laser scanning data. *Canadian Journal of Remote Sensing*, 29, 650–657.
- Hall, S. A., Burke, I. C., Box, D. O., Kaufmann, M. R., & Stoker, J. M. (2005). Estimating stand structure using discrete-return LiDAR: An example from low density, fire prone ponderosa pine forests. *Forest Ecology and Management*, 208, 189–209.
- Harding, D. J., Lefsky, M. A., Parker, G. G., & Blair, J. B. (2001). Laser altimeter canopy height profiles: Methods and validation for closed canopy, broadleaf forests. *Remote Sensing of Environment*, 76, 283–297.
- Hay, G., Niemann, K., & Goodenough, D. (1997). Spatial thresholds, image-objects, and upscaling: A multiscale evaluation. *Remote Sensing of Environment*, 62, 1–19.
- Henry, B. K., Danaher, T., McKeon, G. M., & Burrows, W. H. (2002). A review of the potential role of greenhouse gas abatement in native vegetation management in Queensland rangelands. *Rangeland Journal*, 24, 112–132.
- Hodgson, M. E., & Bresnahan, P. (2004). Accuracy of airborne LiDAR-derived elevation: Empirical assessment and error budget. *Photogrammetric Engineering and Remote Sensing*, 70, 331–339.
- Holmgren, J., Nilsson, M., & Olsson, H. (2003). Estimation of tree height and stem volume on plots — Using airborne laser scanning. *Forest Science*, 49, 419–428.
- Hyypä, J., Kelle, O., Lehtikoinen, M., & Inkinen, M. (2001). A segmentation-based method to retrieve stem volume estimates from 3-D tree height models produced by laser scanners. *IEEE Transactions on Geoscience and Remote Sensing*, 39, 969–975.
- Ishii, H. T., Tanabe, S. I., & Hiura, T. (2004). Exploring the relationships among canopy structure, stand productivity, and biodiversity of temperate forest ecosystems. *Forest Science*, 50, 342–355.
- Jelinski, D. E., & Wu, J. (1996). The modifiable areal unit problem and implications for landscape ecology. *Landscape Ecology*, 11, 129–140.
- Jerez, M., Dean, T. J., Cao, Q. V., & Roberts, S. D. (2005). Describing leaf area distribution in Loblolly pine trees with Johnson's SB function. *Forest Science*, 51, 93–101.

- Jupp, D. L. B., & Walker, J. (1997). Detecting structural and growth changes in woodlands and forests: The challenge for remote sensing and the role of geometric-optical modelling. In H. L. Gholz, K. Nakane, & H. Shimoda (Eds.), *The use of remote sensing in the modelling of forest productivity* (pp. 75–108). Dordrecht, The Netherlands: Kluwer Academic Publishers.
- Leckie, D., Gougeon, F., Hill, D., Quinn, R., Armstrong, L., & Shreenan, R. (2003). Combined high-density LiDAR and multispectral imagery for individual tree crown analysis. *Canadian Journal of Remote Sensing*, 29, 633–649.
- Lee, A., Chikumbo, O., Davey, S., & Tickle, P. K. (2001, 10–13 December). Enhanced visualisation capability for forest management optimisation results. *Proceedings, International Congress on Modelling & Simulation (ModSim), Vol. 4.* (pp. 1739–1744). Canberra, Australia: Modelling and Simulation Society of Australia and New Zealand.
- Lee, A., Lucas, R., & Brack, C. (2004). Quantifying vertical forest stand structure using small footprint LiDAR to assess potential stand dynamics. *International Archive of Photogrammetry, Remote Sensing and Spatial Information Sciences*, 36 - 8/W2, 213–217.
- Lefsky, M. A., Harding, D., Cohen, W. B., & Parker, G. G. (1999). Surface LiDAR remote sensing of basal area and biomass in deciduous forests of eastern Maryland, USA. *Remote Sensing of Environment*, 67, 83–98.
- Lefsky, M. A., Hudak, A. T., Guzy, M., & Cohen, W. B. (2005). Combining LiDAR estimates of biomass and Landsat estimates of stand age for spatially extensive validation of modelled forest productivity. *Remote Sensing of Environment*, 95(4), 549–558.
- Lim, K. S., & Treitz, P. M. (2004). Estimation of above ground forest biomass from airborne discrete return laser scanner data using canopy-based quantile estimators. *Scandinavian Journal of Forest Research*, 19, 558–570.
- Lim, K., Treitz, P., Wulder, M., St-Onge, B., & Flood, M. (2003). LiDAR remote sensing of forest structure. *Progress in Physical Geography*, 27, 88–106.
- Lovell, J. L., Jupp, D. L. B., Culvenor, D. S., & Coops, N. C. (2003). Using airborne and ground-based ranging LiDAR to measure canopy structure in Australian forests. *Canadian Journal of Remote Sensing*, 29(5), 607–622.
- Lovell, J. L., Jupp, D. L. B., Newnham, G. J., Coops, N. C., & Culvenor, D. S. (2005). Simulation study for finding optimal LiDAR acquisition parameters for forest height retrieval. *Forest Ecology and Management*, 214, 398–412.
- Lucas, R. M., Cronin, N., Lee, A., Moghaddam, M., Witte, C., & Tickle, P. (2006). Empirical relationships between AIRSAR backscatter and LiDAR-derived forest biomass, Queensland, Australia. *Remote Sensing of Environment*, 100, 407–425.
- Lucas, R. M., Lee, A., & Williams, M. L. (2006). Enhancing SAR simulations using LiDAR for understanding the relations between forest structure and SAR imagery. *IEEE Transactions on Geoscience and Remote Sensing*, 44 (10), 2736–2754.
- Lucas, R. M., Moghaddam, M., & Cronin, N. (2004). Microwave scattering from mixed species woodlands, central Queensland, Australia. *IEEE Transactions on Geoscience and Remote Sensing*, 42(10), 2142–2159.
- MacArthur, R. H., & Horn, H. S. (1969). Foliage profiles by vertical measurements. *Ecology*, 50, 802–804.
- Magnussen, S., & Boudewyn, P. (1998). Derivations of stand heights from airborne laser scanner data with canopy-based quantile estimators. *Canadian Journal of Forest Research*, 28, 1016–1031.
- Maltamo, M., Eerikainen, K., Pitkanen, J., Hyypä, J., & Vehmas, M. (2004). Estimation of timber volume and stem density based on scanning laser altimetry and expected tree size distribution functions. *Remote Sensing of Environment*, 90, 319–330.
- McDonald, R. C., Isbell, R. F., Speight, J. G., Walker, J., & Hopkins, M. S. (1998). *Australian soil and land survey field handbook*, (2nd ed.). Melbourne: Inkata Press 198 pp.
- Nelson, R. (1997). Modelling forest canopy heights: The effects of canopy shape. *Remote Sensing of Environment*, 60(3), 327–334.
- Nilson, T., & Ross, J. (1997). Modeling radiative transfer through forest canopies: Implications for canopy photosynthesis and remote sensing. In H. L. Gholz, K. Nakane, & H. Shimoda (Eds.), *The use of remote sensing in the modelling of forest productivity* (pp. 23–60). Dordrecht, The Netherlands: Kluwer Academic Publishers.
- Parker, G. G. (1995). Structure and microclimate of forest canopies. In M. Lowman, & N. Nadkarni (Eds.), *Forest canopies — a review of research on a biological frontier* (pp. 73–106). San Diego: Academic Press.
- Patenaude, G., Milne, R., & Dawson, T. P. (2005). Synthesis of remote sensing approaches for forest carbon estimation: Reporting to the Kyoto Protocol. *Environmental Science & Policy*, 8, 161–178.
- Peel, D. R., Pitman, A. J., Hughes, L. A., Narisma, G. T., & Pielke, R. A., Sr (2005). The impact of realistic biophysical parameters for eucalypts on the simulation of the January climate of Australia. *Environmental Modelling & Software*, 20(5), 595–612.
- Popescu, S. C., & Wynne, R. H. (2004). Seeing the trees in the forest: Using LiDAR and multispectral data fusion with local filtering and variable window size for estimating tree height. *Photogrammetric Engineering & Remote Sensing*, 70(5), 589–604.
- Popescu, S. C., Wynne, R. H., & Nelson, R. F. (2003). Measuring individual tree crown diameter with LiDAR and assessing its influence on estimating forest volume and biomass. *Canadian Journal of Remote Sensing*, 29, 564–577.
- Popescu, S. C., Wynne, R. H., & Scriver, J. A. (2004). Fusion of small-footprint lidar and multispectral data to estimate plot-level volume and biomass in deciduous and pine forests in Virginia, USA. *Forest Science*, 50, 551–565.
- Pouliot, D. A., King, D. J., & Pitt, D. G. (2005). Development and evaluation of an automated tree detection–delineation algorithm for monitoring regenerating coniferous forests. *Canadian Journal of Forest Research*, 35, 2332–2345.
- Research Working Group. (1999). In Wood, Turner, & Brack (Eds.), *Code of forest mensuration practise: A guide to good tree measurement practise in Australia and New Zealand* URL: <http://sres.anu.edu.au/associated/mensuration/rwg2/code/3-4-2.htm>, (Accessed December 2005).
- Riaño, D., Meier, E., Allgower, B., Chuvieco, E., & Ustin, S. L. (2003). Modeling airborne laser scanning data for the spatial generation of critical forest parameters in fire behavior modelling. *Remote Sensing of Environment*, 86, 177–186.
- Riaño, D., Valladares, F., Condés, S., & Chuvieco, E. (2004). Estimation of leaf area index and covered ground from airborne laser scanner (LiDAR) in two contrasting forests. *Agricultural and Forest Meteorology*, 124, 269–275.
- Specht, R. L., & Specht, A. (1999). *Australian plant communities: Dynamics of structure, growth and biodiversity*. : Oxford University Press.
- Stone, C., Coops, N. C., & Culvenor, D. S. (2000). Conceptual development of a eucalypt canopy condition index using high resolution spatial and spectral remote sensing imagery. *Journal of Sustainable Forestry*, 11, 23–45.
- Suárez, J. C., Ontiveros, C., Smith, S., & Snape, S. (2005). Use of airborne LiDAR and aerial photography in the estimation of individual tree heights in forestry. *Computers and Geosciences*, 31, 253–262.
- Tickle, P. K., Lee, A., Lucas, R. M., Austin, J., & Witte, C. (2006). Quantifying Australian forest floristics and structure using small footprint LiDAR and large scale aerial photography. *Forest Ecology and Management*, 223, 379–394.
- Todd, K. W., Csillag, F., & Atkinson, P. M. (2003). Three-dimensional mapping of light transmittance and foliage distribution using LiDAR. *Canadian Journal of Remote Sensing*, 29, 544–555.
- Turner, W., Spector, S., Gardiner, N., Fladeland, M., Sterling, E., & Steininger, M. (2003). Remote sensing for biodiversity science and conservation. *Trends in Ecology & Evolution*, 18, 306–314.
- Wiegand, T., Kissling, W. D., Cipriotti, P. A., & Aguiar, M. R. (2006). Extending point pattern analysis to objects of finite size and irregular shape. *Journal of Ecology*, 94, 825–837.
- Wiegand, T., & Moloney, K. A. (2004). Rings, circles, and null-models for point pattern analysis in ecology. *Oikos*, 104(2), 209–229.
- Wulder, M., Niemann, K. O., & Goodenough, D. G. (2000). Local maximum filtering for the extraction of tree locations and basal area from high spatial resolution imagery. *Remote Sensing of Environment*, 73, 103–114.
- Wulder, M. A., & Seemann, D. (2003). Forest inventory height update through the integration of LiDAR data with segmented Landsat imagery. *Canadian Journal of Remote Sensing*, 29, 536–543.

## Retrieving forest biomass through integration of CASI and LiDAR data

R. M. LUCAS\*†, A. C. LEE‡ and P. J. BUNTING†

†Institute of Geography and Earth Sciences, The University of Wales, Penglais Campus,  
Aberystwyth, Ceredigion SY23 3DB, UK

‡School of Resources, Environment and Society, Australian National University,  
Canberra, ACT, 0200, Australia

(Received 10 November 2006; in final form 4 July 2007)

To increase understanding of forest carbon cycles and stocks, estimates of total and component (e.g. leaf, branch and trunk) biomass at a range of scales are desirable. Focusing on mixed species forests in central south-east Queensland, two different approaches to the retrieval of biomass from small footprint Light Detection and Ranging (LiDAR) and Compact Airborne Spectrographic Imager (CASI) hyperspectral data were developed and compared. In the first, stems were located using a LiDAR crown openness index, and each was associated with crowns delineated and identified to species using CASI data. The component biomass for individual trees was then estimated using LiDAR-derived height and stem diameter as input to species-specific allometric equations. When summed to give total above-ground biomass (AGB) and aggregated to the plot level, these estimates showed a reasonable correspondence with ground (plot-based) estimates ( $r^2=0.56$ ,  $RSE=25.3 \text{ Mg ha}^{-1}$ ,  $n=21$ ) given the complex forest being assessed. In the second approach, a Jackknife linear regression utilizing six LiDAR strata heights and crown cover at the plot-scale produced more robust estimates of AGB that showed a closer correspondence with plot-scale ground data ( $r^2=0.90$ ,  $RSE=11.8 \text{ Mg ha}^{-1}$ ,  $n=31$ ). AGB aggregated from the tree-level and Jackknife regression plot-based AGB estimates (for 270 plots—each of 0.25 ha) compared well for more mature homogeneous and open forests. However, at the tree level, AGB was overestimated in taller forests dominated by trees with large spreading crowns, and underestimated AGB where an understorey with a high density of stems occurred. The study demonstrated options for quantifying component biomass and AGB through integration of LiDAR and CASI data but highlighted the requirement for methods that give improved estimation of tree density (by size class distributions) and species occurrence in complex forests.

### 1. Introduction

Forest biomass is a key biophysical property that describes the carbon content of vegetation. Quantification at various scales is critical for understanding the stocks and fluxes associated with forest clearance, degradation, and regeneration, particularly given current concerns regarding global climate change (Barrett *et al.* 2001). Knowledge of carbon dynamics is crucial when addressing issues relating to carbon accounting, including quantifying carbon for credit schemes (Patenaude *et al.* 2005). National reporting of carbon sources and sinks is also required to fulfill

---

\*Corresponding author. Email: rml@aber.ac.uk

obligations to international agreements such as the United Nations Framework Convention on Climate Change (Rosenqvist *et al.* 2003). Despite these requirements, there is still much uncertainty in biomass estimation at a range of scales and in particular on how much carbon is cycled through the Earth's forests. Scenario development to assess whether this cycling might change as a result of forest alteration (e.g. degradation induced by climate change) is also needed and is becoming increasingly important as a research field (Brack *et al.* 2006).

Forest biomass can be quantified at scales ranging from the local to global depending on the research or reporting requirements. Different units of measurement can be utilized that relate to within-tree components (e.g. leaves, branches, and trunks), individual (whole) trees, clusters of trees, forest inventory plots, forest stands or patches and landscape-scale descriptions such as communities or biomes. When remote sensing data are used to quantify biomass, the level of detail obtained depends largely upon the spatial resolution of the observing sensor, the regions of the electromagnetic spectrum within which observations are recorded, and whether the sensor is active (e.g. Synthetic Aperture Radar (SAR) or Light Detection and Ranging (LiDAR)) or passive (e.g. optical sensors). Indeed, several sets of remote sensing data are often required for biomass estimation, alongside algorithms that allow their effective integration. Even so, the above-ground biomass (AGB) has, to date, only been measured indirectly from remote sensing data (e.g. through transfer functions or from surrogates for biomass such as height or canopy cover). Reliable estimation of component (e.g. leaf, branch or trunk) biomass has rarely been achieved.

To advance the estimation of biomass from remote sensing data, this research aimed to establish whether:

1. tree size estimates from LiDAR integrated with species classifications from hyperspectral Compact Airborne Spectrographic Imager (CASI) data can be used as input to species-specific allometric equations to estimate the AGB and component biomass of individual trees identified from these data;
2. the resulting estimates, when aggregated to the plot-level, compare favourably (or otherwise) with those generated either from forest (plot-based) inventory or through empirical-based relationships with LiDAR data; and
3. differences in species type, height, crown cover and stem density influence retrieval using this approach.

Scaling biomass from the individual tree level was considered, as empirical relationships with remotely sensed data generally allow only for the estimation of total AGB and not component biomass. This is largely because the inherent relationship between these components (e.g. leaf and branch biomass) introduces uncertainties in their retrieval (Lucas *et al.* 2000). However, information on the distribution and allocation of biomass to components is desirable, particularly for understanding vegetation dynamics relating to plant health, identifying growth stage, and quantifying productivity and carbon/nitrogen cycling (Gastellu-Etchegorry *et al.* 1995, Zagolski *et al.* 1996). Estimates are also useful for interpreting data acquired by remote sensing instruments operating within wavelength regions known to be sensitive to different forest components. For example, L-band microwaves (~25 cm wavelength) transmitted by Synthetic Aperture Radar (SAR) interact preferentially with the woody components of forests, and backscatter can be related directly to the biomass of the branches and/

or trunks if this information is available (Lucas *et al.* 2004). Similarly, the reflectance of forests in the visible portion of the spectrum is dictated largely by the amount of photosynthetic pigments within leaves forming the canopy, and hence relationships with photosynthetic activity can be established. For these reasons, the study sought also to demonstrate the retrieval of component biomass as well as AGB.

## 2. Background

### 2.1 Biomass estimation from ground survey

Biomass estimates from ground data are generally calculated using allometric equations. These equations are typically nonlinear and relate measures of tree size (e.g. diameter at breast height (DBH), top height, crown area) to the dry weight of the above (leaves, branches, and trunks) and/or below (fine, coarse roots) ground components of biomass or the sum of these (i.e. the total). Equations are determined typically for a particular species by destructively harvesting trees across the size (e.g. stem diameter) range, as observed in the field or from independently collected forest inventory data. Often, the components are separated during the harvesting operation such that equations relating to their individual biomass can be formulated. While height is sometimes used as input to allometric equations, most utilize stem diameter, which is typically measured at 130 cm above ground level (i.e. DBH). However, in Australia, the height at which diameter is measured may be lower (e.g. 30 cm above ground level) where multitemmed individuals occur (Burrows *et al.* 2000). For this reason, DBH is referred to as  $D_{130}$  in this study to clarify the measure used. In many cases, diameter can be estimated using generalized or species-specific relationships with height, which can be established at the time of harvesting. Crown area is sometimes used as an input to allometric equations, particularly where individual trees support a large number of stems (e.g. Harrington 1979), although obtaining reliable ground-based measures of crown area for use in these functions is often problematic.

Although some equations are interchangeable between species (Eamus *et al.* 2001, Burrows *et al.* 2002), many require trees to be similar in terms of architecture if the allometric equation for one species is to be successfully applied to another. For example, equations generated for coniferous species will underestimate the amount of leaf and branch material if applied to most broadleaved species (Lucas *et al.* 2004). Even within species, equations may differ. For example, those generated for species in more productive environments are often not applicable when applied to the same species in an environment that is less conducive to growth. Inter- and intra-specific variation in the specific gravity of the wood in trees also introduces error when applying a standard allometric equation (Chave *et al.* 2004). Often, however, users are not given a wide choice of species-specific allometric equations, as these are expensive to generate in terms of costs, labour, and resources, and hence very few exist. For this reason, a common approach is simply to apply the equation that best represents the species types occurring within the forest, with the resulting increased likelihood of error in the biomass estimates (Richards 2002). Error also increases if the allometrics are applied to trees that are outside the size range of the original calibration data, as overestimation of biomass may result. Careful consideration therefore needs to be given to the development and application of these functions.

## 2.2 Remote sensing for biomass estimation

With the advent of fine-spatial-resolution remote sensing data, the capacity for retrieving information on forest floristics and structure has increased. This capacity has been demonstrated for a range of forested environments and at a range of scales from individual trees up to landscapes and biomes (Lefsky *et al.* 1999, Popescu and Wynne 2004, Lefsky *et al.* 2005, Chasmer *et al.* 2006a,b). For tree-level biomass estimation, species typing is needed for appropriate application of available species-specific allometric equations and is best provided by hyperspectral data (e.g., Clark *et al.* 2005, Zhang *et al.* 2006). However, independent variables relating to tree size (e.g. height) have generally proved more difficult to obtain from optical data (unless appropriate stereo data are available; Lucas *et al.* 2002, Mitchell *et al.* 2007) and therefore need to be derived from other sources.

Increasingly, studies have found that the three-dimensional structure of forest canopies can be measured to high levels of accuracy using airborne LiDAR data (Lim, *et al.* 2003, Lim and Treitz 2004). Specifically, LiDAR data have been shown to produce estimates of tree height that are considered to be at least equivalent to and often more accurate than those obtained at the ground level using more traditional approaches (e.g. clinometers, laser rangefinders; Tickle *et al.* 2006). This occurs partly because of the difficulty with ground-based measurements in sighting the tops of crowns that are expansive or occur in forests where the canopy is dense. Even so, LiDAR-derived tree top heights can be less accurate (although error magnitudes are often better than ground-based survey) for trees where the crown tapers to a point (e.g. conifers), unless a very high LiDAR sampling rate is used or variations in the collection parameters are accounted for (Gaveau and Hill 2003, Lovell, *et al.* 2005). As with optical data, LiDAR can be used to estimate planimetric cover but additionally facilitate retrieval of cover at different layers within the forest volume

Although species and structural measures can be obtained using a combination of optical and LiDAR data, quantifying biomass at the tree level through application of allometric equations is problematic because individuals have to be located, identified to species, and attributed with a size measurement. Difficulties in extracting such information arise when data of a spatial resolution coarser than that of individual crown areas are used (e.g. a pixel area  $>10 \times 10$  m or  $100 \text{ m}^2$ ), as individual tree crowns are more difficult to distinguish and attribute. In these cases, it is often necessary to assume that multiple stems as well as different species may occur within a pixel area, especially in heterogeneous forests. As a consequence, any estimates of biomass generated using allometric equations are likely to be in error, particularly as neither the independent variables (e.g. height, diameter) for individuals nor estimates of stem density are generally available. Conversely, tree level assessment is also problematic using finer (e.g. a pixel area  $<2 \times 2$  or  $4 \text{ m}^2$ ) spatial resolution data. In these cases, individual crowns are often discernible, but they are frequently composed of several pixels with highly variable reflectance because of differences in illumination (i.e. the occurrence of sunlit and shaded portions of the crown). Therefore, traditional pixel-based approaches to classification are often unsatisfactory. For this reason, object-orientated algorithms that allow the delineation of tree crowns (as objects) and which then extract some component of the reflectance that allows best discrimination of trees to the species level are desirable (Lobo 1997, Burnett and Blaschke 2003, Leckie *et al.* 2005).

The retrieval of key attributes for biomass estimation at the tree level is therefore complex, and many approaches to mapping (particularly at landscape scales) have necessarily reverted to the use of empirical relationships between total AGB and remotely sensed data (e.g. Dobson *et al.* 1995, Means *et al.* 1999, dos Santos *et al.* 2003). In such cases, the leaf, branch and trunk biomass cannot be retrieved separately using component-specific empirical relationships with remote sensing data because of the proportional linkages between components and also the total (Lucas *et al.* 2000, 2004). In many cases, total AGB assessments are sufficient, but the demand for more detailed assessments of biomass distributions (e.g. for carbon accounting) is increasing.

### 3. Study area and datasets

The study focused on a  $37 \times 60$  km area (latitude  $25^{\circ}32'$  south, longitude  $147^{\circ}32'$  east) of mixed species forests located near the township of Injune and within the Southern Brigalow Belt, a biogeographic region of south-east central Queensland, Australia (figure 1). Common tree species (Lucas *et al.* 2004) include brigalow (*Acacia harpophylla*), poplar box (*Eucalyptus. populnea*), white cypress pine (*Callitris glaucophylla*), silver-leaved ironbark (*E. melanaphloia*) and smooth-barked apple (*Angophora leiocarpa*). Forests were observed in varying states of degradation and regeneration as a result of prior disturbance (e.g. broad scale clearing, altered fire regimes and spread of exotic species). The forests were also structurally similar (in terms of broad National Forest Inventory classifications) to over 70% of those occurring in Australia (Tickle *et al.* 2006) and comprised woodlands (10–30% Foliage Projected Cover or FPC) and open forests (30–70% FPC; Specht and Specht 1999) of varying density and canopy cover.

### 4. Remote sensing data acquisition

A systematic sampling scheme was used within the study area to collect coincident field and fine-spatial-resolution remotely sensed data. This consisted of one hundred and fifty  $500 \times 150$  m Primary Sampling Units (PSUs), spaced 4 km apart. Each PSU was subdivided into thirty  $50 \times 50$  m Secondary Sampling Units (SSUs), providing 4500 plots (0.25 ha in area) that were equivalent in size to those used commonly in forest inventory. From the 4500 SSUs, 33 forested plots were selected for detailed ground survey (Lucas *et al.* 2004) based on a representative sample of the structure,

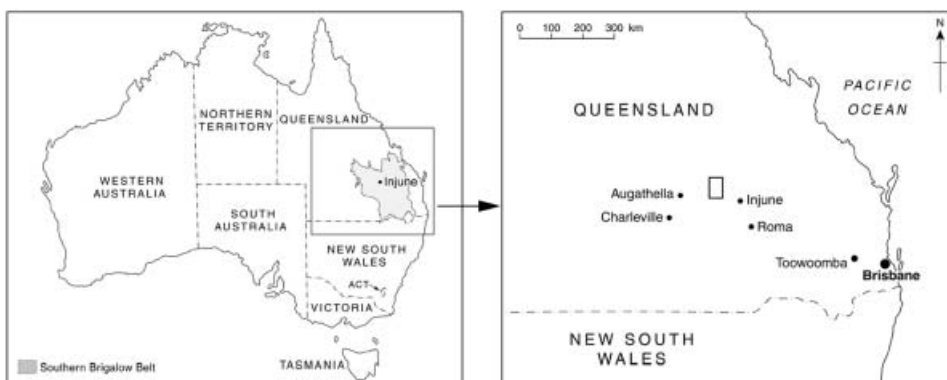


Figure 1. Location of the study area near Injune, central south-east Queensland, Australia.



composition and biomass of forests occurring within the study area (Tickle *et al.* 2006).

Small-footprint discrete return LiDAR data were acquired over each PSU using an Optech 1020 scanner mounted on a Bell Jet Ranger helicopter (Tickle *et al.* 2006). Data were acquired in an east–west direction, at a flying height of 250 m and over a week commencing 24 August 2000. The Optech 1020 measured 5000 first and last returns per second, each with intensity in the near-infrared (1047 nm) part of the electromagnetic spectrum, a beam divergence of 0.3 milliradians, an approximate footprint of 7.5 cm, and an average sample interval <1 m. Using full differential Global Positioning System (dGPS) correction (a base station was setup for the flights) and an Inertial Navigation System (INS) supplying pitch, yaw, and roll, coordinates with an absolute accuracy of <1 m in the  $x$  and  $y$  axis and <0.15 m in the  $z$  axis were provided.

CASI data (nominally 1 m spatial resolution) were also obtained over each of the 150 PSUs on either 29 August or 1 September 2000. The data were acquired in a north–south direction at a flying height of approximately 500 m and in 14 wavelength regions (12 bit) covering the visible to near-infrared regions of the electromagnetic spectrum, including several along the red edge (Bunting and Lucas 2006a). Following acquisition, the CASI data were converted to surface reflectance (per cent) using the ENVI empirical line calibration (Research Systems Inc. 2003) method and reflectance spectra collected from ground calibration targets at the time of the overflights. A more comprehensive overview of the LiDAR and CASI acquisition and pre-processing is given in Lucas *et al.* (2004), Bunting and Lucas (2006a), and Tickle *et al.* (2006).

## 5. Methods

To retrieve and map AGB and component biomass at the individual tree/cluster level from LiDAR and CASI data and scale-up to the plot or stand, algorithms were developed for:

1. automatically registering the CASI and LiDAR data using canopy height and band ratios, respectively;
2. delineating tree crowns/crown-clusters observed within the CASI data;
3. classifying tree species based on CASI spectra extracted from delineated crowns/crown-clusters;
4. mapping associated stem locations and attributing with a height and diameter using LiDAR data;
5. estimating the component biomass and AGB by utilizing LiDAR-derived estimates of height and diameter as input to the available species-specific allometric equations.

While appearing complex, all algorithms and procedures have been fully automated such that they can be applied routinely using CASI and LiDAR data, either singularly or in combination. The sequence of processing is outlined in figure 2 and described in more detail in the following sections.

### 5.1 Automated registration of CASI and LiDAR data

As is common in many studies, the CASI and LiDAR sensors were mounted on different aircraft. Although the data were acquired over a similar time period with

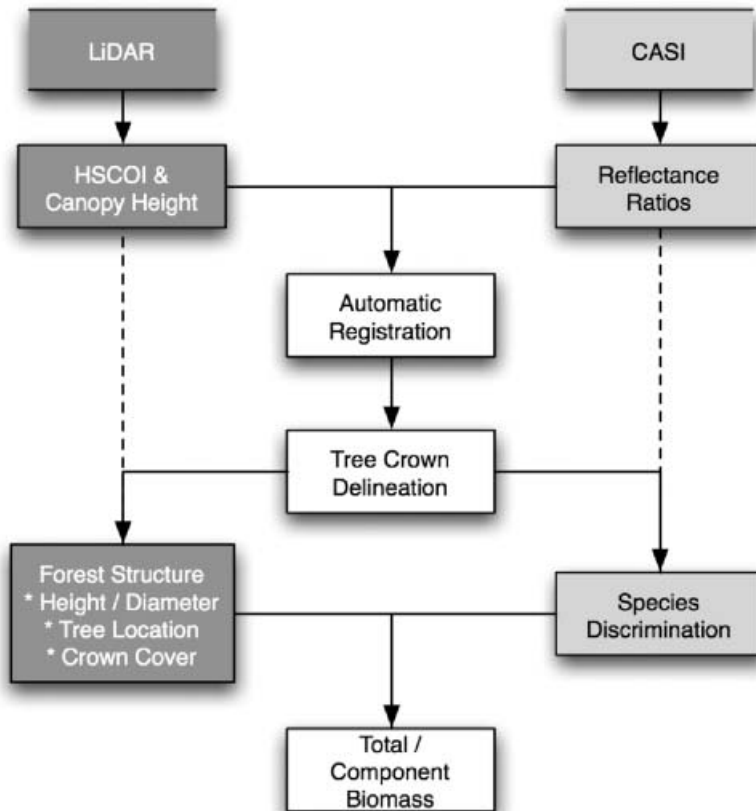


Figure 2. Overview of processing sequences implemented for estimating total above-ground and component biomass at the individual tree/cluster level.

differential Global Positioning Systems (dGPS) and Inertial Navigation Systems (INS), differences between data types, flying conditions and flight paths led to inconsistencies in registration between images. While manual interactive procedures based on ground control point (GCP) selection provided reasonable registration between the LiDAR and CASI data, these were time-consuming and automated registration procedures (Zitová and Flusser 2003, Inglada and Giros 2004) were therefore developed and implemented (Bunting 2007).

An appearance-based method to the automated registration of these two datasets was adopted, whereby matching of the pixel intensity values was performed on windows of image data. A number of metrics (e.g. Euclidean distance and Mutual Information) were evaluated, but the correlation coefficient proved to be more robust (Bunting 2007). The registration process used a multiscale approach through an image pyramid where an adapted self-organizing (Kohonen) network (Kohonen 2001) related neighbouring tie points to one another. The process of registration commenced in the upper level of the pyramid (associated with the coarsest spatial resolution). As tie points were progressively moved into their final position, each of the neighbouring tie points within all levels of the network was updated as the identified transform propagated through the network. Following registration at the upper level and using the tie points established here, the process continued

progressively through to the lower levels, thereby allowing the registration at the lowest level (finest spatial resolution) to be refined. Once registered, the tie points at this lowest level were extracted as GCPs. Registration of the CASI to the LiDAR reference data was based on the identified GCPs and undertaken within IDL ENVI using a nearest-neighbour interpolation and triangulation transformation.

## 5.2 Delineation of tree crowns from CASI data

Using the registered CASI datasets, an algorithm was developed within eCognition (Definiens) Developer (Definiens 2005) to delineate tree crowns of varying dimension. This algorithm, which is fully described in Bunting and Lucas (2006a), first differentiates forest, non-forest, and understorey using a Forest Discrimination Index (FDI) that combines the near-infrared, red edge, and blue reflectance channels. The forested area is then segmented into large objects, which are then allocated to one of several forest types based on their spectral reflectance characteristics. Within each of these, the object maxima are identified using the band ratio C1 and iteratively expanded using the ratio C2 (Carter 1994) to create sub-objects, where:

$$C1 = \frac{\rho_{741}}{\rho_{680}} \quad (1)$$

$$C2 = \frac{\rho_{741}}{\rho_{714}}, \quad (2)$$

and  $\rho$  represents reflectance in selected wavebands (e.g. centred at 741 nm). The expanded objects (containing the maxima) are classified subsequently into crown or crown/cluster classes based on a series of measures relating to, for example, shape and spectral indices that reflect the structural characteristics of crowns of different tree types. Further iterative splitting of unclassified objects is then undertaken using a progressive set of rules to delineate more crowns/crown-clusters. Where objects are oversplit into crowns or crown/clusters, these are identified based largely on rules relating to the relative position of the object maxima in relation to the object boundary. With reference to ground data, the delineation process provided accuracies averaging  $\sim 70\%$  (range 48–88%) for individuals or clusters of trees of the same species with  $D_{130} \geq 10$  cm (senescent and dead trees excluded). The lower accuracies were associated with stands containing a higher density of individuals and several canopy layers.

## 5.3 Discrimination to species

Once delineated, crowns/crown-clusters needed to be associated with a species type so that species-specific allometric equations could be applied appropriately. A number of studies (e.g. Gougeon and Leckie 2003, Huang *et al.* 2004, Leckie *et al.* 2005) have extracted spectra from individual pixels or the meanlit (sunlit) proportions of crowns to classify species, with these defined using selected bands (e.g. the green reflectance channel; Leckie *et al.* 2005). Bunting *et al.* (2006), using the Injune dataset, established that the mean lit spectra extracted using the C2 ratio increased the accuracy of classification of tree species by  $\sim 10\%$  compared with when other measures (e.g. single band reflectance data) were used. The classification was performed using Multiple (Stepwise) Discriminant Analysis (MDA) within SPSS

where the Mahalanobis Distance was used with probabilities of  $F$  set at 0.05 for entry and 0.1 for removal of variables (Bunting and Lucas 2006b). For species of the genera *Eucalyptus*, *Angophora*, *Acacia*, *Callitris*, and *Eremophila*, accuracies of classification were typically greater than 87% and 77% based on reference to training and validation sets, respectively (established through observations in the field and from aerial photography). An example of the classification output for PSU 144 is shown in figure 3.

#### 5.4 LiDAR stem mapping and attribution

To generate tree-level estimates of biomass, measures of tree size (e.g. stem diameter ( $D_{130}$ ) and top height ( $H$ )) for all stems within a unit area were required for input to allometric equations. While LiDAR Canopy Height Models (CHMs) can be used to generate stem maps, they generally only identify the upper strata trees (Hyyppa *et al.* 2001). Within the study area, a wide range of forests at various stages of regeneration occurred, and as a result, many stems were found in the sub-canopy (often beneath large crowns). Hence, these sub-canopy stems were omitted when mapping using a traditional CHM. For this reason, a LiDAR-derived Height-Scaled Crown Openness Index (HSCOI) surface was used to identify stems in both the overstorey and in the sub-canopy. The development of the HSCOI method and its application to SAR simulation are presented in Lucas *et al.* (2006b) and fully described in Lee and Lucas (2007). However, a brief overview of the method will be presented here.

The HSCOI provides a spatial representation of the density of crown components (i.e. leaves, branches, and trunks) by quantifying the penetration of LiDAR returns in three dimensions. The penetration distance of each return with respect to the top of the canopy is scaled by the maximum height of the stand. For example, returns that reach the ground have 100% penetration distance, while those that return from the top of the canopy may have only 10–20% penetration, with respect to the maximum height of the stand. The percentage penetration or openness is then mapped onto a two-dimensional raster surface (herein referred to as the HSCOI surface). Areas of tree crowns that return most of the LiDAR pulses from the upper canopy (i.e. above the trunk and the larger portions of major branches) are generally associated with lower HSCOI values, which are represented as local minima in the

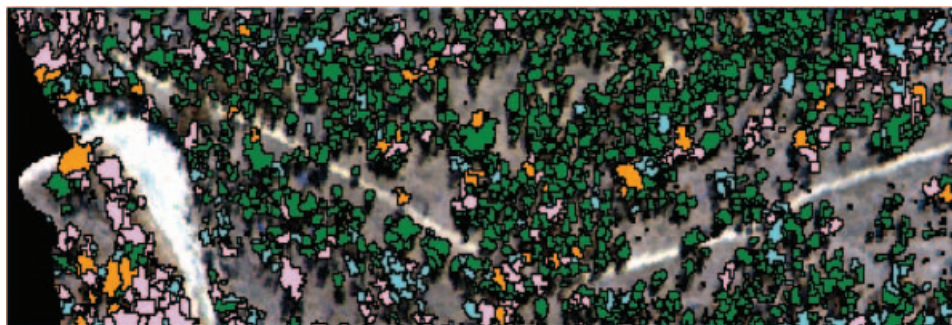


Figure 3. Distribution of *Eucalyptus melanophloia* (cyan), *E. populnea* (orange), *E. chlorochlada* (pink), and *Callitris glaucophylla* (dark green) mapped from the CASI data for PSU 144 (centre of image 147.47° E, -25.789° S; 500 m × 150 m in the east–west and north–south directions, respectively).

surface. As the edges of crowns tended to be more open, LiDAR pulses can penetrate better to the ground, thus resulting in higher HSCOI values, even though the height above the ground is often close to the tree top height.

To locate and map stems, two different smoothing kernels were applied initially to the 1-m-spatial-resolution HSCOI surface; a 1-m-radius circular and a 5-m square kernel. In the first application, local minima were associated with both overstorey stems and smaller trees (typically with  $D_{130} \leq 10$  cm), many of which were adjacent to or below larger crowns. Stems in the sub-canopy were identified largely because the relatively open structure of the overstorey crowns allowed sufficient LiDAR returns to penetrate and hence record the presence of vegetation at lower levels. For the second application, a 5-m square kernel was used. The larger smoothing kernel resulted in fewer HSCOI minima, but these were found to be associated with larger individuals forming the upper canopy and occurring within crown-clusters. By combining the minima from the two HSCOI surfaces, the locations of trees forming both the overstorey and sub-canopy could be identified and differentiated. A CHM was also generated as part of the HSCOI modelling by using an initial raster layer containing the tallest LiDAR value in each  $1\text{m}^2$  HSCOI column. A  $3 \times 3$  kernel was then applied to the initial height raster, which assigned the tallest LiDAR value within the kernel to the central cell, resulting in the final CHM. The smoothing was undertaken to reduce small within-crown gaps caused by the LiDAR sampling rate. Figure 4 illustrates the

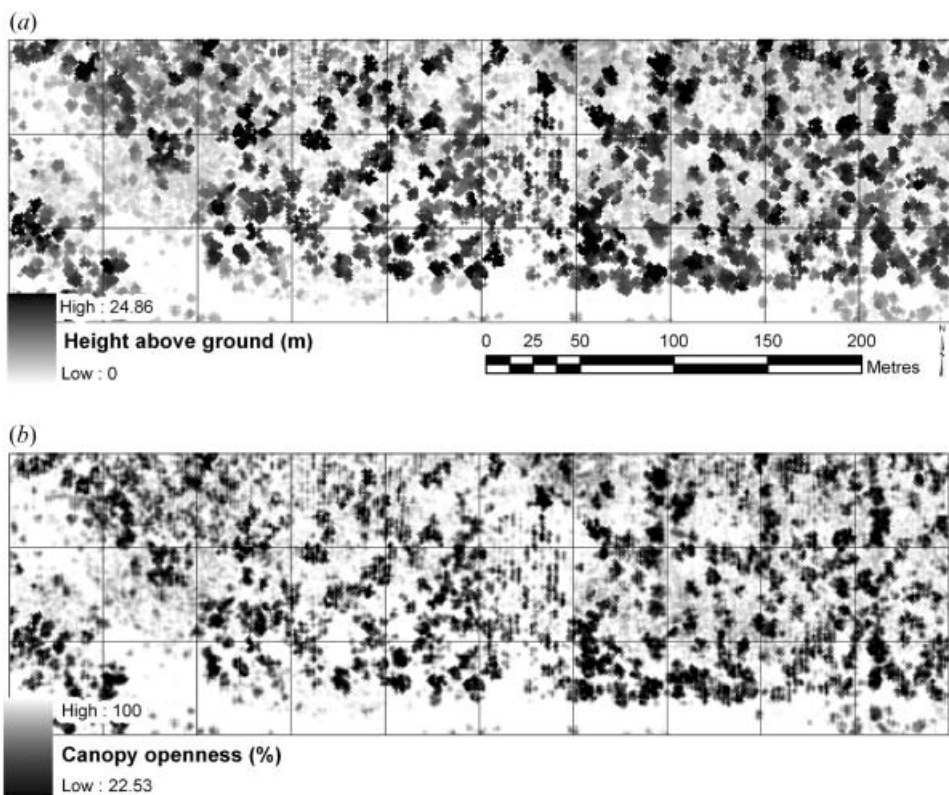


Figure 4. 1 m spatial resolution LiDAR-derived (a) CHM and (b) HSCOI layers generated for PSU 58. The darkest areas in the HSCOI layer are minima associated with tree stem locations.

CHM and HSCOI (smoothed with the 1 m circular kernel) for PSU 58. The stem map derived from the HSCOI for this PSU is shown in figure 7 (§6). A contour that bounded 90% of LiDAR returns  $\geq 2$  m in height was extracted from the HSCOI layer and was found to correspond well to the crown edge boundary and also to plot-scale estimates of crown cover. The crown cover estimates generated using this approach were used subsequently in stepwise and Jackknife linear regression models for estimating plot-scale biomass.

While not directly measured, diameter can be derived through relationships with height. For overstorey crowns/crown-clusters, height is determined traditionally from the CHM values. However, for trees located in the sub-canopy, the heights derived from the CHM were found to have greater error, as only height from the outer canopy surface was extracted. Therefore, height was retrieved for both overstorey and sub-canopy stems by:

1. First, intersecting stems with the CHM and assigning the height from this layer to the stem. Where a single stem occurred within the crown, the maximum CHM value found within the delineated crown area was assigned.
2. Using an empirical relationship established between tree height (derived from the CHM for trees with a single stem) and the minimum HSCOI (Lucas *et al.* 2006b) to assign all remaining stems with a second height estimate.

The height assigned to stems using both methods was then compared, and when these were within an arbitrary 20% of each other, the CHM-derived height was assigned to the stem. Where the two height measures diverged by a greater amount, the stem was assumed to be a sub-canopy tree, and the HSCOI-derived height was assigned.

Stem diameter (at 130 cm) was estimated from tree height using a general empirical nonlinear function that was generally applicable across the main genus types. A random sample (80%,  $n=3016$ ) of ground-measured live trees with  $D_{130} \geq 5$  cm, (from 33 field plots) was used, such that:

$$D_{130} = 3.9806 \exp^{(0.1189H)}. \quad (3)$$

When evaluated against the remaining 20% of live trees ( $D_{130} \geq 5$  cm,  $n=755$ ), predictions of  $D_{130}$  were reasonable ( $r^2=0.60$ ,  $RSE=5.97$  cm, with the slope and intercept of the best-fit line being 1.06 and 0.43, respectively). While some scatter was evident, the slope of the best-fit line indicated that stem  $D_{130}$  derived from  $H$  measurements approximated actual ground-measured  $D_{130}$ . The function could be further refined using species-specific data. Following attribution of LiDAR stems with  $D_{130}$ , an independent validation set of 119 randomly selected ground-measured trees ( $D_{130} \geq 5$  cm) from 30 field plots were matched to the LiDAR stems (using location, height, crown area, and  $D_{130}$ ), and a useful correspondence was observed (table 1).

### 5.5 Tree-scale estimation of component biomass and AGB

To assign individual trees with an estimate of component (leaf, branch, and trunk) biomass, allometric equations for *E. populnea* and *E. melanaphloia* (Burrows *et al.* 2000), *C. glaucophylla* (Burrows *et al.* 2001), *A. harpophylla* (Scanlan 1991), and a range of sub-canopy and understorey species (e.g. *Eremophila mitchelli*; Harrington 1979) were used. The equations and coefficients are summarized in Lucas *et al.* (2006a) and required either circumference (at 30 cm or 130 cm) or height (m) as

Table 1. Relationships established between tree height and diameter based on 119 randomly selected trees from 30 field plots.

Comparison	$R^2$ (RSE*)	Function
Tree height†	0.71 (3.19 m)	$y=0.587x+3.6$
Tree diameter‡	0.65 (6.9 cm)	$y=0.793x+4.4$

\*Residual standard error.

† $x$ =diameter.

‡ $x$ =height.

input. To apply the allometric equations appropriately, crown/crown-cluster objects representing single species and containing more than one stem were first identified, and stems with heights within 10% of the maximum (as determined from the CHM) were then assigned to the crown/crown-cluster object and given an associated species code. Generally, objects with several stems were associated with species supporting larger, more expansive crowns (e.g. *A. leiocarpa* or *E. melanophloia*). All remaining stems within the object were then associated with sub-canopy trees, and were necessarily linked to species (e.g. *C. glaucophylla*) of lower stature occurring in proximity to the object being considered. The circumference (determined from  $D_{130}$ ) or heights of both the overstorey and sub-canopy stems were then used as input to the species-specific allometric equations for estimating component biomass. Adjustments were made for species where the diameter at 30 cm ( $D_{30}$ ) was the required independent variable, through the use of empirical relationships between  $D_{130}$  and  $D_{30}$ . The AGB associated with individual stems was calculated by summing the leaf, branch and trunk biomass. The AGB associated with delineated crowns/crown-cluster objects was then calculated as the sum of the AGB of the stems contained within each object.

To generate estimates of AGB for the 30 0.25 ha ( $50 \times 50$  m) SSUs contained within each of the PSUs being sampled, the AGB associated with each delineated crown/crown-cluster was summed. Where a SSU boundary intersected a crown, the AGB assigned to each SSU was based on the proportion of the crown area found within the SSU. All estimates were expressed in terms of  $\text{Mg ha}^{-1}$ . Although ground data were collected from 13 PSUs, three were excluded for the analysis as follows:

1. PSU 59: contained small trees (typically less than 2 m in height) that were regenerating following recent clearance (i.e. the area was considered to be largely non-forest);
2. PSU 144: portions of the LiDAR data were adversely affected by strong winds during the acquisition;
3. PSU 148: the large number of species observed reduced confidence in discrimination and hence subsequent calculation of AGB.

Of the 300 SSUs remaining, 30 were associated with non-forest and were also excluded from further analyses.

## 5.6 Validation and comparison

To provide an independent assessment of AGB at the plot scale, a set of estimates was generated using a Jackknife linear regression between field measures of AGB and both LiDAR-derived crown cover and the frequency of returns within a range of canopy height levels. Canopy heights were determined from apparent vertical

profiles of LiDAR returns, with the use of three heights each from both understorey and overstorey (where present).

The model form and parameter selection were developed initially through stepwise linear regression (Lucas *et al.* 2006a). However, this approach was limited because all plots were included in the calibration, and none were available for independent validation because of the small number of field plots and wide range of forest types occurring. To refine the estimates of variance and derive robust estimates of standard errors in the model, Jackknife techniques were applied subsequently. Jackknifed statistics are created by systematically omitting subsets of data one at a time and assessing the resulting variation in the studied parameter (Mooney and Duval 1993). This allowed the refinement of parameter selection, resulting in substitution of two parameters from the initial regression model. Parameter estimates were refined through examination of the replicates histogram, where plots of the observed parameter value and mean of the replicates highlighted the estimated bias. Jackknifed statistics also provided information on the influence of each observation on the model. The final function had the form and parameters listed in equation (4):

$$\text{Biomass}(\text{Mg}\cdot\text{ha}^{-1}) = [-44.4\text{ht}_{.5\%}] + [57.98\text{ht}_{.10\%}] + [-18.8\text{ht}_{.20\%}] + [8.3\text{ht}_{.50\%}] + [-34.98 \times \text{ht}_{.75\%}] + [32.2\text{ht}_{.80\%}] + [0.86\text{Crown\_Cover}^0] - 20.68, \quad (4)$$

where  $\text{ht}_x\%$  is the height at which the LiDAR data ( $>0.5$  m in height and sorted lowest to highest) reaches the cumulative percentage of returns. Once all iterations were complete, the mean parameter values were used to calculate AGB for the field plots. The observed, mean, bias and standard error estimates for the parameters are shown in table 2. Table 3 shows the correlation between the coefficients used in the regression analysis and were used to establish if any multicollinearity between parameters might exist. As expected, some metrics were correlated, but this only occurred for a minority of the parameter combinations (assuming a  $\pm 0.7$  correlation threshold). However, as there is little correlation between the different overstorey and understorey sampling parameters, this correlation between some metrics is considered to be a relatively minor issue.

Estimates of AGB generated using the Jackknife regression were calibrated with ground data at the plot scale. The regression equation was considered to be sufficiently robust ( $r^2=0.90$ ,  $\text{RSE}=11.8 \text{ Mg ha}^{-1}$ ,  $n=31$ ; figure 5) for application across the landscape using the PSU grid. The Jackknife method compared well with a previous iteration of the plot-scale biomass estimated using a stepwise linear

Table 2. Jackknife results for the plot scale regression parameters.

Parameter	Observed*	Bias*	Mean*	Standard error*
Height_05%	-44.48	1.31	-44.43	18.80
Height_10%	58.04	-1.72	57.98	20.33
Height_20%	-18.82	0.49	-18.81	5.45
Height_50%	8.33	-0.18	8.32	3.47
Height_75%	-35.13	4.56	-34.98	17.07
Height_80%	32.32	-4.35	32.18	14.98
Crown cover %	0.86	0.05	0.86	0.23
Intercept	-20.68	0.01	-20.68	11.41

\*Rounded to two decimal places for clarity.



Table 3. Correlation of Coefficients for Jackknife analysis

	(Intercept)	HSCOI-CC	HT@05%	HT@10%	HT@20%	HT@50%	HT@75%
HSCOI-CC	0.11	–					
HT@05%	0.40	0.17	–				
HT@10%	0.32	0.14	0.94	–			
HT@20%	0.20	0.08	0.54	0.76	–		
HT@50%	0.09	0.00	0.06	0.13	0.45	–	
HT@75%	0.10	0.25	0.09	0.03	0.21	0.79	–
HT@80%	0.18	0.33	0.16	0.10	0.14	0.70	0.99

regression method that also corresponded well with ground data of ( $r^2=0.92$ ,  $SE=12.06 \text{ Mg ha}^{-1}$ ,  $n=32$ ; Lucas *et al.* 2006a). Note that one plot was omitted from the jackknife regression because the coverage of LiDAR returns within the field plot was insufficient, and this resulted in greater uncertainty with the field calibration. The resulting large dataset (estimates for all 4500 SSUs) provided a reference against which estimates of tree-summed plot AGB could be cross-checked across a wide range of different forest types and structures.

## 6. Results

### 6.1 AGB estimates: comparisons with ground data

The comparison of tree-summed plot AGB estimated through integration of LiDAR and CASI data with ground (plot) data provided an overall correspondence ( $r^2=0.56$ ,  $RSE=25.3$ ,  $n=21$ ; figure 6). For 10 plots, this correspondence was close (within 10%), and within these, the density of trees ( $D_{130} \geq 5 \text{ cm}$ ) was lower (average= $360 \text{ stems ha}^{-1}$ ,  $\delta=34.2$ , range 210–670; table 4), trees were taller, and their crowns were more widely spaced. Large individuals, particularly *A. leiocarpa*, also contributed the majority of the basal area. However, within the remaining 11

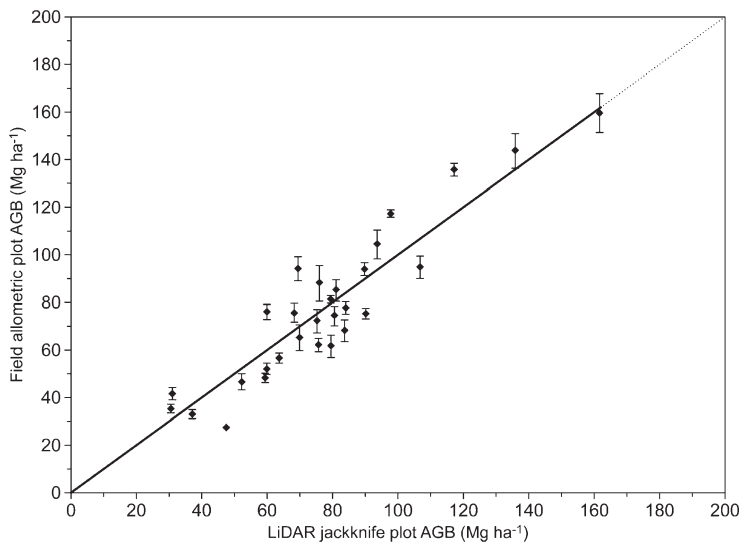


Figure 5. Correspondence between AGB ( $\text{Mg ha}^{-1}$ ) estimated from field measurements and using the plot scale jackknife linear regression ( $R^2=0.90$ ,  $RSE=11.8 \text{ Mg ha}^{-1}$ ).

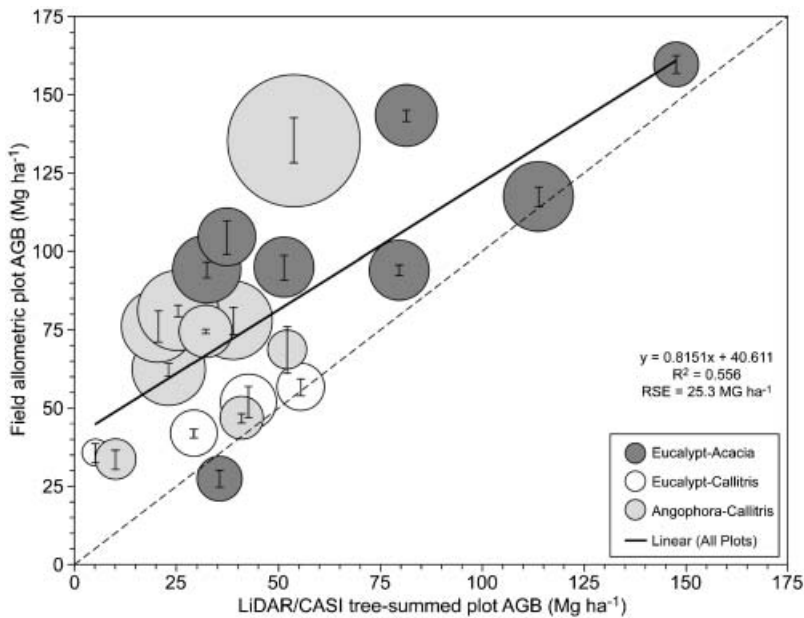


Figure 6. Comparison of AGB estimated from field data and by summing the AGB of individual trees estimated through LiDAR-CASI integration. Circle size is proportional to plot stem density, and the shading relates to co-dominant genera, as determined from basal area measurements. Field data error bars represent the 95% confidence level.

plots, the AGB was underestimated using LiDAR-CASI data. Within these plots, the density of trees was greater (average = 700 stems  $\text{ha}^{-1}$ ,  $\delta = 145.2$ , range 100–2310), and many contained regenerating understorey layers dominated by *C. glaucophylla*. Table 4 presents the different forest structures observed in the 21 field plots.

## 6.2 AGB estimates: comparisons across the landscape

Across 10 PSUs, the biomass (leaf, branch, trunk, and AGB) was estimated and mapped at the individual crown/crown-cluster level. Figure 7 illustrates the component and total AGB maps for PSU 58.

When the AGB was summed at the individual tree level for 270 SSUs, the comparison with the AGB estimated using the Jackknife regression suggested an overall correspondence ( $r^2 = 0.47$ ,  $\text{RSE} = 24.4 \text{ Mg ha}^{-1}$ ), with the slope and intercept of the best-fit line being 0.65 and 37.05, respectively. To test for possible autocorrelation between adjacent SSUs with the PSUs, the Durbin–Watson statistic was applied using the residuals. This gave a  $d$  value of 1.152, which was outside the confidence bounds for the number of samples used with 1 regressor term and at the 1% significant level. As a Durbin–Watson statistic of 2 indicates no autocorrelation, while a 0 indicates large positive autocorrelation, the result generated from the 270 SSUs indicates some positive autocorrelation between SSUs. However, as the input data list sequence is not a complete representation of the spatial arrangement because of some non-adjacent SSUs and PSUs being considered as adjacent, then a further comparison was undertaken. Here, two equal sets of SSUs were selected from the 270, such that there were no adjacent SSUs in either set. A further test randomly selected two equal sets of SSUs. The correspondences for the two

Table 4. Differences in forest structure observed for plots where estimates of AGB generated using LiDAR and CASI data compared well ( $n=10$ ) or otherwise ( $n=11$ ).

Field plot	Stem count			Crown cover %	Predominant plot height (m)	Co-dominant genus
	<i>Callitris/</i> <i>Acacia</i>	<i>Eucalyptus/</i> <i>Angophora</i>	Total stems			
142-02	28	46	74	23.8	10.9	<i>Eucalypt-Acacia</i>
142-13	4	59	63	31.7	12.4	<i>Eucalypt-Callitris</i>
114-12	53	16	69	28.6	14.2	<i>Callitris-Angophora</i>
142-20	58	47	105	42.2	14.7	<i>Eucalypt-Acacia</i>
142-18	2	51	53	40.0	15.1	<i>Eucalypt-Callitris</i>
23-16	37	37	74	48.7	15.6	<i>Angophora-Acacia</i>
83-20	52	48	100	43.2	15.6	<i>Eucalypt-Callitris</i>
111-18	146	21	167	68.5	19.8	<i>Callitris-Angophora</i>
23-24	84	35	119	59.4	19.8	<i>Angophora-Callitris</i>
81-11	63	7	70	62.7	21.5	<i>Angophora-Callitris</i>
Mean of plots ( $\leq 10\%$ )	53	37	89	44.9	16.0	10
131-18	12	13	25	18.6	11.1	<i>Eucalypt-Acacia</i>
83-12	3	52	55	25.6	12.7	<i>Eucalypt-Callitris</i>
138-21	51	122	173	47.3	14.5	<i>Eucalypt-Callitris</i>
23-20	84	27	111	34.9	14.9	<i>Angophora-Callitris</i>
138-16	36	135	171	56.0	15.0	<i>Eucalypt-Callitris</i>
23-15	70	136	206	67.6	15.1	<i>Eucalypt-Callitris</i>
124-06	136	75	211	52.9	15.7	<i>Callitris-Eucalypt</i>
111-12	550	27	577	77.1	17.5	<i>Callitris-Eucalypt</i>
81-16	93	24	117	62.6	18.0	<i>Angophora-Callitris</i>
114-04	138	14	152	40.5	18.0	<i>Callitris-Angophora</i>
124-19	110	19	129	49.9	18.2	<i>Angophora-Callitris</i>
Mean of field plots ( $>10\%$ )	117	59	175	48.5	15.5	11

non-adjacent SSU sets were ( $r^2=0.42$ ,  $RSE=26.1 \text{ Mg ha}^{-1}$ ,  $n=135$ , slope=0.58, intercept=41.1) and ( $r^2=0.53$ ,  $RSE=22.4 \text{ Mg ha}^{-1}$ ,  $n=135$ , slope=0.72, intercept=32.9). The correspondence for the two randomly selected SSU sets was ( $r^2=0.47$ ,  $RSE=24.1 \text{ Mg ha}^{-1}$ ,  $n=135$ , slope=0.63, intercept=35.4) and ( $r^2=0.48$ ,  $RSE=24.5 \text{ Mg ha}^{-1}$ ,  $n=135$ , slope=0.66, intercept=39.3). A Student  $t$ -test comparing the residuals for both selections found no significant difference between the means.

Given the similarity in result between the full 270 SSU and the subsequent non-adjacent and randomly selected samples, it was concluded that any spatial autocorrelation bias that existed was very minor. This was also considered because the AGB comparisons were made between different data sources within SSUs, rather than between SSUs. Therefore, SSU spatial arrangement and adjacency should only have an indirect and minor influence on the correspondence.

To assist in the interpretation of the different sources and interactions of potential error, these 270 points were divided into three classes (figure 8). Specifically, tree-summed plot AGB generated through integration of LiDAR and CASI data were considered to be overestimated by  $>10\%$  compared with the Jackknife regression estimate (Class 1,  $n=37$ ), within  $\leq 10\%$  of each other (Class 2,  $n=40$ ), or underestimated by  $>10\%$  (Class 3,  $n=193$ ).

The results presented in figure 8 are described further in table 5. Within Class 1, most of the stands contained *C. glaucophylla* and *E. melanophloia* species (both in the

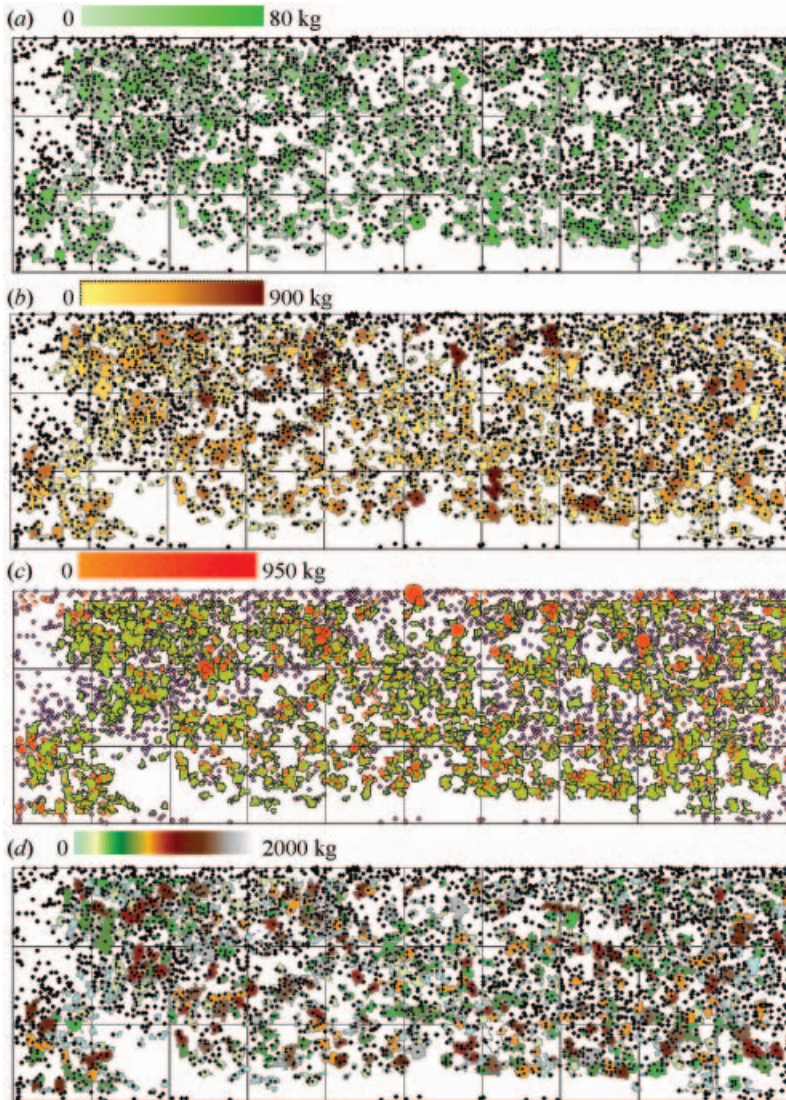


Figure 7. Maps of (a) leaf, (b) branch, (c) trunk (proportional symbols in red), and (d) total AGB (kg) generated from CASI and LiDAR data for PSU 58.

overstorey and sub-canopy) along with other taller trees (e.g. *A. leiocarpa*), many of which supported larger crowns. Here, large crowns are defined as those with an area  $>100\text{ m}^2$ . Generally, the basal area of the sub-canopy was lower (an average of 7% of plot basal area) compared with Class 2 forests. The overestimation of AGB was therefore attributed to the greater interaction of LiDAR pulses with the upper canopy of these taller overstorey trees and hence overestimation of stem height (and thus diameter) in the sub-canopy. Additionally, the overstorey stems of large individuals were likely to have exaggerated AGB values because of the height/diameter being outside the range of the allometric equations for these species. This was particularly the case for some species (namely *Angophora*), as allometrics were not available, and equations from other species were necessarily substituted. Where

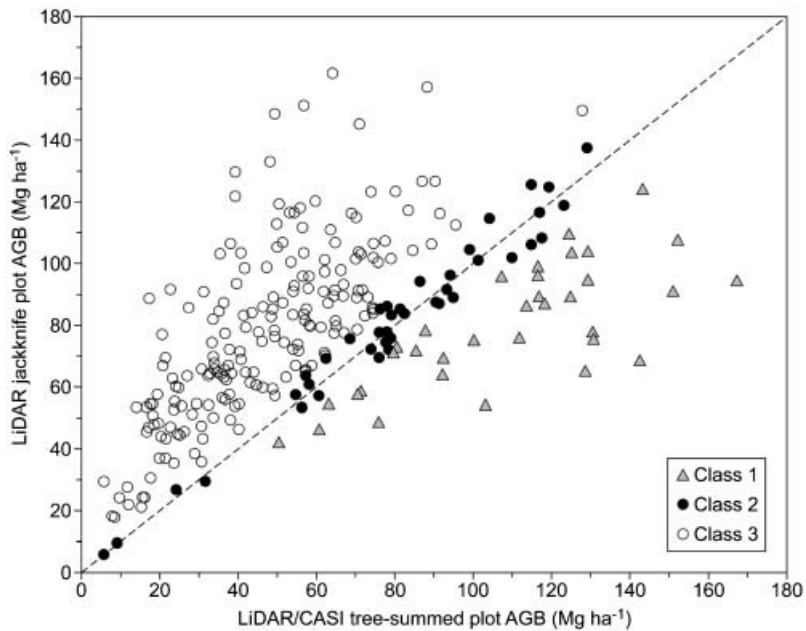


Figure 8. Comparison of AGB estimated at the plot scale using a Jackknife regression (y-axis) and by summing tree-level AGB (x-axis) obtained through integration of LiDAR and CASI data, for each of the 270 SSUs.

Table 5. Comparison of mean structural attributes ( $n=270$ ) associated with classes 1, 2, and 3.

Error class	1		2		3	
	Overestimate		≤ 10%		Underestimate	
Error class range	>10%		≤ 10%		>10%	
Count	37		40		193	
% of SSU's	13.7		14.8		71.5	
Structural attribute	Mean	SD	Mean	SD	Mean	SD
Jackknife AGB ( $\text{Mg ha}^{-1}$ )	78.7	24.1	81.3	29.5	78.0	28.7
Tree-scaled AGB ( $\text{Mg ha}^{-1}$ )	107.5	35.0	80.9	29.2	46.5	21.1
% of SSU composed of large crown area	12.7	14.3	9.7	12.5	6.0	10.7
% basal area in understorey	7.4	9.8	9.9	12.9	11.9	10.2
% stems ( <i>C. glaucophylla</i> / <i>E. melanaphloia</i> )	80.7	23.9	71.7	30.4	61.4	35.3
% understorey stems ( <i>C. glaucophylla</i> / <i>E. melanaphloia</i> )	32.9	13.9	31.0	16.1	27.3	19.4
SSU Predominant height (m)	17.2	3.4	15.4	3.6	14.2	3.2
% basal area SLI/CP in understorey	5.6	5.6	7.2	10.2	7.4	9.4
SSU crown cover %	48.8	13.4	46.8	14.4	44.2	16.6
% understorey stems (5–10 cm dbh)	41.2	16.5	42.7	14.2	44.2	17.0
LiDAR stem density ( $\text{stems ha}^{-1}$ )	438	136	425	143	424	173

Attributes listed after AGB are ranked in order of percentage difference between error classes.

the AGB was underestimated (Class 3), the forests were less mature, as indicated by their lower plot predominant height and crown cover, and there were fewer larger crowns present. These SSUs were also highly variable in terms of their structure and species composition. The SSUs in this class were differentiated from Class 1 SSUs in that the plot basal area of the understorey was greater (average of 12% of plot basal area), and a higher number of other species were found in this stratum. In this case, the underestimation of AGB was attributed largely to the inability to locate all stems using the LIDAR-derived HSCOI because of their high density (often several per m<sup>2</sup>). Where there was agreement in the AGB estimates (Class 2), these forests had a similar density to Class 3 forests but supported less understorey. The trees contained were tall but supported less expansive crowns compared with those found in Class 1 forests.

The selection of the 10% threshold to represent 'correct' estimation was arbitrary. Furthermore, the use of percentage difference as an indicative measure can inflate the apparent error for plots with low AGB. For example, consider a plot that has an AGB estimate of 20 Mg ha<sup>-1</sup> from the Jackknife regression, and 10 Mg ha<sup>-1</sup> from the tree-summed plot AGB estimates. The difference in estimates (10 Mg ha<sup>-1</sup>) is 50% of the Jackknife plot estimate. Now, consider another plot that has greater biomass, where the Jackknife AGB estimate is 160 Mg ha<sup>-1</sup> and the tree-summed plot AGB is 150 Mg ha<sup>-1</sup>. The 10 Mg ha<sup>-1</sup> difference between estimates is now only 6.25% of the Jackknife plot estimate. Therefore, an apparently small difference in estimates (e.g. 10 Mg ha<sup>-1</sup>) can give the impression of large error if percentage differences are only used for lower biomass plots. Consideration of the practical application and error requirements, as well as the distribution of plot biomass across the landscape is needed to determine the most appropriate assessment strategy.

For these reasons, a number of other thresholds were used (table 6), and this suggested that, at best without further model refinement, 50% of the AGB could be estimated by scaling from the individual tree level. The analysis also indicated that because of the complexity of forests occurring within the study area resulting from different species and successional stages (and hence crown architectures), accurate estimates of AGB are perhaps very difficult to achieve if scaling from trees identified and attributed using LiDAR and CASI data.

## 7. Discussion

For forest inventory, landscape estimation of structural attributes, biomass, and species composition at the tree level is desirable but has been difficult to achieve

Table 6. Assessment of the accuracy of modelling using different thresholds of potential error based on 270 SSUs.

Error Class	1		2		3	
	Count	%	Count	%	Count	%
10% threshold (table 4)	37	14	40	15	193	71
20% threshold	26	10	76	28	168	62
Greater than plot scale RSE for field plots*	29	11	76	28	165	61
Greater than plot vs tree scale RSE for 270 SSU plots†	19	7	134	50	117	43

\*12 Mg ha<sup>-1</sup>.

†24 Mg ha<sup>-1</sup>; RSE=residual standard error.

through ground (plot-based) measurement alone because of logistical constraints. This research has demonstrated an approach for specifically estimating biomass from fine spatial resolution airborne data within an integrated landscape-scale sampling scheme. The approach utilized a sequence of separate procedures aimed at retrieving structural (i.e. stem diameter, height, and density) and species information from LiDAR and CASI data, respectively. These derived data were then used in conjunction with available allometric equations to estimate AGB and component biomass. Such information could not have been obtained using either dataset alone. The approach presented is also complementary or even partially supplementary to ground survey, particularly as landscape-level assessments can be achieved over large areas and often in shorter time frames. The approach also contrasts with many previous biomass estimation methods that have focused primarily on extrapolating plot-based measures across the landscape. These methods have been based largely upon empirical relationships established with, for example, LiDAR (e.g. Lucas *et al.* 2006a), optical (Steininger 2000), or radar remote sensing data (e.g. dos Santos *et al.* 2003).

The methods developed in this research can be used to support biomass assessment at scales from the tree to the landscape, although further refinement is needed for successful retrieval in the more complex forests. Table 7 outlines some of the refinements that are needed and how these might be addressed in the future. While not offering a full solution to the consistent retrieval of biomass, the research has set a methodological baseline against which the success of future work can be

Table 7. Refinements necessary for improving AGB estimation through integration of LiDAR and CASI data.

Requirement	Potential solution
Discriminating tree species in the overstorey	<ul style="list-style-type: none"> <li>• Refinements to crown delineation</li> <li>• Inclusion of shortwave infrared data (Lucas <i>et al.</i> 2006c)</li> </ul>
Discriminating tree species in the sub-canopy	<ul style="list-style-type: none"> <li>• Spectrally unmix delineated crowns/crown clusters</li> <li>• Utilize structural information from LiDAR (e.g. Moffiet <i>et al.</i> 2005) as well as known community association for different environments (soils, terrain, etc.)</li> </ul>
Detecting multiple stems	<ul style="list-style-type: none"> <li>• Develop rules based on, for example, stem number versus height/crown area and species relationships</li> </ul>
Estimating stem density	<ul style="list-style-type: none"> <li>• Further refine methods that use the HSCOI for locating stems (Lee and Lucas 2007)</li> <li>• Establish empirical relationships between delineated crown/cluster area and height and stem density</li> <li>• Utilize LiDAR data acquired at a higher sampling rate, or smaller footprint size to allow greater penetration to sub-canopy</li> </ul>
Estimating the height of sub-canopy trees	<ul style="list-style-type: none"> <li>• Further evaluate relationships with the HSCOI</li> <li>• Utilize full waveform LiDAR, if available</li> </ul>
Estimating diameter	<ul style="list-style-type: none"> <li>• Utilize species specific empirical relationships between diameter and height and crown area</li> <li>• Utilize relationships that consider environmental influences (e.g. soils, topography) on growth form</li> </ul>
Estimating AGB and component biomass	<ul style="list-style-type: none"> <li>• Develop allometric equations for new species and for the full range of size classes across different environments, through further destructive harvesting and/or by using terrestrial laser scanners</li> </ul>

gauged and has also provided insight into some of the limitations of such an approach and obstacles that need to be overcome.

The majority of the procedures implemented in this research are generally applicable to other forests provided that remote sensing data of a similar form are available. Knowledge of the species composition of the forests is, however, necessary for implementing parts of the crown delineation algorithms, training the multiple stepwise discriminant analysis, appropriately applying allometric equations for AGB and component biomass estimation, and for retrieving structural attributes (e.g. diameter and height) based on species-specific empirical relationships (Lee and Lucas 2007). Nevertheless, once established for a particular forest region, the procedures can be applied routinely, although some independent validation would, of course, be necessary.

## 8. Conclusions

This study has provided a preliminary evaluation of the integration of LiDAR and CASI data for estimating AGB and component biomass at the individual tree or tree cluster level. When summed to a plot scale, a close correspondence with the AGB estimated within the field and using a Jackknife regression with LiDAR data was observed. When tree-scale LiDAR-CASI AGB estimates were evaluated, greater correspondences were observed for forests where the tree density was generally lower, individuals were widely spaced, trees were tall with crowns of a moderate size, and more mature individuals dominated the basal area. However, for plots where these structural conditions did not occur, the AGB was overestimated in forests where a large number of tall trees with expansive crowns occurred. Underestimation occurred in less mature forests of lower stature, and which were dominated by trees with smaller crowns, or containing a higher stem density of individuals usually in the understorey. Clusters containing a higher stem density consisted primarily of the species *C. glaucophylla* across all plots.

The approach was automated and allowed rapid estimation of AGB and component biomass across the landscape at a level unachievable through plot-based survey alone. While estimation at the individual crown-cluster level appears to be an involved process with the potential for significant improvement, advantages over more general methods that relate remote sensing data (e.g. reflectance at coarser spatial resolution) to biomass through empirical relationships (e.g. with plot-based summaries) were evident. For example, a better understanding of allocation of biomass to different plant components can be obtained, even though there is large apparent variability in some results. This is to be expected, given the complex relationship between components and the total biomass, which, in turn, complicates retrieval using remote sensing data (Lucas *et al.* 2000, 2004). The approaches outlined in this paper present the necessary initial steps to better understand these inherent relationships by first mapping the biomass components, and then using multiscale analyses to interpret, refine, and ultimately improve the algorithms for their estimation.

The algorithms developed for the characterization and reconstruction of the selected forests have a direct application for forest assessment in other regions of Australia and also overseas. The data and products have already been used to support the development of forest mapping using other remote sensing datasets including (1) a 3D forest quantitative reconstruction for coherent SAR simulation (Williams *et al.* 2003, Lucas *et al.* 2006b), (2) a better understanding of microwave



interaction with different components of the forest and the importance of sensor parameters (frequency, polarization, and incidence angle) for biomass retrieval (Lucas *et al.* 2004, 2006a), (3) improved techniques for mapping woody regrowth using a combination of lower frequency radar and Landsat-derived FPC data (Lucas *et al.* 2006c), and (4) interpretation of coarser spatial resolution hyperspectral (e.g. HyMap) data for forest classification and assessment of tree species diversity (Bunting and Lucas 2006b). In future work, the algorithms will be implemented across the Injune study area to provide baseline datasets of forest biomass, structure, and species to support regional and national mapping using spaceborne remotely sensed data including that provided by Japan's Advanced Land Observing Satellite (ALOS), as well as ICESat large footprint laser data.

### Acknowledgements

The authors would like to thank the Australian Research Council, Queensland Department of Natural Resources and Mines (QDNR&M), Queensland Herbarium, Bureau of Rural Sciences (BRS), Australian Greenhouse Office, Cooperative Research Centre (CRC) for Greenhouse Accounting, and Queensland Department of Primary Industries (QDPI) Tropical Beef Centre. Ursula Benz and Definiens AG are especially thanked for providing the facilities and software for Peter Bunting, who was funded by an EU AMPER Training Network Scholarship and by the Institute of Geography and Earth Sciences and Computing Science Department, University of Wales Aberystwyth. Ball Aims are thanked for acquiring the CASI data.

### References

- BARRETT, D.J., GALBALLY, I.E. and GRAETZ, R.D., 2001, Quantifying uncertainty in estimates of C emissions from above ground biomass due to historical land-use change to cropping in Australia. *Global Change Biology*, **7**, pp. 883–902.
- BRACK, C., RICHARDS, G. and WATERWORTH, R., 2006, Integrated and comprehensive estimation of greenhouse gas emissions from land systems. *Sustainability Science*, **1**, pp. 91–106.
- BUNTING, P.J. and LUCAS, R.M., 2006a, The delineation of tree crowns in Australian mixed species forests using hyperspectral Compact Airborne Spectrographic Imager (CASI) data. *Remote Sensing of Environment*, **101**, pp. 230–248.
- BUNTING, P.J. and LUCAS, R.M., 2006b, Landscape classification of Australian forest communities using hyperspectral HyMap and CASI data. In *Proceedings, IUFRO Landscape Ecology Conference*, 26–29 September, 2006, Locorotondo, Bari, Italy (Vienna: IUFRO), pp. 457–462.
- BUNTING, P.J., PATERSON, M. and LUCAS, R.M., 2006, Discrimination of tree species in Australian woodlands using hyperspectral CASI data. In *Proceedings, Workshop on 3D Remote Sensing in Forestry*, 14–15 February, Vienna (Vienna: University of Natural Resources and Applied Life Sciences), pp. 287–290.
- BUNTING, P.J., 2007, Integration of remote sensing data for the characterisation of Australian forests. Unpublished PhD thesis, University of Wales, Aberystwyth.
- BURNETT, C. and BLASCHKE, T., 2003, A multi-scale segmentation/object relationship modelling methodology for landscape analysis. *Ecological Modelling*, **168**, pp. 233–249.
- BURROWS, W.H., HOFFMAN, M.B., COMPTON, J.F. and BACK, P.V., 2001, *Allometric Relationships and Community Biomass Stocks in White Cypress Pine (Callitris glaucophylla) and Associated Eucalypts of the Carnarvon Area, Central Queensland* (Canberra: Australian Greenhouse Office) National Carbon Accounting System (NCAS) Technical Report 33, pp. 17.

- BURROWS, W.H., HOFFMAN, M.B., COMPTON, J.F., BACK, P.V. and TAIT, L.J., 2000, Allometric relationships and community biomass estimates for some dominant eucalyptus in central Queensland woodlands. *Australian Journal of Botany*, **48**, pp. 707–714.
- BURROWS, W.H., HENRY, B.K., BACK, P.V., HOFFMAN, M.B., TAIT, L.J., ANDERSON, E.R., MENKE, N., DANAHER, T., CARTER, J.O. and MCKEON, G.M., 2002, Growth and carbon stock change in eucalypt woodlands in north-east Australia: ecological and greenhouse sink implications. *Global Change Biology*, **8**, pp. 1–16.
- CARTER, G.A., 1994, Ratios of leaf reflectance in narrow wavebands as indicators of plant stress. *International Journal of Remote Sensing*, **15**, pp. 697–703.
- CHASMER, L., HOPKINSON, C. and TREITZ, P., 2006a, Examining the influence of changing laser pulse repetition frequencies on conifer forest canopy returns. *Photogrammetric Engineering and Remote Sensing*, **72**, pp. 1359–1367.
- CHASMER, L., HOPKINSON, C. and TREITZ, P., 2006b, Investigating laser pulse penetration through a conifer canopy by integrating airborne and terrestrial lidar. *Canadian Journal of Remote Sensing*, **32**, pp. 116–125.
- CHAVE, J., CONDIT, R., AGUILAR, S., HERNANDEZ, A., LAO, S. and PEREZ, R., 2004, Error propagation and scaling for tropical forest biomass estimates. *Philosophical Transactions of the Royal Society of London*, **359**, pp. 409–420.
- CLARK, M.L., ROBERTS, D.A. and CLARK, D.B., 2005, Hyperspectral discrimination of tropical rain forest tree species at leaf to crown scales. *Remote Sensing of Environment*, **96**, pp. 375–398.
- DEFINIENS, 2005, *eCognition Version 5 Object Oriented Image Analysis User Guide* (Munich: Definiens AG).
- DOBSON, M.C., ULABY, F.T., PIERCE, L.E., SHARIK, T.L., BERGEN, K.M., KELLNDORFER, J., KENDRA, J.R., LI, E., LIN, Y.C., NASHASHIBI, A., SARABANDI, K. and SIQUEIRA, P., 1995, Estimation of forest biophysical characteristics in northern Michigan with SIR-C/X-SAR. *IEEE Transactions on Geoscience and Remote Sensing*, **33**, pp. 8877–8895.
- DOS SANTOS, J.R., FREITAS, C.C., ARUAJO, L.S., DUTRA, L.V., MURA, J.C., GAMA, F.F., SOLER, L.S. and SANT'ANNA, J.S., 2003, Airborne P-band SAR applied to above ground biomass studies in the Brazilian tropical forest. *Remote Sensing of Environment*, **87**, pp. 482–493.
- EAMUS, D., MCGUINNESS, K. and BURROWS, W.H., 2001, *Review of allometric relationships for estimating woody biomass for Queensland, the Northern Territory and Western Australia* (Canberra: Australian Greenhouse Office) National Carbon Accounting System (NCAS) Technical Report 33, pp. 5a, 64 pp.
- GASTELLU-ETCHEGORRY, J.P., ZAGOLSKI, F., MOUGIN, E., MARTY, G. and GIORDANO, G., 1995, An assessment of canopy chemistry with AVIRIS—a case study in the Landes Forest, South-west France. *International Journal of Remote Sensing*, **16**, pp. 487–501.
- GAVEAU, D.L.A. and HILL, R.A., 2003, Quantifying canopy height underestimation by laser pulse penetration in small-footprint airborne laser scanning data. *Canadian Journal of Remote Sensing*, **29**, pp. 650–657.
- GOUGEON, F.A. and LECKIE, D.G., 2003, *Forest Information Extraction from High Spatial Resolution Images Using an Individual Tree Crown Approach* (Victoria: Natural Resources Canada, Canadian Forest Service) Information Report BC-X-396.
- HARRINGTON, G., 1979, Estimation of above ground biomass of trees and shrubs in *Eucalyptus populnea* (F. Muell). Woodland by regression of mass on trunk diameter and plant height. *Australian Journal of Botany*, **2**, pp. 135–143.
- HUANG, Z., TURNER, B.J., DURY, S.J., WALLIS, I.R. and FOLEY, W.J., 2004, Estimating foliage nitrogen concentration from HyMap data using continuum removal analysis. *Remote Sensing of Environment*, **93**, pp. 18–29.
- HYYPPIA, J., KELLE, O., LEHIKONEN, M. and INKINEN, M., 2001, A segmentation-based method to retrieve stem volume estimates from 3-D tree height models produced by laser scanners. *IEEE Transactions on Geoscience and Remote Sensing*, **39**, pp. 969–975.

- INGLADA, J. and GIROS, A., 2004, On the possibility of automatic multisensor image registration. *IEEE Transactions on Geoscience and Remote Sensing*, **42**, pp. 2104–2120.
- KOHONEN, T., 2001, *Self-organizing maps* (Heidelberg: Springer).
- LECKIE, D.G., GOUGEON, F.A., TINIS, S., NELSON, T., BURNETT, C.N. and PARADINE, D., 2005, Automated tree recognition in old growth conifer stands with high resolution digital imagery. *Remote Sensing of Environment*, **94**, pp. 311–326.
- LEE, A.C. and LUCAS, R.M., 2007, A LiDAR-derived canopy density model for tree stem and crown mapping in Australian forests. *Remote Sensing of Environment*, **111**, pp. 493–518.
- LEFSKY, M.A., HARDING, D., COHEN, W.B. and PARKER, G.G., 1999, Surface LIDAR remote sensing of basal area and biomass in deciduous forests of eastern Maryland, USA. *Remote Sensing of Environment*, **67**, pp. 83–98.
- LEFSKY, M.A., HUDAK, A.T., GUZY, M. and COHEN, W.B., 2005, Combining LiDAR estimates of biomass and Landsat estimates of stand age for spatially extensive validation of modelled forest productivity. *Remote Sensing of Environment*, **95**, pp. 549–558.
- LIM, K., TREITZ, P., WULDER, M., ST-ONGE, B. and FLOOD, M., 2003, LiDAR remote sensing of forest structure. *Progress in Physical Geography*, **27**, pp. 88–106.
- LIM, K.S. and TREITZ, P.M., 2004, Estimation of above ground forest biomass from airborne discrete return laser scanner data using canopy-based quantile estimators. *Scandinavian Journal of Forest Research*, **19**, pp. 558–570.
- LOVELL, J.L., JUPP, D.L.B., NEWNHAM, G.J., COOPS, N.C. and CULVENOR, D.S., 2005, Simulation study for finding optimal LiDAR acquisition parameters for forest height retrieval. *Forest Ecology and Management*, **214**, pp. 398–412.
- LOBO, A., 1997, Image segmentation and discriminant analysis for the identification of land cover units in ecology. *IEEE Transactions on Geoscience and Remote Sensing*, **35**, pp. 1136–1145.
- LUCAS, R.M., CRONIN, N., LEE, A., WITTE, C. and MOGHADDAM, M., 2006a, Empirical relationships between AIRSAR backscatter and forest biomass, Queensland, Australia. *Remote Sensing of Environment*, **100**, pp. 407–425.
- LUCAS, R.M., CRONIN, N., MOGHADDAM, M., LEE, A., ARMSTON, J., BUNTING, P. and WITTE, C., 2006c, Integration of radar and Landsat-derived foliage projected cover for woody regrowth mapping, Queensland, Australia. *Remote Sensing of Environment*, **100**, pp. 407–425.
- LUCAS, R.M., LEE, A. and WILLIAMS, M., 2006b, The role of LiDAR data in understanding the relationship between forest structure and SAR imagery. *IEEE Transactions in Geoscience and Remote Sensing*, **44**, pp. 2736–2754.
- LUCAS, R.M., MILNE, A.K., CRONIN, N., WITTE, C. and DENHAM, R., 2000, The potential of Synthetic Aperture Radar (SAR) data for quantifying the above ground biomass of Australia's woodlands. *Rangeland Journal*, **22**, pp. 124–140.
- LUCAS, R.M., MITCHELL, A., DONNELLY, B., MILNE, A.K., ELLISON, J. and FINLAYSSON, M., 2002, Use of stereo aerial photography for assessing changes in the extent and height of mangrove canopies in tropical Australia. *Wetlands Ecology and Management*, **10**, pp. 161–175.
- LUCAS, R.M., MOGHADDAM, M. and CRONIN, N., 2004, Microwave scattering from mixed species woodlands, central Queensland, Australia. *IEEE Transactions on Geoscience and Remote Sensing*, **42**, pp. 2142–2159.
- MEANS, J.E., ACKER, S.A., HARDING, D.A., BLAIR, B.J., LEFSKY, M.A., COHEN, W.B., HARMON, M. and MCKEE, W.A., 1999, Use of large footprint scanning airborne LIDAR to estimate forest stand characteristics in the western Cascades of Oregon. *Remote Sensing of Environment*, **67**, pp. 298–308.
- MITCHELL, A.L., LUCAS, R.M., DONNELLY, B.E., PFIZNER, K., MILNE, A.K. and FINLAYSON, M., 2007, A new map of mangroves for Kakadu National Park,

- Northern Australia, based on stereo aerial photography. *Aquatic Conservation*, in press.
- MOFFIET, T., MENGERSEN, K., WITTE, C., KING, R. and DENHAM, R., 2005, Airborne laser scanning: Exploratory data analysis indicates potential variables for classifying vegetation according to species. *ISPRS Journal of Photogrammetry and Remote Sensing*, **59**, pp. 289–309.
- MOONEY, C.Z. and DUVAL, R.D., 1993, *Bootstrapping. A Nonparametric Approach to Statistical Inference* (Newbury Park, CA: Sage University Paper series on Quantitative Applications in the Social Sciences), pp. 07–095.
- PATENAUDE, G., MILNE, R. and DAWSON, T.P., 2005, Synthesis of remote sensing approaches for forest carbon estimation: reporting to the Kyoto Protocol. *Environmental Science and Policy*, **8**, pp. 161–178.
- POPESCU, S.C. and WYNNE, R.H., 2004, Seeing the trees in the forest: using lidar and multispectral data fusion with local filtering and variable window size for estimating tree height. *Photogrammetric Engineering and Remote Sensing*, **70**, pp. 589–604.
- RICHARDS, G.P. (Ed.), 2002, *Biomass estimation: Approaches for Assessment of Stocks and Stock change. NCAS Technical Report* (Canberra: Australian Greenhouse Office) No. 27.
- ROSENQVIST, A., MILNE, A.K., LUCAS, R.M., IMHOFF, M. and DOBSON, C., 2003, A review of remote sensing technology in support of the Kyoto Protocol. *Environment, Science and Policy*, **6**, pp. 441–455.
- SCANLAN, J.C., 1991, Woody overstorey and herbaceous understorey biomass in *Acacia harpophylla* (brigalow) woodlands. *Australian Journal of Ecology*, **16**, pp. 521–529.
- SPECHT, R.L. and SPECHT, A., 1999, *Australian Plant Communities: Dynamics of Structure, Growth and Biodiversity* (Melbourne: Oxford University Press).
- STEININGER, M.K., 2000, Secondary forest structure and biomass following short and extended land-use in central and southern Amazonia. *Journal of Tropical Ecology*, **16**, pp. 689–708.
- TICKLE, P.K., LEE, A., LUCAS, R.M., AUSTIN, J. and WITTE, C., 2006, Quantifying Australian forest and woodland structure and biomass using large scale photography and small footprint LiDAR. *Forest Ecology and Management*, **223**, pp. 379–394.
- WILLIAMS, M.L., MANNINEN, T., KELLOMÄKI, S., IKONEN, V., SIEVÄNEN, R., LEHTONEN, M., NIKINMAA, E. and VESALA, T., 2003, Modelling the SAR response of pine forests in southern Finland. Proceedings, IEEE International Geoscience and Remote Sensing Symposium (IGARSS03), **2**, pp. 1350–1352.
- ZAGOLSKI, F., PINEL, V., ROMIER, J., ALCAYDE, D., FONTANARI, J., GASTELLU-ETCHEGORRY, J.P., GIORDANO, G., MARTY, G., MOUGIN, E. and JOFFRE, R., 1996, Forest canopy chemistry with high spectral resolution remote sensing. *International Journal of Remote Sensing*, **17**, pp. 1107–1128.
- ZHANG, J., RIVARD, B., SÁNCHEZ-AZOFEIFA, A. and CASTRO-ESAU, K., 2006, Intra- and inter-class spectral variability of tropical tree species at La Selva, Costa Rica: Implications for species identification using HYDICE imagery. *Remote Sensing of Environment*, **105**, pp. 129–141.
- ZITOVÁ, B. and FLUSSER, J., 2003, Image registration methods: A survey. *Image and Vision Computing*, **21**, pp. 977–1000.

---

## APPENDIX D

---

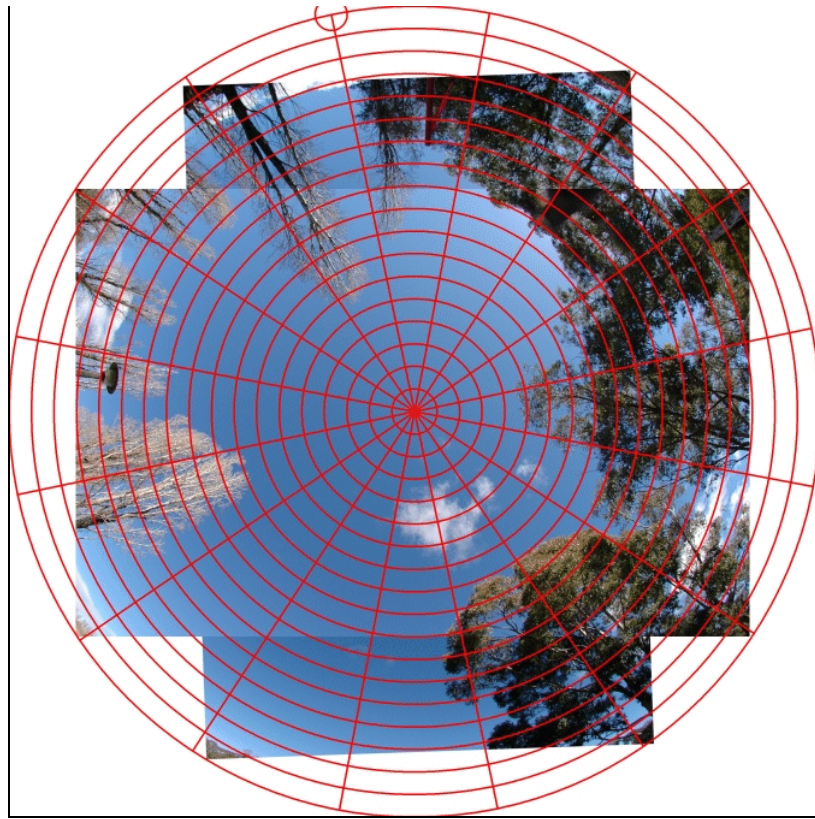
### **Hemispherical photo calibration methodology overview**

#### *Hemispherical Photo Cover Calibration*

An alternative method to assess crown/foilage cover is through the use of “fisheye” or hemispherical canopy photos. This method is effective for LiDAR cover validation as both LiDAR and photos sample a wider extent of the plot than with point based transect methods. This method has been widely used, for example (Frazer *et al.*, 2001; Lovell *et al.*, 2003; Coops *et al.*, 2004; Hill *et al.*, 2006; MacFarlane *et al.*, 2007a;~, 2007b) and for assessing the light penetration through canopy. The images can also be converted to crown openness images that are also used, for example Walker *et al.*, (1988), and McDonald *et al.*, (1998). Circular fisheye images were gathered in the NE Victorian field plots, however as the lens was an adapter, not a prime lens, the quality is not optimal, though sufficient for the purposes of this research. The Queensland datasets have used a 10.5 mm full frame prime hemispherical lens designed for digital cameras, so the image quality is very good (Figure 117). Estimates of foliage cover and LAI for both Queensland and NE Victorian plots were generated using Gap Light Analyzer (Version 2) software (Frazer *et al.*, 1999). For each Injune field plot the photo closest to the centre was used. However in plots with highly variable cover, that is, the initial photo estimate differed from the field transect or LiDAR cover estimate by more than 15%, then the centre photo from each of the three transects was selected and the cover and LAI estimate calculated as the average of the three photos. All measurements were taken at 1 m ( $\pm$  20cm) above the ground.

The full-frame nature of the Nikon lens used for the Injune study site images does not give a full 180° image view (i.e. circular). This is because an 180° view is only present along the diagonal (Figure 117) using calibration images taken at the Australian National University (ANU). As a result two images were required to better approximate the area of a full 180° circular image. Therefore photos were collected oriented both in north-south and east-west directions and merged to create a composite image. However this still resulted in some gaps in

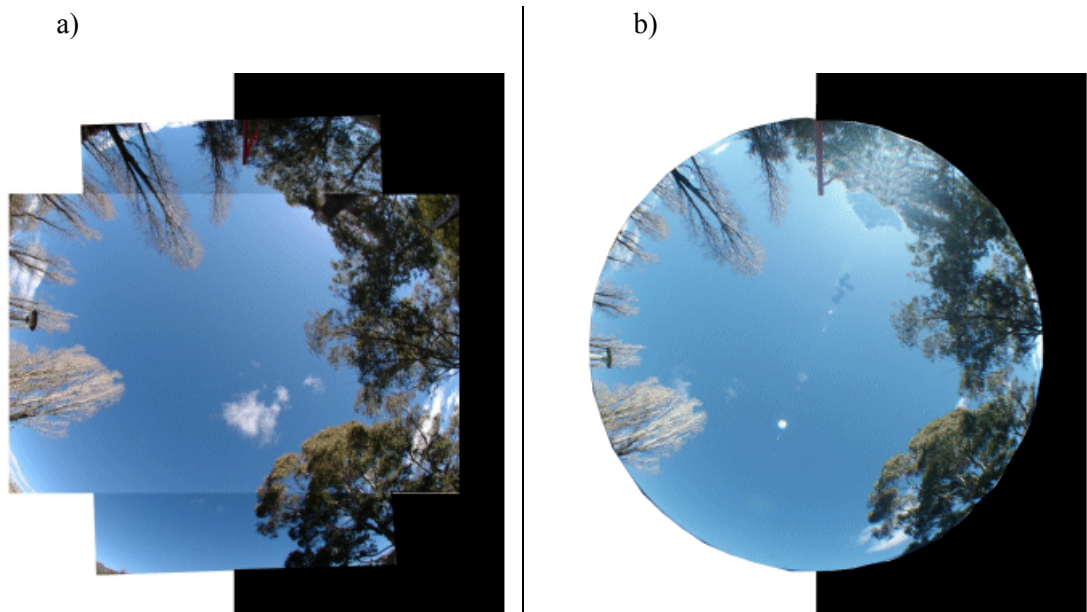
photo coverage at the edges. When examined in the GIS the total circle area was 358,699 pixels, with the photo area equal to 277,479 pixels. Therefore the estimation of the gap in photo coverage was calculated to be 22.65%, with the photo area being 77.35% of the full circular area out to 90 degrees zenith. Therefore if a 70 degree zenith is used, then the composite image allows 100% of the circular area to be used.



**Figure 117: Registration of calibration images using Nikon fisheye lens, showing effective view area, zenith rings, and gaps in extent with the merged photos.**

It was initially assumed that the Minolta lens imaged a full circular extent out to 90 degree zenith. However this assumption was tested in the interests of complete calibration and in order to understand any potential biases that may arise when comparing cover estimates between photos from the two lenses. When the actual view extent (i.e. what canopy elements were evident at the edge of the image) was compared (Figure 118) between the Nikon composite image and the Minolta image, it was observed that the effective Minolta view equated to the 70 degree zenith ring in the Nikon composite image. Therefore it can be concluded that both images completely image the same effective area, with the Nikon composite partially imaging further out towards the 90 degree zenith ring.

As the hemispherical photo analyses software was optimised for processing circular images that are assumed to image out to the 90 degree zenith angle, further processing of the images was undertaken. In this instance, because it is unknown if the edge of the photo would have been predominantly sky or canopy, the effective bias of choosing either was minimised by dividing the area outside the photo extent into equal area panels of black and white. This meant the contribution of the non-photo area to the cover / sky estimate will cancel out. In some cases this may introduce some bias from the actual result, as more sky (in very open woodland environments) or canopy (in dense forests) may be present, so the cover estimate will be an over-estimate or under-estimate respectively.



**Figure 118: Calibration images taken at ANU showing area imaged, and the same effective view extent with (a) Nikon lens, and (b) Minolta lens.**

To determine the potential effect of using a split black and white panel may have on cover estimates from hemispherical photography from the two lenses, a calibration exercise was undertaken using the ANU image. Here the images from both lenses were analysed with three different backing panel combinations: fully white, half black and white, and fully black. Then a full range of pixel brightness threshold values were used, to remove any potential user bias (Cescatti, 2007). The result of this analysis is shown in Figure 119.

Another issue that arose from assessing the images was that the sun disk was visible in many photos. This was due to the need to collect many samples in a short amount of time, as

well as the trunks and shiny leaves of some tree species (for example *E. populnea*) may be very similar to cloud or bright parts of the sky, introducing error when pixel brightness thresholding is undertaken. To resolve this, manual masking or pixel changes were required in cases where the sun disk and/or bright and shiny trunks and leaves were present.

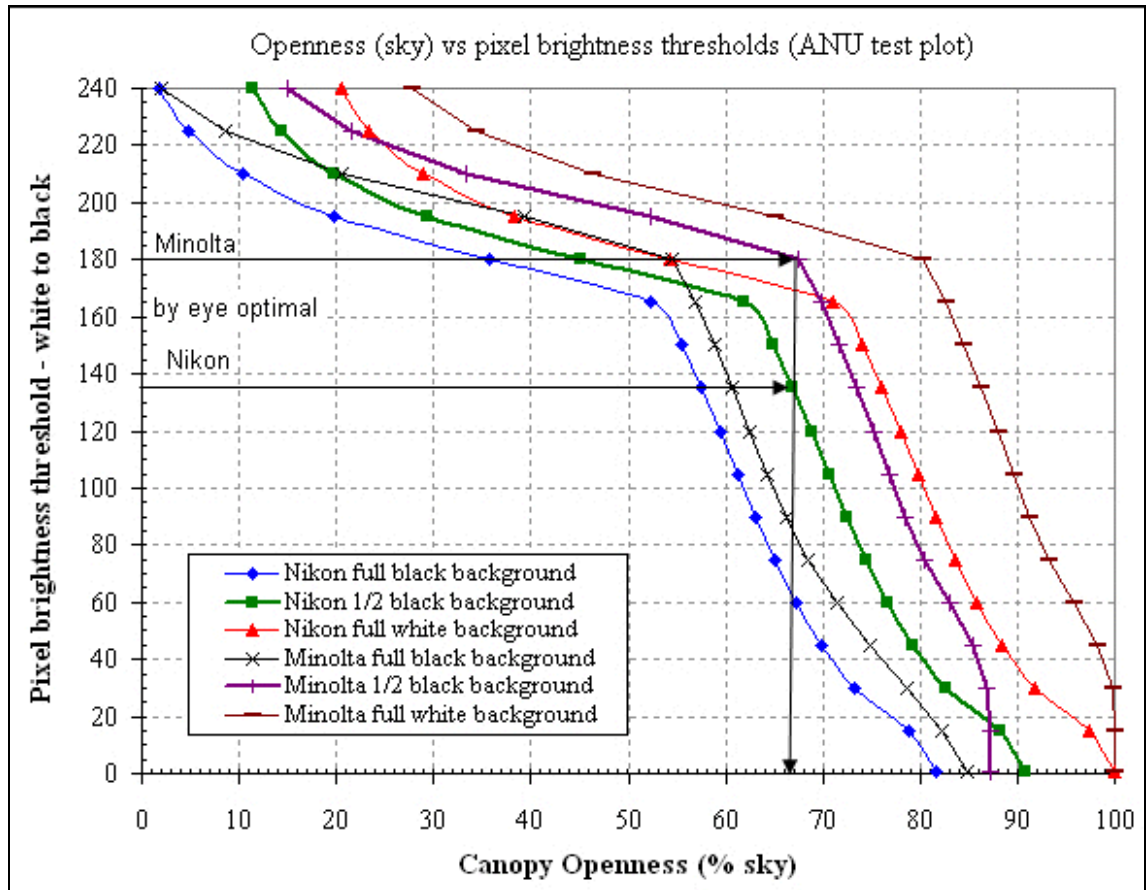


Figure 119: Effect of background colour and pixel brightness threshold in hemispherical photo analysis on cover estimates, using Nikon and Minolta lenses.

An assessment of the geographic extent visible in photos was undertaken to ensure the LiDAR used in the comparison also encompasses the same view area (Figure 120). This was also done to ensure that the same available view extent is used in both Victorian and Queensland datasets. Also, the heights that tree elements have to be observed in the photo, at the plot edge, given the “view” angle.



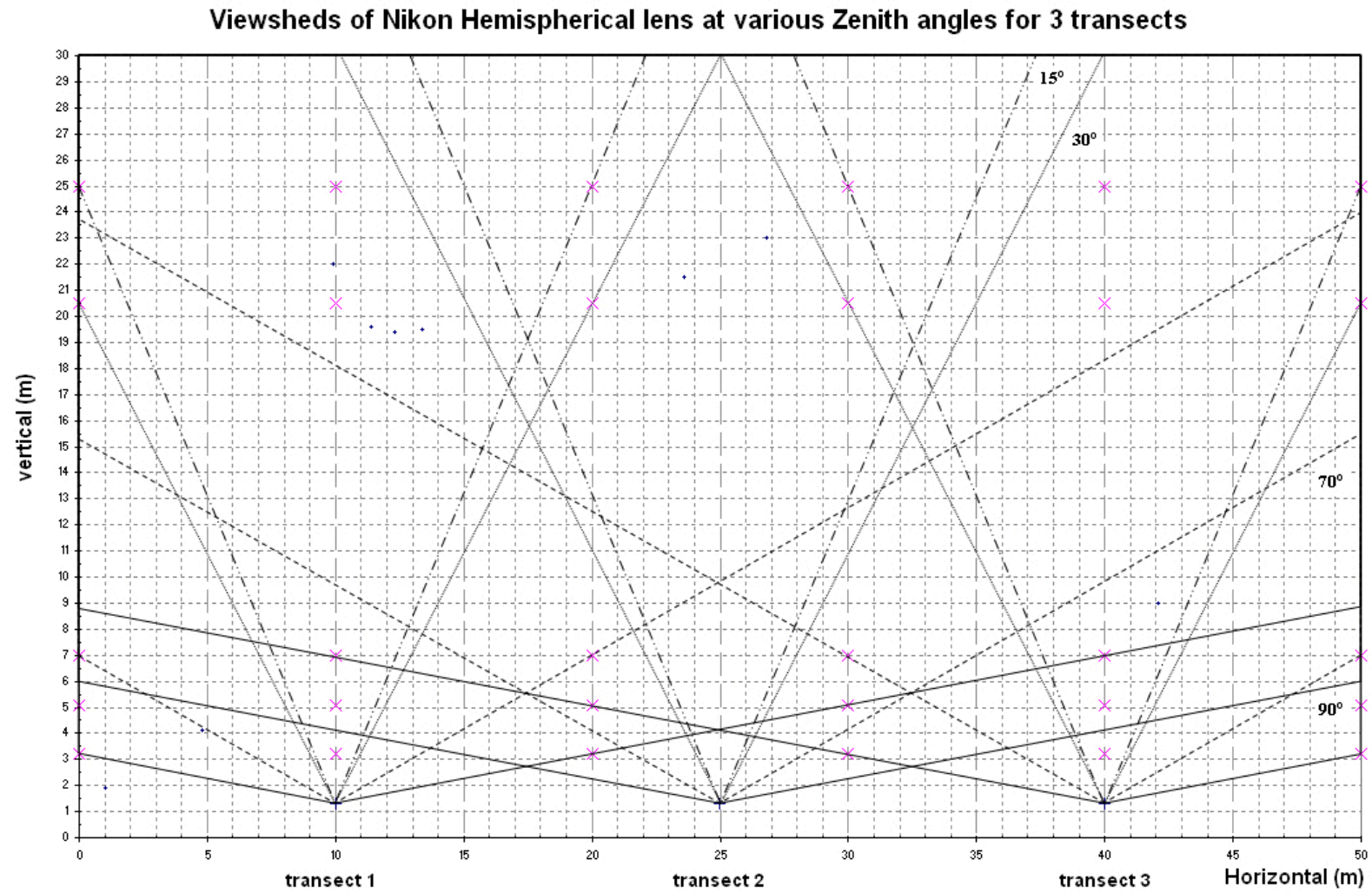
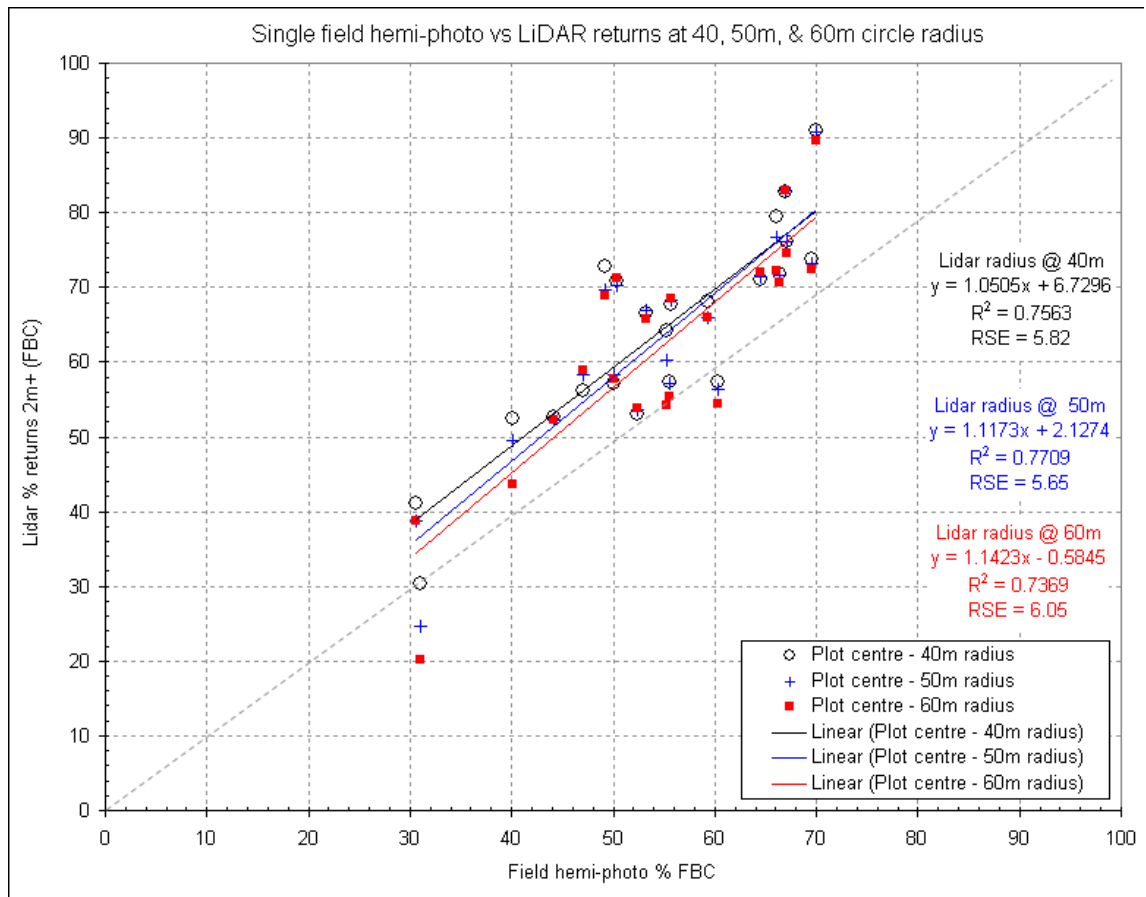


Figure 120: Simulated viewsheds at different zenith angles for Nikon fisheye photos when taken along Qld transects within a field plot

In a similar manner to the Injune processing, analyses of photo view extent were also undertaken for the NE Victorian plots. The analyses differed due to the different plot size and transect sampling methods used in the CFMF trial. It was noted that the actual visible extent of the hemispherical photos is not precisely known for each plot, as this varies with forest density. For example, in a more open forest the canopy elements from further away will be observed. The analysis of the LiDAR data involved calculating the cover estimate for a range of distances out from the plot centre. This utilised two research questions:

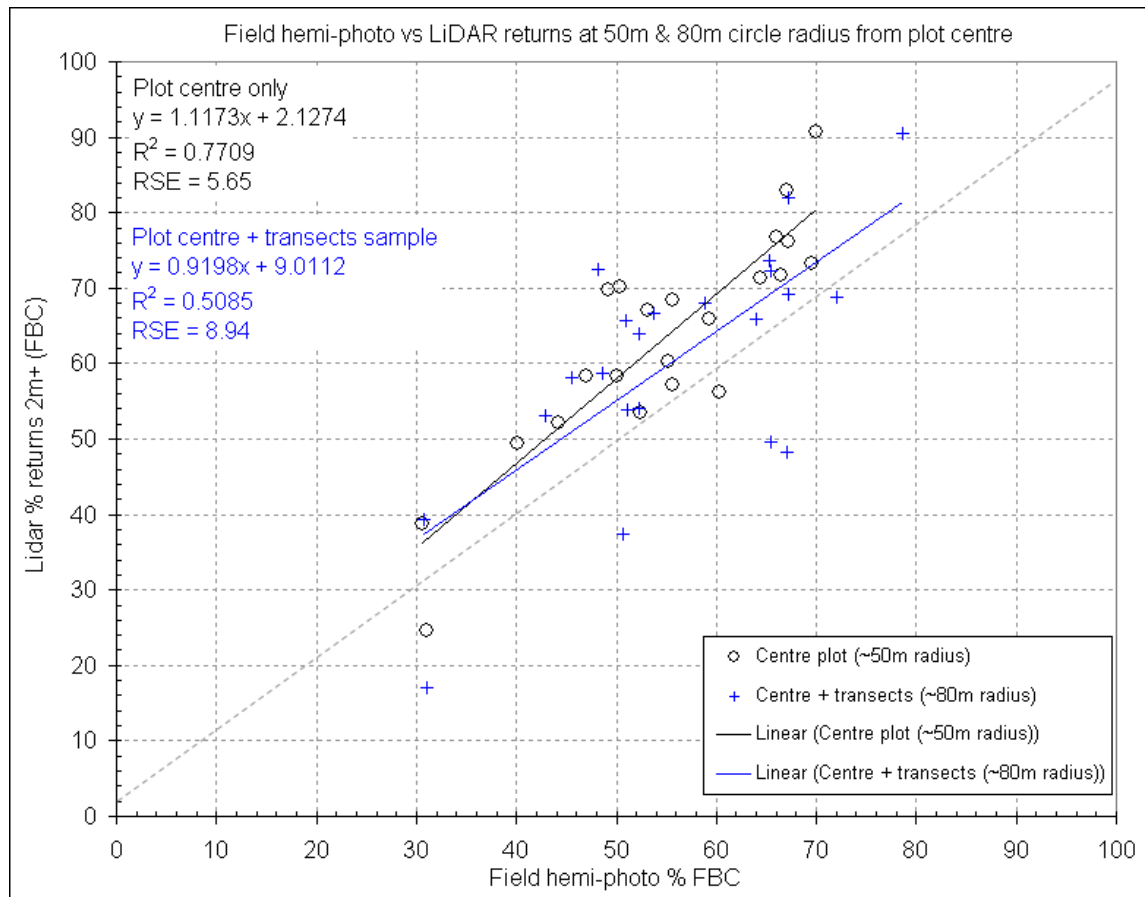
- What is the most likely distance that a single hemispherical photo is observing, such that there is a close correspondence with the LiDAR cover estimate? Initial calibration of the hemispherical photos at ANU indicated that the nominal view extent of the photo was between 40-50m from the camera location. Therefore the LiDAR was analysed at 40, 50, and 60m circle radii distances from the plot centre to see if this distance could be more precisely quantified.
- Given the assumed optimal hemispherical photo observing distance, do the additional transect photos collected as part of the CFMF sampling strategy adequately sample the wider one hectare transect area?

A distance of 50m for a single photo has the smallest residual error, and best  $r^2$ , though the difference from the other distances are small (Figure 121). The results observed are also close to calibration measurements undertaken. There appears to be a consistent underestimation of cover (as compared to the LiDAR estimate) by the photo method of approximately 10% on average. This may be a result of the photo not having a full 180° view angle. The view calibration exercise identified that at the edge of the photo it is actually observing canopy that is approximately 7m tall, with this height difference progressively reducing as the distance from the centre of the photo reduces. The LiDAR estimate includes all canopy strikes 2m+ in height throughout the assessment area, therefore the apparently greater cover results from the LiDAR may well be from the additional canopy that is below the view angle of the photo. To test this explanation, more detailed modeling of the LiDAR data that would simulate the removal of canopy elements below the photo view angle would need to be developed undertaken.



**Figure 121: Assessing potential hemispherical photo view areas for NE Victorian plots against of LiDAR returns (FBC) clipped at a range of circular areas.**

To test the sampling of photos along the transects, against LiDAR across the whole transect area (one hectare), further analyses were done. Here, the photos that were taken 20 m in from the end of each of the four transects were processed for cover, and combined with the plot centre photo estimate. This estimate was compared with LiDAR returns (foliage-branch cover%) clipped to a circle with an 80 m radius from the plot centre. The observed relationship shows much scatter (Figure 122) and this would appear to indicate that, with the current transect photo locations and orientation, that the wider transect area is not sampled adequately for cover, when compared to a LiDAR sample. It may be that different photo placements within the wider stand are required to better sample the forest for foliage and branch cover, to more closely emulate the LiDAR estimate for the given area..



**Figure 122: Assessing view area of NE Victorian plot hemispherical photos against LiDAR (FBC) % circular area assessment for plot and transect areas respectively.**